Synthesis of Mechanically Light-Responsive Materials for the Application in Photoswitchable Adhesives

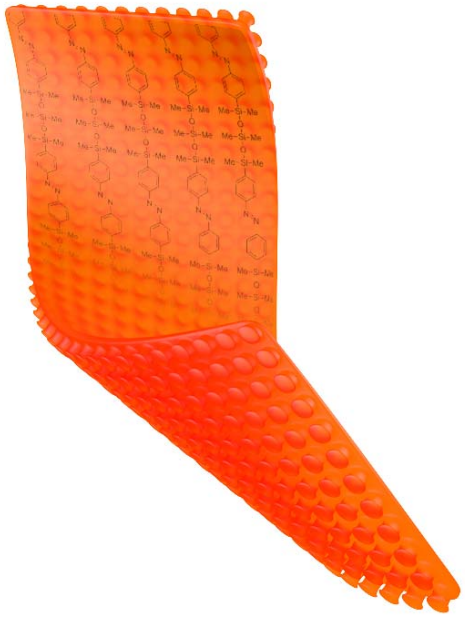

Dissertation

Zur Erlangung des Doktorgrades

der Mathematisch-Naturwissenschaftlichen Fakultät

der Christian-Albrechts Universität zu Kiel

vorgelegt von

Jan Strüben

Kiel 2015

1. Gutachterin: Prof. Dr. Anne Staubitz

2. Gutachterin: Prof. Dr. Thisbe K. Lindhorst

Tag der mündlichen Prüfung: 12.03.2015

Zum Druck genehmigt:

Die vorliegende Arbeit wurde unter Anleitung von

Prof. Dr. Anne Staubitz

am Otto-Diels-Institut für Organische Chemie

der Christian-Albrechts-Universität zu Kiel

in der Zeit von Oktober 2010 bis Januar 2015 angefertigt.

Hiermit erkläre ich, Jan Strüben, an Eides statt, dass ich die vorliegende Dissertation selbstständig und nur mit den angegebenen Hilfsmitteln angefertigt habe. Inhalt und Form dieser Arbeit sind, abgesehen von der Beratung durch meine Betreuerin Prof. Dr. Anne Staubitz, durch mich eigenständig erarbeitet und verfasst worden. Die Arbeit entstand unter Einhaltung der Regeln guter wissenschaftlicher Praxis der Deutschen Forschungsgemeinschaft. Weder die gesamte Arbeit noch Teile davon habe ich an anderer Stelle im Rahmen eines Prüfungsverfahrens eingereicht. Dies ist mein erster Promotionsversuch.

Kiel, den 22. Januar 2015 _____

(Jan Strüben)

Danksagung

Zunächst möchte ich mich bei meiner Doktormutter Prof. Dr. Anne Staubitz bedanken, dass ich an diesem interessanten und herausfordernden Thema arbeiten durfte. Über all die Jahre hat sie immer kreatives Arbeiten und auch ungewöhnliche Ideen unterstützt und gefördert. Ich bedanke mich auch bei Prof. Dr. Thisbe K. Lindhorst für die Übernahme der Zweitkorrektur.

Bei meinen Kooperationspartnern Dr. Xin Jin (AK Prof. Dr. Rainer Adelung) und Emre Kizilkan (AK Prof. Dr. Stanislav N. Gorb) möchte ich mich herzlich für die gute Zusammenarbeit, den regen Ideenaustausch und die Hilfe bei materialwissenschaftlichen Fragestellungen in den letzten Jahren bedanken.

Besonders bedanken möchte ich mich bei meinem Laborkollegen Hauke Kobarg für die gute Zeit im Labor über die letzten Jahre und bei Jan-Ole Springer, der im Rahmen seiner Masterarbeit mit viel Motivation Ergebnisse zu dieser Arbeit beigetragen hat sowie den Austauschstudenten Colin Gould und David Presa-Soto.

Ich möchte mich auch beim ganzen AK Staubitz und AK Soennichsen bedanken, insbesondere bei Mathias (Matti) Schulz und Matthias (Matze) Lipfert für die viele Unterstützung, die lustigen Kaffeepausen und das Korrekturlesen der Arbeit.

Bedanken möchte ich mich auch bei Prof. Dr. Frank Sönnichsen und seinen Mitarbeitern, insbesondere Gitta Kohlmeyer-Yilmaz, Marion Höftmann und Holger Franzen, die auch meine ungewöhnlichsten NMR–Wünsche voll unterstützt haben und für die nette Gesellschaft während der länger dauernden NMR-Experimente. Ich bedanke mich auch bei Dr. Paul J. Gates (University of Bristol) für die Anfertigung unzähliger Massenspektren.

Ich danke dem gesamten Institut für die gute Zeit und die große Hilfsbereitschaft über die letzten Jahre.

Natürlich möchte ich mich auch bei all meinen Freunden bedanken für die gute und lustige Zeit während des Studiums und der Promotion.

Zu guter Letzt möchte ich natürlich meiner Familie danken, ohne die weder das Studium noch die Promotion möglich gewesen wäre.

Kurzzusammenfassung

In dieser Arbeit wurde ein Konzept zur Herstellung eines photoschaltbaren Adhäsivs auf Basis eines photomechanisch responsiven Polymers untersucht. Hierzu wurde zunächst eine Methode entwickelt, ohne chemische Veränderung Materialien niedriger Oberflächenenergie miteinander zu verbinden. Mittels tetrapodischer Mikropartikel aus Zinkoxid konnten so zwei Filme aus Polydimethylsiloxan (PDMS) und Polytetrafluorethylen (PTFE), als klassische Extrembeispiele für geringe Hafteigenschaften, effektiv aneinandergeklebt werden. Desweiteren wurde der Einfluss von Porösität auf ein literaturbekanntes photomechanisch responsives Material untersucht.

Der zentrale Aspekt der vorliegenden Arbeit war die Synthese eines photoresponsiven, prozessierbaren Siloxans mit Azobenzoleinheiten in der Hauptkette. Für die Synthese eines entsprechenden Polymers musste zunächst eine synthetische Methode zur effektiven Metallierung und Silylierung von Azobenzolen entwickelt werden, da dies bis dato nur in niedrigen Ausbeuten möglich war. Der erste Schritt hierbei war eine neue Methode, Azobenzol mittels einer übergangsmetallkatalysierten Kreuzkupplung in sehr hohen Ausbeuten effizient zu stannylieren. Auf Basis der so erhaltenen Verbindungen war es zudem möglich, Azobenzole in sehr hohen Ausbeuten durch Zinn-Lithium-Austausch zu lithiieren, was zuvor nur in geringen Ausbeuten möglich war und ein notwendiger Schritt zur Funktionalisierung des Azobenzols mit Silicium ist. Für die zinnfunktionalisierten Azobenzole konnte ebenfalls gezeigt werden, dass sie sich sehr gut als Nucleophile in Stille Kreuzkupplungen eignen. Bei der Zinn-Lithium-Austausch Reaktion treten anders als bei bislang etablierten Methoden keine Reduktionen der Diazen Gruppe als Nebenreaktionen auf. Der Zinn-Lithium-Austausch wurde sowohl mechanistisch als auch synthetisch untersucht. Die Methode zur quantitativen Lithiierung von Azobenzol erlaubte die Synthese verschiedener Silanol funktionalisierter Azobenzole. Diese ließen sich zu einem prozessierbaren, hochmolekularen Copolymer aus Azobenzolen und Siloxaneinheiten umsetzen. Die so erhaltenen Materialien wurden auf sowohl ihre chemischen als auch photochemischen Eigenschaften untersucht.

Abstract

In this work, the concept of a photoswitchable adhesive based on a mechanically photoresponsive material was developed. Initially, a methodology was established to connect two materials with low surface energy without chemical modification. Poly(tetrafluoroethylene) (PTFE) and poly(dimethylsiloxane) (PDMS) are classic examples of materials with very low surface energies and non-sticking properties. Using tetrapodal zinc oxide microparticles, two films of PDMS and PTFE could be joined together. The influence of porosity on literature known photomechanical responsive polymers was studied.

The central point of this thesis was the synthesis of a new photoresponsive type of polymer: A poly(siloxane) with azobenzene units in the main chain. For the synthesis of such a material, several methodologies for the metalation of azobenzene had to be developed to obtain appropriate monomers for a polymerization. As a first step, a synthetic route for the stannylation of azobenzenes was developed and those compounds served as good nucleophiles in Stille cross coupling reactions. Furthermore they proved to be very suitable starting materials for lithiation reactions that proceeded in high yields. To date, the lithiation of azobenzenes could be performed only in low yields because of the sensitivity of the diazene group to organolithium reagents. The lithiation reaction was studied mechanistically and synthetically. This efficient route for a lithiation allowed the synthesis of a di-silanol functionalized azobenzene. This compound could be copolymerized to an alternating azobenzene siloxane polymer in high molecular weight and a very good solubility in all common organic solvents. The obtained polymers were characterized concerning their chemical and photochemical properties.

Table of Contents

1. Introduction

1.1 Photoswitchable Adhesives

Insects, spiders and even geckos can adhere to a variety of surfaces. Just with the contact area of their feet, the adhesion forces are strong enough that those animals can carry their own body weight multiple times without the need for a supporting “glue”: A spider sticks to a wall due to “dry adhesion” (Figure 1).

Figure 1. Tokay gecko (*gekko gecko*) and a housefly (*musca domestica*) sticking to a wall. (Rights of use purchased at *Shutterstock Inc.*)

The explanation for this ability is found in the special structure of their feet. They are covered with millions of microscopic hair-like adhesive setae which interact with the substrate by van der Waals forces.[1] In contrast to a continuous contact area, animals with such setae have many small subcontacts to the surface they are sticking to. A major advantage of the subcontacts is that a crack at the adhesive interface of a spider to the wall cannot propagate as it could with a continuous interface.[2] Besides a more stable adhesion, fibrillar systems can better adapt to rough surfaces and show a stronger adhesion than a continuous interface.[3] Typically, the adhesive systems of animals have a hierarchical architecture. The setae branch into finer setulae. The feet of the tokay gecko (*gekko gecko; Figure 1*) for example contain up to four hierarchical levels. This architecture prevents a clustering of the setae and increases the ability to adapt to different roughnesses of the substrates.[2a, 3a, 3b, 4] The geometry of the setae is essential for their adhesion. Biological systems which are designed for a long-term adhesion typically have mushroom shaped contact geometry (Figure 2).[5] Fast running insects,

spiders and geckos have spatula shaped setae.[5] Spatula shaped setae only show adhesion when a shear force is applied. This allows animals to quickly detach from a substrate but requires a permanent muscle force during adhesion.[3d, 6] The tokay gecko has about tree million setae on its toes which produce a clinging ability of 20 Newtons.[1a] This corresponds to a weight of approximately 2 kg.

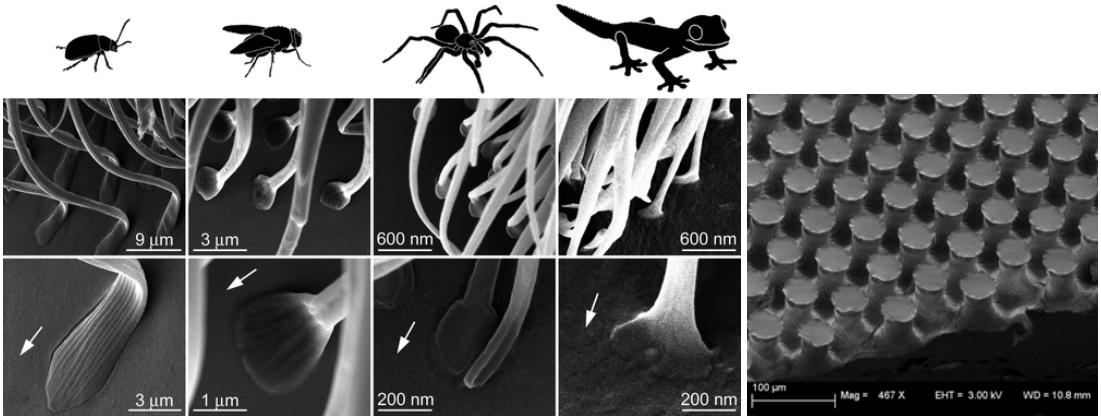

Figure 2. Scanning electron microscopical image of the spatula shaped satae of various animals (left) and an artificial microstructured Gecko®-Tape with a mushroom structure. Model of hypothesized relationships. (left) adapted from "Spatulate structures in biological fibrillar adhesion" by M. Varenberg, N. M. Pugno, S. N. Gorb, 2010, *Soft Matter, 6,* 3269. Copyright 2010 by the Royal Society of Chemistry. Adapted with permission. (right)) Used with the permission of Dr. Xin Jin, Institute of Materials Science, University of Kiel. Copyright Dr. Xin Jin 2014.

Inspired by those biological systems, materials were developed which emulate the stickiness of gecko feet. Products with mushroom shaped synthetic satae are already commercially available. Most products are silicone-based tapes with a microstructured surface. (e.g. Gecko® Nanoplast® with about 29000 mushrooms/cm^2). However, those materials only show a passive adhesion. The use of those adhesive features in intelligent functional materials is highly desirable.

The goal of this thesis was the development of a photoswitchable dry adhesive in form of a tape. Two conceptional designs were planned for such a device. One design is a microstructured tape made of poly(dimethylsiloxane) (PDMS) with a macroscopically, mechanically photoresponsive polymer attached to the back side of the tape. The shape change of the photoresponsive polymer is supposed to detach the tape from a surface. (Figure 3, a). The other design uses a microstructured macroscopically photoswitching polymer with a PDMS layer on the back side of the photoresponsive polymer (Figure 3, b)

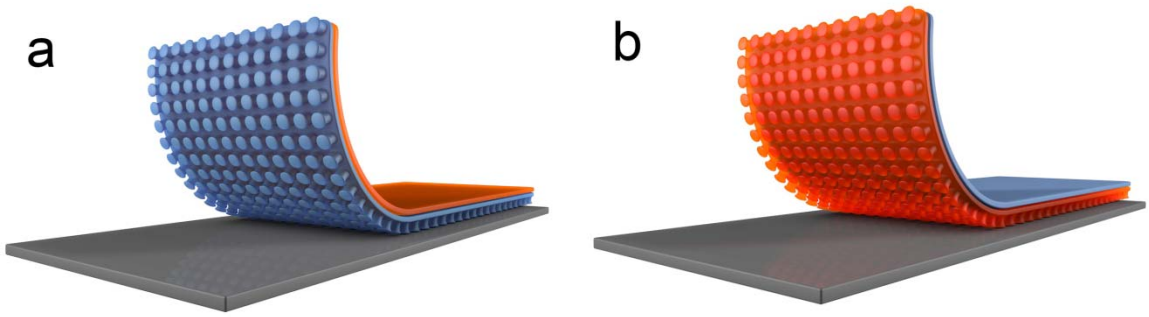

Figure 3. Two conceptional designs for a photoswitchalbe dry adhesive: a) a microstructured PDMS layer (blue) with a photoresponsive polymer attatched to its back side (orange) b) a microstructured photoresponsive polymer (orange) with a PDMS layer on its back side (blue).

However, these simple designs of such a device lead to various challenges in chemistry and materials science. A methodology was needed that allowed to attach polymers, where at least one of them (PDMS) would have a very non-sticky behavior, to each other without the need for chemical modification. Furthermore, a material needed to be developed which is processable and shows reversible and efficient shape changes when irradiated with a specific wavelength of light. Moreover, the material's properties (e.g. porosity, composites with other materials) and the influence on its photomechanic behavior needed to be investigated.

A photoresponsive material for such an application needs to fulfill four main requirements:

1) The material must show an efficient switching behavior with relatively large forces to be functionable in a composite material. Therefore, the materials should comprise **as many photoswitching units per volume unit as possible.**
2) A polymer film of the material must be soft enough to perform shape changes and allow a switching of the photoswitches. For this reason, **a low glass transition temperature (T_g)** is desirable.
3) The material must show **elastomeric properties** to perform **reversible** shape changes.
4) Photoswitching units must be **aligned** along one direction for an addition of the molecular forces.

Especially requirements 1, 2 and 4 might be incompatible:

An alignment of molecules along a preferred direction is typically achieved with liquid crystalline systems. Substances which can form liquid crystals are usually rigid rod like molecules.[7] As more rigid units the material contains, the more the glass transition temperature (T_g) of the material increases. With high T_g, the material might not be flexible enough to perform a shape change. When a polymer is heated above the glass transition temperature, the free volume of a polymer increases and provides the flexibility for molecular motion such as conformation and isomerization: The central requirement for photoswitching in the bulk material. A high number of rigid photoswitches in the material therefore needs to be compensated by more flexible linkers, such as siloxanes, in-between the photoswitches. If the number of photoswitching units is decreased, the material might be soft but not efficient enough to work in a composite material.

We envisioned that a copolymer with an efficient and durable photoswitching unit, such as azobenzene, and siloxane units as flexible linkers would fulfill the requirements described above. Azobenzene can form liquid crystals and is thermally very stable and resistant against photobleaching.[8] Its rigidity should be compensated by very flexible dimethylsiloxane-linkers. The hypothesis is that such a dimethylsiloxane-azobenzene copolymer (Scheme 1) allows a very high percentage of azobenzene units within the material until a critical stiffness is reached at ambient temperatures. The photoswitching units in the main chain should lead to an increased photoresponsiveness.[9]

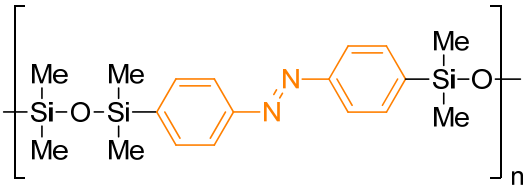

Scheme 1. A dimethylsiloxane-azobenzene copolymer.

1.2 Siloxanes

Poly(siloxanes) are probably the most deeply studied materials in the field of inorganic polymers. Because of their unique properties, they are widely used for countless applications: Especially their high chemical inertness,[10] biocompatibility[11] and flexibility[12] make poly(siloxanes) ideal for medical applications such as implants, catheters or artificial organs.[10, 13] Because of their high thermal stability they are often used as materials for high temperature application like cake pans, electric insulators or simply as sealants or as anti- friction agents (Figure 4).

Figure 4. Applications of poly(siloxanes) in daily life (rights of use purchased at *Shutterstock* Inc.)

Besides their advantageous unique physical properties, industrial production is very cost effective because poly(siloxanes) combine the most abundant elements on the planet, Silicon and Oxigen.[14] There are two main routes for synthesizing poly(siloxanes):

a) By a controlled hydrolysis of chlorosilanes (Scheme 2)

b) By anionic ring opening polymerization (Scheme 3).

The hydrolysis-polycondensation route, a step growth mechanism, generally leads to a mixture of linear and cyclic poly- and oligo(siloxanes) with low molecular weights and high polydispersities (Scheme 2).[10, 13]

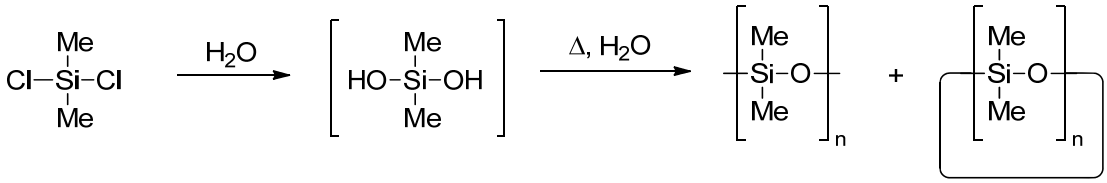

Scheme 2: Hydrolysis of dichlorodimethylsiloxane.

Poly(siloxanes) are typically synthesized from those cyclic siloxanes using an anionic ring opening polymerization (Scheme 3).[10, 13] In contrast to the hydrolytic polycondensation, the anionic polymerization is a chain-growth mechanism which allows a precise control of the molecular weight and leads to a low polydispersity.[13]

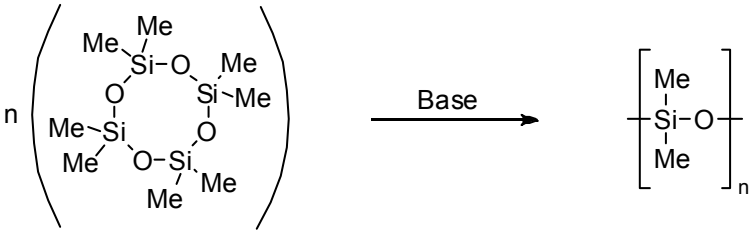

Scheme 3: Anionic ring opening polymerizaton of PDMS.

The backbone of a poly(siloxane) shows an extraordinary flexibility. This is a consequence of the special structural features of those materials. The most important property is the character of the silicon oxygen bond. Compared to a carbon-carbon bond which is 1.53 Å long, the silicon oxygen bond is with 1.64 Å significantly longer.[15] This decreases effects of sterical hindrance within the siloxane backbone. The flexibility is further supported by the divalency of the oxygen, which does not bear any side groups with potential sterical effects and facilitates conformative rotation and flexible bond angles.[15] The most intensively studied poly(siloxane) is PDMS.[10] The torsional barrier for rotations around the Si-O bond is very low. It is almost zero and the rotation virtually energy barrier free.[16] As comparison, the rotational energy for a C-C bond in an organic polymer is 13.8 kJ/mol.[16] With 143 °, the Si-O-Si bond angle is significantly wider than the tetrahedral bonding, which is typically 110 °. Torsional rotations can occur without a significant increase of energy.[12a, 15] PDMS shows one of the lowest glass transition temperatures (-125 °C) known because of this flexibility (Figure 5).[10, 17] Linear PDMS is a transparent liquid and is also known as silicon oil.

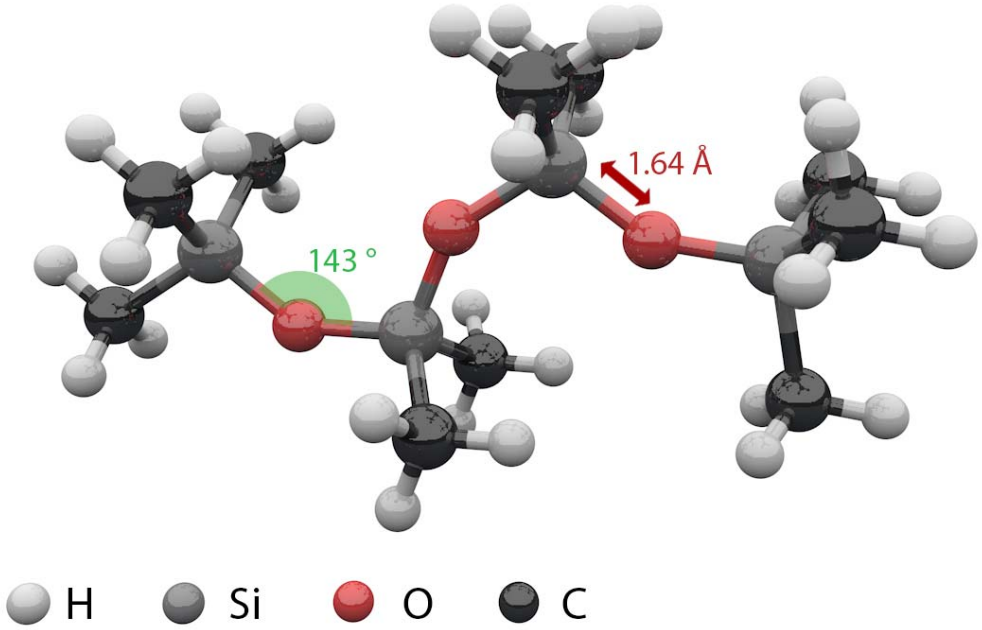

Figure 5. 3D-Structure of a trisiloxane with formerly discussed bond lengths and angles. The divalency of the oxygen and the bond length of Si-O reduces steric hindrance in conformation. (Bond angle and length from Ref.[10])

Because of the low viscosity of linear PDMS, the use is limited to fluid applications such as anti-friction agents. By modification of poly(siloxanes), important physical properties such as the glass transition temperature or the rigidity can be precisely adjusted. This makes poly(siloxanes) ideal for applications across a wide range of temperatures. There are several ways to modify poly(siloxanes). Especially for the production of elastomers or gels, the rigidity and the glass transition temperature are adjusted by cross-linking the polymer chains (Scheme 4, **b**). The higher the degree of cross-linking is, the higher is the rigidity and the glass transition temperature.[18] Cross-linked polymers are never soluble. If solubility is required, the linear polymer needs to be modified by the use of copolymers with varying substituents on the silicon units.[10, 18] Linear PDMS has a glass transition of -125 °C whereas poly(methylphenylsiloxane) shows a much higher glass transition of -28 °C (Scheme 4, **a**).[19] Besides side chain modifications, the physical properties can also be influenced by a main chain modification. Possible modifications are copolymers with non-siloxane units in the backbone, such as block copolymers, randomly copolymerized systems or alternating poly(aryl-siloxanes) (Scheme 4, **c**). Especially in the field of copolymers with various units in the backbone, the siloxane units increase the flexibility of the whole polymer chain. This

typically increases solubility and decreases glass transition temperatures of such systems, compared to the carbon based analogs.[20] Especially in the field of liquid crystalline polymers, siloxane units are used as spacers in-between mesogenic units to facilitate the formation of liquid crystalline phases.[7]

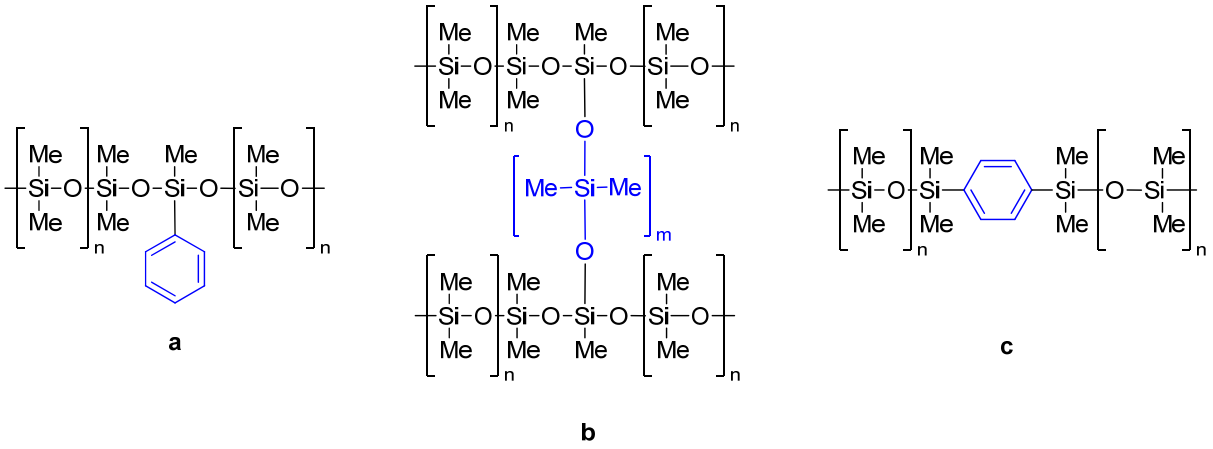

Scheme 4. Modifications of PDMS for the adjustment of physical properties.[18] a) co-polymers with repeating units with different side groups b) crosslinking of polymer chains c) more rigid co-monomers in the main chain.

1.3 Azobenzene

Azobenzene is one of the first known photoswitchable compounds in organic chemistry. Its photoswitchability was discovered in 1937 by S. Hartley.[21] About 70% of the world's commercial dyes are azobenzene based.[22] It is widely used because of its thermal stability[8b] and resistance to photo bleaching.[8a] By irradiation with UV light (365 nm), it isomerizes reversibly from its thermally stable *trans* form to the meta stable *cis* form; by irradiation with blue light (440 nm), azobenzene switches back to its *trans* form.[23] This photoisomerization leads to a significant change in the geometry and the electronic properties of azobenzene. The *trans* azobenzene shows a planar geometry and no dipole moment. The *cis* state is not planar and shows a dipole-moment of 3.2 Debye.[24] Mechanistic studies of the switching process have shown that the photoisomerization occurs very fast on a pico second time scale.[25] However, the isomerization mechanism of azobenzene is still of interest in current research, almost 80 years after the discovery of its photochemical properties. Several mechanisms have been discussed to date.[26] Most widely accepted are a rotational mechanism[26c] around the

diazene group or an inversion mechanism[26d] over one of the nitrogen atoms of the diazene group (Figure 6).

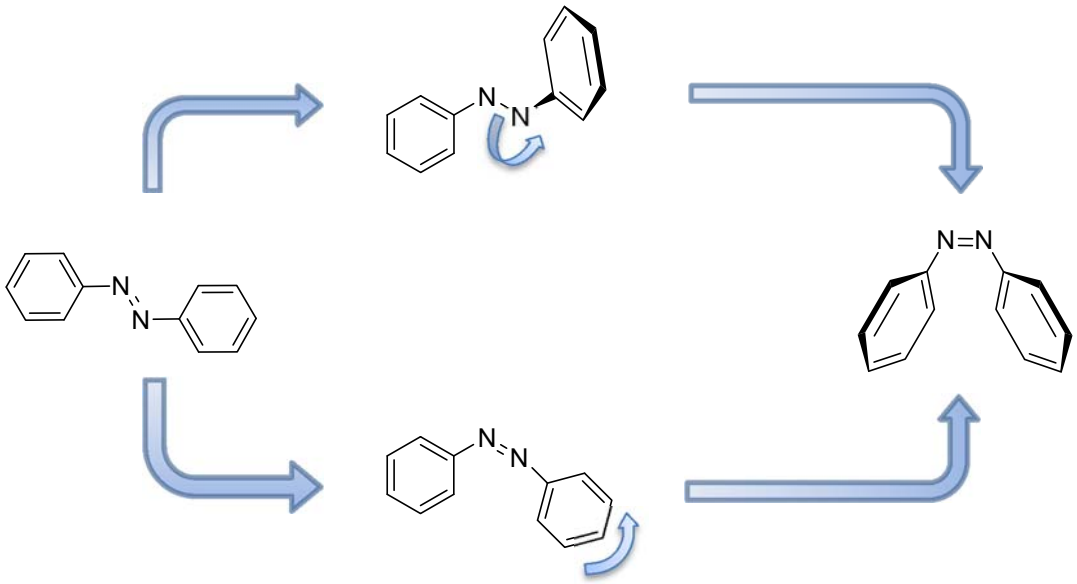

Figure 6. Rotational (top) and inversion mechanism (bottom) of the isomerization of azobenzene from its *trans* form to the *cis* form.[27]

Compared to the *cis*-isomer of azobenzene, the *trans* isomer is about 50 kJ/mol more stable. The energy barrier to convert the *trans* form to the *cis* state is about 200 kJ/mol.[27] Besides to a photo induced backswitching, azobenzenes re-isomerize to the *trans* state by thermal relaxation. Especially the planar geometry and the resulting increased delocalization of the π-electrons make *trans*-azobenzene energetically favorable. The absorption wavelengths for photoisomerization and especially the half-life of the *cis* state are strongly dependent on the substitution pattern of the azobenzene's phenyl rings and can range from seconds to days. By irradiation with UV light, a competition of the formation of the *cis* form and the thermal relaxation leads to a steady state mixture of *trans* and *cis* azobenzenes, the so-called photostationary equilibrium.[27] The ratio of *trans* and *cis* isomers is characteristic for each azobenzene based system and depends on many factors, such as whether the material is dissolved and in which solvent or if it is analyzed as bulk material, on the temperature, on steric effects, etc.[27]

1.4 Chemistry of Azobenzene

There is a variety of synthetic routes for synthesizing azobenzenes. Common synthetic routes are oxidative couplings of aniline derivatives[28] (Scheme 5, **a**) or reductive couplings of nitrobenzene derivatives[28b, 29] (Scheme 5, **b**). These routes are typically one-pot reactions, which are very effective for the synthesis of symmetric azobenzenes. However, due to the nature of the reactions, they cannot be used for asymmetric azobenzenes and would lead to statistical product mixtures.[28b] For such compounds, the most common reaction pathways are the route via a Mills reaction by coupling a nitrosoarene with an aniline[28b, 30] (Scheme 5, **c**) or via diazonium salts (Scheme 5, **d**).[28b, 31]

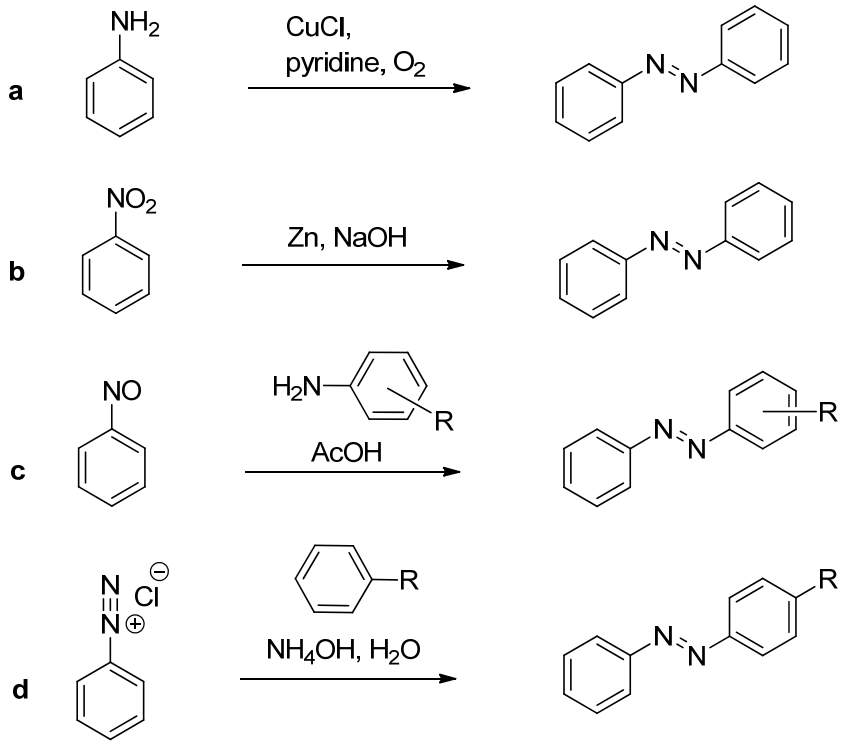

Scheme 5. Common synthetic pathways to azobenzenes. a) Oxidative coupling of anilines[28a] b) reductive coupling of nitrobenzenes[29] c) synthesis via Mills reactions[30] d) synthesis via diazonium intermediates.[31]

In most cases, the starting materials are prefunctionalized and subsequently coupled to the desired azobenzene derivative.[28b] Although the diazene group is very resistant to even harsh pH conditions, high temperatures and many chemical environments, it is sensitive towards

certain other commonly used reaction conditions: Especially by oxidation but also by reducing agents such as organo-alkali compounds, the diazene group is often attacked.[32] Azobenzenes with functionalities that are too sensitive to survive a diazene coupling reaction without the possibility for protection groups are rarely found in literature. Typical examples are metal functions such as organotin or organosilicon groups. In contact with strong oxidating agents (e.g. peroxides,[33] perchloric acid,[34] ozone[35]), the diazene bonds are oxidized to diazene oxides or even nitro compounds (Scheme 6). Strong reductive substances such as organo-alkali[32] reagents and hydrides[36] lead to a reduction of the diazene group do hydrazine derivatives or amines. Also a palladium catalyzed hydrogenation leads to hydrazines or amines (Scheme 6).

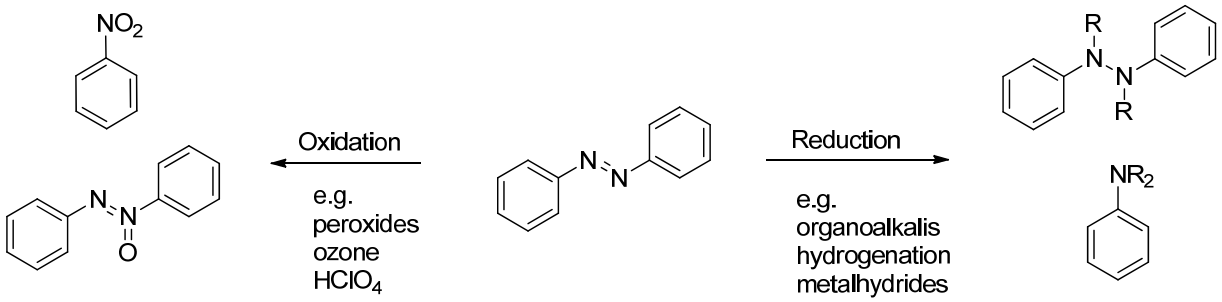

Scheme 6. Decomposition of azobenzenes by oxidation or reduction.

1.5 Liquid Crystallinity

Liquid crystallinity is an aggregated state that can occurs besides the solid, liquid and gas phase for some substances. In contrast to typical crystallinity, liquid crystals do only show a short range order and conformation.[7] Substances which show those additional phase transitions are called mesogens. Liquid crystallinity occurs between the solid phase and an isotropic melt; such liquid crystalline phases are called mesophases. Compared to an usual isotropic melt, liquid crystals show an anisotropy of the mesogens in this state.[7] If mesogens are present, liquid crystalline phases can be achieved using two main approaches. The thermotropic approach leads to mesogenic states by varying the temperature. Mesophases are then observed in a specific temperature range. The second possibility is reaching a lyotropic state by varying the composition of a multi-component system (e.g. addition/removal of a solvent).

The most common mesophase is the nematic phase (Figure 7). In this phase, the mesogenes do not show a positional order but a long range order concerning their direction along the molecule axis and they are aligned nearly parallel to each other.[37] Typically at lower temperatures, the smectic phase is found: Besides the axial orientation, the mesogens are positionally ordered and form layers along one direction.[37]

In addition to those phases, chiral mesogens can form cholesteric phases. Cholesteric phases show a twisting of the molecules perpendictular to the director.[37]

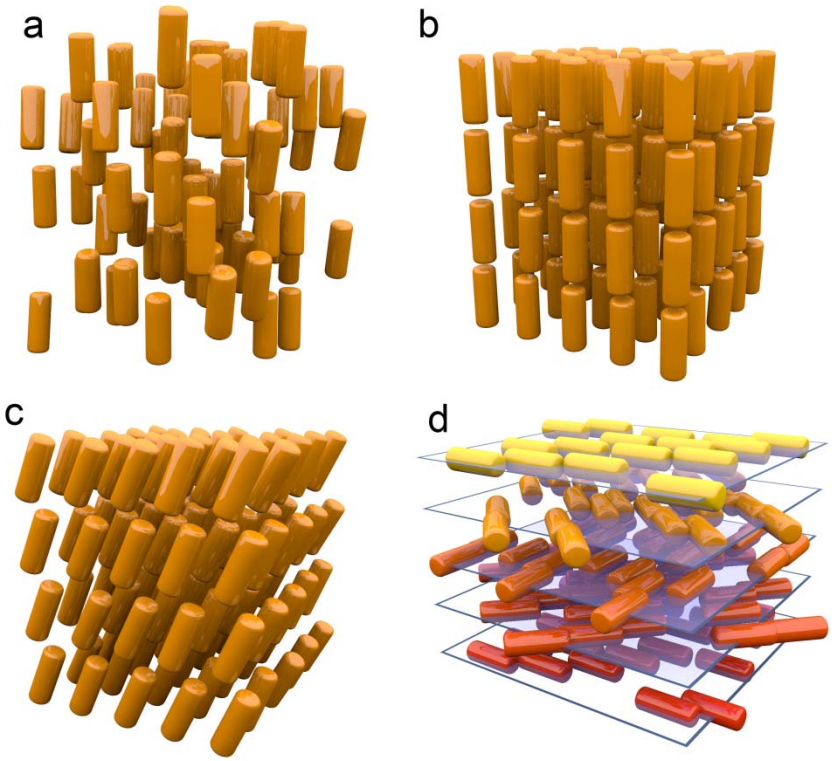

Figure 7. Most common LC phases[37] a) nematic b) smectic A c) smectic C d) cholesteric.

Liquid crystallinity requires certain basic structural properties. Most mesogens can be regarded as rigid rods. Their length is greater than their width. Typically, a mesogen consists of a side group and aromatic rings. Additionally, they can include a terminal group and a linking group[38] (Figure 8).

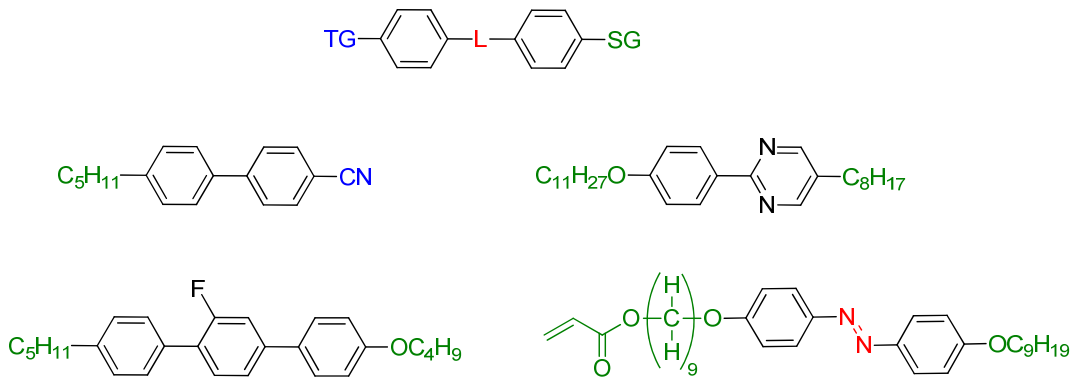

Figure 8. Basic architecture of calamitic mesogens with side group (green), terminal group (blue), linker (red) and examples of liquid crystalline substances.[38]

Liquid crystalline compounds commonly consist of a rigid unit which consists of two or more aromatic rings such as biphenyl or triphenyl units. The rigid structure is essential for the formation of anisotropy in a LC phase.[38-39] However, liquid crystalline phases are typically only observed for substances which bear a side chain. Most common side groups are alkyl, alkoxy, alkenyl and akenyloxy groups.[38] Whether mesophases occur or not and which type is observed strongly depends on the flexibility and the length of the side chain. A general observation is that liquid crystalline phases do not occur in systems bearing side chains shorter than 4 carbons.[7, 38] With increasing length of the side chain, nematic phases occur. With even longer side chains, smectic phases can be observed. Besides the length of the side chain, the mesophases are affected depending on whether the number of carbons in the side chain is even or odd. Odd carbon numbers in the side chain induce significantly higher phase transition temperatures than even carbon numbers.[7, 38] The terminal group as found in many commercial liquid crystals primarily influences dielectric anisotropy and optical properties and does not influence the mesophase in general.[38-39]

1.6 Liquid Crystalline Polymers

For liquid crystalline polymer (LCP) systems, the most important aspect is the occurrence of phase transitions. Liquid crystalline states may be found between the glassy state and an isotropic melt. Depending on the specific properties of the material, the range between the glass transition and an isotropic melt can vary from a few degrees Celsius to hundreds of degrees Celsius. Small molecule LC systems are typically quite easy to observe, because single molecules can easily arrange themselves to mesophases. For polymers, the degree of freedom

of the mesogens is much more limited and shows various dependencies on the polymeric structure such as the flexibility of the backbone, molecular weight, and on how the mesogens are incorporated (polymer architecture) etc.[7]

Liquid crystalline polymers are generally subdivided in two main groups. The side chain liquid crystalline polymers (SCLCP) and main chain liquid crystalline polymers (MCLCP) (Figure 9). SCLCPs bear the mesogenic groups in the side chain of the polymer while MCLCPs bear them in their backbone. The main difference compared to small liquid crystalline molecules is the reduced degree of freedom of the mesogens to orient to form a liquid crystalline phase.[7] The main effect which is observed for SCLCPs as well as for MCLCPs is an increase of the glass transition temperature due to the incorporation of rigid mesogenic groups compared to the incorporation of non-mesogenic groups.[7]

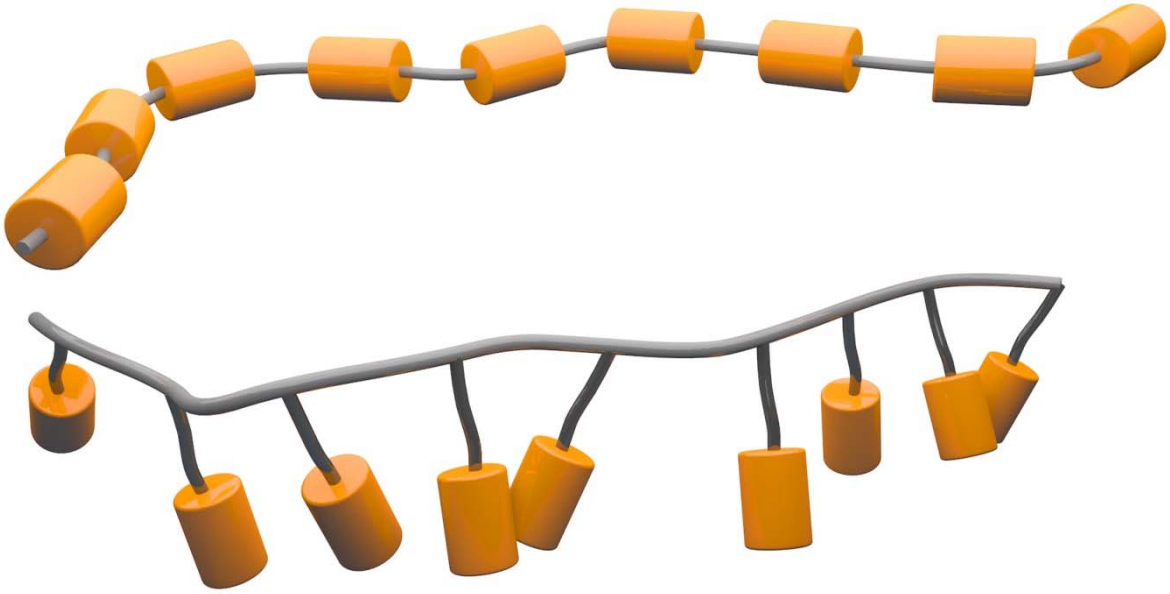

Figure 9. Illustration of a main chain (top) and a side chain liquid crystalline polymer (bottom).

In SCLCPs, linker units are used to connect the mesogens to the polymer's backbone. Those linkers serve as equivalents to the side chains of rigid rod liquid crystalline molecules (see chapter 1.5).[7] Without a linker, the glass transition increases significantly and prevents the formation of a liquid crystalline phase because the packing of the polymers backbone prevents the efficient orientation of the side groups. Nonetheless liquid crystallinity can achieved for such systems by bulk polymerization of a liquid crystalline phase of the monomers. However, once the resulting polymer is heated above the glass transition temperature, the LC phase is

irreversibly lost.[7] To avoid this problem, the mesogenic groups need to be decoupled from the polymers backbone.[7] Flexible spacers are used to achieve this. In most cases methylene groups serve as spacers. Independently from the packing of the main chain, the mesogens mimic the LC behavior similar to small molecules.[7] The polymer backbones are normally very flexible systems such as acrylates, methacrylates and siloxanes.[7, 40] Especially acrylates and methacrylates, which are both polyolefins, allow a simple synthesis of SCLCPs by performing a radical bulk polymerization of a mesophase of the monomers.[7, 40]

The more flexible the backbone, the lower the glass transition temperature, but the higher is the phase transition from an LC phase to an isotropic state. An effect of the chain length is only relevant for short oligomers with less than ten repeating units. With increasing molecular weight the observable effect on phase transitions is reduced.[7] In general, SCLCPs have several advantages: Due to the spacers and the flexible backbone, polymers with relatively low glass transition temperatures can be produced and the polymer synthesis can often be easily achieved by a radical polymerization.[40] But the need for spacers with a minimum length of four methylene groups limits the volumetric percentage of mesogens which can be incorporated in such a material.

In contrast to this, main chain liquid crystalline polymers bear the mesogen in the main chain of the polymer. Due to the rigid structure of mesogenic molecules, the glass transition temperature and the occurrence of thermotropic phases are very high and often above the decomposition temperature of the material. To reduce the transition temperatures which are typically in a range of several hundred degrees Celsius, MCLCPs are often modified by incorporating flexible spacers in the backbone.[7] Commonly, methylene groups are used as spacers. The length and the conformational properties of the spacers show a strong influence on the phase transitions within the material.

Since a thermotropic approach is in most cases impractical for a MCLCP, phase transitions are induced by the lyotrophy of the material:[7] In such systems, the phase transition depends on the temperature as well as the concentration of the solvent. A phase diagram of a lyotropic system normally shows three phases. An isotropic phase at low concentrations and a mixed liquid crystalline and isotropic phase at higher polymer concentrations and a liquid crystalline phase (Figure 10). At which point a liquid isotropic state is obtained in a lyotropic system

depends strongly on the flexibility of the polymer. The critical LC concentration increases with an increasing flexibility of the polymer.[7]

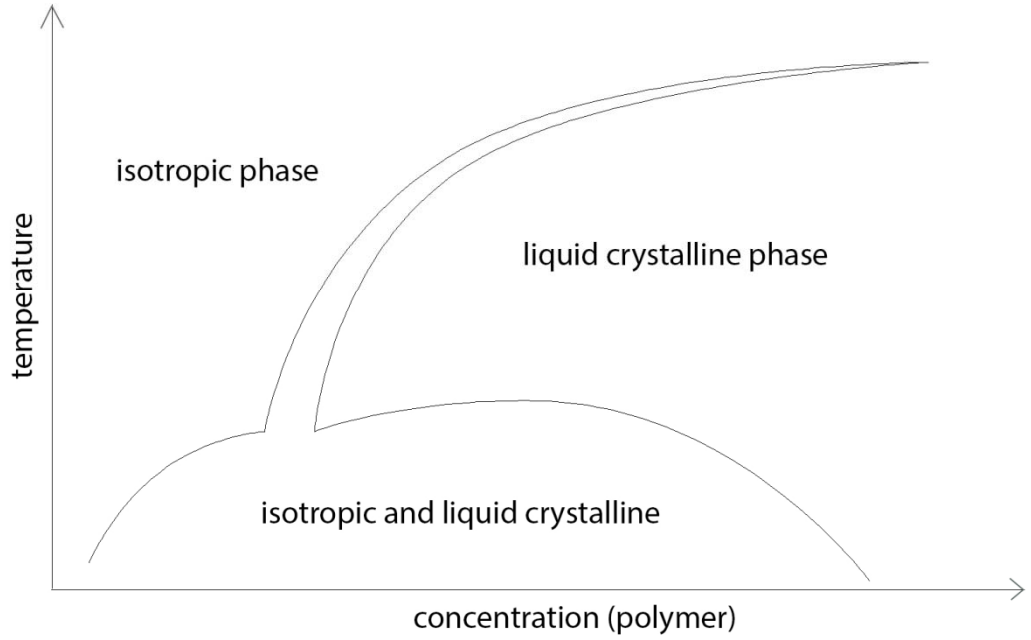

Figure 10. Schematic phase diagram of a lyotropic liquid crystalline polymer and its biphasic "chimney" towards the polymer concentration axis at high temperatures.[41]

1.7 Azobenzenes in Mechanically Photoresponsive Polymers

During the last decades, many intelligent polymeric materials have been developed such as materials which response to external stimuli like pH,[42] temperature,[43] mechanical force[44] or light.[45] While most of the effects in such materials occur on the microscopic scale, one of the most fascinating class of such materials are polymers which convert light into mechanical work which is macroscopically visible by a shape change of the material.

In 1966, Ernest Merian observed a contraction of a nylon fiber colored with azobenzene based dyes when irradiated it with UV light. It was the first published example that azobenzenes can transform light into a mechanical force.[46] This effect was observed for other azobenzene based materials but the effect was very small and with a response time of several hours very slow.[47] Single molecule force spectroscopy experiments showed that by the isomerization from the *trans* to the *cis* form, a force in pico Newton scale is generated.[48] This property of

azobenzene leads to a variety of concepts such as light induced transportation processes on surfaces[49] or light switchable rotaxanes as proton pumps.[50] While those concepts take advantage of generated forces in microscopic scale, the challenge was to combine the individual molecular forces to a macroscopic force. To generate a macroscopic force, an alignment of azobenzenes is needed to enable an addition of the forces generated by each azobenzene. Such alignments are typically achieved by the formation of mesophases.

The first polymer which showed a strong photomechanical response was published by Tomiki Ikeda in 2003.[51] His research-group demonstrated a polymer film which shows a reversible strong macroscopic bending when irradiated with UV light (Figure 11). The polymer was prepared by using liquid crystalline monomers. The alignment in the mesophase was "fixed" by a radical bulk polymerization in this state and further stabilized by a certain degree of cross linking. A liquid crystalline elastomer (LCE) was obtained.[51-52]

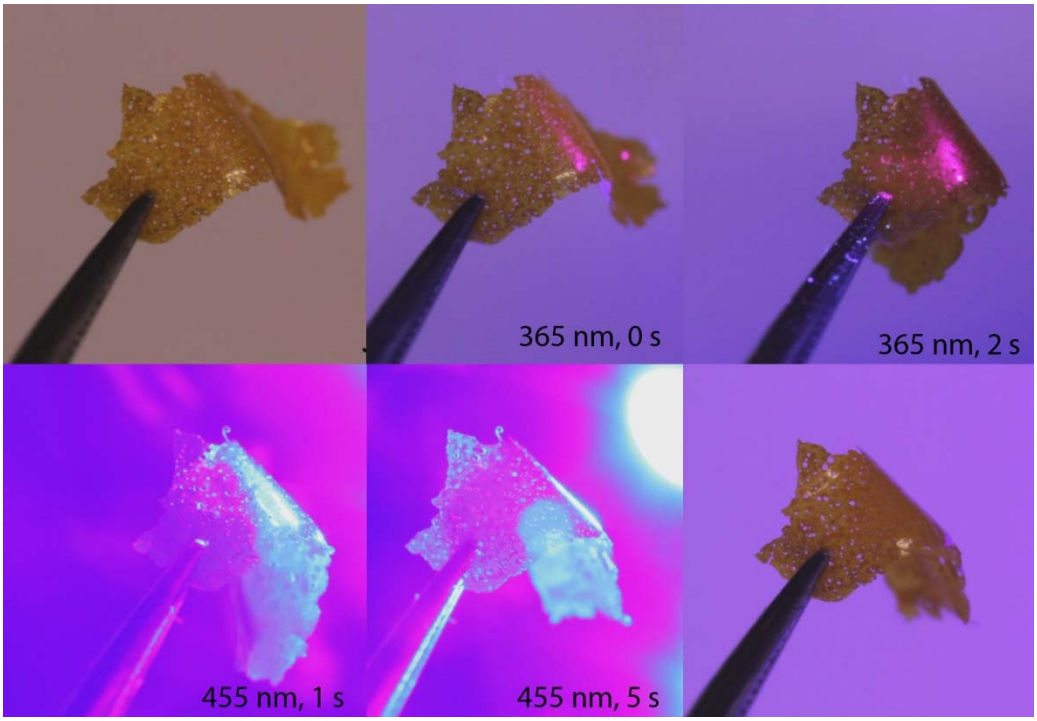

Figure 11. Photomechanical bending of an „Ikeda"-like polymer[52] produced during this thesis (Soft Matter, **2015**, *to be submitted*).

Since Ikeda's polymer, a number of materials were developed which show either a light-induced contraction or -bending.[53] Even more complex moving behavior such as the photoinduced formation of an helical polymer film[54].

Most of the materials published to date are side chain liquid crystalline elastomers. As described in chapter 1.5, side chain liquid crystalline polymers require long spacers between the polymer backbone and the mesogenic units and a flexible polymer backbone to keep the glass transition low. A low glass transition is essential that a shape change of the material can occur. Materials which glass transition temperature is above room temperature need to be heated to observe the photoresponsive effect[55] (except for thin filaments or micrometer scale). The strength of the photomechanical effect is dependent on the elastomeric properties of the material. As more the material is cross-linked, the more intense is the photomechanical effect.[53d, 56] However, with an increased cross-linking, the glass transition temperature of a material greatly increases, too.

The bending motion of SCLCP based photoresponsive polymer films can be compared to a bimetallic motion. The UV light penetrates the material only in the upper layer (penetration depth < 1 µm).[57] Only in this layer switching occurs and due to the contraction/expansion of this layer, a bending is caused. In case of the azobenzene based materials, the alignment strongly affects the motion. Homeotropic aligned azobenzenes lead to a bending away from the light source. Homogeneous aligned azobenzenes lead to a bending towards the light source (Figure 12).[57-58]

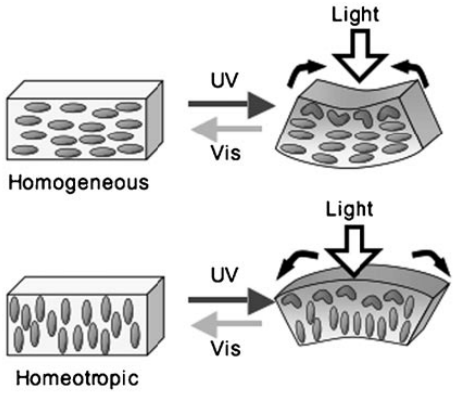

Figure 12. Illustration of the bending motion of azobenzene based SCLCEs and the effect of the alignment of the azobenzenes.[58] Homogeneously aligned azobenzenes induce a bending towards the light. A homeotropic alignment causes a bending away from the light source. Adapted from "*How Does the Initial Alignment of Mesogens Affect the Photoinduced Bending Behavior of Liquid-Crystalline Elastomers?*" by M. Kondo, Y. Yu, T. Ikeda, 2006, *Angewandte Chemie Int. Edit., 118,* 1378-1382. Copyright 2006 by John Wiley and Sons. Adapted with permission.

The use of the mesogenic unit in the main chain of the polymer would allow the incorporation of a higher number of photoswitchable units per volume unit, because the mesogens do not need to be decoupled from a polymer backbone, but only few main chain liquid crystalline materials have been reported to date. All of these materials show very high glass transition temperatures, that a macroscopic deformation can be observed only in very thin filaments or on micrometer scale due to the rigidity.[59]

2. Results and Discussion

2.1 Synthetic Challenges

The synthesis of a poly(siloxane) with azobenzene units in the main chain (**1**) brings several synthetic challenges. As monomer, hydroxydimethylsilyl difunctionalized azobenzene (**2**) is desired for use in a copolymerization with suitable siloxane monomers (Scheme 8).

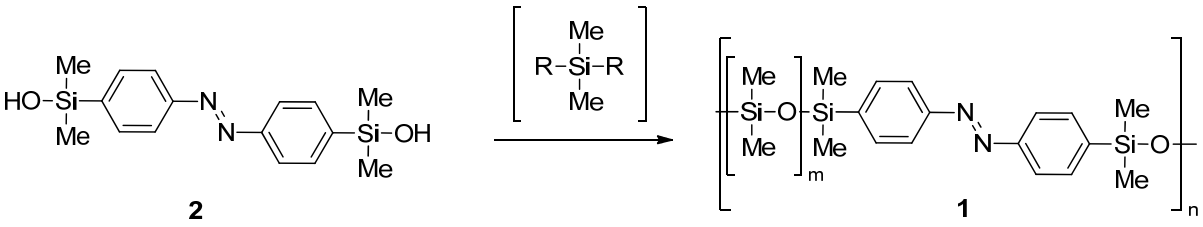

Scheme 8. Synthesis of an azobenzene/siloxane copolymer.

For the synthesis of such a monomer, a completely new synthetic route had to be developed. Silicon functionalizations on aromatic groups are commonly introduced by a prior lithiation and a subsequent quenching reaction with an organosilicon chloride. However, as described in chapter 1.4, azobenzenes are very sensitive to organolithium and organomagnesium reagents. Lithiation reactions on azobenzene using halogen lithium exchange reactions give very low yields because there is a competitive reaction on the azo group. For this reason, there is hardly any literature on the metalation of azobenzenes. In synthesis, especially oranotin groups often show a very good selectivity in transmetallation reactions with lithium. However, to investigate if a transmetallation from tin to a lithiated azobenzene would be successful, first a methodology had to be developed to stannylate azobenzene avoiding lithiation through halogen-lithium exchange (*Chem.- Eur. Chem. J.* **2015**, *submitted*).

Tin functionalized azobenzenes could be obtained from iodinated azobenzenes in quantitative yields by a Stille-Kelly cross-coupling reaction with hexamethyldistannane (**3**). Furthermore it could be shown that they react well as nucleophiles in Stille cross coupling reactions (J. Strueben, P. J. Gates, A. Staubitz, *J. Org. Chem.* **2014**, *79*, 1719-1728 – chapter 2.2) and also allow the transmetalation from tin to lithium selectively without attacking the diazene group.

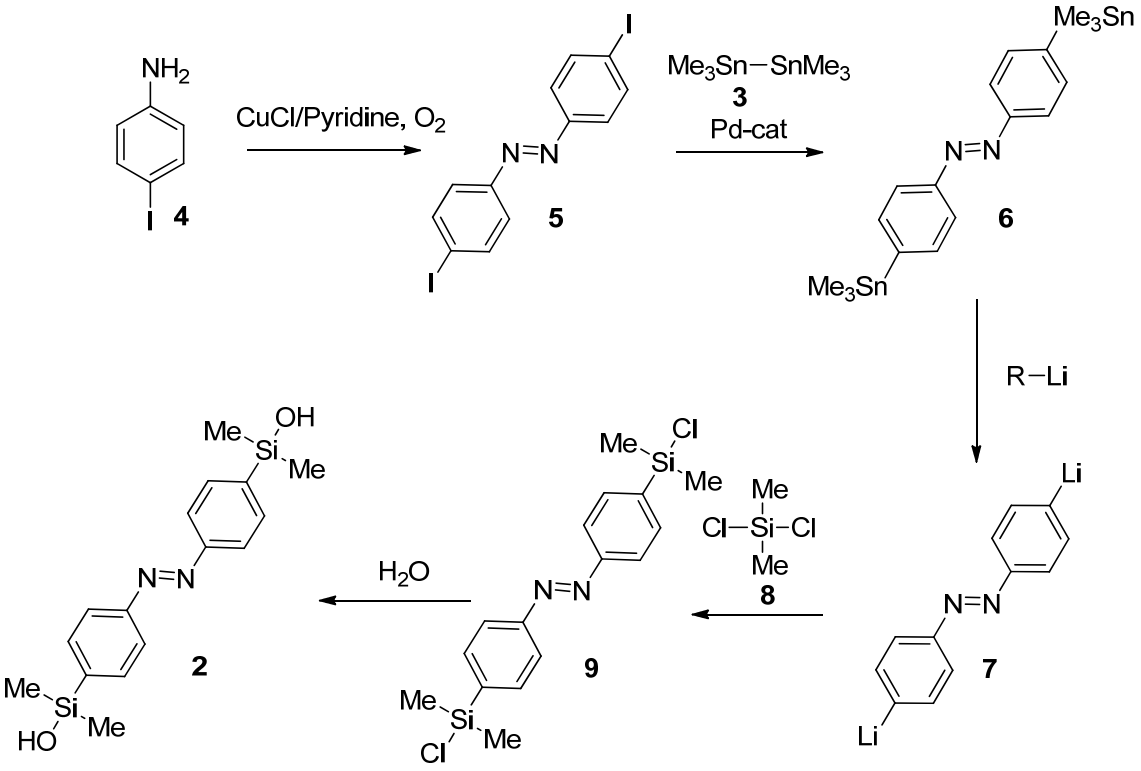

Scheme 9. Synthetic route to a suitable monomer for a copolymerization with siloxane

The optimization and detailed investigation of these synthetic methodologies allowed the difunctionalization of azobenzene with hydroxydimethylsilyl groups. (Scheme 9). 4-Iodoaniline (**4**) was converted to 4,4-*bis*(iodo)azobenzene (**5**). Using the microwave assisted stannylation methodology (chapter 2.2) the iodo functionalized azobenzene **5** could be converted to 4,4'-*bis*(trimethylstannyl)azobenzene (**6**). A tin-lithium exchange (chapter 2.3) allowed the dilithiation of azobenzene to **7**. By quenching this intermediate with dichlorodimethyl silane (**8**), the chlorosilyl functionalized species **9** could be obtained. By hydrolosis, the desired monomer **2** could be obtained. This compound could be finally polymerized to **1** (chapter 2.4).

2.2 High Yielding Stannylation of Azobenzenes

(*J. Org. Chem.* **2014**, *79*, 1719-1728)

J. Strueben, P. J. Gates, A. Staubitz *J. Org. Chem.* **2014**, *79*, 1719-1728.

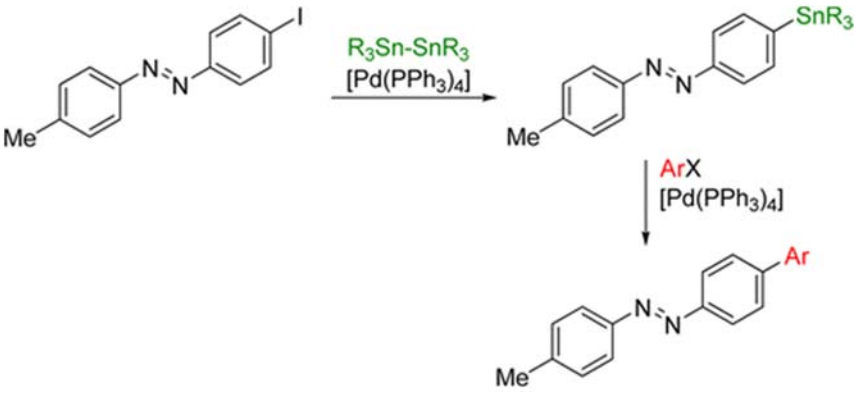

The metalation of azobenzene by halogen metal exchange typically leads to a reduction of the azo group to give hydrazine derivatives as major byproducts, instead of the desired metalated azobenzene species. In cross-coupling reactions, azobenzenes therefore usually serve as electrophiles, which greatly limit the scope of the reaction. To solve this problem, we have developed a mild and fast method to stannylate azobenzenes in high yields. This research shows that these stannylated azobenzenes can be used as nucleophilic components in Stille cross-coupling reactions with aryl bromides. The cross-coupling products were obtained in high yields ranging from 70 to 93%. With this reversal of the nucleophilic and electrophilic components, cross-coupling products are now accessible in which the aromatic rings coupled to the azobenzene bear functional groups that are sensitive to metalation.

Scientific contribution to this publication

For this publication, I carried out all syntheses and experimental work. Paul J. Gates recorded all high resolution mass spectra. Anne Staubitz and I wrote the article together.

JOC The Journal of Organic Chemistry

Article

pubs.acs.org/joc

Tin-Functionalized Azobenzenes as Nucleophiles in Stille Cross-Coupling Reactions

Jan Strueben,[†] Paul J. Gates,[‡] and Anne Staubitz*[,†]

[†]Otto-Diels-Institute for Organic Chemistry, University of Kiel, Otto-Hahn-Platz 4, 24098 Kiel, Germany

[‡]School of Chemistry, University of Bristol, Cantock's Close, Bristol BS8 1TS, U.K.

Supporting Information

ABSTRACT: The metalation of azobenzene by halogen−metal exchange typically leads to a reduction of the azo group to give hydrazine derivatives as major byproducts, instead of the desired metalated azobenzene species. In cross-coupling reactions, azobenzenes therefore usually serve as electrophiles, which greatly limits the scope of the reaction. To solve this problem, we have developed a mild and fast method to stannylate azobenzenes in high yields. This research shows that these stannylated azobenzenes can be used as nucleophilic components in Stille cross-coupling reactions with aryl bromides. The cross-coupling products were obtained in high yields ranging from 70 to 93%. With this reversal of the nucleophilic and electrophilic components, cross-coupling products are now accessible in which the aromatic rings coupled to the azobenzene bear functional groups that are sensitive to metalation.

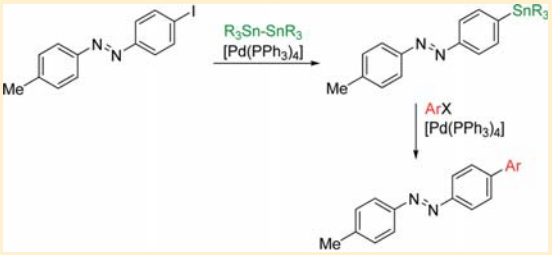

INTRODUCTION

Azobenzene and its derivatives are bistable systems (with their *trans* and their *cis* form)[1] that are comparatively resistant to photobleaching[2] and thermal decomposition.[3] Therefore, they are widely used as effective photoswitchable units in molecular systems and polymers[4] with potential applications ranging from biochemical[5] and medical uses,[6] to photoswitchable bulk materials,[7] to smart surfaces[8] and lithographic applications.[9] A further interest lies in their potential to couple both mechanical and photochemical work in one molecule.[1a,7,10] The effective functionalization of azobenzenes, which enables their connection to other functional molecules or tuning photophysical properties, is therefore essential.

The most versatile approach to functionalize aromatic rings to form CC bonds is by transition-metal-catalyzed cross-coupling methods. While the use of halogen- or pseudohalogen-functionalized azobenzenes as the electrophilic component in this type of reaction is an established synthetic route,[11] there are hardly any nucleophilic azobenzenes known. While a metalation *ortho* to the azo group is facilitated by directed *ortho*-metalation,[12] yields are typically low. Moreover, this feature cannot be used for the synthesis of *para*-substituted analogues. For *para*-substituted azobenzenes, pinacol borane substituted azobenzene derivatives have been described that served as a nucleophile in Suzuki cross-coupling reactions.[13] Lithiated species can be prepared in situ by halogen−metal exchange, but the reported yields are very low (maximal 42% for *para*[14] and 47% for *ortho*[15]). For Grignard compounds, a patent exists that reports the synthesis of the symmetrical *para*-magnesiated azobenzene.[16] However, elemental magnesium in combination with ammonium chloride has been successfully used for the reduction of *ortho*-, *meta*-, and *para*-halogenated azobenzenes to the halogenated hydrazine analogues in 75−91% yield.[17] However, no other metallic groups in the *para* position that can be used for cross-coupling reactions have been described to date.[18]

The main synthetic challenge of preparing *para*-metalated azobenzenes is their low tolerance toward reductive reaction conditions: Most protocols for introducing nucleophilic functional groups are based on deprotonation followed by transmetalation. Alternatively, and as in the case of azobenzenes, a halogen−metal exchange on compounds such as the *para*-halogenated azobenzene **1** with an organolithium reagent to the 4-lithioazobenzene **2** can be used, followed by a transmetalation with the desired metal chloride or semimetal chloride (Scheme 1). However, a prominent side reaction that is impossible to avoid using the highly nucleophilic alkylorganolithium reagents is the reduction of the azo group to hydrazine derivatives (**3** and **4**).[19]

In this work, an easy-to-use methodology to obtain tin functionalized azobenzene derivatives in very high yields[18] and their applicability for Stille cross-coupling reactions is presented.

RESULTS AND DISCUSSION

Although stannylation reactions of arenes are most often performed by a transmetalation from the corresponding organolithium or organomagnesium compounds, another method for introducing trialkyl tin groups is by a cross-coupling reaction.[20] In such a reaction, an aryl halide is treated with a distannane, $R_3Sn-SnR_3$, using a transition-metal catalyst. For the

Received: December 4, 2013
Published: February 6, 2014

Scheme 1. Halogen−Lithium Exchange (Left); Concomitant Reduction of the Azobenzene 1 to Hydrazine Derivatives 6 and 7 (Middle and Right)[14,19]

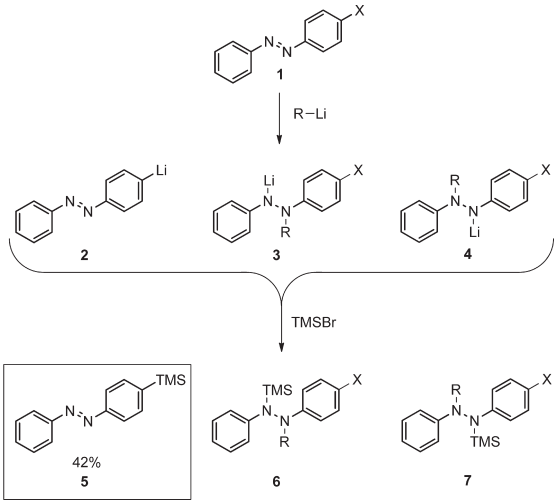

stannylation of nitrophenyl iodide **8**,[21] *n*-hexabutyldistannane as the electrophile and $[Pd(PPh_3)_4]$ as the catalyst in toluene at reflux conditions, a similar reaction had been reported to give product **9** in a yield of 63% (Scheme 2).

Scheme 2. Stannylation of *p*-Nitrophenyl Bromide (8) with Hexa-*n*-butyldistannane to 9 in 63% Yield[21]

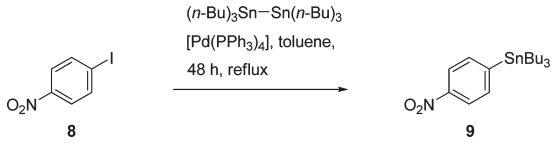

To establish reaction conditions for a stannylation of azobenzene using such a cross-coupling reaction, initially those same reaction conditions for azobenzene **10** as the electrophilic component were used and hexamethyldistannane as electrophile. Compound **11** could be isolated in a yield of 46% (Table 1, entry 1): the trimethylstannylazobenzene **11** proved stable to pH neutral silica gel, and therefore, it could be easily purified by removal of the catalyst with a filtration column. This product **11** was then used as a calibrant for the development of a gas chromatographic (GC) method which allowed us to monitor the reaction and optimize it efficiently. The reaction was performed in different solvents at different temperatures with $[Pd(PPh_3)_4]$ as catalyst (Table 1). For the thermal reactions at 70 °C, the reaction progress was monitored in regular intervals, and the time given in Table 1 represents the time when no further conversion was observed. The reaction turned out to be highly temperature and solvent dependent. For all solvents, a reaction temperature of 70 °C using conventional heating led to significantly longer reaction times than heating to 150 °C in the microwave. (Compare Table 1, entries 2−7, with entries 8 to 13, respectively.) At 70 °C, DMF and DMSO turned out to be very suitable for the reaction to give a full conversion and a GC yield of 91% and 84%, respectively (Table 1, entries 2 and 3). Although pyridine and toluene as solvents led

Table 1. Optimization of the Stannylation of 4-Iodo-4′-methylazobenzene (10) with 2 mol % of $[Pd(PPh_3)_4]$ as Catalyst

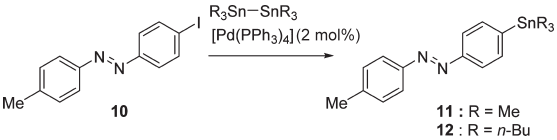

entry	R	solvent	*T* (°C)	time	yield[a] (%)
1	Me	toluene	reflux[b]	48 h	46[c]
2	Me	DMF	70[b]	9 h	91
3	Me	DMSO	70[b]	13 h	84
4	Me	pyridine	70[b]	11 h	54
5	Me	toluene	70[b]	14 h	64
6	Me	dioxane	70[b]	12 h	39
7	Me	THF	70[b]	16 h	43
8	Me	DMF	150[d]	10 min	21
9	Me	DMSO	150[d]	10 min	27
10	Me	pyridine	150[d]	10 min	82
11	Me	toluene	150[d]	10 min	>99
					95[c]
12	Me	dioxane	150[d]	10 min	94
13	Me	THF	150[d]	10 min	>99
14	*n*-Bu	toluene	150[d]	35 min	74[c]

[a]GC yield unless noted otherwise; calibrated with the product **11** using triisoprobylbenzene as the internal calibration standard. [b]Conventional heating. [c]Isolated yield. [d]Microwave heating.

to adequate yields (54%, entry 5 and 64% entry 1, respectively), starting material could still be observed. Dioxane and THF as solvents led to the lowest yields under those reaction conditions (39% and 43%, entries 6 and 7) and did not lead to a full conversion of the starting material. However, in all reactions no side products were observed, only the starting material **10** and product **11**. As byproduct formation was not a significant issue at 70 °C, and in order to reduce the reaction time and increase the product yield, the reaction was performed at higher temperatures in a sealed reaction vessel in a microwave at 150 °C (Table 1, entries 8−13). For each solvent, the reaction was stopped after 10 min; the mixture was analyzed by GC to determine the conversion of the starting material. Although no decomposition or side products could be observed under any of the reaction conditions, there were significant differences with respect to conversion compared to the reactions performed at 70 °C. Under the microwave conditions, DMF and DMSO, which were the most suitable solvents for conventional heating at 70 °C, only led to low yields of 21% and 27% (Table 1, entries 8 and 9). Toluene and THF, on the other hand, led to an almost quantitative product yield of >99% each, respectively (Table 1, entries 11 and 13). The same was true for dioxane and pyridine (Table 1, entries 12 and 10). The optimized conditions for the monostannylation of azobenzene in toluene (Table 1, entry 11) were transferred to the coupling reaction of *n*-hexabutyldistannane to azobenzene in toluene in the microwave to give **12**. Although THF also led to a quantitative yield for the stannylation, toluene was selected because this solvent does not carry the risk of forming explosive peroxides when stored.[22] The stannylation of **10** to give **12** was monitored by thin layer chromatography because we could not observe a signal in GC/MS. After 10 min, the reaction was incomplete, presumably due to the lower reactivity of

dx.doi.org/10.1021/jo402598u | J. Org. Chem. 2014, 79, 1719−1728

$(n\text{-Bu})_3\text{Sn}-\text{Sn}(n\text{-Bu}_3)$ as compared to the sterically more accessible $Me_3Sn-SnMe_3$. The reaction time in the microwave was therefore increased to 35 min. Although the product could be isolated in an adequate yield of 74% (Table 1, entry 14), the purification required a Kugelrohr distillation at very high temperatures of 180 °C and a pressure of 9.4×10^{-2} mbar, which probably led to a partial decomposition of the material.

Having established high-yielding reaction conditions, 4,4′-bis(iodo)azobenzene (**13**) was stannylated with both hexamethyldistannane and *n*-hexabutyldistannane to give products **14** and **15** (Scheme 3). As for the monostannylated species, the

Scheme 3. Distannylation of 4,4′-Bis(iodo)azobenzene (13) with 4 mol % of $[Pd(PPh_3)_4]$ as a Catalyst to Products 14 and 15

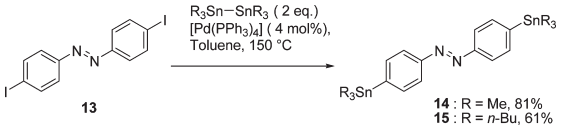

bis-trimethylstannylated azobenzene (**14**) was obtained in a very good yield of 81%. For the bis(tri-*n*-butyl)stannylated species **15**, the isolated yield was somewhat lower, at 61%. Whereas the methylstannylated azobenzenes could be purified by filtration on silica and subsequent evaporation of the hexamethyldistannane without a noticeable loss of yield, **15** had to be performed by Kugelrohr distillation. We assume that this process caused the observed lower yield for this product.

With both the trimethylstannyl- and tri-*n*-butylstannylazobenzenes **11** and **12** in hand, we explored their usefulness in Stille cross-coupling reactions with various aromatic bromides as reaction partners (Table 2). All of these Stille coupling reactions were performed at a moderate temperature of 70 °C. The reaction progress was monitored by GC/MS, and the reaction was terminated when no starting material could be detected any more. Initially, all reactions were performed with the trimethylstannylazobenzene **11** as the nucleophile. As expected, the use of electron-deficient benzene derivatives gave excellent yields: *para*-bromonitrobenzene (**16**) was fully converted within 6 h, giving the product **17** in a yield of 89% (Table 2, entry 1). Similarly, the electron-deficient *para*-cyanobenzene bromide **18** and *para*-bromophenyl methyl ketone **19** required only a short reaction time of 8 h to give the products **20** and **21** in good yields of 82% and 87%, respectively. The reaction worked equally well for electron-rich aromatic cycles. Although the electrophile **24** bears an aldehyde group, the furan heterocycle is very electron rich, which explains the longer reaction time of 16 h which was required for this compound, and a yield of 73% of **25** could be isolated. Electron-rich electrophiles typically required longer reaction times of more than 19 h (compare, for example, 3-methoxy bromide **28**, 2,4-dimethoxide **29**, and benzodioxolyl bromide **30** with bromobenzene **22**; Table 2, entries 7, 8, 9, and 4), but the furan ester **27** showed a full conversion after only 14 h and could be isolated in a yield of 84% (Table 2, entry 6). In reactions with bromothiophenes, 2-bromothiophene (**34**) gave **35** with a yield of 88% in only 11 h, which is significantly faster compared to the less reactive[23] 3-bromothiophene (**36**) with a reaction time of 14 h to give **37** in an isolated yield of 83%. (Table 2, entries 10, and 11). The *para*-bromoaniline **38** showed full conversion to product **39** after 19 h with a yield of 72%.

Stille cross-coupling reactions with the tri-*n*-butylstannyl azobenzene derivative were also performed with the electron-deficient *para*-nitrophenyl bromide (**16**) and the electron-rich 3-methoxyphenyl bromide (**28**). As this starting material, tri-*n*-butylstannyl azobenzene could not be observed by our GC/MS, the reaction was monitored by thin-layer chromatography. The yields with this nucleophile were significantly lower than the product yield with the methylstannylated species: Product **17** could only be isolated in a yield of 71% (18% lower than with nucleophile **11**), and product **31** gave only a yield of 54% (25% lower than with nucleophile **11**) (Table 2, entries 1 (b) and 7 (b)). We attribute this to the lower reactivity of the nucleophile **12** to the increased sterical hindrance of the *n*-butyl groups as compared to the methyl groups.

Several of the aryl bromides were used for the Stille coupling reactions in this work are highly sensitive to typical metalation reactions using organolithium or organomagnesium reagents. For example, nitrophenyl bromide and cyanophenyl bromide (**16**, **18**) are unstable when treated with *n*-butyllithium, and the aldehyde-, ketone-, and ester-functionalized aryl bromides (**19**, **24**, and **26**[24]) would be attacked by the butyl nucleophile and be reduced. To circumvent this problem, protection groups can be used, but as this increases the number of steps in a synthesis, and causes more waste, it is advantageous if protection groups can be avoided in a synthetic process. With our newly developed stannylated azobenzenes, aromatic bromides bearing these sensitive functional groups (nitro, cyano, carbonyl) can now be used as the much more easily accessible electrophilic cross-coupling partner for a carbon−carbon bond formation with an azobenzene. The carbonyl functionalized arylbromides gave yields from 73 to 87% (Table 2 entries 3, 5, and 6).

CONCLUSION

In conclusion, we have developed a highly efficient methodology to prepare mono- and distannylated azobenzene derivatives with tri-*n*-butylstannyl and trimethylstannyl substituents. This reaction involves a palladium-catalyzed cross-coupling reaction with reagents of the type $R_3Sn-SnR_3$ and the easily accessible iodinated azobenzene derivatives as starting materials. It was also shown that such tin-functionalized azobenzenes are effective nucleophiles in Stille cross-coupling reactions with a range of functionalized aryl bromides. Electron-rich and electron-deficient electrophiles were efficiently cross-coupled in similarly high yields ranging from 70 to 93%. Of particular interest are electrophiles FG−Ar−Br with functional groups (FG) such as aldehydes, ketones, or nitro groups. Previously, corresponding nucleophiles, FG−Ar−M, could be reacted with the easily accessible azobenzene halides using established procedures. However, such compounds FG−Ar−M can be difficult to prepare in this form if a metalation procedure would lead to an attack of the nucleophile on these electrophilic functional groups. Because azobenzene stannanes are now available, these electrophiles can be used as the much more easily accessible electrophilic component. This newly established method therefore complements the established procedures by introducing a new synthon for nucleophilic azobenzenes.

EXPERIMENTAL SECTION

All reagents used were commercially available and used without further purification. For their purities see the Supporting Information. All solvents that were used in the stannylation and Stille reactions were dried prior to use. For the exact drying procedures see Supporting Information.

dx.doi.org/10.1021/jo402598u | J. Org. Chem. 2014, 79, 1719−1728

Table 2. Stille Coupling of Various Aryl Bromides with 4-Methyl-4′-(trimethylstannyl)azobenzene (11) or 4-Methyl-4′-(tri-*n*-butylstannyl)azobenzene (12)

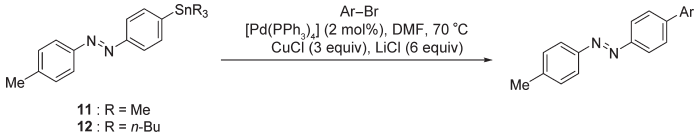

11 : R = Me
12 : R = *n*-Bu

Entry	Electrophile	Product	t/h	Yield [%]
1	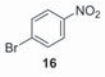 **16**	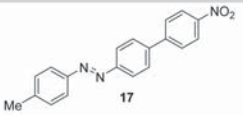 **17**	6 17	89[a] 71[b]
2	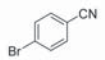 **18**	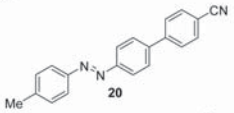 **20**	8	82
3	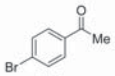 **19**	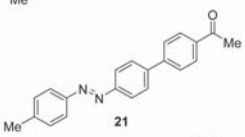 **21**	8	87
4	 **22**	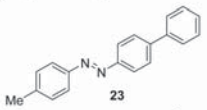 **23**	12	93
5	 **24**	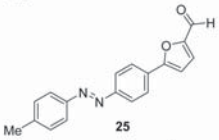 **25**	16	73
6	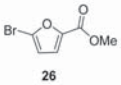 **26**	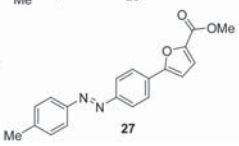 **27**	14	84
7	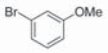 **28**	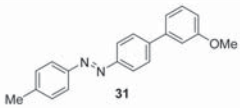 **31**	19 25	79[a] 54[b]
8	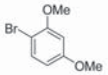 **29**	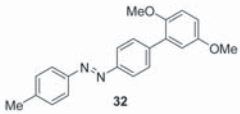 **32**	26	70
9	 **30**	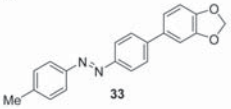 **33**	24	70
10	 **34**	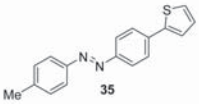 **35**	11	88
11	 **36**	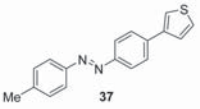 **37**	14	83
12	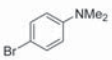 **38**	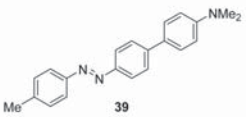 **39**	19 h	72

[a]Reaction with 4-methyl-4′(trimethylstannyl)azobenzene. [b]Reaction with tri-*n*-butylstannylazobenzene.

All preparations for the stannylation reactions were performed in a nitrogen-filled glovebox and carried out in a sealed vial under nitrogen. All Stille couplings were carried out using standard Schlenk techniques under a nitrogen atmosphere.

All NMR spectra were recorded on a 500 MHz spectrometer (with respect to the proton resonance). ^{1}H NMR and ^{13}C NMR spectra were referenced against the solvent residual proton signals (^{1}H) or the solvent itself (^{13}C). ^{119}Sn NMR spectra were referenced externally against $CDCl_3$.

The exact assignment of the peaks was performed by two-dimensional NMR spectroscopy such as ^{1}H COSY, ^{1}H/^{13}C HSQC, or ^{1}H/^{13}C HMBC when possible.

All microwave syntheses were performed on a Biotage Initiator+ SP Wave (Organic Synthesis Mode). The temperature was measured with an external IR sensor during microwave heating.

Due to the toxicity of organotin compounds,[25] certain precautions should be observed: All manipulations should be performed in a well-vented fume cupboard, wearing standard eye protection, lab coats, and nitrile gloves with the following specification: EN374-1:2003 "Protection against chemical splash."

Care needs to be taken to observe proper disposal procedures for all waste products, according to the health and safety procedures in place. Under no circumstances should these compounds be disposed of in the drains or allowed to leak in any other way into the environment.

Representative Procedure for the Optimization of the Stannylation of 4-Iodo-4′-methylazobenzene. *Thermal Syntheses.* A solution of 4-iodo-4′-methylazobenzene (177 mg, 550 μmol), hexamethyldistannane (180 mg, 550 μmol), [$Pd(PPh_3)_4$] (12.7 mg, 2 mol %), and the internal reference 1,3,5-triisopropylbenzene (112 mg, 550 μmol) in toluene (4 mL) was heated to 70 °C. In regular intervals, a sample (0.1 mL) was taken from the reaction vial and filtered through a short column of silica (5 × 3 mm; eluent: DCM) and a PTFE syringe filter (pore size = 45 μm) before the sample was analyzed by GC.

For all other reaction conditions, the parameters were varied as specified in Table 1.

Microwave syntheses. A solution of 4-iodo-4′-methylazobenzene (177 mg, 0.55 mmol), hexamethyldistannane (180 mg, 0.55 mmol), [$Pd(PPh_3)_4$] (12.7 mg, 2 mol %), and the internal reference 1,3,5-triisopropylbenzene (112 mg, 550 μmol) in toluene (4 mL) was heated to 150 °C in a microwave apparatus. Every 10 min, a sample (0.1 mL) was taken from the reaction vial and filtered through a short column of silica (5 × 3 mm; eluent: DCM) and a PTFE syringe filter (pore size = 45 μm), before the sample was analyzed by GC.

For all other reaction conditions, the parameters were varied as specified in Table SI 1 (Supporting Information).

dx.doi.org/10.1021/jo402598u | *J. Org. Chem.* 2014, 79, 1719−1728

*4-Iodo-4′-methylazobenzene (**10**).*[26]

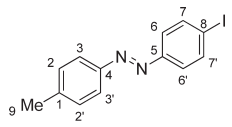

This compound has also been synthesized by J. Tour and co-workers using a different method.[26] *para*-Toluidine (26.0 g, 243 mmol) was dissolved in DCM (100 mL) at 20 °C. A solution of K_2SO_5 (300 g, 488 mmol) in water (600 mL) was added, and the reaction was stirred for 4 h at 20 °C. The dark green organic phase was separated and washed with 1 M hydrochloric acid (2 × 150 mL), a saturated aqueous solution of hydrogen carbonate (1 × 150 mL), and water (1 × 200 mL). The organic phase was dried over magnesium sulfate. After evaporation of the solvent and without further purification, a solution of 4-iodoaniline (53.2 g, 243 mmol) in acetic acid (250 mL) was added to the crude product and stirred for 16 h at 20 °C. The precipitate was separated by filtration and dissolved in DCM (50 mL). The solution was washed 1 M hydrochloric acid (2 × 150 mL), a saturated solution of hydrogen carbonate in water (1 × 150 mL), and water (1 × 200 mL). The combined organic phases were dried over magnesium sulfate. After evaporation of the solvent, 42.3 g (54%, lit.[26] 93%) of an orange solid was obtained. Mp: 160 °C (lit.[27] mp 160 °C. ^{1}H NMR (500 MHz, $CDCl_3$): 7.86 (d, ^3J = 8.5 Hz, 2 H, H-3,3′), 7.83 (d, ^3J = 8.5 Hz, 2 H, H-7,7′), 7.64 (d, ^3J = 8.5 Hz, 2 H, H-6,6′), 7.32 (d, ^3J = 8.5 Hz, 2 H, H-2,2′), 2.45 (s, 3H, H-9) ppm. ^{13}C NMR (125 MHz, $CDCl_3$): 152.0 (C-5), 150.6 (C-4), 142.0 (*C-1*), 138.3 (C-7,7′), 129.8 (C-2,2′), 124.4 (C-6,6′), 123.0 (C-3,3′), 97.2 (*C-8*), 21.5 (*C-9*) ppm. IR (ATR): 3021 (w), 2978 (w), 2912 (w), 1600 (m), 1381 (m), 1105 (m), 1065 (m), 830 (s), 763 (s), 711 (s), 512 (s) cm^{-1}. HRMS (CI-sector) *m/z*: $[M + H]^+$ calcd for $[C_{13}H_{11}N_2I + H]^+$ 323.0045, found 323.0050.

*4-Methyl-4′-(trimethylstannyl)azobenzene (**11**).*

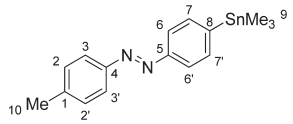

4-Iodo-4′-methylazobenzene (3.00 g, 9.31 mmol), hexamethyldistannane (3.05 g, 9.31 mmol), and $[Pd(PPh_3)_4]$ (215 mg, 186 μmol, 2 mol %) were dissolved in toluene (19 mL). The reaction vessel was heated to 170 °C for 10 min in a microwave. The solvent was evaporated, and the crude product was purified by filtration through silica with cyclohexane/ethyl acetate (v/v, 2/3). The solvent and the remaining hexamethyldistannane were evaporated at 6.4 × 10^{-2} mbar and 70 °C over the course of 17 h. 3.12 g (95%) of red solid was obtained. Mp: 62 °C. ^{1}H NMR (500 MHz, $CDCl_3$): 7.87 (d, ^3J = 8.2 Hz, 2 H, H-3, 3′), 7.84 (d, ^3J = 8.3 Hz, 2 H, H-6, 6′), 7.66 (d, ^3J = 8.3 Hz, 2 H, H-7,7′), 7.32 (d, ^3J = 8.2 Hz, 2 H, H-2, 2′), 2.45 (s, 3 H, H-10), 0.35 (s, 9 H, H-9) ppm. ^{13}C NMR (126 MHz, $CDCl_3$): 152.7 (*C-5*), 150.9 (*C-4*), 146.7 (*C-8*), 141.5 (*C-1*), 136.6 (*C-7, 7′*), 129.7 (*C-2, 2′*), 122.9 (*C-6, 6′*) 122.9 (*C-3, 3′*), 21.5 (*C-10*) −9.5 (*C-9*) ppm. ^{119}Sn NMR (187 MHz, $CDCl_3$): −25.25 ppm. IR (ATR): 3023 (w), 2980 (w), 2910 (w), 1600 (w), 1380 (w), 1156 (m), 1065 (m), 1010 (m), 830 (s), 783 (s), 711 (s), 526 (s) cm^{-1}. HRMS (ESI-FTMS) *m/z*: $[M + H]^+$ calcd for $[C_{16}H_{20}N_2Sn + H]^+$ 361.0721, found 361.0735.

*4-Methyl-4′-(tributylstannyl)azobenzene (**12**).*

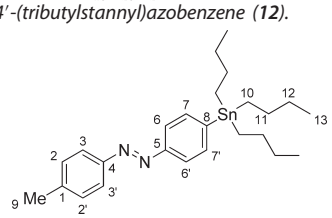

4-Iodo-4′-methylazobenzene (1.00 g, 3.10 mmol), hexa-*n*-butyldistannane 1.80 g (3.10 mmol), and $[Pd(PPh_3)_4]$ (64.3 g, 55.0 μmol, 2 mol %) were dissolved in toluene (19 mL). The reaction vessel was heated to 150 °C for 35 min in a microwave apparatus, and then the solvent was evaporated. The crude product was dissolved in DCM and filtered over a short plug of silica. The solvent was evaporated, and the remaining oil was purified by Kugelrohr distillation (9.43 × 10^{-2} mbar, 150 °C, 20 min). The residue was dissolved in DCM and filtered over a short plug of silica. After evaporation of the solvent, 998 mg (74%) of a red oil was obtained. ^{1}H NMR (500 MHz, $CDCl_3$): 7.87 (d, ^3J = 8.1 Hz, 2 H, H-3, 3′), 7.86 (d, ^3J = 8.2 Hz, 2 H, H-6, 6′), 7.65 (d, ^3J = 8.2 Hz, 2 H, H-7,7′), 7.33 (d, ^3J = 8.1 Hz, 2 H, H-2, 2′), 2.34 (s, 3 H, H-9), 1.66−1.49 (m, 6 H, H-11), 1.41−1.32 (m, 6 H, H-12), 1.19−1.05 (m, 6 H, H-10), 0.91 (t, ^3J = 7.3 Hz, 9 H, H-13) ppm. ^{13}C NMR (126 MHz, $CDCl_3$): 152.7 (*C-5*), 150.9 (*C-4*), 146.7 (*C-8*), 141.3 (*C-1*), 137.1 (*C-7, 7′*), 129.7 (*C-2, 2′*), 122.9 (*C-6,6′*) 122.8 (*C-3,3′*), 29.1 (*C-11*), 27.4 (*C-12*), 21.5 (*C-9*), 13.7 (*C-13*), 9.7 (*C-10*) ppm. ^{119}Sn NMR (187 MHz, $CDCl_3$): −39.9 ppm. IR (ATR): 3020 (w), 2955 (s), 2921 (s), 2870 (m), 2852 (m), 1600 (w), 1462 (m), 1376 (m), 1964 (m), 1013 (m), 960 (m), 873 (m), 829 (s), 658 (s) cm^{-1}. HRMS (ESI-FTMS) *m/z*: $[M + H]^+$ calcd for $[C_{25}H_{38}N_2Sn + H]^+$ 487.2130, found 487.2149.

*4,4′-Bis(iodo-)azobenzene (**13**).*[28]

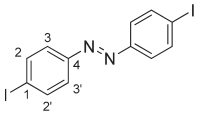

This compound has also been synthesized by Roncali and coworkers.[28] For the preparation of the catalyst, copper chloride (5.00 g, 45.7 mmol) was dissolved in pyridine (50 mL), and the mixture was stirred for 30 min at 20 °C. An insoluble residue which remained was removed by filtration before addition of 4-iodoaniline (14.3 g, 65.3 mmol) in one portion to the solution. The reaction mixture was stirred for 9 h at 20 °C while air was bubbled through the reaction mixture with the help of a frit. Then, diethyl ether (150 mL) was added, and the organic phase was washed with water (3 × 200 mL), 2 M aqueous hydrochloride acid (2 × 200 mL), and water (1 × 100 mL). The organic phase was dried over sodium sulfate. After evaporation of the solvent, the crude product was recrystallized from ethanol to give 8.64 g (61%, lit.[28] 87%) of a red solid. Mp: 210 °C (lit.[28] mp 210−211 °C). ^{1}H NMR (500 MHz, $CDCl_3$): δ= 8.07 (d, ^3J = 8.7 Hz, 4 H, H-2, 2′), 7.79 (d, ^3J = 8.7 Hz, 4 H, H-3,3′) ppm. ^{13}C NMR (126 MHz, $CDCl_3$): 151.8 (*C-4*), 138.4 (*C-2, 2′*), 124.5 (*C-3, 3′*), 98.1 (*C-1*) ppm. IR (ATR): 3078 (w), 1560 (m), 1573 (m), 1469 (m), 1393 (m), 1156 (m), 1051 (m), 1001 (m), 833 (s), 539 (s) cm^{-1}. HRMS (CI-sector) *m/z*: $[M + H]^+$ calcd for $[C_{12}H_8N_2I_2 + H]$ 434.8855, found 434.8848.

*4,4′-Bis(trimethylstannyl)azobenzene (**14**).*

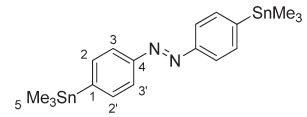

4,4′-*Bis*(iodo)azobenzene (1.00 g, 2.30 mmol), hexamethyldistannane (1.15 g, 4.61 mmol), DMSO (2 mL), and $[Pd(PPh_3)_4]$ (106 μg, 92.0 μmol, 4 mol %) were dissolved in toluene (19 mL). The reaction vessel was heated to 150 °C for 10 min in a microwave apparatus. Then the solvent was evaporated, and the crude product was purified by filtration on silica with DCM. The solvent was evaporated, and the remaining hexamethyldistannane was evaporated at 5.3 × 10^{-2} mbar and 70 °C over 39 h. 946 mg (81%) of red solid was obtained. Mp: 54 °C. ^{1}H NMR (500 MHz, $CDCl_3$): 7.87 (d, ^3J = 8.2 Hz, 4 H, H-3, 3′), 7.65 (d, ^3J = 8.2 Hz, 4 H, H-2, 2′), 0.34 (s, 18 H, H-5) ppm. ^{13}C NMR (126 MHz, $CDCl_3$): 152.8 (*C-4*), 147.1 (*C-1*), 136.6 (*C-2, 2′*), 122.0 (*C-3, 3′*), −9.4 (*C-5*) ppm. ^{119}Sn NMR (187 MHz, $CDCl_3$): δ = −25.20 ppm. IR (ATR): 3067 (w), 3024 (w), 2987 (w), 2917 (w), 1925 (w), 1437 (m), 1383 (m), 1306 (m), 1067 (m), 1011 (m), 831 (s), 761 (s), 583 (s), 508 (s) cm^{-1}. HRMS (ESI-FTMS) *m/z*: $[M + H]^+$ calcd for $[C_{18}H_{26}N_2Sn_2 + H]^+$ 511.0213, found 511.0227.

dx.doi.org/10.1021/jo402598u | *J. Org. Chem.* 2014, 79, 1719−1728

*4,4′-Bis(tributylstannyl)azobenzene (**15**).*

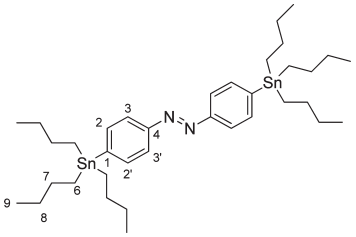

4,4′-*Bis*(iodo)azobenzene (1.00 g, 2.30 mmol), hexa-*n*-butyldistannane (2.67 g, 4.60 mmol), DMSO (2 mL), and $[Pd(PPh_3)_4]$ (106 mg, 92.0 μmol, 4 mol %) were dissolved in toluene (19 mL). The reaction vessel was heated to 150 °C for 60 min in a microwave apparatus. The solvent was evaporated. The crude product was dissolved in DCM and filtered over a short plug of silica. The solvent was evaporated, and the remaining oil was purified by removing the byproducts by Kugelrohr distillation (7.93×10^{-2} mbar, 150 °C, 30 min). The residue was dissolved in DCM and filtered over a short plug of silica. 1.07 g (61%) of a red oil was obtained. ^{1}H NMR (500 MHz, $CDCl_3$): 7.85 (d, ^3J = 8.2 Hz, 4H, H-3, 3′), 7.64 (d, ^3J = 8.2 Hz, 4H, H-2, 2′), 1.66−1.49 (m, 12H, H-7), 1.41−1.32 (m, 12 H, H-8), 1.19−1.05 (m, 12 H, H-6), 0.91 (t, ^3J = 7.3 Hz, 18 H, H-9) ppm. ^{13}C NMR (126 MHz, $CDCl_3$): 152.7 (*C-4*), 147.0 (*C-1*), 137.1 (*C-3, 3′*), 121.8 (*C-2, 2′*), 29.1 (*C-7*), 27.4 (*C-8*), 13.7 (C-9), 9.7 (*C-6*) ppm. ^{119}Sn NMR (187 MHz, $CDCl_3$): −40.0 ppm. IR (ATR): 3074 (w), 2955 (s), 2922 (s), 2850 (s), 1921 (w), 1462 (m), 1376 (m), 1064 (m), 1012 (m), 830 (s) cm^{-1}. HRMS (ESI-FTMS) *m/z*: $[M + H]^+$ calcd for $[C_{36}H_{62}N_2Sn_2 + H]^+$ 763.3030, found 763.3023.

*4-(4-Nitrophenyl)-4′-methylazobenzene (**17**).*

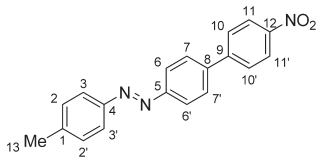

Method A. 4-Methyl-4′-(trimethylstannyl)azobenzene (200 mg, 0.557 mmol), *para*-nitrophenyl bromide (113 mg, 0.557 mmol), $[Pd(PPh_3)_4$ (12.9 mg, 0.011 mmol, 2 mol %), copper chloride (165 mg, 1.67 mmol,] 3 equiv), and lithium chloride (142 mg, 3.34 mmol, 6 equiv) were dissolved in DMF (15 mL). The reaction mixture was heated to 70 °C for 6 h. After the reaction mixture had cooled to 20 °C, chloroform (80 mL) was added, and the mixture was extracted with 2 M hydrochloric acid (2 × 150 mL), a saturated sodium carbonate solution (1 × 150 mL), and water (1 × 150 mL). The combined organic phases were dried over sodium sulfate. The product was recrystallized from EtOH. Orange crystals (157 mg, 89%) were obtained.

Method B. 4-Methyl-4′-(tri-*n*-butylstannyl)azobenzene (270 mg, 0.557 mmol), *para*-nitrophenyl bromide (113 mg, 0.559 mmol), $[Pd(PPh_3)_4]$ (12.9 mg, 11.2 μmol, 2 mol %), copper chloride (165 mg, 1.67 mmol, 3 equiv), and lithium chloride (142 mg, 3.34 mmol, 6 equiv) were dissolved in DMF (15 mL). The reaction mixture was heated to 70 °C for 17 h. After the reaction mixture had cooled to 20 °C, chloroform (80 mL) was added, and the mixture was extracted with 2 M hydrochloric acid (2 × 150 mL), a saturated sodium carbonate solution (1 × 150 mL), and water (1 × 150 mL). The combined organic phases were dried over sodium sulfate. The solvent was evaporated. The crude product was recrystallized from cyclohexane. An orange solid (125 mg, 71%) was obtained. Mp: 104 °C. ^{1}H NMR (500 MHz, $CDCl_3$): 8.24 (d, ^3J = 8.9 Hz, 2 H, H-11, 11′), 7.93 (d, ^3J = 8.7 Hz, 2H, H-6, 6′), 7.78 (d, ^3J = 8.2 Hz, 2H, H-3,3′), 7.71 (d,^3J = 8.9 Hz, 2H, H-10, 10′), 7.68 (d, ^3J = 8.7 Hz, 2H, H-7, 7′), 7.26 (d, ^3J = 8.2 Hz, 2 H, H-2, 2′), 2.37 (s, 3 H, H-13) ppm. ^{13}C NMR (125 MHz, CD_2Cl_2): 152.8 (*C-5*), 150.8 (*C-4*), 147.4 (*C-12*), 146.6 (*C-9*), 142.1 (*C-8*), 140.6 (*C-1*), 129.8 (*C-2, 2′*), 128.1 (*C-7, 7′*), 127.9 (*C-10, 10′*), 124.2 (*C-11, 11′*), 123.5 (*C-6, 6′*), 123.0 (*C-3, 3′*), 21.6 (*C-13*) ppm. IR (ATR): 3023 (w), 2979 (w), 2912 (w), 1382 (m), 1067 (m), 832 (m), 1065 (m), 832 (s), 760 (s), 583 (s), 520 (s) cm^{-1}. HRMS (ESI-FTMS) *m/z*: $[M + H]^+$ calcd for $[C_{19}H_{15}N_3O_2 + H]^+$ 318.1237, found 318.1245.

*4-(4-Cyanophenyl-) 4′-methylazobenzene (**20**).*

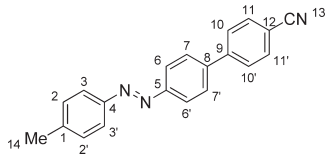

4-Methyl-4′-(trimethylstannyl)azobenzene (200 mg, 0.557 mmol), 4-bromobenzonitrile (101 mg, 0.557 mmol), $[Pd(PPh_3)_4]$ (12.9 mg, 11.2 μmol, 2 mol %), copper chloride (165 mg, 1.67 mmol, 3 equiv), and lithium chloride (142 mg, 3.34 mmol, 6 equiv) were dissolved in DMF (15 mL). The reaction mixture was heated to 70 °C for 8 h. After the reaction mixture had cooled to 20 °C, chloroform (80 mL) was added, and the mixture was extracted with 2 M hydrochloric acid (2 × 150 mL), a saturated sodium carbonate solution (1 × 150 mL), and water (1 × 150 mL). The combined organic phases were dried over sodium sulfate. The product was purified by column chromatography on silica with toluene as eluent. The solvent was evaporated, and an orange solid (136 mg, 82%) was obtained. Mp: 207 °C. ^{1}H NMR (500 MHz, $CDCl_3$): 8.01 (d, ^3J = 8.7 Hz, 2H, 6, 6′), 7.86 (d, ^3J = 8.2 Hz, 2H, 3, 3′), 7.81−7.74 (m, 6 H, H-7, 7′, 10, 10′, 11, 11′), 7.36 (d, ^3J = 8.2 Hz, 2H, 2,2′), 2.45 (s, 3 H, CH_3) ppm. ^{13}C NMR (125 MHz, CD_2Cl_2) (due to significant signal overlap in the ^{1}H NMR spectrum, it was impossible to assign all ^{13}C NMR signals using HMQC and HMBC): 152.7 (*C-5*), 150.9 (*C-4*), 144.65, 142.4 (*C-1*), 141.3, 132.8 (*C-2, 2′*), 123.0, 128.2, 127.9, 123.5 (*C-6, 6′*), 123.0 (*C-3, 3′*), 118.9, 111.6, 21.4 (*C-14*) ppm. IR (ATR): 3071 (w), 3045 (w), 2925 (w), 2225 (m), 1598 (m), 1417 (m), 1378 (m), 1233 (m), 1208 (m), 1158 (m), 1109 (m), 1003 (m), 830 (s), 718 (m), 639 (m), 546 (s) cm^{-1}. HRMS (CI-sector) *m/z*: $[M + H]^+$ calcd for $[C_{20}H_{15}N_3 + H]^+$ 298.1344, found 298.1347.

*4-(4-Acetylphenyl)-4′-methylazobenzene (**21**).*

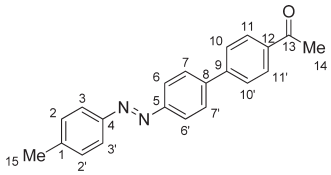

4-Methyl-4′-(trimethylstannyl)azobenzene (200 mg, 0.557 mmol), 4-bromoacetophenone (111 mg, 0.557 mmol), $[Pd(PPh_3)_4]$ (12.9 mg, 11.2 μmol, 2 mol %), copper chloride (165 mg, 1.67 mmol, 3 equiv), and lithium chloride (142 mg, 3.34 mmol, 6 equiv) were dissolved in DMF (15 mL). The reaction mixture was heated to 70 °C for 8 h. After the reaction mixture had cooled to 20 °C, chloroform (80 mL) was added, and the mixture was extracted with 2 M hydrochloric acid (2 × 150 mL), a saturated sodium carbonate solution (1 × 150 mL), and water (1 × 150 mL). The combined organic phases were dried over sodium sulfate. The solvent was evaporated. The crude product was purified by column chromatography with toluene as eluent. An orange solid (152 mg, 87%) was obtained. Mp: 186 °C. ^{1}H NMR (500 MHz, CD_2Cl_2): 8.05 (d, ^3J = 8.6 Hz, 2 H, H-11, 11′), 8.01 (d, ^3J = 8.7 Hz, 2 H, H-6, 6′), 7.86 (d, ^3J = 8.1 Hz, 2 H, H-3, 3′), 7.82 (d, ^3J = 8.7 Hz, 2 H, H-7, 7′), 7.79 (d, ^3J = 8.6 Hz, 2 H, H-10, 10′), 7.36 (d, ^3J = 8.1 Hz, 2 H, H-2, 2′), 2.63 (s, 3 H, H-14), 2.45 (s, 3 H, H-15) ppm. ^{13}C NMR (125 MHz, $CDCl_3$): 197.7 (*C-13*), 152.75 (*C-5*), 151.2 (*C-4*), 144.9 (*C-9*), 142.50 (*C-8*), 142.4 (*C-1*), 136.8 (*C-12*), 130.2 (*C-2, 2′*), 129.3 (*C-11, 11′*), 128.4 (*C-7, 7′*), 127.6 (*C-10, 10′*), 123.7 (*C-6, 6′*), 123.2 (*C-3, 3′*), 26.9 (*C-14*), 21.6 (*C-15*) ppm. IR (ATR): 3348 (w), 3027 (w), 2917 (w), 2859 (w), 1925 (w), 1674 (s), 1599 (m), 1355 (m), 1231 (m), 957 (m), 824 (s), 720 (m) cm^{-1}. HRMS (ESI-FTMS) *m/z*: $[M + Na]^+$ calcd for $[C_{21}H_{18}N_2O + Na]^+$ 337.1311, found 337.1318.

dx.doi.org/10.1021/jo402598u | *J. Org. Chem.* 2014, 79, 1719−1728

*4-Phenyl-4′-methylazobenzene (**23**).*

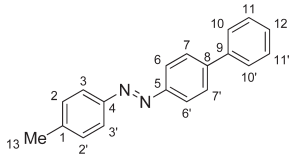

4-Methyl-4′-(trimethylstannyl)azobenzene (200 mg, 0.557 mmol), bromobenzene (87,5 mg, 0.557 mmol), $[Pd(PPh_3)_4]$ (12.9 mg, 11.2 μmol, 2 mol %), copper chloride (165 mg, 1.67 mmol, 3 equiv), and lithium chloride (142 mg, 3.34 mmol, 6 equiv) were dissolved in DMF (15 mL). The reaction mixture was heated to 70 °C for 10 h. After the reaction mixture had cooled to 20 °C, chloroform (80 mL) was added, and the mixture was extracted with 2 M hydrochloric acid (2 × 150 mL), a saturated sodium carbonate solution (1 × 150 mL), and water (1 × 150 mL). The combined organic phases were dried over sodium sulfate. The solvent was evaporated. The crude product was purified by column chromatography with toluene as eluent. The solvent was evaporated, and an orange solid (141 mg, 93%) was obtained. Mp: 198 °C. ^{1}H NMR (500 MHz, CD_2Cl_2): 7.99 (d, ^3J = 8.7 Hz, 2 H, H-6, 6′), 7.86 (d, ^3J = 8.1 Hz, 2 H, H-3, 3′), 7.78 (d, ^3J = 8.7 Hz, 2 H, H-7, 7′), 7.70 (dd, J = 8.5, 1.2 Hz, 2 H, H-10, 10′), 7.49 (t, ^3J = 8.5 Hz, 2 H, H-11, 11′), 7.42−7.38 (m, 1 H, H-12), 7.36 (d, ^3J = 8.1 Hz, 2 H, H-2, 2′), 2,45 (s, 3 H, H-15) ppm. ^{13}C NMR (125 MHz, CD_2Cl_2): 152.2 (*C-5*), 151.24 (*C-4*), 143.8 (*C-8*), 142.3 (*C-1*), 140.5 (*C-9*), 130.2 (*C-2, 2′*), 129.3 (*C-11, 11′*), 128.3 (*C-12*), 128.1 (*C-7, 7′*), 127.5 (*C-10, 10′*), 123.6 (*C-6, 6′*), 123.2 (*C-3, 3′*), 21.6 (C-13) ppm. IR (ATR): 3023.7 (w), 2914 (w), 1599 (m), 1483 (m), 1405 (m), 1157 (m) 847 (s), 763 (s), 687 (s) cm^{-1}. HRMS (CI-sector) *m/z*: $[M + H]^+$ Calcd for $[C_{19}H_{16}N_2 + H]^+$ 273.1392; Found 273.1391.

*4-(2-Furanyl-5-aldehyde)-4′-methylazobenzene (**25**).*

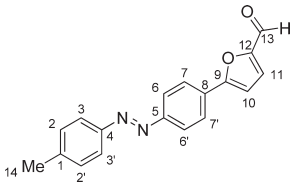

4-Methyl-4′-(trimethylstannyl)azobenzene (200 mg, 0.557 mmol), 2-bromo-5-furaldehyde (97.5 mg, 0.557 mmol), $[Pd(PPh_3)_4]$ (12.9 mg, 11.2 μmol, 2 mol %), copper chloride (165 mg, 1.67 mmol, 3 equiv), and lithium chloride (142 mg, 3.34 mmol, 6 equiv) were dissolved in DMF (15 mL). The reaction mixture was heated to 70 °C for 16 h. After the reaction mixture had cooled to 20 °C, chloroform (80 mL) was added, and the mixture was extracted with 2 M hydrochloric acid (2 × 150 mL), a saturated sodium carbonate solution (1 × 150 mL), and water (1 × 150 mL). The combined organic phases were dried over sodium sulfate. The product was purified by column chromatography with DCM as eluent. The solvent was evaporated, and an orange solid (155 mg, 73%) was obtained. Mp: 163 °C. ^{1}H NMR (500 MHz, CD_2Cl_2): 9.67 (s, 1 H, H-13) 7.98 (m, 4 H, H-6,6′,7,7′), 7.85 (d, ^3J = 8.2 Hz, 2 H,H- 3,3′), 7.38−7.34 (m, 3 H, 2, 2′, H-11), 6.99 (d, ^3J = 3.7 Hz, 1 H, H-12), 2.45 (s, 3 H, H-14) ppm. ^{13}C NMR (125 MHz, CD_2Cl_2): 177.3 (*C-13*), 158.4 (*C-9*), 153.0 (*C-12*), 152.7 (*C-5*), 150.9 (*C-4*), 142.5 (*C-1*), 131.0 (C-8), 129.0 (*C-2, 2′*), 127.9 (C-11), 126.0 (*C-7, 7′*), 123.5 (*C-6, 6′*), 123.1 (*C-3, 3′*), 109.1 (*C-10*), 21.4 (*C-15*) ppm. IR (ATR): 3137 (w), 3057 (w), 2922 (w), 2852 (w), 1683 (s), 1477 (s), 1257 (s), 1151 (s), 1104 (s), 1040 (s), 966 (s), 815 (s), 546 (m), 529 (m) cm^{-1}. HRMS (ESI-FTMS) *m/z*: $[M + Na]^+$ calcd for $[C_{18}H_{14}N_2O_2 + Na]^+$ 313.0947, found 313.0956.

*4-(5-Methylcarboxylate-2-furanyl)-4′-methylazobenzene (**27**).*

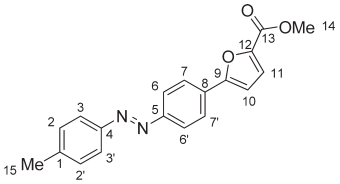

4-Methyl-4′-(trimethylstannyl)azobenzene (200 mg, 0.557 mmol), 5-bromo-2-furancarboxylic acid methyl ester (114 mg, 0.557 mmol), $[Pd(PPh_3)_4]$ (12.9 mg, 11.2 μmol, 2 mol %), copper chloride (165 mg, 1.67 mmol, 3 equiv), and lithium chloride (142 mg, 3.34 mmol, 6 equiv) were dissolved in DMF (15 mL). The reaction mixture was heated to 70 °C for 14 h. After the reaction mixture had cooled to 20 °C, chloroform (40 mL) was added, and the mixture was extracted with water (3 × 150 mL). The combined organic phases were dried over sodium sulfate. The product was purified by column chromatography with toluene as eluent. The solvent was evaporated, and an orange solid (185 mg, 84%) was obtained. Mp: 161 °C. ^{1}H NMR (500 MHz, CD_2Cl_2): 7.98 (d, ^3J = 8.8 Hz, 2 H, H-7, 7′), 7.93 (d, ^3J = 8.8 Hz, 2 H, H-6, 6′), 7.85 (d, ^3J = 8.3 Hz, 2 H, H-3, 3′), 7.35 (d, ^3J = 8.3 Hz, 2 H, H 2, 2′), 7.28 (d, ^3J = 3.6 Hz, 1 H, H-11), 6.90 (d, ^3J = 3.6 Hz, 1 H, H-10), 3.91 (s, 3 H, H-14), 2.45 (s, 3 H, H-15) ppm. ^{13}C NMR (125 MHz, CD_2Cl_2): 159.3 (*C-13*), 156.98 (*C-12*), 152.9 (*C-8*), 151.2 (*C-4*), 144.7 (*C-9*), 142.6 (*C-1*), 131.8 (*C-5*), 130.2 (*C-2, 2′*), 125.8 (*C-7, 7′*), 123.7 (*C-6, 6′*), 123.4 (*C-3, 3′*), 120.3 (*C-11*), 108.6 (*C-10*), 52.2 (*C-14*), 21.6 (*C-15*) ppm. IR (ATR): 3403 (w), 3243 (w), 3122 (w), 3034 (w), 2954 (m), 2848 (2), 1703 (s), 1527 (m), 1299 (s) 1133 (s), 1027 (m), 992 (m), 923 (m), 808 (s), 759 (s), 553 (s) cm^{-1}. HRMS (ESI-FTMS) *m/z*: $[M + Na]^+$ calcd for $[C_{19}H_{16}N_2O_3 + Na]^+$ 343.1053, found 343.1062.

*4-(3-Methoxyphenyl-) 4′-methylazobenzene (**31**).*

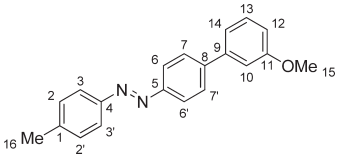

Method A. 4-Methyl-4′-(trimethylstannyl)azobenzene (200 mg, 0.557 mmol), 1-bromo-5-methoxybenzene (104 mg, 0.557 mmol), $[Pd(PPh_3)_4]$ (12.9 mg, 11.2 μmol, 2 mol %), copper chloride (165 mg, 1.67 mmol, 3 equiv), and lithium chloride (142 mg, 3.34 mmol, 6 equiv) were dissolved in DMF (15 mL). The reaction mixture was heated to 70 °C for 19 h. After the reaction mixture had cooled to 20 °C, chloroform (80 mL) was added, and the mixture was extracted with 2 M hydrochloric acid (2 × 150 mL), a saturated sodium carbonate solution (1 × 150 mL), and water (1 × 150 mL). The combined organic phases were dried over sodium sulfate. The solvent was evaporated, and the crude product was purified by column chromatography with toluene as solvent. An orange solid (133 mg, 79%) was obtained.

Method B. 4-Methyl-4′-(tri-*n*-butylstannyl)azobenzene (270 mg, 0.557 mmol), 1-bromo-5-methoxybenzene (104 mg, 0.557 mmol), $[Pd(PPh_3)_4]$ (12.9 mg, 11.2 μmol, 2 mol %), copper chloride (165 mg, 1.67 mmol, 3 equiv), and lithium chloride (142 mg, 3.34 mmol, 6 equiv) were dissolved in DMF (15 mL). The reaction mixture was heated to 70 °C for 25 h. After the reaction mixture had cooled to 20 °C, chloroform (80 mL) was added, and the mixture was extracted with 2 M hydrochloric acid (2 × 150 mL), a saturated sodium carbonate solution (1 × 150 mL), and water (1 × 150 mL). The combined organic phases were dried over sodium sulfate. The solvent was evaporated. The crude product was purified by Kugelrohr distillation (150 °C, 9.74 × 10^{-2} mbar) for 30 min. The residue was purified by column chromatography. An orange solid (91 mg, 54%) was obtained. Mp: 81 °C. ^{1}H NMR (500 MHz, CD_2Cl_2): 7.99 (d, ^3J = 8.7 Hz, 2 H, H-6, 6′), 7.87 (d, ^3J = 8.1 Hz, 2 H, H - 3, 3′), 7.78 (d, ^3J = 8.7 Hz, 1 H, H-7, 7′), 7.40 (t, ^3J = 7.9 Hz, 1 H, H-13), 7.36 (d, ^3J = 8.1 Hz,

dx.doi.org/10.1021/jo402598u | *J. Org. Chem.* 2014, 79, 1719−1728

2 H, H-2, 2′), 7.28 (ddd, *J* = 8.2, 2.6, 0.9 Hz, 1 H, H-14), 7.22 (dd, *J* = 2.6 Hz, 0.9 Hz, 1 H, H-10), 6.95 (ddd, *J* = 8.2, 2.6, 0.9 Hz, 1 H, H-12), 3.88 (s, 3 H, H-15), 2.46 (s, 3 H, H-16) ppm. ^{13}C NMR (125 MHz, CD_2Cl_2): 160.6 (*C*-11), 152.3 (*C*-5), 151.3 (*C*-4), 143.7 (*C*-8), 142.7 (*C*-1), 142.0 (*C*-9), 130.3 (*C*-10), 130.2 (*C*-13), 128.2 (*C*-7, 7′), 123.6 (*C*-6, 6′), 123.2 (*C*-3, 3′), 120.0 (*C*-2,2′), 113.7 (*C*-12), 113.2 (*C*-10), 55.7 (*C*-15), 21.6 (*C*-16) ppm. IR (ATR): 3080 (w), 3009 (w), 2947 (m), 2844 (m), 1925 (w), 1598 (s), 1583 (s), 1480 (s), 1295 (s), 1213 (s), 1152 (s), 1023 (s), 846 (s), 836 (s), 823 (s) 780 (s), 736 (m), 692 (s)545 (s) cm^{-1}. HRMS (CI-sector) *m*/*z*: [M + H]$^+$ calcd for [$C_{20}H_{18}N_2O$ + H]$^+$ 303.1497, found 303.1500.

*4-(2,5-Methoxyphenyl)-4′-methylazobenzene (**32**).*

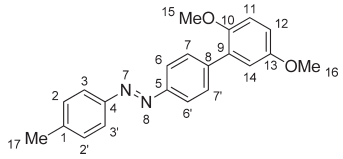

4-Methyl-4′-(trimethylstannyl)azobenzene (200 mg, 0.557 mmol), 1-bromo-2,5-dimethoxybenzene (120 mg, 0.557 mmol), [$Pd(PPh_3)_4$] (12.9 mg, 11.2 μmol, 2 mol %), copper chloride (165 mg, 1.67 mmol, 3 equiv), and lithium chloride (142 mg, 3.34 mmol, 6 equiv) were dissolved in DMF (15 mL). The reaction mixture was heated to 70 °C for 26 h. After the reaction mixture had cooled to 20 °C, chloroform (80 mL) was added, and the mixture was extracted with 2 M hydrochloric acid (2 × 150 mL), a saturated sodium carbonate solution (1 × 150 mL), and water (1 × 150 mL). The combined organic phases were dried over sodium sulfate. The crude product was purified by column chromatography with toluene as solvent. The solvent was evaporated, and an orange solid (137 mg, 74%) was obtained. Mp: 74 °C. ^{1}H NMR (500 MHz, CD_2Cl_2): 7.94 (d, ^3J = 8.7 Hz, 2 H, H-6, 6′), 7.86 (d, ^3J = 8.3 Hz, 2 H, H-3, 3′), 7.70 (d, ^3J = 8.7 Hz, 2 H, H-7, 7′), 7.36 (d, ^3J = 8.3 Hz, 2 H, H-2, 2′), 6.98 (d, ^3J = 8.9 Hz, 1 H, H-11), 6.97 (d, ^4J = 2.9 Hz, 1 H, H-14), 6.91 (dd, *J* = 8.9, 3.2 Hz, 1 H, H-12), 3.82 (s, 3 H, H-15), 3.79 (s, 3 H, H-16), 2.46 (s, 3 H, H-17) ppm. ^{13}C NMR (125 MHz, CD_2Cl_2): 154.7 (*C*-10), 152.3 (*C*-5), 151.3 (*C*-13), 151.2 (*C*-4), 142.6 (*C*-1), 142.0 (*C*-8), 131.1 (*C*-7, 7′), 130.6 (*C*-2, 2′), 130.2 (*C*-9), 123.6 (*C*-3, 3′), 123.1 (*C*-6, 6′), 117.3 (*C*-14), 114.5 (*C*-12), 113.6 (*C*-11), 57.0 (*C*-15), 56.6 (*C*-16), 22.0 (*C*-17) ppm. IR (ATR): 3093 (w), 3001 (w), 2954 (m), 2830 (m), 1593 (m), 1488 (s), 1459 (s), 1296 (m), 1208 (s), 1178 (s), 1023 (s), 1010 (s), 852 (s), 811 (s), 727 (s). HRMS (CI-sector) *m*/*z*: [M + H]$^+$ calcd for [$C_{21}H_{20}N_2O_2$ + H]$^+$ 333.1603, found 333.1604.

*4-(5-1,3-Benzodioxolyl)-4′-methylazobenzene (**33**).*

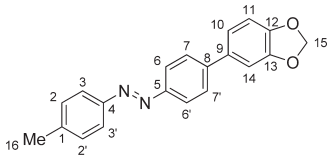

4-Methyl-4′-(trimethylstannyl)azobenzene (200 mg, 0.557 mmol), 5-bromo-1,3-benzodioxole (112 mg, 0.557 mmol), [$Pd(PPh_3)_4$] (12.9 mg, 0.011 mmol, 2 mol %), copper chloride (165 mg, 1.67 mmol, 3 equiv), and lithium chloride (142 mg, 3.34 mmol, 6 equiv) were dissolved in DMF (15 mL). The reaction mixture was heated to 70 °C for 24 h. After the reaction mixture had cooled to 20 °C, chloroform (80 mL) was added, and the mixture was extracted with water (3 × 150 mL). The combined organic phases were dried over sodium sulfate. The crude product was purified by column chromatography with toluene as solvent. A red solid (123 mg, 70%) was obtained. Mp: 144 °C. ^{1}H NMR (500 MHz, CD_2Cl_2): 7.95 (d, ^3J = 8.5 Hz, 2 H, 6,6′), 7.84 (d, ^3J = 8.2 Hz, 2 H, 3,3′), 7.69 (d, ^3J = 8.5 Hz, 2 H, 7,7′), 7.35 (d, ^3J = 8.2 Hz, 2 H, 2,2′), 7.19−7.16 (m, 2 H, H-11, 14), 6.84 (d, ^3J = 7.8 Hz, 1 H, H-10), 6.03 (s, 2 H, H-15), 2.45 (s, 3 H, H-16) ppm. ^{13}C NMR (125 MHz, CD_2Cl_2): 151.7 (*C*-5), 151.0 (*C*-4), 148.5 (*C*-12), 147.9 (*C*-13), 143.3 (*C*-8), 141.9 (*C*-1), 134.5 (*C*-9), 129.9 (*C*-2, 2′), 127.5 (*C*-7, 7′), 123.3 (*C*-3, 3′), 122.9 (*C*-6, 6′), 121.0 (*C*-11), 108.7 (*C*-10), 107.5 (*C*-14), 101.7 (*C*-15), 21.4 (*C*-16) ppm. IR (ATR): 3022 (w), 2912 (w), 2859 (w), 2720 (w), 1920 (w), 1696 (m), 1477 (m), 1242 (m), 1307 (m), 823 (s), 731 (m), 547 (m) cm^{-1}. HRMS (CI-sector) *m*/*z*: [M + H]$^+$ calcd for [$C_{20}H_{16}N_2O_2$ + H]$^+$ 317.1290, found 317.1291.

*4-(2-Thiophene-yl)-4′-methylazobenzene (**35**).*

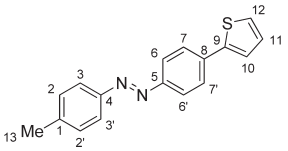

4-Methyl-4′-(trimethylstannyl)azobenzene (200 mg, 0.557 mmol), 2-bromothiophene (90.8, 0.557 mmol), [$Pd(PPh_3)_4$] (12.9 mg, 11.2 μmol, 2 mol %), copper chloride (165 mg, 1.67 mmol, 3 equiv), and lithium chloride (142 mg, 3.34 mmol, 6 equiv) were dissolved in DMF (15 mL). The reaction mixture was heated to 70 °C for 11 h. After the reaction mixture had cooled to 20 °C, chloroform (80 mL) was added, and the mixture was extracted with 2 M hydrochloric acid (2 × 150 mL), a saturated sodium carbonate solution (1 × 150 mL), and water (1 × 150 mL). The combined organic phases were dried over sodium sulfate. The crude product was dissolved in DCM and filtered through a short plug of silica. The solvent was evaporated and dried at 5 × 10^{-2} mbar for 19 h. An orange solid (173 mg, 88%) was obtained. Mp: 153 °C. ^{1}H NMR (500 MHz, CD_2Cl_2): 7.93 (d, *J* = 8.7 Hz, 2 H, H-6,6′), 7.84 (d, *J* = 8.2 Hz, 1H, H-3, 3′), 7.78 (d, *J* = 8.7 Hz, 2 H, H-7, 7′), 7.46 (dd, *J* = 3.6, 1.1 Hz, 1 H, H-10), 7.38 (dd, *J* = 5.1, 1.1 Hz, 1 H, H-12), 7.35 (d, *J* = 8.2 Hz, 1H, H- 2,2′), 7.14 (dd, *J* = 5.1, 3.6 Hz, 1 H, H-11), 2.45 (s, 3 H, H-13) ppm. ^{13}C NMR (125 MHz, CD_2Cl_2): 152.1 (*C*-5), 151.2 (*C*-4), 143.8 (*C*-9), 142.3 (*C*-1), 137.0 (*C*-8), 130.2 (*C*-2), 128.8 (*C*-11), 126.7 (*C*-7), 126.3 (*C*-12), 124.5 (*C*-10), 123.8 (*C*-6), 123.2 (*C*-3), 21.6 (*C*-13) ppm. IR (ATR): 3104 (w), 3027 (w), 2914 (m), 2856 (m), 1928 (w), 1735 (m), 1598 (m), 1157 (m), 1110 (m), 1011 (m), 846 (s), 824 (s), 780 (s), 728 (s), 690 (m), 531 (s) cm^{-1}. HRMS (CI-sector) *m*/*z*: [M + H]$^+$ calcd for [$C_{17}H_{14}N_2S$ + H]$^+$ 279.0956, found 279.0953.

*4-(3-Thiophene-yl)-4′-methylazobenzene (**37**).*

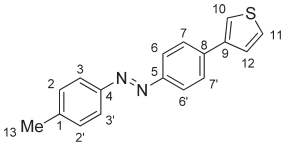

4-Methyl-4′-(trimethylstannyl)azobenzene (200 mg, 0.557 mmol), 3-bromothiophene (90.8 mg, 0.557 mmol), [$Pd(PPh_3)_4$] (12.9 mg, 11.2 μmol, 2 mol %), copper chloride (165 mg, 1.67 mmol, 3 equiv), and lithium chloride (142 mg, 3.34 mmol, 6 equiv) were dissolved in DMF (15 mL). The reaction mixture was heated to 70 °C for 14 h. After the reaction mixture had cooled to 20 °C, chloroform (80 mL) was added, and the mixture was extracted with 2 M hydrochloric acid (2 × 150 mL), a saturated sodium carbonate solution (1 × 150 mL), and water (1 × 150 mL). The combined organic phases were dried over sodium sulfate. The crude product was dissolved in DCM (5 mL) and filtered through a short plug of silica. The solvent was evaporated, and the product was dried at 5 × 10^{-2} mbar for 21 h. An orange solid (164 mg, 83%) was obtained. Mp: 178 °C. ^{1}H NMR (500 MHz, CD_2Cl_2): 7.95 (d, *J* = 8.7 Hz, 2 H, H-6, 6′), 7.84 (d, *J* = 8.1 Hz, 2 H, H-3, 3′), 7.78 (d, *J* = 8.7 Hz, 2 H, H-7, 7′), 7.62 (dd, *J* = 2.9, 1.4 Hz, 1 H, H-10), 7.50 (dd, *J* = 5.0, 1.4 Hz, 1 H, H-11), 7.46 (dd, *J* = 5.0, 2.9 Hz, 1 H, H-12), 7.35 (d, *J* = 8.1 Hz, 2 H, H-2, 2′), 2.45 (s, 3 H, H-13). ^{13}C NMR (125 MHz, CD_2Cl_2): 152.0 (*C*-5), 151.2 (*C*-4), 142.2 (*C*-1), 141.8 (*C*-9), 138.4 (*C*-8), 130.2 (*C*-2), 127.3 (*C*-7), 127.0 (*C*-12), 126.6 (*C*-11), 123.7 (*C*-6), 123.1 (*C*-3), 121.8 (*C*-10), 21.6 (*C*-13) ppm. IR (ATR): 3104 (w), 3027 (w), 2914 (m), 2856 (m), 1928 (w), 1735 (m), 1598 (m), 1157 (m), 1110 (m), 1011 (m), 846 (s), 824 (s), 780 (s), 728 (s), 690 (m), 531 (s) cm^{-1}. HRMS (CI-sector) *m*/*z*: [M + H]$^+$ calcd for [$C_{17}H_{14}N_2S$ + H]$^+$ 279.0956, found 279.0951.

*4-(4-N,N-Dimethylaminophenyl)-4′-methylazobenzene (**39**).*

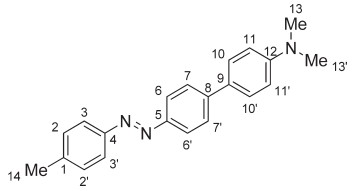

4-Methyl-4′-(trimethylstannyl)azobenzene (200 mg, 0.557 mmol), 4-bromo-*N*,*N*-dimethylaniline (111 mg, 0.557 mmol), [$Pd(PPh_3)_4$] (12.9 mg, 11.2 μmol, 2 mol %), copper chloride (165 mg, 1.67 mmol, 3 equiv), and lithium chloride (142 mg, 3.34 mmol, 6 equiv) were dissolved in DMF (15 mL). The reaction mixture was heated to 70 °C for 19 h. After the reaction mixture had cooled to 20 °C, chloroform (80 mL) was added, and the mixture was extracted with 2 M hydrochloric acid (2 × 150 mL), a saturated sodium carbonate solution (1 × 150 mL), and water (1 × 150 mL). The combined organic phases were dried over sodium sulfate. The solvent was evaporated, and the crude product was purified by column chromatography with toluene as solvent. An orange solid (126 mg, 72%) was obtained. Mp: 124 °C. ^{1}H NMR (500 MHz, CD_2Cl_2): 7.93 (d, ^3J = 8.6 Hz, 2 H, H-6, 6′), 7.83 (d, ^3J = 8.3 Hz, 2 H, H-3, 3′), 7.73 (d, ^3J = 8.6 Hz, 1 H, H-7, 7′), 7.60 (d, ^3J = 8.9 Hz, 2 H, H-10, 10′), 7.36 (d, ^3J = 8.0 Hz, 2 H, H-2, 2′), 7.36 (d, ^3J = 8.9 Hz, 2 H, H-11, 11′), 3.01 (s, 6 H, H-13), 2.44 (s, 3 H, H-14) ppm. ^{13}C NMR (125 MHz, CD_2Cl_2):[2] 151.3 (C-5), 151.2 (C-4), 150.9 (C-12), 143.9 (C-8), 141.9 (C-1), 130.1 (C-2,2′), 129.7 (C-9), 128.0 (C-7,7′), 126.7 (C-10,10′), 123.6 (C-6,6′), 123.0 (C-7,7′), 112.9 (C-11,11′), 40.6 (C-13,13′), 21.6 (C-14) ppm. IR (ATR): 3031 (w), 2921 (w), 2852 (w), 2801 (w), 1591 (m), 1537 (m), 1492 (m), 1364 (m), 1286 (m), 1210 (m), 1153 (m), 950 (m), 826 (s), 812 (s) 716 (m) cm^{-1}. HRMS (CI-sector) *m*/*z*: $[M + H]^+$ calcd for $[C_{21}H_{21}N_3 + H]^+$ 316.1814, found 316.1809.

■ ASSOCIATED CONTENT

Ⓢ Supporting Information

GC calibration, purities of the compounds used, drying procedures for the solvents, and ^{1}H and ^{13}C NMR spectra for all compounds This material is available free of charge via the Internet at http://pubs.acs.org.

■ AUTHOR INFORMATION

Corresponding Author

*E-mail: astaubitz@oc.uni-kiel.de.

Notes

The authors declare no competing financial interest.

■ ACKNOWLEDGMENTS

This project was supported by the Special Research Area 677 "Function by Switching" of the Deutsche Forschungsgemeinschaft (DFG), Project C10.

■ REFERENCES

(1) (a) Hugel, T.; Holland, N. B.; Cattani, A.; Moroder, L.; Seitz, M.; Gaub, H. E. *Science* **2002**, *296*, 1103. (b) Bandarab, H. M. D.; Burdette, S. C. *Chem. Soc. Rev.* **2012**, *41*, 1809. (c) Bushuyev, O. S.; Tomberg, A.; Friščič, T.; Barrett, C. J. *J. Am. Chem. Soc.* **2013**, *135*, 12556.

(2) Lagrasta, C.; Bellobono, I. R. *J. Photochem. Photobiol. A* **1997**, *110*, 201.

(3) Yesodha, S. K.; Pillaia, C. K. S.; Tsutsumi, N. *Prog. Polym. Sci.* **2004**, *29*, 45.

(4) (a) Altomare, A.; Ciardelli, F.; Tirelli, N.; Solaro, R. *Macromolecules* **1997**, *30*, 1298. (b) Yager, K. G.; Barrett, C. J. *J. Photochem. Photobiol. A: Chemistry* **2006**, *182*, 250. (c) Tanchak, O. M.; Barrett, C. J. *Macromolecules* **2005**, *38*, 10566. (d) Nathanson, A.; Rochon, P. *Chem. Rev.* **2002**, *102*, 4139. (e) Kumar, G. S.; Neckers, D. C. *Chem. Rev.* **1989**, *89*, 1915.

(5) (a) Chandrasekaran, V.; Lindhorst, T. K. *Chem. Commun.* **2012**, *48*, 7519. (b) Chandrasekaran, V.; Kolbe, K.; Beiroth, F.; Lindhorst, T. K. *Beilstein J. Org. Chem.* **2013**, *9*, 223. (c) Hartmann, M.; Papavlassopoulos, H.; Chandrasekaran, V.; Grabosch, C.; Beiroth, F.; Lindhorst, T. K.; Röhl, C. *FEBS Lett.* **2012**, *586*, 1459. (d) Goulet-Hanssens, A.; Lai Wing Sun, K.; Kennedy, T. E.; Barrett, C. J. *Biomacromolecules* **2012**, *13*, 2958.

(6) (a) Beharry, A. A.; Sadovski, O.; Woolley, G. A. *J. Am. Chem. Soc.* **2011**, *133*, 19684. (b) Beharry, A. A.; Woolley, G. A. *Chem. Soc. Rev.* **2011**, *40*, 4422. (c) Tochitsky, I.; Banghart, M. R.; Mourot, A.; Yao, J. Z.; Gaub, B.; Kramer, R. H.; Trauner, D. *Nature Chem.* **2012**, *4*, 105. (d) Szymanski, W.; Beierle, J. M.; Kistemaker, H. A. V.; Velema, W. A.; Feringa, B. L. *Chem. Rev.* **2013**, *113*, 6114. (e) Wachtveitl, J.; Zumbusch, A. *ChemBioChem* **2011**, *12*, 1169. (f) Venkataramani, S.; Jana, U.; Dommaschk, M.; Sönnichsen, F. D.; Tuczek, F.; Herges, R. *Science* **2011**, *331*, 445.

(7) (a) Yu, Y.; Nakano, M.; Ikeda, T. *Nature* **2003**, *425*, 145. (b) Aemissegger, A.; Kräutler, V.; van Gunsteren, W. F.; Hilvert, D. *J. Am. Chem. Soc.* **2005**, *127*, 2929.

(8) (a) Wang, S.; Song, Y.; Jiang, L. *J. Photochem. Photobiol. C: Photochem. Rev.* **2007**, *8*, 18. (b) Ambrosio, A.; Marrucci, L.; Borbone, F.; Roviello, A.; Maddalena, P. *Nature Commun.* **2012**, *3*, 1996/1. (c) Baisch, B.; Raffa, D.; Jung, U.; Magnussen, O. M.; Nicolas, C.; Lacour, J.; Kubitschke, J.; Herges, R. *J. Am. Chem. Soc.* **2009**, *131*, 442. (d) Gopakamur, T. G.; Davran-Candan, T.; Bahrenburg, J.; Maurer, R. J.; Temps, F.; Reuter, K.; Berndt, R. *Angew. Chem., Int. Ed.* **2013**, *52*, 11007. (e) Yager, K. G.; Barrett, C. J. *Macromolecules* **2006**, *39*, 9320. (f) Bian, S.; Williams, J. M.; Kim, D. Y.; Li, L.; Balasubramanian, S.; Kumar, J.; Tripathy, S. *J. Appl. Phys.* **1999**, *86*, 4498.

(9) (a) Kravchenko, A.; Shevchenko, A.; Ovchinnikov, V.; Priimagi, A.; Kaivola, M. *Adv. Mater.* **2011**, *23*, 4174. (b) Fukuda, T.; Matsuda, H.; Shiraga, T.; Kimura, T.; Kato, M.; Viswanathan, N. K.; Kumar, J.; Tripathy, S. K. *Macromolecules* **2000**, *33*, 4220.

(10) (a) Bléger, D.; Yu, Z.; Hecht, S. *Chem. Commun.* **2011**, *47*, 12260. (b) Thies, S.; Sell, H.; Schuett, C.; Bornholdt, C.; Naether, C.; Tuczek, F.; Herges, R. *J. Am. Chem. Soc.* **2011**, *133*, 16243. (c) Bushuyev, O. S.; Singleton, T. A.; Barrett, C. J. *Adv. Mater.* **2013**, *25*, 1796.

(11) See, for example: (a) Nguyen, T.-T.-T.; Türp, D.; Wang, D.; Nölscher, B.; Laquai, F.; Müllen, K. *J. Am. Chem. Soc.* **2011**, *133*, 11194. (b) Khan, A.; Hecht, S. *Chem.—Eur. J.* **2006**, *12*, 4764. (c) Yu, B.-C.; Shirai, Y.; Tour, J. M. *Tetrahedron* **2006**, *62*, 10303. (d) Sasaki, T.; Tour, J. M. *Org. Lett.* **2008**, *10*, 897. (e) Shirai, Y.; Sasaki, T.; Guerrero, J. M.; Yu, B.-C.; Hodge, P.; Tour, J. M. *ACSNano* **2008**, *2*, 97. (f) Zeitouny, J.; Belbakra, A.; Llanes-Pallas, A.; Barbieri, A.; Armaroli, N.; Bonifazi, D. *Chem. Commun.* **2011**, *47*, 451.

(12) (a) Lahiri, G. K.; Bhattacharya, S.; Mukherjee, M.; Mukherjee, A. K.; Chakravorty, A. *Inorg. Chem.* **1987**, *26*, 3359. (b) Bergbreiter, D. E.; Osburn, P. L.; Li, C. *Org. Lett.* **2002**, *4*, 737. (c) Dutta, S.; Peng, S.-M.; Bhattacharya, S. *J. Chem. Soc., Dalton Trans.* **2000**, 4623.

(13) Harvey, J. H.; Butler, B. K.; Trauner, D. *Tetrahedron Lett.* **2007**, *48*, 1661.

(14) Koźlecki, T.; Syper, L.; Wilk, K. A. *Synthesis* **1997**, 681.

(15) Yoshino, J.; Furuta, A.; Kambe, T.; Itoi, H.; Kano, N.; Kawashima, T.; Ito, Y.; Asashima, M. *Chem.—Eur. J.* **2010**, *16*, 5026.

(16) Zhu, H.; Zheng, Z.; Wang, J.; Ren, B.; Huang, Y.; Wu, D.; , Process for preparation of 4,4′-dimercaptoazobenzene. CN 101880251 A, Nov 10, 2010.

(17) Sridhara, M. B.; Srinivasa, G. R.; Channe Gowda, D. *J. Chem. Res.* **2004**, 74.

(18) During our work on this project, a very versatile method for introducing trialkylstannanes into highly functionalized molecules via a Sandmeyer-type reaction was published. This work included a stannylated azobenzene which was isolated in 61% yield: Qiu, D.; Meng, H.; Jin, L.; Wang, S.; Tang, S.; Wang, X.; Mo, F.; Zhang, Y.; Wang, J. *Angew. Chem., Int. Ed.* **2013**, *52*, 11581.

(19) Katritzky, A. R.; Wu, J.; Verin, S. V. *Synthesis* **1995**, 651.

(20) For a review, see: (a) Farina, V.; Krishnamurthy, V.; Scott, W. J. *Organic Reactions: The Stille Reaction*; Wiley: Hoboken, 1997. For examples where this reaction has been used in synthesis, see: (b) Yue, W.; Lv, A.; Gao, J.; Jiang, W.; Hao, L.; Li, C.; Li, Y.; Polander, L. E.; Barlow, S.; Hu, W.; Di Motta, S.; Negri, F.; Marder, S. R.; Wang, Z. *J. Am. Chem. Soc.* **2012**, *134*, 5770. (c) Benaglia, M.; Ponzini, F.; Woods, C. R.; Siegel, J. S. *Org. Lett.* **2001**, *3*, 967. (d) Jevric, M.; Broman, S. L.; Nielsen, M. B. *J. Org. Chem.* **2013**, *78*, 4348.
(21) (a) Mee, S. P. H.; Lee, V.; Baldwin, J. E. *Chem.—Eur. J.* **2005**, *11*, 3294. The coupling reaction between aryl halides and hexaalkylditin reagents was first discovered in 1976: (b) Azarian, D.; Dua, S. S.; Eaborn, C.; Walton, D. R. M. *J. Organomet. Chem.* **1976**, *117*, C55. The reaction was further developed by Migita and co-workers: (c) Kosugi, M.; Shimizu, K.; Ohtani, A.; Migita, T. *Chem. Lett.* **1981**, 829. (d) Kosugi, M.; Ohya, T.; Migita, T. *Bull. Chem. Soc. Jpn.* **1983**, *56*, 3855.
(22) Ogata, Y.; Tomizawa, K.; Ikeda, T. *J. Org. Chem.* **1980**, *45*, 1320.
(23) Swanston, J. *Ullmann's Encyclopedia of Industrial Chemistry*; Wiley-VCH Verlag: Weinheim, 2000.
(24) Linshoeft, J.; Heinrich, A. C. J.; Segler, S. A. W.; Gates, P. J.; Staubitz, A. *Org. Lett.* **2012**, *14*, 5644.
(25) (a) Appel, K. E. *Drug Metab. Rev.* **2004**, *36*, 763. (b) Dopp, E.; Hartmann, L. M.; Florea, A.-M.; Rettenmeier, A. W.; Hirner, A. V. *Crit. Rev. Toxicol.* **2004**, *34*, 301.
(26) Yu, B.-C.; Shirai, Y.; Tour, J. M. *Tetrahedron* **2006**, *62*, 10303.
(27) Qu, D.-H.; Wang, Q.-C.; Ren, J.; Tian, H. *Org. Lett.* **2004**, *6*, 2085.
(28) Jousselme, B.; Blanchard, P.; Gallego-Planas, N.; Levillain, E.; Delaunay, J.; Allain, M.; Richomme, P.; Roncali, J. *Chem.—Eur. J.* **2003**, *9*, 5297.

2.3 Lithiation of Azobenzenes by Tin-Lithium Exchange

(*Chem. –Eur. J.* **2015**, *submitted*)

J. Strueben, M. Lipfert, J.-O. Springer, Colin A. Gould, P. J. Gates, F. Soennichsen, A. Staubitz. Manuscript submitted to „Chemistry – A European Journal“

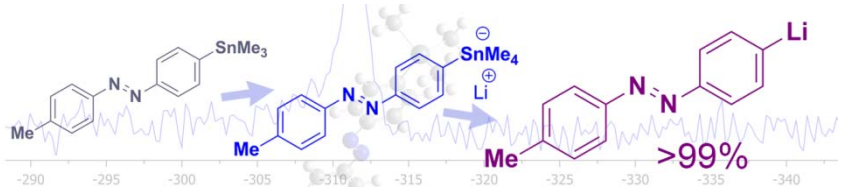

A mild and efficient method for the near quantitative lithiation of azobenzenes in any position is reported. It proceeds via a tin-lithium exchange, which could be monitored by low T ^{119}Sn NMR spectroscopy. The lithiated azobenzenes were able to react with a wide variety of electrophiles in yields ranging from 71% to 98% for mono-substitutions of azobenzenes. In addition, di- and even tri- azobenzene-functionalized compounds were obtained in good yields.

Scientific contribution to this publication

For this publication, I developed and optimized the synthetic route for a quantitative lithiation of azobenzenes by a tin-lithium exchange. I synthesized all stannylated azobenzenes used in this work and also synthesized various compounds (**8a,b,c – 11a,b,c**; **14a,b**; **17a,b**; **18b**; **20b**; **23b**) by quenching with different electrophiles. Furthermore I developed a practical methodology to follow fast lithiation reactions at very low temperatures in an NMR spectrometer. M. Lipfert developed highly optimized NMR settings for following very low concentrated species by ^{119}Sn NMR. Under my supervision, J. O. Springer screened various electrophiles (**19 a,b; 29a; 22a; 23a; 24a,b; 25a-28b**) with the optimized reaction conditions and isolated the products for his M. Sc. thesis. Colin A. Gould supported me as a DAAD RISE Student helping me carrying out some of first optimization reactions for the lithiation of azobenzenes under my supervision. A. Staubitz performed DFT calculations on the reaction mechanism of the tin-lithium exchange. A. Staubitz and I wrote the article together.

High Yielding Lithiation of Azobenzenes by Tin-Lithium Exchange

Jan Strueben[a], Matthias Lipfert[a]‡, Jan-Ole Springer[a] ‡, Colin A. Gould[a], Paul J. Gates[b], Frank D. Sönnichsen[a], Anne Staubitz[a]*

Abstract: The lithiation of halogenated azobenzenes by a halogen-lithium exchange commonly leads to a substantial degradation of the azo-group to give hydrazine derivatives besides the desired aryl-lithium species. Yields for quenching reactions with electrophiles are therefore low. This work shows that a transmetalation reaction of easily accessible stannylated azobenzenes with methyl lithium leads to a near-quantitative lithiation of azobenzenes in *para*, *meta* and *ortho* position. To investigate the scope of the reaction, various lithiated azobenzenes species were quenched with a variety of electrophiles. Furthermore, mechanistic ^{119}Sn NMR spectroscopic studies on the formation of lithiated azobenzenes are presented. A tin-ate complex of the azobenzene could be detected at low temperatures. The findings from this study are supported by DFT calculations.

Introduction

Azobenzene derivatives are very important compounds in many fields of research on dyes[1,2] or photoswitchable systems: They undergo a reversible photoisomerization by irradiation with ultraviolet light from their *trans* form to their *cis* form, resulting in substantial changes in their electronic and geometric properties.[3,4] Furthermore, azobenzenes show a high resistance against photobleaching[5] and thermal decomposition.[6] These properties have led to a wide use of azobenzenes in biochemical research,[7,8] e. g. in photoswitchable cell adhesion,[9,10] in medical research e. g. photoswitchable contrast media for magnetic resonance imaging,[11] and in materials and polymer science e. g. photoresponsive polymer materials.[12-18] To be able to tailor the properties of azobenzenes exactly to their intended application, flexible and effective methodologies for the functionalization of azobenzenes are essential.

For the functionalization of aromatic rings in general, a common synthetic strategy is to convert them into organolithium or organomagnesium species and to subsequently quench the reaction with an appropriate electrophile.[19] For these systems, a metalation is usually achieved in situ by a halogen-metal exchange, direct insertion into a carbon-halogen bond or by deprotonation. Halogen-metal exchange reactions are especially selective, so long as the starting material does not contain competing halide functional groups.[20] However, if the molecule contains other electrophilic groups, these are often attacked by the lithiating reagent.[21]

In the case of the lithiation of azobenzenes, the protocols reported in literature all employ a halogen-lithium exchange reaction.[22-27] Typically, the yields are quite low (maximally 53%[22] for the *para* position, 47% for the *ortho* position, and 54 %[28] for the *meta* position). The reason for these poor yields is the low tolerance of the azo group towards reductive conditions: In competition with the halogen-lithium exchange, a nucleophilic attack by the alkyl lithium species on the azo group occurs, leading to hydrazine analogs (**3**, **4** and after quenching with TMSBr, **6** and **7**) of the starting material (Scheme 1).[29-33]

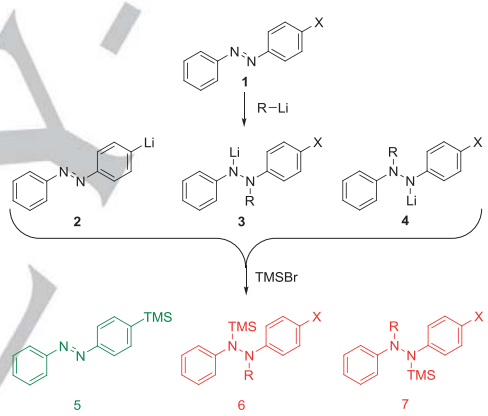

Scheme 1. Lithiation of *para*-iodoazobenzene and subsequent quenching with trimethyl bromo silane.[22]

For a successful, selective lithiation of azobenzene, the lithiation reaction on the aromatic ring must be kinetically preferred over the attack on the diazene group: the desired aryl lithium species should be much less nucleophilic than an alkyl lithium reagent. We reasoned that if a tin-lithium exchange reaction on a stannylated azobenzene of type **9** would be faster than the attack of the lithiating reagent on the diazo group, then a selective lithiation should be possible. We recently demonstrated the stannylation of azobenzenes by a Stille-Kelly cross coupling reaction of the corresponding iodinated azobenzenes **8**, catalyzed by [Pd(PPh$_3$)$_4$], using hexamethyldistannane as the nucleophilic component (Scheme 2).[34]

[a] J. Strueben, M. Lipfert, J.-O. Springer, C. A. Gould, Dr. P. J. Gates, Prof. Dr. F. D. Sönnichsen, Prof. Dr. A. Staubitz
Otto-Diels-Institute for Organic Chemistry, University of Kiel, Otto-Hahn-Platz 4, 24098 Kiel (Germany)
E-mail: astaubitz@oc.uni-kiel.de
[b] School of Chemistry, University of Bristol, Cantock's Close, Bristol BS7 1TS (UK)
‡ These authors contributed equally.

Supporting information for this article is given via a link at the end of

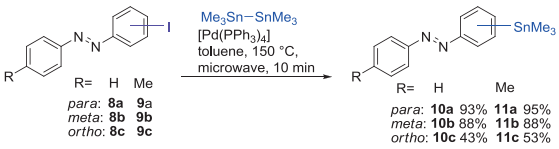

Scheme 2. Stannylation of mono iodinated azobenzenes. Compounds **8a-c**,[35] **9a**,[35] **9b-c**,[36] **10a**,[37] **11a**[34] have been reported previously, the other stannylated azobenzenes are described in this work.

In this work, we demonstrate that a transmetalation from trimethyl tin to lithium leads to a rapid and effective lithiation of azobenzenes in the *para*, *meta* and *ortho* positions without any decomposition of the azo-group. This protocol increases the yield of the lithiated species substantially and allows easy access to compounds that are difficult to obtain by other means.

Reaction Optimization

The three most important factors that influence the selectivity of the two types of competing reactions (i. e. attack of the organolithium reagent on the azo group vs. tin-lithium exchange) are: a) the reactivity of the functional group which should be exchanged by lithium (halogen vs. trialkyl tin) b) the temperature, and c) the reactivity of organolithium complexes in the reaction solvent. We hypothesized that it should be possible to find reaction conditions where the formation of a lithium-stannate complex **11** and a subsequent rearrangement to the lithiated azobenzene **12** would be fast compared to the nucleophilic attack of the alkyllithium reagents on the azo group: As a large group 14 element, tin is able to react with nucleophiles by expanding its coordination sphere to give a penta-coordinated reactive ate-complex. Such intermediates have been described before,[38-43] and, in one instance, have even been isolated.[43] Lithium stannates typically have a lower reactivity towards electrophiles than is observed for other organolithium reagents.[40,46] We further hypothesized that the resulting lithiated azobenzene would have a significantly reduced nucleophilicity, as compared to the alkyl lithium species, and would not be capable of attacking the azo group (Scheme 3).

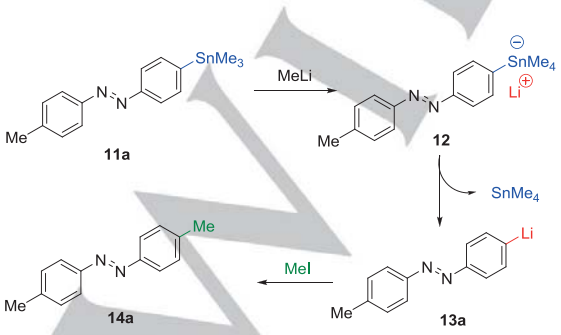

Scheme 3. Proposed lithiation of 4-methyl-4'-trimethyl-stannylazobenzene (**11a**) and subsequent quenching with methyl iodide.

Methyl lithium was chosen as a lithiation reagent be-cause of its high nucleophilicity. A further advantage is its comparatively high stability in tetrahydrofurans, as compared to butyl lithium reagents; [44, 45] the latter show a very short half live in THF of 107 min at 20 °C.[44, 46]

The reaction conditions were analyzed with respect to solvent, temperature and lithiation time (Table 1). To analyze the efficiency of the lithiation, methyl iodide was used as an effective electrophilic quenching reagent and the conversion was determined by quantitative gas chromatographic (GC) analysis (for details see Supporting Information - SI). All other possible side products could be expected to be chemically and thermally stable and thus suitable for GC and GC-MS analysis. To establish reaction conditions for a selective transmetalation from tin to lithium, very low temperatures of -130 °C were initially chosen. MeTHF was selected as a solvent because it has a lower freezing point than THF, -136 °C as compared to -108 °C, while maintaining comparable properties of activating organolithium reagents through deaggregation.[47,48]

At -130 °C, after 4 min of lithiation, the reaction showed no side reactions but a conversion of only 72% (Table 1, entry 1). When the temperature was raised to -78 °C, the transmetalation in MeTHF showed a full conversion to the desired product without observable side reactions (Figure 1). The same was true for THF (Table 1, entries 2, 3). To evaluate the stability of the lithiated intermediate, the total lithiation time was increased to 30 min, but no side products were detected (Table 1 entry 4). In the temperature range from -100 to -43 °C in THF, full conversion to the desired product could be observed. At -16 °C however, the reaction produced various side products: Although it was not possible to isolate these side products individually in pure form and to quantify them, they could be identified as hydrazine derivatives by GC-MS (table 1, entry 4).[49] In contrast to MeTHF and THF as solvents, the reaction proceeded entirely differently in diethyl ether: Using the same reaction conditions as for THF at -100 °C and -78 °C, the yields and the conversion were much lower with 29% and 32%, respectively (Table 1, entries 8, 9). The gas chromatograms of the reactions showed that the lithiation in diethyl ether produced various side products (Figure 1). To ensure the correct identification of the main side products, which we assumed to be the hydrazine derivatives, the lithiation reaction in ether was performed on a larger scale to isolate the side products. As a quenching reagent, methyl iodide was used. Besides the intended product **14a**, the main side product in the crude ^{1}H NMR spectrum could be identified as the hydrazine species **15**. A subsequent column chromatography gave hydrolyzed[50] species **16** in a purity of 90% and an isolated yield of 34%.[51]

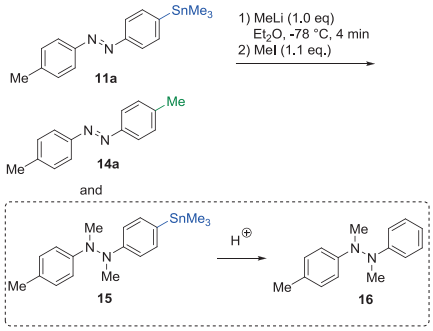

Scheme 4. Lithiation reaction in diethyl ether, followed by quenching with methyl iodide.

The different reaction kinetics were also visible with the naked eye: In THF and MeTHF, the reaction mixture turned black immediately after adding the methyl lithium solution in THF, indicating the formation of an aryl-lithium species. In diethyl ether on the other hand, no significant color change could be observed at -100 °C or -78 °C. Only when the reaction mixture was allowed to warm to temperatures higher than -20 °C, an intense color change to black occurred. As the absence of by-products in THF at temperatures as high as -43 °C was striking, the tin-lithium exchange reaction was performed using an *n*-butyl lithium solution in hexanes. *n*-Butyl lithium is more commonly available and cheaper. Because of the low stability of this reagent in THF, the reaction was performed in reverse order by adding a solution of 4-methyl-4'-trimethylstannylazobenzene to a solution of *n*-butyl lithium in THF at -78 °C. This reaction led to full conversion of the starting material, but unselective transmetalation of the tin group was observed: GC-MS analysis indicated a butylation of the azo group, corresponding to the side reaction in diethyl ether methyl lithium and the hydrazine synthesis as described by Katritzky and coworkers[30] (Table 1, entry 5; Scheme 4).

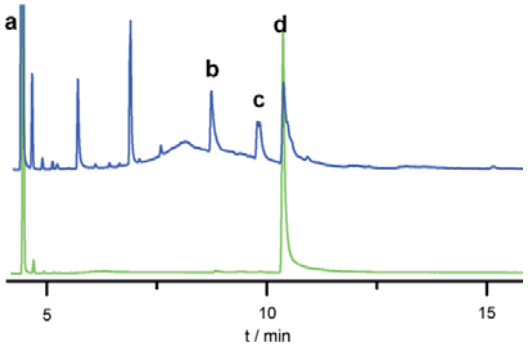

Figure 1. Gas chromatogram of the reaction mixtures after the lithiation of 4-methyl-4'-trimethylstannyl azobenzene (**11a**) in THF (table 1, entry 3) (green) and diethyl ether (table 2, entry 8) (blue). Signal a) triisopropylbenzene; b) 4-methylazobenzene; c) hydrazine **16;** d) product **14a**.

Table 1. GC optimization of the lithiation of 4-ethyl-4'-trimethylstannylazobenzene **(11a)**.

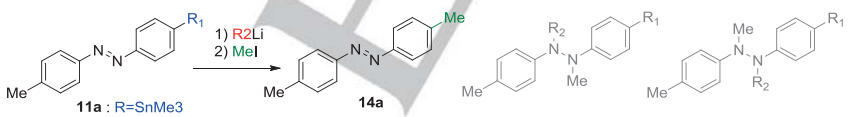

Entry	Solvent	T / °C	R	RLi	t/min	Starting Material / %	Yield of **14**/%
1	MeTHF	-130	$SnMe_3$	MeLi	4	25	72
2	MeTHF	-78	$SnMe_3$	MeLi	4	<1	>99
3	THF	-78	$SnMe_3$	MeLi	4	<1	>99
4	THF	-78	$SnMe_3$	MeLi	30	<1	98
5	THF	-16	$SnMe_3$	MeLi	4	<1	63
6	THF	-78	$SnMe_3$	*n*-BuLi	4	<1	43
7	Diethyl ether	-100	$SnMe_3$	MeLi	4	<1	29
8	Diethyl ether	-78	$SnMe_3$	MeLi	4	<1	32
9	THF	-78	I	MeLi	4	22[a]	54
10	THF	-78	I	*n*-BuLi	30	<1	27

[a] Isolated from the reaction mixture, no GC quantification (see SI).

To provide a direct comparison with the tin-lithium exchange reaction to halogen-lithium exchange reactions, which are standard in the literature, the reaction was also performed with 4-iodo-4'-methylazobenzene. By adding either methyl lithium or butyl lithium to the iodinated azobenzene **10**, dissolved in THF,

the conversion to the products was incomplete and the reaction showed various side products (Table 1, entries 9, 10).

NMR Studies

To support the mechanistic hypothesis for the reaction and to investigate why the reaction proceeded with much less selectivity in diethyl ether, in situ NMR experiments were performed. As the reaction progress in MeTHF at -130 °C was slow, those conditions were chosen to mix the reactants in a NMR tube in a glove box and immediately freeze the NMR tube within the glove box with liquid nitrogen. In this way, any reaction progress could be avoided before inserting the NMR tube into the pre-cooled NMR spectrometer (see supporting information for a detailed protocol). The reactions were then followed by ^{119}Sn NMR spectroscopy because the fast relaxation behavior of this nucleus allowed efficient sampling of the experiments. A fast scanning method was needed because of the low concentration of the ate-complex in the reaction mixture. Because of the different relaxation behaviors of symmetric and asymmetric tin species,[52] the parameters for the asymmetric, fast relaxing species could be optimized (pre-scan delay of 30 µs, relaxation delay of 1 ms).

This granted a fast recording of 3000-6000 scans with an overall recording of 132 s / 264 s per spectrum. There-fore, integration of the signals could not be correlated to the concentration of the species observed in solution and only qualitative statements can be made.

The spectra were initially recorded at -103 °C[53] and then the temperature was raised stepwise by 10 K monitoring the reaction progress. First the reaction of *para* stannylated azobenzene **11a** in MeTHF was investigated.

At -103 °C, the starting material **11a** showed a chemical shift of -27 ppm. After 4 minutes, two new species appeared (Figure 2). One showed a signal at 0 ppm, which is consistent with tetramethylstannane.[54] A further ^{119}Sn NMR signal was visible at -312 ppm. This signal was assigned to the ate-complex **12**, based on literature precedent.[41,55] At -103 °C, the relative intensity for the signal of the ate-complex stayed constant, whilst the signal due to the the starting material continued to disappear and tetramethylstannane formed at the same rate (based on the percentage change of the integral of each species). The signal corresponding to the tin-ate-complex could be observed at temperatures of up to -88 °C, but when the reaction was warmed up further to -70 °C, the signal could no longer be observed. After warming up to -60 °C, the starting material had entirely disappeared and only the signal for tetramethylstannane was visible (Figure 2 and Figure SI-5 in the supporting information).

The transmetalation reactions were recorded in a similar manner for the corresponding *meta*- and *ortho*- substituted species. 4-Methyl-3'-trimethylstannylazobenzene (**11b**) showed a chemical shift of -27 ppm at -103 °C. As for the *para* congener, two new species appeared at 0 ppm[56] and -313 ppm,) also corresponding to tetramethylstannane and a lithium-tin ate-complex (**12b**). The reaction for the transmetalation in the *meta*-position was very similar to the reaction of 4-methyl-4'-trimethylazobenzene (**11a**), but appeared to be faster. The reaction was already completed at -78 °C (Figure SI-6 in the supporting information). For the reaction of 4-methyl-2'-trimethylstannylazobenzene (**11c**), the starting material showed a chemical shift at -43 ppm. Although the signal corresponding to tetramethylstannane at 0 ppm appeared, no signal for the tin-ate-complex was detectable in the temperature range of -103 °C up to -58 °C. At this temperature the reactions for the *para* and *meta* species **11a** and **11b** were almost completed, whereas the reaction for the *ortho* position only began to take place. However, as for the reaction in the *para* and *meta* positions, only tetramethylstannane could be observed as the final tin containing product, which indicates a selective tin lithium exchange. In diethyl ether, a completely different reaction progress was observed: For the treatment of 4-methyl-4'-trimethylstannylazobenzene (**11a**) with methyllithium, at -103 °C, the starting material could be observed at 27 ppm. However, after the reaction mixture had melted at -103 °C, neither a signal for tetramethylstannane nor a signal for the ate-complex could be observed. Only after warming up to -44 °C, a signal at 0 ppm, assigned to tetramethylstannane, became visible. No further changes were observed up to -15 °C. At this temperature however, the reaction displayed the formation of a third, heretofore unobserved signal at -36 ppm (Figure 2). At 27 °C, the starting materials had disappeared and only tetramethylstannane and this new stannyl species could be observed. The chemical shift of this signal indicated an aryl-stannylated compound. The reaction in the NMR tube was eventually quenched with methyl iodide. Analysis by GCMS indicated the same side products as described in Figure 1. Based on this quenching experiment in combination with the isolated by-products (Scheme 4), the signal occurring at 36 ppm must be the *N*-lithium salt of the hydrazine derivatives, which becomes methylated upon quenching. The different reactivity of the tin-lithium exchange in diethyl ether and THF can be explained by different complexation of the lithiation agents and the different reactivity of organolithium compounds in THF/MeTHF and diethyl ether. THF shows a significantly stronger de-aggregation effect on organolithium compounds than diethyl ether.[57] This activation of the organolithium reagents enables reactions at much lower temperatures compared to diethyl ether. The reactions in MeTHF were already completed at -73 °C, whereas the reactions in diethyl ether only started at -15 °C.

However, at this increased temperature, the reactivity of all reactants was higher, leading to a decreased selectivity: At such high temperatures, the alkylation / metalation of the azo group can compete with the transmetalation of the trimethylstannyl group.

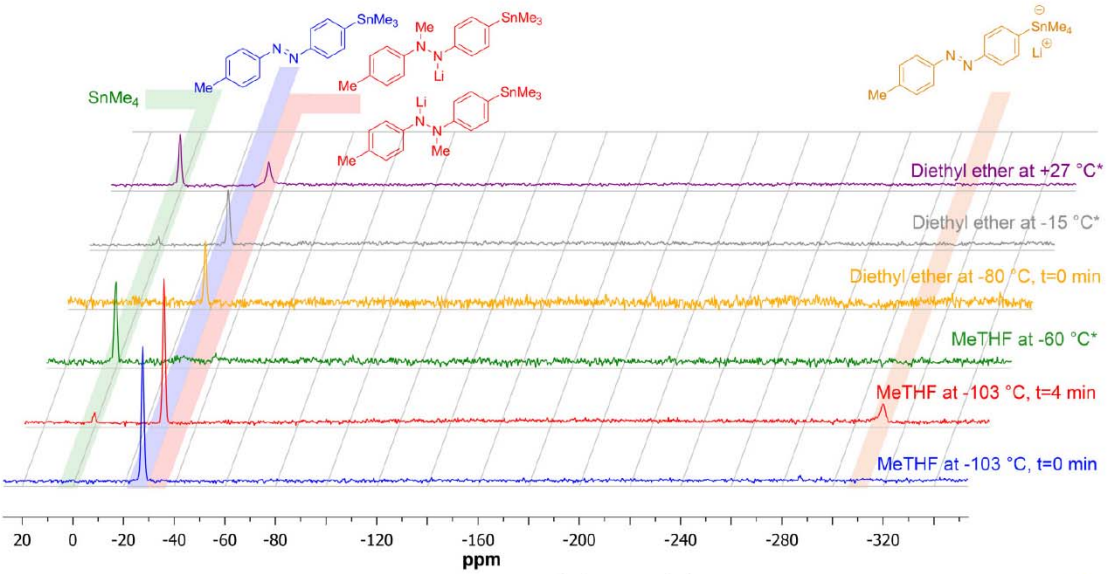

Figure 2. MeTHF: ^{119}Sn NMR signals for the reaction of the *para* stannylated azobenzene at -103 at t=0 (t=0) (blue) A reaction progress and the formation of the tin-stannate complex could be observed at -103 °C (t=4 min) (red), 26.85 °C the reaction is finished and only tetramethylstannane is visible (green); diethyl ether: The starting material **11a** at -80 °C (yellow), -15 °C the reaction started (grey) and 27 °C the reaction finished and tetramethylstannane and the sideproduct is visible (magenta). *= First spectrum of at this temperature, the average heating rate of the NMR was 0.2 °C/min.

DFT Calculations

To further support the proposed mechanism and to understand the differences that were observed for the lithiation of the *para*-*meta*- and *ortho*-positions, DFT calculations were performed. As a basis, 6-31g was used for all atoms except tin. For tin, the lanl2dz basis was used with the corresponding pseudo potential. All structures were optimized in the gas phase, followed by a frequency calculation to identify minima (only positive frequencies) and transition states (one negative frequency). The frequency calculation also allowed to estimate corrections to obtain zero-point energies, enthalpies and Gibbs free energies at 25 °C (for computational details, full citations for the computational methods and Gaussian calculation program see SI).[58,59]

As the tin-ate-complexes for the *meta* and *para* azobenzenes were only visible in low concentrations in the ^{119}Sn NMR spectrum, and the *ortho*-tin-ate complex was not visible at all, no ^{119}Sn-^{13}C coupling constants could be obtained. Such coupling constants allow the determination of the geometry of the ate-complex. Tin-ate-complexes are typically trigonal bipyramidal, and all reports in the literature place aromatic substituents at the apical position, whereas alkyl substituents occupy equatorial positions.[41,43] Our calculations agree with these observations; For the *para*-ate-complex with the azo group in equatorial position, the zero-point corrected energy (E_{ZPE}) is 3.6 kcal/mol higher (corrected for THF as the solvent; ΔG_{PCM} = 7.2 kcal/mol) than for the corresponding complex with the azobenzene in the apical position; for *meta*, the difference was ΔE_{ZPE} = 2.8 kcal/mol, and in the *ortho* case, no stable ate complex with the azobenzene in equatorial position could be found, due to steric hindrance. When the complexes with the azobenzene in the apical position were compared, the *para*-ate-complex was lowest in energy, followed by the *meta*-ate complex (ΔE_{ZPE} = 1.6 kcal/mol and ΔG_{PCM} = 3.6 kcal/mol compared to the *para*-ate-complex). The *ortho*-ate complex was highest in energy (ΔE_{ZPE} = 6.5 kcal/mol and ΔG_{PCM} = 11.9 kcal/mol compared to the *para*-ate-complex) (Figure 3).

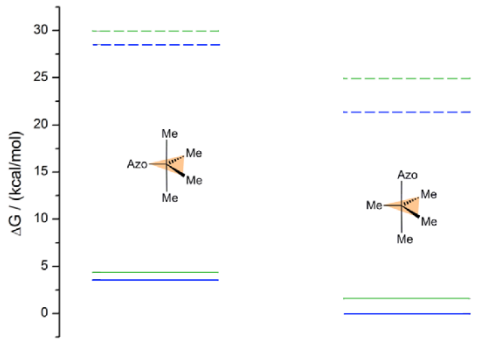

Figure 3. Energy diagram of the equatorial and apical ate complexes in *para* position (blue) and *meta* position

(green), calculated in the gas phase (solid lines) and corrected for the solvent THF (PCM, dashed line).

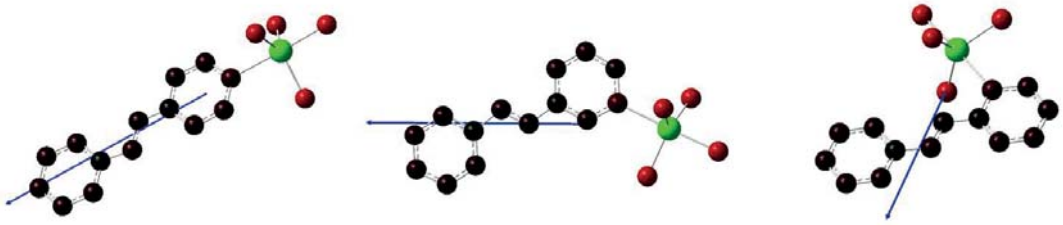

Figure 4. 3D geometries, charge distributions and dipole vectors of the *para*, *meta* and *ortho* tin-ate complexes. Hydrogens atoms were omitted for clarity. The atoms are colored by charge; green: positive; red: negative; black: neutral.

large solvent effect is likely due to the decreasing dipole moment for these compounds (*para*: 7.99 Debye; *meta:* 7.97 Debye, *ortho:* 4.81 Debye) (Figure 4).[60]

However, the formation of the tin-ate-complexes from methyllithium and the corresponding stannylated azobenzenes proved to be difficult to calculate in absolute terms: In this step, two ionic compounds form, the lithium cation and the tin-ate-complex. The energy of ionic species is difficult to simulate in the gas phase. In addition, even factoring in the solvation of these species did not yield satisfactory results: In the case of coordinating solvents such as THF, the polarized continuum model is insufficient, as it only takes into account polarization and cavitation, but not the specific complexation events that are well-documented for the solubilization of organolithium species. Furthermore, it was impossible to find any transition states for any possible trajectories of approach of the nucleophile to the tin compounds. We therefore computed the stannylated azobenzene with an associated methyllithium molecule positioned in the trajectory of the attack on the tin center. Minima could be found in all cases, with a distance of the lithium ion to the Sn atom of ca 4.4 Å in all cases (*para*: 4.4 Å; *meta:* 4.4 Å; *ortho:* 4.5 Å). Then, the distance between the carbon atom and the Sn atom was consistently shortened by 0.15 Å and the geometries were optimized at every step. Scanning the approach in this way showed that in all cases, there was either no distinct transition state or that the transition state was too flat to be detected by the calculation. Therefore, the rate of formation of the ate-complexes is a direct function of the energy of the ate-complex. Because the *ortho*-tin-ate complex is considerably higher in energy than the corresponding *para* or *meta* complexes, this explains the observation that the tin-lithium exchange proceeds only at much higher temperatures in the *ortho* case, as compared with the *meta* and *para* cases.

The last step in the reaction sequence was the insertion of the lithium cation into the azobenzene-carbon-tin bond. The lithium cation, as one of the reactants, may again lead to error in determining the energies for these transition states. However, in the transition state that we could determine, the geometry around the lithium center already suggests partial desolvation, due to steric congestion. In these transition states, the *para*- and the *meta*-azobenzene-tin-ate complexes are very similar in energy (*para*: ΔE_{ZPE} = 2.3 kcal/mol, ΔG_{PCM} = 25.8 kcal/mol; *meta:* ΔE_{ZPE} = 2.1 kcal/mol, ΔG_{PCM} = 25.1 kcal/mol, with respect to the respective starting materials).[61] The transition state for the *ortho*-case however is much lower with ΔE_{ZPE} = 7.0 kcal/mol, ΔG_{PCM} = 12.7 kcal/mol (with respect to the respective starting materials). The same trend is observed for the lithiated azobenzene products with *para*: ΔE_{ZPE} = 4.0 kcal/mol, ΔG_{PCM} = 13.0 kcal/mol; *meta* = ΔE_{ZPE} = -4.0 kcal/mol, ΔG_{PCM} = -12.9 kcal/mol and *ortho:* ΔE_{ZPE} = -19.2 kcal/mol, ΔG_{PCM} = -33.1 kcal/mol. From the structures of both transition states and products, it is clear that this substantial additional stabilization of the *ortho* species is a direct consequence of a neighboring group effect of the lone pair of the nitrogen atom in the diazene group, which coordinates the lithium atom. Therefore, these calculations explain why the *ortho*-tin-ate complex could not be observed by NMR spectroscopy: It is much more reactive than the *meta* or *para* –tin-ate complex and immediately rearranges into the lithiated azobenzene once it has formed.

Synthetic Scope

The reaction of 4-lithio-4'-methylstannyl azobenzene (**13a**) with methyl iodide, as used in the optimization reactions, gave an excellent isolated yield of 96% of **14a**. The reaction conditions were transferred to 4-methyl-3'-trimethylstannyl azobenzene (**11b**) and a comparable yield of 95% of **14b** could be isolated (Table 2, entry 1). However, a good reaction conversion does not only depend on a successful lithiation: The electrophile used for quenching is also an important factor. To show that our newly developed methodology for the lithiation of azobenzenes is of general practical use, a variety of quenching agents were used for 4-lithio-4'-methylstannyl (**11a**) azobenzene and 4-lithio-4'-methylstannyl (**11b**) azobenzenes (Table 2).

Quenching with trimethylsilyl chloride showed yields with 94% for **17a** and 95% for **17b** (entry 2). This compares favorably to previous protocols for a silylations of azobenzenes via halogen-lithium exchange: The yields reported for these reactions average around 20%[62] to a maximum yield of 42%[12] using a trimethylsilyl halogenide electrophile.

Table 2: Range of electrophiles employed for the reaction with the lithiated azobenzenes and the resulting products.

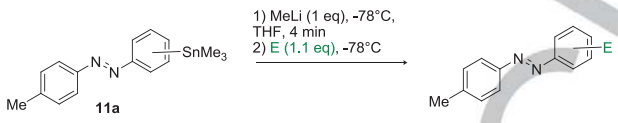

Entry	E	Product	Yield/ %	Product	Yield/ %
1	MeI	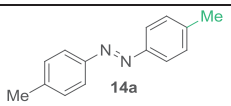 **14a**	96	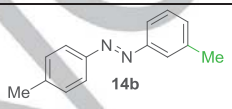 **14b**	95
2	TMSCl	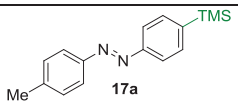 **17a**	94	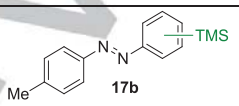 **17b**	95
3		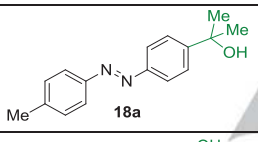 **18a**	89	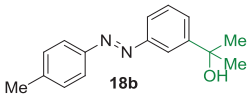 **18b**	83
4	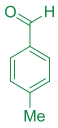	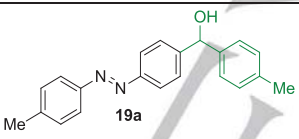 **19a**	95	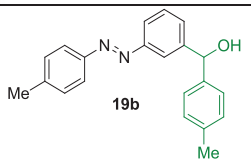 **19b**	89
5		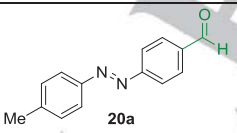 **20a**	89	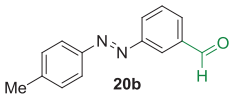 **20b**	83
6	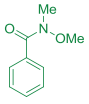 **22**	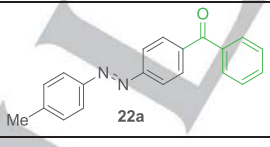 **22a**	98	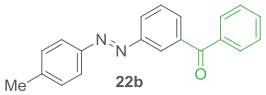 **22b**	71
7		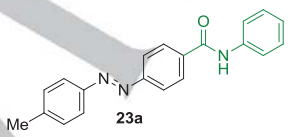 **23a**	77	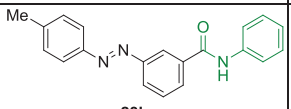 **23b**	76
8		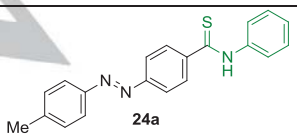 **24a**	80	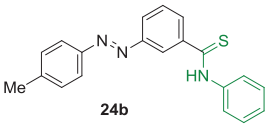 **24b**	81

Lithiation reactions are also often used for the introduction of functional groups such as alcohols, carbonyls or amides. The quenching reaction with acetone gave alcohol **18a** with a yield of 88% and **18b** in a slightly lower yield of 79 % (entry 3). The reaction of tolulaldehyde gives **19a** and **19b** in excellent yields ranging from 89 to 95 % (table 2, entry 4). The aldehyde functionalization by quenching with *N,N*-dimethyl formamide gave product **20a** in a yield of 89% and the *meta*-compound **20b** in a yield of 83%.(entry 5). A further classical methodology of synthesizing ketones from organolithium reagents is the use of Weinreb's amide (**21**).[63] In reaction with the lithiated azobenzenes, it provided the ketones **22a** and **22b** in yields of up to 98% (entry 6).

The synthesis of amides and thioamides from aryl lithium species are typically performed by the use of phenyl isocyanate or phenyl isothiocyanate. Those compounds were also appropriate electrophiles and gave very good yields of 77% and 76%, respectively, for the *para*-lithiated species and 80% and 81%, respectively, for the *meta* lithiated species (entries 7 and 8). While simple electrophiles can only react once, other electrophiles are capable of multiple reactions. Such electrophiles are very attractive for the synthesis of dyes with multiple chromophoric groups. Various methane derivatives with two azobenzene units on one carbon atom have been reported in the literature.[64-68]

Typically, these compounds are synthesized from diamine precursors and a subsequent azocoupling.[64,66,68]

With benzoyl chloride as an electrophile, two equivalents of the lithiated azobenzenes could be added to the electrophile, where 96% of **25a** and 71% of **25b** could be obtained. Product **26a** and **26b** could be obtained by using an analogous ester that gives the product in both the *para* and *meta* positions in good yields of 79%.

Only two protocols for the synthesis of triple azobenzene functionalized methane derivatives have been reported to date: In one procedure, the product was obtained by a condensation reaction of nitrosobenzene with tri(4-aminophenyl)methane in a yield of 35%, followed by a subsequent oxidation of the corresponding (triphenylazo)triphenyl methanol, an analog of **27a**, in a yield of 30% (which corresponds to an overall yield of 10%).[64] The second protocol entails condensation of an aldehyde functionalized azobenzene with unsubsituted azobenzenes via an electrophilic substitution in sulfuric acidutilizing very harsh conditions. No yield was reported.[65]

When three equivalents of 4-methyl-4'-trimethylstannyl azobenzene were lithiated and quenched with one equivalent of diethyl carbonate the main product was a triple azobenzene functionalized methanol derivative **27a** in a yield of 52%, and the bis-azobenzene functionalized ketone **28a** in a yield of 35%. The same reaction quenched with one equivalent of oxalyl chloride gave the triple azobenzene substituted methanol **27a** in a yield of 54% and the ketone **28a** in a yield of 23% (Table 3, entry 4).

The *meta*-substituted azobenzene analogs could be obtained in a yield of 49% for the tri-substituted methanol **27b** and 28% for the di-substituted ketone **28a** (Table 3, entry 3).

Table 3. Products with multiple azobenzenes.

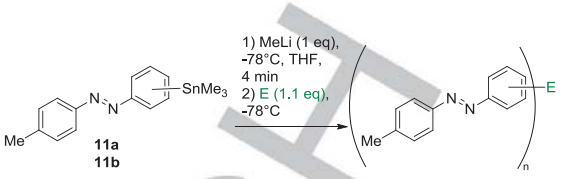

11a
11b

Entry	E	Products	Yield/%
1a	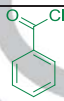	25a	96
1b		25b	71
2a		26a	79
2b		26b	79
3a		27a	52
		28a	35
3b		27b	28
		28b	49
4a		27a	23
4b		28a	54

Although the *para*- and *ortho*-lithiated azobenzenes did not show a significant difference in their reactivity towards electrophiles, we suspect that this might be different for the *ortho*-lithiated azobenzene: Steric hinderence by the azo group could affect the formation of the analogous products. On the other hand, the lithiated species might be particularly stable due to additional complexation of the lithium by the lone pair of the adjacent nitrogen atom. In the literature, *ortho* lithiations typically give higher yields than a lithiation in *meta* or *para* position due to this effect.[33] When the *ortho* lithiated azobenzene was quenched with methyl iodide, the isolated yield of the *ortho* methylated azobenzene derivative **11c** was almost quantitative (99%). Even the more sterically hindered trimethyl silyl electrophiles gave the silylated product **17c** in good 82% yield. (Scheme 6). For further *ortho*-products, see the supporting information.

Scheme 5. Products with multiple azobenzenes. For yields, see Table 3.

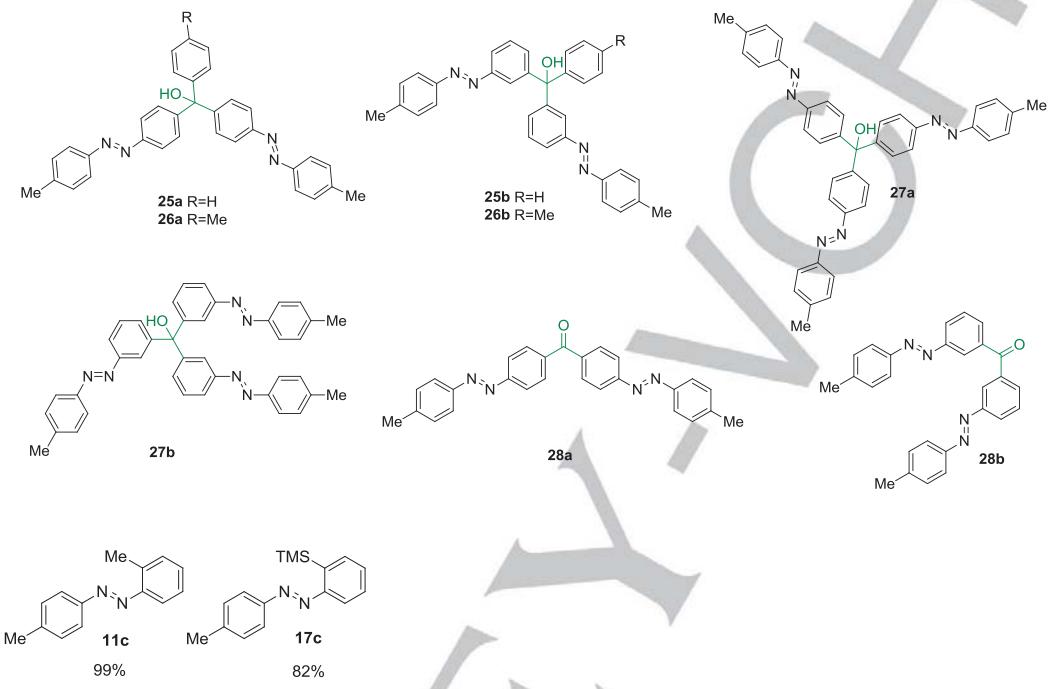

Scheme 6. *Ortho*-functionalized azobenzenes.

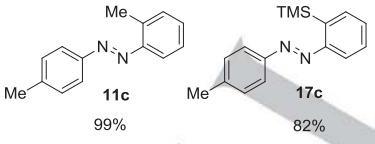

Conclusions

The transmetalation of stannylated azobenzenes with methyl lithium in THF led to a rapid and selective ex-change of the trimethylstannyl group without any attack on the azo group. NMR spectroscopy showed that the reaction proceeded via a lithium-tin-ate complex prior to a rearrangement to the lithiated species. Analysis by gas chromatography and NMR spectroscopy showed that the reaction was rapid and selective in THF and MeTHF, but unselective in diethyl ether; in this solvent hydrazine derivatives were formed due to an attack of the organolithium reagent on the diazo group. Furthermore, optimized reaction conditions for performing the lithiation reaction in THF at -78 °C could be applied as a high yielding, general method for lithiating azobenzenes in *ortho*, *meta* and *para* positions. The lithiated azobenzenes were quenched with a wide variety of electrophiles. Products containing one azobenzene unit could be obtained in yields ranging from 71% to 98%. Quenching the lithiated azobenzenes with electrophiles with functional groups of multiple reactivity allowed the synthesis of di- and even tri- azobenzene-functionalized compounds in good yields.

Experimental Section

Representative lithiation procedure for 4,4'-dimethylazobenzene (**14a**): To a solution of 4-methyl-4'-(trimethylstannyl)-azobenzene (1.00 eq, 250 mg, 700 µmol) in THF (10 mL), a solution of methyllithium (0.99 eq, 440 µL, 700 µmol, 1.58 M in diethyl ether), diluted in THF (1.58 mL) was added at -78 °C over the course of 4 min. After 2 min, a solution of methyl iodide (1.10 eq, 50.0 µL, 800 µmol) in THF (0.32 mL) was added and the reaction mixture was warmed to 20 °C. After 6 h stirring the solvent was evaporated and the residue purified using column chromatography with DCM (Rf = 0.7) as eluent. The solvent was evaporated and yellow crystalline needles (140 mg, 666 µmol, 96%) were obtained. ^{1}H NMR (500 MHz, CDCl3): δ = 7.82 (d, 3J = 8.4 Hz, 4 H, H-2),

7.32 (d, 3J = 8.4 Hz, 4 H, H-3), 2.44 (s, 6 H, H-5) ppm. ^{13}C NMR (125 MHz, CDCl3): δ = 150.8 (C-1), 141.2 (C-4), 129.7 (C-2), 122.7 (C-3), 21.5 (C-5) ppm. IR (ATR): ṽ = 3023 (w), 2921 (w), 1601 (m), 1502 (m), 1306 (w), 1237 (w), 1149 (m), 1012 (m), 883 (m), 839 (m), 821 (s), 794 (m), 710 (m), 683 (s), 535 (m), 504 (s) 492 (s) cm^{-1}. HRMS (EI-sector): *m/z* = $[M]^+$ calcd. for $[C_{14}H_{14}N_2$ 210.1157$]^+$; found 210.1156. Mp: 145 °C.

Acknowledgements

This project was supported by the Special Research Area 677 "Function by Switching" of the Deutsche Forschungsgemeinschaft (DFG), Project C10.

The authors thank Hans J. Reich, University of Wisconsin, for helpful discussions.

Keywords: Azo compounds• lithiation • tin • metalation • NMR spectroscopy

[1] K. L. Hunger, *Industrial Dyes: Chemistry, Properties, Applications*, Wiley-VCH, Weinheim, Germany, **2003**.
[2] B. L. Feringa, W. R. Browne, *Molecular Switches*, 2nd ed.,Wiley-VCH, Weinheim, Germany, **2011**.
[3] E. J. Wei-Guang Diau, *Phys. Chem. A* **2004**, *108*, 950.
[4] N. Siampiringue, G. Guyot, S. Monti, P.J. Bortolus, *Photochem.* **1987**, *37*, 185.
[5] S. K. Yesodha, C. K. S. Pillai, N. Tsutsumi, *Prog. Polym. Sci.* **2004**, *29*, 45.
[6] C. Lagrasta, I. R. Bellobono, M. J. Bonardi, *Photochem. Photobiol.* **1997**, *110*, 201.
[7] M. Izquierdo-Serra, M. Gascón-Moya, J. J. Hirtz, S. Pittolo, K. E. Poskanzer, È. Ferrer, R. Alibés, F. Busqué, R. Yuste, J. Hernando, P. Gorostiza, *J. Am. Chem. Soc.* **2014**, *136*, 8693.
[8] V. Chandrasekaran, T. K. Lindhorst, *Chem. Comm.* **2012**, *48*, 7519.
[9] J. Auernheimer, C. Dahmen, U. Hersel, A. Bausch, H. Kessler, *J. Am. Chem. Soc.* **2005**, *127*, 16107.
[10] A. Goulet-Hanssens, K. Lai Wing Sun, T. E. Kennedy, C. J. Barrett, *Biomacromolecules* **2012**, *13*, 2958.
[11] S. Venkataramani, U. Jana, M. Dommaschk, F. D. Soennichsen, F. Tuczek, R. Herges, *Science* **2011**, *331*, 445.
[12] G. S. Kumar, D. C. Neckers, *Chem. Rev.* **1989**, *89*, 1915.
[13] A. Natansohn, P. Rochon, *Chemical Reviews* **2002**, *102*, 4139.
[14] R. D. Mukhopadhyay, V. K. Praveen, A. Ajayaghosh, *Materials Horizons* **2014**, *1*, 572.
[15] Y. Deng, N. Li, Y. He, X. Wang, *Macromolecules* **2007**, *40*, 6669.
[16] Y. Yu, T. Maeda, J. I. Mamiya, T. Ikeda, *Angew. Chem. Int. Ed.* **2007**, *46*, 881.
[17] Y. Yu, M. Nakano, T. Ikeda, *Nature* **2003**, *425*, 145.
[18] Y. Zhao, T. Ikeda, *Smart Light-Responsive Materials: Azobenzene-Containing Polymers and Liquid Crystals*; Wiley-VCH, Weinheim, Germany, **2009**.
[19] M. Schlosser, *Organometallics in Synthesis - Third Manual*; Wiley-VCH, Weinheim, Germany, **2013**.
[20] S. El Sheikh, H.-G. Schmalz, *Curr. Opin. Drug Discov. Devel.* **2004**, *7*, 882.
[21] T. Imamoto, T. Kusumoto, Y. Tawarayama, Y. Sugiura, T. Mita, Y. Hatanaka, M. Yokoyama, *J. Org. Chem.* **1984**, *49*, 3904.
[22] F. A. Garlichs-Zschoche, K. H. Dötz, *Organometallics* **2007**, *26*, 4535.
[23] D.-H. Qu, Q.-C. Wang, X. Ma, H. Tian, *Chem. Eur. J.* **2005**, *11*, 5929.
[24] A. K. Flatt, S. M. Dirk, J. C. Henderson, D. E. Shen, J. Su, M. A. Reed, J. M. Tour, *Tetrahedron* **2003**, *59*, 8555.
[25] T. Soga, Y. Jimbo, K. Suzuki, D. Citterio, *Anal. Chem.* **2013**, *85*, 8973.
[26] T. Kozlecki, L. Syper, K. A. Wilk, *Synthesis* **1997**, *6*, 681.
[27] M. Unno, K. Kakiage, M. Yamamura, T. Kogure, T. Kyomen, M. Hanaya, *Appl. Organometal. Chem* **2010**, *24*, 247.
[28] M. D. Segarra-Maset, P. W. N. M. van Leeuwen, Z. Freixa, *Eur. J. Inorg. Chem.* **2010**, *2010*, 2075.
[29] Y. Zhang, T. Qiang M. Luo, *Org. Biomol. Chem.* **2011**, *9*, 4977.
[30] A. R. Katritzky, J. Wu, S. V. Verin, *Synthesis* **1995**, *1995*, 651.
[31] E. Ciganek, *Organic Reactions*, John Wiley & Sons, Inc. **2004**.
[32] T. T. T. Nguyen, A. Boussonnière, E. Banaszak, A.-S. Castanet, K. P. P. Nguyen, J. Mortier, *J. Org. Chem.* **2014**, *79*, 2775.
[33] Compound **5** was also synthesized with our method in 93% yield (compound **SI-5** in the supporting information).
[34] J. Strueben, P. J. Gates, A. Staubitz *J. Org. Chem.* **2014**, *79*, 1719.
[35] B.-C. Yu, Y. Shirai, J. M. Tour, *Tetrahedron* **2006**, *62*, 10303.
[36] J. Yamamoto, R. Yamawakiy, Y. Sumi, R. Okamoto, M. Saito, M. Kato, A. Shibata, *Nippon Kagaku Kaishi* **1992**, *1992*, 1508.
[37] D. Qiu, H. Meng, L. Jin, S. Wang, S.Tang, X. Wang, F. Mo, Y. Zhang, J. Wang, *Angew. Chem. Int. Ed.* **2013**, *52*, 11581; *Angew. Chem.* **2013**, *125*, 11795. In this report, the com-pound was synthesized via an Sandmeyer type reaction. In this work, it was synthesized analogous to reference 34.
[38] A. Maercker, H. Bodenstedt, L. Brandsma, *Angew. Chem.***1992**, *104*, 1387.
[39] M. Saito, S. Imaizumi, T. Tajima, *Eur. J. Inorg. Chem.* **2010**, *14*, 2153.
[40] N. H. Phillips, H. J. Reich, *Pure Appl. Chem.* **2009**, 59, 1021.
[41] N. H. Phillips, H. J. Reich, *J. Am. Chem. Soc.* **1986**, *108*, 2102.
[42] J. P. Borst, H. J. Reich, *J. Am. Chem. Soc.* **1991**, *113*, 1835.
[43] M. Saito, S. Imaizumi, T. Tajima, K. Ishimura, S. Nagase, *J. Am. Chem. Soc.* **2007**, *129*, 10974.
[44] T. L. Rathman, J. A. Schwindeman, *Org. Proc. Res. Dev.* **2014**, *18*, 1192.
[45] H. Gilman, B. J. Gaj, *J. Org. Chem.* **1957**, *22*, 1165.
[46] D. Mihovilovic, P. Stanetty, *J. Org. Chem.* **1997**, *62*, 1514.
[47] J. Clayden, *Organolithiums: Selectivity for Synthesis*, Pergamon: Amsterdam, Netherlands, 2003.
[48] H. J. Reich, *Chem. Rev.* **2013**, *113*, 7130.
[49] NMR spectroscopic analysis of a fraction from an attempt to purify these compounds by column chromatography lent further support to their identification (Scheme 4 and supporting information).
[50] Protodestannylation of aromatic trimethyl tin species is common: J. Linshoeft, A. C. J. Heinrich, S. A. W. Segler, P. J. Gates, A. Staubitz, *Org. Lett.* **2012**, *14*, 5644.
[51] Substance was contaminated with starting material **11a** and product **14a** (see supporting information for details and spectra).
[52] R. R. Sharp, J. W. Tolan, *J. Chem. Phys.* **1976**, *65*, 522.
[53] At this low temperature, no temperature stability can be granted. The temperature varied by 7 K. This fact prevented quantitative kinetic studies, because of the sensitivity of the resonance of the ^{119}Sn nucleus to small temperature variations.
[54] J. Holeček, K. Handlíř, , V. Černý, M. Nádvorník, A. Lyčka, *Polyhedron* **1987**, *6*, 1037.
[55] H. J. Reich, B. Ö. Gudmundsson, D. P. Green, M. J. Bevan, I. L. Reich, *Helv. Chim. Acta* **2002**, *85*, 3748.
[56] Because of the temperature variations and $SnMe_4$ as product for this reaction, no external references were added and the spectra were referenced on $SnMe_4$.
[57] H. J. Reich, D. P. Green, M. A. Medina, W. S. Goldenberg, B. Ö. Gudmundsson, R. R. Dykstra, N. H. Phillips, *J. Am. Chem. Soc.* **1998**, *120*, 7201.
[58] Gaussian 09, Revision D.01, M. J. Frisch, G. W. Trucks, H. B. Schlegel, G. E. Scuseria, M. A. Robb, J. R. Cheeseman, G. Scalmani, V. Barone, B. Mennucci, G. A. Petersson, H. Na-katsuji, M. Caricato, X. Li, H. P. Hratchian, A. F. Izmaylov, J. Bloino, G. Zheng, J. L. Sonnenberg, M. Hada, M. Ehara, K. Toyota, R. Fukuda, J. Hasegawa, M. Ishida, T. Nakajima, Y. Honda, O. Kitao, H. Nakai, T. Vreven, J. A. Montgomery, Jr., J. E. Peralta, F. Ogliaro, M. Bearpark, J. J. Heyd, E. Brothers, K. N. Kudin, V. N. Staroverov, T. Keith, R. Kobayashi, J. Nor-mand, K. Raghavachari, A. Rendell, J. C. Burant, S. S. Iyengar, J. Tomasi, M. Cossi, N. Rega, J. M. Millam, M. Klene, J. E. Knox, J. B. Cross, V. Bakken, C. Adamo, J. Jaramillo, R. Gomperts, R. E. Stratmann, O. Yazyev, A. J. Austin, R. Cammi, C. Pomelli, J. W. Ochterski, R. L. Martin, K. Morokuma, V. G. Zakrzewski, G. A. Voth, P. Salvador, J. J. Dannenberg, S. Dapprich, A. D. Daniels, O. Farkas, J. B. Foresman, J. V. Ortiz, J. Cioslowski, and D. J. Fox, Gaussian, Inc., Wallingford CT, 2013.
[59] Gaussian, Inc. 340 Quinnipiac St Bldg 40, Wallingford, CT 06492 USA, Copyright 2000-2008 Semichem. Inc. Authors: R. D. Dennington II, T. A. Keith, J. M. Millan.
[60] The dipole moments are based on a natural bond order (NBO) calculation, as these are considered more rubust than Mulliken charges. NBO Version 3.1, E. D. Glendening, A. E. Reed, J. E. Carpenter, and F. Weinhold.
[61] The very high solvent free energies are again most likely a computational artifact due to the specific THF-transition state interactions that are not taken into account.
[62] Average from SciFinder results from *para*-trimethylsilyl substituted azobenzene derivatives at the time of writing.
[63] M. Mentzel, H. M. R. Hoffmann, *Prakt. Chem.* **1997**, *339*, 517.

[64] D. Hellwinkel, H. Fritsch, *Chem. Ber.* **1990**, *123*, 2207
[65] R. N. Sen, B. Sett, *J. Am. Chem. Soc.* **1924**, *46*, 111.
[66] S. Sengupta, S. K. Sadhukhan, *B. Chem. Soc. Jpn.* **2003**, 76, 1223.
[67] S. Timofei, L. Kurunczi, T. Suzuki, W. M. F. Fabian, S. Mureşan, *Dyes Pigments* **1997**, *34*, 181.
[68] S. Miao, H. Li, Q. Xu, Y. Li, S. Ji, N. Li, L. Wang, J. Zheng, J. Lu, *Adv. Mater.* **2012**, *24*, 6210.

Entry for the Table of Contents

Layout 2:

FULL PAPER

A mild and efficient method for the near quantitative lithiation of azobenzenes in any position is reported. It proceeds via a tin-lithium exchange, which could be monitored by low T ^{119}Sn NMR spectroscopy. The lithiated azobenzenes were able to react with a wide variety of electrophiles in yields ranging from 71% to 98% for mono-substitutions of azobenzenes. In addition, di- and even tri- azobenzene-functionalized compounds were obtained in good yields.

*J. Strueben, M. Lipfert, J.-O. Springer, C. A. Gould, P.J. Gates, F.D. Sönnichsen, A. Staubitz**

Page No. – Page No.

High Yielding Lithiation of Azobenzenes by Tin-Lithium Exchange

2.4 Synthesis of Exactly Alternating Azobenzene-Siloxane Copolymers

The development of a suitable pathway for the lithiation of azobenzenes as described in chapter 2.3 allowed the synthesis of a suitable silanol functionalized azobenzene **2** for the use as co-monomer for alternating azobenzene-siloxane polymers (Scheme 10). Following an analogous route, di-iodinated azobenzene was firstly distannylated in a Stille-Kelly reaction with hexamethyldistannane.[60] Compound **6** could be obtained in a yield of 91%. The distannylated azobenzene was dilithiated with the reaction conditions developed in chapter 2.3 and quenched using an excess of dichlorodimethyl silane. The resulting chlorosilyl functionalized azobenzene **9** is highly sensitive to moisture, and for this reason it was used without further purification. A direct hydrolosis would lead to a condensation of chlorosilyl groups with silanol groups. The solvent and unreacted dichlorodimethylsilane were evaporated under Schlenk conditions and directly transformed to the corresponding methoxysilyl compound and subsequently hydrolyzed to the silanol **2**. Following this route, the desired monomer could be isolated in a yield of 35%. A crystal structure of the monomer could be obtained (see experimental part, chapter 4.3)

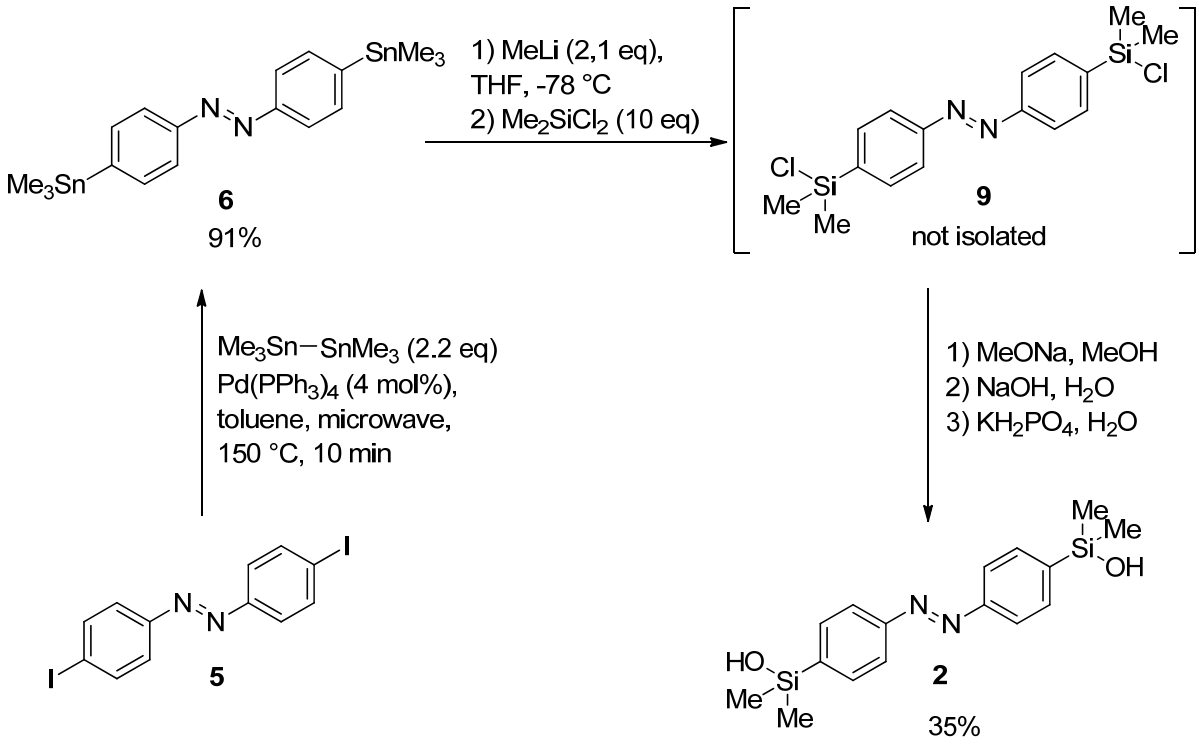

Scheme 10. Synthesis of 4,4'-*bis*(hydroxydimethylsilyl)azobenzene (**2**).

Syntheses of siloxane copolymers with different units in the main chain is typically performed using a step growth mechanism in a polycondensation reaction.[13] For a non- crosslinked polymer, high molecular weights are desired which are only achieved having a very high conversion of the starting material. Silane **11** was chosen as co-monomer, and synthesized according to Dvornic and coworkers in 92% yield (Scheme 11).[61] Silane **11** was synthesized starting from dichlorodimethylsilane which was converted to *bis*(pyrrolinyl)silane (**10**) using an excess of pyrrolidine in a nucleophilic substitution reaction.[62] The *bis*(pyrrolinyl)silane (**10**) was subsequently transformed to monomer **18** in reaction with phenyl isocyanate.[61]

This reactant (**11**) is typically used in chlorobenzene as solvent. The advantage of this monomer (**11**) as compared to dimethyldichlorosilane (**9**) is its reactivity and the low solubility of the side product (an urea derivative) in chlorobenzene. Due to its precipitation and high chemical stability, the side product cannot interfere with the reaction. This leads to linear, regularly alternating aryl-siloxane polymers with high molecular weights.[61, 63]

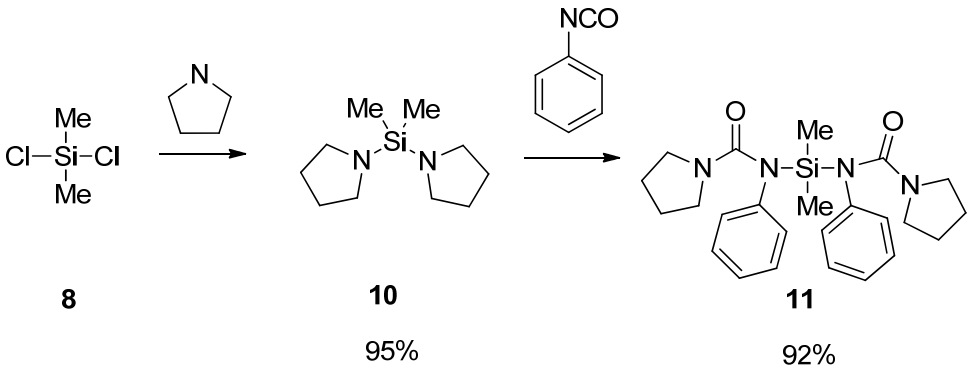

8 **10** 95% **11** 92%

Scheme 11. Synthesis of bis(*N*-phenyl-*N*'-pyrrodinyl)dimethylsilane (**11**).

The polymerization with the monomer **2** was performed analogously to Dvornic and coworkers in chlorobenzene.[63] The addition of the reactants was performed by the use of a syringe pump to slowly increase the stoichiometric amounts of the silane **11**. The reaction progress was monitored by gel permeation chromatography (GPC) every 24 h. The GPC was calibrated against polystyrene. After 24 h, high molecular weights of M_n= 25 kDa, M_w = 49 kDa and a PDI of 1.9 could be observed. The reaction was considered complete when no further increase of the molecular weight could be monitored. In this case, the reaction ended after 8 d. After precipitation of polymer **1** in methanol, a red rubber like material was obtained in a

yield of 55%. The molecular weight was determined by GPC to be M_n = 32 kDa Da, M_w = 53 kDa and a PDI of 1.7 was calculated (Figure 15).

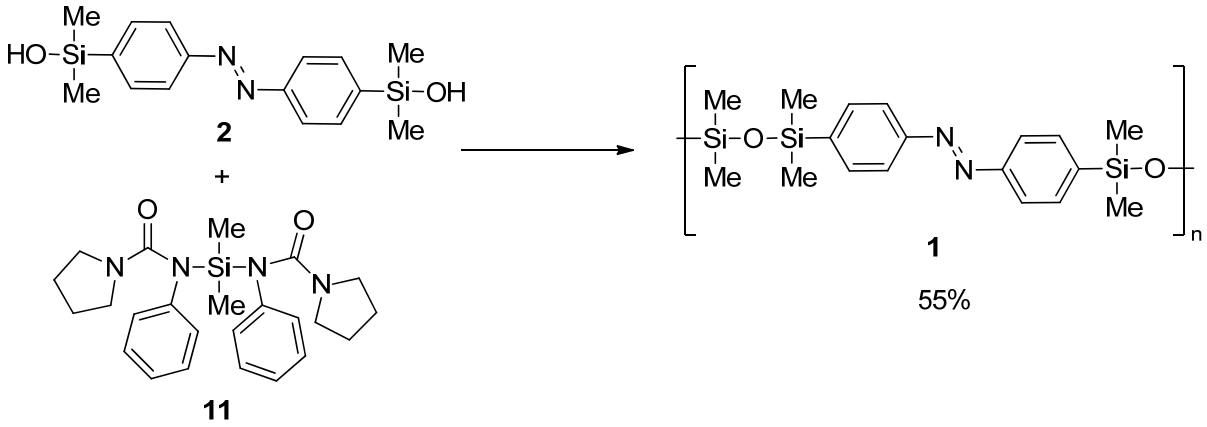

Scheme 12. Synthesis of poly[azobenzene-tri(dimethylsiloxane)] (**1**).

To investigate if the material showed any thermotropic behavior, phase transitions were analyzed using dynamic scanning calorimety (DSC) (Figure 13). Polymer **1** showed a glass transition temperature of ca. 23 °C. No further phase transitions were observed up to 200 °C (DSC for this temperature range, see experimental part, chapter 4.3). The material showed a very good thermal stability. The degradation temperature of the material was determined by DTA-TG with 419 °C. This observation was consistent with the properties of many main chain liquid crystalline polymers in which the phase transition from a LC phase state to an isotropic melt increases by an increased flexibility of the spacers connecting the mesogens.[7]

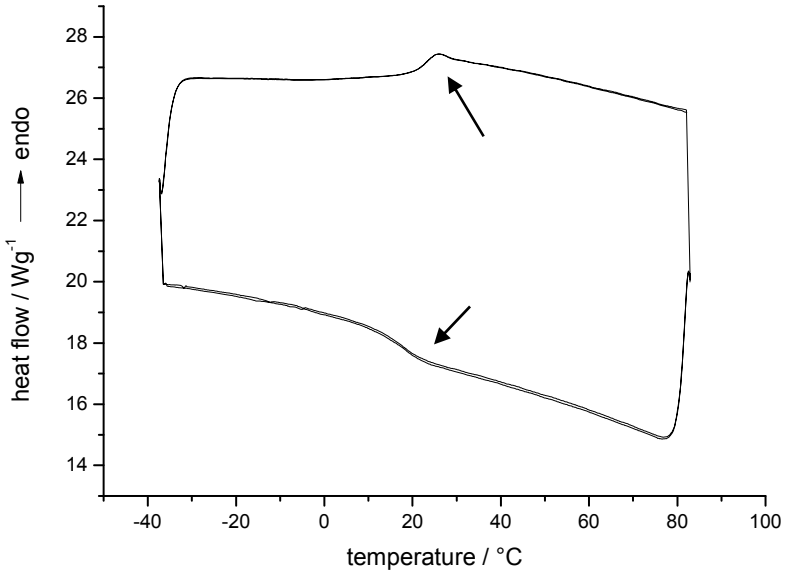

Figure 13. DSC of Polymer **1**. Three cycles were performed at a heating rate of 10 °C in a temperature range of -40°C to 80°C. The glass transition temperature was determined with T_g = 22.67 °C; T_{gO}^{E} = 20.09 °C.

However, investigating the presence of liquid crystallinity in main chain liquid crystalline materials is not trivial. While small molecule systems and side chain liquid crystalline polymers (which mimic the behavior of small molecular mesophases)[7] can be easily observed through a polarization microscope, main chain liquid crystalline polymers often do not show this birefringence.[7] The analysis by ^{1}H NMR spectroscopy showed a very small line width for a polymer of such a high molecular weight. This indicates a high isotropy and low aggregation at low concentrations (10 mg/550 µL). The critical concentration when lyotropic systems form liquid crystalline phases increases with the flexibility of the polymer chain.[7] At a higher concentration (35 mg/60 µL), next to an increased line width, a shift of the aromatic signals towards high field could be observed. This indicated an aggregation of the polymer at higher concentrations. Whether the aggregation is anisotropic or not could not be determined by ^{1}H NMR spectroscopy (Figure 14).

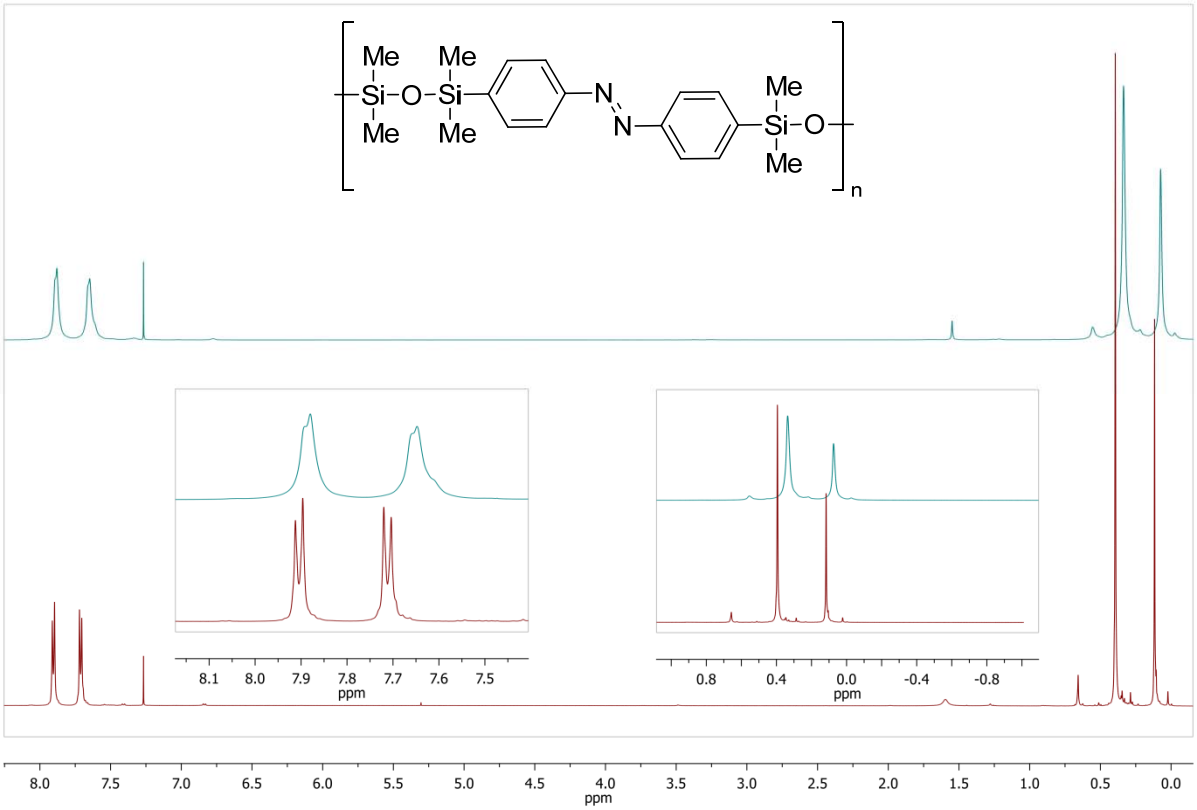

Figure 14. ^{1}H NMR spectra of polymer **1** at a low concentration (10 mg/550 µL; $CDCl_3$) (red) and at high concentration (35 mg/60 µL; $CDCl_3$) (blue). Below and above the critical concentration for the formation of a liquid crystalline and isotropic state. Intensities of both samples were adjusted (measured on a Bruker DRX 500 (500 MHz) spectrometer).

To find indicators for a liquid crystallinity, the polymer film was measured by X-ray diffraction. In a liquid crystalline polymer certain indications of a regularity should be detectable. The X-ray diffraction of the material shows a low angle reflex at 2Θ = 4.5° and a reflex at 2Θ = 14.1°. The low angle reflex corresponds to d = 2.0 nm for the reflex at 4.5° and d = 0.6 nm for the reflex at 14.1 °. This indicates a microcrystallinity of the material (Figure 15).

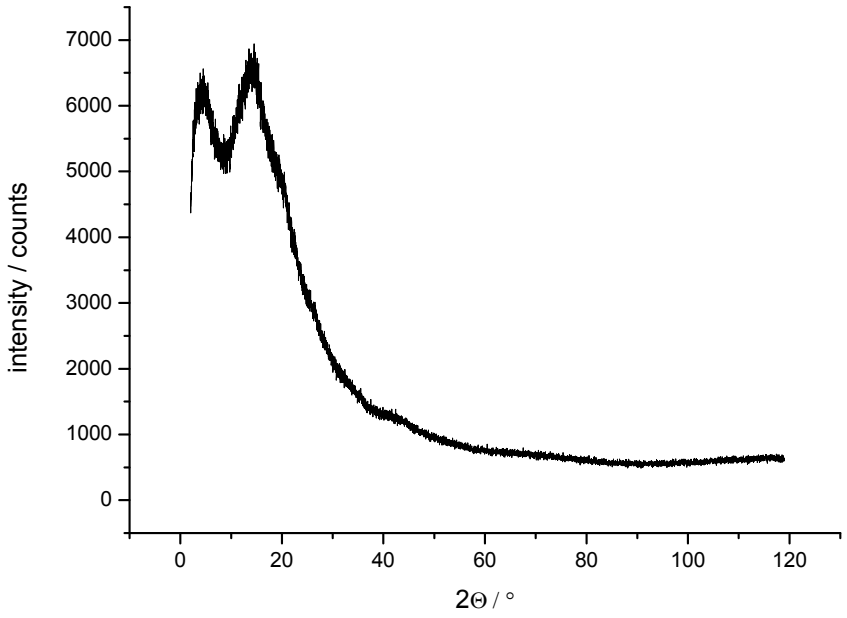

Figure 15. XRD of Polymer **1**. Two reflexes can be observed at at *2Θ* = 4.5° and *2Θ* = 14.1°.

The optical properties of the material were investigated using NMR and UV/vis spectroscopy. Initially, the photostationary equilibrium was determined by NMR spectroscopy. A solution of the polymer was irradiated for 3 h with a wavelength of 365 nm. The ratio of the integrals of the specific aromatic signals of the *cis*-state were used to determine the photostationary equilibrium (Figure 16). A photostationary equilibrium of *trans : cis* = 3 : 5 was found. The half-life in the *cis* state was determined by the change of the integral of a specific *cis*-azobenzene signal (see experimental section for details, chapter 4.3). The half-life in solution could be determined as 480 min (see experimental section for details, chapter 4.3).

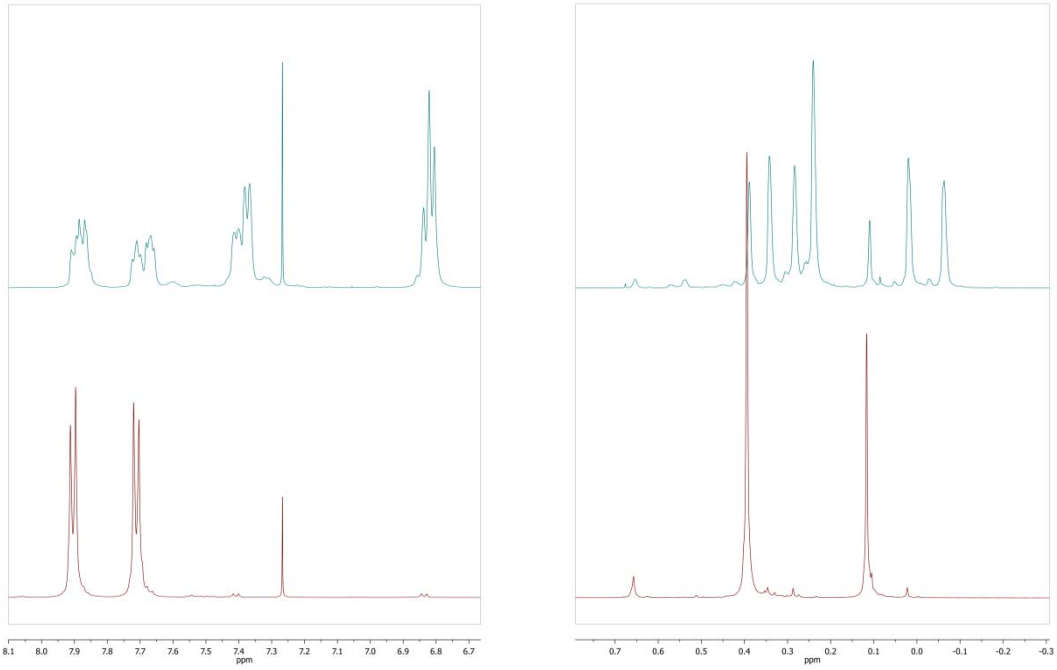

Figure 16. NMR Spectra of polymer **1** at the photostationary equilibrium (blue) and in the *trans*-state (red). Intensities of the aromatic and alkylic region were adjusted for plotting purposes.

Especially the optical properties of the solid material such as the absorption wavelength and half-life are of interest. For determination of the half-life and absorption maxima in solid state, a solution of the polymer was irradiated with UV light until the photostationary equilibrium was reached. This solution was casted onto a quartz glass slide (see experimental section for details, chapter 4.3). The relaxation of the polymer film was followed by UV/vis spectroscopy. Absorption maxima were found at 450 nm and 330 nm. The π-π* transition (330 nm) appeared to be shifted to significantly shorter wavelengths compared to the typical absorption of 360 nm of *trans*-azobenzene.[27] The half-life of the *cis* state in solid phase was determined to be 380 min and was significantly shorter than in solution, where a half-life of 480 min was found (Figure 17).

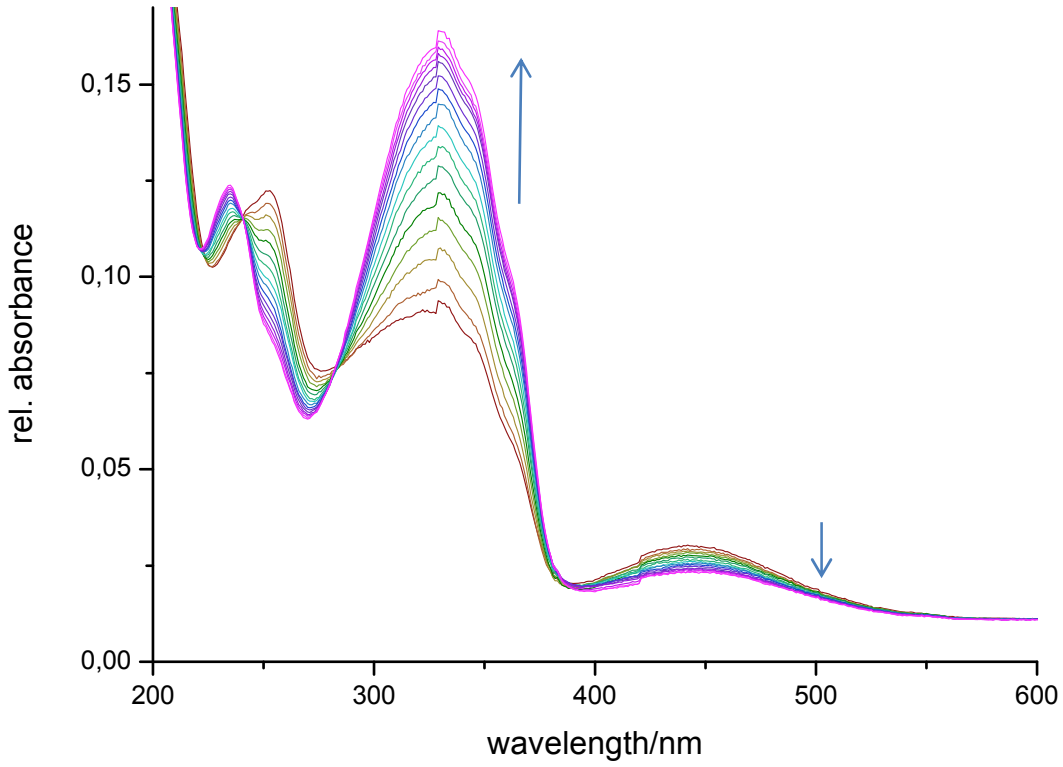

Figure 17. a) UV Spectra of a bulk polymer film in the *cis*-state, measured over the course of 14 h. One spectrum per hour is displayed. The absorption maxima are at 330 nm and 450 nm. The artifact at 327 nm is due to the change to the deuterium lamp in the spectrometer.

In solution, the hydrodynamic radius significantly changes when the polymer is switched to the photostationary equilibrium in solution. The retention time on a GPC column depends on the hydrodynamic radius of the analyzed polymer. All molecular weights are determined against polystyrene standards. The apparent molecular weight of the switched material determined by GPC is significantly lower compared to the molecular weight of the *trans*-state. The retention time for the *trans* state was 14.18 min (corresponding to M_n =32 kDa; M_w = 53 kDa) the retention time for the *cis*-state at the photostationary equilibrium was 14.43 min (corresponds to M_n=27 kDa, M_w = 41 kDa) (Figure 18).

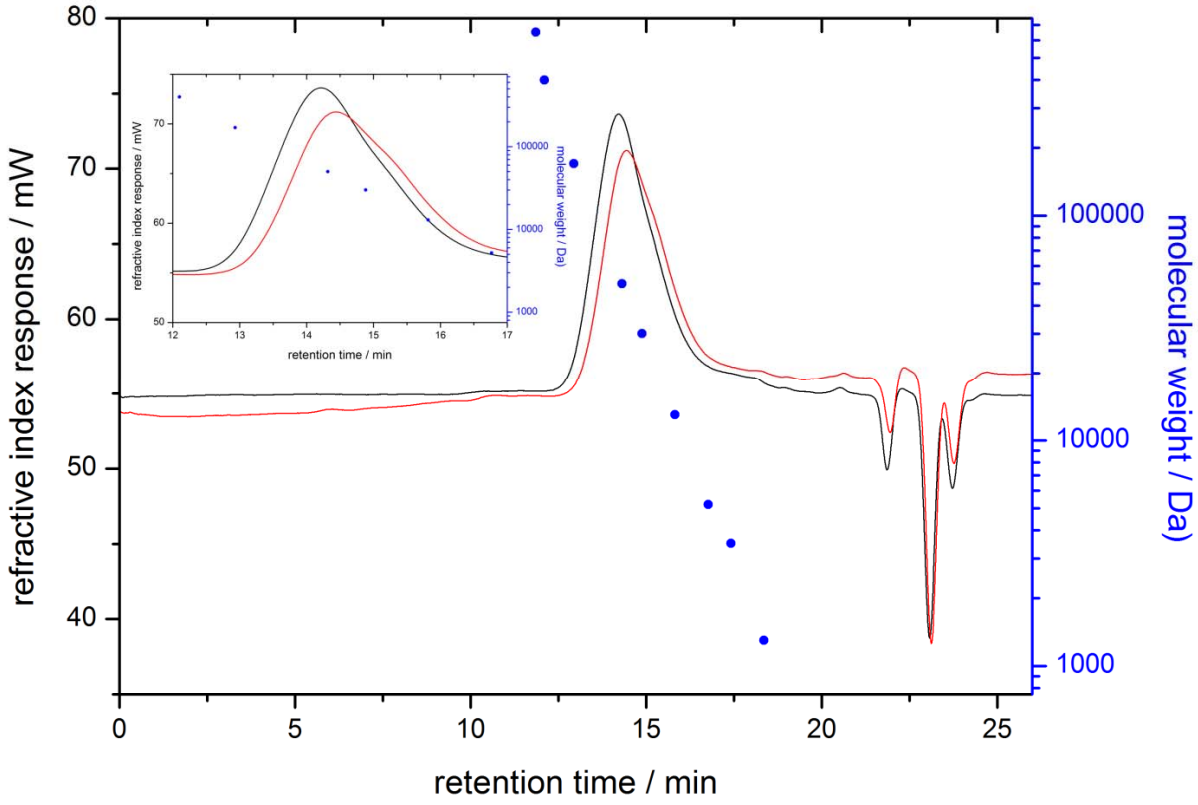

Figure 18. GPC Chromatograms of polymer **2** in the *trans* state (black) and at the photostationary equilibrium (red). The maxima of the signals were at 14.18 min for the *trans* state and at 14.42 min for the *cis* state. The blue points show the polystyrene calibration standards.

Elastomericity is essential for a material to perform a macroscopic shape change.[53d, 56] However, elastomeric properties in polymers are usually caused by a cross linking in the material. Linear polymers often show flowing properties but due to physical interactions of the polymer chains with each other (e.g. liquid crystallinity[64]), an elastic behavior can occur. This phenomenon is called viscoelasticity. To investigate if material **1** shows an viscoelasticity, tensile tests were performed on the material for allowing a reproducable stretching. For this purpose, a molded piece of the polymer with defined dimensions (see chapter 4.3) was placed in a tensile device and was slowly stretched (20 mm/min) until the material failed. The material could be streched to 210 % of its original length. However, after the material failed at a critical strain, the material nearly regained into its original shape after some time. This indicates a strong viscoelasticity of the material. (Figure 19).

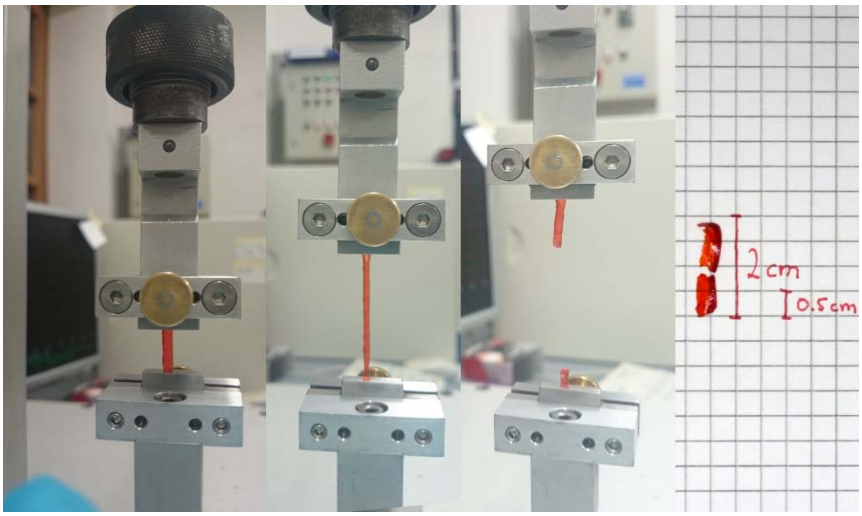

Figure 19. Tensile test on poly[azobenzene-tri(dimethylsiloxane)] (**2**). The material was stretched with a speed of 20 mm/min. 15 min after polymer film failure, it returned almost to the original length.

The polymer showed a macroscopic response to UV light (365 nm, 500 mW). During irradiation, a strong deformation of the polymer films could be observed (Figure 20). However, the material could not be switched back reversibly into its original shape, neither by irradiation with visible light (450 nm), nor by thermal relaxation. A movement due to thermal effects can be excluded since the irradiation was performed using an IR filter. A possible explanation for this behavior is the fact that the material is not chemically cross-linked. The high elasticity of the material indicates a strong interaction of the polymer chains which each other. The material does not show a flowing behavior which is often found in linear polymers. It is assumed that the liquid crystalline character of the material leads to an efficient packing of the azobenzenes in short range ordered domains. Those domains allow a strong π-stacking of the *trans*-azobenzenes. Thus the material is physically cross-linked. By irradiation with UV light, a contraction of the polymer chains which are exposed to the light occurs and a macroscopic deformation could be observed. However, the liquid crystallinity of the material and its order depend on the mesogenic character of the *trans*-azobenzene. By isomerization to the non-mesogenic[57] *cis*-state, the liquid crystalline alignments get irreversibly lost. When the azobenzenes re-isomerize to the *trans*-state, this effect does not cause a macroscopical effect.

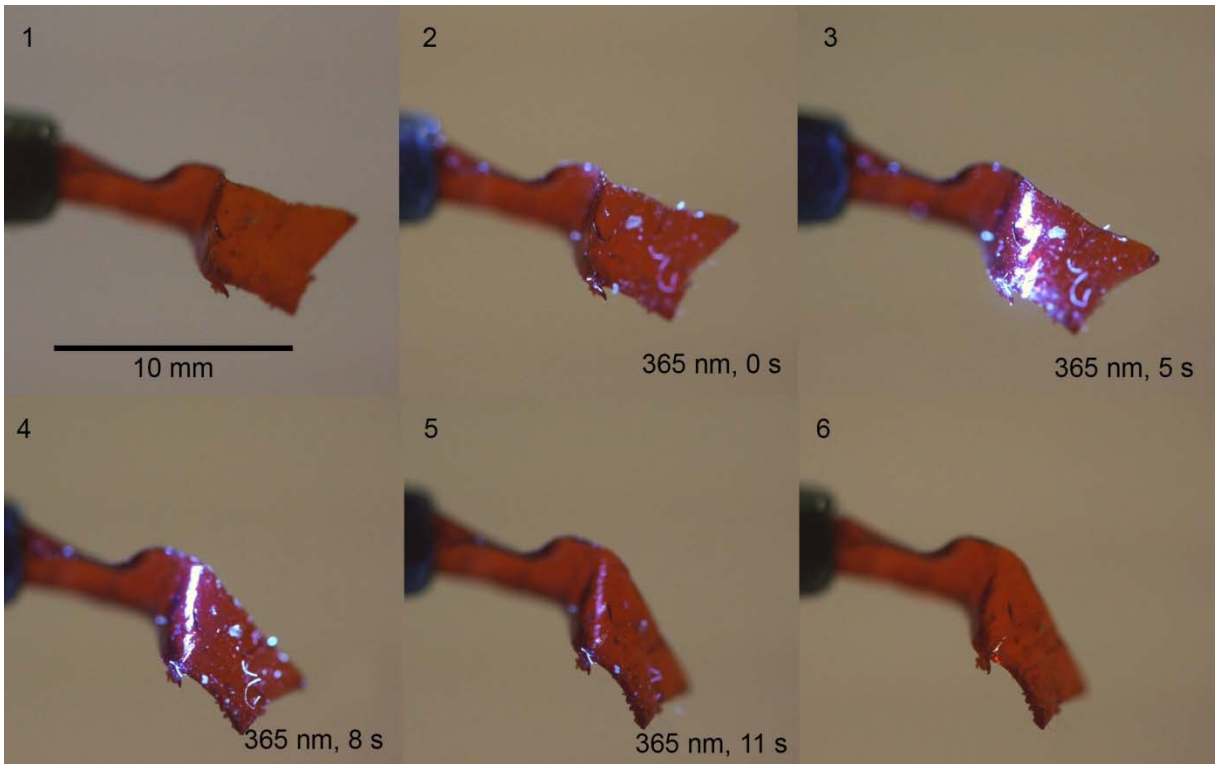

Figure 20. Photoinduced deformation of polymer **1** by irradiation with UV light (365 nm).

Besides the *para* silanol functionalized azobenzene **2**, *meta* analog **12** was synthesized. Compared to the *para* substituted monomer, the distance change of the *meta*-carbons in azobenzene is shorter. The distance of the *para* carbons in azobenzene changes from 9 Å in the *trans* form to 5.5 Å in the *cis* form. The change of the distance of the *meta* carbons in azobenzene is with 8.2 Å to 6.6 Å siginifantcly lower (determined from single crystal data of *trans*[65] and *cis*[66]-azobenzene). Accordingly, a contraction of a polymer chain should be significantly lower. With different ratios of *para* and *meta* substituted azobenzenes, it should be possible to adjust the mechanical response of the material. The *meta* substituted monomer was synthesized analogously to monomer **2** starting from 3,3'-*bis*(iodo)azobenzene (**13**) (Scheme 13). The compound was stannylated in a Stille Kelly reaction. 3,3'-Bis(trimethylstannyl)azobenzene (**14**) could be synthesized in a yield of 70%. Compared to the *para* silanol (yield = 35%), the yield of the *meta* analog **12** is with 20% significantly lower and needs to be further optimized. A single crystal structure of 3,3'-bis(hydroxydimethylsilyl)azobenzene (**12**) could be obtained (see experimental part, chapter 4.3).

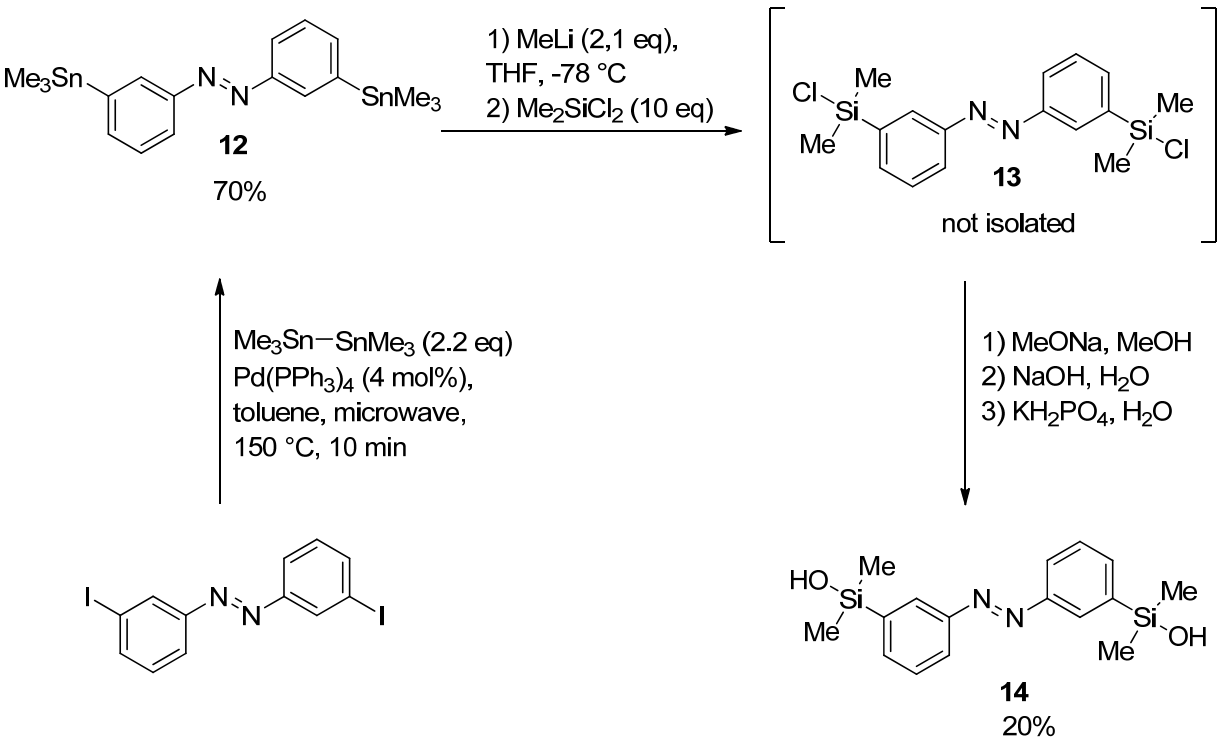

Scheme 13. Synthetic route to 3,3'bis(hydroxydimethylsilyl)azobenzene (**14**).

2.5 Porous Liquid Crystalline Elastomers

Emre Kizilkan, Jan Strueben, Xin Jin, Clemens Schaber, Rainer Adelung, Anne Staubitz,* Stanislav N. Gorb* **2015**, *to be submitted to Soft Matter*.

Azobenzene based liquid crystal elastomers have been produced with different porosities. A high porosity led to an improved photomechanical response of the free standing films. This has been demonstrated in terms of bending angles and forces under alternate illumination of ultraviolet and visible light.

Scientific contribution to this publication.

I performed all polymer syntheses, and the chemical characterizations. Precursors were prepared by the project students Jennifer Paasch and Nicole vom Stein. Emre Kizilkan measured the bending angles and forces of the films. Xin Jin performed all DSC measurements. A. Staubitz and I contributed to writing the article.

Soft Matter

Dynamic Article Links►

Cite this: DOI: 10.1039/c0xx00000x

www.rsc.org/xxxxxx

COMMUNICATION

Photoswitching of Porous Liquid Crystal Elastomer

E. Kizilkan[a],J. Strueben[b], X. Jin[c], C. Schaber[a], R. Adelung[c], A. Staubitz[b], and S. Gorb[a]

Received (in XXX, XXX) XthXXXXXXXXX 20XX, Accepted Xth XXXXXXXXX 20XX

DOI: 10.1039/b000000x

Azobenzene based liquid crystal elastomers have been produced with different porosities. A high porosity has led to an improved bending behaviour of the free standing films. Their photomechanical response has been also demonstrated in terms of forces under alternate illumination of ultraviolet and visible light.

Stimuli-responsive polymers which can be actuated by light[1], or other stimuli[2], have gained much attention in recent years. Light activated shape-memory and shape changing polymers demonstrate reversible macroscopic shape changes through molecular light triggered motion. In particular, liquid crystal elastomers (LCE) with azobenzene moieties as mesogenes have been most widely used as photo-responsive polymers due to their fast response to different proper light wavelengths and strong absorption [3, 4]. By illumination with ultraviolet light with wavelengths of typically 350-370 nm, the *trans* isomer configuration of azobenzene molecule switches to the *cis* isomer thereby it changes its geometry from a molecular length of 9 Å in the *trans* configuration to 5.5 Å in the *cis* configuration[5, 6]. This enormous change in the molecular length leads to a shape change back to stable *trans* configuration thermo-reversibly or by illumination with visible light wavelengths [7, 8]. Through these reversible molecular size changes, macroscopic motions of azobenzene LCE were demonstrated such as robotic arm movement, twisting, high frequency oscillation or switchable bending[4, 9, 10].

Implementing the LCEs into technological applications requires novel modifications or composites of LCE with different materials in order to enhance the photo-responsiveness or bring new functions on present framework. With easy processability, lower density and bigger apparent surface area for external stimuli, porous polymers are more advantageous thus bringing many other functions over bulk polymers[11]. Moreover, the porous media provides capability of 3D incorporation of multiple functional materials with different properties. Therefore, in this work, we have produced photoresponsive azobenzene LCE films with different porosities. The porous LCEs demonstrated improved photomechanical response hereby their bending angle measurements. The results indicated that the higher porosity on the LCE films increases the final bending angle. Moreover, the photoswitchability of highly porous LCE was demonstrated in terms of bending forces generated during the photoisomerisation of azobenzene when the highly porous LCE samples were alternately illuminated by UV and VIS light sources.

In this work ,a material developed by Ikeda[12] and co-workers was used and the synthesis was modified to obtain free standing films of different porosities (Scheme 1).

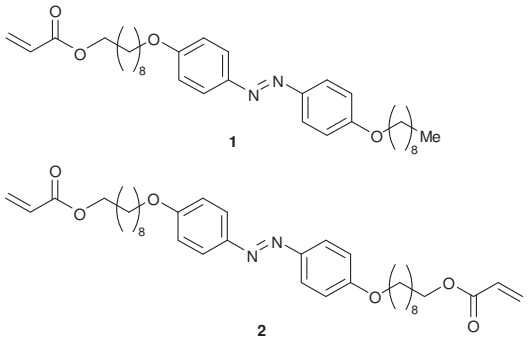

Scheme 1 Chemical structure of monomer 1 and 2 used in this work.

By the use of thermal initiator [1,1′-azobis (cyclohexanecarbonitrile)], the gas evolution during polymerisation yielded porosity on the final LCE films. As result of using thermal initiators with amounts of 1.6 mol% and 2 mol% in polymerization process, two different films of LCE with 5% and 67% porosities were obtained, respectively. The porosity was induced by nitrogen release due to nitrogen containing thermal initiator use during the polymerization processes (for more details, see the supporting information). The porosity consists of 1-70µm and 1-200µm pores for 5% and %67 porous films, respectively. The both films have thickness of 100 µm.

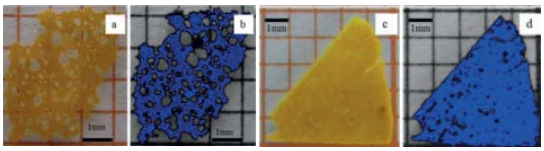

Fig.1 LCE films with porosity on the apparent surface area (a, c). Surface porosities were calculated via colour threshold analysis (b,d).

The photoresponse of the LCE films has been characterized by

applying 30 seconds of UV light (λ = 365nm) and thus measuring the bending of the films in respect to tip displacement angles of the films to the y-axis. The light triggered bendings were recorded in time sequence (Figure 2). The representative samples of 5% and 67% porous LCE free standing films were observed during the illumination with UV light source with 7.5, 6, 3 and 1.1 W/cm^2 light intensities for 30 sec. The observation revealed that the final bending angles for 67% porous films are higher at any intensity than all 5% porous films' bending angles (Video 1 and Video 2). Furthermore, light intensity has an influence on the bending behaviour; higher the intensity, bigger the final bending angles. However, for 67% porous samples, at 7.5 and 6 W/cm^2 intensities, there was not a distinct difference at final bending angle. This can be explained by the diameter of Gaussian beam which provide a bigger diameter of light illumination at 6 W/cm^2 compared to 7.5 W/cm^2. The fluctuations on the bending angles at 3-30 sec are due to highly porous volumes which do not photoisomerise steadily. For 3 and 1.1 W/cm^2 intensities, the final bending was corresponded directly to the intensity of light, in other words, as the light intensity increased, the porous film bent more. The 5% porous samples in average demonstrate smaller final bending angles. As the light intensity decreases, the final bending angle decreases, too. At 1- 5 the second, 67% porous films have reached higher bending angles quicker than 5% porous films. Interestingly, at this time range, the bending angles for the 7.5 and 6 w/cm^2 illuminated 5% porous film were higher than 3 and 1.1 W/cm^2 illuminated 67% porous films because of the quicker photoisomerisation on the appearent surface through the higher light intensities.

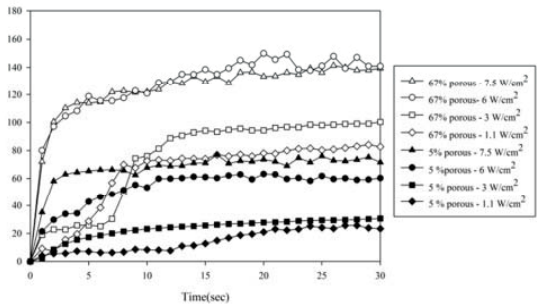

Fig.2 Observation of bending angle change by time. With UV light illumination of different light intensities, the bending angle for LCE films with 5% and 67% porosity.

The Xin's mathematical model

The average final bending angles at these four different intensities were plotted for the 5% and 67% porous films with 10 samples to each. They demonstrated 43.9 ± 17 and 117.8 ± 24 average final bending angles, respectively (Figure 3). The differences in the final bending angles between these two different porous films analysed are statistically highly significant ($P \leq 0.001$, one-way ANOVA, Tukey test).

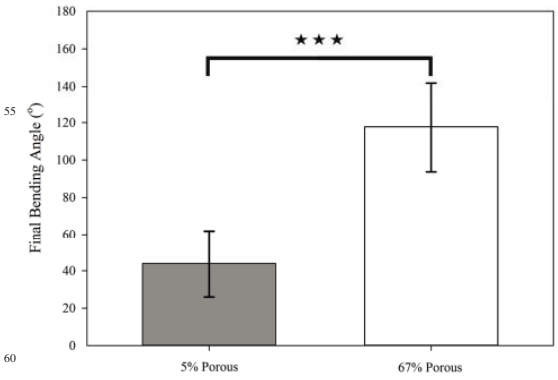

Fig.3 Average final bending angle of %5 and %67 porous LCE films when illuminated with UV light. One wa ANOVA Tukey test resulted a highly significant difference on the final bending angle of porous films when illuminated same amount of time.

The azobenzene LCE films produced are assumed to have polydomain liquid crystal structure with homeotropic aligned mesogenes on the apparent surface based on literature precedent[7, 13] since the LCE films bent away from the direction of UV light source. Under UV light illumination, the homeotropic aligned mesogenes of the azobenzene LCE films change their molecular structure due to trans-cis photoisomerisation that leads to orientational disorder of domain structure on the surface and induces a volume expansion at a certain thickness. Thus, the LCE film demonstrates a bilayer structure and bends to the opposite direction of light source (Figure 4a).

While bringing lower density and bigger framework, porous structure provides wider area for external stimulus. During illumination with UV light source, the ratio of volume in which molecules are photoisomerised to total volume determines the gradient of bending. The porous LCE with its bigger apparent surface area enables light to stimulate a bigger volume (Figure 4b). Thus, the proportion of photoisomerised azobenzene mesogens to non-photoisomerised mesogenes is increased. Moreover, not only on the surface, the pores enables light stimulus to reach azobenzene molecules also throughout the film. Therefore, the volume expansion occuring thickness in bilayer structure increases and leads to bigger final bending angles compared to non porous LCEs.

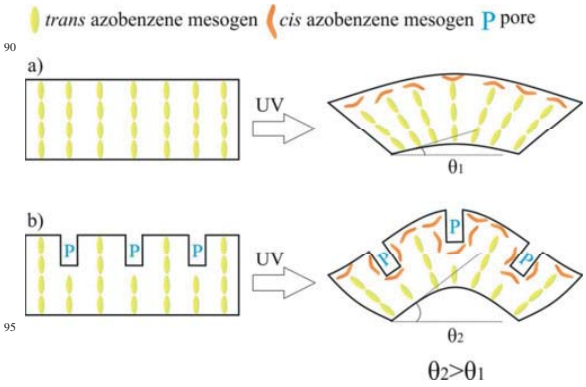

Fig.4 The bending of LCE films which have homeotropic aligned mesogenes a) non-porous film, b) porous film. The porosity provides a relatively bigger illumination area and enables the absorption of the UV light deep into the film. Thus for porous films, proportion the photoisomerized volume to non photoisomerized volume is bigger compared to nonporous films with same thicknesses.

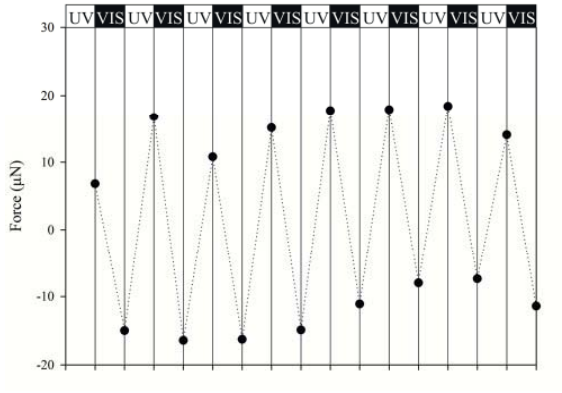

Fig.5 Forces arising by consecutive photoswitching of the 67% porous free standing LCE film. The UV and VL light sources are operated alternatively for 20 sec each.

In particular, the demonstration of this photoresponse in terms of forces is important, even at very small force scales, e.g. for micro/nano mechanical systems or robotic applications where locomotion and low noise, quick mechanical output are necessary. Hence, we have demonstrated the light triggered force actuation of porous LCE film by switching the state of azobenzene from *trans* to *cis* and *cis* to *trans* continuously, as the film bends forth and back when illuminated by UV light (λ = 365nm) and visible light (VIS, λ = 455 nm) sources, respectively (Figure 5). This bending is depicted in terms of forces measured by deflection of encountering the calibrated glass cantilever force probe. We used the 67% porous LCE film to show the responses of the film to light stimuli with UV and VIS light wavelengths, since the higher porous film has demonstrated higher and faster response to light in terms of bending angles. The representative sample of 67% porous film was alternately illuminated by UV and VIS light sources perpendicular to substrate surface with light intensity of 7.5 W/cm^2(for more details, see the supporting information). The film was exposed to the light stimuli for 20 seconds each, since the plateau, on which the bending angle remains constant, has been known to reach. Maximum deflection of calibrated force probe was calculated and converted to force generated when the initial position and final position of force probe encountering the LCE film was compared. Since the homeotropic aligned LCE film bends to the opposite direction of UV light source illumination, the forces generated are labelled as '+' and for VIS light illumination, the bending forces were labelled '-' while the film recovers its initial shape and position. The continuously alternately illumination of UV and VIS light revealed the forces that arise during the photoswitching vary from ±7 to ±18 μN for both directions.

Conclusions

In this work, two different azobenzene containing LCE free standing films with two degrees of porosity were produced. In terms of final bending angle, the porosity increased the photoresponse of the LCE with high significance. It has been also demonstrated the photoswitching by a force measurements when the polymer is illuminated by altering the light stimulus wavelengths. Presumably, when having low density, bigger framework for incorporation of other functionalities, the porous azobenzene LCEs can be utilized in micro/nano systems where precise, quick, low noise mechanical outputs are necessary.

Acknowledgements

This work was funded by the German Research Foundation (DFG) under the grant scheme SFB 677-C10.

Notes and references

[a]*Department of Functional Morphology and Biomechanics, Zoological Institute, Kiel University, Am Botanischen Garten 1-9, 24098, Kiel, Germany;Fax: +49 431 8801389; Tel:+49 431 8804513 E-mail: sgorb@zoologie.uni-kiel.de*
[b]*Otto-Diels-Institute for Organic Chemistry, Kiel University, Otto-Hahn-Platz 4, 24098 Kiel, Germany; Fax: +49 431 8801540; Tel:+49 431 8803697 E-mail: astaubitz@ oc.uni-kiel.dec*
[c]*Institute for Materials Science, Functional Nanomaterials, Kiel University, Kaiserstr. 2, 24143, Kiel, Germany; Fax: +49 431 8806124; Tel: +49 431 8806234 E-mail: ra@ tf.uni-kiel.de*

† *Electronic Supplementary Information (ESI) available: See DOI: 10.1039/b000000x/*

1. Y. Zhao and T. Ikeda, *Smart light-responsive materials: azobenzene-containing polymers and liquid crystals*, John Wiley & Sons, 2009.
2. A. Lendlein and S. Kelch, *Angewandte Chemie International Edition*, 2002, **41**, 2034-2057.
3. C. J. Barrett, J.-i. Mamiya, K. G. Yager and T. Ikeda, *Soft Matter*, 2007, **3**, 1249-1261.
4. Y. Yu, M. Nakano and T. Ikeda, *Nature*, 2003, **425**, 145-145.
5. T. Ikeda and O. Tsutsumi, *Science*, 1995, **268**, 1873-1875.
6. G. S. Kumar and D. Neckers, *Chemical Reviews*, 1989, **89**, 1915-1925.
7. H. Yu, *Journal of Materials Chemistry C*, 2014, **2**, 3047-3054.
8. K. Ichimura, *Chemical reviews*, 2000, **100**, 1847-1874.
9. J. J. Wie, K. M. Lee, M. L. Smith, R. A. Vaia and T. J. White, *Soft Matter*, 2013, **9**, 9303-9310.
10. T. J. White, N. V. Tabiryan, S. V. Serak, U. A. Hrozhyk, V. P. Tondiglia, H. Koerner, R. A. Vaia and T. J. Bunning, *Soft Matter*, 2008, **4**, 1796-1798.
11. D. Wu, F. Xu, B. Sun, R. Fu, H. He and K. Matyjaszewski, *Chemical reviews*, 2012, **112**, 3959-4015.
12. M. Yamada, M. Kondo, J.-i. Mamiya, Y. Yu, M. Kinoshita, C. J. Barrett and T. Ikeda, *Angewandte Chemie*, 2008, **120**, 5064-5066.
13. A. Emoto, E. Uchida and T. Fukuda, *Polymers*, 2012, **4**, 150-186.

2.6 Adhesion Between Low Surface Energy Polymers

(*Adv. Mater.* **2012**, *24*, 5676-5680.)

As prelimary work for the design of devices (figure 21), a methodology was required to attach the photoresponsive materials to PDMS, a material with very non-sticky properties. It was desired that the attachment could be performed without the need for a chemical modification, especially regarding the photoresponsive materials. For this purpose, a technique to join two polymers together by the use of tetrapodal zinc oxide microparticles. To demonstrate the efficiency of this method, PTFE and PDMS layers were joined together. These materials could not be joined before because of their low surface energies.

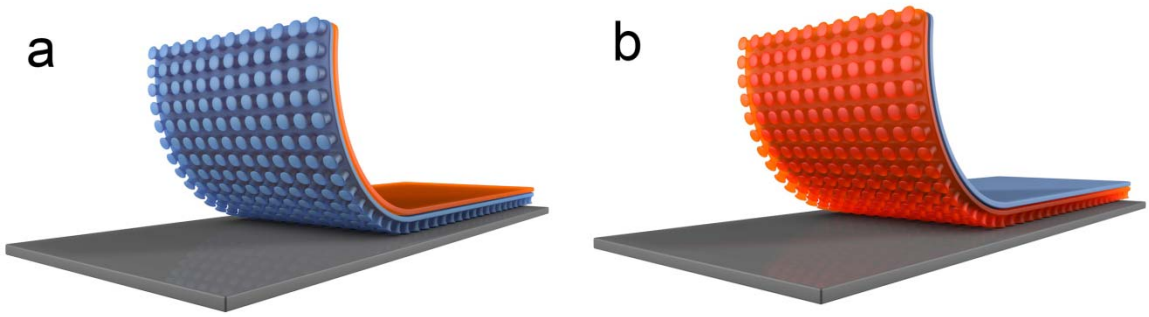

Figure 21. Two conceptional designs for a photoswitchalbe dry adhesive: a) a microstructured PDMS layer (blue) with a photoresponsive polymer attatched to its back side (orange) b) a microstructured photoresponsive polymer (orange) with a PDMS layer on its back side (blue).

Joining the Un-Joinable: Adhesion Between Low Surface Energy Polymers Using Tetrapodal ZnO Linkers

X. Jin, J. Strueben, L. Heepe, A. Kovalev, Y. K. Mishra, R. Adelung, S. N. Gorb, A. Staubitz, *Adv. Mater.* **2012**, *24*, 5676-5690.

highlighted in *Nature* **2012**, 489, 9.

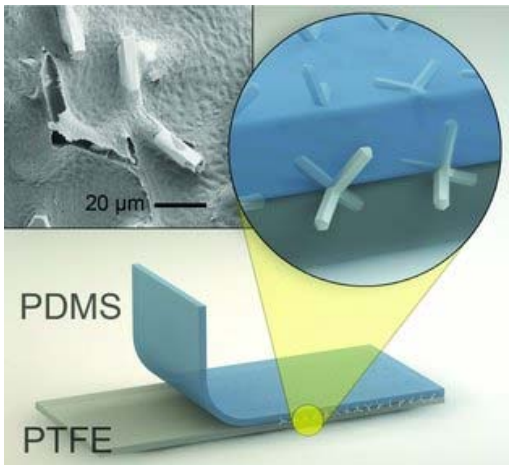

Tetrapodal ZnO crystals are used for mechanical interlocking of PTFE and cross-linked PDMS, classically non-adhesive polymers. This novel approach is straightforward and easily applicable and leads to a peel strength that is higher than 200 Nm^{-1} without chemical modification of the surfaces. The shape of these fillers emerged as a crucial aspect of the interlocking mechanism.

Scientific contribution to this publication

For this publication, I contributed the idea to attach PTFE and PDMS as two extreme examples for non-adhesive polymers to demonstrate the effect of the ZnO microparticles. Furthermore I developed the procedure of preparing PTFE films containing ZnO particles. A. Staubitz and I contributed to writing the article.

ADVANCED MATERIALS
www.advmat.de

Materials Views
www.MaterialsViews.com

Joining the Un-Joinable: Adhesion Between Low Surface Energy Polymers Using Tetrapodal ZnO Linkers

Xin Jin, Jan Strueben, Lars Heepe, Alexander Kovalev, Yogendra K. Mishra, Rainer Adelung, Stanislav N. Gorb,* and Anne Staubitz**

Joining polymer materials is an important challenge in materials engineering. Ideally, two polymers can be firmly affixed to each other, while at the same time preserving the highly optimized and specialized properties of each individual polymer.[1] However, in many cases, the chemical and physical properties of polymers to be connected render them incompatible to conventional methods for facilitating a firm attachment between them. Often, this can only be achieved with difficulty or not at all.

One of the most extreme cases is the combination of poly(tetrafluorethylene) (PTFE) and cross-linked poly(dimethylsiloxane) (PDMS). PTFE, also known as Teflon, is a thermoplastic material with high chemical inertness and is well known for its non-adhesive properties (for example in frying pans).[2] Similarly, cross-linked PDMS (often used in backing paper of sticky labels)[3] is, together with PTFE, among the materials with the lowest surface energy known to date.[4] Due to their unique chemical and physical properties, the combination of these two materials is required for many applications, such as for membranes for pervaporation technology,[5] biocompatible microelectronic and optofluidic devices,[6] or in medical implants.[7]

In general, adhesion between two surfaces may result from van der Waals interactions, diffusion, chemical interactions, and mechanical interlocking.[8] Because PTFE and PDMS have the lowest known surface energies, van der Waals interactions are insufficient for joining the materials. Diffusive adhesion can also be excluded: not only is PDMS cross-linked but PTFE is also insoluble in all but perfluorinated solvents and materials.[4] In addition, chemical interactions are also negligible for the provision of an adhesion mechanism, because both polymers are chemically inert.

Substantial effort has been made to achieve strong adhesion between polymers and other materials, such as wet chemical treatments,[9] plasma treatments,[10] ion beam treatment,[11] and graft polymerization.[12] Crucially, a strong joint of PTFE and cross-linked PDMS by these methods has never been demonstrated to the best of our knowledge. Even on high surface energy substrates, the adhesion of these low surface energy polymers is recognized to be a difficult task. For example, the peel strength of a PTFE/epoxy adhesive system could be increased from 25 to 280 N m^{-1} by plasma treatment[13] which is a typical value.[14] Ion beam treatment of the same system could further increase the peel strength to 800 N m^{-1}; however in this case, substantial morphological modification occurred, which was found to induce mechanical interlocking, leading to the high value obtained. Typical peel strengths for polymer-metal adhesion enhanced by ion beam treatment are around 150 to 300 N m^{-1}.[15] The peel strength between a silicone and acrylic adhesive tape was increased to about 350 N m^{-1} by reactive gas plasma treatment.[16] Despite their usefulness, these treatments have disadvantages: the surface chemical modification, often leading to degradation and loss of special properties,[12c,17] safety issues, especially for fluoropolymers,[18] and often the need for specialized equipment and tightly controlled process environments. Moreover, these techniques have never been shown to be effective on two low surface energy polymers such as PDMS and PTFE.

Adhesion by simple mechanical interlocking is a potentially very straightforward process that can avoid chemical modification of the surface and appears to be the only solution to join two low surface energy polymers. However, to date, it has not gained much attention because of its relatively low effectiveness.[14] The traditional treatments to increase mechanical interlocking, such as grit blasting and grinding are only used as surface pre-treatments before the application of other bonding methods.[19] Micro- and nanoparticles have been widely employed as reinforcement fillers for polymer matrices in composite materials studies[20] but as adhesion facilitators they have not received much attention.[21]

In this work, we present a new approach to effect a strong joint between PTFE and cross-linked PDMS as prime examples for typically non-sticky polymers. We show that tetrapodal ZnO crystals (T-ZnO) can be used as powerful mechanical adhesion facilitators in a straightforward and easily applicable way. The peel strength attained by this approach is at least of the same order of magnitude as obtained by plasma etching methods (for more adhesive polymer combinations)[13,14] and can be

X. Jin, Dr. Y. K. Mishra, Prof. R. Adelung
Institute for Materials Science
Functional Nanomaterials
University of Kiel, Kaiserstr. 2, 24143 Kiel, Germany
E-mail: ra@tf.uni-kiel.de
J. Strueben, Prof. A. Staubitz
Otto-Diels-Institute for Organic Chemistry
University of Kiel
Otto-Hahn-Platz 3/4, 24118 Kiel, Germany
E-mail: astaubitz@oc.uni-kiel.de
L. Heepe, Dr. A. Kovalev, Prof. S. N. Gorb
Department of Functional Morphology and Biomechanics
Zoological Institute
University of Kiel
Am Botanischen Garten 1–9, 24098 Kiel, Germany
E-mail: sgorb@zoologie.uni-kiel.de

DOI: 10.1002/adma.201201780

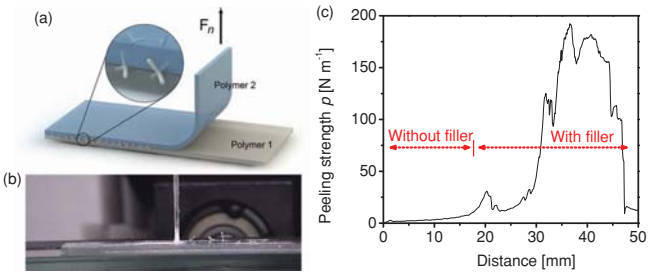

Figure 1. Peeling experiment setup. (a) Two polymers were layered on top of each other in the presence of T-ZnO particles embedded between them. (b) The peel strength for the separation of the two layers was measured in a 90° peel test. (c) Peeling strength of a PTFE/PDMS sample with T-ZnO as a filler with a filling factor of 0.008 ± 0.001 g cm^{-2} (Errors were estimated from the instrument precision; details are provided in the Supporting Information).

seen as a viable, simple alternative to these methods, especially when chemical modification of the polymer surface needs to be avoided. Furthermore, we provide mechanistic insight into the adhesion and failure mechanisms on the meso-scale and demonstrate the crucial importance of the shape of the crystals with respect to the reinforcement mechanism.

Our hypothesis was that instead of using classical *convex* filler particles such as short fibers or particulates, *concave* particles could act as a form of "micro/nano Velcro" filler at the polymer/polymer interface, leading to high adhesion strengths without a chemical interaction. In order to classify a particle as concave or convex, we use the mathematical definition of these geometries: In a convex particle, the surface bends outwards at all points (all intersecting planes on the surface display angles >180°), whereas in a concave particle, part of its surface bends inwards (some intersecting planes on the surface with angles <180°), leading to mechanical interlocking. Concave T-ZnO crystals are ideally suited to this requirement and can be produced in high quantities at low cost by a simple flame transport method.[22]

In order to test this hypothesis, samples were prepared where two polymer layers were placed on top of each other, with varying amounts of T-ZnO between them. The samples were typically prepared by slip-casting one polymer from a solution or dispersion onto a glass substrate, followed by heating. On one half of the polymer film, T-ZnO fillers were sprinkled, whereas the other part was shaded and served as a reference area for no treatment conditions. The second polymer (PDMS) was subsequently flow-coated on top. The assemblies were heated at 100 °C for 40 min to cure the second layer and they were then allowed to cool to ambient temperature before testing the adhesion strength with a peeling tester. The sample configuration was such that the top polymer layer was peeled at a 90° angle at a speed of 0.5 mm s^{-1} (**Figure 1**a,b). An inelastic backing tape (Tesafilm Transparent, Tesa AG, Hamburg, Germany) was attached to the top layer to reduce elongation during measurement.

In the experiments, the peeling strength, p, was calculated as $p = \frac{F}{b}$,[23] where F is the peeling force, and b is the sample width. The filling factor (ff) was calculated as $ff = \frac{m}{A}$, where m and A were the filler weight and filled area respectively. In a typical experiment, the peeling strength was very low when the peeling force was applied to the control area without filler (Figure 1c; peeling test for a PTFE/PDMS sample, position 0 to ca. 18 mm). Some adhesion could be observed in this area with a slightly increasing force across the filled region. This was mainly due to the bending of the upper polymer layer, because when a layered control PTFE/PDMS sample without any filler at all was prepared, the layers separated before the measurement could be performed. This observation confirms the expected extremely low adhesion between the two polymers by the van der Waals, diffusive or chemical adhesion mechanism. However, when the propagating peel front reached the filled region, the peel strength increased significantly to about 190 N m^{-1}. Because the filler particles were directly added to the first polymer layer without any dispersion agent (i.e., no chemical pre-treatment) and only with the help of a sieve, some statistical dispersion of the filler distribution was unavoidable. It is likely that the variance of the peel strength may be associated with this variance of the filler distribution. It is gratifying therefore that despite this variation, such a significant increase of peeling strength was reproducibly obtained by this very simple sample preparation technique.

This approach proved not only suitable for an extremely non-adhesive polymer combination such as PTFE and PDMS but also between PDMS and polyvinyl butyral (PVB), which has a highly adhesive surface (**Figure 2**d) and is commonly used as glue.[4]

In general, the peeling strength between glue and substrate can be enhanced by increasing interface roughness and thereby the contact area. Since the addition of filler particles has the effect of roughening the interface, additional experiments were performed in order to examine the specific effect of the shape of the filler. T-ZnO particles were ground into short fibers and particulate shapes (G-ZnO) and were used as a comparison to T-ZnO. Scanning electron microscope (SEM) images of T-ZnO and G-ZnO (Figure 2a,b) show the shape of the tetrapodal filler, T-ZnO, with four "legs" pointing out.

The peeling strengths for both PTFE/PDMS and PVB/PDMS samples were tested with the two different types of fillers or no fillers as a control (Figure 2c,d). For the latter, the peeling strength for the PTFE/DMS sample was below the detection limit of the test setup (see Figure 2c) and was therefore set to 0 N m^{-1}. For both the PVB/PDMS and PTFE/PDMS samples, it was shown that the peeling strength was improved by both types of fillers. A maximum peeling strength of more than 220 N m^{-1} at a ff of 0.008 g cm^{-2} for T-ZnO in the PTFE/PDMS samples could be observed. In fact, the polymers were so firmly joined together that the measurement was limited by the lower polymer layer (PTFE) being sheared up from the underlying adhesive tape. Therefore, the increase in adhesion by applying the T-ZnO crystals is likely to be even higher than this value. In the PVB samples, the maximum peeling strength was found for

ADVANCED MATERIALS
www.advmat.de

www.MaterialsViews.com

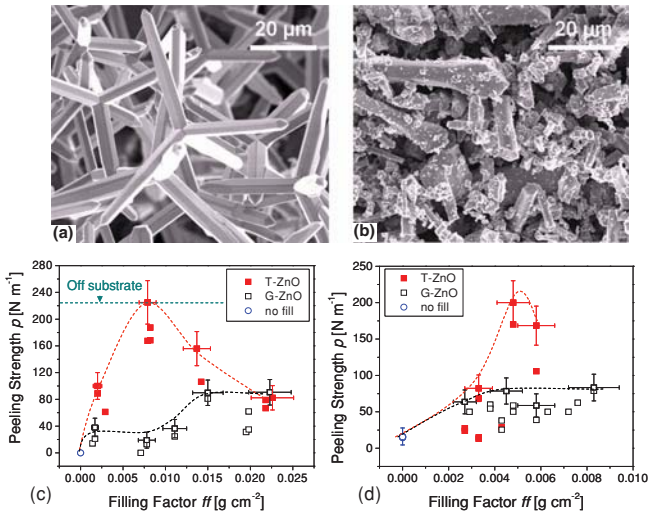

Figure 2. SEM images of (a) T-ZnO (concave) and (b) G-ZnO (mainly convex). Peeling strength vs. filling factor for (c) PTFE/PDMS samples and (d) PVB/PDMS samples. Each data point indicates the maximum peeling strength of a sample during a measurement (details of the error estimation in the Supporting Information). The dashed lines are guides for the eye only.

a *ff* of around 0.005 g cm^{-2}. In this case, cohesive failure of the PDMS layer was observed. The addition of more filler reduced the peeling strength. For both PTFE/PDMS and PVB/PDMS in combination with G-ZnO, the peeling strength increased only marginally with the filling factor (black line in Figure 2c). Samples with higher filling factors could not be prepared because the additional fillers did no longer attach to the surface of the first polymer layer. From these data values, it is clear that T-ZnO provided a much higher enforcement than G-ZnO at similar filling factors, despite the fact that G-ZnO has a higher surface to volume ratio. This trend was particularly pronounced in the combination of PTFE and PDMS.

A peel test is a mechanical test and does not directly provide the adhesion force between interfaces, because energy is dissipated through material deformation.[24] However, the peel strength provides an estimate of how much stress the joint of two materials can withstand before failure. In order to analyze the specific effects induced by the special shape of filler, the interface between two polymers before and after peeling was investigated by SEM (**Figure 3**a–d).

The analysis of the peeling interface and the fillers embedded at the interface reflects the forces that act on them, such as tension, bending, adhesion, compression, etc.[20b,25] In order to provide a clear interpretation of our results, we considered only failure modes classified by separated surfaces and cohesive failure of one material. In general, for the separation of the two polymer layers with fillers embedded in them, four locations exist where failure can occur. Firstly the filler itself may undergo cohesive failure (failure mode 1). Secondly, polymer cohesive failure may occur (failure mode 2). A third situation would arise from polymer/polymer interfacial failure (failure mode 3). Finally, a fourth failure mode is the polymer/filler interfacial failure (failure mode 4). Failure modes 1 and 2, as cohesive failures, generally are more energy consuming. Failure modes 3 and 4 are determined by interfacial interactions of the materials (commonly van der Waals interaction, diffusion, chemical interaction and mechanical interlocking). As pointed out in the introduction, the first three interactions between PDMS and PTFE (and between these polymers and ZnO) are very weak. In fact, this polymer/polymer adhesion is so fragile that the polymers separate immediately after solidification (0 N m^{-1} in Figure 2c). In other words, failure mode 3 (polymer/polymer interfacial failure) consumes negligible energy. The energy consumption of failure mode 4 depends strongly on the filler geometry. For G-ZnO, failure mode 4 consumes also very little energy, and, together with mode 3 would lead to failure well before modes 1 (cohesive failure of the ceramic) and 2 (cohesive failure of the polymer) can occur. Therefore, for G-ZnO, failure modes 3 and/or 4 dominate the observed low strength peeling process. However, for T-ZnO, the situation is different. The filler geometry leads to strong mechanical interlocking: If the filler is pulled out (failure mode 4: polymer/filler failure), the tetrapodal shaped filler will involve a significant bending of the legs or deformation of the polymer in many embedding situations, if the legs are not pointing into the direction of the pulling force. Therefore, failure mode 4 needs to consume additional energy, which can be significant. (Images are shown in the Supporting Information (Figure S2) for the bending of tetrapod leg in the polymer matrix under stress). If the local energy consumption for failure mode 4 is *higher* than failure modes 1 and 2, the latter two cohesive modes can also occur. Such extreme cases were observed on the peeled surfaces. We observed both mode 1 failure (fracture of the filler, Figure 3e) and cohesive failure of the polymer (mode 2) (Figure 3c). Mode 4 was visible in those cases where there was only a small part of the tetrapodal leg embedded in the other polymer layer (Figure 3f). For this reason, the peeling strength of samples with T-ZnO are higher than that of samples with G-ZnO.

In the discussion above, we considered a *single* filler particle's interaction with the polymer matrices. However, it is also necessary to evaluate the effect of the interaction of the filler particles with each other. Especially at high filling factors, the tetrapods can interlock with each other (Figure 3g) and dissipate the peeling energy into larger volume, and hence strengthen the joint of the two layers. This effect should compete with the decreasing relative polymer volume at the interface. Therefore, an optimum filling factor for the peeling strength was observed. Similar situations were found for PVB/PDMS samples (Figure 2d and Figure S1 in the Supporting Information).

In summary, we report a substantial increase of the peeling strength between two non-adhesive polymers by the addition of concave tetrapodal ZnO crystals at the interface. The highest

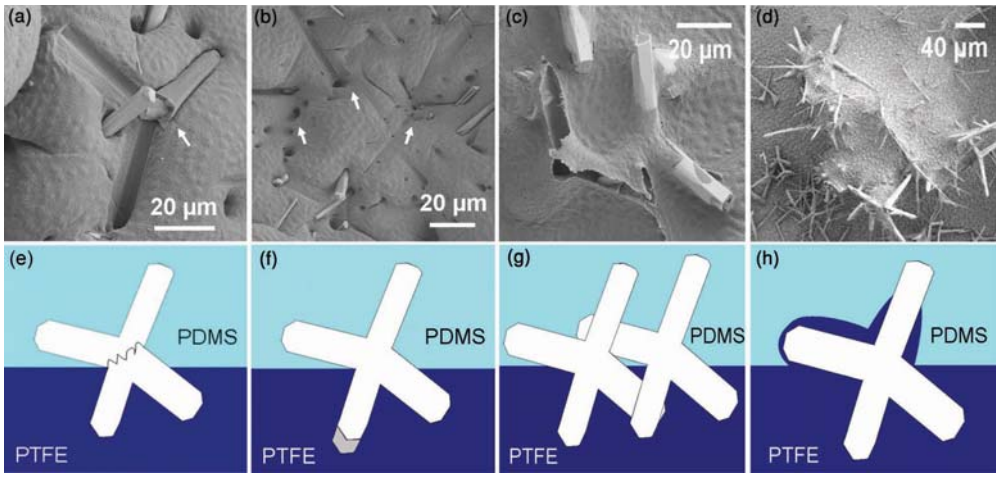

Figure 3. (a–d) SEM observation of different adhesive interfaces obtained in the course of experiments and (e–h) illustrations of important failure modes and origin of increased peel strength. (a) Peeled PDMS surface of a PTFE/PDMS sample. One leg of a tetrapod was broken off, indicating the bridging effect of filler. Also visible in (b) is the imprint of the filler peeled PDMS surface. The black holes correspond to the cavities remaining after pulling-out the tetrapod legs. (c) PTFE surface after peeling. The tetrapod on the right side remained but the one appeared to have been be pulled out by tearing the polymer. Polymer/polymer fracture has occurred in all cases; there are no fragments of the other polymer left on the peeling surface. (d) PTFE surface without addition of a second layer; joint formation by good wetting with the aqueous polymer dispersion of a group of T-fillers during processing. (e) Cohesive failure of the filler. (f) Adhesive failure between filler and polymer. (g) Interlocking between fillers. (h) Strong wetting of the filler by the polymer dispersion due to the tetrapodal shape of filler leading to polymer interlocking (increased surface roughness).

peeling strength for PTFE/PDMS samples was well above 200 N m^{-1} with T-ZnO, but below the detection limit without filler. The shape of the fillers was shown to be of critical importance: Whereas convex particles (G-ZnO) increased the peeling force required to separate the layers only slightly at higher filling factors, the re-enforcing effect was dominant for T-ZnO, despite the higher surface to volume ratio of the crystals. By SEM analysis of the fracture surface after peeling, we observed different failure modes: cohesive failure of the filler, cohesive failure of one of the polymers, interfacial polymer/filler failure and interfacial polymer-polymer failure. As the polymer layers were always cleanly separated, the latter always occurred first, leading to joint disintegration with no filler present (at ca. 0 N m^{-1}). For G-ZnO fillers, the only additional mechanism of adhesion is weak interfacial polymer/filler adhesion, whose energy requirement is slightly higher but by far not high enough to observe cohesive failure. However, in the case of T-ZnO, the joint was reinforced to such a degree that the two higher energy failure modes also played a role, cohesive failure of the polymer or of the filler. This is based on their concave shape, which serves as a hook, resisting being pulled out of the polymer matrix. In addition, interlocking between the tetrapods themselves leads to increased energy dissipation and also higher energy failure modes. We therefore suggest that polymer mechanical interlocking facilitated by concave particles could be a cost-effective, simple, yet versatile technique for joining polymer materials together that may complement established techniques, such as plasma methods, providing an increase in adhesion of the same order of magnitude. More importantly, in cases where other methods typically fail, low surface energy polymers such as PTFE/PDMS can be joint with significant peel strength using concave shaped tetrapodal ZnO linkers.

Experimental Section

Peel Test Sample Preparation: For PTFE/PDMS samples, a PTFE dispersion was coated onto a glass slide by slip-casting and heated on a hotplate at 120 °C for 10 min for the removal of residual water, then at 290 °C for 10 min in order to remove the surfactant (Tergitol tmn-10) present in the PTFE dispersion, and finally at 350 °C for 30 min when melting occurred. Heating was stopped and the PTFE layer was allowed to solidify. This process was repeated for a second layer, but before heating, ZnO fillers were added with the help of a sieve, shielding part of the sample as a reference for no filler. After allowing the assembly to cool to 20 °C, the PDMS prepolymer and crosslinker mixture (10:1 by weight) was flow coated on top, then heated on a hotplate at 100 °C for 40 min for curing.

For PVB/PDMS samples, a solution of PVB in ethanol was prepared with weight ratio of 1 part PVB: 3 parts ethanol. The solution was slip cast on a glass substrate and ZnO fillers added as described for PTFE above. Another glass slide was placed on top of the ZnO region for a few seconds to press the filler into the viscous PVB solution layer. Ethanol was then evaporated at 20 °C for 24 h and the PDMS layer was coated on top as described above.

Peel Test: Samples were cut into 10 or 20 mm wide sheets. The upper polymer layer (PDMS) was about 1 mm thick and was back-taped with Tesa pressure sensitive adhesive tape (Tesafilm Transparent, Tesa AG, Hamburg, Germany) before the peeling. The sample was fixed on

ADVANCED MATERIALS
www.advmat.de
www.MaterialsViews.com

the peeling tester stage (DS4-Peeling Tester, Tetra GmbH, Ilmenau, Germany) with double-sided tesa tape (Tesa Doppelband AG, Hamburg, Germany). The peeling angle was set at 90° and peeling speed was 0.5 mm s^{-1} with an acceleration rate of 5 mm s^{-2}. The peeling tester was equipped with an additional force sensor sensitive in the direction perpendicular to the direction of peeling, which sends a signal to a feedback circuit for the control system to adjust the speed of horizontal stage movement to ensure a constant peeling angle. In this way, the forces in the perpendicular direction which arise from bending or torsion of the peeled layer were minimized.

Scanning Electron Microscopy (SEM): Before imaging, the sample surfaces were sputter-coated with a 4 nm thick layer of gold and palladium. Images were obtained with a Hitachi-4800 high resolution scanning electron microscope (Hitachi High-Technologies Corp., Tokyo, Japan) at an accelerating voltage of 3 kV.

Supporting Information

Supporting Information is available from the Wiley Online Library or from the author.

Acknowledgements

This project was funded by the German Research Foundation (DFG) under the grant scheme, SFB 677-C10. Y.K.M. thanks the Humboldt Foundation for a Postdoctoral Research Fellowship. R.A. gratefully acknowledges a Heisenberg Professorship by the DFG. Fruitful discussion with Prof. Dr. Franz Faupel is sincerely acknowledged.

Received: May 2, 2012
Revised: July 12, 2012
Published online: August 24, 2012

[1] a) K. G. Budinski, M. K. Budinski, *Engineering Materials: Properties and Selection*, Pearson, London **2009**; b) *High Performance Polymers and Engineering Plastics* (Ed: V. Mittal) John Wiley & Sons, Hoboken NJ **2011**; c) Handbook of Plastics Joining: A Practical Guide (Ed: M. J. Troughton), Plastics Design Library, New York **2008**.
[2] W. Georgette, Gregoire, *French Patent, FR 1 119 221*, **1956**; T. Soc, *French Patent, FR 1 156 405*, **1958**.
[3] J. Comyn, in *Handbook of Adhesives and Sealants*, Vol. *2* (Ed: P. Cognard), Elsevier Science & Technology, Kidlington, UK **2006**.
[4] J. E. Mark, *Polymer Data Handbook*, Oxford University Press, New York **1999**.
[5] a) W. Zhang, W. Sun, J. Yang, Z. Ren, *Appl. Biochem. Biotechnol.* **2010**, *160*, 156–167; b) Y. Mori, T. Inaba, *Biotechnol. Bioeng.* **1990**, *36*, 849–853.
[6] a) Y. Xiu, L. Zhu, D. Hess, C. Wong, "Superhydrophobic Silicone/PTFE Films for Biocompatible Application in Encapsulation of Implantable Microelectronics Devices", presented at *Electronic Components and Technology Conference*, San Diego, USA**2006**; b) C. Sung Hwan, J. Godin, L. Yu-Hwa, *IEEE Photon. Technol. Lett.* **2009**, *21*, 1057–1059.
[7] a) M. Crombez, P. Chevallier, R. C. Gaudreault, E. Petitclerc, D. Mantovani, G. Laroche, *Biomaterials* **2005**, *26*, 7402–7409; b) M. E. Jabbour, F. Desgrandchamps, E. Angelescu, P. Teillac, A. L. Duc, *J. Endourol.* **2001**, *15*, 611–614.
[8] W. Brockmann, P. L. Geiß, J. Klingen, B. Schröder, in *Adhesive Bonding*, Wiley-VCH Verlag, Weinheim, Germany **2009**, pp. 11–28.
[9] a) L. Penn, H. Wang, *Polym. Adv. Technol.* **1994**, *5*, 809–817; b) E. Kang, K. Tan, K. Kato, Y. Uyama, Y. Ikada, *Macromolecules* **1996**, *29*, 6872–6879.
[10] a) N. Inagaki, *Plasma Surface Modification and Plasma Polymerization*, Technomic Pub. Co., Lancaster, USA **1996**; b) *Plasma Surface Modification of Polymers: Relevance to Adhesion* (Eds: M. Strobel, C. S. Lyons, K. Mittal) VSP, Zeist, The Netherlands**1994**; c) K. Chau, B. Millare, A. Lin, S. Upadhyayula, V. Nuñez, H. Xu, V. Vullev, *Microfluid. Nanofluid.* **2011**, *10*, 907–917.
[11] S. W. Lee, J. W. Hong, M. Y. Wye, J. H. Kim, H. J. Kang, Y. S. Lee, "Surface Modification and Adhesion Improvement of PTFE Film by Ion Beam Irradiation", presented at *International Conference on Ion Beam Analysis*, Albuquerque, USA **2003**.
[12] a) S. Wu, E. Kang, K. Neoh, H. Han, K. Tan, *Macromolecules* **1999**, *32*, 186-193; b) K. Kato, E. Uchida, E. T. Kang, Y. Uyama, Y. Ikada, *Prog. Polym. Sci.* **2003**, *28*, 209–259; c) M. Okubo, M. Tahara, Y. Aburatani, T. Kuroki, T. Hibino, *IEEE Trans. Ind. Appl.* **2010**, *46*, 1715–1721.
[13] S. R. Kim, *J. Appl. Polym. Sci.* **2000**, *77*, 1913–1920.
[14] E. Liston, L. Martinu, M. Wertheimer, *J. Adhes. Sci. Technol.* **1993**, *7*, 1091–1127.
[15] V. Zaporojtchenko, J. Zekonyte, S. Wille, U. Schuermann, F. Faupel, *Nucl. Instrum. Methods Phys. Res., Sect. B* **2005**, *236*, 95–102.
[16] J. Y. Lai, Y. Y. Lin, Y. L. Denq, J. K. Chen, *J. Adhes. Sci. Technol.* **1996**, *10*, 231–242.
[17] a) C. Oehr, M. Müller, B. Elkin, D. Hegemann, U. Vohrer, *Surf. Coat. Technol.* **1999**, *116–119*, 25–35; b) K. Watari, T. Iwao, M. Yumoto, *Elect. Eng. Jpn.* **2012**, *178*, 1–7.
[18] S. Ebnesajjad, P. R. Khaladkar, *Fluoropolymers Applications in Chemical Processing Industries: the Definitive User's Guide and Databook*, William Andrew Publishing, New York **2005**.
[19] *Handbook of Adhesi on* (Ed: D. E. Packham), John Wiley & Sons, Chichester, UK **2005**.
[20] a) D. M. Bigg, *Polym. Compos.* **1987**, *8*, 115–122; b) F. L. Matthews, R. D. Rawlings, *Composite Materials: Engineering and Science*, Woodhead Publishing Ltd, Cambridge, UK **1999**.
[21] G. M. Su, K. Best, T. Ranganathan, T. Emrick, A. J. Crosby, *Macromolecules* **2011**, *44*, 5256–5261.
[22] a) R. Adelung, S. Kaps, Y. K. Mishra, M. Claus, T. Preusse, C. Wolpert, *German Patent, DE 2011/000282*, **2011**; b) M. Mecklenburg, A. Schuchardt, Y. K. Mishra, S. Kaps, R. Adelung, A. Lotnyk, L. Kienle, K. Schulte, *Adv. Mater.* **2012**, *24*, 3437–3437.
[23] K. Kendall, *Science* **1994**, *263*, 1720–1725.
[24] a) O. Allix, P. Ladeveze, *Compos. Struct.* **1992**, *22*, 235–242; b) *Fracture Mechanics Testing Methods for Polymers, Adhesives, and Composites*, Vol. *28* (Eds: D. R. Moore, A. Pavan, J. G. Williams), Elsevier Science, Kidlington, UK **2001**.
[25] N. G. McCrum, C. Buckley, C. B. Bucknall, *Principles of Polymer Engineering*, Oxford University Press, New York **1997**.

3. Summary and Outlook

A high yielding mild procedure for the stannylation of azobenzenes using a microwave enhanced Stille Kelly reaction with hexamethyldistannane was developed. The suitability of tin functionalized azobenzes as nucleophiles for Stille cross coupling reactions could be demonstrated. Furthermore, tin functionalized azobenzenes offer access to quantitative lithiation of azobenzenes by tin-lithium exchange (*Chem.-Eur. J.* **2015**, *submitted*). It could be shown that the methodology of lithiating azobenzenes by transmetalation from tin is of general practical use by offering a synthetic route to a huge variety of azobenzene derivatives. In addition the lithiation of azobenzene offers an efficient pathway to the functionalization with silanes. Using this methods, silanol functionalized azobenzenes could be synthesized which served as monomer for main chain liquid crystalline siloxane polymers. This type of polymer deforms strongly when irradiated with UV light. Besides the synthesis of a new polymer type, preliminary work on the design for devices shows that a photomechanical responsive film undergoes a more efficient bending behavior with increasing porosity. For the design of bi-layered composite materials, a methodology was developed to attach polymer films without the need for a chemical modification. The efficiency of this methodology was demonstrated by joining PTFE and PDMS films which usually could not be attached to each other before.

The azobenzenes-siloxane copolymer was able to switch in solid phase and a reversible back switching of the azobenzenes could be observed. During UV irradiation (365 nm), a macroscopical deformation could be observed. During the re-isomerization from *cis* to *trans,* (by irradiation with 450 nm and thermally) no macroscopic shape change was visible. It is assumed that the photoisomerization of the azobenzene to the *cis* form destroys the local order of the azobenzenes within the material in the depth of penetration of the UV light. Due to the loss of the alignment of the azobenzenes, the re-isomerization to the *trans* is invisible on the macroscopic scale. Chemically cross-linked polymers are likely to increase the strength of the photomechanical effect and may aide *reversible* macroscopic switching. They would probably serve as a shape memory which is independent of irradiation with light. To maintain the advantage of the easy processability of the material, a subsequent cross-linking of the material after molding would be favorable. This should be achievable using two main routes.

a) The incorporation of vinyl groups into the polymer chains which allow a subsequent radical or thermal cross linking.
b) The condensation of the end groups with branching curing agents.

Following route a) would allow the efficient cross-linking of high molecular weight polymers. During the polymerization process, a defined percentage of methylvinyl-siloxane groups could be used as cross linkable units which are randomly copolymerized. The synthesis of the vinyl functionalized monomer **15** is analogous to monomer **11** and has already been synthesized in large amounts (see experimental part for details – chapter 4.3). The cross-linking would be initiated by light or the addition of a free radical initiator. This could be a thermal initiator or a photoinitiator. An appropriate amount of vinyl groups has to be found which give the best compromise of an adequate glass transition temperature and photomechanical response. The main advantage is the precise control of the degree of cross linking by the amount of vinyl functionalized monomers.

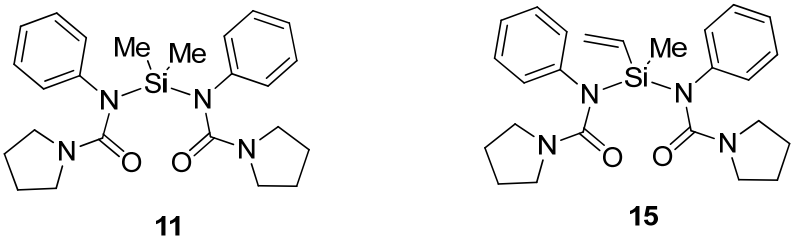

Scheme 14. Monomers for cross-linkable azobenzene-siloxane polymers.

Route b) relies on a cross linking using branches connecting the ends of the polymer chains (Scheme 15). The advantage of this methodology is the easy cross-linking of polymer chains. Typically, a mixture of the polymer and the curing agent is casted as a film and heated. This way of cross linking strongly depends on the molecular weight of the polymer. Especially high molecular weights limit the degree of cross-linking.

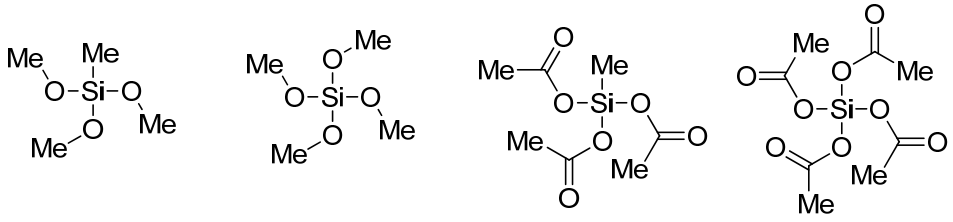

Scheme 15. Possible curing agents for End-group crosslinking.

If a cross-linked material shows a reversible photomechanic switching behavior, an optimal cross linking degree must be found which keeps the glass transition temperature at ambient temperatures and allows an efficient shape change. To improve the switching behavior, a proper alignment technique must be applied to the polymer. As more azobenzenes are oriented in the same direction, the more controlled and efficient the macroscopic switching effect should occur. Alignment techniques for main chain liquid crystalline polymers are e.g. slit coating[67] or blade coating.[68] Alignments and their optimization must be studied by solid state NMR and small angle X-ray scattering. The effect must be characterized by comparison of the bending forces and angles.

In terms of preparing the photoswitchable dry adhesive as outlined in the introduction, the following further steps need to be taken: Zinc oxide microparticles must be added to the material and its effect on the photoresponsivity must be studied. As final step, a bilayered device must be fabricated and the adhesive behavior must be studied. If the concept proves to work, copolymers with different ratios of meta substituted azobenzene units must be produced and studied, whether the mechanical response and the adhesive properties can be affected.

4. Experimental Part

4.1 Supporting Information for *J. Org. Chem.* 2014*, 79, 1719-1728.*

Supporting Information

for

Tin Functionalized Azobenzenes as Nucleophiles in Stille Cross Coupling Reactions

Jan Strueben[1], Paul J. Gates[2], and Anne Staubitz[1,]*

[1]*Otto-Diels-Institute for Organic Chemistry, University of Kiel, Otto-Hahn-Platz 4, 24098 Kiel (Germany)*

[2]*School of Chemistry, University of Bristol, Cantock's Close, Bristol BS8 1TS (UK)*

* *astaubitz@oc.uni-kiel.de*

Abbreviations

A	area
Azo	Azobenzene (and derivatives)
Fur	furanyl
M.p.	melting point
MW	microwave
RF	response factor
s	strong (concerning the intensity) (IR)
w	weak (concerning the intensity) (IR)

Reagents

Reagent	Purity
1-Bromo-4-nitrobenzene	99%
2-Bromo-1,4-dimethoxybenzene	98%
3-Bromoanisole	98%
3-Bromopyridine	99%
4-Bromoacetophenone	98%
4-Bromobenzonitrile	99%
1-Bromo-2,5-dimethoxybenzene	98%
4-Bromo-*N*,*N*-dimethylaniline	97%

5-Bromo-2-furoic acid	99%
5-Bromofuran-2-carbaldehyde	99%
4-Bromo-1,2-(methylenedioxy)benzene	98%
Bromobenzene	99.5%
Copper chloride	97%
Hexamethyldistannane	99%
Hexabutyldistannane	95%
4-Iodoaniline	98%
Magnesium sulfate	99%
4-Methylaniline	99+%
Lithium chloride	99% (anhydrous)
$[Pd(PPh_3)_4]$	>98%
Potassium peroxomonosulfate	>98%

If not otherwise noted, all reagents were used as received.

Due to the toxicity of organo tin compounds, certain precautions should be observed: All manipulations should be performed in a well vented fume cupboard, wearing standard eye protection, lab coats and nitrile gloves with the specification: EN374-1:2003 "Protection against chemical splash."

Care needs to be taken to observe proper disposal procedures for all waste products, according to the health and safety procedures in place. Under no circumstances should these compounds be disposed of in the drains or allowed to leak in any other way into the environment.

GC Optimization Reactions

GC analysis was performed on gas chromatograph equipped with a (5%-phenyl)-methylpolysiloxane column (30 m length, 0.32 mm diameter, 0.25 µm grain size) and a flame ionization detector (FID).

The formation of 4-(4-trimethylstannyl-) 4'-methylazobenzene for the optimization reactions was determined by GC by a multiple point internal standard method. 1,3,5-Triisopropylbenzene was used as reference analyte. Yields were calculated corresponding to the following equation:

$$n(analyte) = \frac{A(analyte)}{A\,(reference)} \frac{n(reference)}{RF}$$

Where *n* is the amount of substance; A the integrated area of a signal and RF a system specific response factor. Standard solutions of different ratios of 4-(4-trimethylstannyl-)4'-(4-methyl-) azobenzene (**1**) and 1,3,5-triisopropylbenzene were measured to obtain the calibration curve. The response factor RF=0.86094 (+/- 0.05249) was obtained from the slope of the following calibration curve (**Figure SI 1**).

Solvents

All solvents were freshly distilled, if used for purification. Where noted, solvents were dried over the specified drying agent by refluxing for several hours before distillation. Dry solvents were degassed by three freeze-pump-thaw cycles and stored in a nitrogen filled glove box over 3 Å molecular sieves.

Solvent	drying procedure
Acetonitrile	Dried over phosphorus pentoxide
Cyclohexane	-
Chloroform	-
DCM	Dried over phosphorus pentoxide
Dioxane	Dried over $LiAlH_4$ with triphenyl methane as indicator.
DMF	Purchased as extra dry, stored over 3 Å molecular sieves, flushed with nitrogen.
DMSO	Purchased as extra dry, stored over 3 Å molecular sieves, flushed with nitrogen.
Ethanol	-
Ethyl acetate	-
Methanol	-
Pyridine	Dried over calcium hydride
THF	Dried over LiAlH4 with triphenyl methane as indicator.
Toluene	Dried over Sodium with benzophenone as indicator.

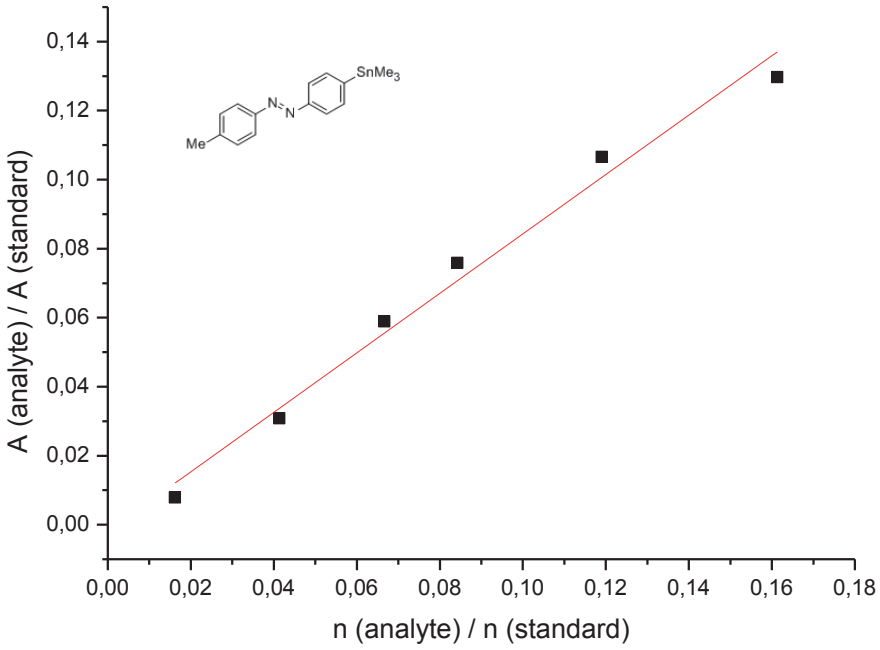

Figure SI 1. Calibration curve for 4-(4-trimethylstannyl-) 4'-methylazobenzene (**1**) using 1,3,5-triisopropylbenzene as an internal reference substance.

NMR Spectra (^{1}H NMR and ^{13}C NMR)

4-Iodo-4'-methylazobenzene (10)

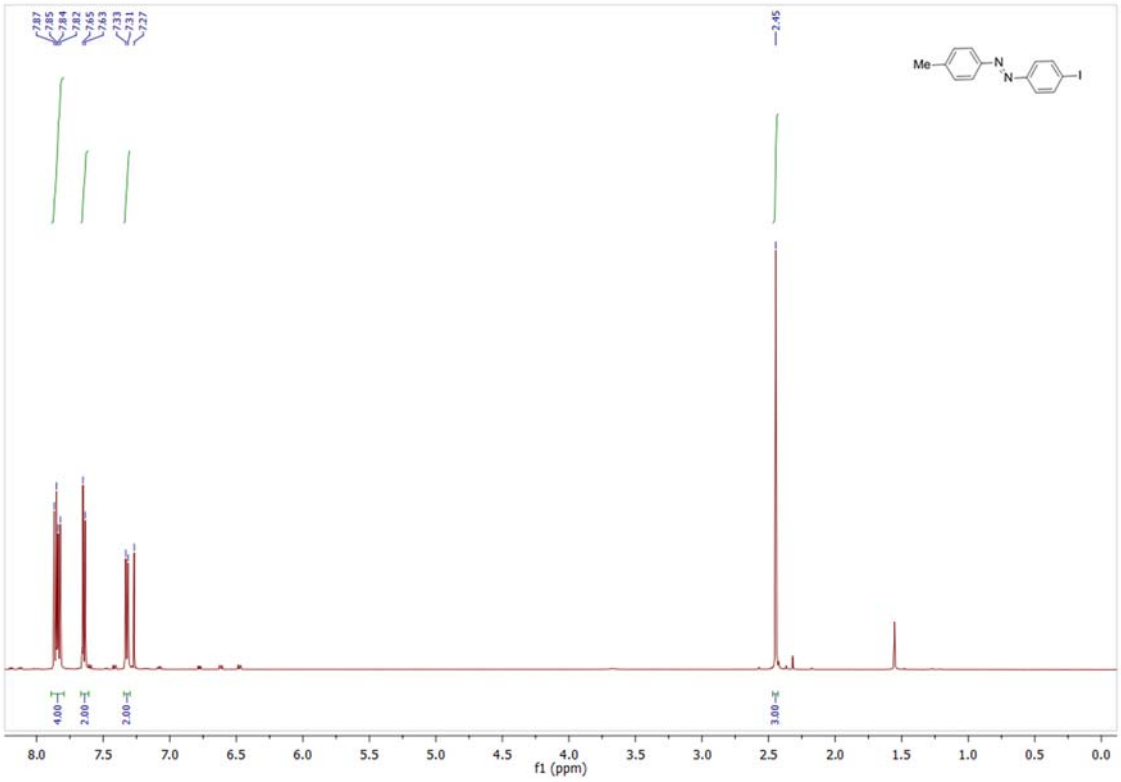

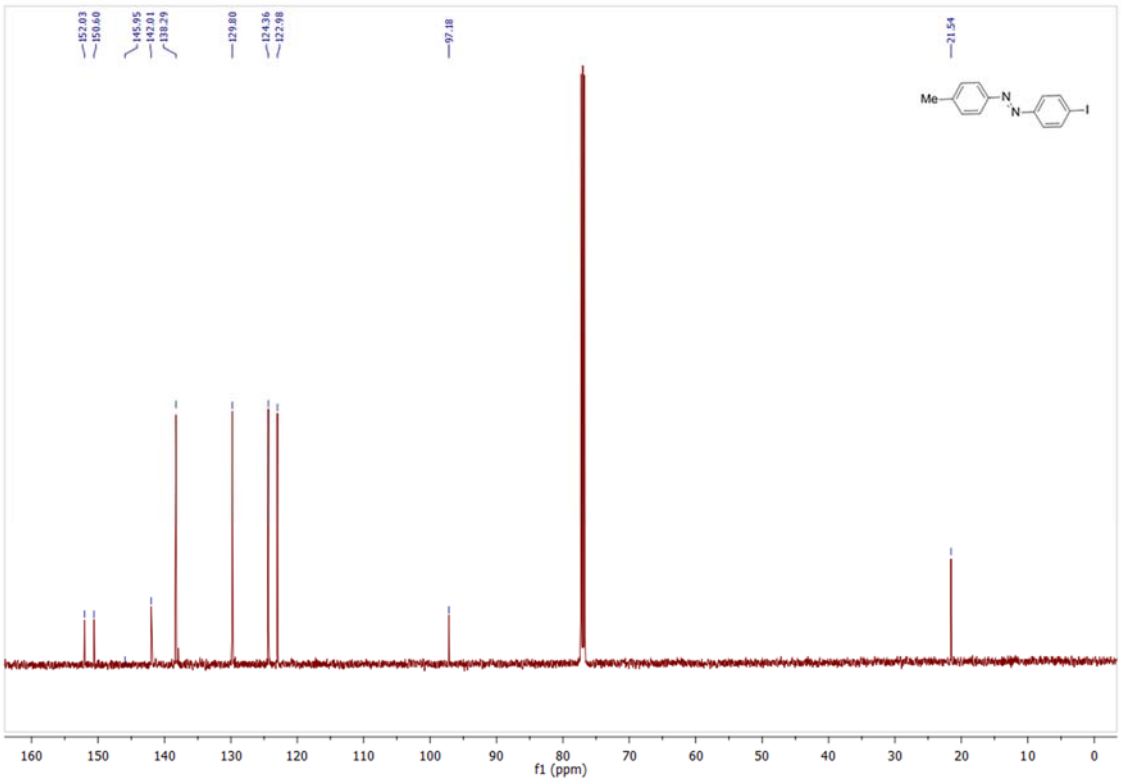

4-Methyl-4'-(trimethylstannyl-)azobenzene (11)

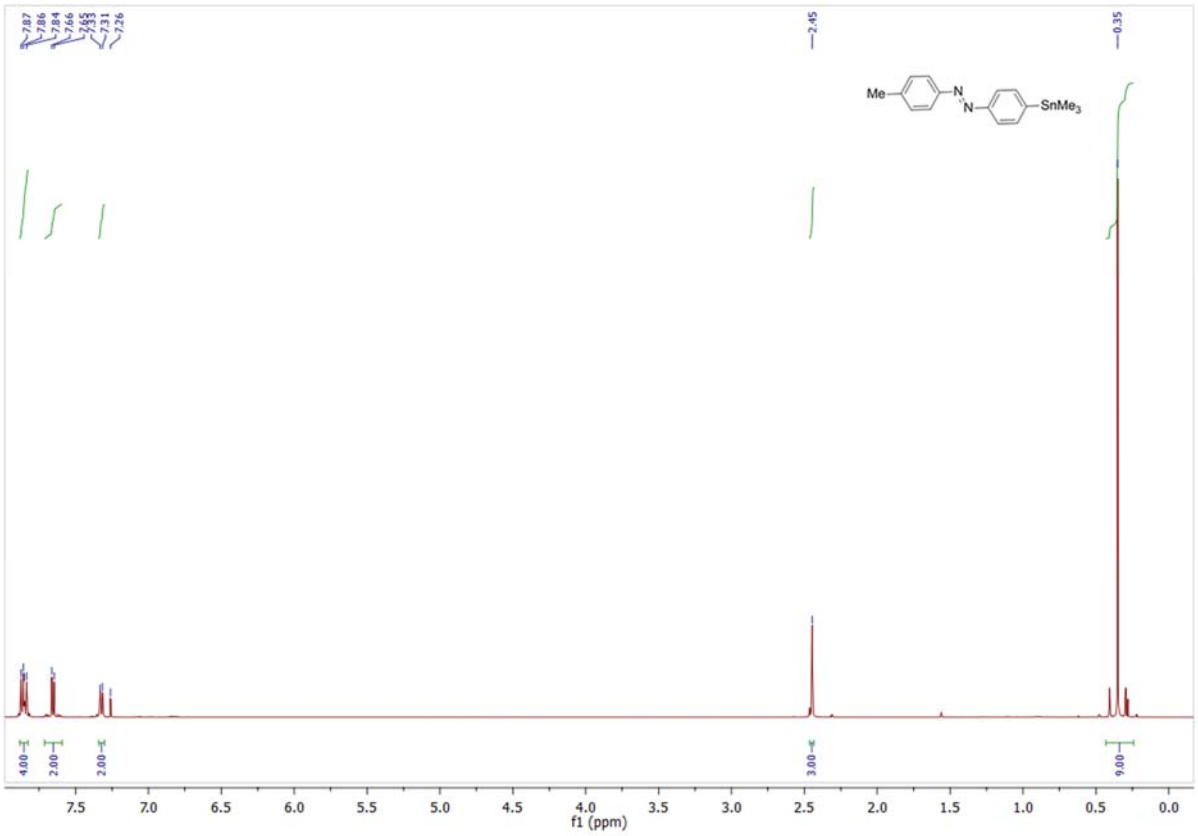

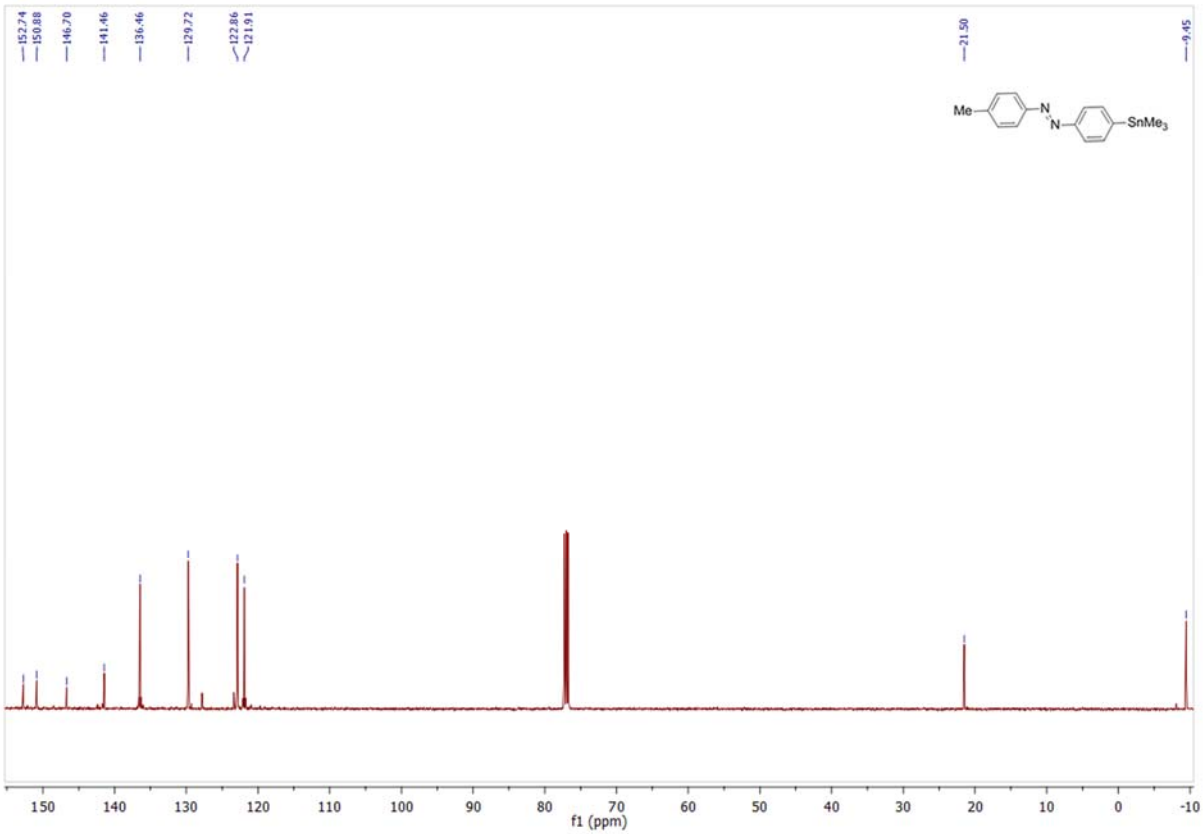

4-Methyl-4'-(tri-*n*-butylstannyl-)azobenzene (12)

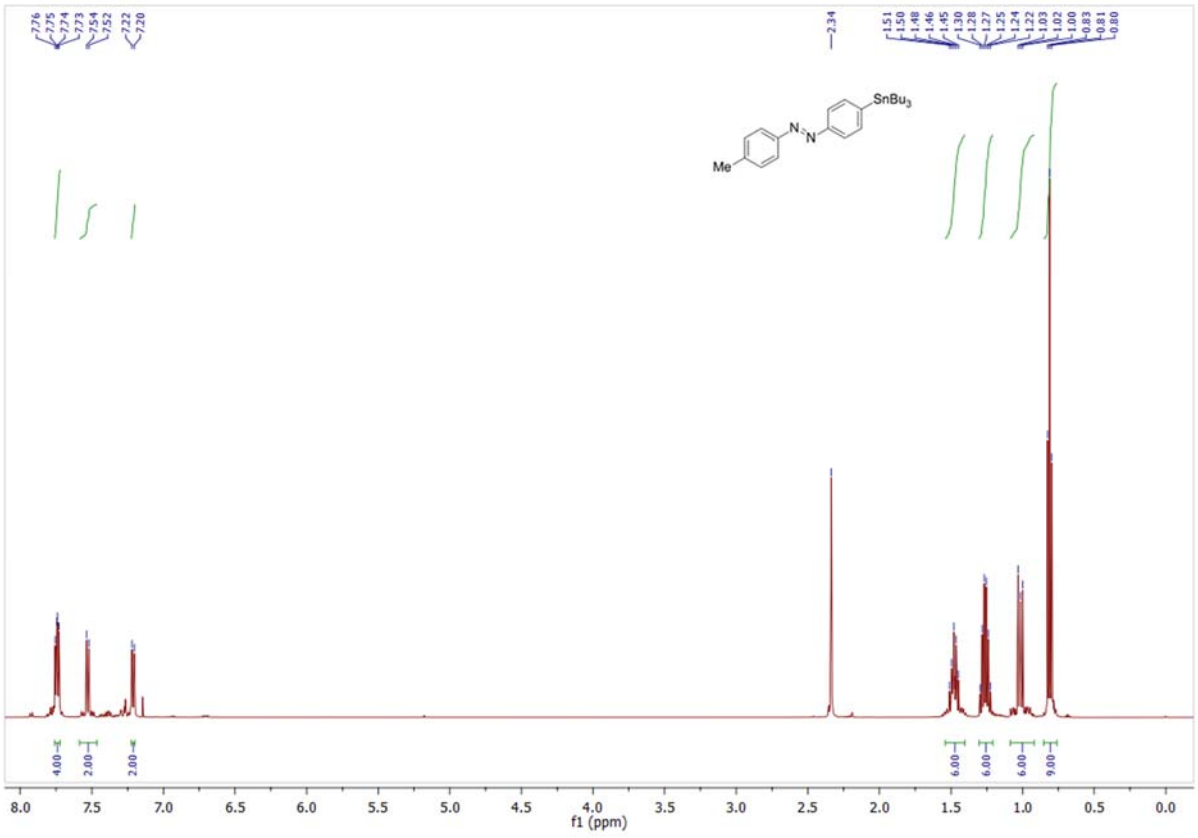

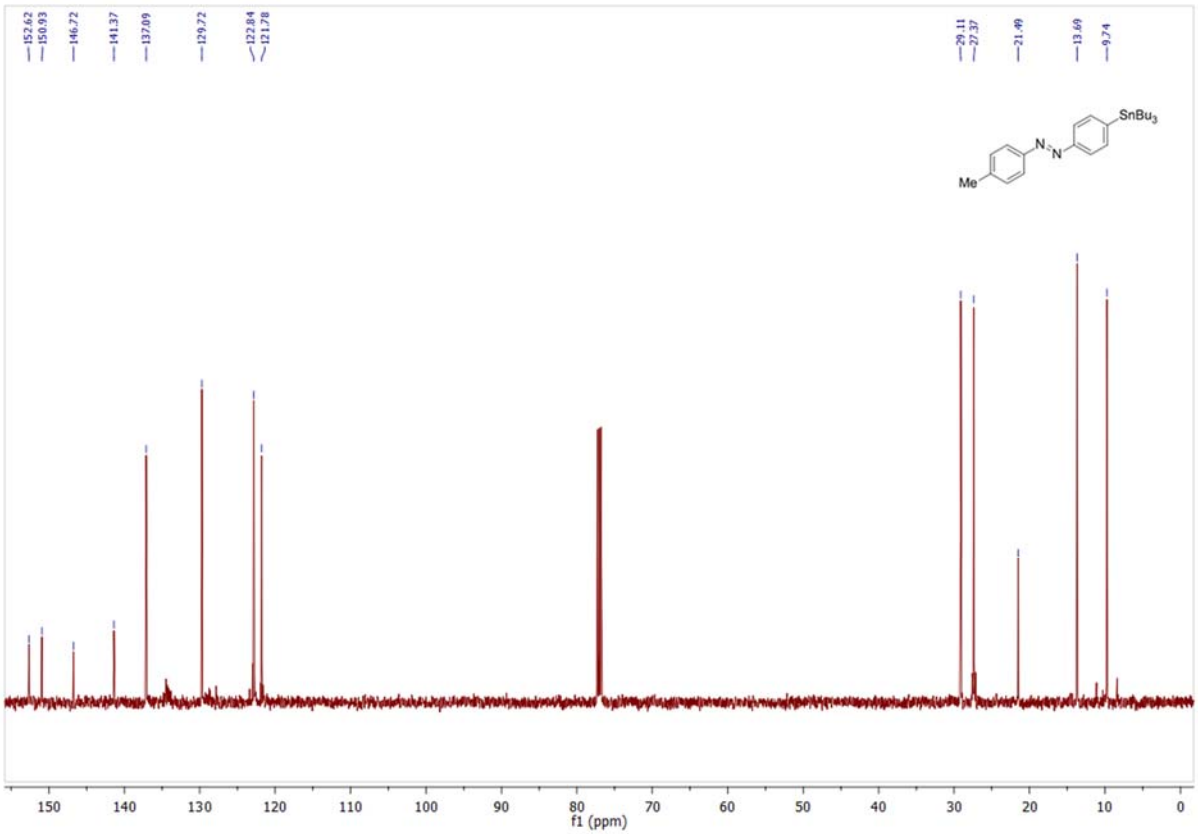

4,4‘-*bis*(Iodo-)azobenzene (13)

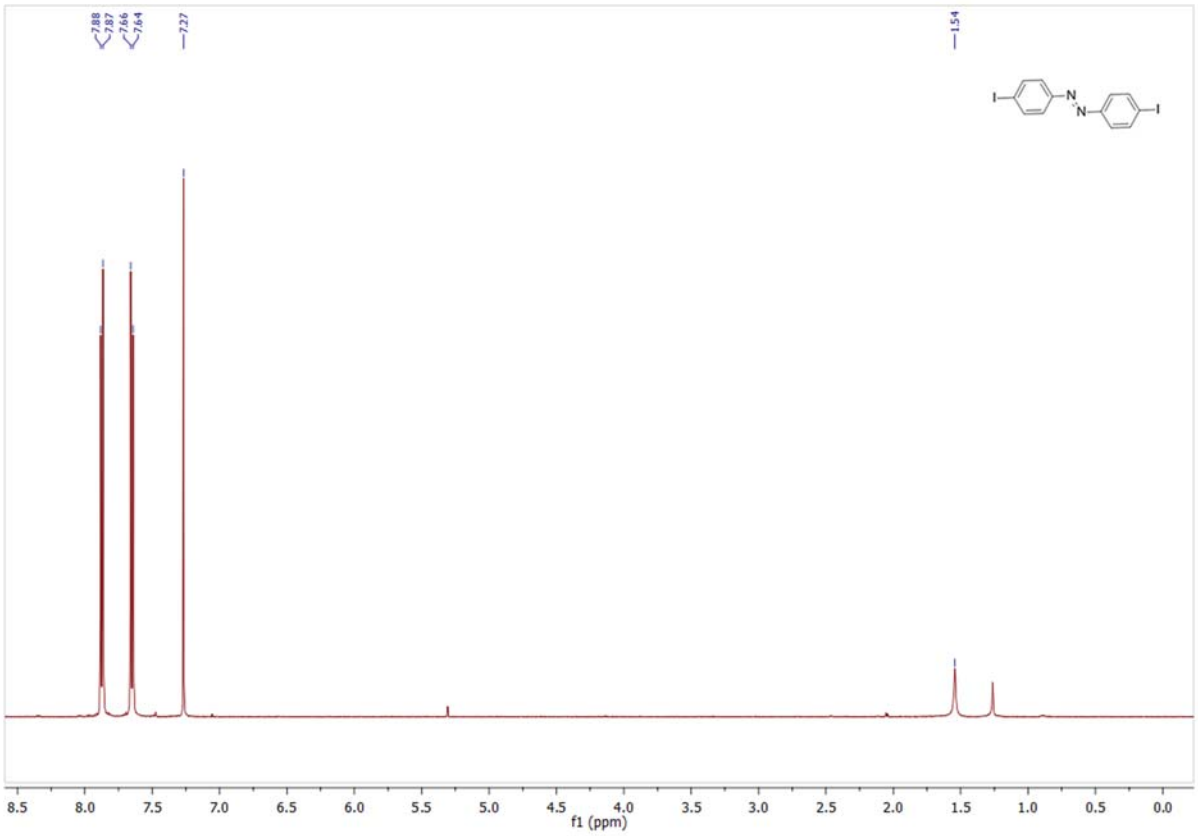

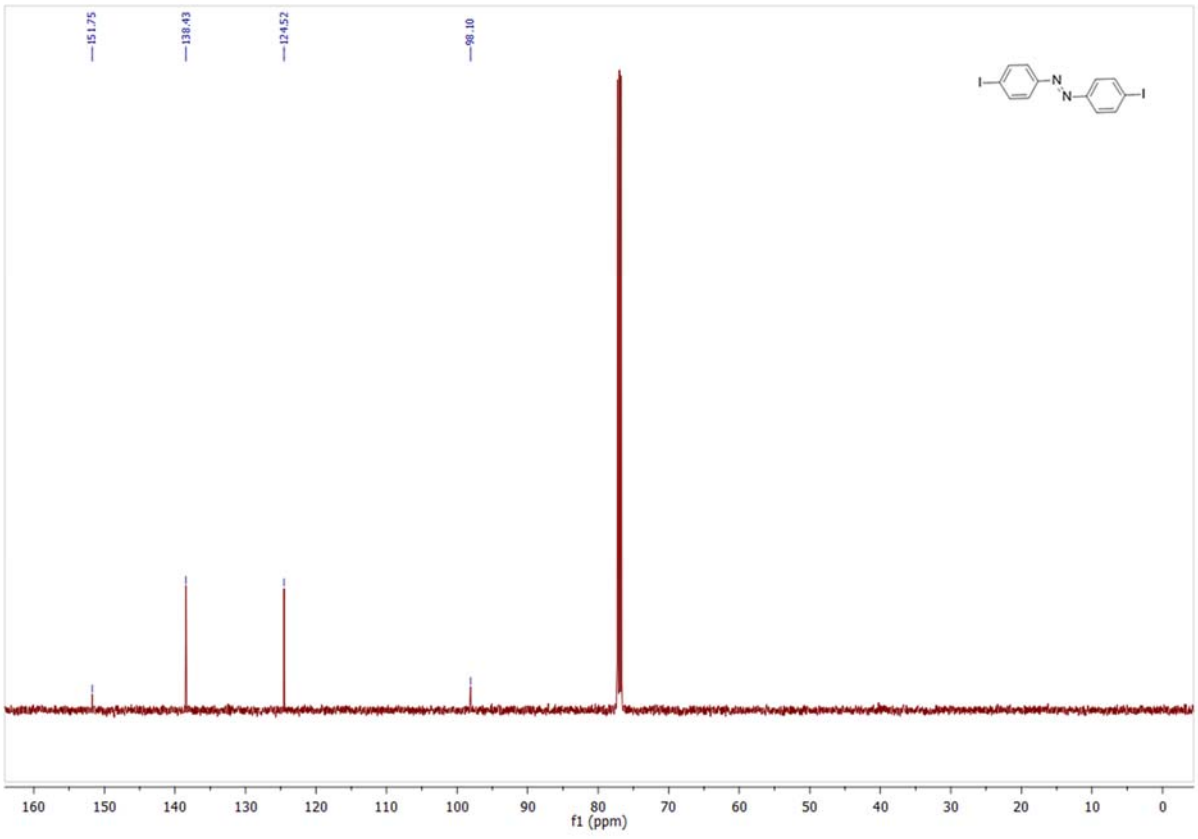

4,4‘-*bis*(Trimethylstannyl-) azobenzene (14)

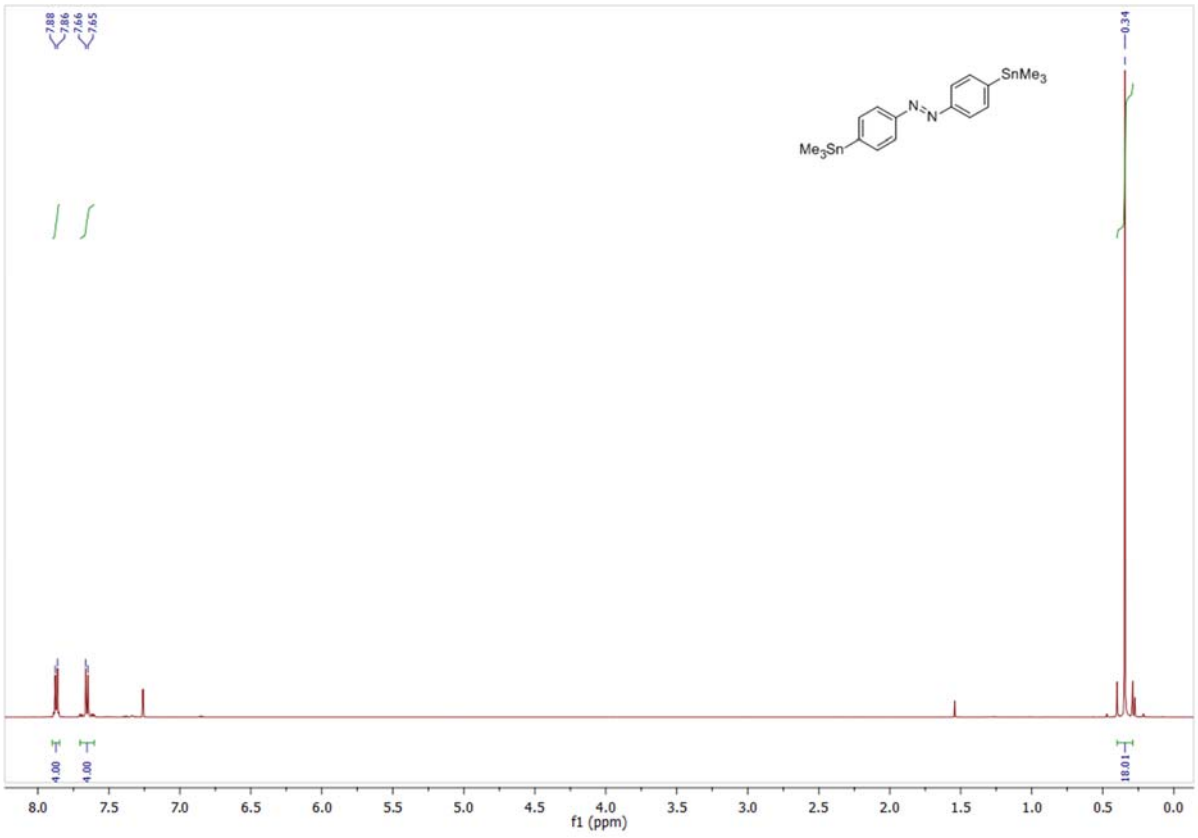

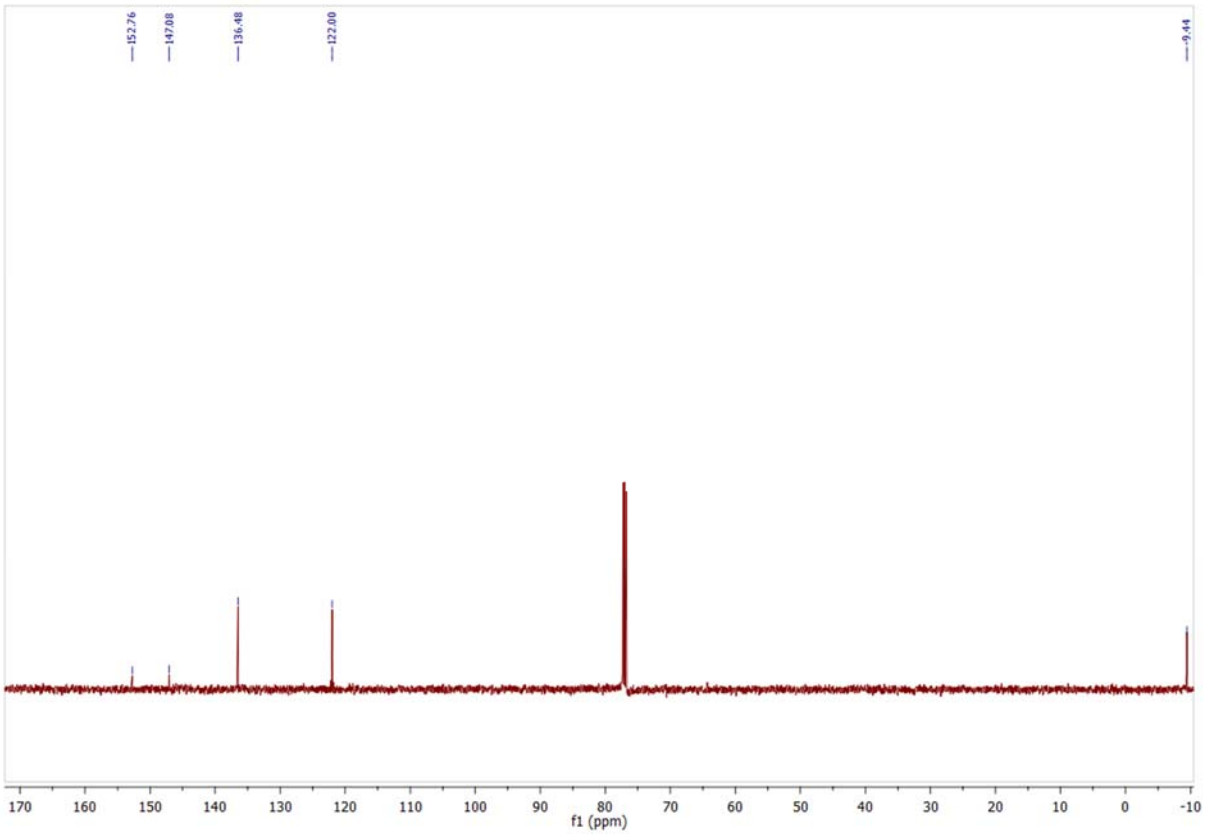

4,4‘-*bis*(Tri-*n*-butylstannyl-)azobenzene (15)

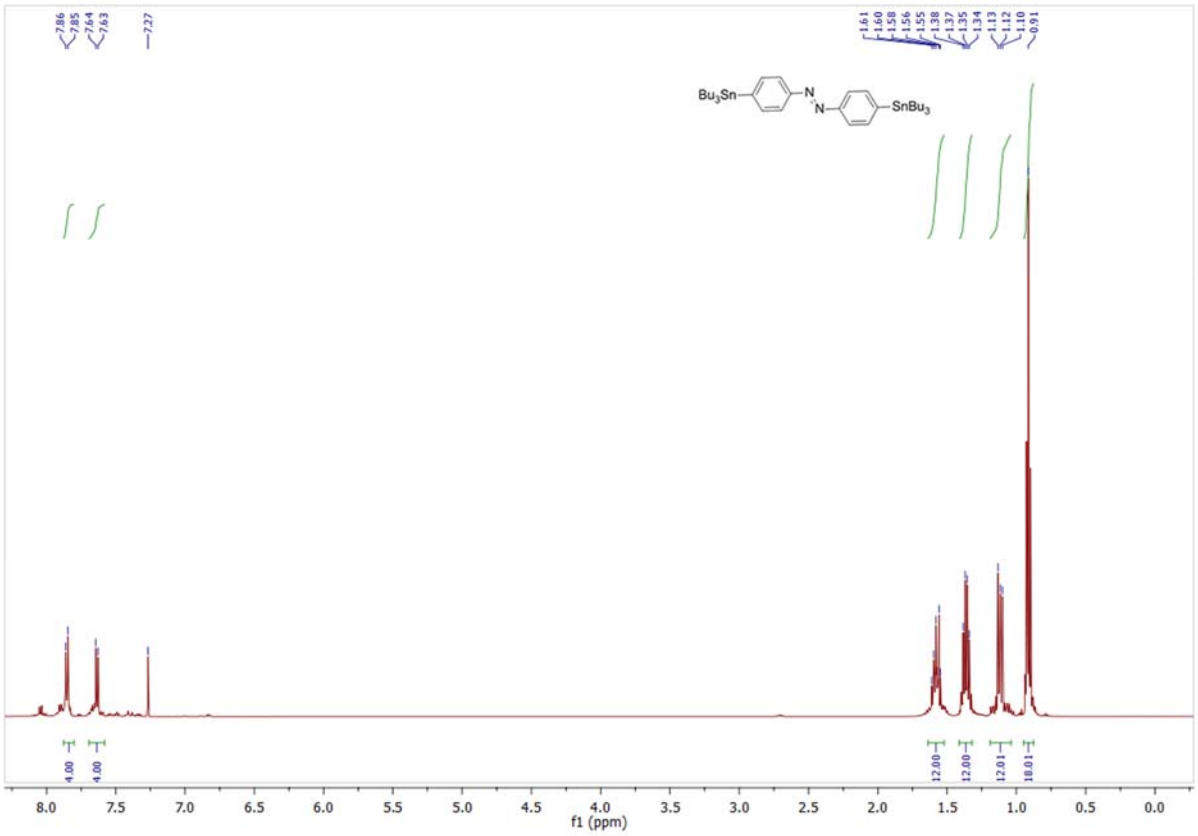

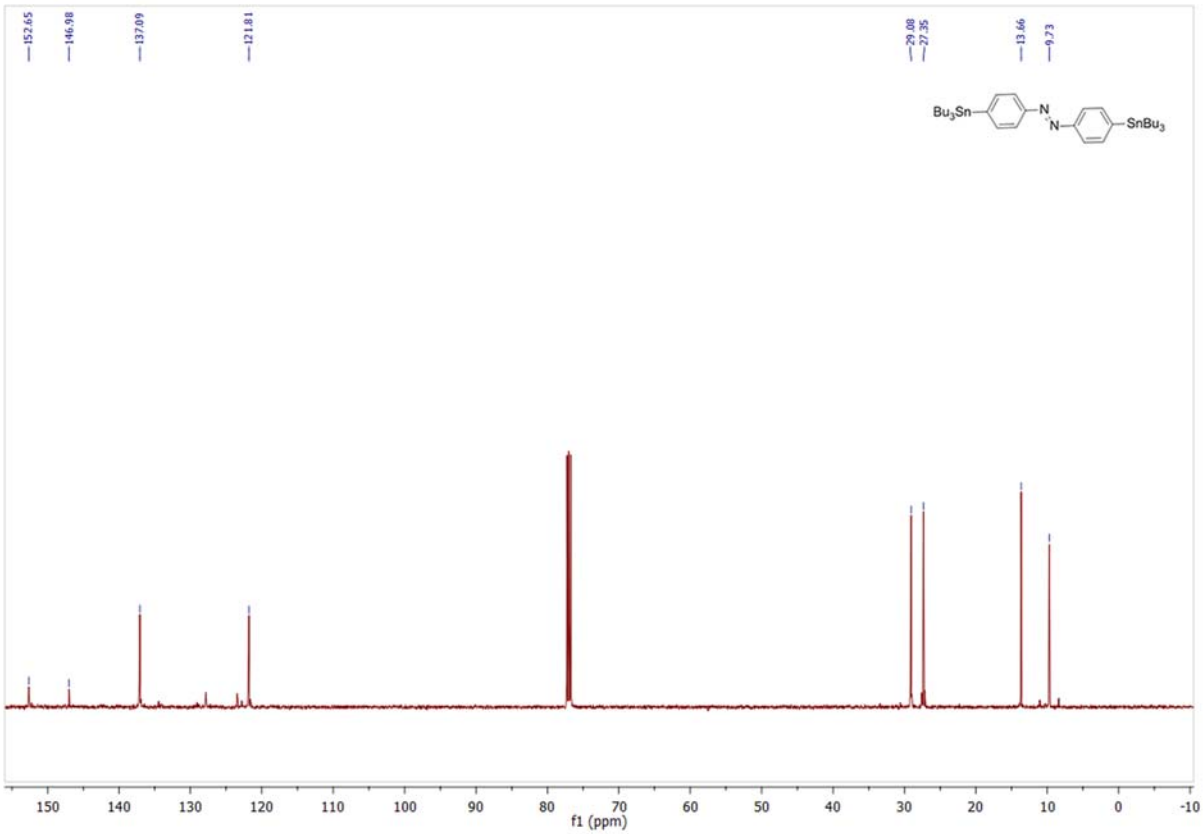

4-(4-Nitrophenyl-) 4'-methylazobenzene (17)

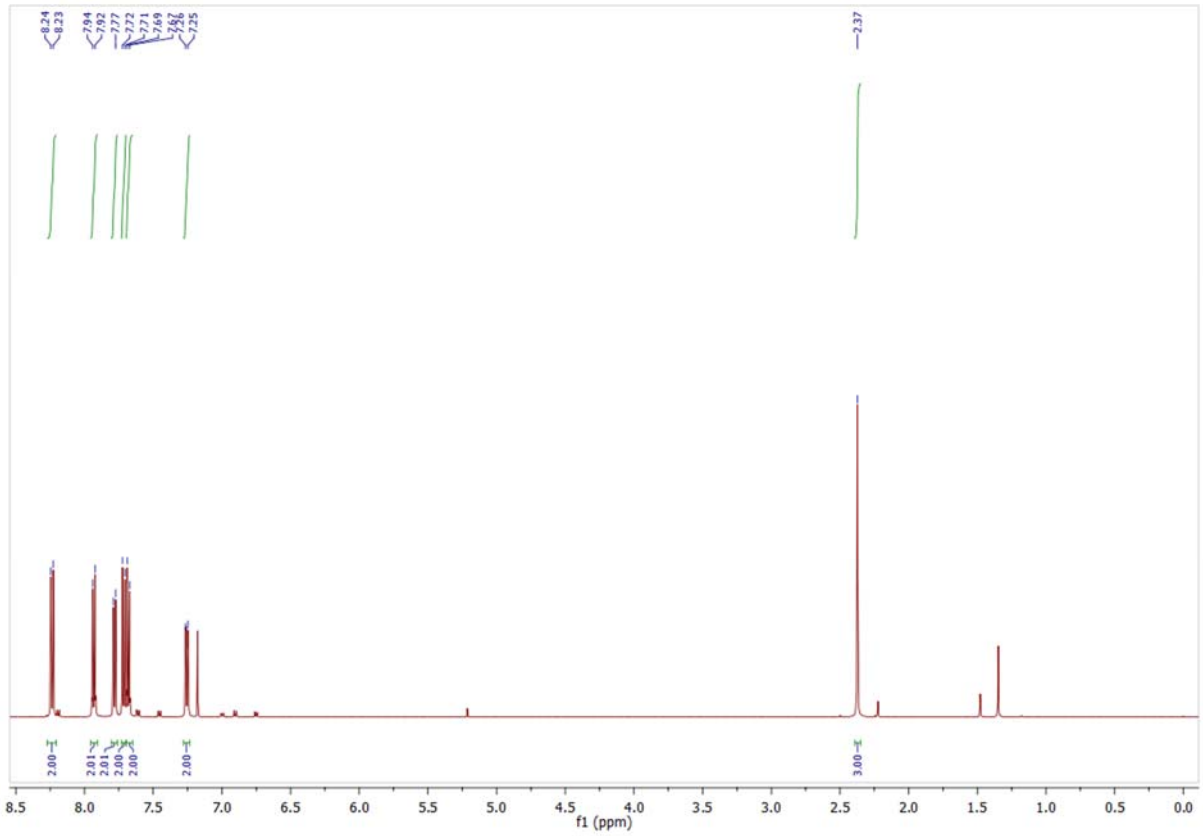

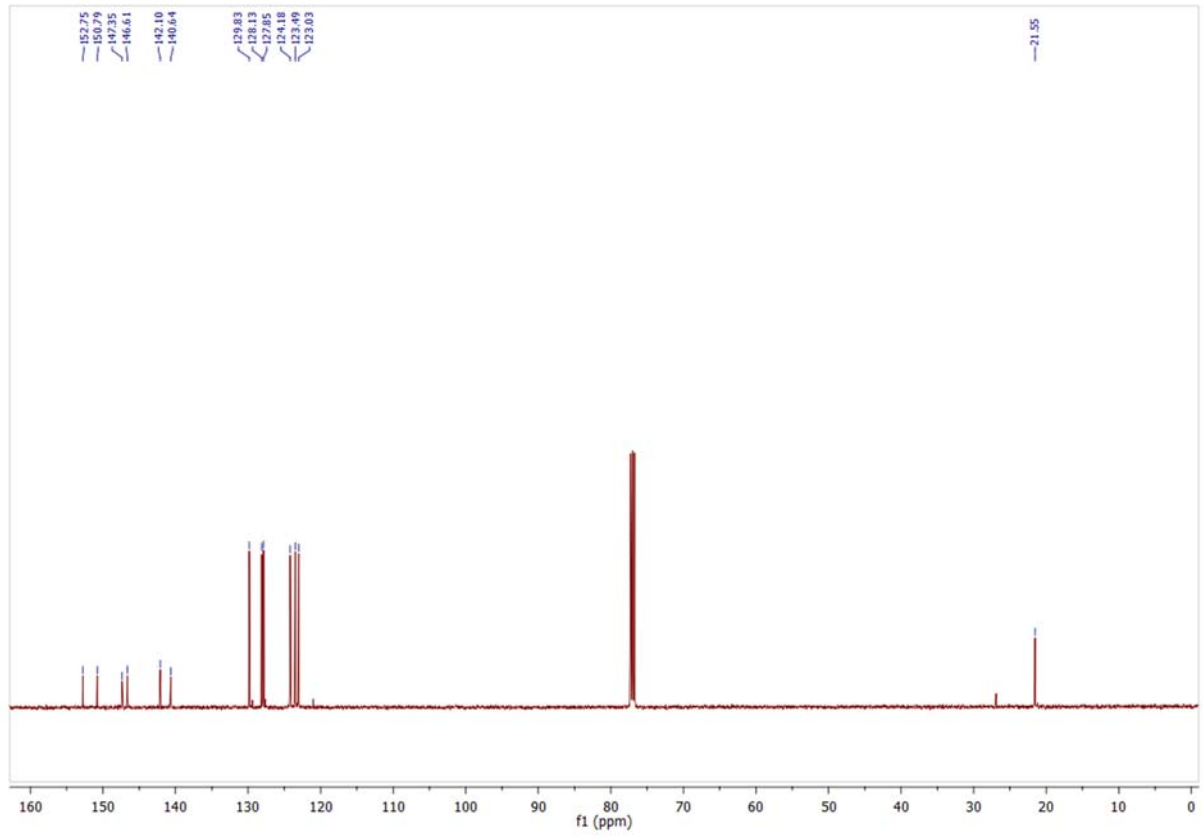

4-(4-Cyanophenyl-) 4’-methylazobenzene (20)

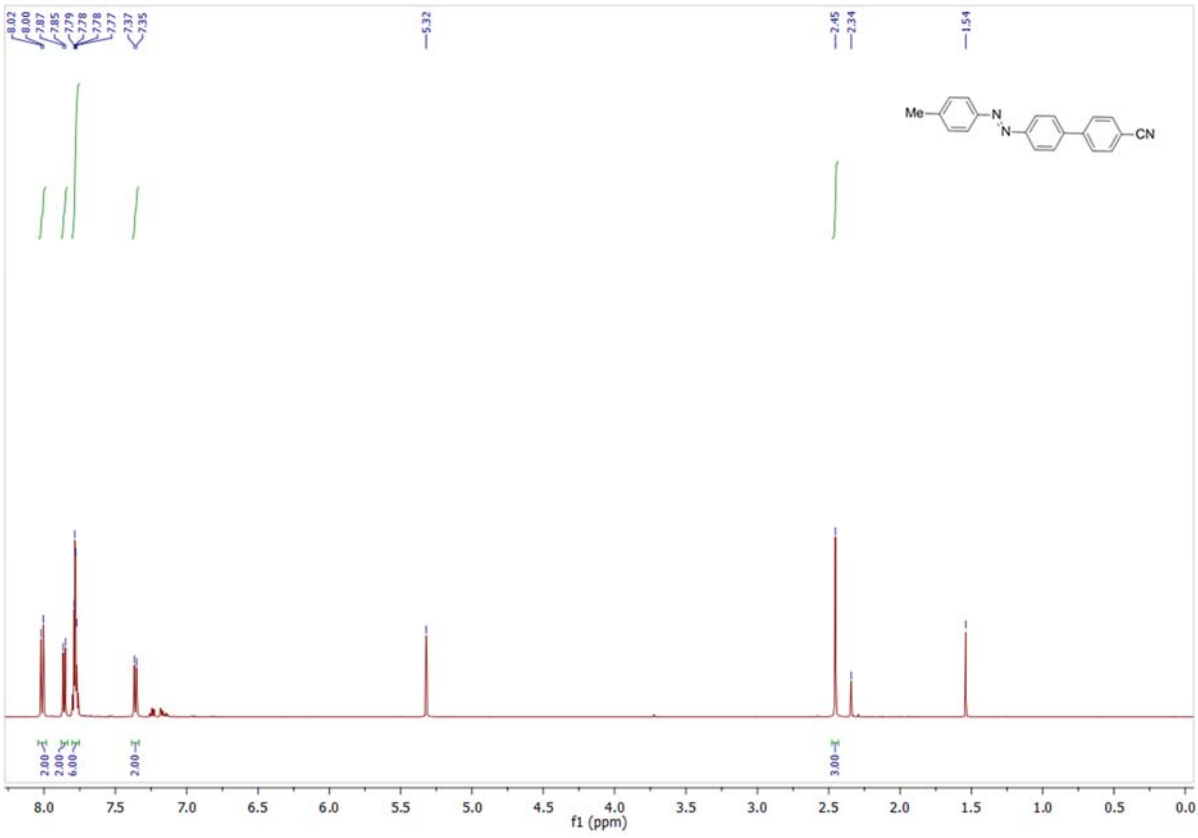

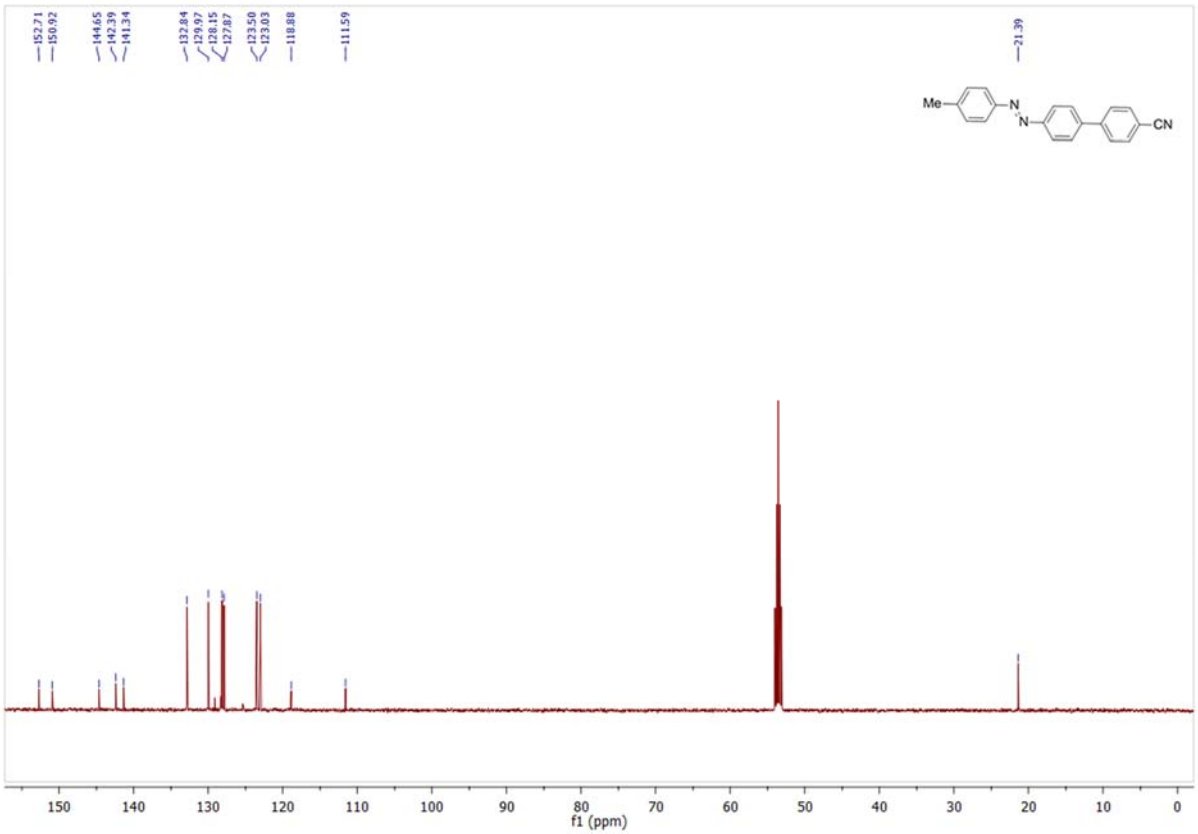

4-(4-Acetylphenyl-) 4’-methylazobenzene (21)

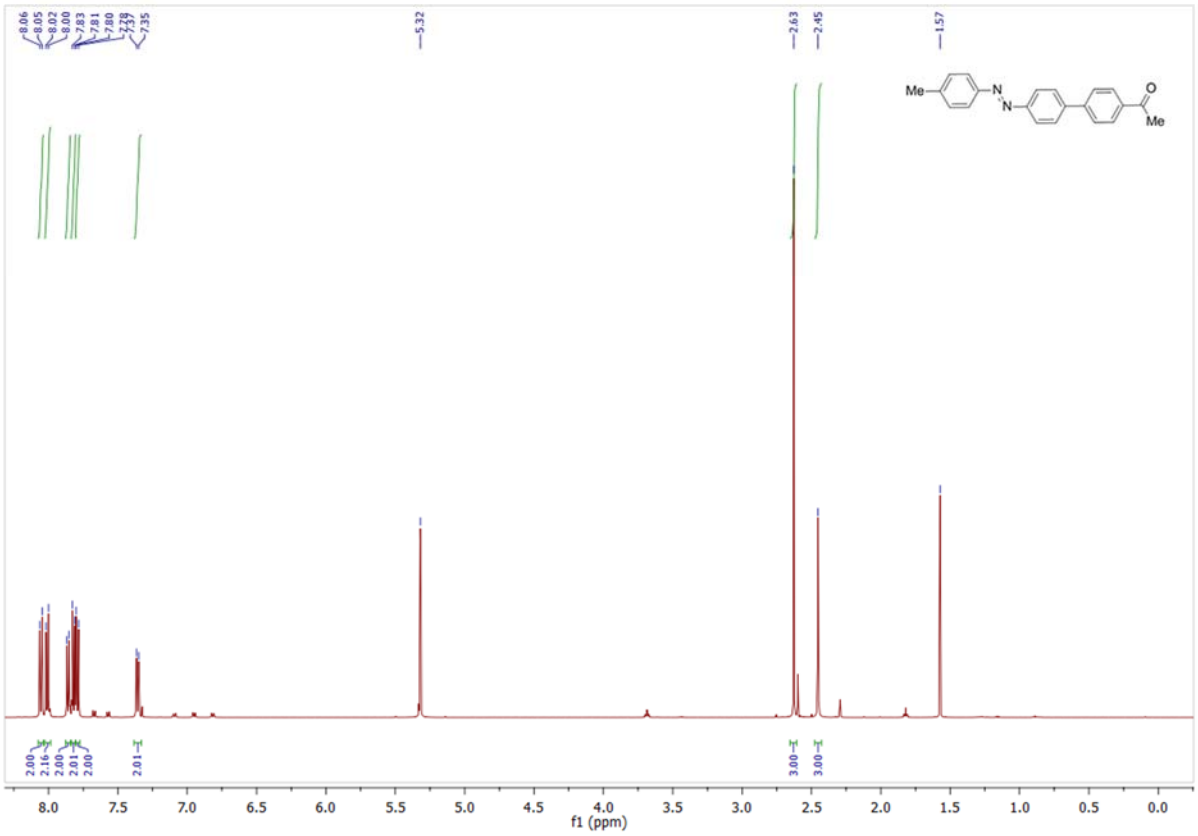

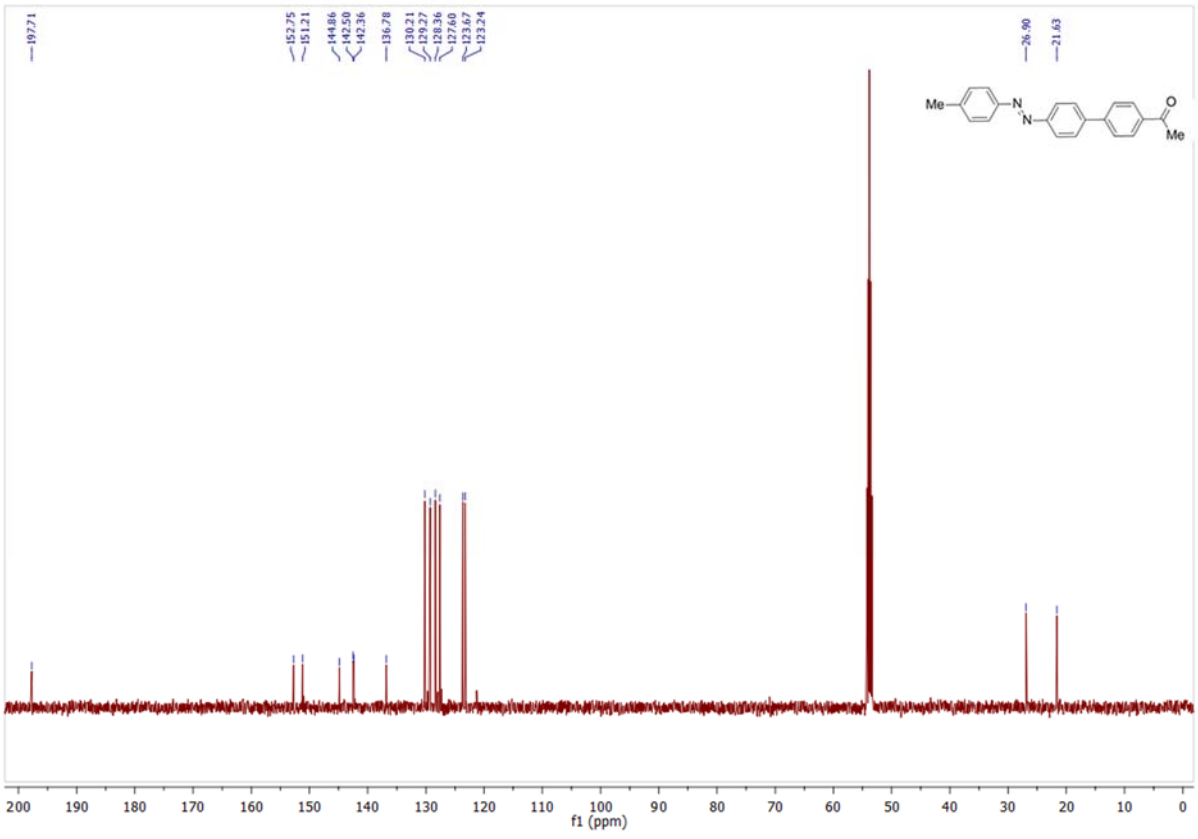

4-Phenyl- 4’ -methylazobenzene (23)

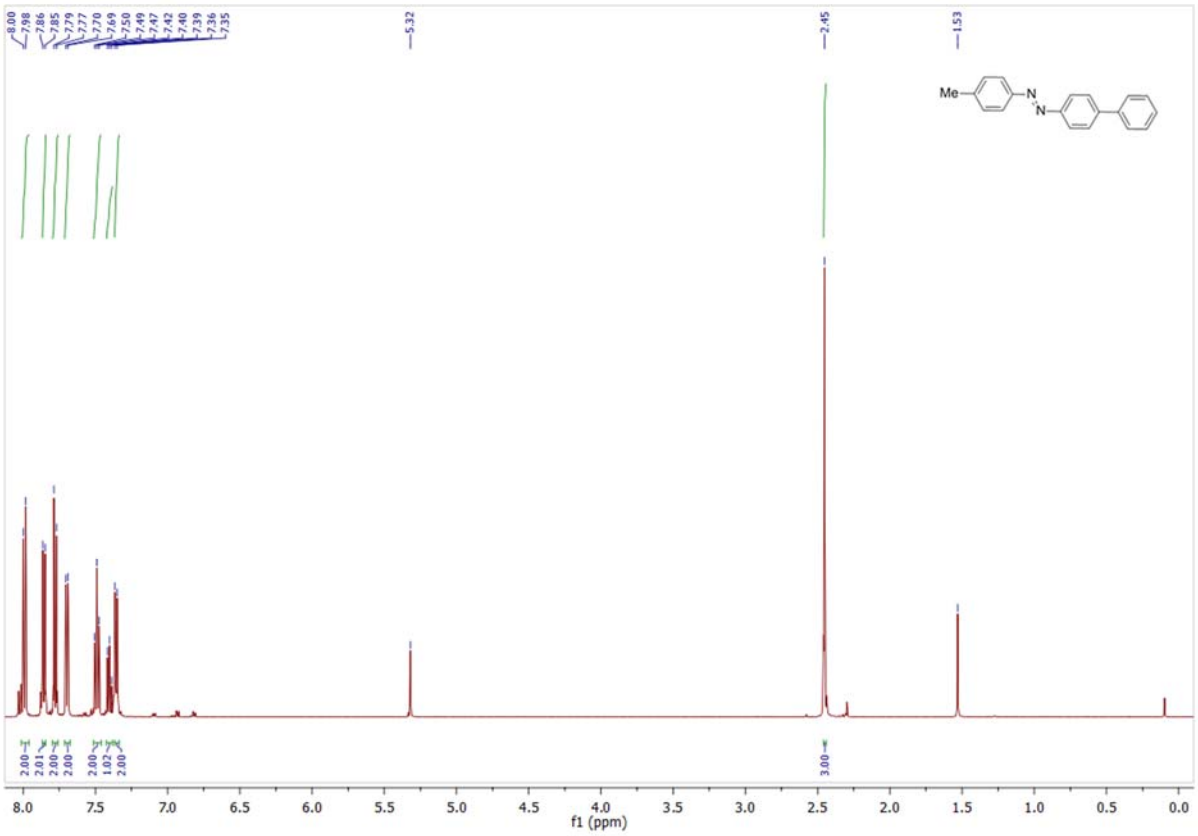

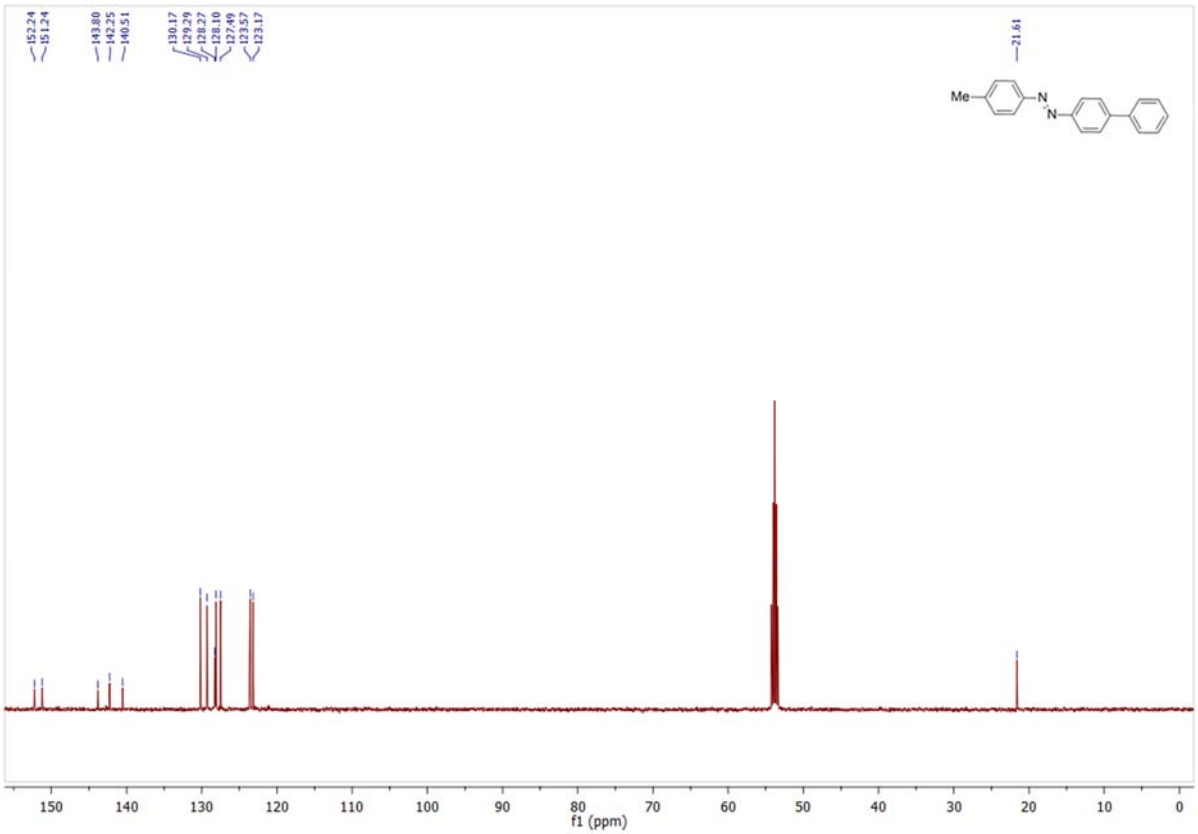

4-(2-Furanyl-5-aldehyd-) 4'-methylazobenzene (25)

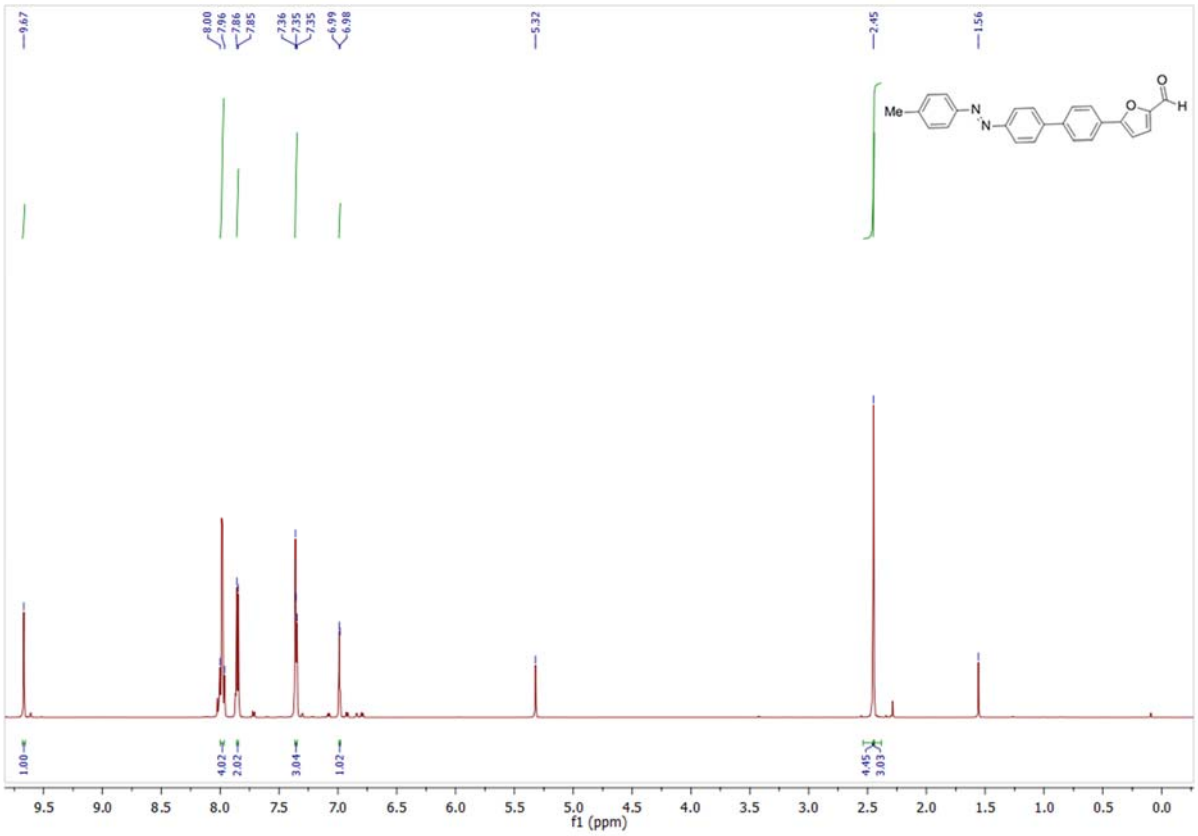

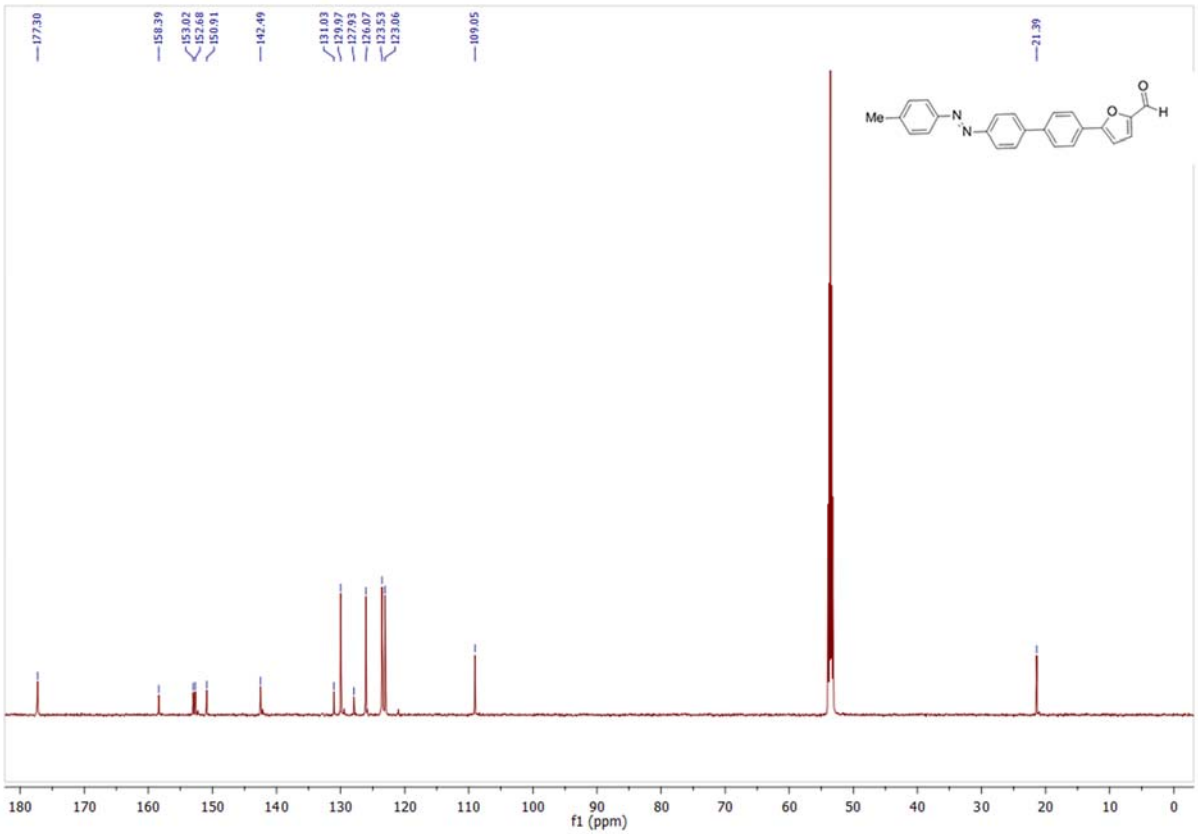

4-(5-Methylcarboxylate-2-furanyl-) 4'-methylazobenzene (27)

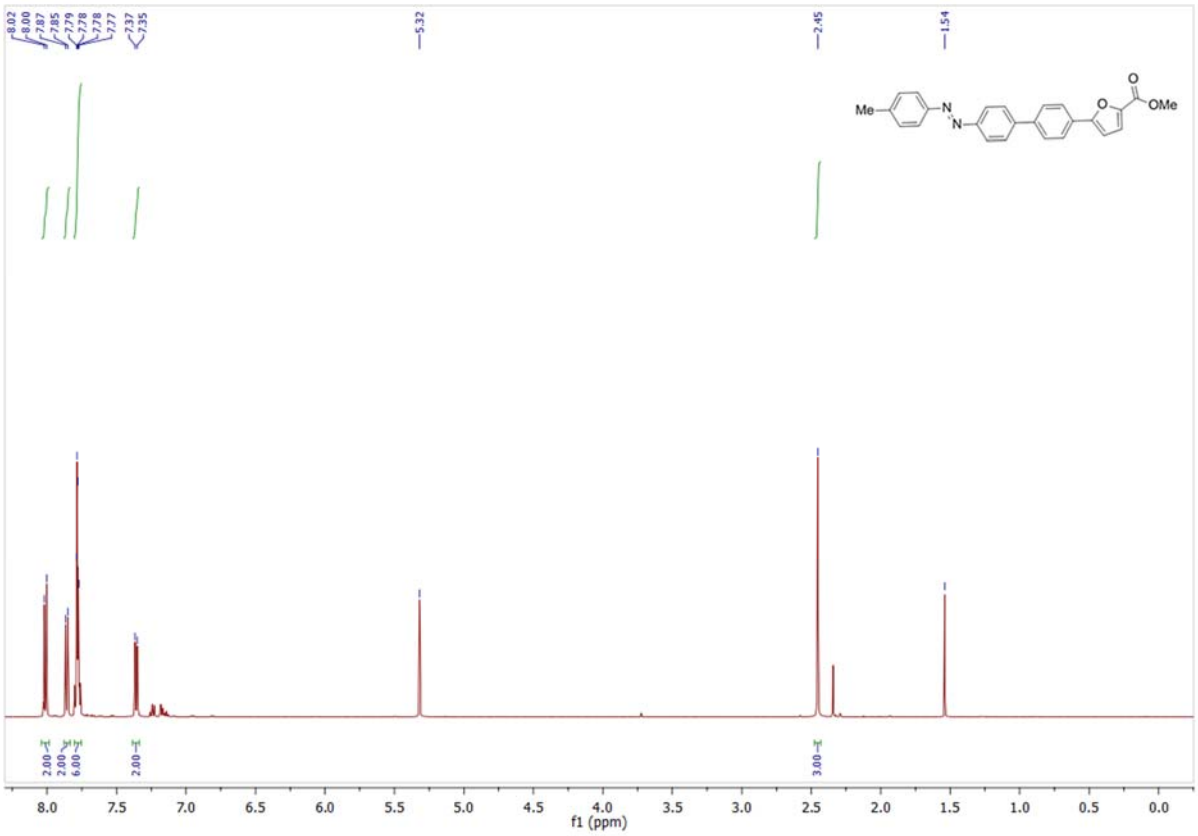

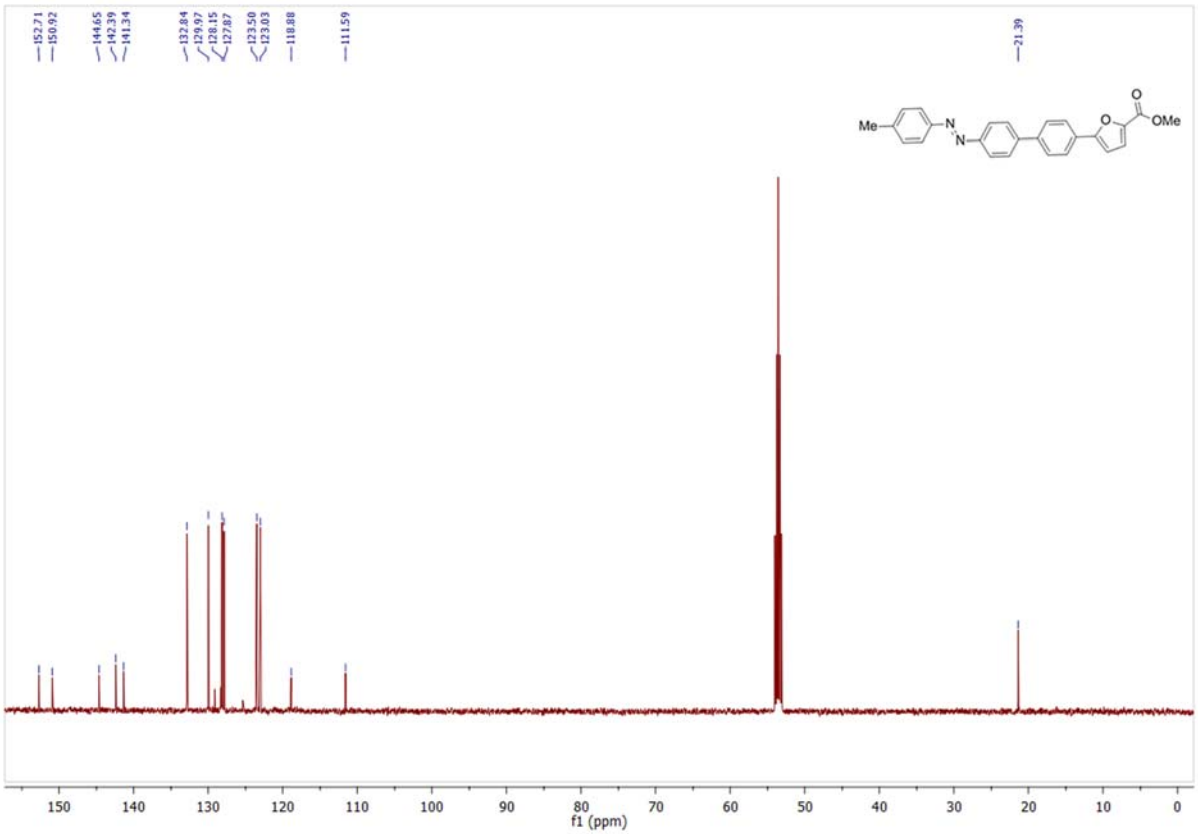

4-(3-Methoxyphenyl-) 4’-methylazobenzene (31)

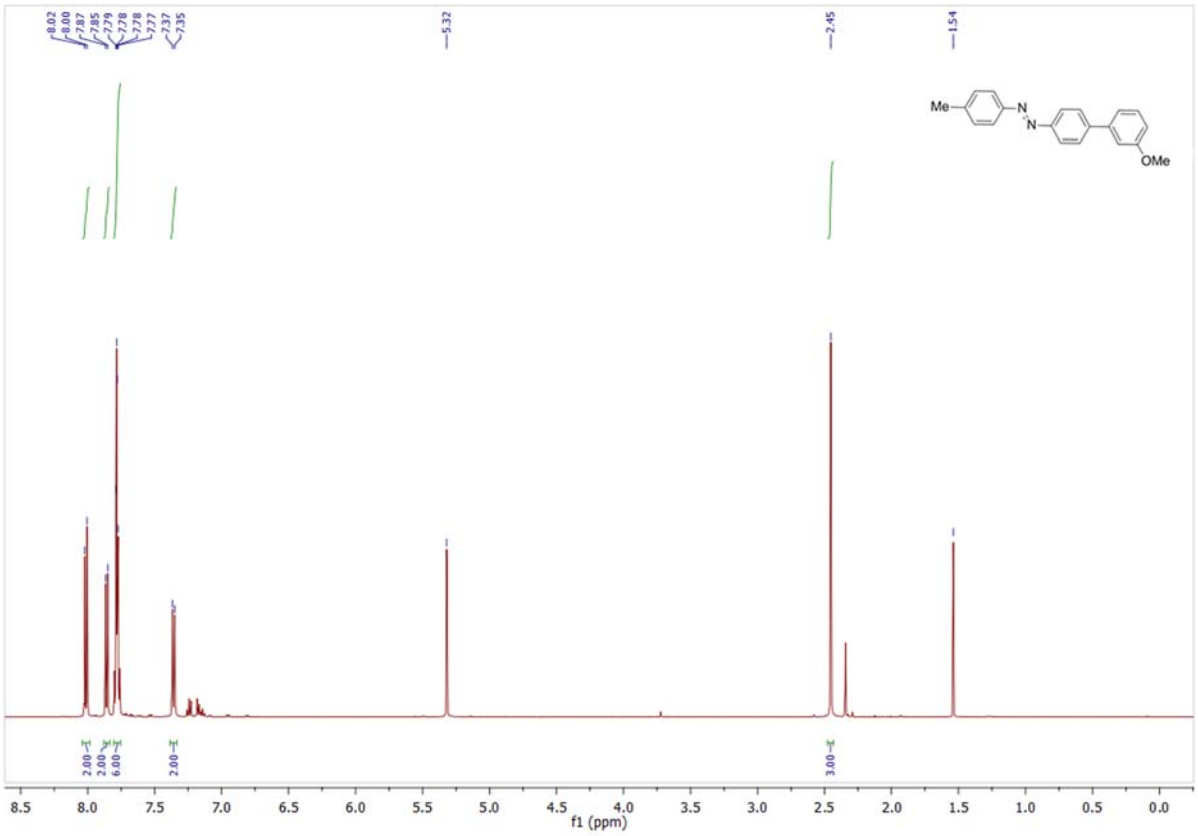

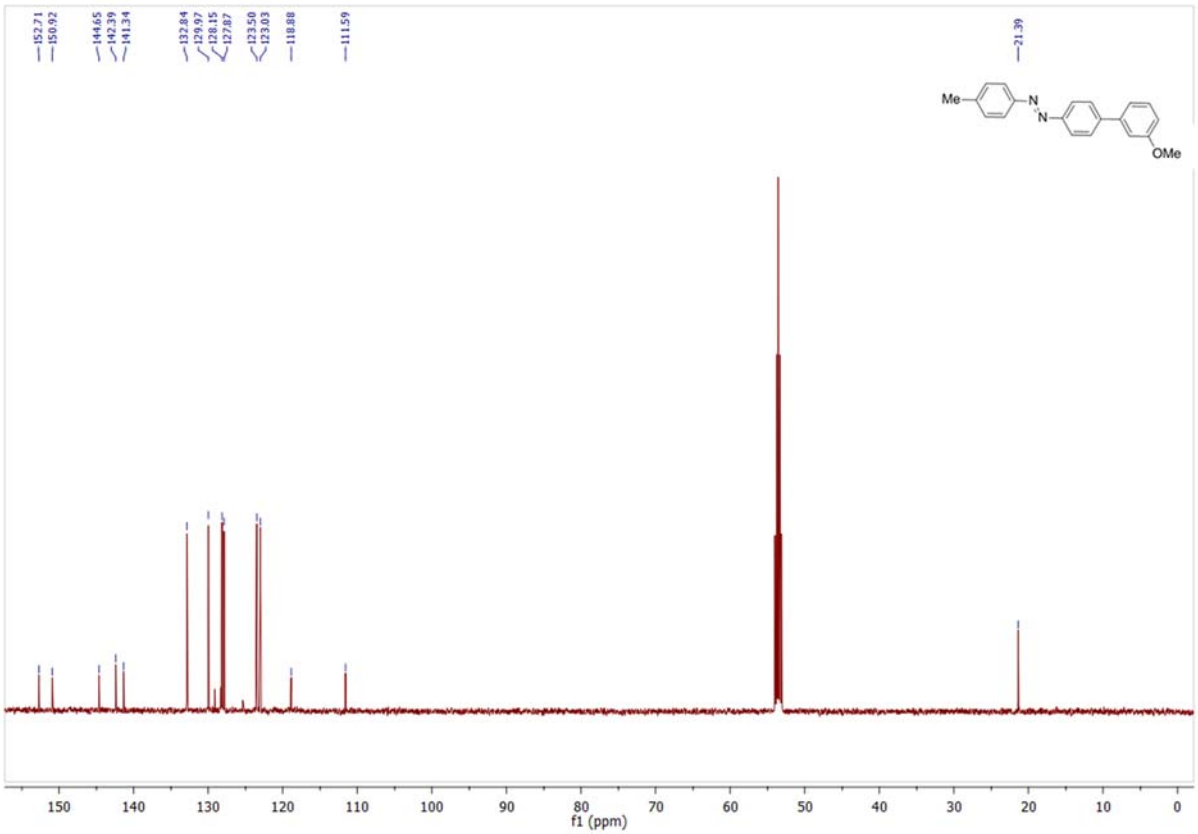

4-(2,5-Methoxyphenyl-) 4'-methylazobenzene (32)

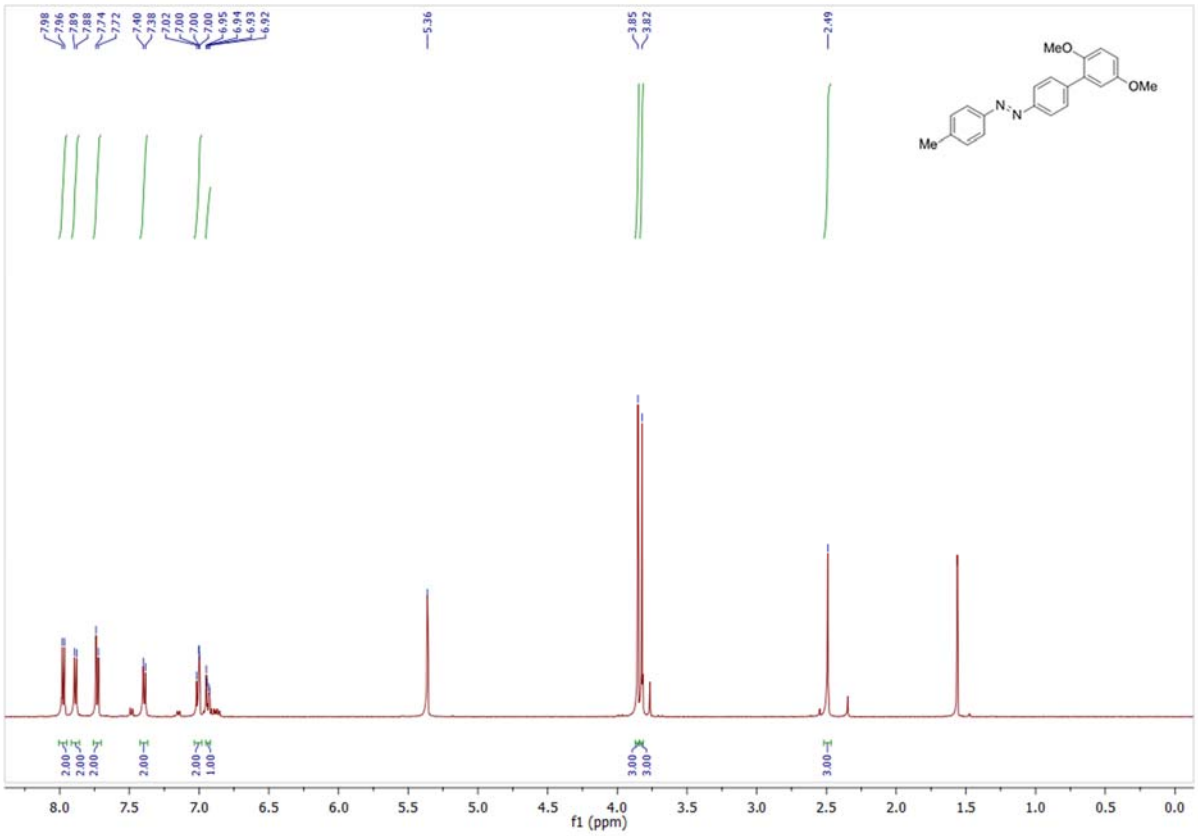

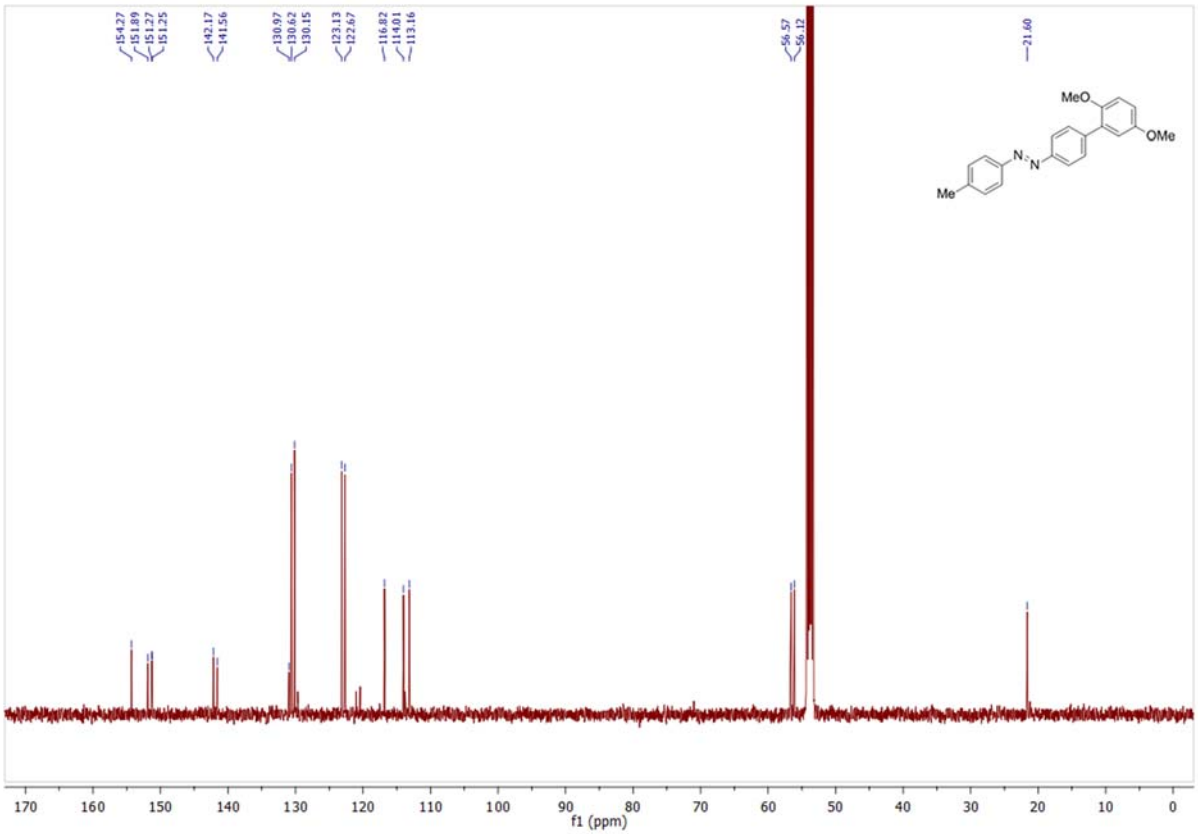

4-(5-1,3-Benzodioxolyl-) 4'-methylazobenzene (33)

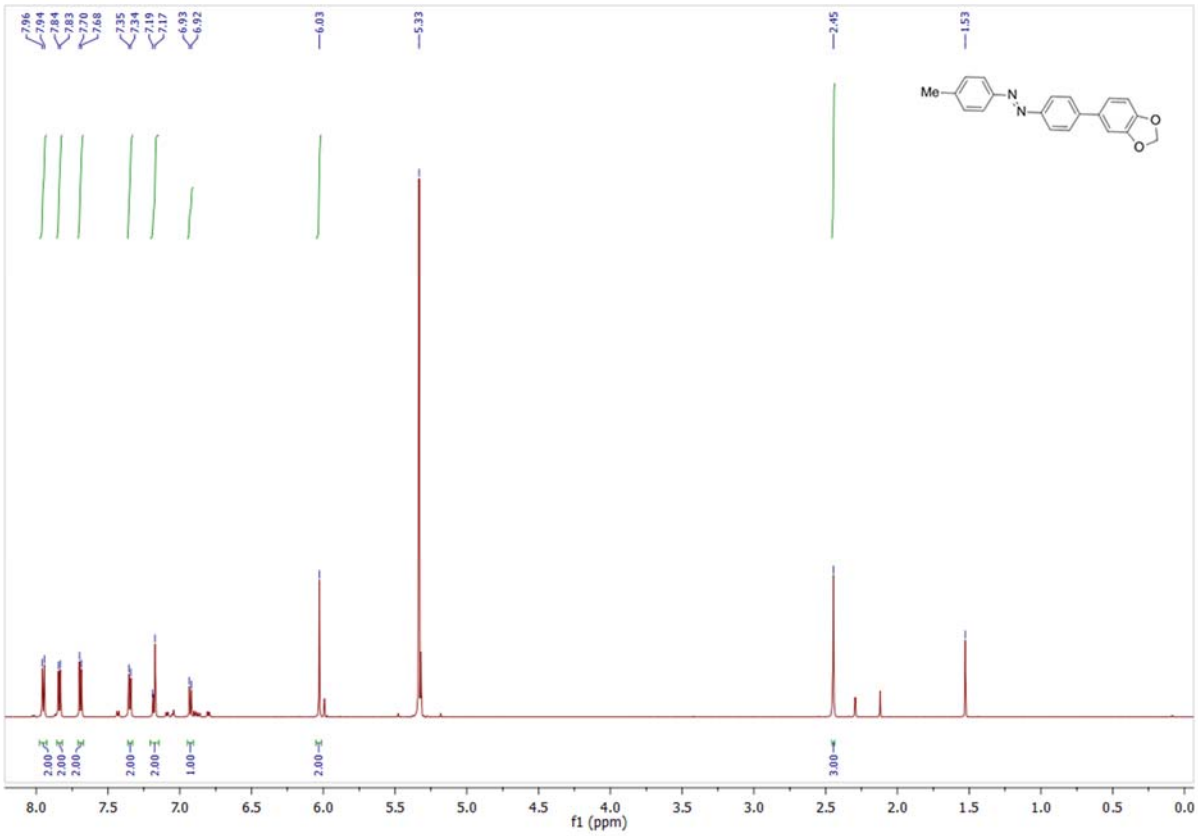

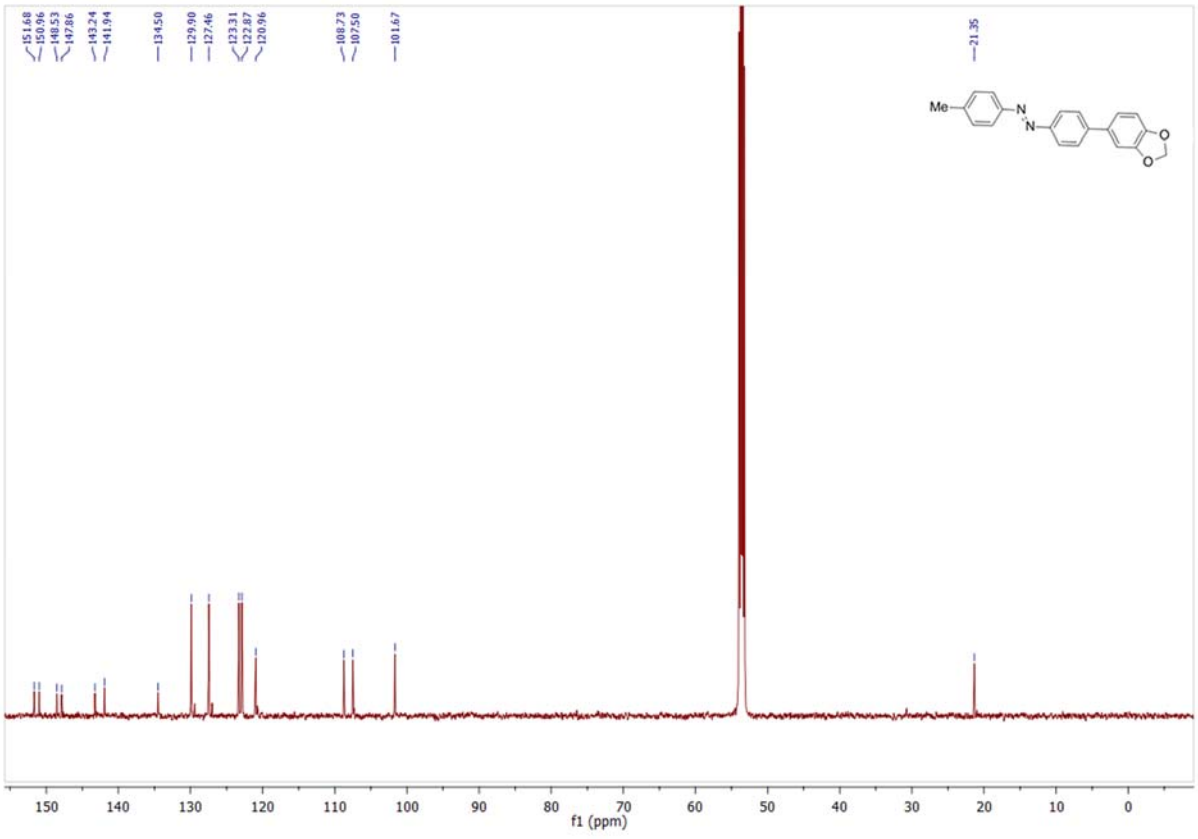

4-(2-Thiophenyl-) 4’-methylazobenzene (35)

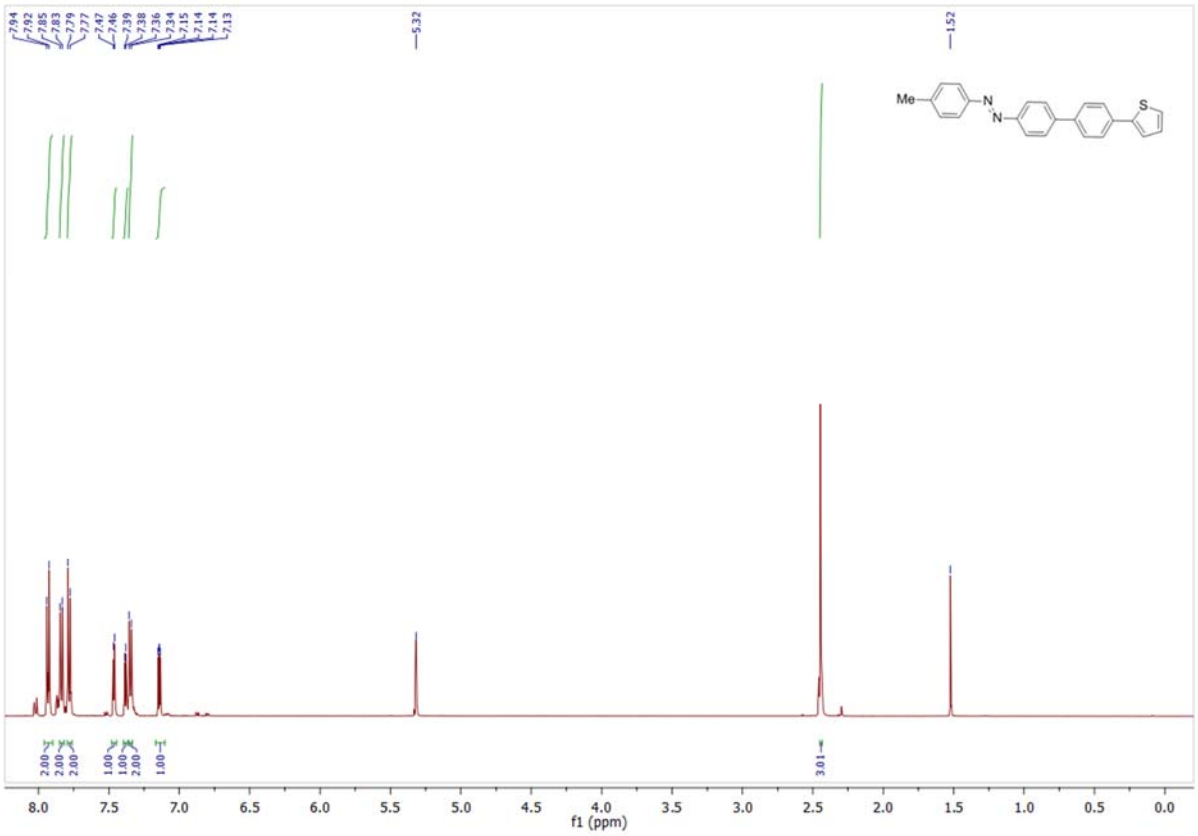

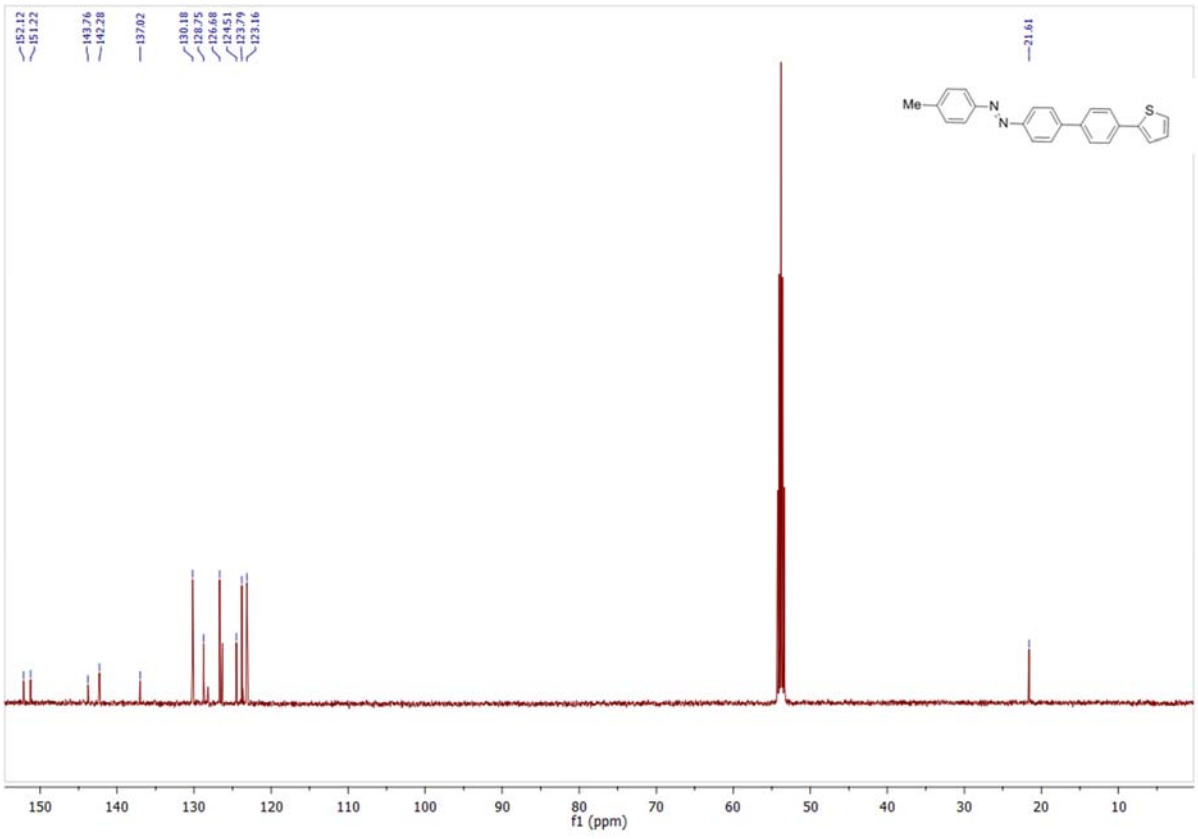

4-(3-Thiophenyl-)- 4'-methylazobenzene (37)

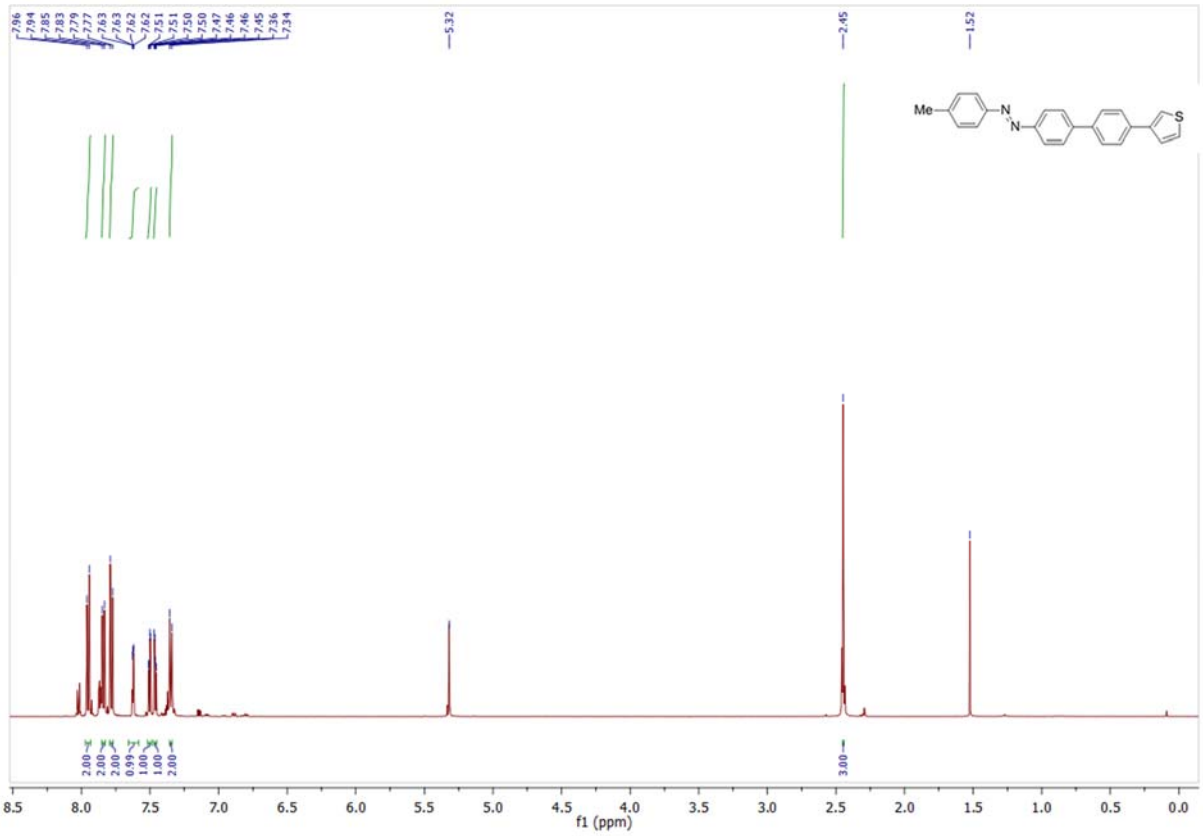

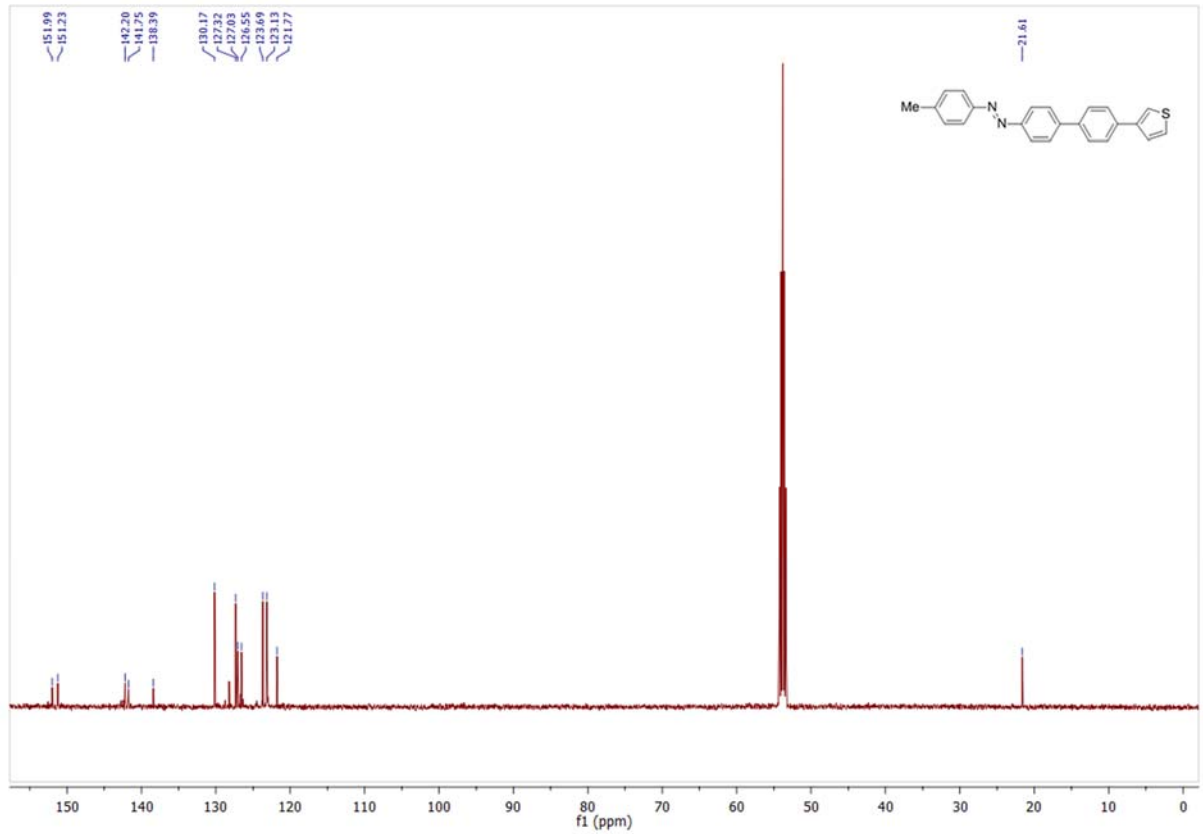

4-(4-Dimethylaminophenyl-) 4'-methylazobenzene (39)

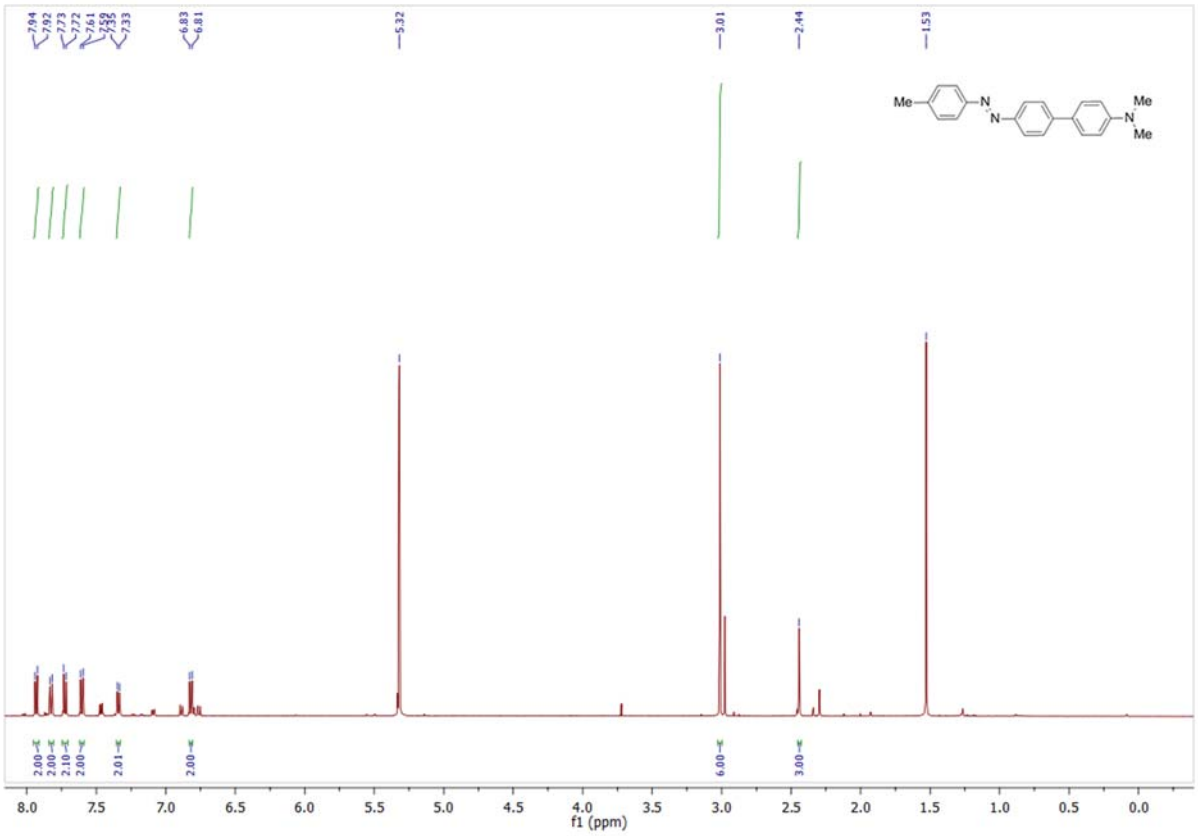

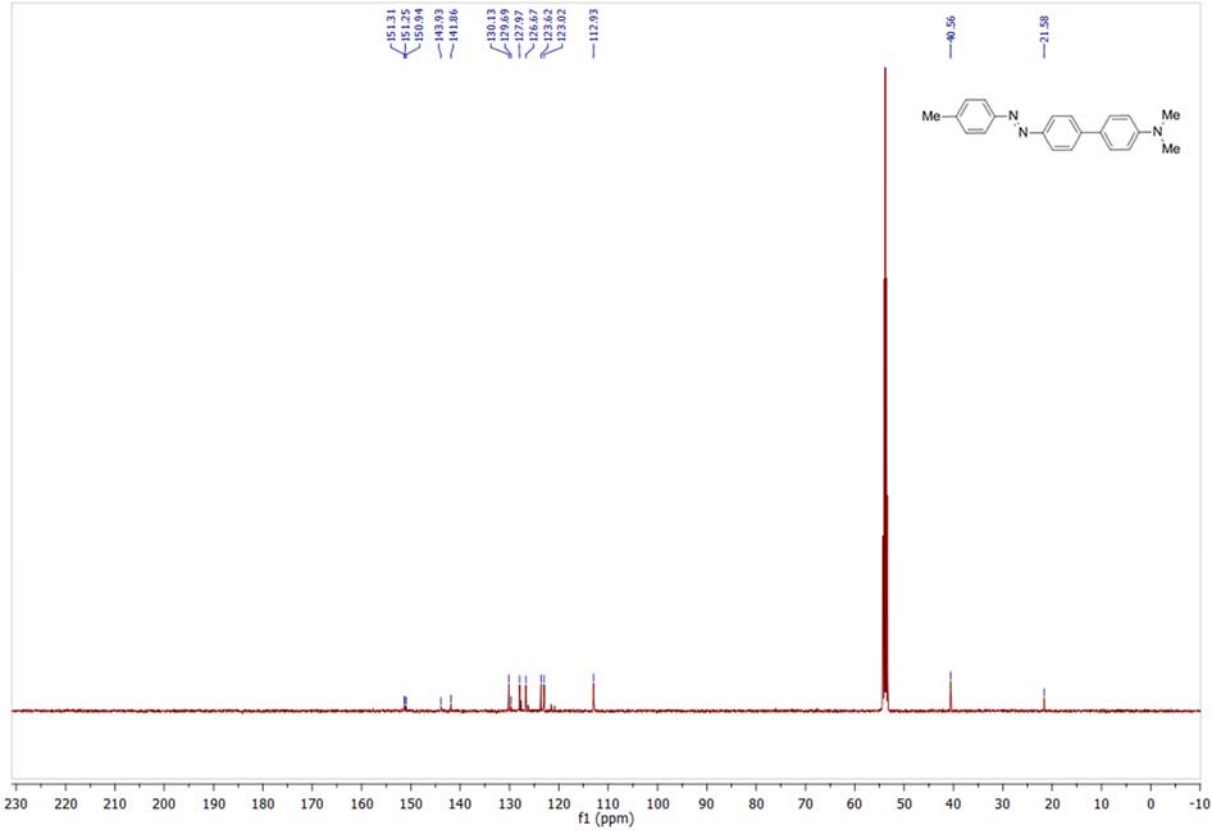

4.2 Supporting Information for *Chem. – Eur. J.* 2015, *submitted.*

4.2.1 Syntheses

Supporting Information

for

High Yielding Lithiation of Azobenzenes by Tin-Lithium Exchange

-Experimental Data-

Jan Strueben[a], Matthias Lipfert[a], Jan-O. Springer [a], Colin A. Gould[a], Paul J. Gates[b], Frank D. Sönnichsen[a], Anne Staubitz[a]*

[a] *Otto-Diels-Institute for Organic Chemistry, University of Kiel, Otto-Hahn-Platz 4, 24098 Kiel (Germany)*
* *astaubitz@oc.uni-kiel.de*
[b] *School of Chemistry, University of Bristol, Cantock's Close, Bristol BS7 1TS (UK)*

Table of Contents

Abbreviations

A	area
Ac	acetate
as	apparent singlett
ATR	attenuated total reflectance
Bu	butyl
calcd.	calculated
CI	chemical ionization
COSY	correlated spectroscopy
d	doublet (NMR)
DCM	dichloromethane
DMF	*N*,*N*-dimethylformamide
DMSO	dimethylsulfoxide
ESI	electrospray ionization
FT-IR	Fourier transform infrared sprectroscopy
GC	gas chromatography
GC/MS	gas chromatography-mass spectrometry
HMBC	heteronuclear multiple bond coherence
HSQC	heteronuclear single quantum coherence
IR	infrared
m	medium (concerning the intensity) (IR)
m	multiplet (NMR)
Me	methyl
MeTHF	methyl tetrahydrofuran
M.p.	melting point
MS	mass spectrometry
MW	microwave
Ph	phenyl
PTFE	polytetrafluoroethylene
RF	response factor
R_f	retention factor
s	strong (concerning the intensity) (IR)
s	singlet (NMR)
t	triplet (NMR)
THF	tetrahydrofuran
w	weak (concerning the intensity) (IR)

General Methods and Materials

All preparations for the stannylation reactions were performed in a nitrogen filled glovebox and carried out in a sealed vial under nitrogen. All reagents and solvents for the lithiation reactions were stored in a nitrogen filled glovebox. Solutions of starting materials and organolithium reagents were prepared in the glovebox. The lithiation reactions were carried out using standard Schlenk techniques under an argon atmosphere. Schlenk glassware and NMR tubes with a J. Young's cap for preparing NMR samples under inert conditions were flame dried prior use. The water and oxygen concentration in the glovebox was below 1 ppm for each reaction. The argon "N46" was dried over a column of activated 3 Å molecular sieves with a diameter of 5 cm and a length of 40 cm. Molecular sieves were activated by heating at 300 °C and under a reduced pressure of 0.05 mbar. The activated molecular sieves were stored in a nitrogen filled glovebox.

Analyses

^{1}H NMR, ^{13}C NMR, ^{119}Sn NMR spectra were recorded at 300 K. ^{1}H NMR spectra were recorded on a Bruker DRX 500 (500 MHz) spectrometer. ^{13}C NMR spectra were recorded on a Bruker DRX 500 (126 MHz) spectrometer or a Bruker Avance 600 (151 MHz) spectrometer. ^{119}Sn NMR spectra were recorded on a Bruker DRX 500 (187 MHz) spectrometer. All ^{1}H NMR and ^{13}C NMR spectra were referenced against the residual proton signals of the solvent (^{1}H) or the solvent itself (^{13}C). ^{119}Sn and ^{29}Si NMR spectra were referenced by comparing the frequency (^{1}H) of the solvent with the ^{1}H NMR frequency of tetramethylsilane for the individual NMR spectrometer. The exact assignment of the peaks was performed by two-dimensional NMR spectroscopy such as ^{1}H COSY, ^{1}H/^{13}C HSQC or ^{1}H/^{13}C HMBC when possible.

Ultra high-resolution ESI mass spectra were recorded on a Bruker Daltonics Apex IV Fourier transform Ion Cyclotron resonance mass spectrometer. EI spectra were recorded on a JEOL ACCUTOF GCV JMS-T100GCV at 70 eV ionization energy. IR spectra were recorded on a Perkin Elmer Paragon 1000 FT-IR spectrometer with a A531-G Golden-Gate-ATR-unit. All melting points were recorded on an electrothermal melting point apparatus LG 1586 and are uncorrected. GC/MS analysis was performed on a Hewlett Packard 5890A gas chromatograph, equipped with a Hewlett Packard 5972A mass selective detector and an Agilent Technologies dimethylpolysiloxane column (19091S-931E, nominal length: 15 m, 0.25 mm diameter, 0.25 µm grain size). The carrier gas was helium, the ionization voltage was 70 eV. GC analysis was performed on an Agilent Technologies 6890N gas

chromatograph, equipped with an Agilent Technologies 7683 Series Injector, an Agilent Technologies (5%-phenyl)-methylpolysiloxane column (19091J-413, 30 m length, 0.32 mm diameter, 0.25 µm grain size) and a flame ionization detector (FID). The carrier gas was nitrogen.

Reagents

All liquid reagents that were used as quenching reagents were dried over 3Å molecular sieves for minimum of 7 d. All reagents used for lithiation reactions and quenching reactions were stored in a nitrogen filled glovebox. If not otherwise noted, all remaining reagents were used as received.

Reagent	Supplier	Purity	Notes
Acetone	Acros Organics	97 %	distilled; degassed[a]
Benzoyl bromide	Merck KGaA	99 %	
n-Butyl lithium[b] nominally 2.5 M in hexanes	Acros Organics	+/- 5 %	titrated[1] conc. 2.50 M
Diethyl carbonate	Merck KgaA	99 %	
N,N-Dimethyl formamide	Acros Organics	99.9 %[c]	
Hexamethyldistannane	Sigma Aldrich Inc.	99 %	
2-Iodoaniline	TCI Inc.	97%	
3-Iodoaniline	Alfa Aesar	98 %	
4-Iodoaniline	Sigma Aldrich Inc.	97 %	
4-Methylbenzaldehyde0	Alfa Aesar	97 %	
Methyl lithiumb, nominally 1.6 M in diethyl ether	Acros Organics	+/- 5 %	titrated [1] conc. 1.58 M
Methyl iodide	ABCR Inc.	99 %	stored over copper[d]
N-Methoxymethylamine	Sigma Aldrich Inc.	98 %	
4-Methyl toluate	Alfa Aesar	99 %	
Nitrosobenzene	Sigma Aldrich	97 %	
Oxalyl chloride	Alfa Aesar	98 %	
Oxone	ABCR Inc.	-	
Phenylisocyanate	Alfa Aesar	98 %	

[a] Degassed by three freeze-pump-thaw cycles.
[b] Organo lithium compounds were stored at -30 °C in a glovebox. Prior use, they were allowed to warm to 20 °C.
[c] Purchased "extra dry"; stored over molecular sieves 3Å and flushed with nitrogen.
[d] Prior to use, the copper powder was removed by the help of a syringe filter (PTFE, 0.45 µm).

Phenylisothiocyanate	Sigma Aldrich Inc.	99 %	
Tetrakis(triphenylphosphine)palladium	Sigma Aldrich Inc.	99 %	
4-Toluidine	ABCR	99 %	
Triethylamine	Acros Organics	99.5 %	
Triisopropylbenzene	TCI Inc.	99.9 %	
Trimethylsilyl chloride	Merck KGaA	99 %	Distilled from calcium hydride

Solvents

All solvents were freshly distilled, if used for purification. Where noted, solvents were dried over the specified drying agent by refluxing for several hours before distillation. Dry solvents were degassed by three freeze-pump-thaw cycles and stored in a nitrogen filled glove box over 3 Å molecular sieves. The water contamination of diethyl ether, DMF, THF and toluene was less than 5 ppm and was determined by Carl Fischer titration on a "Mettler-Toledo C20 Coulometric KF Titrator" with "Hydranal - Coulomat AD" by Fluka.

Solvent	**Supplier; drying procedure**
Acetonitrile	Sigma Aldrich; Dried over phosphorus pentoxide
Acetic acid	Grüssing GmbH
Chloroform	VWR; Dried over phosphorus pentoxide
DCM	BCD; -
Diethyl ether	Merck-Polaro, dried and degassed with an PS-MD-5 by Innovation Technology.
DMF	Acros Organics, extra dry, stored over 3 Å molecular sieves, flushed with nitrogen.
DMSO	Acros Organics, extra dry, stored over 3 Å molecular sieves, flushed with nitrogen.
Methanol	BCD;
Pyridine	Sigma Aldrich; Dried over calcium hydride
THF	Merck-Polaro, dried and degassed with an PS-MD-5 by Innovation Technology.
Toluene	BCD; Sodium with benzophenone as indicator.

Synthetic and Purification Equipment

All microwave syntheses were performed on a CEM Discover Explorer apparatus. Column chromatography of tin functionalized azobenzenes was performed manually using Merck Silica Gel 60 (15 – 40 μm). Thin layer chromatography (TLC) was performed with pre-coated

TLC-sheets from Macherey-Nagel GmbH & Co. KG with silica 60 and fluorescent indicator UV254. TLC was used to monitor reaction progression and find appropriate work up conditions for column chromatography. Column chromatography of all non-stannylated compounds was performed with silica gel 60M from Macherey-Nagel GmbH & Co. KG with a size of 0.040 – 0.063 mm except for the stannylated compounds.

Cooling Baths

For adjusting the reaction temperatures, various different cooling baths were used.

Temperature	**Cooling Mixture**
-130 °C	*n*-Pentane/N_2
-120 °C	Ethyl bromide/N_2
-110 °C	Carbon disulfide/N_2
-98 °C	Methanol/N_2
-78 °C	Acetone/dry ice
-61 °C	Chloroform/dry ice
-41 °C	Acetonitrile/N_2
-15 °C	Ethylene glycol/N_2
0 °C	Ice water

GC Optimization Reactions

The formation of 4,4'-bismethylazobenzene, unconverted 4-(4-trimethylstannyl-)4'-(4-methyl-)azobenzene and hydrolyzed 4-methylazobenzene for the optimization reactions was determined by GC by a multiple point internal standard method. 1,3,5-Triisopropylbenzene was used as reference analyte. Yields were calculated corresponding to the following equation:

$$n(analyte) = \frac{A(analyte)}{A\,(reference)} \frac{n(reference)}{RF}$$

Where *n* is the amount of substance; A the integrated area of a signal and RF a system specific response factor. Standard solutions of different ratios of **1**, **2** and **3** each and 1,3,5-triisopropylbenzene were measured to obtain the calibration curves. Each calibration sample was measured six times and the average value of the samples was used for the calibration curve. The response factor was obtained from the slope of the resulting calibration curves. The response factor of 4,4'-bismethylazobenzene gave RF=0.86 (standard error=0.01) (Figure SI 1), for the starting material 4-methyl-4'-trimethylstannylazobenzene, RF=0.86 (standard error=0.05) (Figure SI 2) and for hydrolyzed material, 4-methylazobenzene, the response factor was RF=0.70 (standard error=0.04)(Figure SI 3).

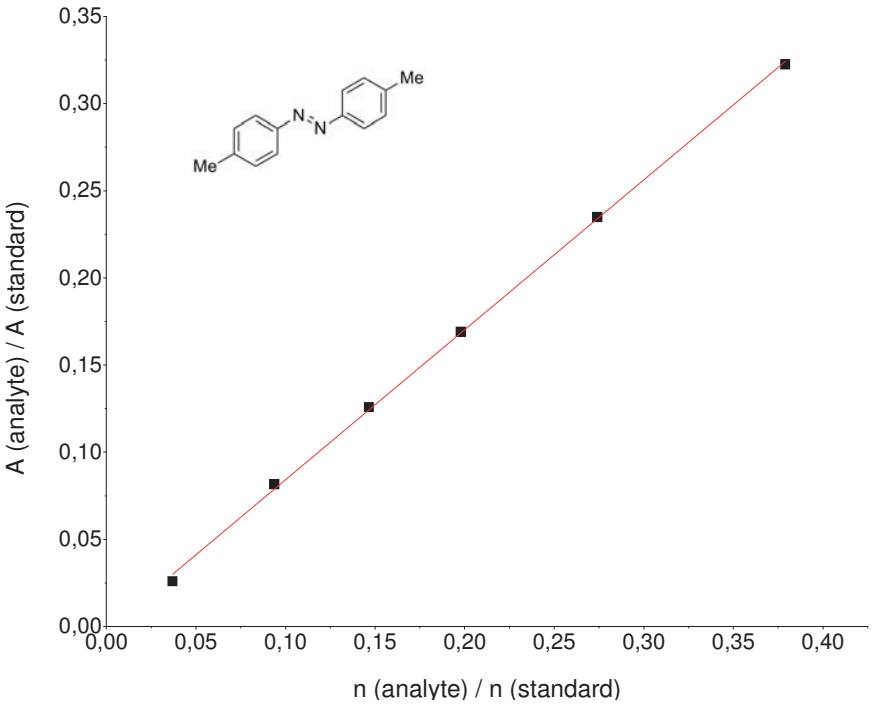

Figure SI 1. Calibration curve for 4,4-bismethylazobenzene (**14a**) using 1,3,5-triisopropyl-benzene as an internal reference substance. RF = 0.86 (standard error=0.01).

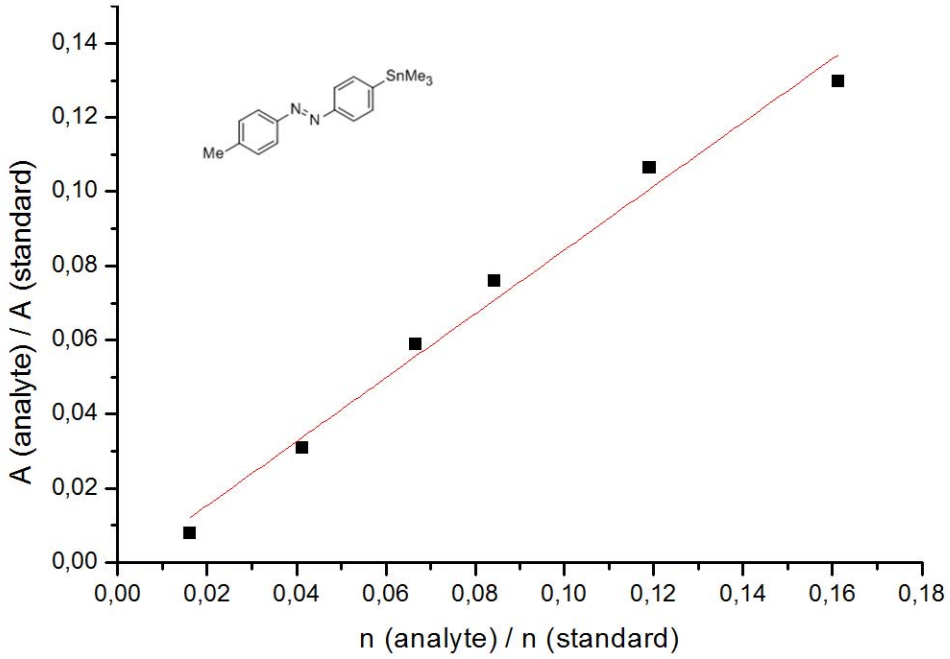

Figure SI 2. Calibration curve for 4-(4-trimethylstannyl-)4'-(4-methyl-)azobenzene (**11a**) using 1,3,5-triisopropylbenzene as an internal reference substance. RF = 0.86 (standard error=0.05).

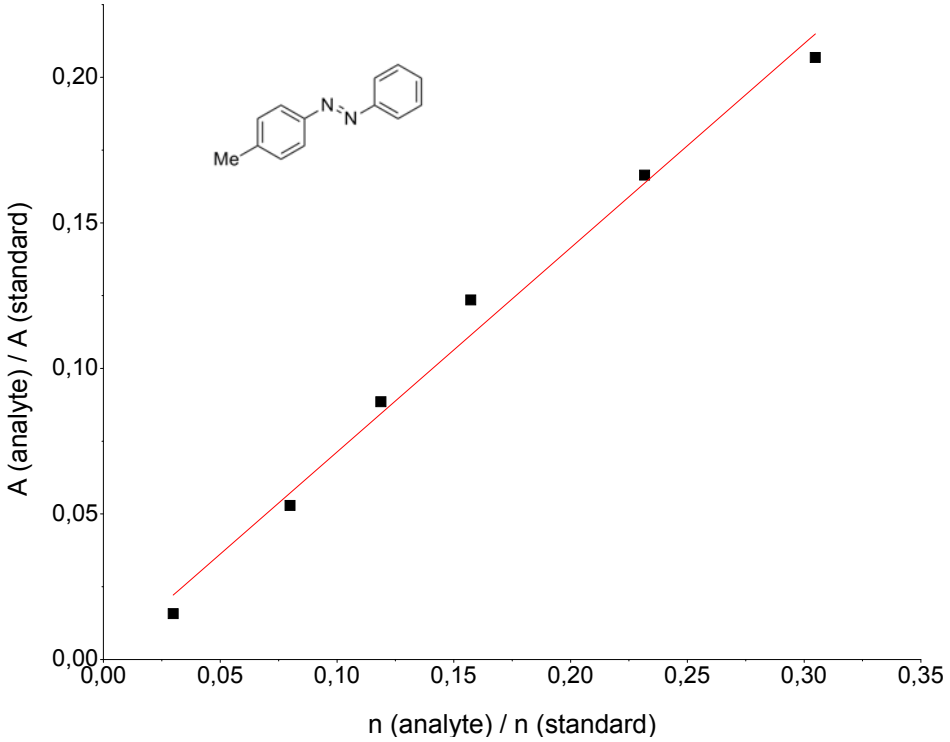

Figure SI 3. Calibration curve for 4-methylazobenzene (**SI-1**) using 1,3,5-triisopropylbenzene as an internal reference substance. RF = 0.70 (standard error=0.04).

Representative Procedure for the Optimization of the Lithiation of 4-Methyl-4'-trimethylstannylazobenzene:

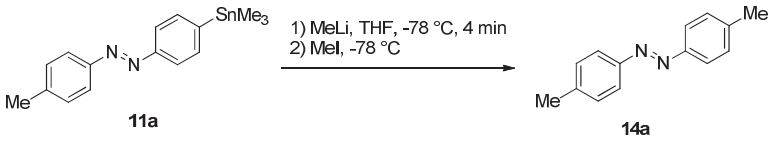

A solution of 4-methyl-4'-trimethylstannylazobenzene (250 mg, 694 µmol) and triisopropylbenzene (141 mg; 694 µmol) in THF (10 mL) was cooled to -78 °C. A solution of methyllithium (0.99 eq, 440 µL, 700 µmol, 1.58 M in diethyl ether) diluted in THF (2 mL) was added at -78 °C over the course of 4 min. The solution was stirred for another 2 min. A solution of methyl iodide (1.10 eq, 48.1 µL, 770 µmol) in THF (900 µL) was added. The reaction mixture was allowed to warm 20 °C by removal of the cooling bath and stirred for 6 h, until the reaction mixture turned orange again. 0.5 mL of the reaction mixture were filtered through a syringe filter (PTFE, pore size 45 µm) and analyzed by GC.

Procedure for the Lithiation of 4-Methyl-4'-trimethylstannylazobenzene in Diethyl Ether for Side-Product Identification

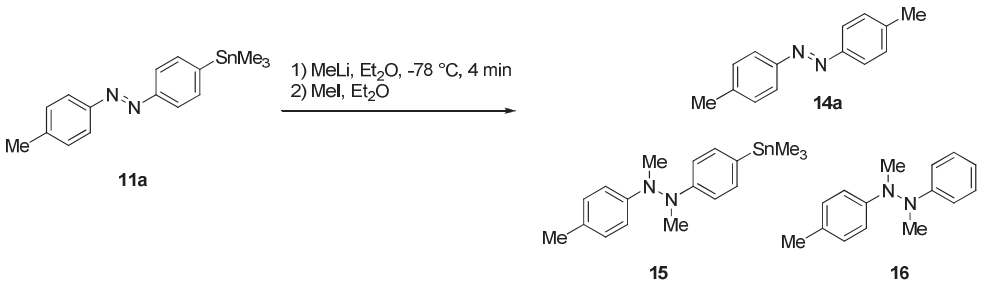

A solution of 4-methyl-4'-trimethylstannylazobenzene (500 mg, 1.38 mmol) in diethyl ether (20 mL) was cooled to -78 °C. A solution of methyl lithium (0.99 eq, 980 µL, 1.40 µmol, 1.58 M in diethyl ether) diluted in diethyl ether (2 mL) was added at -78 °C over the course of 4 min. The solution was stirred for another 2 min. A solution of methyl iodide (1.10 eq, 48.1 µL, 770 µmol) in diethyl ether (900 µL) was added over the course 4 min. The solution was stirred for 12 h. From the crude product, **15** could be identified by NMR but was already contaminated with **16**. For isolation, the solvent was evaporated and the crude product was purified by column chromatography (*n*-pentane, R_f=0.3). hydrazine **16** (the hydrolyzed species of **15**) could be obtained in a purity of 90% and a crude yield of 52% as an brown oil.

Identification of 15 from the Crude ^{1}H NMR Mixture[a]

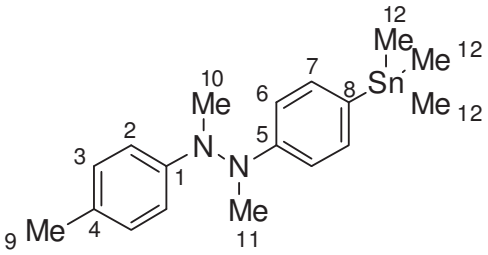

^{1}H NMR (500 MHz, $CDCl_3$): δ = 7.39 (d, *J* = 8.4 Hz, 7.3 Hz, 2H, H-7), 7.08 (d, *J* = 8.4 Hz, H-2), 6.87 (d, *J* = 8.4 Hz, 2 H, H-6), 6.76 (d, *J* = 8.4 Hz, 1 H, H-3), 2.98 (as, H-10,11), 2.98 (s, H-9), 0.27 (s, 9 H, H-12) ppm.

^{13}C NMR (125 MHz, $CDCl_3$): δ = 149.3 (C-5), 146.6 (C-1), 136.8 (C-8), 129.8 (C-4), 129.3 (C-7), 127.8 (C-2), 112.8 (C-3), 112.4 (C-6), 34.2 (C-10 or 11), 33.2 (C-10 or 11), 20.3 (C-9), -9.6 (C-12) ppm.

^{119}Sn NMR (186 MHz, CDCl3)**:** δ = -27.5 ppm.

Side Product 16[b]

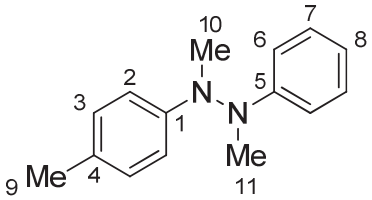

^{1}H NMR (500 MHz, $CDCl_3$): δ = δ = 7.27 (dd, *J* = 8.6 Hz, 7.3 Hz, 2H, H-7), 7.08 (d, *J* = 8.6 Hz, 2 H, H-2), 6.87 (d, *J* = 8.6 Hz, 2 H, H-6) 6.82 (t, *J* = 7.3 Hz, 1 H, H-8) , 6.77 (d, *J* = 8.6 Hz, 1 H, H-3), 2.98 (as, 6 H, H-10,11), 2.30 (s, 3 H, H-9) ppm.

^{13}C NMR (125 MHz, $CDCl_3$): δ = 149.1 (C-5), 146.7 (C-1), 129.8 (C-2), 129.3 (C-7), 127.8 (C-4), 118.3 (C-8), 112.7 (C-3), 112.4 (C-6), 34.0 (C-10 or 11), 33.3 (C-10 or 11), 20.3 (C-9) ppm.

HRMS (EI-sector): *m/z* = $[M]^+$ calcd for $[C_{15}H_{18}N_2]^+$ 226.1470, found 226.1471.

[a] Signal without an assigned integral could not be integrated properly because of overlapping signals. Attempts to identify the substance with mass spectrometry lead to a loss of the trimethyltin group. Only the hydrolyzed product was detected.
[b] Due to the low purity of 90%, the substance was not characterized by IR-spectroscopy.

Table 1: Optimization results of the lithiation of 4-methyl-4'-trimethylstannylazobenzene (11a).

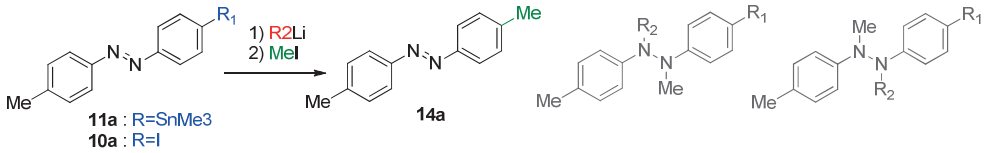

Entry	Solvent	T / °C	R	RLi	t/min	Starting material / %	Yield / %
1	MeTHF	-130	$SnMe_3$	MeLi	4	25	72
2	MeTHF	-130	$SnMe_3$	MeLi	30	10	89
3	MeTHF	-100	$SnMe_3$	MeLi	4	2	98
4	MeTHF	-78	$SnMe_3$	MeLi	4	<1	>99
5	MeTHF	-78	$SnMe_3$	MeLi	30	<1	>99
6	THF	-100	$SnMe_3$	MeLi	4	<1	>99
7	THF	-78	$SnMe_3$	MeLi	4	<1	>99
8	THF	-78	$SnMe_3$	MeLi	30	<1	>99
9	THF	-54	$SnMe_3$	MeLi	4	<1	>99
10	THF	-43	$SnMe_3$	MeLi	4	<1	98
11	THF	-16	$SnMe_3$	MeLi	4	<1	63
12	THF	-100	$SnMe_3$	*n*-BuLi	4	<1	56
13	THF	-78	$SnMe_3$	*n*-BuLi	4	<1	43
14	THF	-100	I	MeLi	4	24	46
15	THF	-78	I	MeLi	4	22	54
16	THF	-78	I	*n*-BuLi	30	<1	27
17	Diethyl ether	-100	$SnMe_3$	MeLi	4	<1	29
18	Diethyl ether	-78	$SnMe_3$	MeLi	4	<1	32

NMR Studies

Representative Procedure for the Lithiation of 4-Methyl-4'-trimethylstannylazobenzene in a Sealed NMR Tube:

A solution of 4-methyl-4'-trimethylstannylazobenzene (30 mg, 83 µmol) in MeTHF (0.4 mL) in a flame dried inert NMR tube was cooled to -130 °C in a nitrogen filled glovebox. A solution of methyl lithium (52 µL, 1.58 M in diethyl ether) MeTHF (100 µL) was added in one portion with the help of a syringe while the solution was mixed with a PTFE rod. Liquid nitrogen was added to the cooling bath so that the reaction mixture in the NMR tube froze immediately. The sealed NMR tube and the cooling bath were taken out of the glove box and directly transferred to the precooled NMR spectrometer. The NMR tube was removed from the cooling bath, water ice crystals were removed with a towel from the outer wall of the NMR tube (within 6 seconds so that the reaction mixture stayed frozen). The NMR tube was inserted into the NMR spectrometer. The NMR tube warmed up to the temperature of the spectrometer (166-173 K) and the reaction progress was observed by ^{119}Sn NMR spectroscopy.

Representative Procedure for the Lithiation of 4-Methyl-4'-trimethylstannylazobenzene in a Sealed NMR Tube in Pictures:

Figure SI 4. (a) A solution of the azobenzene stannane was placed in the NMR-tube with an PTFE stick for mixing; **(b)** the solution was cooled to -130°C in an *n*-pentane/N_2 cooling bath; **(c)** The methyl lithium solution was added via syringe while the reaction was mixed with the PTFE rod; (**d**) the reaction was frozen with liquid N_2; **(e)** the frozen reaction mixture **(f, g);** the NMR tube was removed from the glove box **(h);** the NMR tube was inserted into the NMR spectrometer.

NMR Experiments

^{119}Sn NMR spectra were recorded with Bruker DRX-500 spectrometer using a 5-mm probe head using quadrature detection, simultaneous mode. The FIDs (spectral width of 93 kHz centered at 37 kHz) were recorded with a standard 1D-sequence without any suppressions and were recorded on 1864 data points for 3000 or 6000 scans. The relaxation delay was optimized to 0.001 s with a pre-scan delay of 35 µs. The spectra were processed with an exponential window function using a line broadening of 20 Hz.

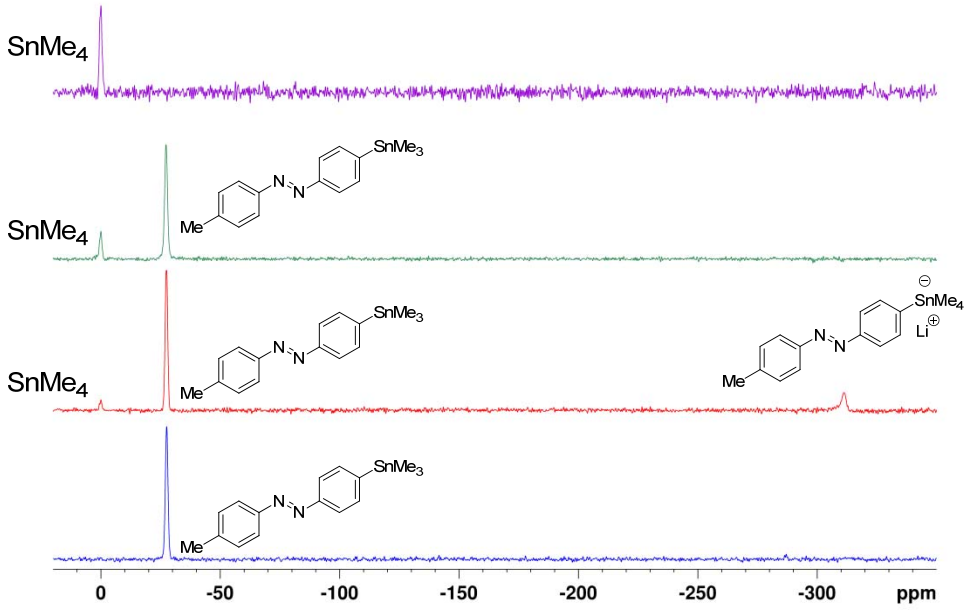

Figure SI 5: ^{119}Sn NMR signals for the reaction of 4-methyl-4'-trimethylstannylazobenzene (11a) in MeTHF: at -103 °C and t=4.5 min (blue) the reaction started, at -103 °C and t=4 min (red) at -90 °C and t = 12min (green) and -60 °C the reaction finished and only $SnMe_4$ was visible (magenta). Heating rate was approx. 0.2 K/min

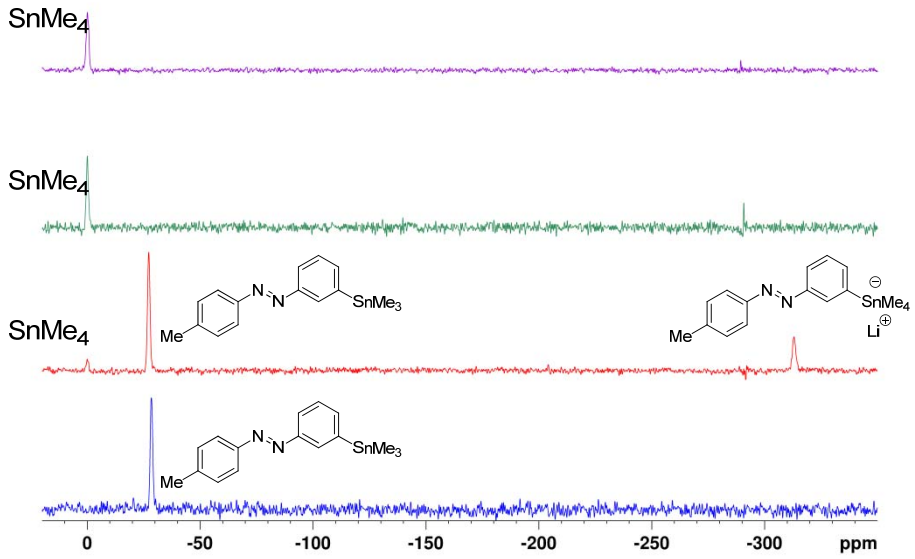

Figure SI 6: ^{119}Sn NMR signals for the reaction of 4-methyl-3'-trimethylstannylazobenzene (11b) in MeTHF: at -103 °C and t=4.3 min (blue) the reaction started, at -103 °C and t=4 min (red) at -78 °C the reaction was completed (green) and 300 K (magenta).

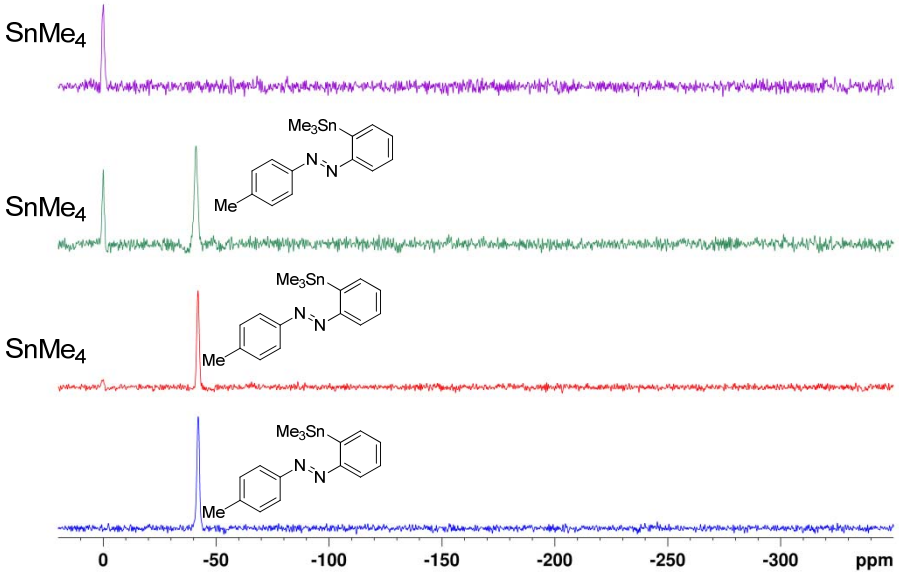

Figure SI 7. ^{119}Sn NMR signals for the reaction 4-methyl-2'-trimethylstannyl azobenzene (11c) in MeTHF: at -103 °C and t=4.3 min (blue) no reaction could be observed, -78 °C and t=12.3 min a slow reaction could be observed (red) at -58 °C, the reaction accelerated rapidly (green) and at -60 °C and t=13 min only $SnMe_4$ was visible (magenta). Heating rate was approx. 0.2 K/min.

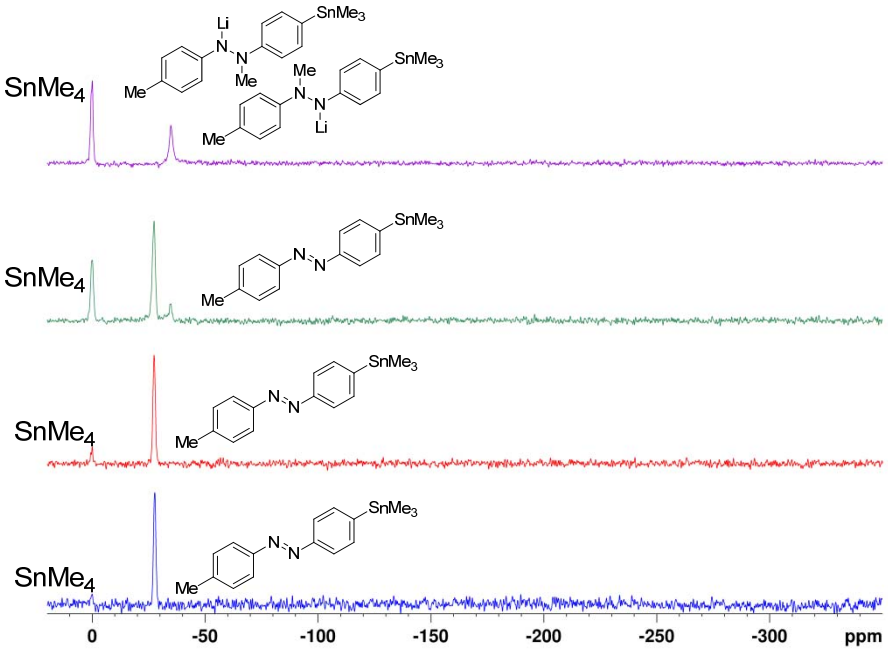

Figure SI 8: ^{119}Sn NMR signals for the reaction of the 4-methyl-4'-trimethylstannylazobenzene (11a) in diethyl ether: at -45 °C (blue) the reaction started at 35 °C (red) but no significant reaction progress could be observed. At -15 °C, a second tin-species appeared (green) and 300 K the reaction finished and $SnMe_4$ and the side product was visible (magenta). The heating rate was approx.. 0.2 °K/min.

Preparation of the Starting Materials

The preparation of the starting materials was performed as follows: iodinated azobenzenes **20a-22b** could be synthesized by an oxidative coupling of nitrosobenzene/nitrosotoluene and the corresponding *ortho*, *meta* or *para* iodinated aniline. The azobenzenes were obtained in yields ranging from 25 to 94%. In the case of the *ortho*-iodinated azobenzenes, the yield was always significantly lower than for *meta* and *para* positions, presumably due to the steric hindrance introduced by the large halide. The subsequent stannylations were carried out using a previously developed procedure[2] and gave yields ranging from 43 to 96% (Scheme SI-1).

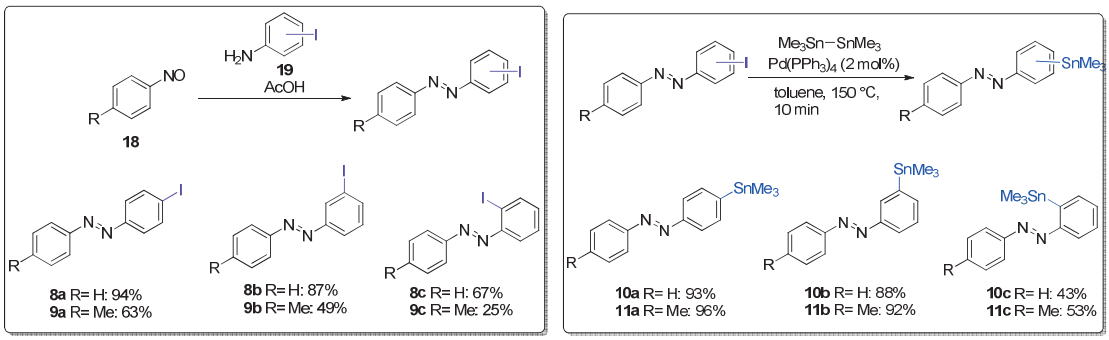

Scheme SI-1. Iodine and tin functionalized azobenzenes.

Lithiation of Non-Methylated Azobenzenes

The methyl group, which all azobenzenes that were described in the main article contained, might affect solubility and electronic properties of the azobenzene. Therefore, the lithiation reaction was also performed with the simplest possible system of mono substituted azobenzene stannanes in *ortho*, *meta* and *para* position. With methyl iodide as the electrophile, the *ortho*, *meta* and *para* methylated products gave yields of 96%, 79% and 84%, respectively. With trimethylsilyl chloride as electrophile, yields of 87%, 85% and 76% could be obtained.

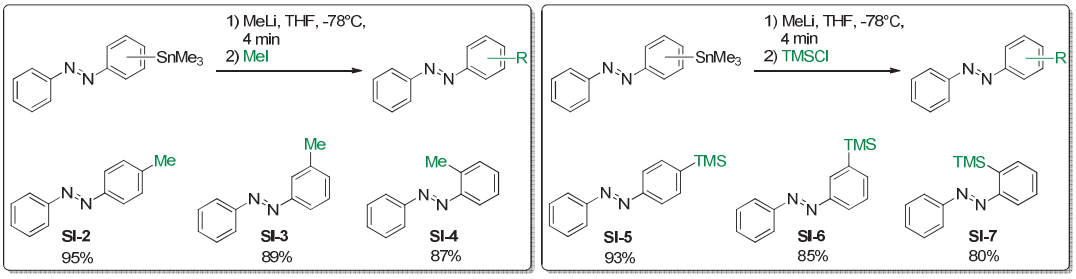

Scheme SI-2. Lithiation of mono substituted azobenzenes.

Syntheses

Overview of the Synthesized Compounds

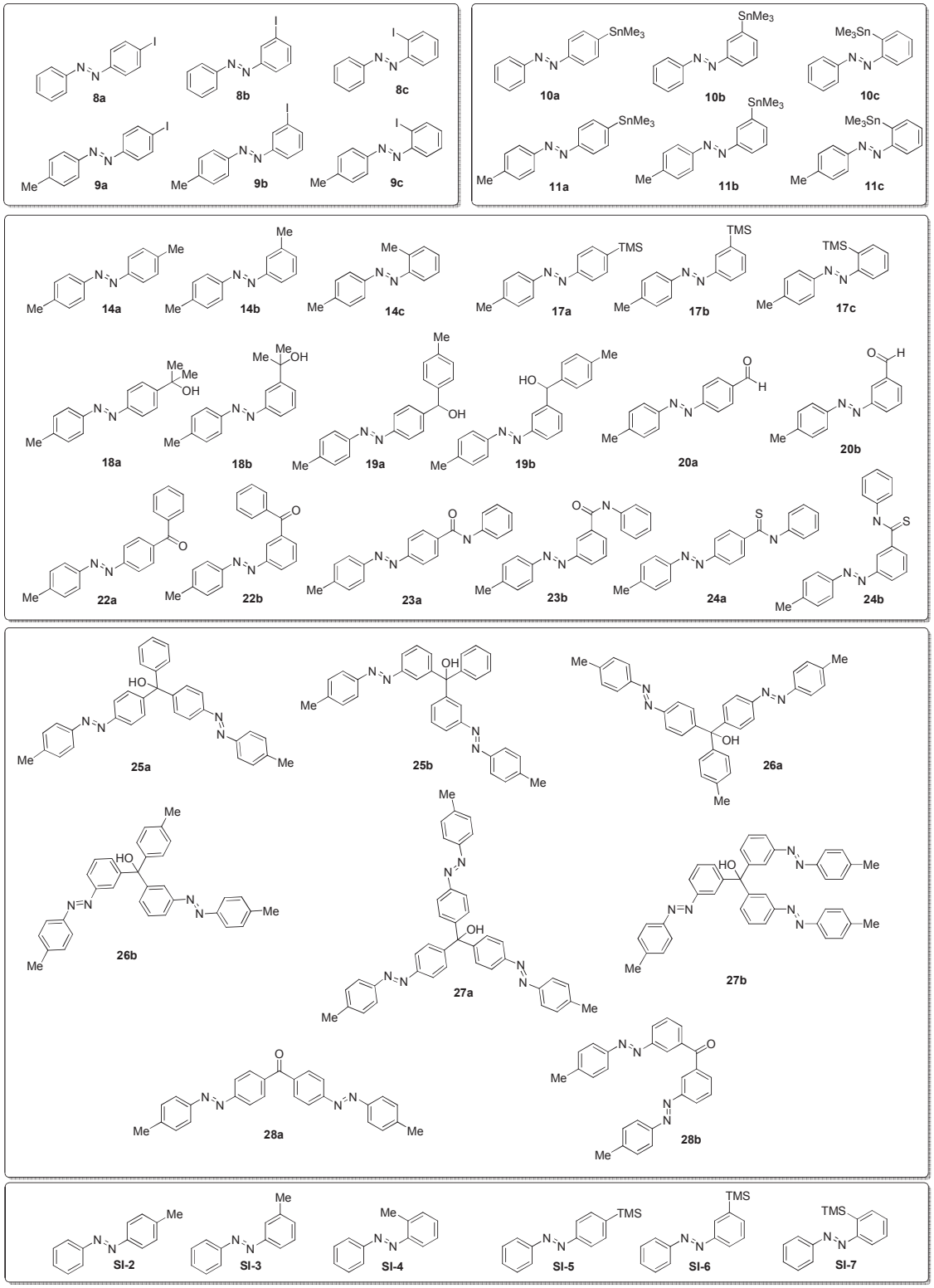

Iodinated Azobenzenes

4-Iodoazobenzene[4] (8a)

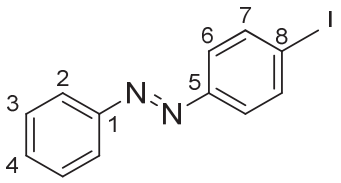

This reaction was not performed under Schlenk conditions. Nitrosobenzene (1.30 eq, 6.58 g, 61.4 mmol) and 3-iodoaniline (1.00 eq, 10.0 g, 45.7 mmol) were stirred in acetic acid (500 mL) for 5 days at 20 °C. The solvent was evaporated, and the crude mixture dissolved in DCM (50 mL). This solution was filtered over silica with DCM as eluent (R_f = 0.6). The solvent was removed *in vacuo* to obtain an orange solid (12.8 g, 41.4 mmol, 91%, Lit.: 85%[4]).

^{1}H NMR (500 MHz, $CDCl_3$): δ = 7.91 (dd, ^3J = 8.2 Hz, ^4J = 1.5 Hz 2 H, H-2), 7.86 (d, ^{3}J= 8.7 Hz, 2 H, H-7), 7.65 (d, ^3J = 8.7 Hz, 2 H, H-6), 7.54-7.46 (m, 3 H, H-3, H-4) ppm.

^{13}C NMR (125 MHz, $CDCl_3$): δ = 152.5 (C-*5*), 152.0 (C-*1*), 138.4 (C-*7*), 131.4 (C-*4*), 129.2 (C-*3*), 124.5 (*C*6), 123.0 (C2), 97.6 (C*8*) ppm.

IR (ATR): $\tilde{\nu}$ = 3039 (w), 2921 (m), 2853 (m), 1563 (s), 1473 (s), 1391 (m), 1293 (m), 1184 (m), 997 (s), 838 (s), 768 (s), 678 (s), 646 (s), 544 (s), 523 (s) cm^{-1}.

HRMS (EI-sector): *m/z* = $[M]^+$ calcd. for $[C_{12}H_9N_2I]^+$ 307.9809; found 307.9809.

Mp: 105 °C.

3-Iodoazobenzene[3] (8b)

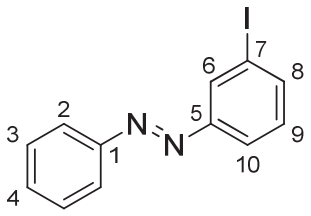

This reaction was not performed under Schlenk conditions. Nitrosobenzene (1.30 eq, 6.58 g, 61.4 mmol) and 3-iodoaniline (1.00 eq, 10.0 g, 45.7 mmol) were stirred in acetic acid (500 mL) for 5 days at 20 °C. The solvent was evaporated, and the crude mixture dissolved in DCM (50 mL). This solution was filtered over silica with DCM as eluent (R_f = 0.6). The

solvent was removed *in vacuo* to obtain an orange solid (13.5 g, 43.7 mmol, 96%, Lit.: 87%[3]).

^{1}H NMR (500 MHz, $CDCl_3$): δ = 8.25 (dd, ^4J = 1.7, 1.7 Hz, 1 H, C6-*H*), 7.93 – 7.90 (m, 3 H, *H-10*, *H-3*), 7.80 (ddd, ^3J = 7.8 Hz, ^4J = 1.7 Hz, 1.0 Hz, 1 H, *H-8*), 7.55 – 7.48 (m, 3 H, *H-4*, *H-2*), 7.27 (dd, ^3J = 7.8 Hz, ^3J = 7.8 Hz, 1 H, *H-9*) ppm.

^{13}C NMR (125 MHz, $CDCl_3$): δ = 153.6 (C*5*), 152.5 (C*1*), 139.7 (C*8*), 131.6 (C*4*), 130.9 (C*9*), 130.8 (*C*6), 129.3 (C*2*), 123.7 (C*10*), 123.2 (C*3*), 94.7 (*C7*) ppm.

IR (ATR): $\tilde{\nu}$ = 3051 (w), 1560 (m), 1459 (m), 1441 (m), 1403 (m), 1205 (m), 1148 (m), 915 (m), 880 (m); 792 (s), 760 (s), 681 (s), 646 (m), 528 (m), 522 (s), 494 (m) cm^{-1}.

HRMS (EI-sector): *m/z* = $[M]^+$ calcd. for $[C_{12}H_9N_2I]^+$ 307.9811; found 307.9809.

Mp: 67 °C.

2-Iodoazobenzene[3] (8c)

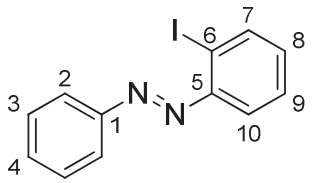

This reaction was not performed under Schlenk conditions. Nitrosobenzene (1.00 eq, 5.00 g, 46.7 mmol) and 2-iodoaniline (1.00 eq, 10.0 g, 45.7 mmol) were stirred in acetic acid (500 mL) for 16 h at 20 °C. The solvent was removed *in vacuo* and the precipitate was purified by column chromatography with DCM as eluent (R_f = 0.6). After evaporation an orange solid was obtained. (3.53 g, 11.5 mmol, 25%, Lit.: 67%[3]).

^{1}H NMR (500 MHz, $CDCl_3$): δ = 8.04 (dd, ^3J = 7.9 Hz, ^4J = 1.3 Hz, 1 H, *H-10*), 8.01 (m, 2 H, *H-3*), 7.64 (dd, ^3J = 8.0 Hz, ^4J = 1.6 Hz, 1 H, *H-7*), 7.53 (m, 3 H, *H-2*, *H-4*), 7.43 (ddd, ^3J = 8.0 Hz, ^3J = 7.3 Hz, ^4J = 1.3 Hz, 1 H, *H-8*), 7.17 (ddd, ^3J = 7.9 Hz, ^3J = 7.3 Hz, ^4J = 1.6 Hz, 1 H, *H-9*) ppm.

^{13}C NMR (125 MHz, $CDCl_3$): δ = 152.5 (*C*1), 151.5 (*C*5), 140.0 (*C*10), 132.3 (*C*9), 131.7 (*C*4), 129.3 (*C*2), 129.1 (*C*8), 123.7 (*C*3), 117.5 (*C*7), 102.6 (*C*6) ppm.

IR (ATR): $\tilde{\nu}$ = 3056 (w), 3011 (w), 1563 (w), 1446 (m), 1420 (w), 1303 (w), 1142 (m), 1015 (m), 919 (w), 771 (s), 708 (m), 681 (s), 636 (m), 549 (m), 534 (s), 489 (m) cm^{-1}.

HRMS (EI-sector): *m/z* = $[M]^+$ calcd for $[C_{12}H_9N_2I]^+$ 307.9810; found 307.9807.

Mp: 59 °C.

4-Iodo-4'-Methylazobenzene[4] (9a)

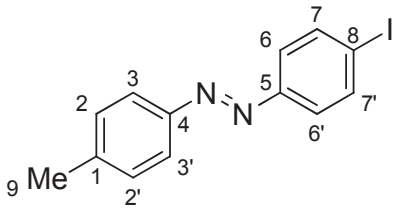

This reaction was not performed under Schlenk conditions. *p*-Toluidine (26.0 g, 243 mmol) was dissolved in DCM (100 mL) at 20 °C. A solution of Oxone (300 g, 488 mmol) in water (600 mL) was added in one portion and the reaction was stirred for 4 h at 20 °C. The dark green organic phase was separated and washed with hydrochloric acid (1 M, 2 x 150 mL), a saturated aqueous solution of hydrogen carbonate (1 x 150 mL) and water (1 x 200 mL). The organic phase was dried over magnesium sulfate. After evaporation of the solvent and without further purification, a solution of 4-iodoaniline (53.2 g, 243 mmol) in acetic acid (250 mL) was added to the crude product, and the reaction mixture was stirred for 16 h at 20 °C. The precipitate was filtered and dissolved in DCM (50 mL). The solution was washed hydrochloric acid (1 M, 2 x 150 mL), a saturated solution of hydrogen carbonate in water (1 x 150 mL) and water (1 x 200 mL). The combined organic phases were dried over magnesium sulfate. After evaporation of the solvent, 42.3 g (54%, Lit.: 93%[4]) of an orange solid was obtained.

^{1}H NMR (500 MHz, $CDCl_3$): 7.86 (d, ^3J = 8.5 Hz, 2 H, H-3,3'), 7.83 (d, ^3J = 8.5 Hz, 2 H, H-7,7'), 7.64 (d, ^3J = 8.5 Hz, 2 H, H-6,6'), 7.32 (d, ^3J = 8.5 Hz, 2 H, H-2,2'), 2.45 (s, 3H, H-9) ppm.

^{13}C NMR (125 MHz, $CDCl_3$): 152.0 (C-5), 150.6 (C-4), 142.0 (*C-1*), 138.3 (C-7,7'), 129.8 (C-2,2'), 124.4 (C-6,6'), 123.0 (C-3,3'), 97.2 (*C-8*), 21.5 (*C-9*) ppm.

IR (ATR): 3021 (w), 2978 (w), 2912 (w), 1600 (m), 1381 (m), 1105 (m), 1065 (m), 830 (s), 763 (s), 711 (s), 512 (s) cm^{-1}.

HRMS (EI-sector**):** *m/z* = $[M]^+$ calcd. for $[C_{13}H_{11}N_2I]^+$ 321.9967; found 321.9965.

Mp.: 160 °C [Lit=160 °C][2]

3-Iodo-4'methylazobenzene[5] (9b)

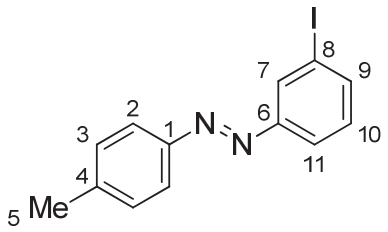

This reaction was not performed under Schlenk conditions. 4-Toluidine (1.00 eq, 16.4 g, 153 mmol) in DCM (60 mL) was added to Oxone (2.00 eq, 190 g, 309 mmol) in H_2O (750 mL) over the course of 30 s and vigorously stirred for 2.25 h at 22 °C. Then, the phases were allowed to separate, and the solvent of the organic phase was evaporated. The crude intermediate 4-methylnitrosobenzene (9.90 g) was used without further purification (4.64 g, 38.3 mmol, 25%). 4-Methyl-nitrosobenzene (1.00 eq, 4.64 g, 38.3 mmol) and 3-iodoaniline (1.10 eq, 8.95 g, 40.9 mmol) were stirred in acetic acid (90 mL) for 16.5 h at 85 °C. The solvent was evaporated and the product was crystallized from methanol as red needles (9.81 g, 30.5 mmol, 80%, Lit.:=23%[5]).

^{1}H NMR (500 MHz, $CDCl_3$): δ = 8.23 (dd, ^4J = 1.8, 1.8 Hz, 1 H, *H-7*), 7.89 (ddd, ^3J = 7.9 Hz, ^4J = 1.8, 1.0 Hz, 1 H, *H-11*), 7.82 (d, ^3J = 8.2 Hz, 2 H, *H-2*), 7.78 (ddd, ^3J = 7.8 Hz, ^4J = 1.8, 1.0 Hz, 1 H, *H-9*), 7.32 (d, ^3J = 8.2 Hz, 2 H, *H-3*), 7.25 (dd, ^3J = 7.9, 7.8 Hz, 1 H, *H-10*), 2.45 (s, 3 H, *H-5*) ppm.

^{13}C NMR (125 MHz, $CDCl_3$): δ = 153.7 (*C*6), 150.7 (*C*1), 142.4 (*C*4), 139.4 (*C*9), 130.8 (*C*7), 130.7 (*C*10), 123.0 (*C*3), 123.6 (*C*11), 123.2 (*C*2), 94.69 (*C*8), 21.7 (*C*5) ppm.

IR (ATR): $\tilde{\nu}$ = 2915 (w), 1741 (w), 1565 (m), 1500 (m), 1443 (m), 1207 (m), 1151 (m), 991 (m), 880 (m), 824 (s), 789 (s), 710 (m), 675 (s), 665 (s), 532 (m), 499 (s), 491 (s) cm^{-1}.

HRMS (EI-sector**):** *m/z* = $[M]^+$ calcd. for $[C_{13}H_{11}N_2I]^+$ 321.9967; found 321.9966;

Mp: 112 °C.

2-Iodo-4'-methyliodoazobenzene (9c)

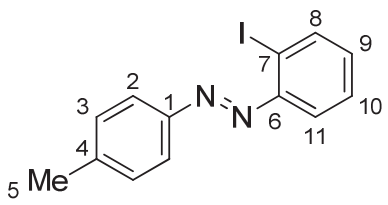

This reaction was not performed under Schlenk conditions. 4-Toluidine (1.00 eq, 16.4 g, 153 mmol) in DCM (60 mL) was added to Oxone (2.00 eq, 190 g, 309 mmol) in H_2O (750 mL) over the course of 30 s and vigorously stirred for 2.25 h at 22 °C. Then, the phases were allowed to separate, the solvent of the organic phase was evaporated. The crude intermediate 4-methylnitrosobenzene (9.90 g) was used without further purification (4.64 g, 38.3 mmol, 25%). 4-Methyl-nitrosobenzene (1.00 eq, 4.64 g, 38.3 mmol) and 3-iodoaniline (1.10 eq, 8.95 g, 40.9 mmol) were stirred in acetic acid (90 mL) for 16.5 h at 85 °C. The solvent was evaporated and the precipitate was recrystallized from methanol to give the product (6.74 g, 20.9 mmol, 55%) as red needles.

^{1}H NMR (500 MHz, $CDCl_3$): δ = 8.02 (dd, ^3J = 7.9 Hz, ^4J =1.3 Hz, 1 H, *H-8*), 7.91 (d, ^3J = 8.6 Hz, 2 H, *H-2*), 7.62 (dd, ^3J = 8.0 Hz, ^4J = 1.6 Hz, 1 H, *H-11*), 7.42 (ddd, ^3J = 8.0, 7.2 Hz, ^4J = 1.3 Hz, 1 H, *H-10*), 7.33 (d, ^3J = 8.6 Hz, 2 H, *H-3*), 7.15 (ddd, ^3J = 7.9, 7.2 Hz, ^3J = 1.6 Hz, 1 H, *H-9*), 2.45 (s, 3 H, *H-5*) ppm.

^{13}C NMR (125 MHz, $CDCl_3$): δ = 151.6 (*C*6), 150.7 (*C*1), 142.4 (*C*4), 139.9 (*C*8), 132.0 (*C*9), 130.0 (*C*3), 129.0 (*C*10), 123.7 (*C*2), 117.5 (*C*11), 102.4 (*C*7), 21.7 (*C*5) ppm.

IR (ATR): $\tilde{\nu}$ = 2915 (w), 1599 (m), 1500 (m), 1454 (m), 1420 (m), 1225 (w), 1147 (m), 1014 (m), 820 (s), 762 (s), 716 (m), 658 (m), 544 (m), 494 (s) cm^{-1}.

HRMS (EI-sector**):** *m/z* = $[M]^+$ calcd. for $[C_{13}H_{11}N_2I]^+$ 321.9967; found 321.9964.

Mp: 58 °C.

Stannylated Azobenzenes

4-(Trimethylstannyl)azobenzene (10a)

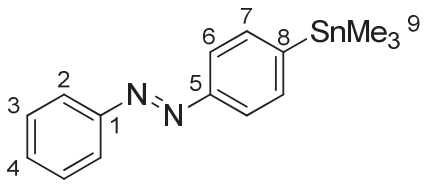

4-Iodo-azobenzene (1.00 eq, 2.39 g, 7.76 mmol), hexamethyldistannane (1.20 eq, 3.05 g, 9.32 mmol) and $Pd(PPh_3)_4$ (2 mol%, 180 mg, 155 µmol) were dissolved in toluene (15 mL) and MeTHF (1 mL). The reaction vessel was heated to 150 °C for 10 min in a microwave apparatus. The solvent was evaporated and the crude product purified by column

chromatography with *n*-hexane (R_f = 0.6). After solvent evaporation an orange oil (2.48 g, 7.19 mmol, 93%, Lit.: 61%[6(a)]) was obtained.

^{1}H NMR (500 MHz, $CDCl_3$): δ = 7.94 (d, ^3J = 7.3 Hz, 2 H, *H-2*), 7.89 (d, ^3J = 8.2 Hz, 2 H, *H-6*), 7.67 (d, ^3J = 8.2 Hz, 2 H, *H-7*), 7.53 (dd, ^3J = 7.3 Hz, ^3J = 7.3 Hz, 2 H, *H-3*), 7.48 (t, ^3J = 7.2 Hz, 1 H, *H-4*), 0.36 (s, 9 H, *H-9*) ppm.

^{13}C NMR (125 MHz, $CDCl_3$): δ = 152.9 (*C*1), 152.8 (*C*5), 147.3 (*C*8), 136.6 (*C*7), 131.0 (*C*4), 129.2 (*C*3), 123.0 (*C*2), 122.2 (*C*6), -9.3 (*C*9) ppm.

^{119}Sn NMR (186 MHz, $CDCl_3$): δ = -25.24 ppm.

IR (ATR): $\tilde{\nu}$ = 3020 (w), 2978 (w), 2915 (w), 2856 (w), 1481 (w), 1381 (w), 1065 (m), 1012 (m), 824 (m), 762 (s), 704 (m), 686 (s), 559 (m), 546 (m), 527 (s), 511 (m) cm^{-1}.

HRMS (EI-sector): *m/z* = $[M - Me]^+$ calcd for $[C_{14}H_{15}N_2Sn]^+$ 331.0257; found 331.0257.

3-(Trimethylstannyl)azobenzene (10b)

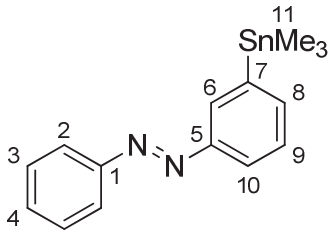

3-Iodo-azobenzene (1.00 eq, 2.39 g, 7.76 mmol), hexamethyldistannane (1.20 eq, 3.05 g, 9.32 mmol) and $Pd(PPh_3)_4$ (2 mol%, 180 mg, 155 µmol) were dissolved in toluene (15 mL). The reaction vessel was heated to 150 °C for 10 min in a microwave apparatus. The solvent was evaporated and the crude product purified column chromatography with *n*-hexane (R_f = 0.5). After solvent evaporation an orange oil (2.35 g, 6.81 mmol, 88%) was obtained.

^{1}H NMR (600 MHz, $CDCl_3$) δ = 8.04 (s, 1 H, *H-6*), 7.93 (d, ^3J = 7.6 Hz, 2 H, *H-2*), 7.84 (d, ^3J = 7.9 Hz, 1 H, *H-10*), 7.59 (d, ^3J = 7.0 Hz, 1 H, *H-8*), 7.52 (dd, ^3J = 7.6, 7.6 Hz, 2 H, *H-3*), 7.51 – 7.45 (m, 2 H, *H-4, H-9*), 0.36 (s, 9 H, *H-11*) ppm.

^{13}C NMR (151 MHz, $CDCl_3$) δ = 153.0 (*C*1), 152.1 (*C*5), 143.8 (*C*7), 138.7 (*C*8), 131.0 (*C*4), 130.7 (*C*6), 129.2 (*C*3), 128.8 (*C*9), 122.9 (*C*2), 122.2 (*C*10), -9.3 (*C*11) ppm.

^{119}Sn NMR (187 MHz, $CDCl_3$) δ = -24.01 ppm.

[a] In this report, the stannylation was performed using a Sandmeyer-Type reaction.

IR (ATR): $\tilde{\nu}$ = 2978 (w), 2911 (w), 1468 (w), 1395 (w), 1189 (w), 1070 (w), 924 (w), 791 (m), 761 (s), 715 (m), 690 (s), 525 (s), 511 (m), 487 (m) cm^{-1}.

HRMS (EI-sector**):** *m/z* = $[M]^+$ calcd. for $[C_{15}H_{18}N_2Sn]^+$ 346.0492; found 346.0492.

2-(Trimethylstannyl)azobenzene (10c)

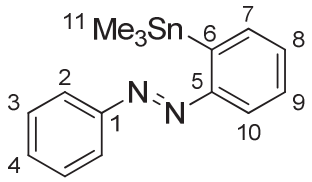

2-Iodo-azobenzene (1.00 eq, 2.39 g, 7.76 mmol), hexamethyldistannane (1.20 eq, 3.05 g, 9.32 mmol) and $Pd(PPh_3)_4$ (2 mol%, 180 µg, 155 µmol) were dissolved in toluene (15 mL) and MeTHF (1 mL). The reaction vessel was heated to 150 °C for 10 min in a microwave apparatus. The solvent was evaporated and the crude product purified by column chromatography with *n*-hexane (R_f = 0.4). The solvent was evaporated to give a red oil (1.16 g, 3.36 mmol, 43%).

^{1}H NMR (500 MHz, $CDCl_3$): δ = 7.96 (ddd, ^3J = 7.9 Hz, ^4J = 1.3 Hz, ^5J = 0.4 Hz, 1 H, *H-10*), 7.94-7.91 (m, 2 H, *H-2*), 7.75 (ddd, ^3J = 7.0 Hz, ^4J = 1.6 Hz, ^5J = 0.4 Hz, 1 H, *H-7*), 7.57-7.53 (m, 2 H, *H-3*), 7.53-7.48 (m, 2 H, *H-4*, *H-9*), 7.48-7.43 (m, 1 H, *H-8*), 0.33 (s, 9 H, *H-11*) ppm.

^{13}C NMR (125 MHz, $CDCl_3$): δ = 157.4 (*C*5), 152.3 (*C*1), 142.7 (*C*6), 136.7 (*C*7), 131.1 (*C*9), 130.5 (*C*8), 129.6 (*C*4), 129.3 (*C*3), 123.0 (*C*2), 121.1 (*C*10), -7.1 (*C*11) ppm.

^{119}Sn NMR (186 MHz, $CDCl_3$): δ = -35.62 ppm.

IR (ATR): $\tilde{\nu}$ = 3056 (w), 2976 (w), 2911 (w), 1449 (w), 1295 (w), 1106 (w), 767 (s), 704 (m), 685 (s), 528 (s), 509 (m), 485 (w) cm^{-1}.

HRMS (EI-sector): *m/z* = $[M - Me]^+$ calcd. for $[C_{14}H_{15}N_2Sn]^+$ 331.0257; found 331.0262.

4-Methyl-4'-(trimethylstannyl)azobenzene[2] (11a)

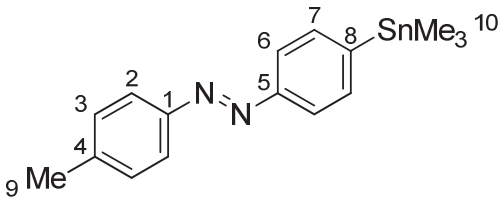

4-Methyl-4'-iodoazobenzene (1.00 eq, 2.50 g, 7.76 mmol), hexamethyldistannane (1.20 eq, 3.05 g, 9.32 mmol) and $Pd(PPh_3)_4$ (2 mol%, 180 mg, 155 µmol) were dissolved in toluene (15 mL). The reaction vessel was heated to 150 °C for 10 min in a microwave apparatus. The solvent was evaporated and the crude product purified by filtration through a pad of silica with DCM as eluent. The solvent was evaporated and the residue purified by column chromatography with *n*-hexane (R_f = 0.5). Evaporation of the solvent gave an orange solid (2.45 g, 6.83 mmol, 88%, Lit.: 95%[2]).

^{1}H NMR (500 MHz, $CDCl_3$): δ = 7.85 (d, ^3J = 8.2 Hz, 2 H, *H-6*), 7.83 (d, ^3J = 8.2 Hz, 2 H, *H-2*), 7.65 (d, ^3J = 8.2 Hz, 2 H, *H-7*), 7.32 (d, ^3J = 8.2 Hz, 2 H, *H-3*), 2.44 (s, 3 H, *H-9*), 0.34 (s, 9 H, *H-10*) ppm.

^{13}C NMR (125 MHz, $CDCl_3$): δ = 152.9 (*C*5), 151.0 (*C*1), 146.8 (*C*8), 141.6 (*C*4), 136.6 (*C*7), 129.9 (*C*3), 123.0 (*C*2), 122.0 (*C*6), 21.7 (*C*9), -9.3 (*C*10) ppm.

^{119}Sn NMR (186 MHz, $CDCl_3$): δ = -25.25 ppm.

IR (ATR): $\tilde{\nu}$ = 3023 (w), 2986 (w), 2913 (w), 1600 (w), 1381 (w), 1157 (w), 1106 (w), 1066 (w), 1011 (w), 829 (s), 764 (s), 711 (m), 547 (s), 526 (s), 513 (s), 479 (m) cm^{-1}.

HRMS (EI-sector): *m/z* = $[M]^+$ calcd for $[C_{16}H_{20}N_2Sn]^+$ 360.0649, found 360.0647.

Mp: 60 °C.

4-Methyl-3'-(trimethylstannyl)azobenzene (11b)

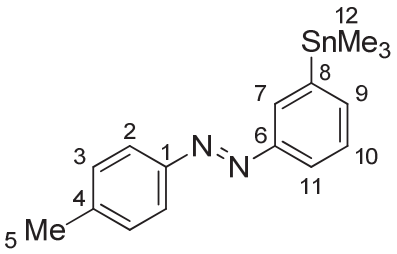

4-Methyl-3'-iodoazobenzene (1.00 eq, 2.50 g, 7.76 mmol), hexamethyldistannane (1.20 eq, 3.05 g, 9.32 mmol) and $Pd(PPh_3)_4$ (2 mol%, 180 mg, 155 µmol) were dissolved in toluene (15 mL). The reaction vessel was heated to 150 °C for 10 min in a microwave apparatus. The solvent was evaporated and the crude product purified by column chromatography with *n*-hexane as eluent (R_f = 0.5). After the solvent was evaporated, the product was obtained as an orange solid (2.46 g, 683 mmol, 88%).

^{1}H NMR (500 MHz, $CDCl_3$): δ = 8.02 (dd, ^4J = 1.2, 0.7 Hz, 1 H, *H-7*), 7.84 (d, ^3J = 8.1 Hz, 2 H, *H-2*), 7.81 (m, 1 H, *H-11*), 7.58 (ddd, ^3J = 7.1 Hz, ^4J = 1.2, 1.1 Hz, 1 H, *H-9*), 7.48 (ddd, ^3J = 7.1, 7.1 Hz, ^4J = 0.7 Hz, 1 H, *H-10*), 7.32 (d, ^3J =8.1 Hz, 2 H, *H-3*), 2.44 (s, 3 H, *H-5*), 0.36 (s, 9 H, *H-12*) ppm.

^{13}C NMR (125 MHz, $CDCl_3$): δ = 152.2 (*C*6), 151.1 (*C*1), 143.7 (*C*8), 141.6 (*C*4), 138.4 (*C*9), 130.6 (*C*7), 129.9 (*C*3), 128.8 (*C*10), 123.0 (*C*2), 122.1 (*C*11), 21.6 (*C*5), -9.3 (*C*12) ppm.

^{119}Sn NMR (186 MHz, $CDCl_3$): δ = -24.32 ppm.

IR (ATR): $\tilde{\nu}$ = 3047 (w), 2978 (w), 2911 (w), 1601 (w), 1501 (w), 1391 (w), 1189 (w), 1158 (w), 1092 (w), 1011 (w), 921 (w), 829 (s), 788 (m), 767 (s) 712 (s), 690 (s), 529 (s), 513 (m), 492 (s), 468 (w) cm^{-1}.

HRMS (EI-sector**):** *m/z* = $[M]^+$ calcd. for $[C_{16}H_{20}N_2Sn]^+$ 360.0648; found 360.0646;

Mp: 67 °C.

4-Methyl-2‘-(trimethylstannyl)azobenzene (11c)

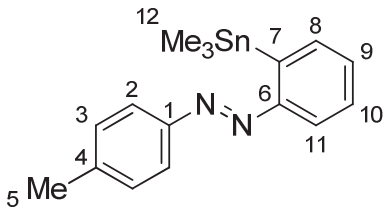

4-Methyl-2’-iodoazobenzene (1.00 eq, 3.00 g, 9.31 mmol), hexamethyldistannane (1.20 eq, 3.66 g, 11.2 mmol) and $Pd(PPh_3)_4$ (2 mol%, 216 mg, 186 µmol) were heated to 150 °C in toluene (15 mL) for 15 min in a microwave apparatus. The solvent was evaporated and the crude product purified by column chromatography with *n*-hexane (R_f = 0.5) as eluent to give a red oil (1.77 g, 4.93 mmol, 53%).

^{1}H NMR (500 MHz, $CDCl_3$): δ = 7.91 (dd, ^3J = 7.9 Hz, ^4J = 1.1 Hz, 1 H, *H-11*), 7.81 (d, ^3J = 8.2 Hz, 2 H, *H-2*), 7.71 (dd, ^3J = 7.2 Hz, ^3J = 1.3 Hz, 1 H, *H-8*), 7.49 (ddd, ^3J = 7.9, 7.2 Hz, ^4J = 1.3 Hz, 1 H, *H-10*), 7.43 (dd, ^3J = 7.2, 7.2 Hz, ^4J = 1.1 Hz, 1 H, *H-9*), 7.33 (d, ^3J = 8.2 Hz, 2 H, *H-3*), 2.45 (s, 3 H, *H-5*), 0.30 (s, 9 H, *H-12*) ppm.

^{13}C NMR (125 MHz, $CDCl_3$): δ = 157.4 (*C*6), 150.4 (*C*1), 142.4 (*C*7), 141.7 (*C*4), 136.6 (*C*8), 130.3 (*C*9), 130.0 (*C*3), 129.5 (*C*10), 123.0 (*C*2), 121.0 (*C*11), 21.6 (*C*5), -7.1 (*C*12) ppm.

^{119}Sn NMR (187 MHz, $CDCl_3$) δ = -36.46 ppm.

IR (ATR): $\tilde{\nu}$ = 2977 (w), 2916 (w), 1601 (w), 1504 (w), 1294 (w), 1149 (m), 1107 (m), 1014 (w), 823 (s), 764 (s), 710 (m), 548 (m), 527 (s), 499 (m) cm^{-1}.

HRMS (EI-sector): *m/z* = $[M]^+$ calcd. for $[C_{16}H_{20}N_2Sn]^+$ 383.0543; found 383.0542.

Compounds with one Azobenzene Unit

4,4'-Dimethylazobenzene (14a)

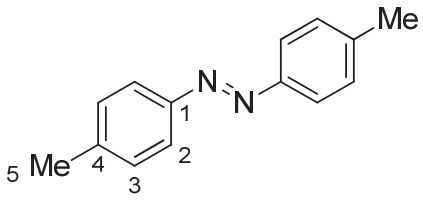

To a solution of 4-methyl-4'-(trimethylstannyl)-azobenzene (1.00 eq, 250 mg, 700 µmol) in THF (10 mL), a solution of methyllithium (0.99 eq, 440 µL, 700 µmol, 1.58 M in diethyl ether), diluted in THF (1.58 mL) was added at -78 °C over the course of 4 min. After 2 min, a solution of methyl iodide (1.10 eq, 50.0 µL, 800 µmol) in THF (0.32 mL) was added and the reaction mixture was warmed to 20 °C. After 6 h stirring the solvent was evaporated and the residue purified using column chromatography with DCM (R_f = 0.7) as eluent. The solvent was evaporated and yellow crystalline needles (140 mg, 666 µmol, 96%) were obtained.

^{1}H NMR (500 MHz, $CDCl_3$): δ = 7.82 (d, ^3J = 8.4 Hz, 4 H, H-2), 7.32 (d, ^3J = 8.4 Hz, 4 H, H-3), 2.44 (s, 6 H, H-5) ppm.

^{13}C NMR (125 MHz, $CDCl_3$): δ = 150.8 (C-1), 141.2 (C-4), 129.7 (C-2), 122.7 (C-3), 21.5 (C-5) ppm.

IR (ATR): $\tilde{\nu}$ = 3023 (w), 2921 (w), 1601 (m), 1502 (m), 1306 (w), 1237 (w), 1149 (m), 1012 (m), 883 (m), 839 (m), 821 (s), 794 (m), 710 (m), 683 (s), 535 (m), 504 (s) 492 (s) cm^{-1}.

HRMS (EI-sector): *m/z* = $[M]^+$ calcd. for $[C_{14}H_{14}N_2$ 210.1157$]^+$; found 210.1156.

Mp: 145 °C

3,4'-Dimethylazobenzene (14b)

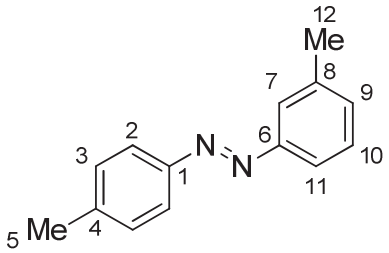

To a solution of 4-methyl-3'-(trimethylstannyl)-azobenzene (1.00 eq, 250 mg, 700 µmol) in THF (10 mL), a solution of methyllithium (0.99 eq, 440 µL, 700 µmol, 1.58 M in diethyl ether),

diluted in THF (1.58 mL) was added at -78 °C over the course of 4 min. After another 2 min, a solution of methyl iodide (1.10 eq, 50.0 µL, 800 µmol) in THF (0.32 mL) was added and the reaction mixture was warmed to 20 °C. After stirring the reaction mixture for 13 h, the solvent was evaporated and the residue purified using column chromatography with DCM (R_f = 0.7) as eluent. Drying *in vacuo* gave an orange solid (140 mg, 666 µmol, 95% Lit.: 38%[7(a)]).

^{1}H NMR (500 MHz, $CDCl_3$): δ = 7.83 (d, ^3J = 8.1 Hz, 2 H, *H-2*), 7.74 – 7.69 (m, 2 H, *H-7, H-11*), 7.40 (dd, ^3J = 8.4, 7.5 Hz, 1 H, *H-10*), 7.32 (d, ^3J = 8.1 Hz, 2 H, *H-3*), 7.28 (d, ^3J = 7.5 Hz, 1 H, *H-9*), 2.46 (s, 3 H, *H-12*), 2.44 (s, 3 H, *H-5*) ppm.

^{13}C NMR (125 MHz, $CDCl_3$): δ = 153.0 (*C*6), 151.0 (*C*1), 141.6 (*C*4), 139.1 (*C*8), 131.6 (*C*9), 129.9 (*C*3), 129.0 (*C*10), 123.0 (*C*2), 122.9 (*C*7), 120.5 (*C*11), 21.6 (*C*5), 21.5 (*C*12) ppm.

IR (ATR): $\tilde{\nu}$ = 3023 (w), 2921 (w), 1601 (m), 1502 (m), 1306 (w), 1237 (w), 1149 (m), 1012 (m), 883 (m), 839 (m), 821 (s), 794 (m), 710 (m), 683 (s), 535 (m), 504 (s) 492 (s) cm^{-1}.

HRMS (EI-sector): *m/z* = $[M]^+$ calcd. for $[C_{14}H_{14}N_2]^+$ 210.1157; found 210.1159.

Mp: 46 °C

2-Methyl-4'-methylazobenzene (14c)

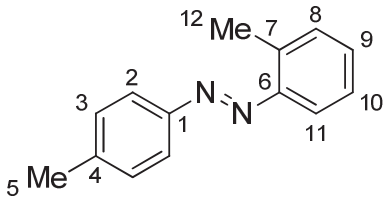

To a solution of 4-methyl-2'-(trimethylstannyl)-azobenzene (1.00 eq, 240 mg, 672 µmol) in THF (10 mL), a solution of methyllithium (0.99 eq, 420 µL, 672 µmol, 1.58 M in diethyl ether), diluted in THF (1.58 mL) was added at -78 °C over the course of 4 min. After another 2 min, a solution of methyl iodide (1.10 eq, 50.0 µL, 800 µmol) in THF (320 µL) was added and the reaction mixture was warmed to 20 °C. After 16 h stirring, solvent was evaporated and the residue filtered over magnesium sulfate with DCM. Drying *in vacuo* gave a red oil (140 mg, 666 µmol, 99%, Lit.: (no yield given)[8(b)].

^{1}H NMR (500 MHz, CD_2Cl_2): δ = 7.84 (d, ^3J = 8.4 Hz, 2 H, *H-2*), 7.62 (d, 1 H, *H-11*), 7.38-7.36 (m, 2 H, *H-8, H-9*), 7.34 (d, ^3J = 8.4 Hz, 2 H, *H-3*), 7.31 – 7.23 (m, 1 H, *H-10*), 2.72 (s, 3 H, *H-12*), 2.45 (s, 3 H, *H-5*) ppm.

[a] In this report, the compound was synthesized by hydrogen transfer using palladium(II) acetylacetonate.
[b] In this report, the compound was synthesized from 2-nitrosotoluene and *para*-toluidine.

^{13}C NMR (125 MHz, CD_2Cl_2): δ = 151.8 (*C*1), 151.3 (*C*6), 142.2 (*C*4), 138.6 (*C*7), 131.8 (*C*8), 131.2 (*C*9), 130.3 (*C*3), 126.9 (*C*10), 123.4 (*C*2), 115.9 (*C*11), 21.8 (*C*5), 17.8 (*C*12) ppm.

IR (ATR): $\tilde{\nu}$ = 3025 (w), 2922 (w), 2865 (w), 1600 (w), 1501 (w), 1451 (w), 1150 (m), 1106 (w), 1039 (w), 1014 (w), 823 (s), 761 (s), 718 (s), 554 (m), 497 (m), 481 (m) cm^{-1}.

HRMS (EI-sector): *m/z* = $[M]^+$ calcd. for $[C_{14}H_{14}N_2]^+$ 210.1157; found 210.1158.

4-Methyl-4'-(trimethylsilyl)azobenzene (17a)

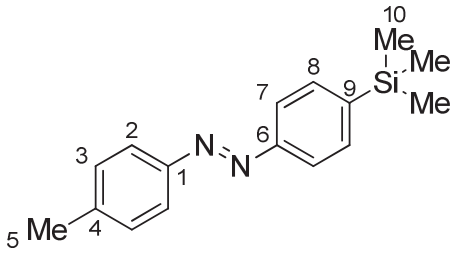

To 4'-trimethylstannyl-4-methylazobenzene (1.00 eq, 250 mg, 700 µmol) in THF (10 mL), a solution of methyllithium (0.99 eq, 44.0 µL, 700 µmol, 1.58 M in diethyl ether) in THF (2 mL) was added at -78 °C over the course of 4 min. After another 2 min, trimethylchlorosilane (1.10 eq, 100 µL, 770 µmol) in THF (900 µL) was added. The reaction mixture was warmed to 20 °C over the course of 15 min and stirred for 12 h. The solvent was removed *in vacuo* and the residue purified using column chromatography with *n*-hexane as eluent (R_f = 0.6). The solvent was evaporated to give an orange solid (144 mg, 540 µmol, 77%).

^{1}H NMR (500 MHz, $CDCl_3$): δ = 7.86 (d, ^3J = 8.3 Hz, 2 H, *H-7*), 7.84 (d, ^3J = 8.0 Hz, 2 H, *H-2*), 7.67 (d, ^3J = 8.3 Hz, 2 H, *H-8*), 7.86 (d, ^3J = 8.0 Hz, 2 H, *H-3*), 2.44 (s, 3 H, *H-5*), 0.32 (s, 9 H, *H-10*) ppm.

^{13}C NMR (125 MHz, $CDCl_3$): δ = 153.2 (*C*6), 151.1 (*C*1), 144.3 (*C*9), 141.7 (*C*4), 134.2 (*C*8), 129.9 (*C*3), 123.0 (*C*2), 121.9 (*C*7), 21.7 (*C*5), -1.0 (*C*10) ppm.

^{29}Si NMR (99 MHz, $CDCl_3$) δ = -3.61 ppm.

IR (ATR): $\tilde{\nu}$ = 3028 (w), 2954 (w), 2900 (w), 1600 (w), 1499 (w), 1385 (w), 1248 (m), 1105 (m), 824 (s), 757 (m), 719 (m), 624 (w), 548 (m) cm^{-1}.

HRMS (EI-sector): *m/z* = $[M]^+$ calcd. for $[C_{16}H_{20}N_2Si]^+$ 268.1396; found 268.1401.

Mp: 48 °C.

4-Methyl-3'-(trimethylsilyl)azobenzene (17b)

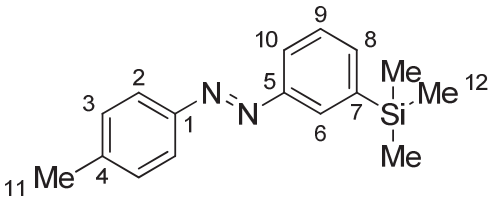

To a solution of 3'-trimethylstannyl-4-methylazobenzene (1.00 eq, 250 mg, 700 µmol) in THF (10 mL), a solution of methyllithium (0.99 eq, 44.0 µL, 700 µmol, 1.58 M in diethyl ether) diluted in THF (2 mL) was added at -78 °C over the course of 4 min. After another 2 min, trimethylchlorosilane (1.10 eq, 100 µL, 770 µmol) in THF (900 µL) was added. The reaction mixture was warmed to 20 °C over the course of 15 min and stirred for 12 h. The solvent was removed *in vacuo* and the residue purified using column chromatography with DCM as eluent (R_f = 0.7). The solvent was evaporated to give a red solid (178 mg, 663 µmol, 95%).

^{1}H NMR (500 MHz, $CDCl_3$): δ = 8.09 – 8.03 (m, 1 H, *H-6*), 7.89 – 7.79 (m, 3 H, *H-2, H-10*), 7.62 (ddd, ^3J = 7.3 Hz, ^4J = 1.2, 1.2 Hz, 1 H, *H-8*), 7.50 (dd, ^3J = 7.3, 7.3 Hz, 1 H, *H-9*), 7.32 (d, ^3J = 8.0 Hz, 2 H, *H-3*), 2.45 (s, 3 H, *H-11*), 0.34 (s, 9 H, *H-12*) ppm.

^{13}C NMR (125 MHz, $CDCl_3$): δ = 152.2 (*C*5), 151.1 (*C*1), 142.0 (*C*7), 141.6 (*C*4), 135.9 (*C*8), 129.9 (*C*3), 128.8 (*C*6), 128.7 (*C*9), 123.0 (*C*2), 122.1 (*C*10), 21.6 (*C*11), -1.0 (*C*12) ppm.

^{29}Si NMR (99 MHz, $CDCl_3$) δ = -3.35 ppm.

IR (ATR): $\tilde{\nu}$ = 3058 (w), 2953 (w), 1601 (w), 1503 (w), 1394 (w), 1249 (s), 1106 (m), 1012 (w), 867 (m), 825 (s), 796 (s), 754 (s), 712 (s), 688 (s), 621 (m), 531 (m), 493 (s) cm^{-1}.

HRMS (EI-sector): *m/z* = $[M]^+$ calcd. for $C_{16}H_{20}N_2Si$ [268.1396]$^+$; found 268.1400.

Mp: 44 °C

4-Methyl-2'-trimethylsilylazobenzene (17c)

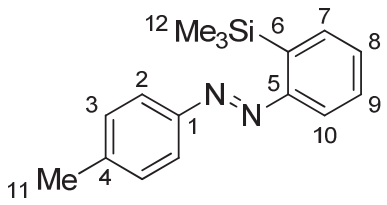

To 2'-trimethylstannyl-4-methylazobenzene (1.00 eq, 150 mg, 560 µmol) in THF (10 mL), a solution of methyllithium (0.99 eq, 35.0 µL, 560 µmol, 1.58 M in diethyl ether) in THF (2 mL) was added at -78 °C over the course of 4 min. After another 2 min, trimethylsilane (1.10 eq, 76.0 µL, 600 µmol) in THF (930 µL) was added. The reaction mixture was warmed to 20 °C over the course of 15 min and stirred for 12 h. Solvent was removed *in vacuo* and the residue filtered over magnesium sulfate with DCM. Evaporation of the solvent gave a dark red oil (123 mg, 459 µmol, 82%).

^{1}H NMR (500 MHz, $CDCl_3$): δ = 7.84 (d, ^{3}J = 8.2 Hz, 2 H, *H-2*), 7.74 (dd, ^{3}J = 7.9 Hz, ^{4}J = 1.1 Hz, 1 H, *H-10*), 7.69 (dd, ^{3}J = 7.2 Hz, ^{4}J = 1.6 Hz, 1 H, *H-7*), 7.47 (ddd, ^{3}J = 7.9 Hz, ^{3}J = 7.4 Hz, ^{4}J = 1.6 Hz, 1 H, *H-9*), 7.42 (ddd, ^{3}J = 7.4 Hz, ^{3}J = 7.2 Hz, ^{4}J = 1.1 Hz, 1 H, *H-8*), 7.34 (d, ^{3}J = 8.2 Hz, 2 H, *H-3*), 2.45 (s, 3 H, *H-11*), 0.38 (s, 9 H, *H-12*) ppm.

^{13}C NMR (125 MHz, $CDCl_3$): δ = 157.6 (*C*5), 150.9 (*C*1), 141.6 (*C*4) 141.6 (*C*6), 134.8 (*C*7), 130.1 (*C*9), 123.0 (*C*3), 123.0 (*C*8), 123.3 (*C*2), 114.9 (*C*10), 21.6 (*C*11), 0.7 (*C*12) ppm.

^{29}Si NMR (99 MHz, $CDCl_3$) δ = -4.17 ppm.

IR (ATR): $\tilde{\nu}$ = 3056 (w), 2953 (w), 1601 (w), 1503 (w), 1419 (w), 1243 (m), 1149 (m), 1117 (m), 833 (s), 822 (s), 766 (m), 750 (m), 720 (s), 687 (m), 549 (m) 494 (m) cm^{-1}.

HRMS (EI-sector**):** *m/z* = $[M]^+$ calcd. for $[C_{16}H_{20}N_2Si]^+$ 268.1396; found 268.1396.

4-(1-Hydroxy-1-methylethyl)-4'-methylazobenzene (18a)

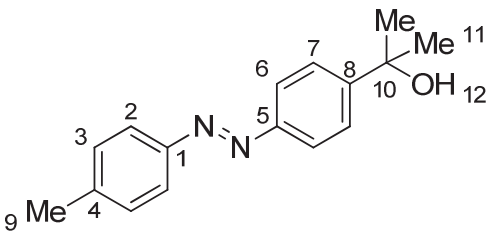

To 4'-trimethylstannyl-4-methylazobenzene (1.00 eq, 250 mg, 700 µmol) in THF (10 mL), a solution of methyllithium (0.99 eq, 440 µL, 700 µmol, 1.58 M in diethyl ether) diluted in THF (2 mL) was added at -78 °C over the course of 4 min. After another 2 min, acetone (1.10 eq, 60.0 µL, 770 µmol) in THF (940 µL) was added. The reaction mixture was warmed to 20 °C over the course of 15 min and then stirred for 12 h. Hydrochloric acid (1 M, 36 mL) was added, and the aqueous phase was extracted with DCM (3 x 30 mL). The combined organic phases were concentrated to obtain an orange oil. The product was purified using column chromatography with DCM as an eluent (R_f = 0.1). The solvent was evaporated to give an orange foamy solid (157 mg, 617 µmol, 88%, Lit.: 11%[9])

^{1}H NMR (500 MHz, $CDCl_3$): δ = 7.88 (d, ^3J = 8.7 Hz, 2 H, *H-6*), 7.83 (d, ^3J = 8.1 Hz, 2 H, -*H-2*), 7.63 (d, ^3J = 8.7 Hz, 2 H, *H-7*), 7.31 (d, ^3J = 8.1 Hz, 2 H, *H-3*), 2.44 (s, 3 H, *H-9*), 1.76 (s, 1 H, -*H*12) 1.63 (s, 6 H, *H-11*) ppm.

^{13}C NMR (125 MHz, $CDCl_3$): δ = 151.9 (*C*5), 151.7 (*C*8), 151.0 (*C*1), 141.6 (*C*4), 129.9 (*C*3), 125.3 (*C*7), 123.0 (*C*2), 122.8 (*C*6), 72.8 (*C*10), 31.9 (*C*11), 21.6 (*C*9) ppm.

IR (ATR): $\tilde{\nu}$ = 3430 (b), 2927 (w), 2931 (w), 1600 (w), 1496 (w), 1403 (w), 1370 (w), 1156 (m), 1129 (m), 1084 (m), 1010 (w), 944 (w), 847 (s), 822 (s), 591 (w), 567 (s), 536 (m) cm^{-1}.

HRMS (EI-sector): *m/z* = $[M]^+$ calcd for $[C_{16}H_{18}N_2O]^+$ 254.1419; found 254.1422.

Mp: 103 °C.

3-(1-Hydroxy-1-methylethyl)-4'-methylazobenzene (18b)

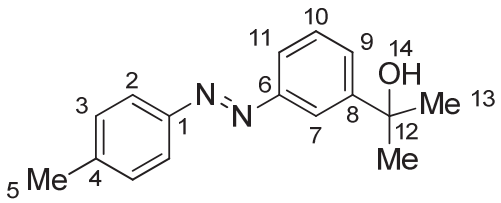

To 4-Methyl-3'-trimethylstannylazobenzene (1.00 eq, 250 mg, 70.0 µmol) in THF (10 mL) was a solution of methyllithium (0.99 eq, 44.0 µL, 70.0 µmol) in THF (2 mL) at -78 °C added over the course of 4 min. Acetone (1.10 eq, 60.0 µL, 77.0 µmol) in THF (940 µL) was added after 2 min. The reaction mixture was warmed to 20 °C over the course of 15 min and stirred for 13 h. Hydrochloric acid (1 M, 36 mL) was added, the aqueous phase was extracted with DCM (3 x 30 mL). The combined organic phases were concentrated to obtain an orange oil. The crude product was purified using column chromatography with DCM as eluent (R_f = 0.2). Removal of the solvent under reduced pressure gave a red oil (140 mg, 554 µmol, 79%).

^{1}H NMR (500 MHz, $CDCl_3$): δ = 8.03 (dd, ^4J = 1.8, 1.8 Hz, 1 H, *H-7*), 7.84 (d, ^3J = 8.2 Hz, 2 H, *H-2*), 7.78 (ddd, ^3J = 7.9 Hz, ^4J = 1.8, 1.1 Hz, 1 H, *H-11*), 7.62 (ddd, ^3J = 7.9 Hz, ^4J = 1.8, 1.1 Hz, 1 H, *H-9*), 7.48 (dd, ^3J = 7.9, 7.9 Hz, 1 H, *H-10*), 7.32 (d, ^3J = 8.2 Hz, 2 H, *H-3*), 2.44 (s, 3 H, *H-5*), 1.80 (s, 1 H, *H*-14), 1.66 (s, 6 H, *H-13*) ppm.

^{13}C NMR (125 MHz, $CDCl_3$): δ = 152.9 (*C*6), 150.9 (*C*1), 150.5 (*C*8), 141.7 (*C*4), 129.9 (*C*3), 129.1 (*C*10), 127.0 (*C*9), 123.0 (*C*2), 121.0 (*C*11), 119.3 (*C*7), 72.8 (*C*12), 31.9 (*C*13), 21.6 (*C*5) ppm.

IR (ATR): $\tilde{\nu}$ = 3398 (b), 2973 (w), 2923 (w), 2862 (w), 1602 (w), 1502 (w), 1364 (w), 1208 (w), 1154 (m), 954 (m), 823 (s), 797 (m), 711 (m), 694 (s), 640 (w), 544 (m), 518 (m) cm^{-1}.

HRMS (EI-sector): *m/z* = $[M]^+$ calcd for $[C_{16}H_{18}N_2O]^+$ 254.1421; found 254.1422.

4-Tolyl-[4-(4-methylphenyl)azo-phenyl)]methanol (19a)

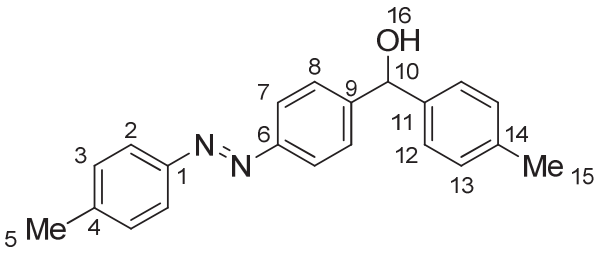

To 4'-trimethylstannyl-4-methylazobenzene (1.00 eq, 250 mg, 700 µmol) in THF (10 mL), a solution of methyllithium (0.99 eq, 44.0 µL, 700 µmol, 1.58 M in diethyl ether) in THF (2 mL) was added at -78 °C over the course of 4 min. After another 2 min, 4-methylbenzaldehyde (1.10 eq, 90.0 µL, 770 µmol) in THF (900 µL) was added. The reaction mixture was warmed to 20 °C over the course of 15 min and stirred for 13 h. Hydrochloric acid (0.1 M, 25 mL) was added. After phase separation, the aqueous phase was extracted with DCM (3 x 30 mL). The combined organic phases were evaporated to obtain an orange oil. The product was purified using column chromatography with DCM as eluent (R_f = 0.4) to give an orange solid (211 mg, 667 µmol, 95%).

^{1}H NMR (600 MHz, $CDCl_3$): δ = 7.87 (d, ^3J = 8.4 Hz, 2 H, *H-7*), 7.81 (d, ^3J = 8.2 Hz, 2 H, *H-2*), 7.53 (d, ^3J = 8.4 Hz, 2 H, *H-8*), 7.31 (d, ^3J = 8.2 Hz, 2 H, *H-3*), 7.28 (d, ^3J = 7.9 Hz, 2 H, *H-12*), 7.16 (d, ^3J = 7.9 Hz, 2 H, *H-13*), 5.89 (s, 1 H, *H-10*), 2.67 (s, 1 H, *H*-16), 2.44 (s, 3 H, *H-5*), 2.34 (s, 3 H, *H-15*) ppm.

^{13}C NMR (150 MHz, $CDCl_3$): δ = 152.2 (*C*6), 150.9 (*C*1), 146.6 (*C*9), 141.7 (*C*4), 140.8 (*C*11), 137.8 (*C*14), 129.9 (*C*3), 129.5 (*C*13), 127.2 (*C*8), 126.8 (*C*12), 123.0 (*C*7), 123.0 (*C*2), 76.0 (*C*10), 21.6 (*C*5), 21.3 (*C*15) ppm.

IR (ATR): $\tilde{\nu}$ = 3559 (b), 2917 (s), 2849 (s), 1600 (w), 1512 (m), 1463 (m), 1152 (m), 1055 (m), 824 (s), 793 (s), 769 (m), 759 (m), 569 (s), 528 (s), 515 (m) cm^{-1}.

HRMS (EI-sector**):** *m/z* = $[M]^+$ calcd. for $[C_{21}H_{20}N_2O]^+$ 316.1576; found 316.1580.

Mp: 118 °C.

4-Tolyl-[3-(4-methylphenyl)azo-phenyl)]methanol (19b)

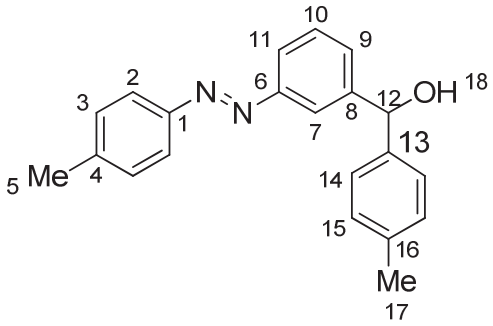

To 3'-trimethylstannyl-4-methylazobenzene (1.00 eq, 250 mg, 700 µmol) in THF (10 mL), a solution of methyllithium (0.99 eq, 44.0 µL, 700 µmol, 1.58 M in diethyl ether) in THF (2 mL) was added at -78 °C over the course of 4 min. After another 2 min, 4-methylbenzaldehyd (1.10 eq, 90.0 µL, 770 µmol) in THF (900 µL) was added. The reaction mixture was warmed to 20 °C over the course of 15 min and stirred for 13 h. Hydrochloric acid (1 M, 12 mL) was added. After phase separation, the aqueous phase was extracted with DCM (3 x 30 mL). The combined organic phases were evaporated to obtain an orange oil. The product was purified using column chromatography with DCM as eluent (R_f = 0.6), concentration gave an orange solid (197 mg, 623 µmol, 89%).

^{1}H NMR (500 MHz, $CDCl_3$): δ = 7.96 (s, 1 H, *H-7*), 7.82 (d, ^{3}J = 8.0 Hz, 2 H, *H-2*), 7.84-7.80 (m, 1 H, *H-11*), 7.52 – 7.43 (m, 2 H, *H-9, H-10*), 7.31 (d, ^{3}J = 8.0 Hz, 4 H, *H-3, H-14*), 7.16 (d, ^{3}J = 8.0 Hz, 2 H, *H-15*), 5.92 (s, 1 H, *H-12*), 2.44 (s, 3 H, *H-5*), 2.34 (s, 3 H, *H-17*), 2.29 (s, 1 H, *H*-18) ppm.

^{13}C NMR (125 MHz, $CDCl_3$): δ = 153.0 (*C*6), 150.9 (*C*1), 145.3 (*C*8), 141.8 (*C*4), 140.8 (*C*13), 137.7 (*C*16), 129.9 (*C*3), 129.5 (*C*15), 129.3 (*C*10), 128.8 (*C*9), 126.8 (*C*14), 123.0 (*C*2), 121.8 (*C*11), 121.0 (*C*7), 76.1 (*C*12), 21.7 (*C*5), 21.3 (*C*17) ppm.

IR (ATR): $\tilde{\nu}$ = 3317 (b), 3027 (w), 2920 (w), 2862 (w), 1601 (w), 1504 (m), 1174 (m), 1150 (m), 1036 (s), 823 (m), 793 (s), 753 (s), 691 (s), 638 (m), 535 (s), 515 (s), 482 (s) cm^{-1}.

HRMS (EI-sector): *m/z* = $[M]^+$ calcd. for $[C_{21}H_{20}N_2O]^+$ 316.1576; found 316.1580.

Mp: 116 °C

4-Formyl-4'-methylazobenzene (20a)

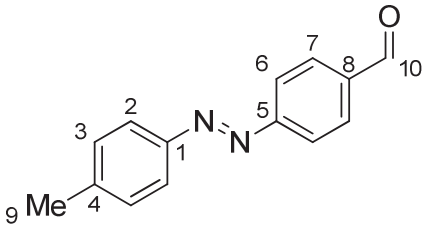

To 4'-trimethylstannyl-4-methylazobenzene (1.00 eq, 250 mg, 700 µmol) in THF (10 mL), a solution of methyllithium (0.99 eq, 44.0 µL, 700 µmol, 1.58 M in diethyl ether) in THF (2 mL) was added at -78 °C over the course of 4 min. After another 2 min, *N,N*-dimethylformamide (1.10 eq, 50.0 µL, 770 µmol) in THF (950 µL) was added. The reaction mixture was warmed to 20 °C over the course of 15 min and stirred for 72 h. Hydrochloric acid (1 M, 6 mL) was added. After phase separation, the aqueous phase was extracted with DCM (3 x 30 mL). The combined organic phases were evaporated to obtain an orange oil. The product was purified using column chromatography with DCM as eluent (R_f = 0.5) to give small orange platelets (139 mg, 620 µmol, 89%, Lit.; 25%[10 (a)]).[b]

^{1}H NMR (500 MHz, $CDCl_3$): δ = 10.10 (s, 1 H, *H-10*), 8.01-8.04 (m, 4 H, *H-6*, *H-7*), 7.87 (d, ^3J = 8.2 Hz, 2 H, *H-2*), 7.43 (d, ^3J = 8.2 Hz, 2 H, *H-3*), 2.46 (s, 3 H, *H-9*) ppm.

^{13}C NMR (125 MHz, $CDCl_3$): δ = 191.8 (*C*10), 156.2 (*C*5), 150.9 (*C*1), 143.0 (*C*4), 137.4 (*C*8), 130.8 (*C7*), 130.1 (*C*3), 123.5 (*C*6), 123.4 (*C*2), 21.8 (*C*9) ppm.

IR (ATR): $\tilde{\nu}$ = 3036 (w), 2925 (w), 2833 (w), 2729 (w), 1694 (s), 1596 (m), 1499 (m), 1306 (m), 1292 (m), 1197 (s), 1135 (m), 808 (s), 760 (m), 720 (m), 659 (m), 546 (s), 523 (m) cm^{-1}.

HRMS (EI-sector): *m/z* = $[M]^+$ calcd. for $[C_{14}H_{12}N_2O]^+$ 224.0950, found 224.0954.

Mp: 176 °C.

[a] In this report, the product was obtained by a reaction of *para*-nitrobenzaldehyde and 5 eq. *para*-methyl phenyl imino dimagnesium.

4-Methyl-4'formylazobenzene (20b)

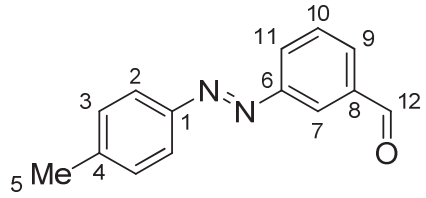

To a solution of 3'-trimethylstannyl-4-methylazobenzene (1.00 eq, 250 mg, 700 µmol) in THF (10 mL), a solution of methyllithium (0.99 eq, 44.0 µL, 700 µmol) in THF (2 mL) was added at -78 °C over the course of 4 min. After another 2 min, *N*,*N*-dimethylformamide (1.10 eq, 50.0 µL, 770 µmol) in THF (950 µL) was added. The reaction mixture was warmed to 20 °C over the course of 15 min and stirred for 12 h. Hydrochloric acid (1 M, 12 mL) was added. After phase separation, the aqueous phase was extracted with DCM (3 x 30 mL). The combined organic phases were dried over magnesium sulfate and concentrated in vacuo. The crude product was purified by column chromatography with DCM as eluent (R_f = 0.8) to give orange platelets (134 mg, 584 µmol, 83%, Lit.: 82%10[(a)]).

^{1}H NMR (500 MHz, $CDCl_3$) δ = 10.13 (s, 1 H, *H-12*), 8.38 (dd, ^4J = 1.7, 1.7 Hz, 1 H, *H-7*), 8.16 (ddd, ^3J = 7.7 Hz, ^4J = 1.7, 1.3 Hz, 1 H, *H-11*), 7.99 (ddd, ^3J = 7.7 Hz, ^4J = 1.7, 1.3 Hz, 1 H, *H-9*), 7.87 (d, ^3J = 8.2 Hz, 2 H, *H-2*), 7.68 (dd, ^3J = 7.7, 7.7 Hz, 1 H, *H-10*), 7.34 (d, ^3J = 8.2 Hz, 2 H, *H-3*), 2.45 (s, 3 H, *H-5*) ppm.

^{13}C NMR (125 MHz, $CDCl_3$) δ = 191.9 (*C*12), 153.2 (*C*6), 150.7 (*C*1), 142.6 (*C*4), 137.5 (*C*8), 130.9 (*C*9), 130.0 (*C*3), 130.0 (*C*10), 128.8 (*C*11), 123.9 (*C*7), 123.3 (*C*2), 21.7 (*C*5) ppm.

IR (ATR): $\tilde{\nu}$ = 3024 (w), 2922 (w), 2840 (w), 1689 (s), 1601 (w), 1580 (m), 1502 (w), 1390 (w), 1193 (m), 1145 (m), 1107 (m), 904 (w), 820 (s), 807 (m), 678 (s), 645 (s), 528 (s), 500 (s), 493 (m) cm^{-1}.

HRMS (EI-sector): *m/z* = $[M]^+$ calcd. for $[C_{14}H_{12}N_2O]^+$ 224.0950; found 224.0951.

Mp: 201 °C

[a] In this report, the product was obtained by a reaction of *para*-nitrobenzaldehyde and 5 eq. *para*-methyl phenyl imino dimagnesium.

***N*-Methoxy-*N*-methylbenzamide (21)[11]**

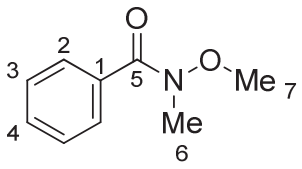

Triethylamine (2.00 eq, 2.80 mL, 20.0 mmol) was slowly added to *N*-methoxymethylamine hydrochloride (1.00 eq, 976 mg, 10.0 mmol) in DCM (25 mL) over the course of 1 min at 0 °C. Benzoylchloride (1.00 eq, 1.16 mL, 10.0 mmol) was added dropwise at 0 °C and then allowed to warm to 22 °C and was stirred for 1 h. After quenching with aqueous sodium hydrogencarbonate solution (15 mL), the organic phase was washed with hydrochloric acid (1 M, 5 mL), brine (5 mL) and dried over sodium sulfate. The crude product was purified by column chromatography with DCM as eluent (R_f = 0.2). The solvent was evaporated to obtain a colorless oil (1.60 mg, 9.69 mmol, 97%, Lit.: 99%11).

^{1}H NMR (500 MHz, $CDCl_3$): δ = 7.66 (d, ^3J = 7.3 Hz, 2 H, *H-2*), 7.44 (t, ^3J = 7.3 Hz, 1 H, *H-4*), 7.39 (dd, ^3J = 7.3 Hz, 7.3 Hz, 2 H, *H-3*), 3.55 (s, 3 H, *H-7*), 3.35 (s, 3 H, *H-6*) ppm.

^{13}C NMR (125 MHz, $CDCl_3$): δ = 170.1 (*C*5), 134.28 (*C*1), 130.67 (*C*4), 128.26 (*C*2), 128.13 (*C*3), 61.15 (*C7*), 33.92 (*C*6) ppm.

IR (ATR): $\tilde{\nu}$ = 2971 (w), 2935 (w), 1637 (s), 1447 (m), 1413 (m), 1374 (m), 1212 (w), 977 (m), 787 (m), 703 (s), 558 (w) cm^{-1}.

HRMS (EI-sector**):** *m/z* = $[M]^+$ calcd. for $[C_9H_{11}NO_2]^+$ 166.0863; found 166.0869.

Phenyl-[4-(4-methylphenyl)azo-phenyl)]ketone (22a)

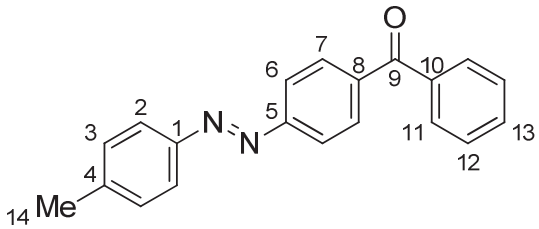

To 4'-trimethylstannyl-4-methylazobenzene (1.00 eq, 250 mg, 700 µmol) in THF (10 mL) a solution of methyllithium (0.99 eq, 440 µL, 700 µmol, 1.58 M in diethyl ether) diluted in THF (2 mL) was added at -78 °C over the course of 4 min. After another 2 min, *N*-methoxy-*N*-methylbenzamide (1.10 eq, 117 µL, 770 µmol) in THF (0.88 mL) was added. The reaction mixture was warmed to 20 °C over the course of 15 min and then stirred for 16 h.

Hydrochloric acid (12 mL, 1 M) was added, the aqueous phase extracted with DCM (2 x 15 mL) and the solvent of the combined organic phases was evaporated to give an orange solid (205 mg, 683 µmol, 98%).

^{1}H NMR (500 MHz, CD_2Cl_2): δ = 7.99 (d, ^3J = 8.7 Hz, 2 H, *H-6*), 7.94 (d, ^3J = 8.7 Hz, 2 H, *H-7*), 7.88 (d, ^3J = 8.3 Hz, 2 H, *H-2*), 7.83 (d, ^3J = 7.6 Hz, 2 H, *H-11*), 7.64 (t, ^3J = 7.6 Hz, 1 H, *H-13*), 7.53 (dd, ^3J = 7.6, 7.6 Hz, 2 H, *H-12*), 7.37 (d, ^3J = 8.3 Hz, 2 H, *H-3*), 2.46 (s, 3 H, *H-14*) ppm.

^{13}C NMR (125 MHz, CD_2Cl_2): δ = 196.3 (*C*9*)*, 155.3 (*C*5*)*, 151.4 (*C*1*)*, 143.3 (*C*4*)*, 139.6 (*C*8*)*, 138.1 (*C*10*)*, 133.1 (*C*13*)*, 131.6 (*C*7*)*, 130.5 (*C*11*)*, 130.5 (*C*3*)*, 129.0 (*C*12*)*, 123.7 (*C*2*)*, 123.0 (*C*6*)*, 21.9 (*C*14*)* ppm.

IR (ATR): $\tilde{\nu}$ = 3030 (w), 2919 (w), 2825 (w), 1643 (m), 1598 (m), 1443 (m), 1303 (m), 1222 (m), 1151 (m), 1012 (m) 921 (m), 843 (m), 822 (s), 764 (m), 706 (m), 684 (s), 545 (s) cm^{-1}.

HRMS (EI-sector): *m/z* = $[M]^+$ calcd. for $[C_{20}H_{16}N_2O]^+$ 300.1263; found 300.1259.

Mp: 115 °C.

Phenyl-[3-(4-methylphenyl)azo-phenyl)]ketone (22b)

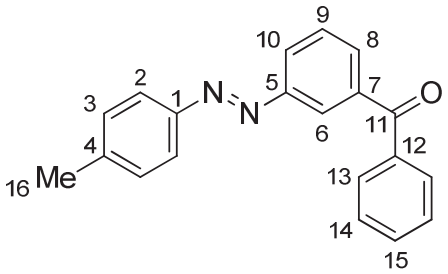

To 3'-trimethylstannyl-4-methylazobenzene (1.00 eq, 250 mg, 700 µmol) in THF (10 mL) a solution of methyllithium (0.99 eq, 440 µL, 700 µmol, 1.58 M in diethyl ether) diluted in THF (2 mL) was added at -78 °C over the course of 4 min. After another 2 min, *N*-methoxy-*N*-methylbenzamid (1.10 eq, 117 µL, 770 µmol) in THF (880 µL) was added. The reaction mixture was warmed to 20 °C over the course of 15 min and then stirred for 13 h. The solvent was evaporated and the crude product purified by column chromatography through silica with DCM as eluent (R_f = 0.9). Evaporation of the solvent gave an orange solid (149 mg, 496 µmol, 71%).

^{1}H NMR (500 MHz, $CDCl_3$): δ = 8.30 (dd, ^4J = 1.8, 1.8 Hz, 1 H, *H-6*), 8.12 (ddd, ^3J = 7.9, ^4J = 1.8, ^4J = 1.2 Hz, 1 H, *H-10*), 7.91 (d, ^3J = 7.6 Hz, 1 H, *H-8*), 7.87 (dd, ^3J = 8.0, ^4J = 1.4

Hz, 2 H, *H-13*), 7.84 (d, ^3J = 8.3 Hz, 2 H, *H-2*), 7.67-7.59 (m, 2 H, *H-9, H-15*), 7.52 (dd, ^3J = 8.0, 8.0 Hz, 2 H, *H-14*), 7.32 (d, ^3J = 8.3 Hz, 2 H, *H-3*), 2.44 (s, 3 H, *H-16*) ppm.

^{13}C NMR (125 MHz, $CDCl_3$): δ = 196.3 (*C*11), 152.6 (*C*5), 150.8 (*C*1), 142.3 (*C*4), 138.8 (*C*7), 137.5 (*C*12), 132.8 (*C*15), 131.9 (*C*8), 130.3 (*C*13), 123.0 (*C*3), 129.3 (*C*9), 128.6 (*C*14), 126.1 (*C*10), 124.7 (*C*6), 123.2 (*C*2), 21.7 (*C*16) ppm.

IR (ATR): $\tilde{\nu}$ = 3059 (w), 3024 (w), 2925 (w), 2868 (w), 1657 (s), 1598 (w), 1280 (m), 1210 (w), 844 (w), 822 (m), 721 (w), 706 (s), 691 (m), 681 (m), 493 (w) cm^{-1}.

HRMS (EI-sector): *m/z* = $[M]^+$ calcd. for $[C_{20}H_{16}N_2O]^+$ 300.1263; found 300.1259.

Mp: 75 °C.

4-Methy-(4'-*N*-Phenylformamid)azobenzene (23a)

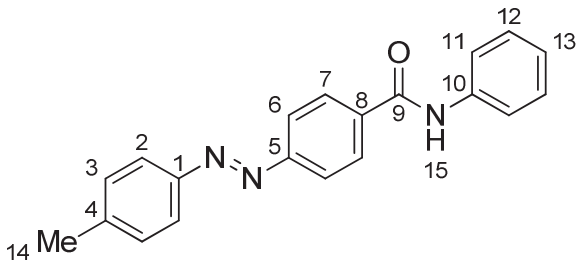

To 4'-trimethylstannyl-4-methylazobenzene (1.00 eq, 250 mg, 700 µmol) in THF (10 mL) a solution of methyllithium (0.99 eq, 440 µL, 700 µmol, 1.58 M in diethyl ether) diluted in THF (2 mL) was added at -78 °C over the course of 4 min. After another 2 min, phenylisocyanate (1.10 eq, 83.0 µL, 770 µmol) in THF (0.92 mL) was added. The reaction mixture was warmed to 20 °C over the course of 15 min and then stirred for 16 h. The solvent was evaporated, the precipitate solved in toluene and filtered over magnesium sulfate. The product crystallised at -20 °C as orange shiny platelets (169 mg, 537 µmol, 77%) from toluene.

^{1}H NMR (500 MHz, THF-d_8): δ = 9.49 (s, 1 H, *H*-15), 8.11 (d, ^3J = 8.5 Hz, 2 H, *H-7*), 7.97 (d, ^3J = 8.5 Hz, 2 H, *H-6*), 7.86 (d, ^3J = 8.4 Hz, 2 H, *H-2*), 7.81 (d, ^3J = 7.6 Hz, 2 H, *H-11*), 7.36 (d, ^3J = 8.4 Hz, 2 H, *H-3*), 7.33 – 7.26 (m, 2 H, *H-12*), 7.05 (t, ^3J = 7.4 Hz, 1 H, *H-13*), 2.43 (s, 3 H, *H-14*) ppm.

^{13}C NMR (125 MHz, THF-d_8): δ = 165.5 (*C*9), 155.3 (*C*5), 152.0 (*C*1), 143.4 (*C*4), 140.8 (*C*10), 138.7 (*C*8), 130.8 (*C*3), 129.5 (*C*7), 129.5 (*C*12), 124.5 (*C*13), 124.0 (*C*2), 123.4 (*C*6), 121.0 (*C*11), 21.66 (*C*14) ppm.

IR (ATR): $\tilde{\nu}$ = 3353 (w), 2365 (w), 2321 (w), 1656 (m), 1598 (m), 1523 (s), 1495 (m), 1438 (m), 1322 (m), 860 (m), 823 (s), 751 (s), 689 (s), 660 (s), 626 (m), 548 (s), 505 (m) cm^{-1}.

HRMS (EI-sector): *m/z* = $[M]^+$ calcd. for $[C_{20}H_{17}N_3O]^+$ 315.1372; found 315.1373.

Mp: 233 °C.

4-Methy-(3'-*N*-Phenylformamid)azobenzene (23b)

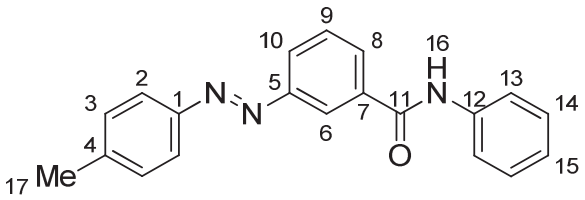

To a solution of 3'-trimethylstannyl-4-methylazobenzene (1.00 eq, 250 mg, 700 µmol) in THF (10 mL) a solution of methyllithium (0.99 eq, 440 µL, 700 µmol, 1.58 M in diethyl ether) diluted in THF (2 mL) was added at -78 °C over the course of 4 min. After another 2 min, phenyl isocyanate (1.10 eq, 83.0 µL, 770 µmol) in THF (0.92 mL) was added. The reaction mixture was warmed to 20 °C over the course of 15 min and then stirred for 15 h. The solvent was evaporated, the precipitate dissolved in toluene and filtered over magnesium sulfate. The product crystallized at -20 °C as small orange crystals (166 mg, 526 µmol, 76%).

^{1}H NMR (500 MHz, $CDCl_3$) δ = 8.33 (dd, ^4J = 1.8, 1.8 Hz, 1 H, *H-6*), 8.09 (ddd, ^3J = 7.8 Hz, ^4J = 1.8, 1.2 Hz, 1 H, *H-10*), 8.03 (ddd, ^3J = 7.8 Hz, ^4J = 1.8, 1.2 Hz, 1 H, *H-8*), 7.96 (s, 1 H, *H*-16), 7.86 (d, ^3J = 8.3 Hz, 2 H, *H-2*), 7.68 (d, ^3J = 8.4 Hz, 2 H, *H-13*), 7.65 (dd, ^3J = 7.8, 7.8 Hz, 1 H, *H-9*), 7.40 (dd, ^3J = 8.4, 7.5 Hz, 2 H, *H-14*), 7.34 (d, ^3J = 8.3 Hz, 2 H, *H-3*), 7.18 (t, ^3J = 7.5 Hz, 1 H, *H-15*), 2.46 (s, 3 H, *H-17*) ppm.

^{13}C NMR (125 MHz, $CDCl_3$) δ = 165.2 (*C*11), 152.8 (*C*5), 150.7 (*C*1), 142.5 (*C*4), 137.9 (*C*12), 136.2 (*C*7), 130.0 (*C*3), 129.9 (*C*9), 129.6 (*C*8), 129.3 (*C*14), 126.5 (*C*10), 124.9 (*C*15), 123.2 (*C*2), 120.5 (*C*13), 120.41 (*C*6), 21.7 (*C*17) ppm.

IR (ATR): $\tilde{\nu}$ = 3252 (m), 3024 (w), 2925 (w), 1650 (s), 1597 (m), 1524 (s), 1499 (s), 1442 (s), 1324 (m), 1241 (w), 1157 (w), 903 (w), 822 (s), 747 (s), 688 (s), 551 (m), 512 (s), 491 (m), 459 (w) cm^{-1}.

Mp: 199 °C.

HRMS (EI-sector): *m/z* = $[M]^+$ calcd. for $[C_{20}H_{17}N_3O]^+$ 315.1372; found 315.1372.

4-Methy-(4'-*N*-Phenylthioformamid)azobenzene (24a)

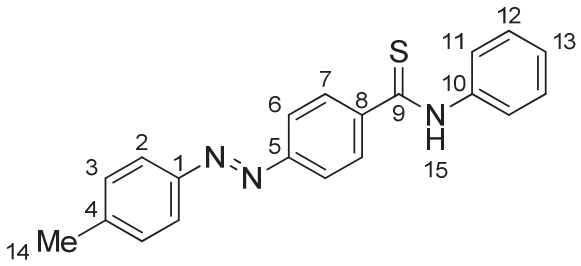

To 4'-trimethylstannyl-4-methylazobenzene (1.00 eq, 250 mg, 700 µmol) in THF (10 mL) a solution of methyllithium (0.99 eq, 440 µL, 700 µmol, 1.58 M in diethyl ether) diluted in THF (2 mL) was added at -78 °C over the course of 4 min. After another 2 min, phenylisothiocyanate (1.10 eq, 92.0 µL, 770 µmol) in THF (0.91 mL) was added. The reaction mixture was warmed to 20 °C over the course of 15 min and then stirred for 16 h. Water (20 mL) were added and the aqueous phase was extracted with toluene (2 x 50 mL). The combined organic phases were filtered over magnesium sulfate and the solvent evaporated. After solving the precipitate in toluene the product crystallized at -20 °C as red-orange shiny platelets (185 mg, 559 µmol, 80%).

^{1}H NMR (500 MHz, THF-d8): δ = 10.92 (s, 1 H, *H*-15), 8.01 (d, ^{3}J = 8.4 Hz, 2 H, *H-7*), 7.95 – 7.88 (m, 4 H, *H-6*, *H-11*), 7.86 (d, ^{3}J = 8.1 Hz, 2 H, *H-2*), 7.39 (m, 2 H, *H-12*), 7.35 (d, ^{3}J = 8.1 Hz, 2 H, *H-3*), 7.22 (t, ^{3}J = 7.4 Hz, 1 H, *H-13*), 2.43 (s, 3 H, *H-14*) ppm.

^{13}C NMR (125 MHz, THF-d8): δ = 198.0 (*C*9), 154.6 (*C*5), 152.0 (*C*1), 146.5 (*C*8), 143.3 (*C*4), 141.7 (*C*10), 130.8 (*C*3), 129.4 (*C*12), 129.2 (*C*7), 127.0 (*C*13), 124.7 (*C*11), 124.0 (*C*2), 123.2 (*C*6), 21.66 (C14) ppm.

IR (ATR): $\tilde{\nu}$ = 3324 (w), 2320 (w), 1594 (w), 1525 (m), 1496 (m), 1439 (w), 1407 (m), 1351 (m), 1282 (m), 1200 (m), 984 (m), 853 (s), 826 (m), 757 (s), 721 (s), 685 (s), 546 (s), 528 (m), 505 (m) cm^{-1}.

Mp: 208 °C.

HRMS (EI-sector) *m/z* = [M]$^{+}$ calcd. for [$C_{20}H_{17}N_3S$]$^{+}$ 331.1143; found 331.1140.

4-Methy-(3'-*N*-Phenylthioformamid)azobenzene (24b)

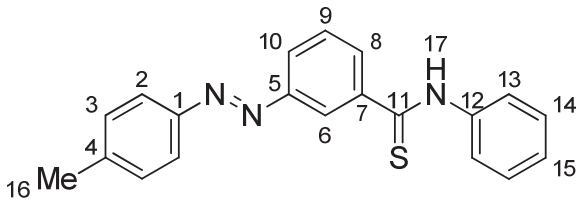

To 3'-Trimethylstannyl-4-methylazobenzene (1.00 eq, 250 mg, 700 µmol) in THF (10 mL) a solution of methyllithium (0.99 eq, 440 µL, 700 µmol, 1.58 M in diethyl ether) diluted in THF (2 mL) was added at -78 °C over the course of 4 min. After another 2 min, phenylisothiocyanate (1.10 eq, 92.0 µL, 770 µmol) in THF (910 µL) was added. The reaction mixture was warmed to 20 °C over the course of 15 min and then stirred for 16 h. Water (20 mL) was added and the aqueous phase was extracted with toluene (2 x 50 mL). The combined organic phases were filtered over magnesium sulfate and the solvent was evaporated. After solving the precipitate in toluene the product crystallized at -20 °C as small orange platelets (188 mg, 567 µmol, 81%).

^{1}H NMR (500 MHz, DMSO-d_6) δ = 11.98 (s, 1 H, *H*-17), 8.28 (dd, ^{4}J = 1.8, 1.8 Hz, 1 H, *H-6*), 8.07 – 7.98 (m, 2 H, *H-8, H-10*), 7.86 (m, 4 H, *H-2,H-13*), 7.69 (dd, J = 7.8, 7.8 Hz, 1 H, *H-9*), 7.46 (dd, ^{3}J = 7.6, 7.6 Hz, 2 H, *H-14*), 7.42 (d, ^{3}J = 8.1 Hz, 2 H, *H-3*), 7.30 (t, ^{3}J = 7.6 Hz, 1 H, *H-15*), 2.42 (s, 3 H, *H-16*) ppm.

^{13}C NMR (125 MHz, DMSO-d_6) δ = 196.4 (*C*11), 151.4 (*C*5), 150.0 (*C*1), 143.7 (*C7*), 142.2 (*C*4), 140.0 (*C*12), 130.1 (*C*3), 130.0 (*C*8), 129.3 (*C*9), 128.5 (*C*14), 126.4 (*C*13), 124.7 (*C*10), 124.1 (*C*15), 122.7 (*C*2), 120.9 (*C*6) 21.1 (*C*16) ppm.

IR (ATR): $\tilde{\nu}$ = 3266 (m), 3049 (w), 2919 (w), 2865 (w), 1650 (w), 1596 (m), 1518 (s), 1498 (m), 1444 (s), 1296 (m), 1153 (m), 999 (s), 818 (s), 755 (m), 702 (s), 684 (s), 663 (s), 564 (m), 531 (s), 494 (s), 476 (m) cm^{-1}.

HRMS (EI-sector): *m/z* = $[M]^+$ calcd. for $[C_{20}H_{17}N_3S]^+$ 331.1143; found 331.1139.

Mp: 128 °C.

Compounds with Multiple Azobenzene Units

4-Phenyl-di-[4-(4-methylphenyl)azo-phenyl)]methanol (25a)

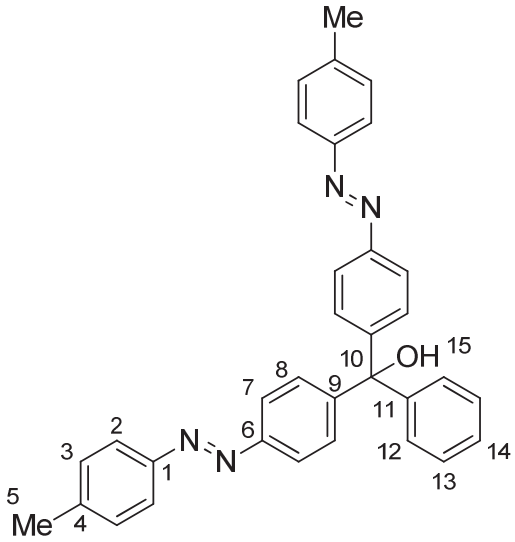

To 4'-trimethylstannyl-4-methylazobenzene (1.00 eq, 250 mg, 700 µmol) in THF (10 mL), a solution of methyllithium (0.99 eq, 44.0 µL, 700 µmol, 1.6 M in diethyl ether) in THF (2 mL) was added at -78 °C over the course of 4 min. Benzoylchloride (2.4 eq, 190 µL, 1.66 mmol) in THF (0.81 mL) was added after 30 s. The reaction mixture was warmed to 20 °C over the course of 15 min and stirred for 18 h. After evaporation of the solvent, the crude product was purified using column chromatography with DCM as eluent (R_f = 0.5) to give an orange foamy solid (168 mg, 340 µmol, 96%).

^{1}H NMR (500 MHz, CD_2Cl_2): δ = 7.87 (d, ^3J = 8.8 Hz, 4 H, *H-7*), 7.83 (d, ^3J = 8.3 Hz, 4 H, *H-2*), 7.50 (d, ^3J = 8.8 Hz, 4 H, *H-8*), 7.39-7.31 (m, 9 H, *H-3, H-12, H-13, H-14*), 3.06 (s, 1 H, *H-15*), 2.44 (s, 6 H, *H-5*) ppm.

^{13}C NMR (125 MHz, CD_2Cl_2): δ = 152.4 (*C*6), 151.4 (*C*1), 149.7 (*C*9), 146.9 (*C*11), 142.6 (*C*4), 130.4 (*C*3), 129.3 (*C*8), 128.8 (*C*12 or 13), 128.5 (*C*12 or 13), 128.3 (*C*14), 123.4 (*C*2), 122.8 (*C*7), 82.4 (*C*10), 21.8 (*C*5) ppm.

IR (ATR): $\tilde{\nu}$ = 3368 (b), 3028 (w), 1602 (w), 1492 (w), 1447 (w), 1153 (w), 1028 (m), 1012 (m), 823 (s), 755 (m), 670 (m), 594 (m), 562 (m) cm^{-1}.

Mp: 162 °C.

HRMS (EI-sector**):** *m/z* = $[M]^+$ calcd. for $[C_{33}H_{28}N_4O]^+$ 496.2263; found 496.2263.

Phenyl-di-[3-(4-methylphenyl)azo-phenyl)]methanol (25b)

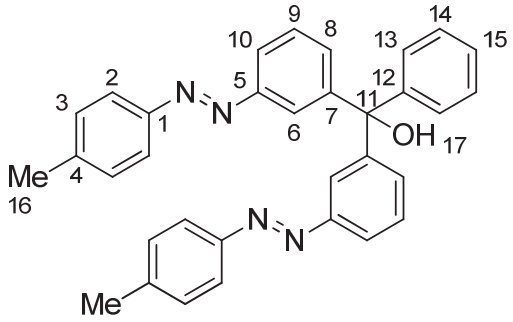

To 4-methyl-3'-trimethylstannylazobenzene (1.00 eq, 250 mg, 700 µmol) in THF (10 mL), a solution of methyllithium (1.58 M in diethyl ether, 0.99 eq, 440 µL, 700 µmol) in THF (2 mL) was added at -78 °C added over the course of 4 min. Benzoylchloride (1.10 eq, 95.0 µL, 770 µmol) in THF (810 µL) was added after 2 min. The reaction mixture was warmed to 20 °C over the course of 15 min and stirred for 18 h. After evaporation of the solvent, the crude product was purified using column chromatography with DCM as eluent (R_f = 0.8) to give a red oil (123 mg, 248 µmol, 71%).

^{1}H NMR (500 MHz, $CDCl_3$): δ = 7.98 (dd, ^4J = 1.8, 1.8 Hz, 2 H, *H-6*), 7.82 (ddd, ^3J = 7.7 Hz, ^4J = 1.8, 1.8 Hz, 2 H, *H-10*), 7.78 (d, ^3J = 8.2 Hz, 4 H, *H-2*), 7.47 (dd, ^3J = 7.7, 7.7 Hz, 2 H, *H-9*), 7.43 (ddd, ^3J = 7.7 Hz, ^3J = 1.8, 1.8 Hz, 2 H, *H-8*), 7.39 – 7.35 (m, 4 H, *H-13, H-14*), 7.34 – 7.32 (m, 1 H, *H-15*), 7.28 (d, ^3J = 8.2 Hz, 4 H, *H-3*), 3.01 (s, *H*-17), 2.42 (s, 6 H, *H-16*) ppm.

^{13}C NMR (125 MHz, $CDCl_3$): δ = 152.8 (*C*5), 150.9 (*C*1), 147.9 (*C*7), 146.5 (*C*12), 141.8 (*C*4), 130.4 (*C*8), 129.9 (*C*3), 128.9 (*C*9), 128.4 (*C*13 or 14), 128.3 (*C*13 or 14), 127.8 (*C*15), 123.5 (*C*6), 123.1 (*C*2), 120.7 (*C*10), 82.1 (*C*11), 21.6 (*C*16) ppm.

IR (ATR): $\tilde{\nu}$ = 3461 (b), 3062 (w), 6036 (w), 2922 (w), 2868 (w), 1600 (m), 1502 (w), 1447 (m), 1151 (s), 1014 (m), 823 (s), 797 (s), 751 (m), 710 (s), 694 (s), 492 (m) cm^{-1}.

HRMS (EI-sector**):** *m/z* = $[M]^+$ calcd. for $[C_{33}H_{28}N_4O]^+$ 496.2263; found 496.2264.

4-Tolyl-di-[4-(4-methylphenyl)azo-phenyl)]methanol (26a)

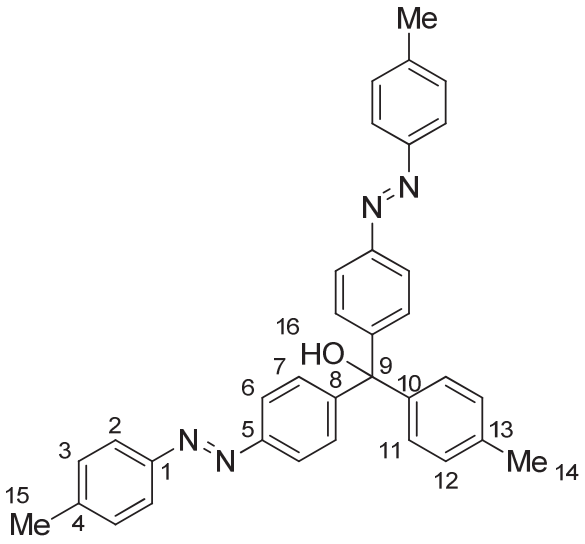

To 4'-trimethylstannyl-4-methylazobenzene (1.00 eq, 250 mg, 700 µmol) in THF (10 mL), a solution of methyllithium (0.99 eq, 44.0 µL, 700 µmol, 1.58 M in diethyl ether) in THF (2 mL) was added at -78 °C over the course of 4 min. Methyl-4-methylbenzoate (0.50 eq, 53.0 mg, 350 µmol) in THF (1.00 mL) was added after 2 min. The reaction mixture was warmed to 20 °C over the course of 15 min and stirred for 13 h. After addition of HCl (1 M, 20 mL), the organic phase was extracted with DCM (3 x 30 mL) and the combined organic phases were evaporated. The product was purified using column chromatography with DCM as eluent (R_f = 0.4) to give an orange oil (142 mg, 278 µmol, 79%).

^{1}H NMR (500 MHz, CD_2Cl_2): δ = 7.86 (d, ^3J = 8.6 Hz, 4 H, *H-6*), 7.82 (d, ^3J = 8.4 Hz, 4 H, -*H-2*), 7.50 (d, ^3J = 8.6 Hz, 4 H, *H-7*), 7.34 (d, ^3J = 8.4 Hz, 4 H, *H-3*), 7.22 (d, ^3J = 8.4 Hz, 2 H, *H-11*), 7.18 (d, ^3J = 8.4 Hz, 2 H, *H-12*), 3.00 (s, 1 H, *H*-16), 2.44 (s, 6 H, *H-15*), 2.36 (s, 3 H, *H-14*) ppm.

^{13}C NMR (125 MHz, CD_2Cl_2): δ = 152.4 (*C*5), 151.4 (*C*1), 149.9 (*C*8), 144.0 (*C*10), 142.5(*C*4), 138.2 (*C*13), 130.3 (*C*3), 129.4 (*C*12), 129.2 (*C*7), 128.3 (*C*11), 123.4 (*C*2), 122.8 (*C*6), 82.2 (*C*9), 21.8 (*C*15), 21.3 (*C*14) ppm.

IR (ATR): $\tilde{\nu}$ = 3465 (b), 2962 (w), 1599 (w), 1495 (w), 1407 (w), 1260 (m), 1145 (m), 1093 (m), 1033 (s), 1010 (s), 822 (s), 806 (s), 736 (m), 709 (m), 583 (s), 561 (m) cm^{-1}.

HRMS (EI**):** *m/z* = $[M]^+$ calcd. for $[C_{34}H_{30}N_4O]^+$ 510.2420; found 510.2417.

4-Tolyl-di-[3-(4-methylphenyl)azo-phenyl)]methanol (26b)

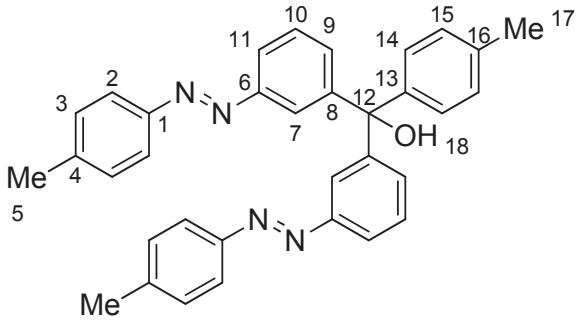

To 3'-Trimethylstannyl-4-methylazobenzene (1.00 eq, 250 mg, 700 µmol) in THF (10 mL) was a solution of methyllithium (0.99 eq, 440 µL, 700 µmol) in THF (2 mL) at -78 °C added over the course of 4 min. methyl 4-toluate (0.50 eq, 53.0 mg, 350 µmol) in THF (1.00 mL) was added after 2 min. The reaction mixture was warmed to 20 °C over the course of 15 min and stirred for 13 h. After addition of hydrochloric acid (1 M, 20 mL), the organic phase was extracted with DCM (3 x 30 mL) and the combined organic phases were evaporated. The product was purified using column chromatography with DCM as eluent (R_f = 0.7) to give a foamy orange solid (281 mg, 551 µmol, 79%).

^{1}H NMR (500 MHz, $CDCl_3$): δ = 7.99 (t, ^4J = 1.7 Hz, 2 H, *H-7*), 7.81 (ddd, ^3J = 7.5 Hz, ^4J = 1.7, 1.7 Hz, 2 H, *H-11*), 7.79 (d, ^3J = 8.1 Hz, 4 H, *H-2*), 7.49 – 7.40 (m, 4 H, *H-9, H-10*), 7.28 (d, ^3J = 8.1 Hz, 4 H, *H-3*), 7.25 (d, ^3J = 8.2 Hz, 2 H, *H-14*), 7.16 (d, ^3J = 8.2 Hz, 2 H, *H-15*), 2.95 (s, 1 H, *H*-18), 2.42 (s, 6 H, *H-5*), 2.36 (s, 3 H, *H-17*) ppm.

^{13}C NMR (125 MHz, $CDCl_3$): δ = 152.7 (*C*6), 150.9 (*C*1), 148.1 (*C*8), 143.7 (*C*13), 141.7 (*C*4), 137.6 (*C*16), 130.4 (*C*9), 129.9 (*C*3), 129.1 (*C*15), 128.8 (*C*10), 128.1 (*C*14), 123.5 (*C*7), 123.0 (*C*2), 120.6 (*C*11), 81.9 (*C*12), 21.6 (*C*5), 21.2 (*C*17) ppm.

IR (ATR): $\tilde{\nu}$ = 3401 (b), 3030 (w), 2918 (w), 1600(w), 1502 (w), 1152 (m), 1033 (m), 1015 (m), 823 (s), 802 (s), 770 (m), 711 (m), 697 (m), 493 (m) cm^{-1}.

HRMS (EI-sector): *m/z* = $[M]^+$ calcd. for $[C_{34}H_{30}N_4O]^+$ 510.2420; found 510.2419.

Mp: 68 °C

Tri-[4-(4-methylphenyl)azo-phenyl)]methanol (27a)

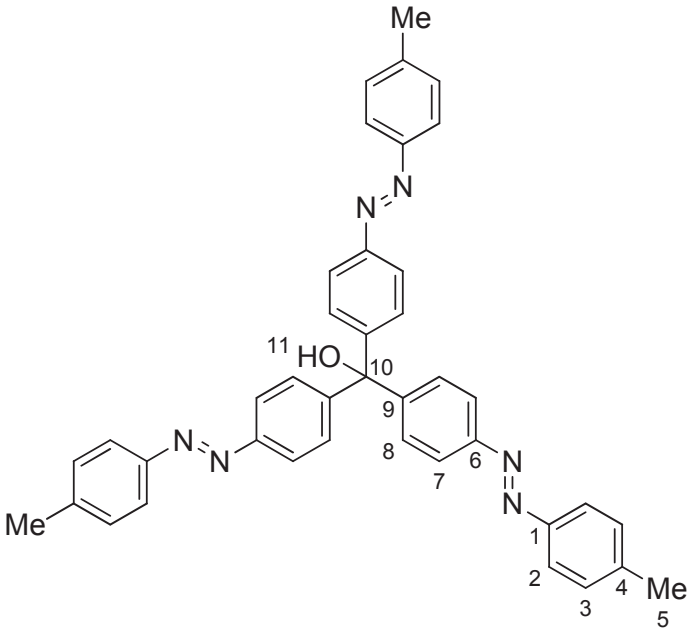

Method 1:

To 4'-trimethylstannyl-4-methylazobenzene (3.00 eq, 750 mg, 2.10 mmol) in THF (10 mL) a solution of methyllithium (3.00 eq, 1.32 mL, 2.10 mmol, 1.58 M in diethyl ether) diluted in THF (2 mL) was added at -78 °C over the course of 4 min. After another 2 min, diethylcarbonate (0.99 eq, 84.0 µL, 700 µmol) in THF (916 µL) was added. The reaction mixture was warmed to 20 °C over the course of 15 min and then stirred for 16 h. The solvent was evaporated and the precipitate was purified using column chromatography with DCM gave the product (R_f = 0.1) as foam orange solid (225 mg, 366 µmol, 52%) and the side product (R_f = 0.4) as small orange platelets (103 mg, 246 µmol, 35%).

Method 2:

To 4'-trimethylstannyl-4-methylazobenzene (4.00 eq, 1.00 g, 2.80 mmol) in THF (10 mL) a solution of methyllithium (4.00 eq, 1.76 mL, 2.80 mmol, 1.58 M in diethyl ether) diluted in THF (1.24 mL) was added at -78 °C over the course of 4 min. After another 2 min, oxalylchloride (0.99 eq, 60.0 µL, 700 µmol) in THF (0.94 mL) was added. The reaction mixture was warmed to 20 °C over the course of 15 min and then stirred for 15 h. Hydrochloric acid (12 mL, 1 M) was added, the aqueous phase extracted with DCM (2 x 15 mL) and the solvent of the combined organic phases was evaporated. The crude product was purified using column chromatography to give an orange solid (R_f = 0.1) (319 mg, 380 µmol, 54%) after solvent evaporation and a side product, see below (R_f = 0.6) (72 mg, 161 µmol, 23%).

^{1}H NMR (500 MHz, DMSO-d_6) δ = 7.86 (d, ^4J = 8.7 Hz, 6 H, *H-7*), 7.79 (d, ^4J = 8.2 Hz, 6 H, *H-2*), 7.52 (d, ^4J = 8.7 Hz, 6 H, *H-8*), 7.39 (d, ^4J = 8.2 Hz, 6 H, *H-3*), 7.02 (s, 1 H, *H-11*), 2.40 (s, 9 H, *H-5*) ppm.

^{13}C NMR (125 MHz, DMSO-d_6) δ = 150.8 (*C*6), 150.1 (*C*1), 149.9 (*C*9), 141.8 (*C*4), 130.0 (*C*3), 128.8 (*C*8), 122.6 (*C*2), 122.0 (*C*7), 80.4 (*C*10), 21.0 (*C*5) ppm.

IR (ATR): $\tilde{\nu}$ = 3431 (b), 2919 (w), 1602 (w), 1495 (w), 1408 (w), 1159 (m), 1145 (m), 1011 (m), 825 (s), 768 (m), 726 (m), 564 (m), 543 (m), 534 (m) cm^{-1}.

Mp: 167 °C.

HRMS (ESI-TOF**):** *m/z* = [M]$^+$ calcd. for [$C_{40}H_{34}N_6NaONa$]$^+$ 637.2686; found 637.2680. (method 1)

HRMS (ESI-TOF**):** *m/z* = [M]$^+$ calcd. for [$C_{40}H_{34}N_6NaONa$]$^+$ 637.2686; found 637.2681. (method 2)

Side product: Di-[4-(4-methylphenyl)azo-phenyl)]ketone (28a)

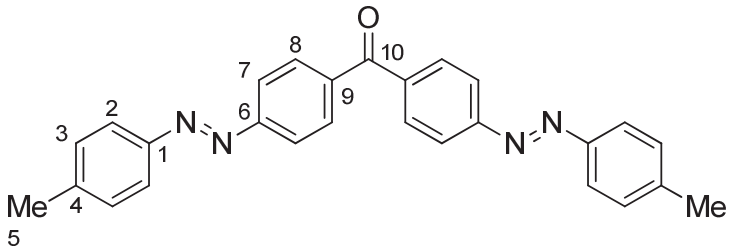

^{1}H NMR (500 MHz, $CDCl_3$) δ = 8.06 – 7.94 (m, 8 H, *H-7* + *H-8*), 7.89 (d, ^4J = 8.1 Hz, 4 H, *H-2*), 7.35 (d, ^4J = 8.1 Hz, 4 H, *H-3*), 2.46 (s, 6 H, *H-5*) ppm.

^{13}C NMR (125 MHz, $CDCl_3$) δ = 195.4 (*C*10), 154.9 (*C*6), 150.8 (*C*1), 142.6 (*C*4), 138.7 (*C*9), 131.1 (*C7* or C*8*), 129.9 (*C*3), 123.3 (*C*2), 122.6 (*C7* or *C*8), 21.6 (*C*5) ppm.

IR (ATR): $\tilde{\nu}$ = 3052 (w), 2910 (w), 2887 (w), 1639 (s), 1597 (m), 1498 (w), 1407 (w), 1304 (s), 1280 (m), 1107 (m), 1012 (m), 932 (s), 868 (s), 823 (s), 772 (m), 765 (m), 711 (s), 549 (s), 530 (s), 509 (m) cm^{-1}.

Mp: 257 °C.

HRMS (EI-sector**):** *m/z* = [M]$^+$ calcd. for [$C_{27}H_{22}N_4O$]$^+$ 418.1794; found 418.1800. (method 1)

HRMS (EI-sector**):** *m/z* = $[M]^+$ calcd. for $[C_{27}H_{22}N_4O]^+$ 418.1794 found 418.1803. (method 2)

Tri-[3-(4-methylphenyl)azo-phenyl)]methanol (27b)

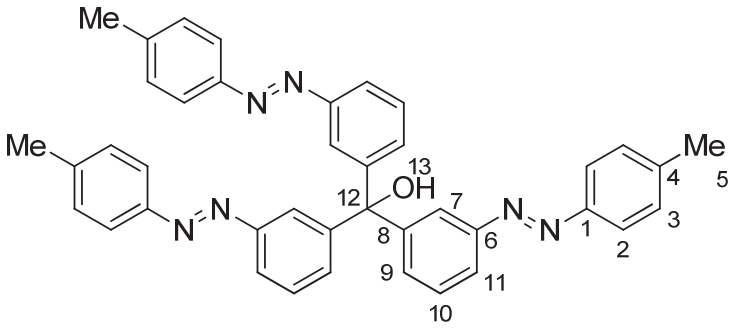

To 3'-trimethylstannyl-4-methylazobenzene (3.00 eq, 750 mg, 2.10 mmol) in THF (10 mL) a solution of methyllithium (3.00 eq, 1.32 mL, 2.10 mmol, 1.58 M in diethyl ether) diluted in THF (2 mL) was added at -78 °C over the course of 4 min. After another 2 min, diethyl carbonate (0.99 eq, 84.0 µL, 700 µmol) in THF (916 µL) was added. The reaction mixture was warmed to 20 °C over the course of 15 min and then stirred for 16 h. The solvent was evaporated and the precipitate was purified using column chromatography with DCM gave the product (R_f = 0.1) as an orange solid (225 mg, 366 µmol, 52%) and the side product (R_f = 0.4) as orange solid (103 mg, 246 µmol, 35%).

^{1}H NMR (500 MHz, DMSO-d_6) δ = 7.93 (dd, ^4J = 1.9 Hz, 1.9 Hz, 3 H, *H-7*), 7.82 (ddd, ^3J = 7.8 Hz, ^4J = 1.9, 1.1 Hz, 3 H, *H-11*), 7.76 (d, ^3J = 8.4 Hz, 6 H, *H-2*), 7.59 (dd, ^3J = 7.8, 7.8 Hz, 3 H, *H-10*), 7.46 (ddd, ^3J = 7.8 Hz, ^4J = 1.9, 1.1 Hz, 3 H, *H-9*), 7.36 (d, ^3J = 8.4 Hz, 6 H, *H-3*), 7.12 (s, 1 H, *H*-13), 2.38 (s, 9 H, *H-5*) ppm.

^{13}C NMR (126 MHz, DMSO-d_6) δ = 151.6 (*C*6), 150.0 (*C*1), 148.5 (*C*8), 141.9 (*C*4), 130.7 (*C*9), 130.0 (*C*3), 129.0 (*C*10), 122.6 (*C*2), 122.0 (*C*7), 120.9 (*C*11), 80.4 (*C*12), 21.0 (*C*5) ppm.

IR (ATR): $\tilde{\nu}$ = 3027 (w), 1600 (w9, 1502 (w), 1421 (w), 1152 (m), 1033 (m), 1014 (m), 896 (w), 821 (s), 796 (s), 711 (s), 693 (s), 540 (m), 491 (m), 458 (m) cm^{-1}.

HRMS (EI sector): *m/z* = $[M]^+$ calcd. for $[C_{40}H_{34}N_6O]^+$ 614.2794; found 614.2787.

Mp: 79 °C

Side product: **Bis-[3-(4-methylphenyl)azo-phenyl)]ketone (28b)**

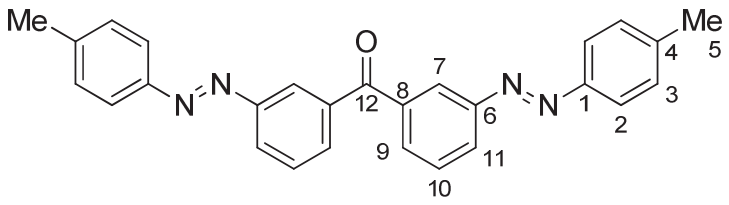

^{1}H NMR (500 MHz, $CDCl_3$) δ = 8.36 (dd, ^4J = 1.7, 1.7 Hz, 2 H, *H-7*), 8.14 (ddd, ^3J = 7.8 Hz, ^4J = 1.7, 1.2 Hz, 2 H, *H-11*), 7.95 (ddd, ^3J = 7.8 Hz, ^4J = 1.7, 1.2 Hz, 2 H, *H-9*), 7.84 (d, ^3J = 8.4 Hz, 4 H, *H-2*), 7.66 (dd, ^3J = 7.8, 7.8 Hz, 2 H, *H-10*), 7.32 (d, ^3J = 8.4 Hz, 4 H, *H-3*), 2.44 (s, 6 H, *H-5*) ppm.

^{13}C NMR (126 MHz, $CDCl_3$) δ = 195.7 (*C*12), 152.8 (*C*6), 150.8 (*C*1), 142.3 (*C*4), 138.6 (*C*8), 131.9 (*C*9), 130.0 (*C*3), 129.4 (*C*10), 126.3 (*C*11), 124.8 (*C*7), 123.2 (*C*2), 21.7 (*C*5) ppm.

IR (ATR): $\tilde{\nu}$ = 3024 (w), 2922 (w), 1658 (m), 1600 (m), 1574 (m), 1430 (m), 1282 (m), 1150 (s), 1012 (m), 906 (m), 821 (s), 751 (m), 709 (s), 645 (m), 555 (s), 532 (m), 495 (m) cm^{-1}.

HRMS (EI-sector): *m/z* = $[M]^+$ calcd. for $[C_{27}H_{22}N_4O]^+$ 418.1794; found 418.1794.

Mp: 182 °C.

Mono Substituted Azobenzenes

4-Methylazobenzene (SI-2)

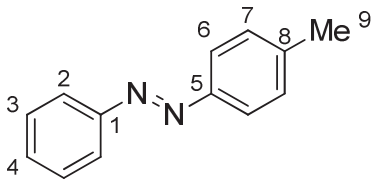

To 4-(trimethylstannyl-azobenzene (1.00 eq, 242 mg, 700 µmol) in THF (10 mL), a solution of methyl lithium (0.99 eq, 440 µL, 700 µmol, 1.58 M in diethyl ether), diluted in THF (2 mL) was added at -78 °C over the course of 4 min. After another 2 min, a solution of methyl iodide (1.10 eq, 50.0 µL, 800 µmol) in THF (950 µL) was added and the reaction mixture was warmed to 20 °C. After 13 h stirring the solvent was evaporated and the residue purified

using column chromatography with *n*-hexane as eluent (R_f = 0.4). Drying the product *in vacuo* gave an orange solid (116 mg, 591 µmol, 85%, Lit.: 95%[12(a)]).

^{1}H NMR (600 MHz, $CDCl_3$) δ = 7.91 (d, ^3J = 8.0 Hz, 2 H, *H-2*), 7.84 (d, ^3J = 8.1 Hz, 2 H, *H-6*), 7.52 (dd, ^3J = 8.0, 7.3 Hz, 2 H, *H-3*), 7.46 (t, ^3J = 7.3 Hz, 1 H, *H-4*), 7.32 (d, ^3J = 8.1 Hz, 2 H, *H-7*), 2.45 (s, 3 H, *H-9*) ppm.

^{13}C NMR (151 MHz, $CDCl_3$) δ = 152.9 (*C*1), 150.9 (*C*5), 141.7 (*C*8), 130.8 (*C*4), 129.9 (*C*7), 129.2 (*C*3), 123.0 (*C*6), 122.9 (*C*2), 21.6 (*C*9) ppm.

IR (ATR): $\tilde{\nu}$ = 3036 (w), 2922 (w), 1602 (w), 1486 (w), 1442 (w), 1302 (w), 1220 (w), 1150 (m), 1034 (m), 821 (s), 763 (s), 707 (m), 681 (s), 546 (s), 525 (s), 492 (s) cm^{-1}.

HRMS (EI-sector) = *m/z*= $[M]^+$ calcd. for $[C_{13}H_{12}N_2]^+$ 196.1000; found 196.1003.

3-Methylazobenzene (SI-3)

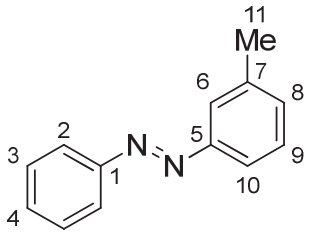

To 3-(trimethylstannyl-azobenzene (1.00 eq, 242 mg, 700 µmol) in THF (10 mL), a solution of methyl lithium (0.99 eq, 440 µL, 700 µmol, 1.58 M in diethyl ether), diluted in THF (2 mL) was added at -78 °C over the course of 4 min. After another 2 min, a solution of methyl iodide (1.10 eq, 50.0 µL, 800 µmol) in THF (950 µL) was added and the reaction mixture was warmed to 20 °C. After 13 h stirring the solvent was evaporated and the residue purified using column chromatography with *n*-hexane as eluent (R_f = 0.5). Drying the product *in vacuo* gave an orange solid (122 mg, 622 µmol, 89%, Lit.:[13],[14(b)]).

^{1}H NMR (500 MHz, $CDCl_3$) δ = 7.96 (d, ^3J = 7.2 Hz, 2 H, C2-*H*), 7.80 – 7.75 (m, 2 H, C6-*H* + C10-*H*), 7.55 (dd, ^3J = 7.2, 7.2 Hz, 2 H, C3-*H*), 7.49 (t, ^3J = 7.2 Hz, 1 H, C4-*H*), 7.44 (dd, ^3J = 7.4, 8.4 Hz, 1 H, C9-*H*), 7.32 (d, ^3J = 7.4 Hz, 1 H, C8-*H*), 2.49 (s, 3 H, C11-*H*) ppm.

^{13}C NMR (126 MHz, $CDCl_3$) δ = 152.9 (*C*5), 152.8 (*C*1), 139.1 (*C*7), 131.9 (*C*8), 131.0 (*C*4), 129.2 (*C*3), 129.0 (*C*9), 123.1 (*C*10), 122.9 (*C*2), 120.6 (*C*6), 21.5 (*C*11) ppm.

[a] In this report, the products were prepared by a reaction of 4-methylbenzenediazonium *ortho*-benzenedisulfonimides with triphenylindium.
[b] In both publications no yields are mentioned.

IR (ATR): $\tilde{\nu}$ = 3059 (w), 2921 (w), 1599 (w), 1585 (w), 1482 (w), 1453 (w), 1150 (w), 920 (w), 787 (m), 766 (m), 688 (s), 537 (m), 493 (w) cm^{-1}.

HRMS (EI-sector**):** *m/z* = $[M]^+$ calcd. for $[C_{13}H_{12}N_2]^+$ 196.1000; found 196.0999.

2-Methylazobenzene (SI-4)

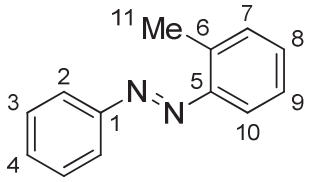

To 2-(trimethylstannyl-azobenzene (1.00 eq, 242 mg, 700 µmol) in THF (10 mL), a solution of methyl lithium (0.99 eq, 440 µL, 700 µmol, 1.58 M in diethyl ether), diluted in THF (2 mL) was added at -78 °C over the course of 4 min. After another 2 min, a solution of methyl iodide (1.10 eq, 50.0 µL, 800 µmol) in THF (950 µL) was added and the reaction mixture was warmed to 20 °C. After 13 h stirring the solvent was evaporated and the residue purified using column chromatography with *n*-hexane as eluent (R_f = 0.4). Drying the product *in vacuo* gave an orange solid (132 mg, 672 µmol, 96%, Lit.: 87%[15 (a)]).

IR (ATR): $\tilde{\nu}$ = 3060 (w), 2925 (w), 1742 (w), 1598 (w), 1480 (m), 1456 (m), 1302 (w), 1150 (w), 1070 (w), 1034 (w), 771 (s), 755 (m), 740 (m), 714 (s), 687 (s), 569 (w), 496 (w) cm^{-1}.

^{1}H NMR (500 MHz, $CDCl_3$) δ = 7.92 (d, ^3J = 7.8 Hz, 2 H, C2-*H*), 7.63 (d, ^3J = 7.9 Hz, 1 H, C10-*H*), 7.52 (dd, ^3J = 7.8, 7.2 Hz, 1 H, C3-*H*), 7.47 (t, ^3J = 7.2 Hz, 1 H, C4-*H*), 7.39 – 7.32 (m, 2 H, C8-*H* + C7-*H*), 7.30 – 7.22 (m, 1 H, C9-*H*), 2.73 (s, 3 H, C11-*H*).

^{13}C NMR (126 MHz, $CDCl_3$) δ = 153.2 (*C*1), 150.9 (*C*5), 138.2 (*C*6), 131.4 (*C*7), 131.1 (*C*8), 130.9 (*C*4), 129.2 (*C*3), 126.6 (*C*9), 123.1 (*C*2), 115.6 (*C*10), 17.7 (*C*11) ppm.

HRMS (EI-sector**):** *m/z* = $[M]^+$ calcd. for $[C_{13}H_{12}N_2]^+$ 196.1000; found 196.0999.

M.p.: 56 °C

[a] In this report, the product was synthesized from phenyldiazonium fluoborate and 1-bromo-2-methylbenzene.

4-(Trimethylsilyl)azobenzene (SI-5)

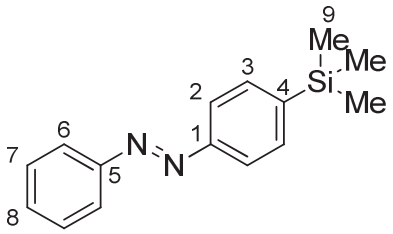

To 4-trimethylstannylazobenzene (1.00 eq, 242 mg, 700 µmol) in THF (10 mL), a solution of methyl lithium (0.99 eq, 44.0 µL, 700 µmol, 1.58 M in diethyl ether) in THF (2 mL) was added at -78 °C over the course of 4 min. After another 2 min, trimethylchlorosilane (1.10 eq, 100 µL, 770 µmol) in THF (900 µL) was added. The reaction mixture was warmed to 20 °C over the course of 15 min and stirred for 12 h. The solvent was removed *in vacuo* and the residue purified using column chromatography with *n*-hexane as eluent (R_f = 0.4). The solvent was evaporated to give an orange oil (166 mg, 652 µmol, 93%).

^{1}H NMR (600 MHz, $CDCl_3$) δ = 7.96 (d, ^{3}J = 7.3 Hz, 2 H, C6-*H*), 7.92 (d, ^{3}J = 8.3 Hz, 2 H, C2-*H*), 7.70 (d, ^{3}J = 8.3 Hz, 2 H, C3-*H*), 7.54 (dd, ^{3}J = 7.3, 7.3 Hz, 2 H, C7-*H*), 7.49 (t, ^{3}J = 7.3 Hz, 1 H, C8-*H*), 0.35 (s, 9 H, C9-*H*) ppm.

^{13}C NMR (151 MHz, $CDCl_3$) δ = 153.1 (*C*1), 152.9 (*C*5), 144.6 (*C*4), 134.2 (*C*3), 131.1 (*C*8), 129.2 (*C*7), 123.0 (*C*6), 122.0 (*C*2), -1.0 (*C*9) ppm.

^{29}Si NMR (99 MHz, $CDCl_3$) δ = -3.54 ppm.

IR (ATR): $\tilde{\nu}$ = 3022 (w), 2954 (w), 2896 (w), 1484 (w), 1444 (w), 1384 (w), 1248 (m), 1107 (m), 838 (s), 825 (s), 766 (s), 715 (m) 756 (s), 628 (m), 549 (m) cm^{-1}.

HRMS (EI-sector**):** *m/z* = $[M]^+$ calcd. for $[C_{15}H_{18}N_2Si]^+$ 254.1239; found 254.1232.

3-(Trimethylsilyl)azobenzene (SI-6)

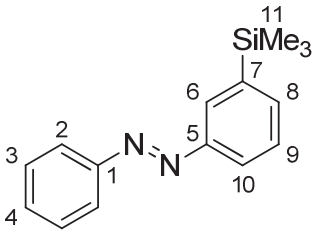

To 3-trimethylstannylazobenzene (1.00 eq, 242 mg, 700 µmol) in THF (10 mL), a solution of methyl lithium (0.99 eq, 44.0 µL, 700 µmol, 1.58 M in diethyl ether) in THF (2 mL) was added at -78 °C over the course of 4 min. After another 2 min, trimethylchlorosilane (1.10 eq, 100 µL, 770 µmol) in THF (900 µL) was added. The reaction mixture was warmed to 20 °C over the course of 15 min and stirred for 12 h. The solvent was removed *in vacuo* and the residue purified using column chromatography with *n*-hexane as eluent (R_f = 0.5). The solvent was evaporated to give an orange oil (152 mg, 598 µmol, 85%).

^{1}H NMR (500 MHz, $CDCl_3$) δ = 8.12 (dd, ^4J = 1.0, 1.1 Hz, 1 H, C6-*H*), 7.96 (d, ^3J = 7.1 Hz, 2 H, C2-*H*), 7.91 (ddd, ^3J = 7.9 Hz, ^4J = 2.0, 1.0 Hz, 1 H, C10-*H*), 7.66 (ddd, ^3J = 7.2 Hz, ^4J = 2.0, 1.1 Hz, 1 H, C8-*H*), 7.58 – 7.45 (m, 4 H, C3-*H* + C9-*H* + C4-*H*), 0.37 (s, 9 H, C11-*H*) ppm.

^{13}C NMR (126 MHz, $CDCl_3$) δ = 152.8 (*C*1), 152.0 (*C*5), 141.9 (*C*7), 136.0 (*C*8), 130.9 (*C*4), 129.1 (*C*3), 128.8 (*C*6), 128.6 (*C*9), 122.8 (*C*2), 122.1 (*C*10), -1.1 (*C*11) ppm.

^{29}Si NMR (99 MHz, CDCl3) δ = -3.29 ppm.

IR (ATR): $\tilde{\nu}$ = 3060 (w), 2954 (w), 2895 (w), 1586 (w), 1398 (w), 1263 (w), 1248 (m), 1109 (w), 1069 (w), 866 (m), 832 (s), 764 (m), 753 (s), 687 (s), 621 (m), 525 (m) cm^{-1}.

HRMS (EI-sector**):** *m/z* = $[M]^+$ calcd. for $[C_{15}H_{18}N_2Si]^+$ 254.1239; found 254.1238.

2-(Trimethylsilyl)azobenzene (SI-7)

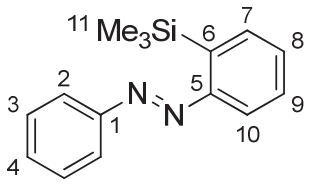

To 2-(trimethylstannyl)azobenzene (1.00 eq, 242 mg, 700 µmol) in THF (10 mL), a solution of methyl lithium (0.99 eq, 44.0 µL, 700 µmol, 1.58 M in diethyl ether) in THF (2 mL) was added at -78 °C over the course of 4 min. After another 2 min, trimethylchlorosilane (1.10 eq, 100 µL, 770 µmol) in THF (900 µL) was added. The reaction mixture was warmed to 20 °C over the course of 15 min and stirred for 12 h. The solvent was removed *in vacuo* and the residue purified using column chromatography with *n*-hexane as eluent (R_f = 0.4). The solvent was evaporated to give an orange oil (160 mg, 629 µmol, 90%, Lit.: 80%[16 (a)]).

^{1}H NMR (600 MHz, $CDCl_3$) δ = 7.96 (d, ^3J = 7.4 Hz, 2 H, C2-*H*), 7.79 (d, ^3J = 7.6 Hz, 1 H, C10-*H*), 7.73 (d, ^3J = 7.0 Hz, 1 H, C7-*H*), 7.56 (dd, ^3J = 7.4, 7.4 Hz, 2 H, C3-*H*), 7.52 – 7.48 (m, 2 H, C4-*H* + C9-*H*), 7.46 (dd, J = 7.6 Hz, 7.6 Hz, 1 H, C8-*H*), 0.42 (s, 9 H, C11-*H*) ppm.

^{13}C NMR (151 MHz, $CDCl_3$) δ = 157.5 (*C*5), 152.7 (*C*1), 142.0 (*C*6), 134.9 (*C*7), 131.1 (*C*4), 130.2 (*C*8), 130.1 (*C*9), 129.3 (*C*3), 123.3 (*C*2), 114.9 (*C*10), 0.7 (*C*11) ppm.

^{29}Si NMR (99 MHz, $CDCl_3$) δ = -4.05 ppm.

IR (ATR): $\tilde{\nu}$ = 3055 (w), 2953 (w), 2897 (w), 1583 (w), 1473 (w), 1448 (w), 1243 (m), 1118 (m), 1069 (w), 834 (s), 777 (s), 718 (s), 685 (s), 621 (m), 539 (m) cm^{-1}.

HRMS (EI-sector**):** *m/z* = $[M]^+$ calcd. for $[C_{15}H_{18}N_2Si]^+$ 254.1239; found 254.1235.

[a] In this report, the product was obtained by the lithiation of 2-iodoazobenzene with *n*-BuLi and quenching with TMSCl.

References

[1] A. F. Burchat, M. J. Chong, N. Nielsen, *J. Organomet. Chem.* **1997**, *542*, 281.

[2] J. Strueben, P. J. Gates, A. Staubitz, *J. Org. Chem.* **2014**, 79, 1719.

[3] M. Teraguchi, T. Masuda, *Macromolecules* **2000**, *33*, 240.

[4] B.-C. Yu, Y. Shirai, J. M. Tour, *Tetrahedron* **2006**, 62, 10303.

[5] J. Yamamoto, R. Yamawakiy, Y. Sumi, R. Okamoto, M. Saito, M. Kato, A. Shibata, *Nippon Kagaku Kaishi* **1992**, 1992, 1508.

[6] D. Qiu, H. Meng, L. Jin, S. Wang, S. Tang, X. Wang, F. Mo, Y. Zhang, J. Wang, *Angew. Chem. Int. Ed.* **2013**, *52*, 11581*; Angew. Chem.* **2013**, *125*, 11795.

[7] X. Wang, J. Wang, F. Qi, L. Hu, X. Li, X. Cao, H. Gu, *Chinese J. of Catal.* **2013**, *34*, 2084.

[8] G. E. Lewis, M. A.G. Osman, *Aust. J. Chem.* **1964**, *17*, 498.

[9] C. J. Byrne, D. A. R. Happer, M. P. Hartshorn, H. K. J. Powell, *J. Chem. Soc. Perk. Trans. 2* **1987**, 1649.

[10] M. Okubo, H. Aratani,T. Gondo, K. Koga, *Bull. Chem. Soc. Jpn.* **1983**, *56*, 788.

[11] W. J. Kerr, A. J. Morrison, M. Pazicky, T. Weber, *Org. Lett.* **2012**, *14*, 2250.

[12] M. Barbero, S. Cadamuro, S. Dughera, C. Giaveno, *Eur. J. Org. Chem.* **2006**, 4884.

[13] M. Kaiser, S. P. Leitner, C. Hirtenlehner, M. List, A. Gerisch, U. Monkowius, *Dalton Trans.* **2013**, *42*, 14749.

[14] M. Sharma, *Arch. Appl. Sci. Res.* **2011**, 3, 51.

[15] M. E. Garst, D. Lukton, *Synth. Commun.* **1980**, *10*, 155.

[16] N. Kano, F. Komatsu, M. Yamamura, T. Kawashima, *J. Am. Chem. Soc.* **2006**, *128*, 7097.

Supporting Information

for

High Yielding Lithiation of Azobenzenes by Tin-Lithium Exchange

-NMR Spectra-

Jan Strueben[a], Matthias Lipfert[a], Jan-O. Springer[a], Colin A. Gould[a], Paul J. Gates[b], Frank D. Sönnichsen[a], Anne Staubitz[a]*

[a] *Otto-Diels-Institute for Organic Chemistry, University of Kiel, Otto-Hahn-Platz 4, 24098 Kiel (Germany)*
* astaubitz@oc.uni-kiel.de

[b] *School of Chemistry, University of Bristol, Cantock's Close, Bristol BS7 1TS (UK)*

1.1 Iodinated Azobenzenes

4-Iodoazobenzene (8a) in chloroform-*d*

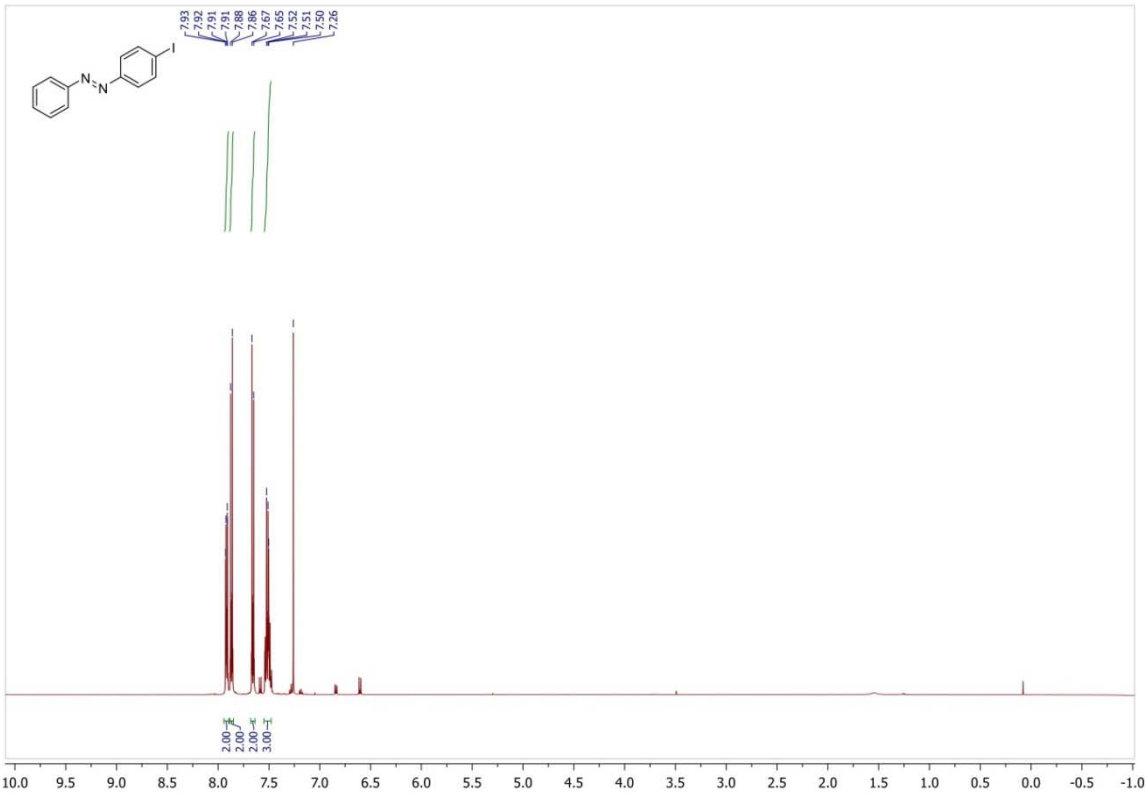

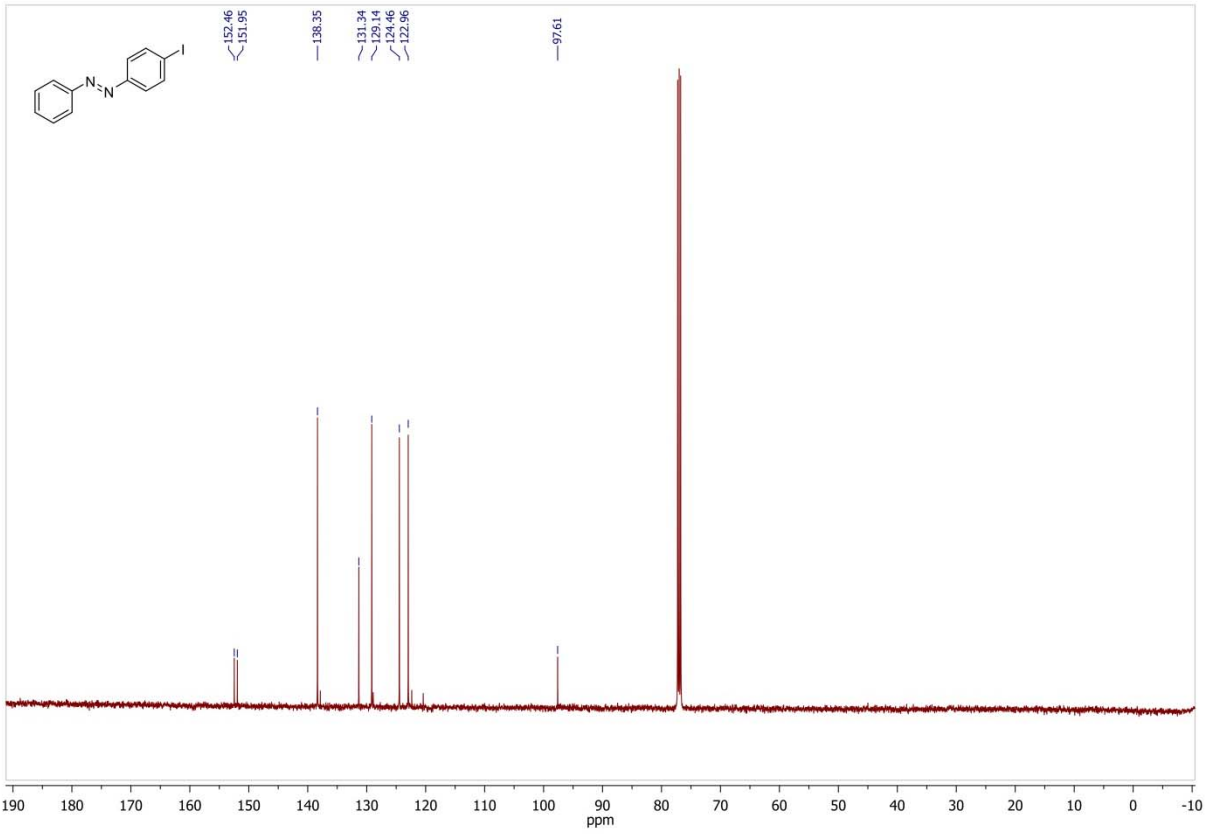

3-Iodoazobenzene (8b) in chloroform-*d*

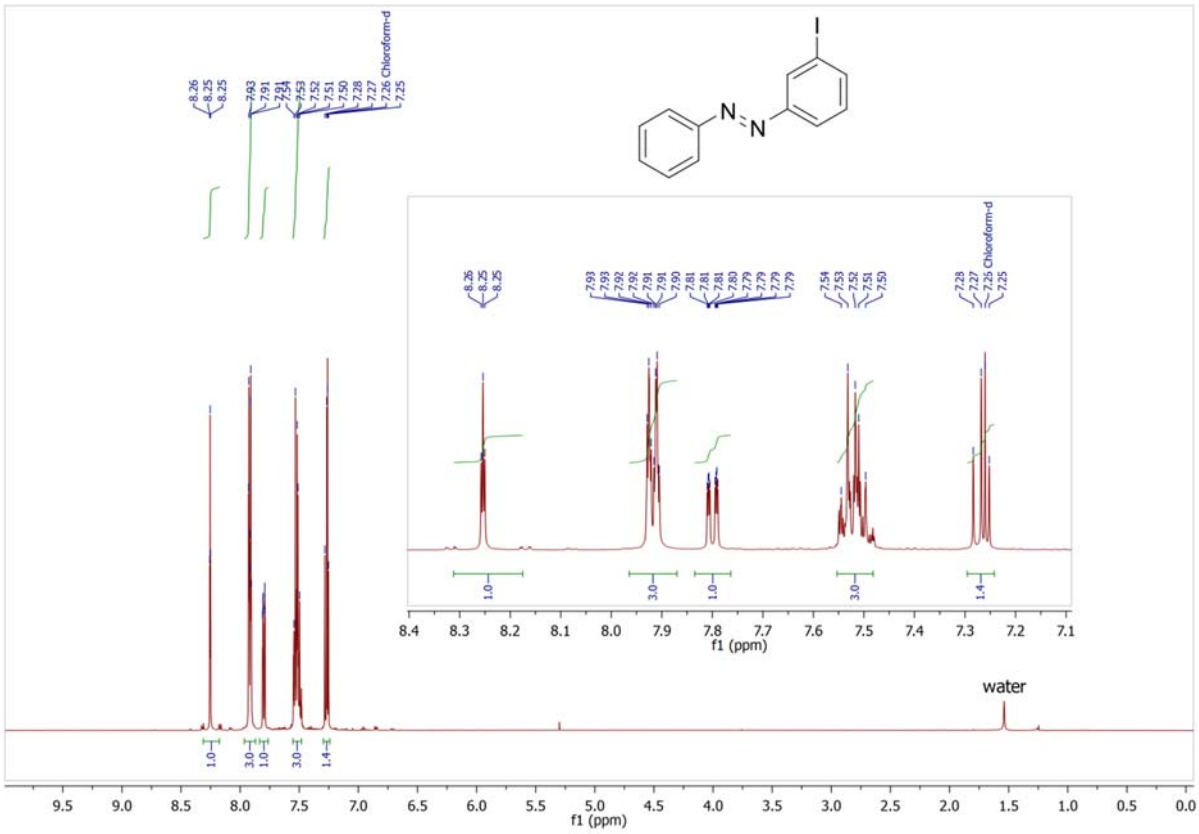

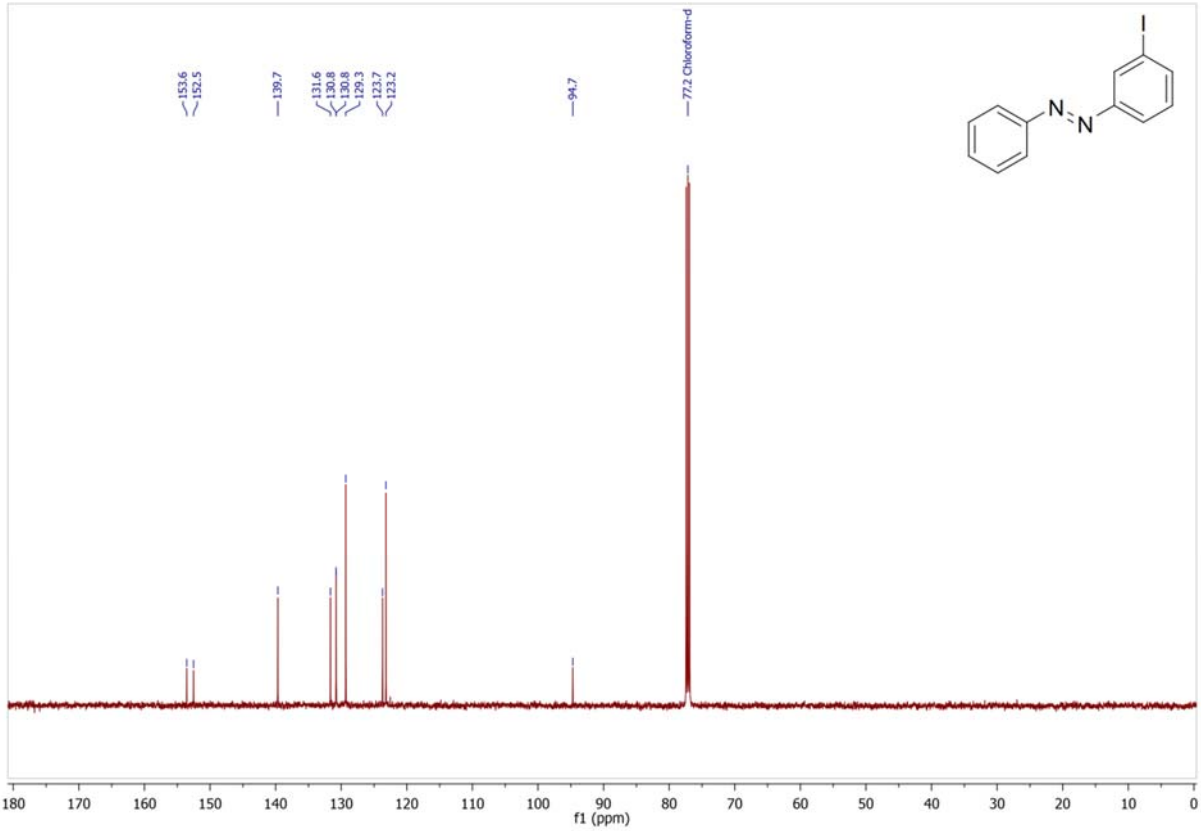

2-Iodoazobenzene (8c) in chloroform-*d*

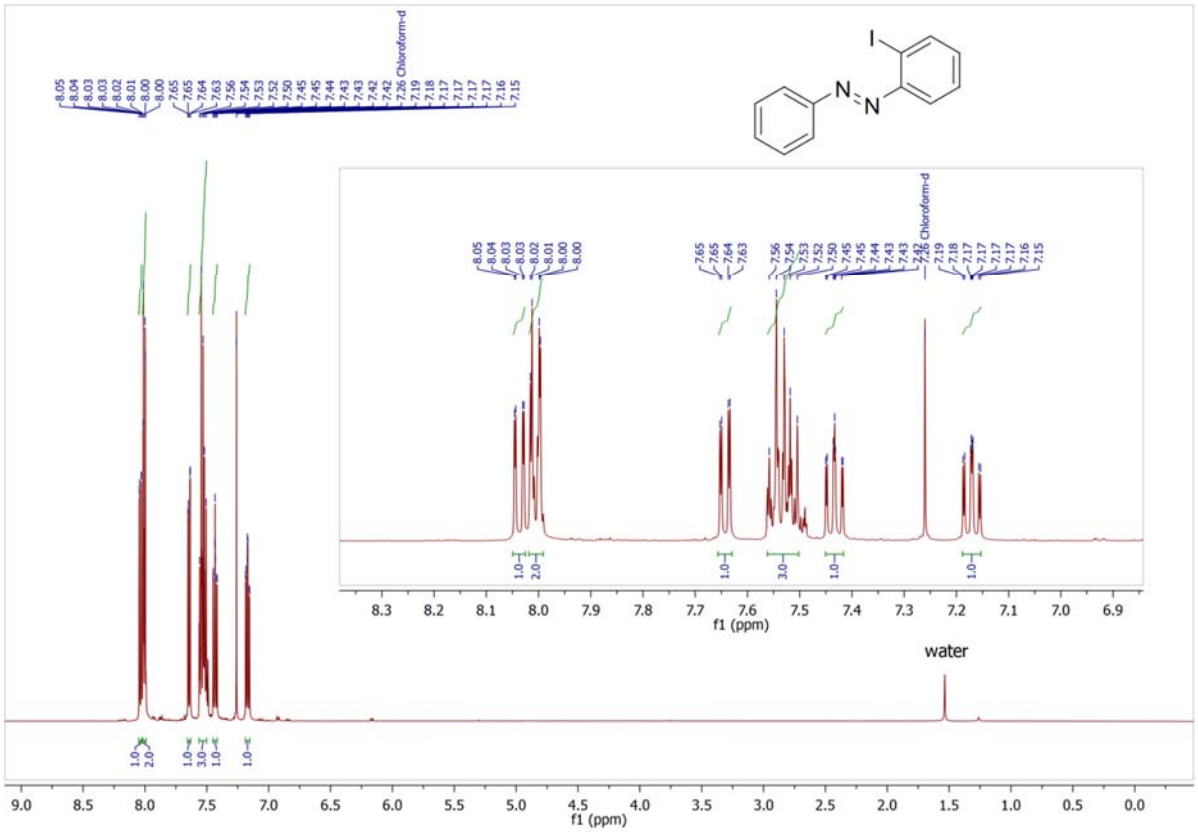

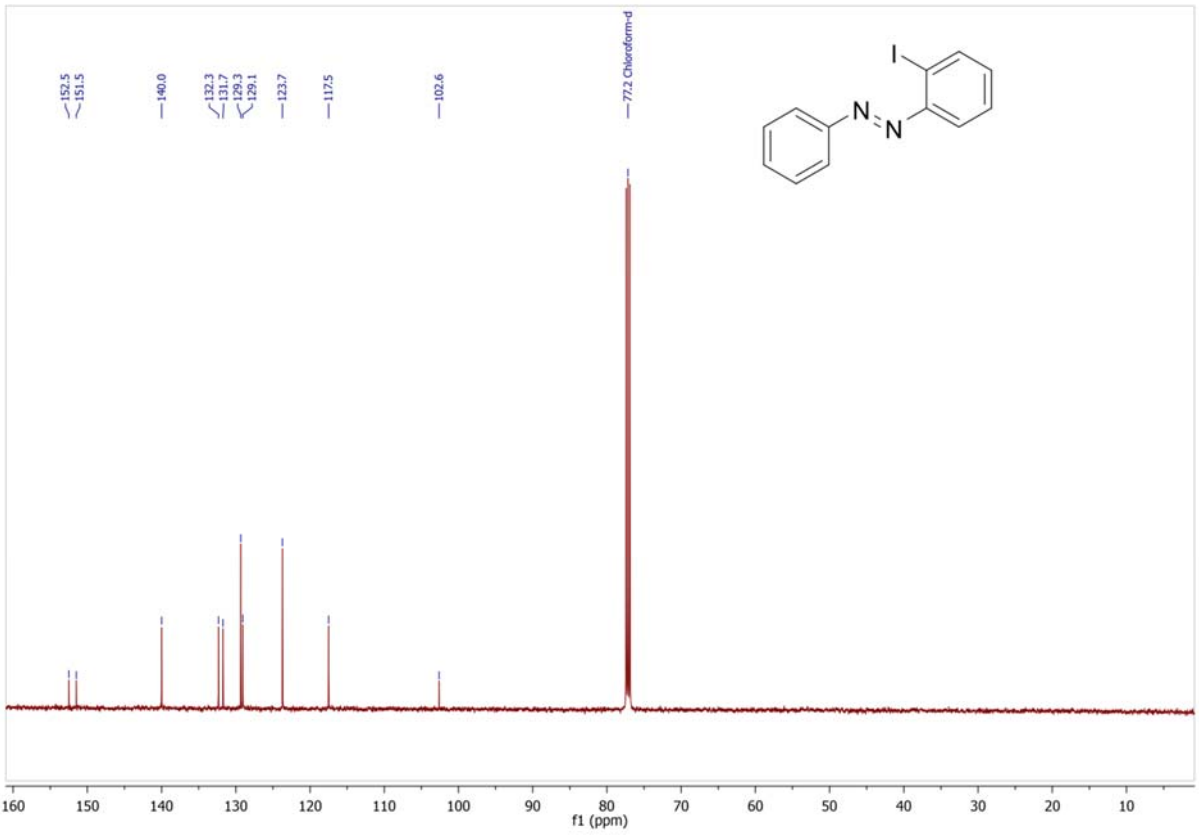

4-Iodo-4’-methylazobenzene (9a) in chloroform-*d*

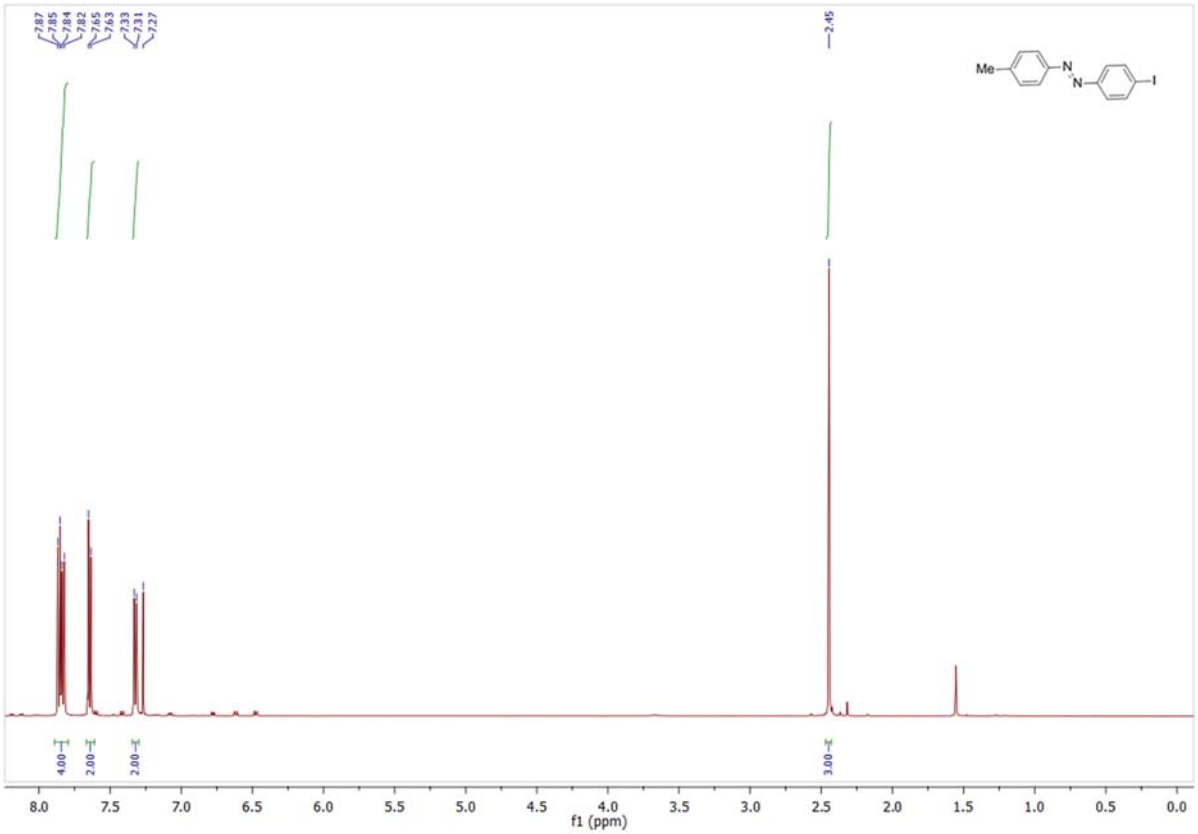

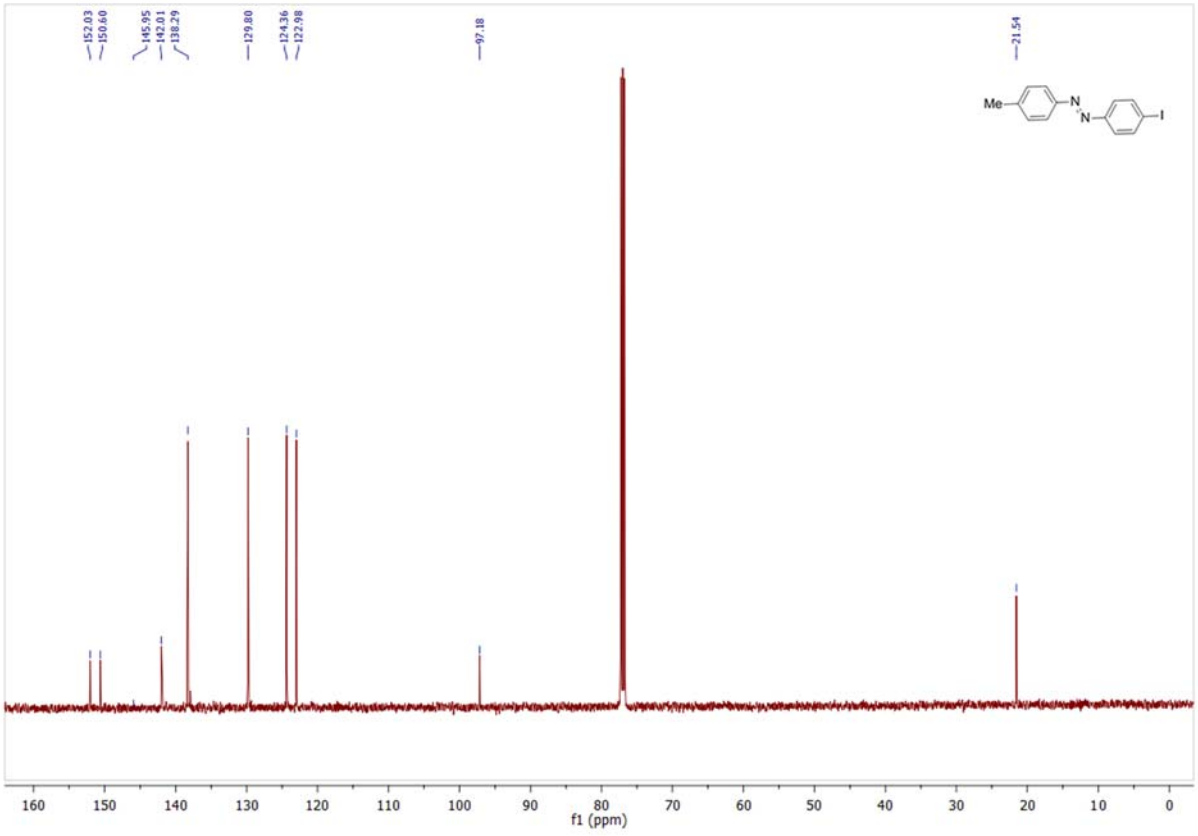

3-Iodo-4'methylazobenzene in (9b) chloroform-*d*

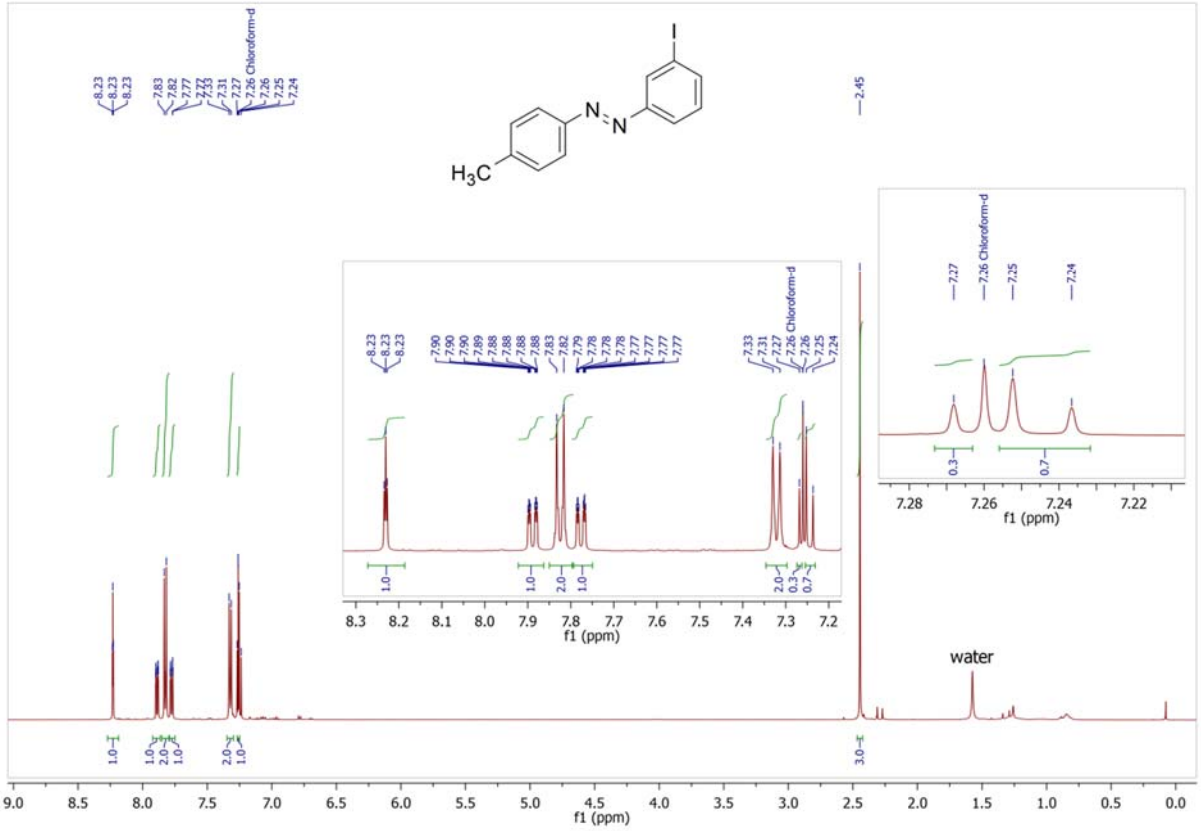

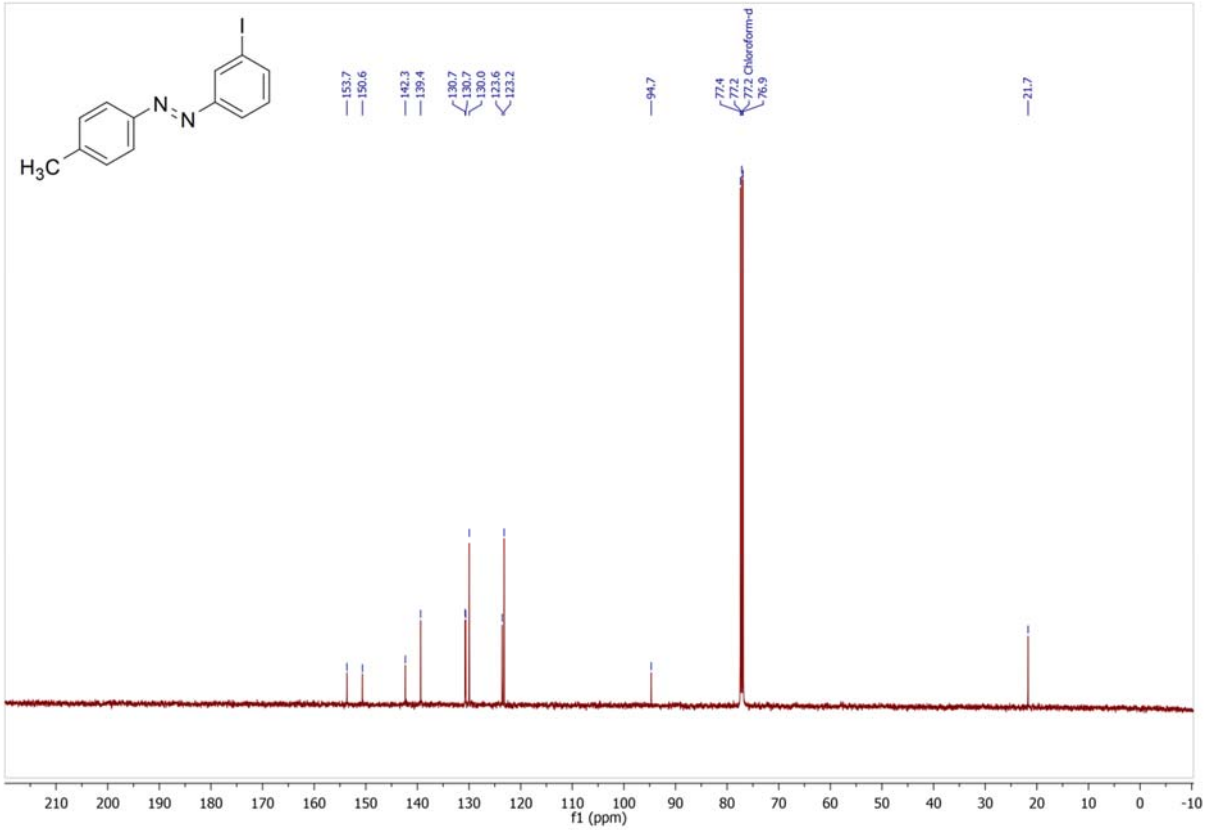

2-Iodo-4‘-methyliodoazobenzene (9c) in chloroform-*d*

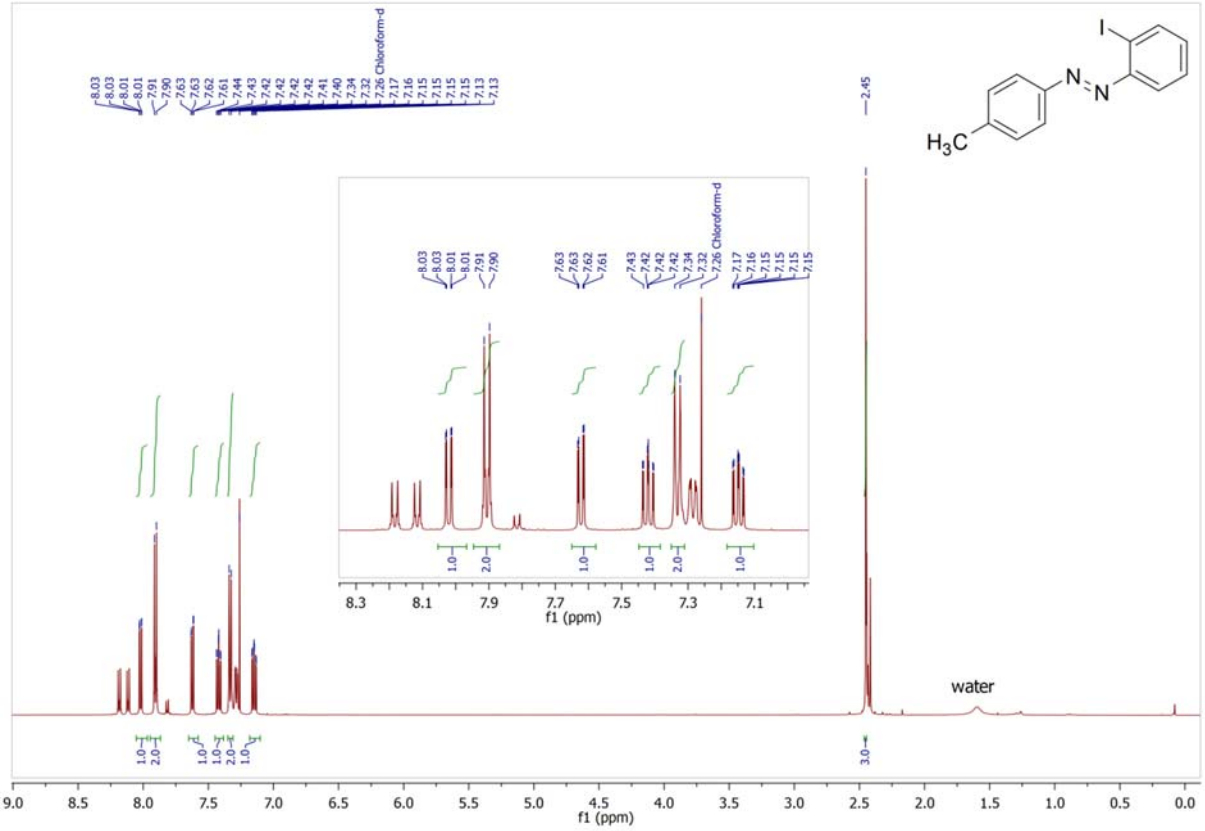

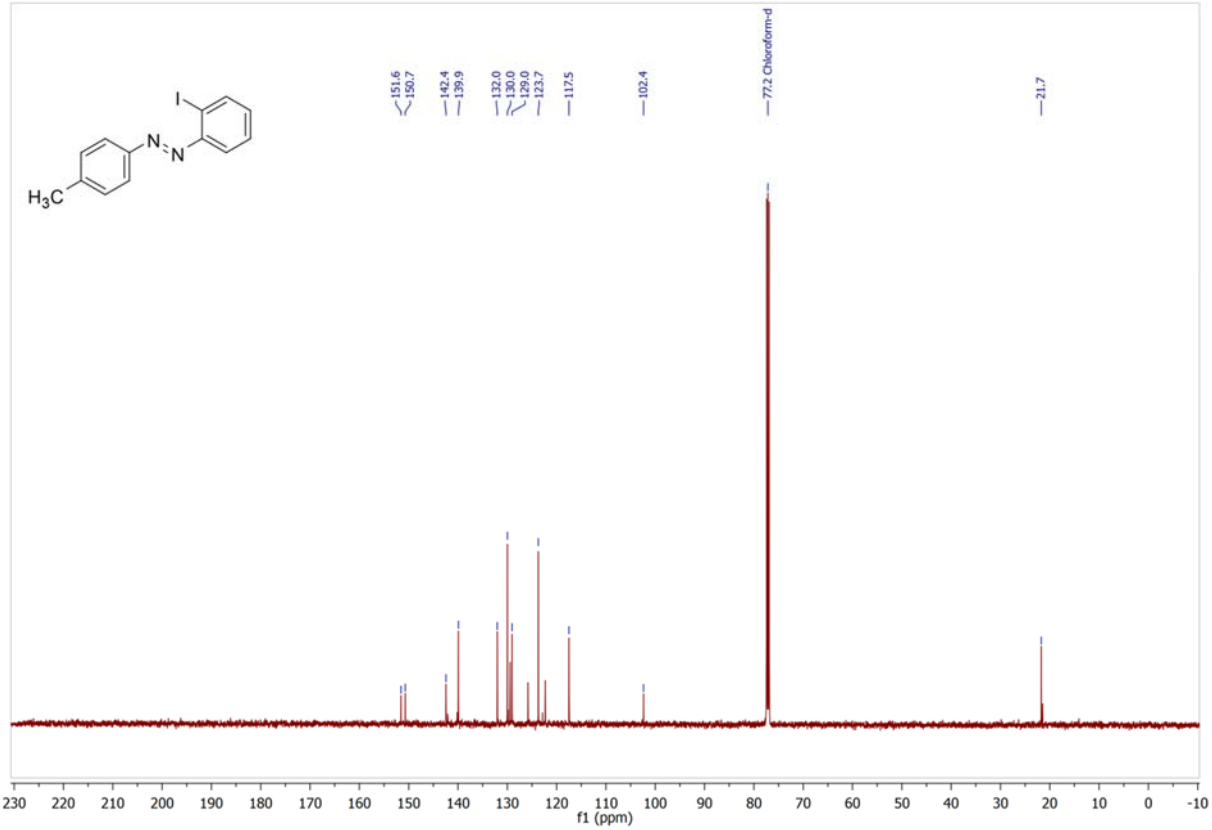

1.2 Stannylated Azobenzenes

4-(Trimethylstannyl)azobenzene (10a) in chloroform-*d*

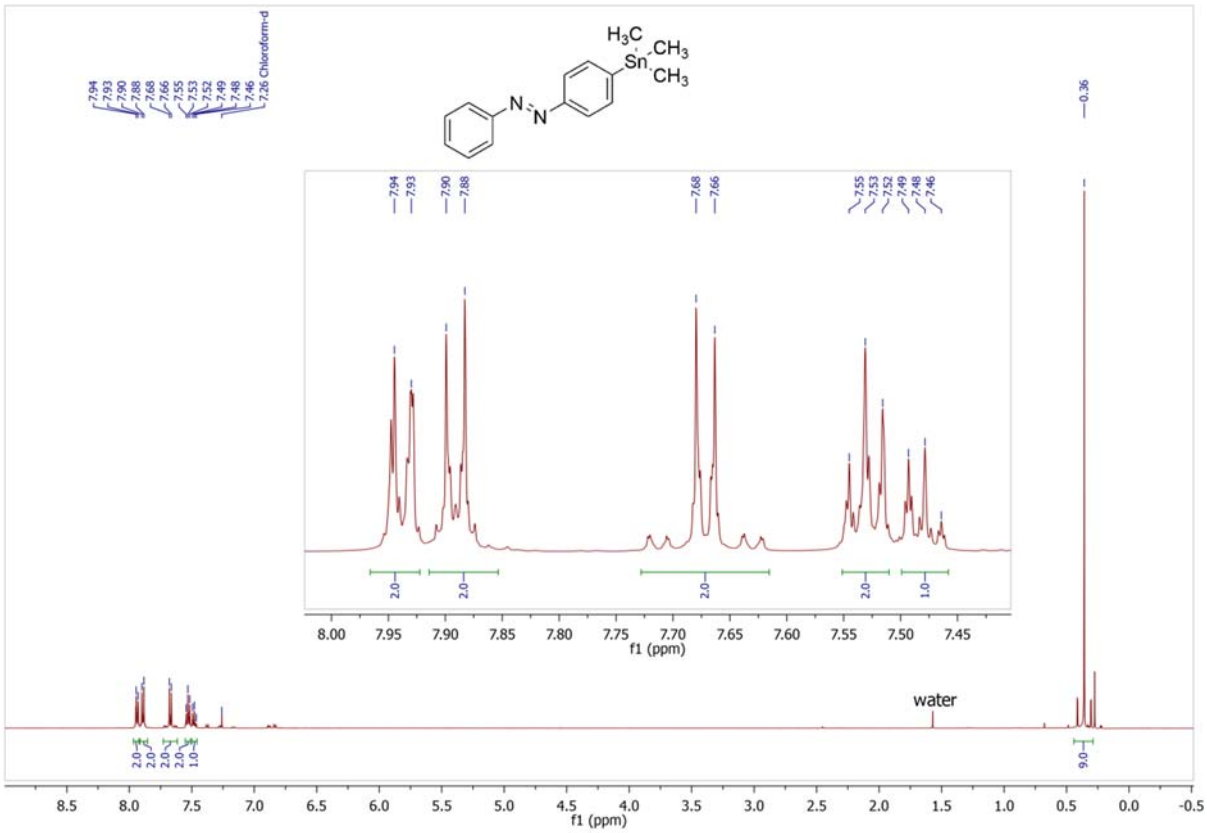

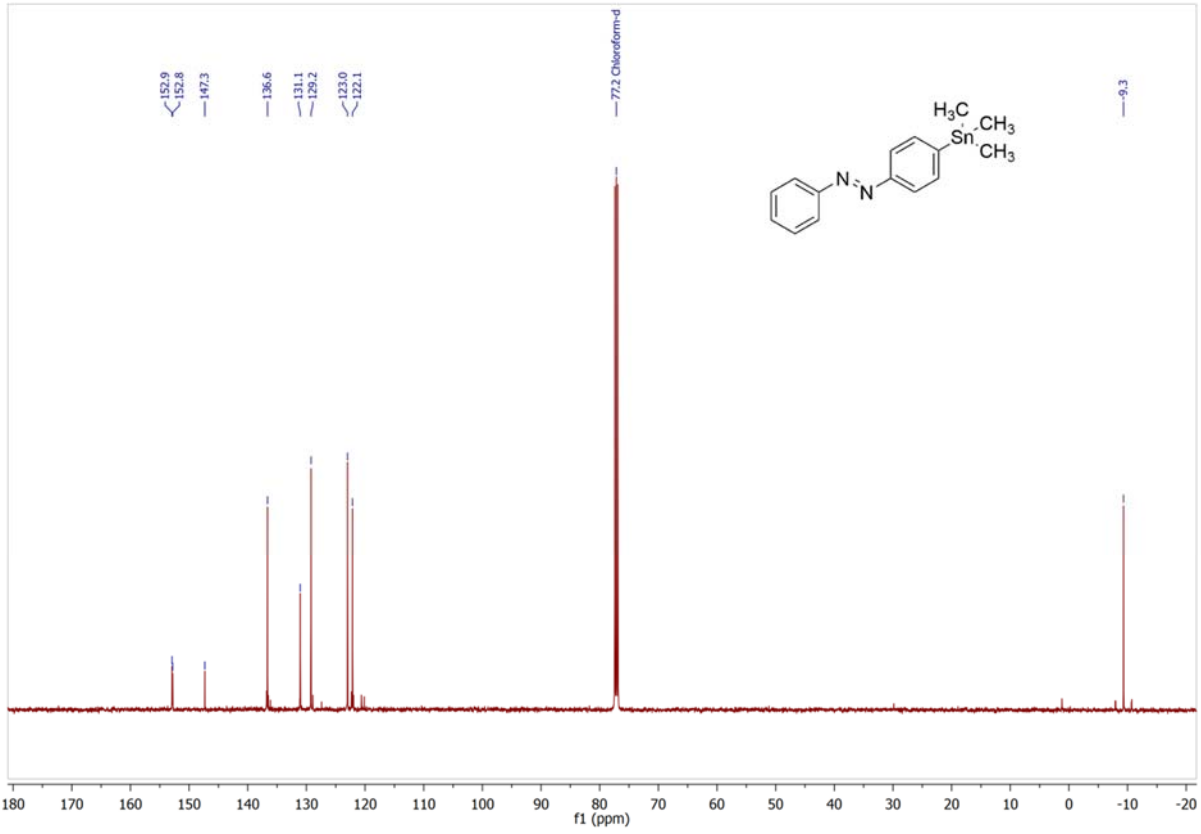

3-(Trimethylstannyl)azobenzene (10b) in chloroform-*d*

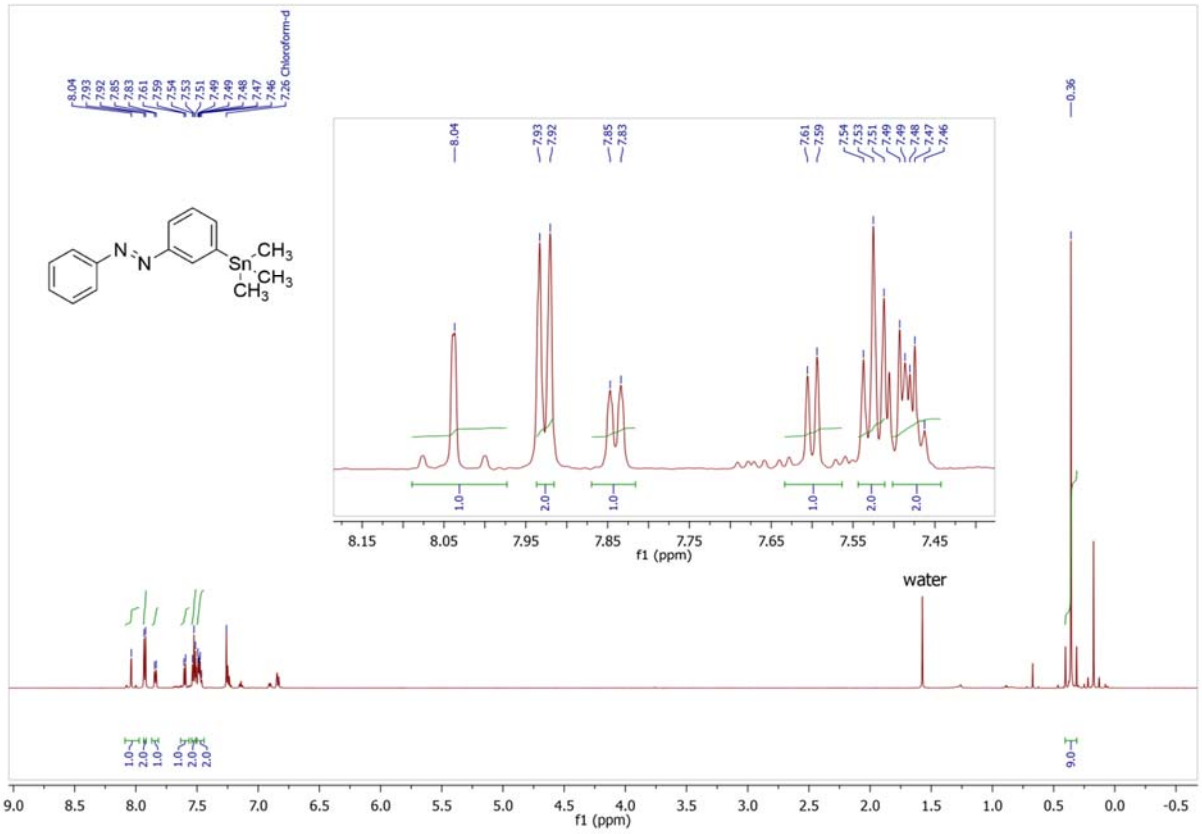

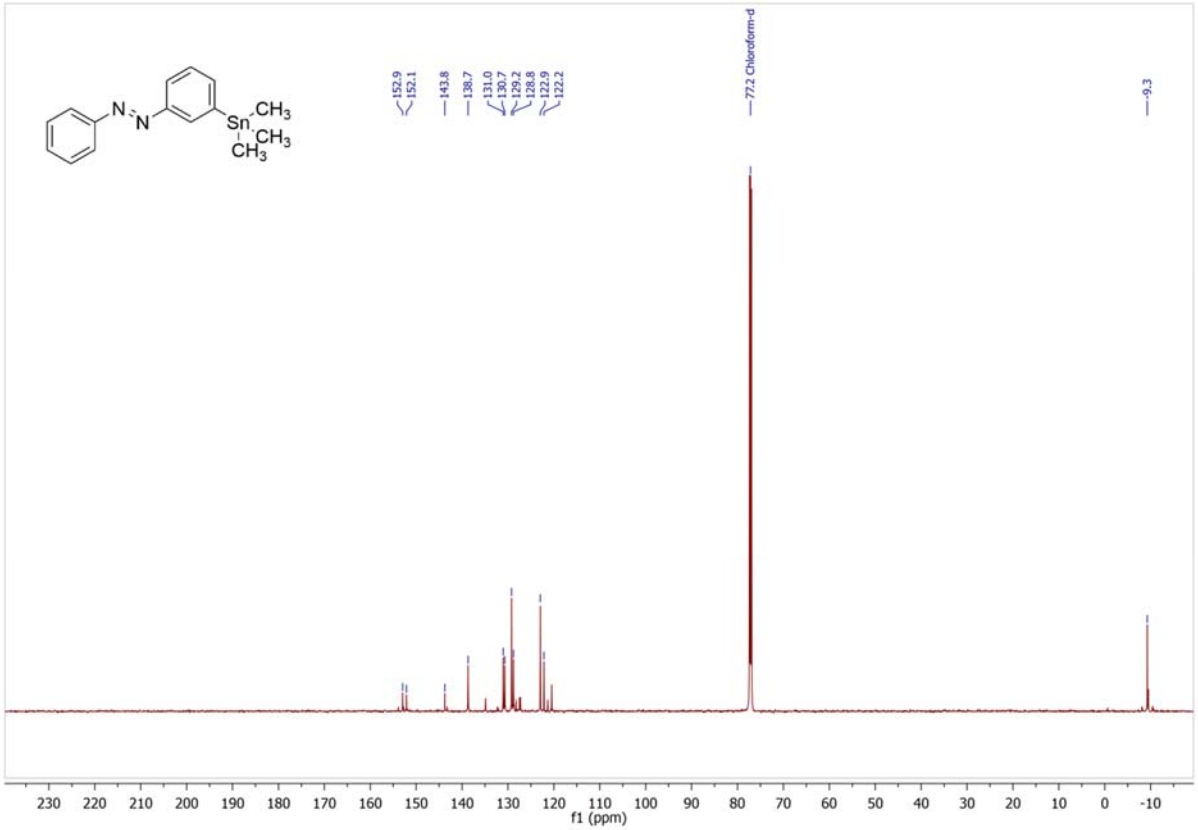

2-(Trimethylstannyl)azobenzene (10c) in chloroform-*d*

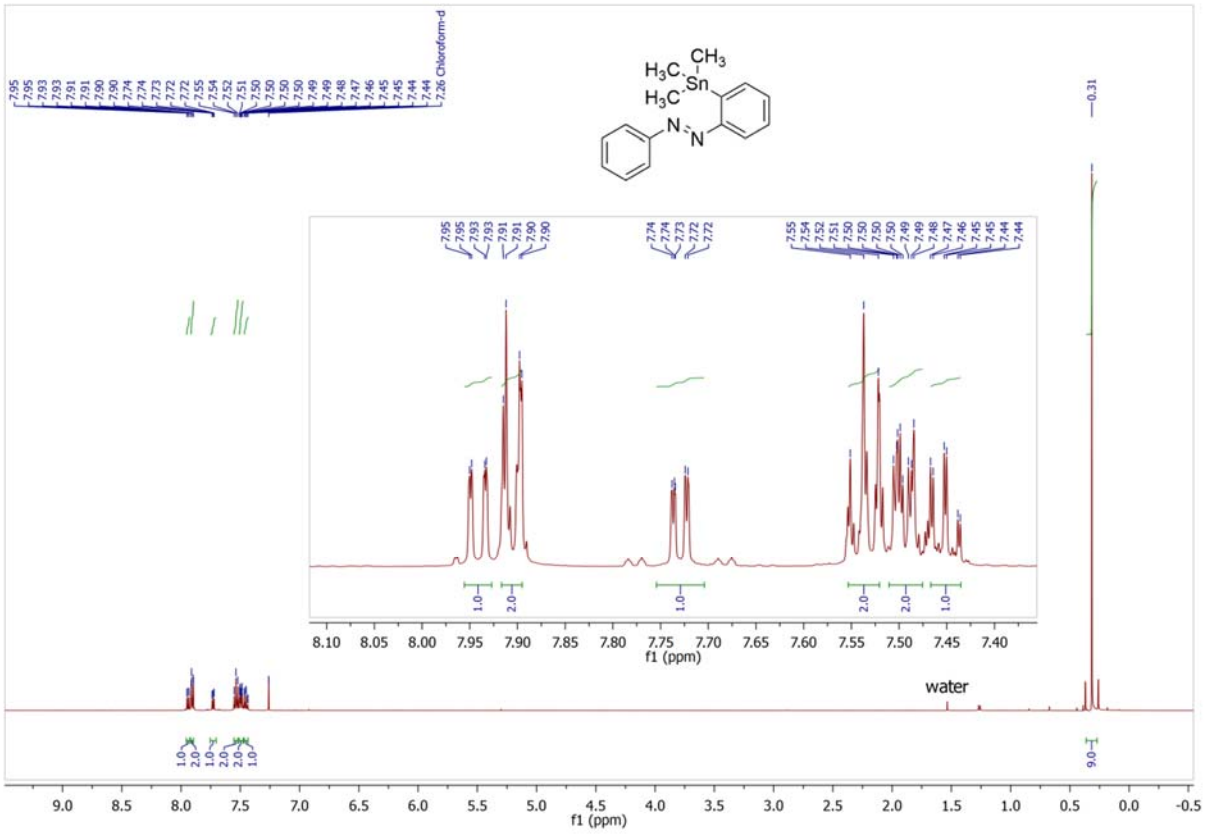

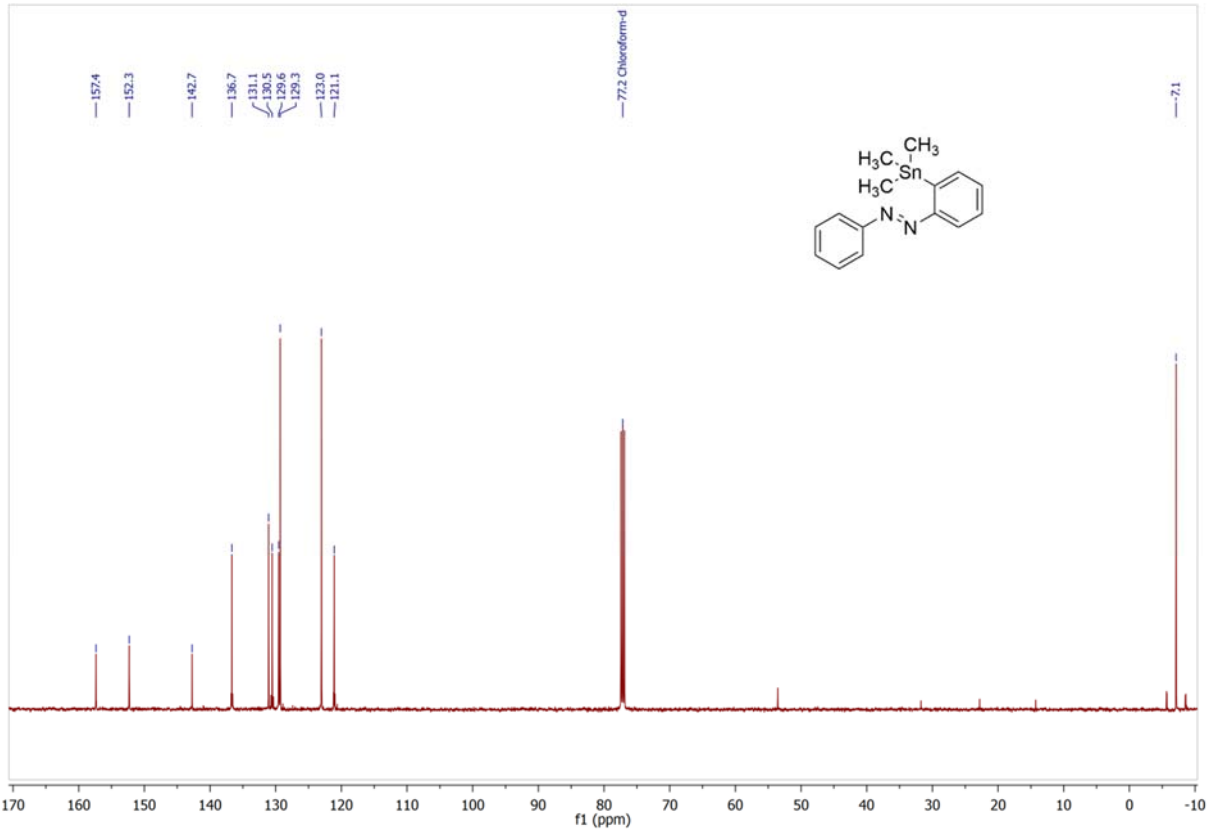

4-Methyl-4'-(trimethylstannyl)azobenzene (11a) in chloroform-*d*

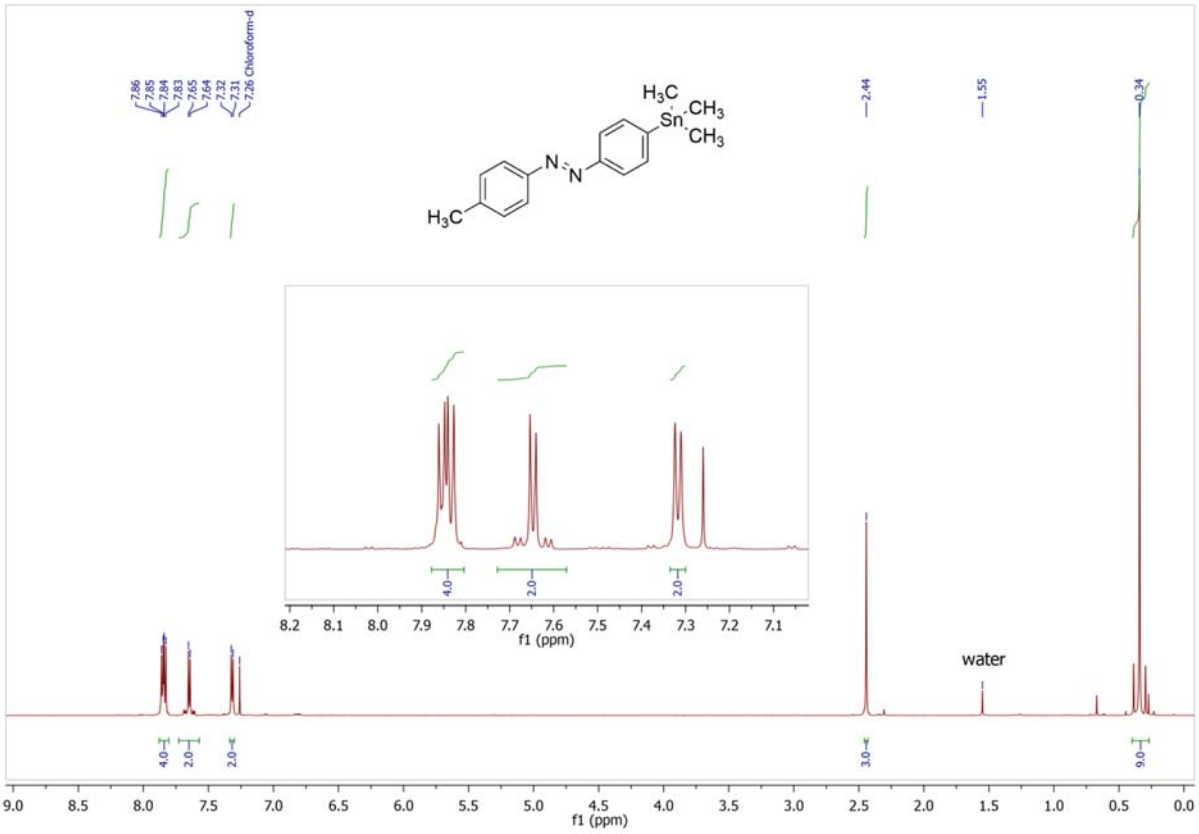

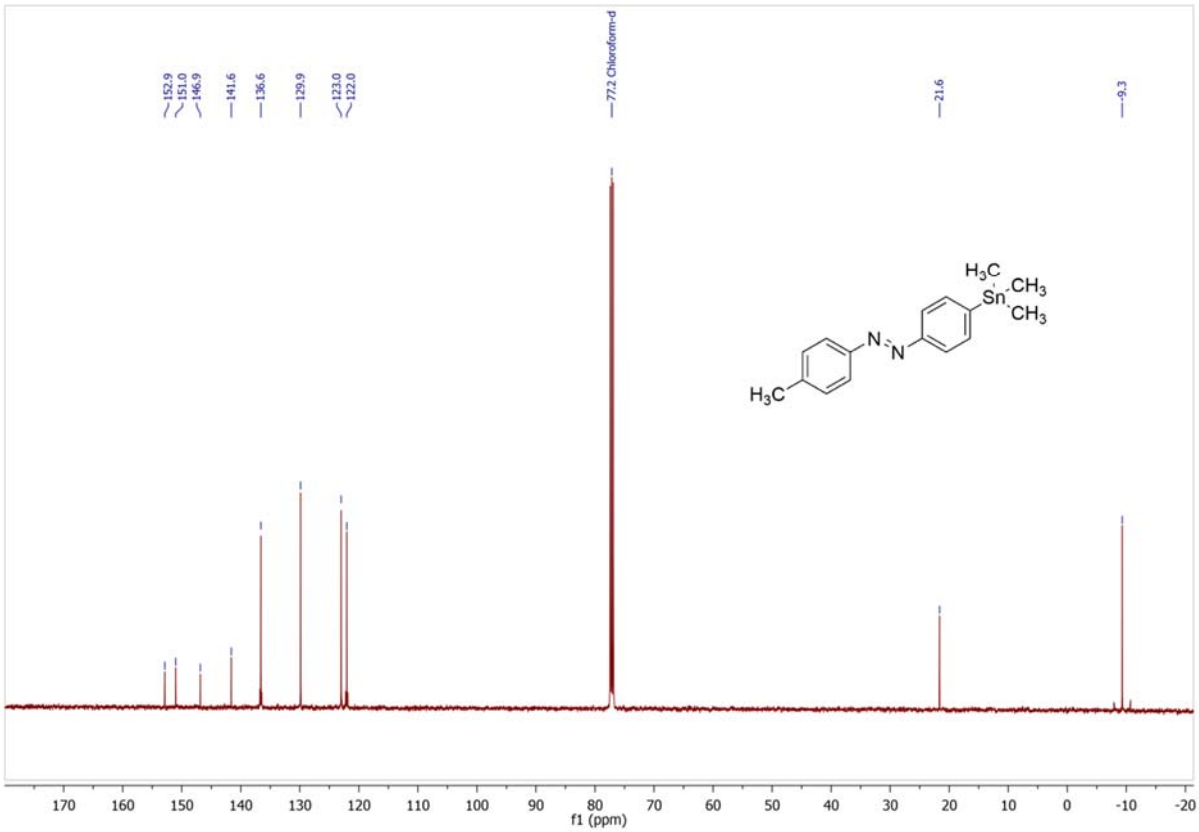

4-Methyl-3'-(trimethylstannyl)azobenzene (11b) in chloroform-*d*

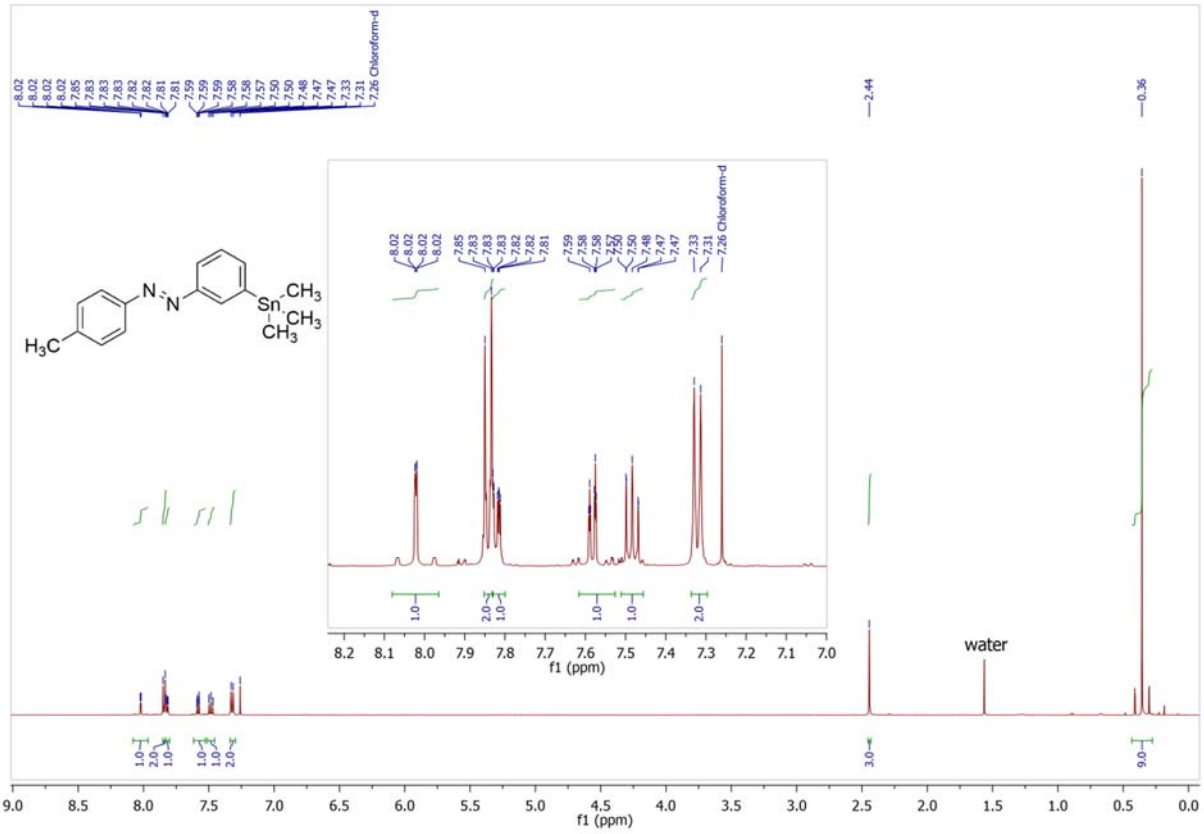

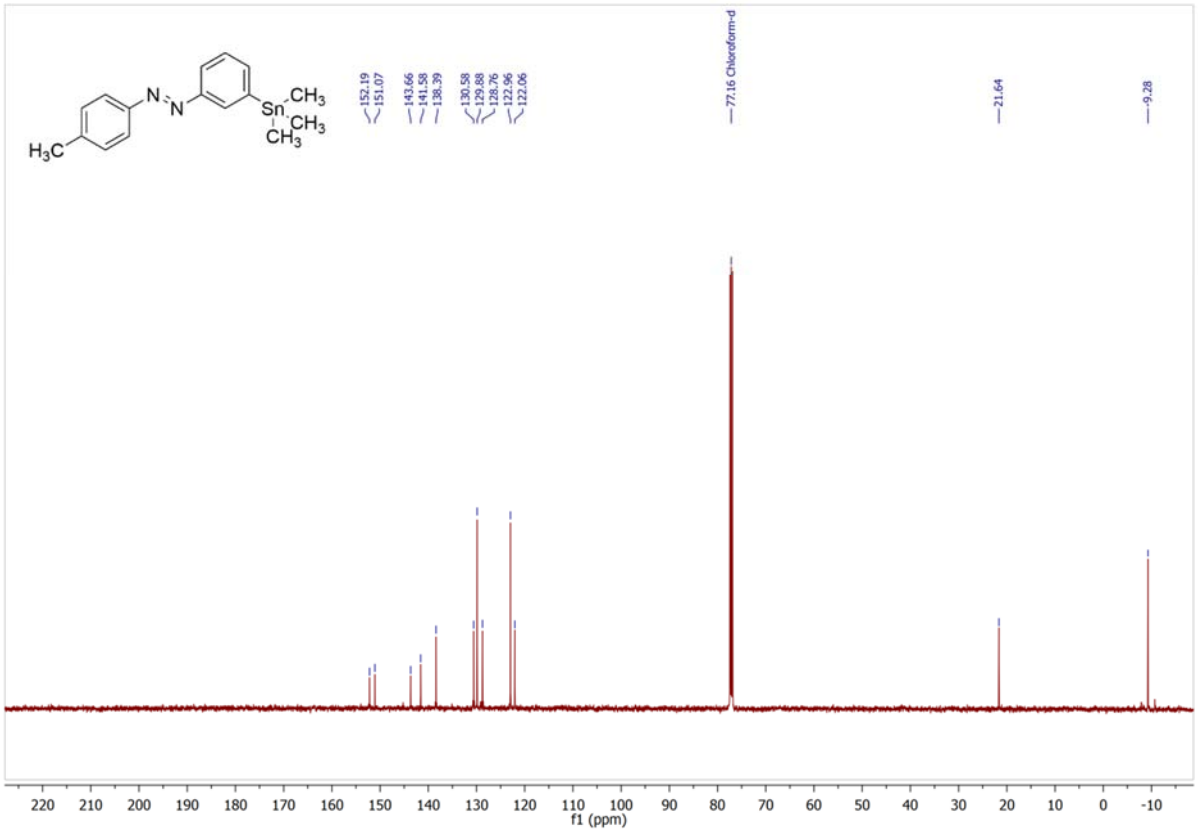

4-Methyl-2‘-(trimethylstannyl)azobenzene (11c) in chloroform-*d*

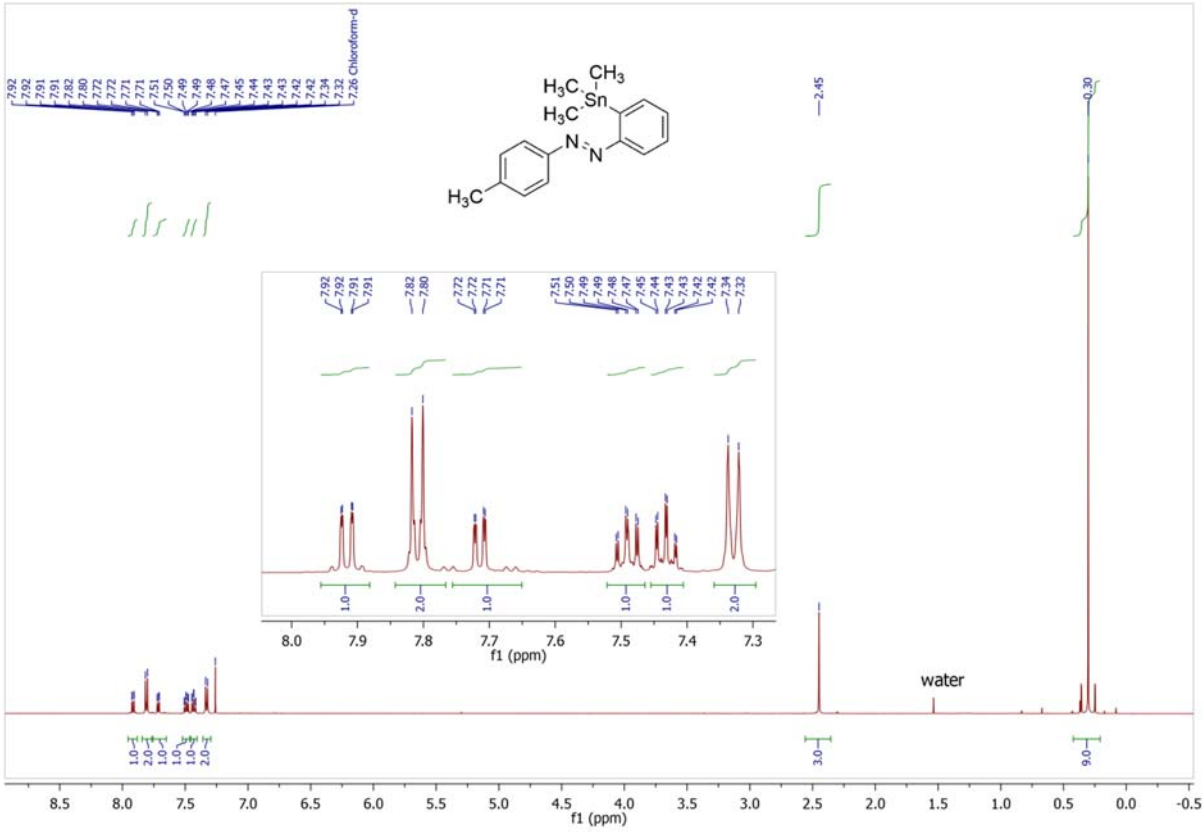

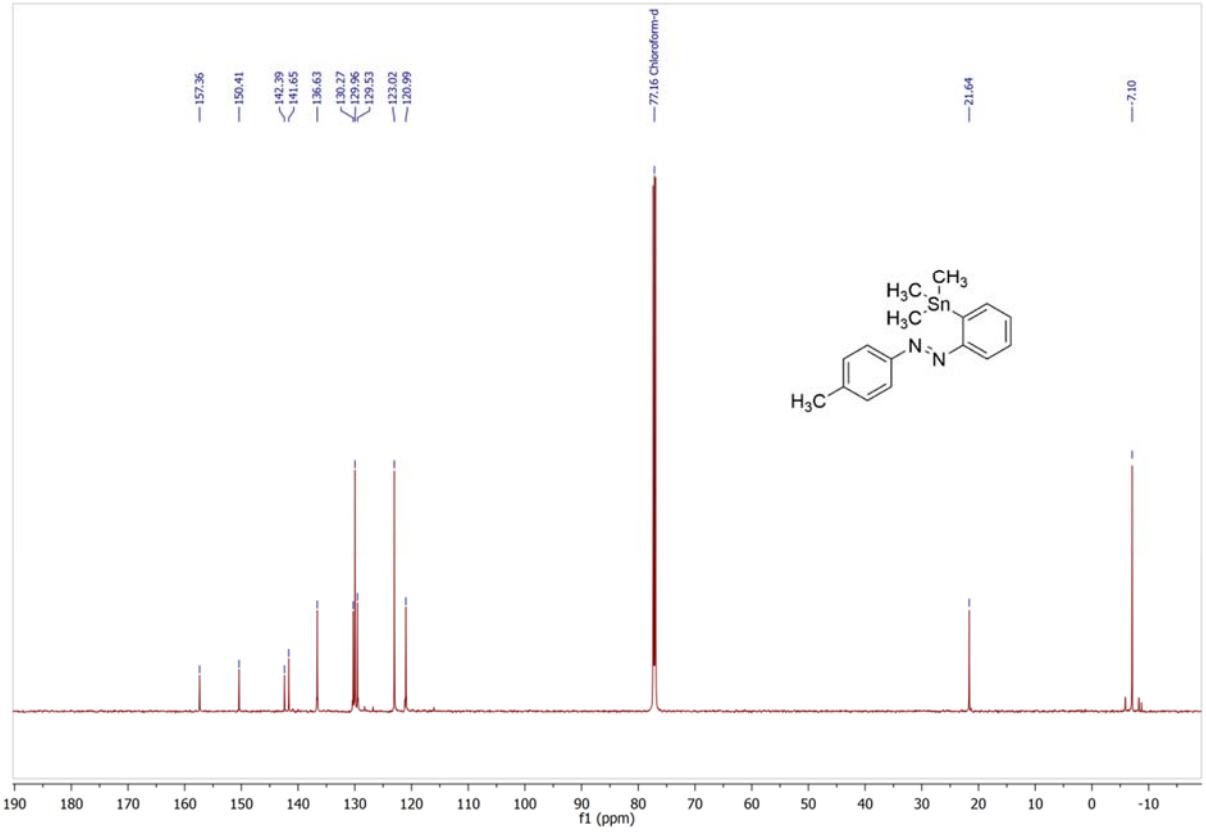

1.3 Compounds with one Azobenzene Unit

4,4'-Dimethylazobenzene (14a) in chloroform-*d*

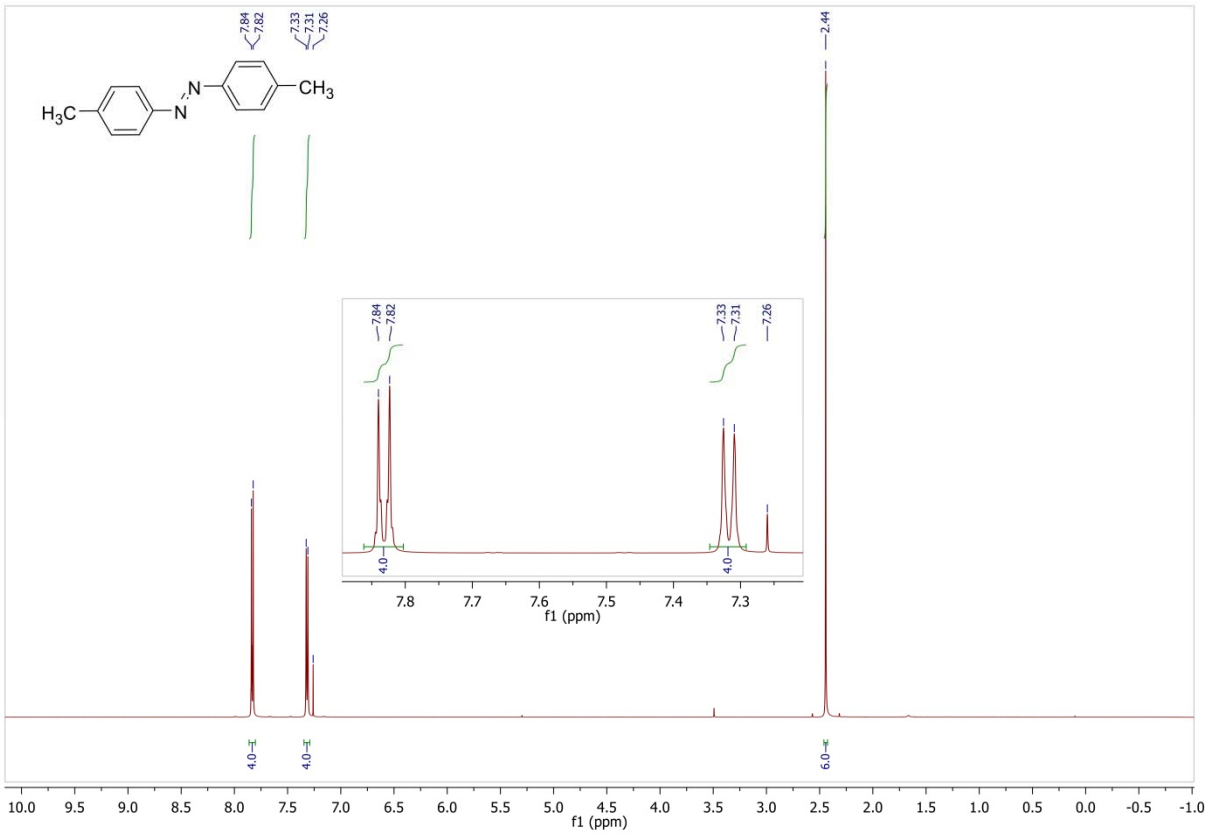

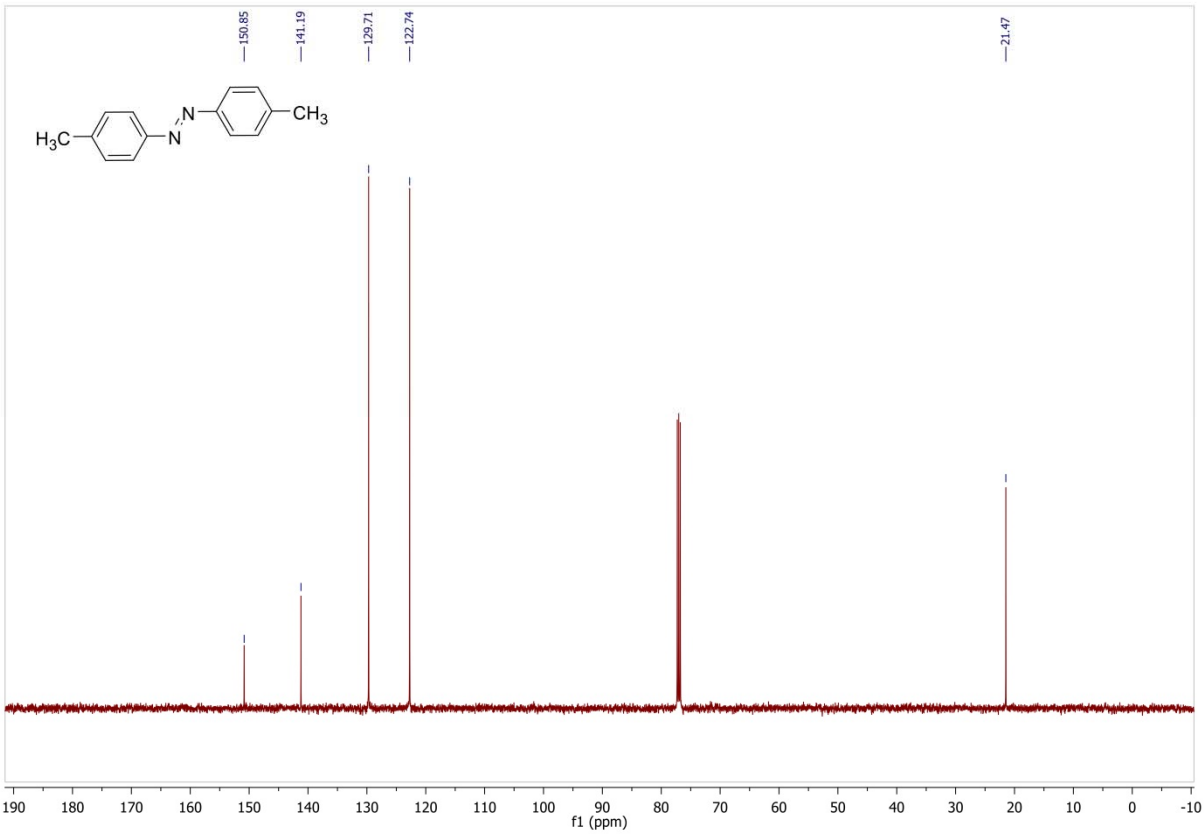

3,4'-Dimethylazobenzene (14b) in chloroform-*d*

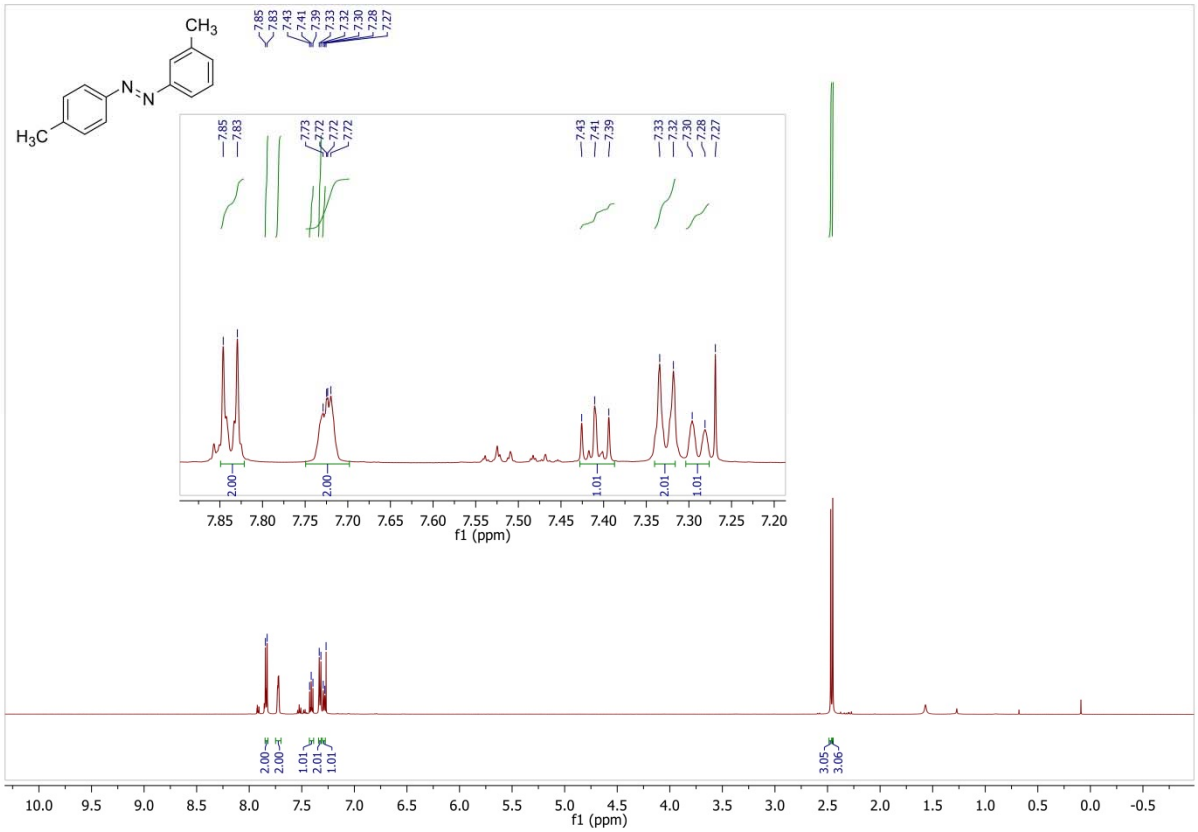

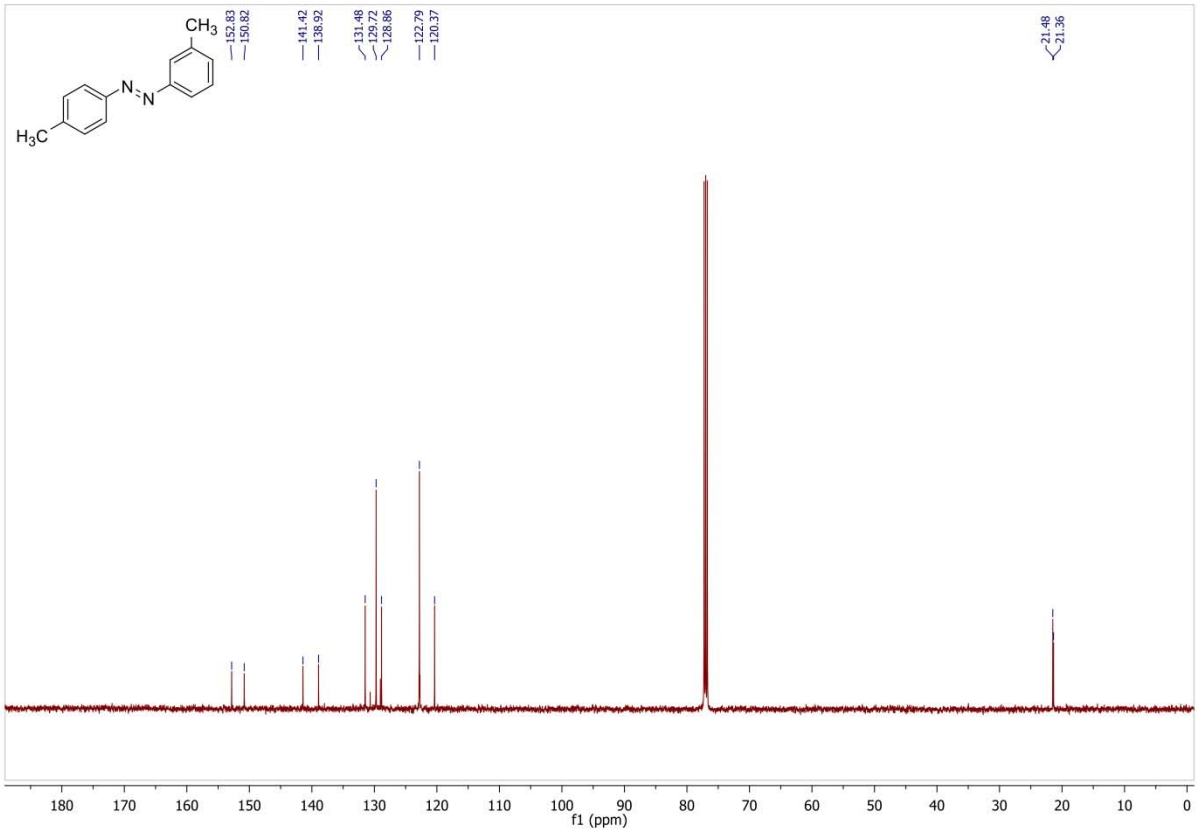

2-Methyl-4'-methylazobenzene (14c) in dichloromethane-d_2

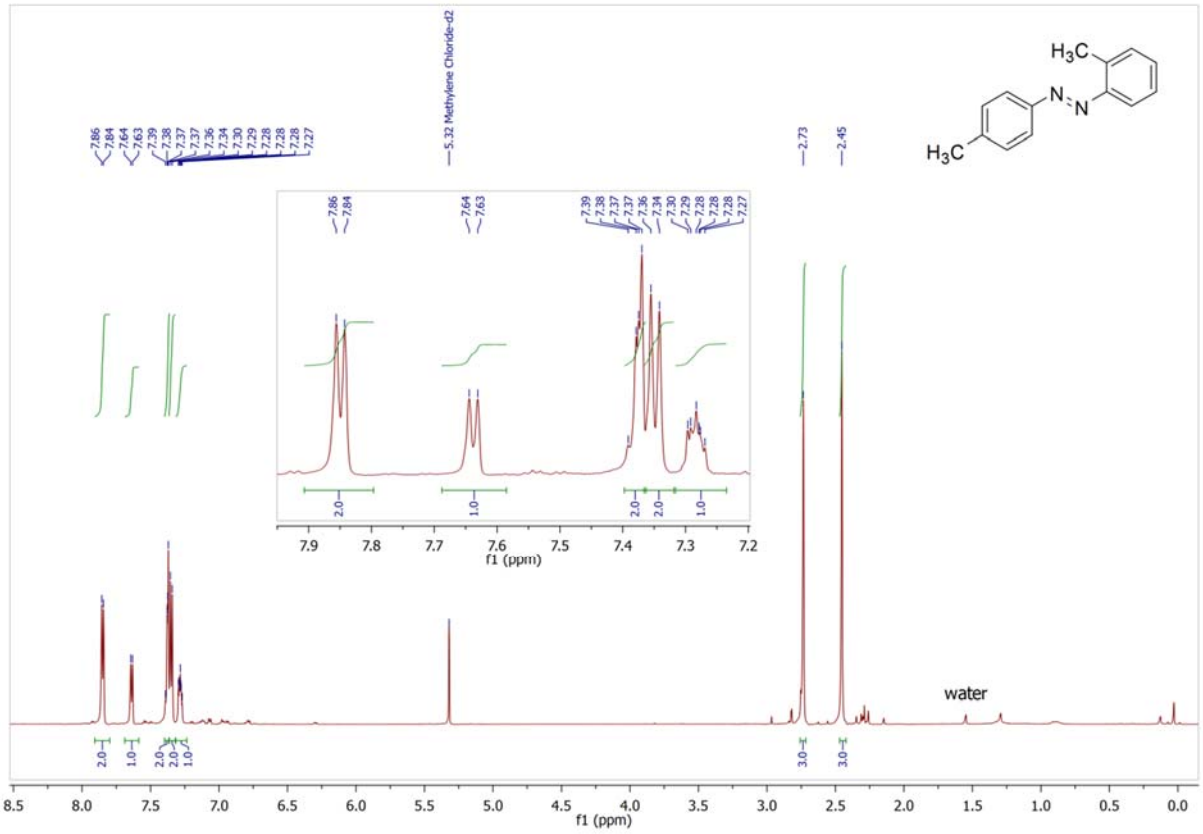

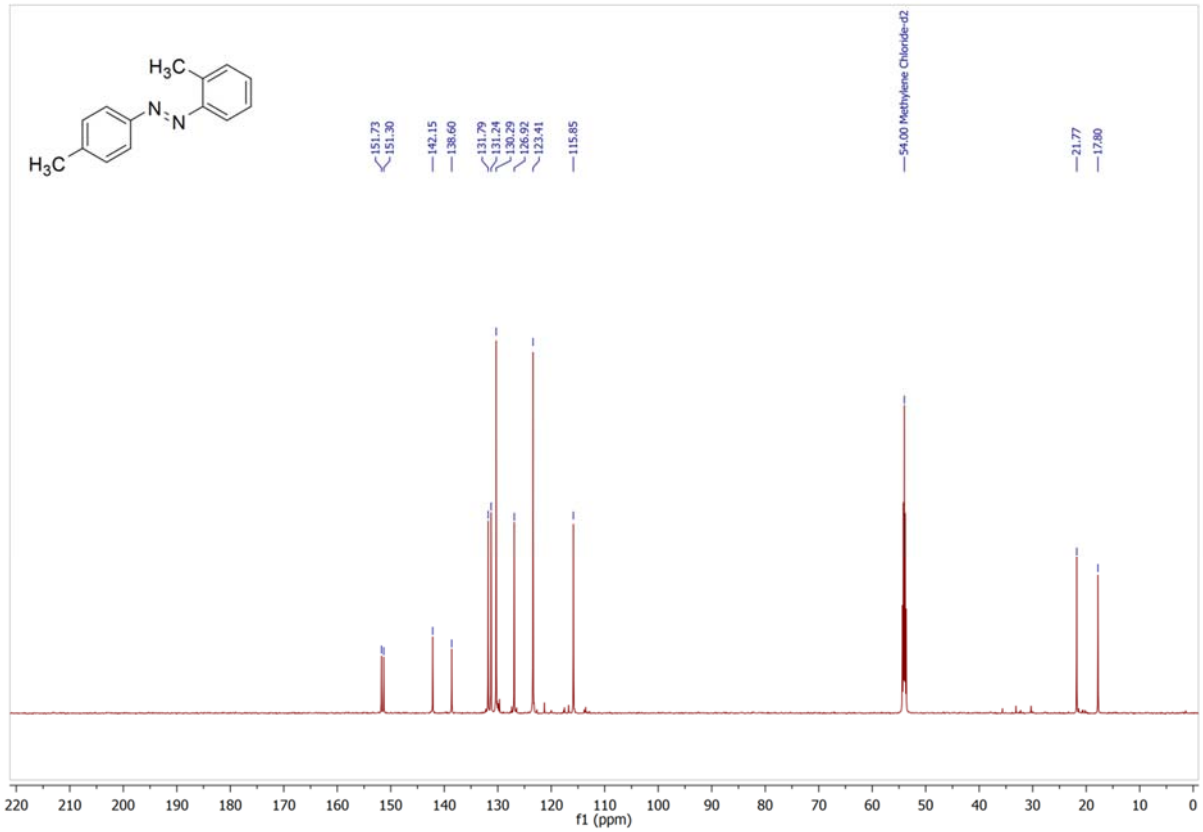

Side product 15 – crude spectra in chloroform-*d*

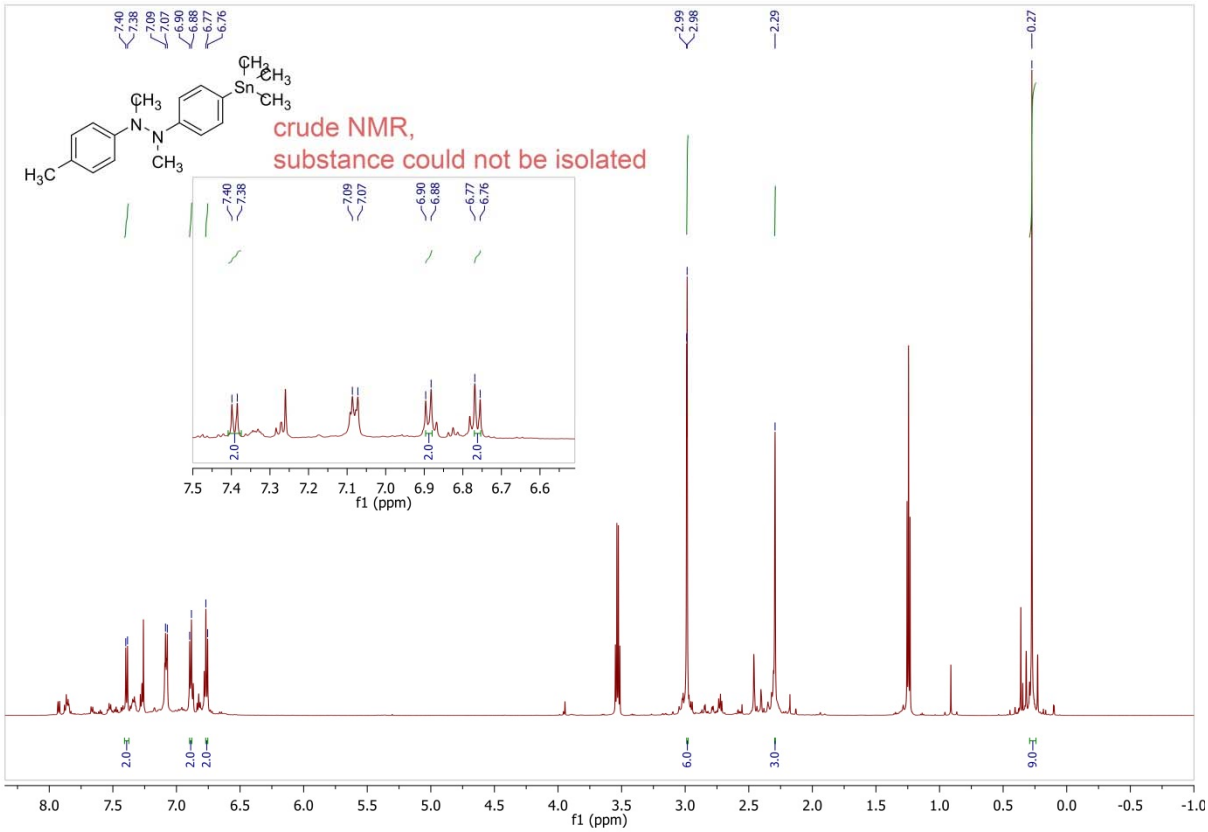

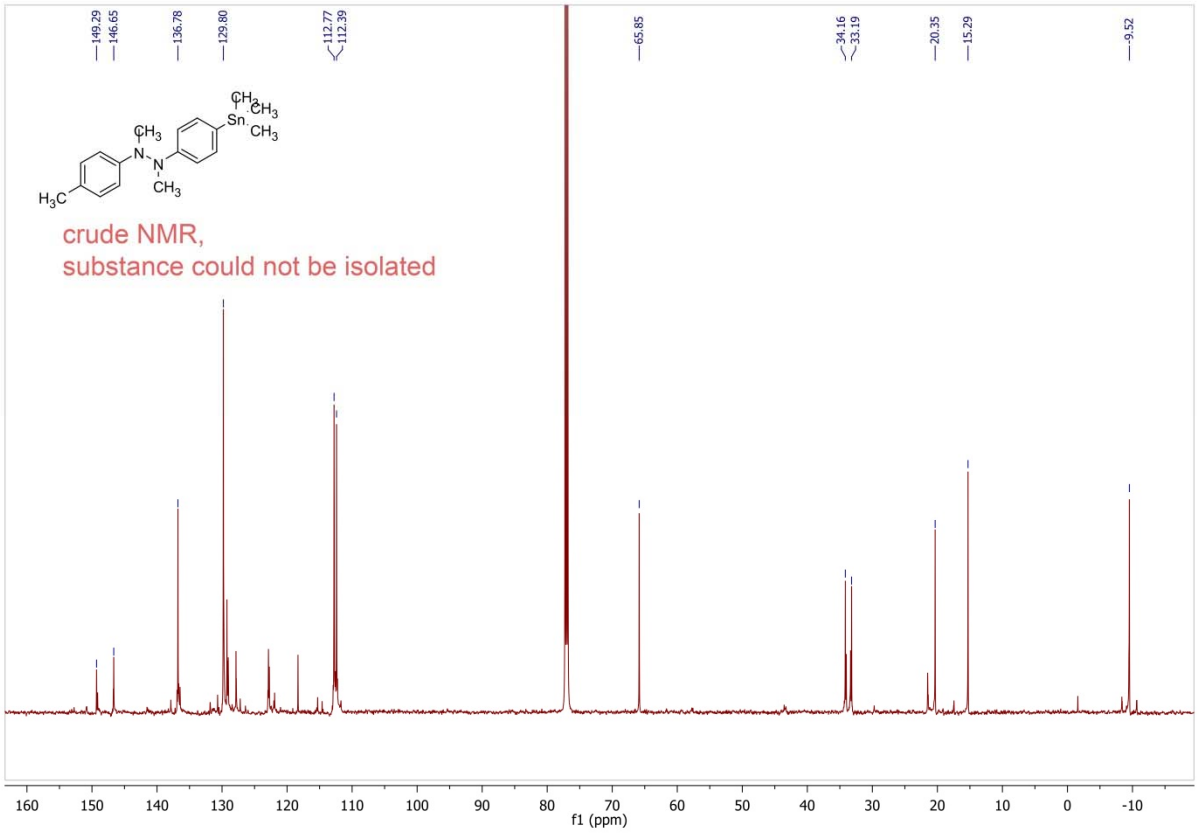

Side product 16 – purity 90% - chloroform-*d*

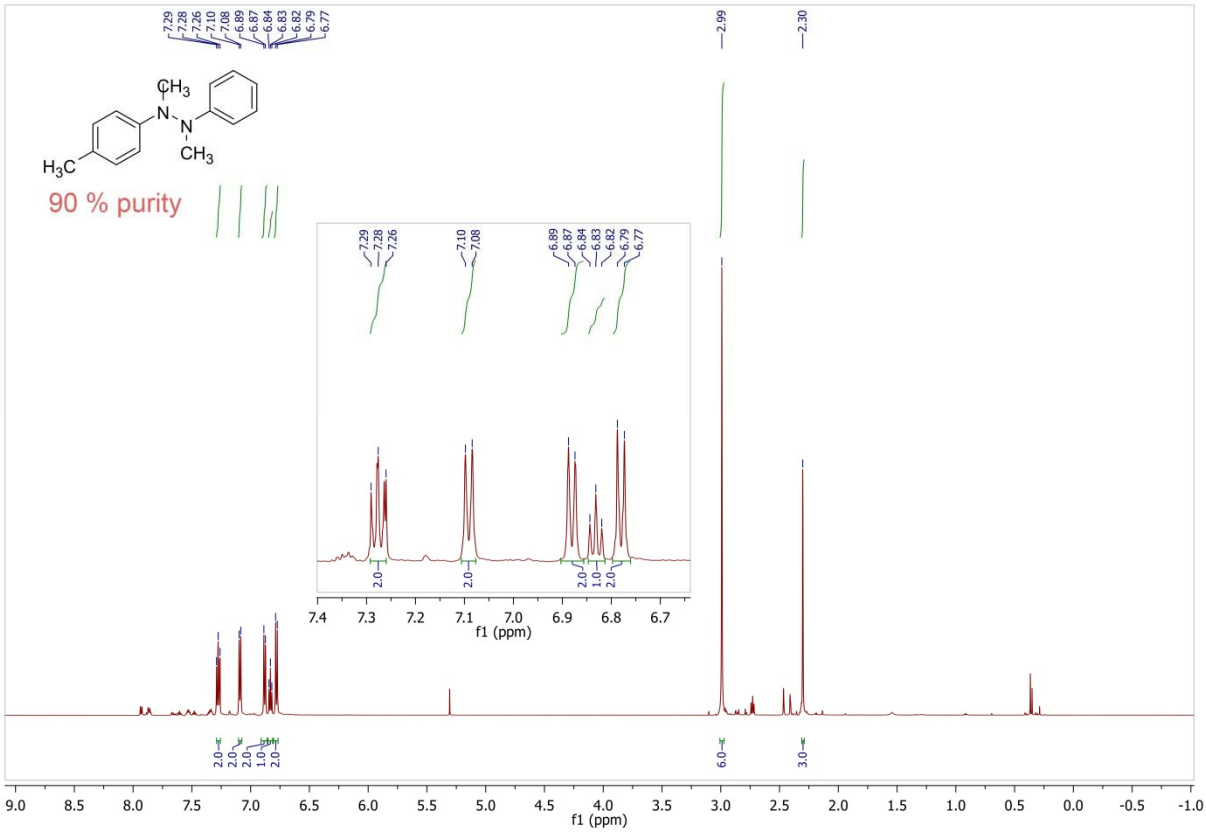

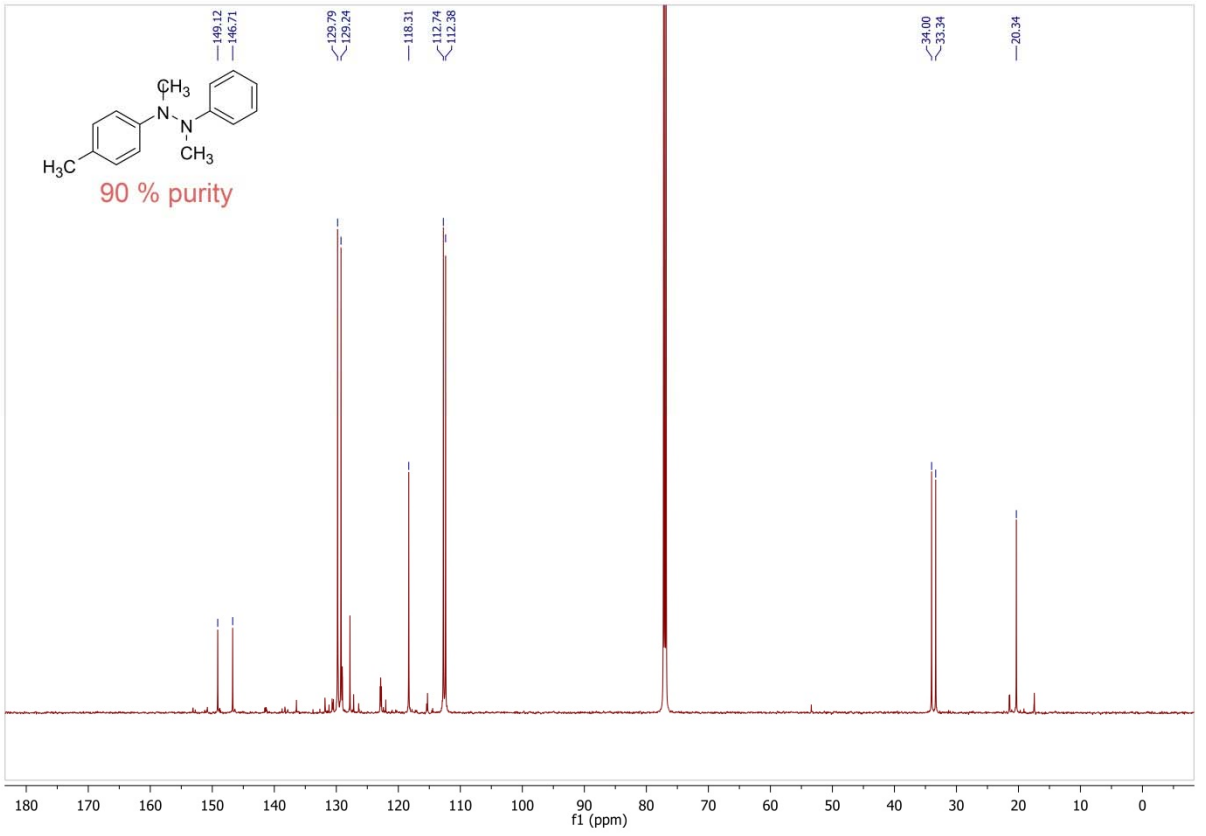

4-Methyl-4‘-(trimethylsilyl)azobenzene (17a) in chloroform-*d*

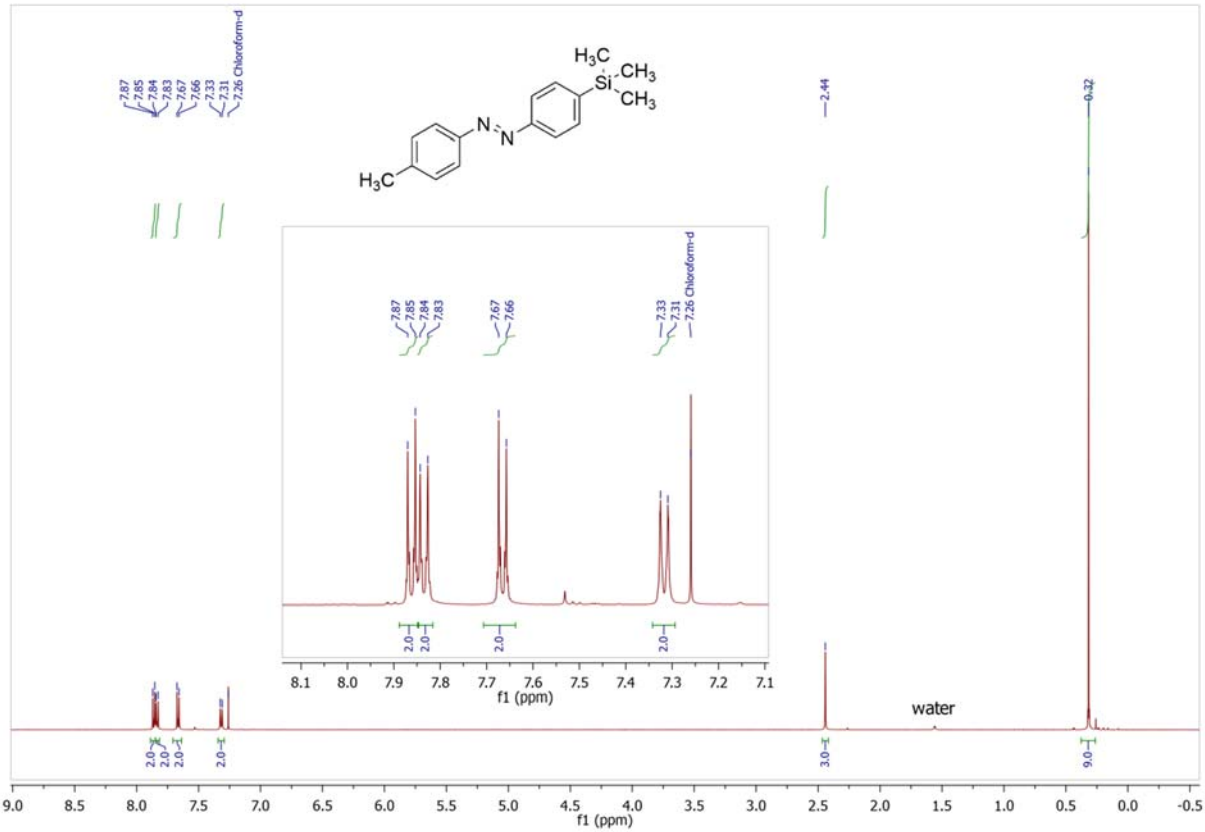

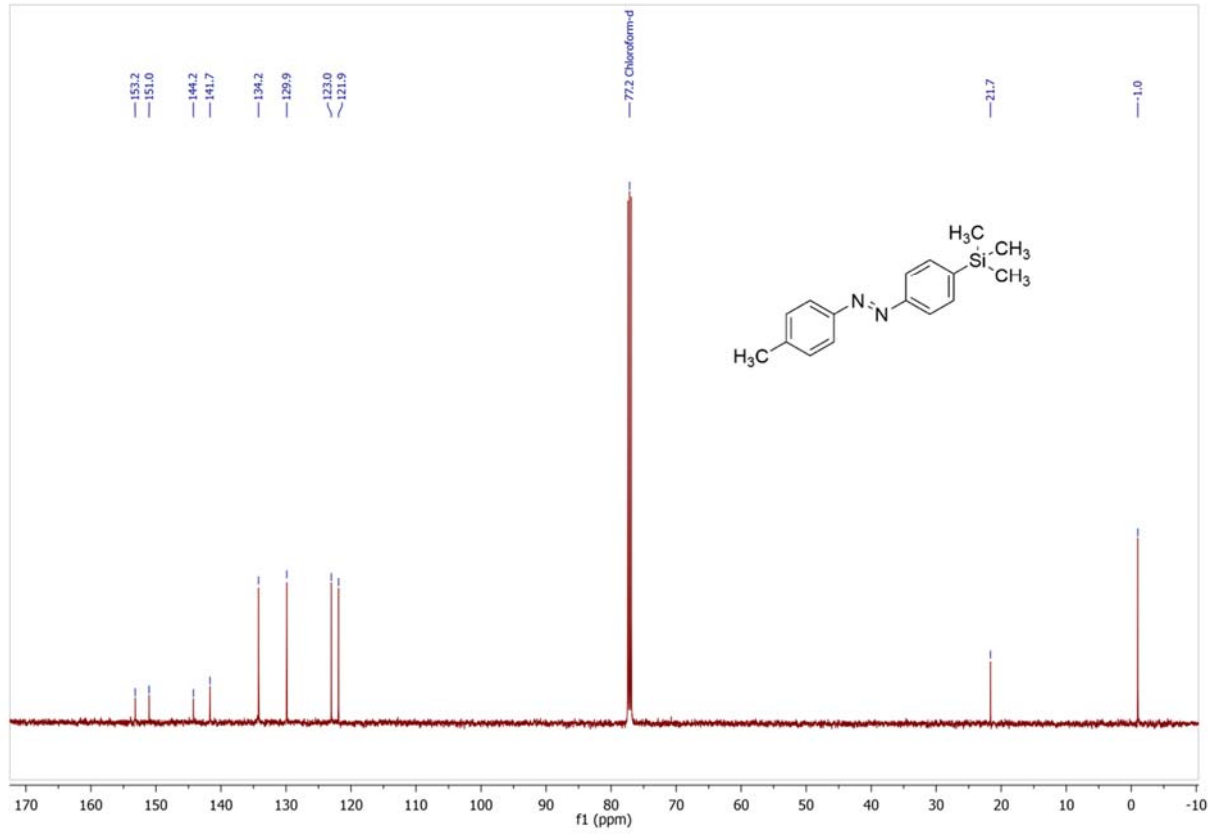

4-Methyl-3'-(trimethylsilyl)azobenzene (17b) in chloroform-*d*

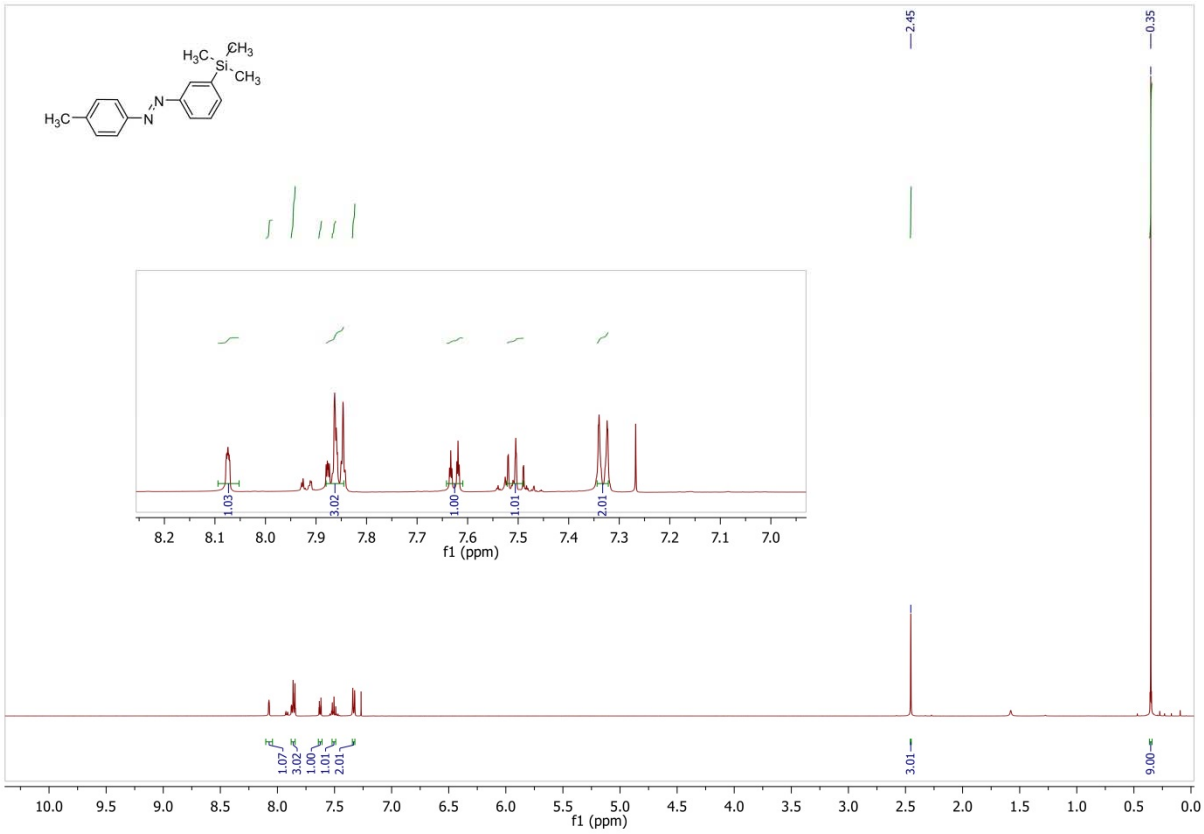

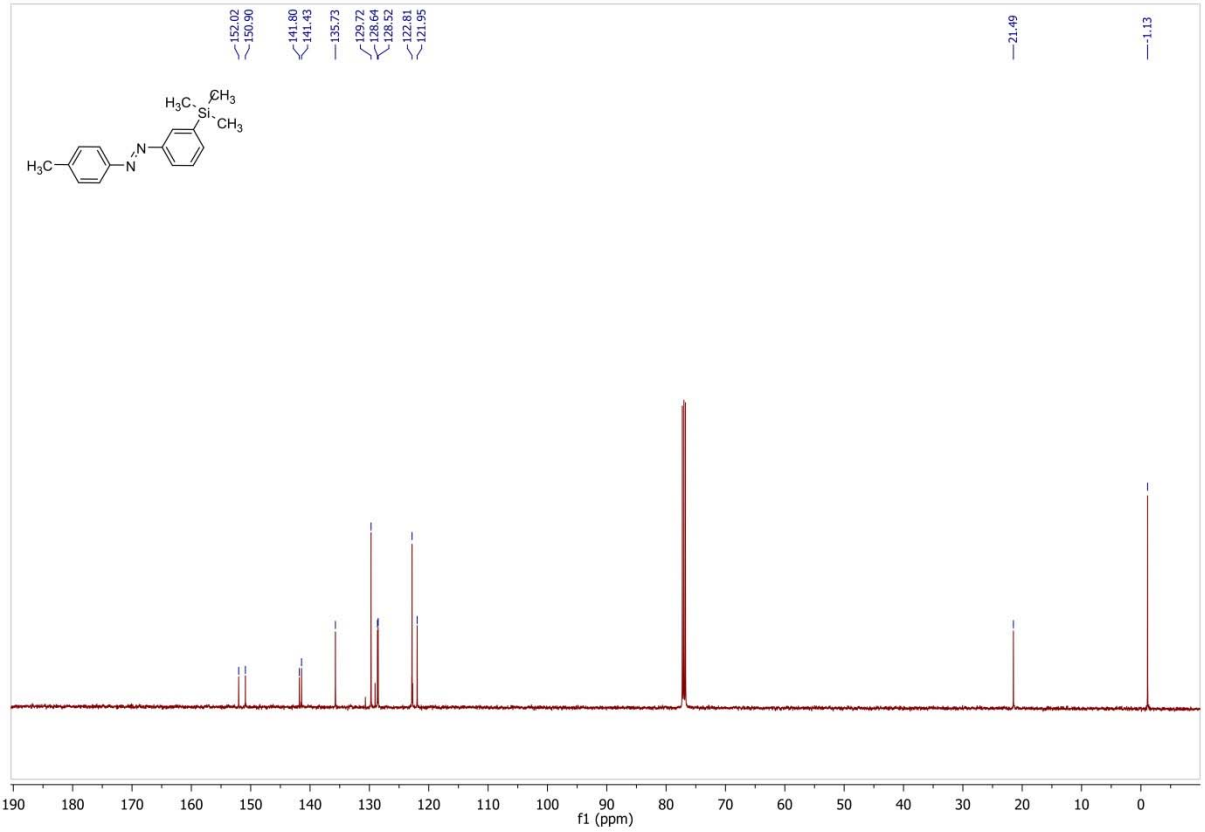

4-Methyl-2’-trimethylsilylazobenzene (17c) in chloroform-*d*

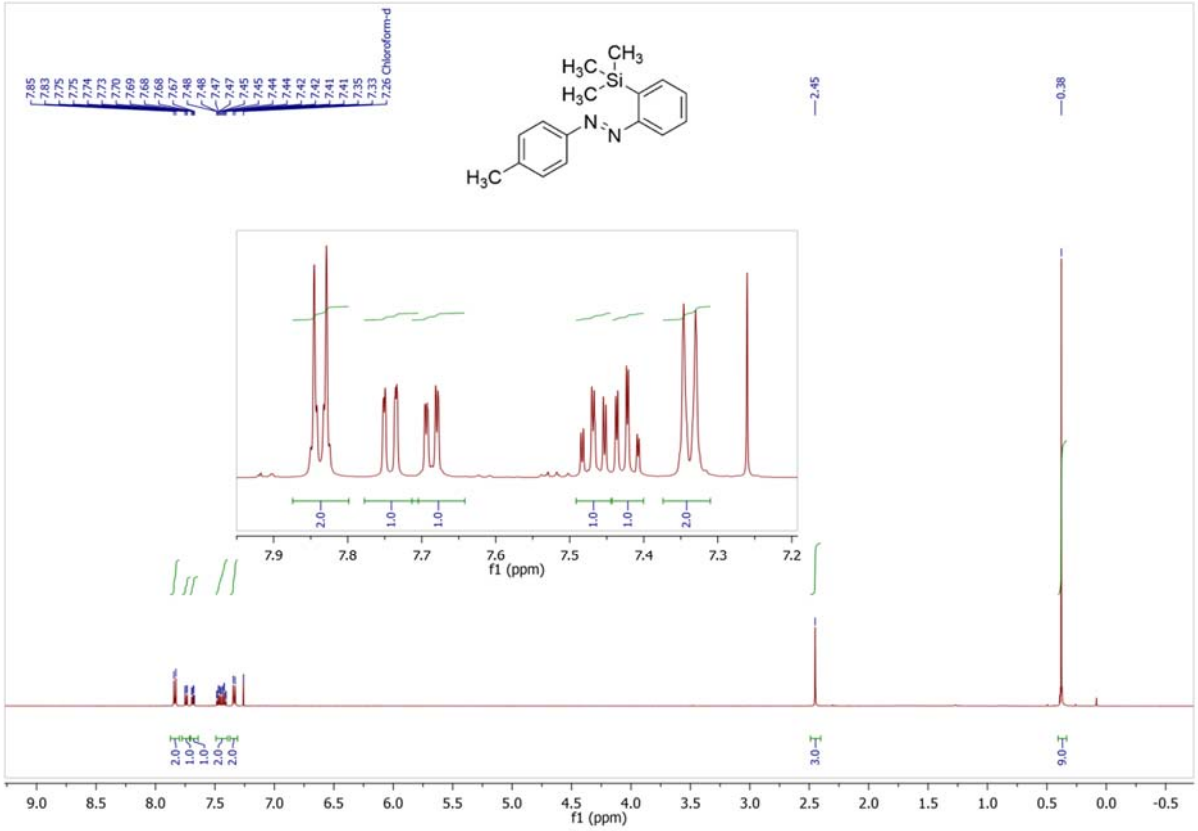

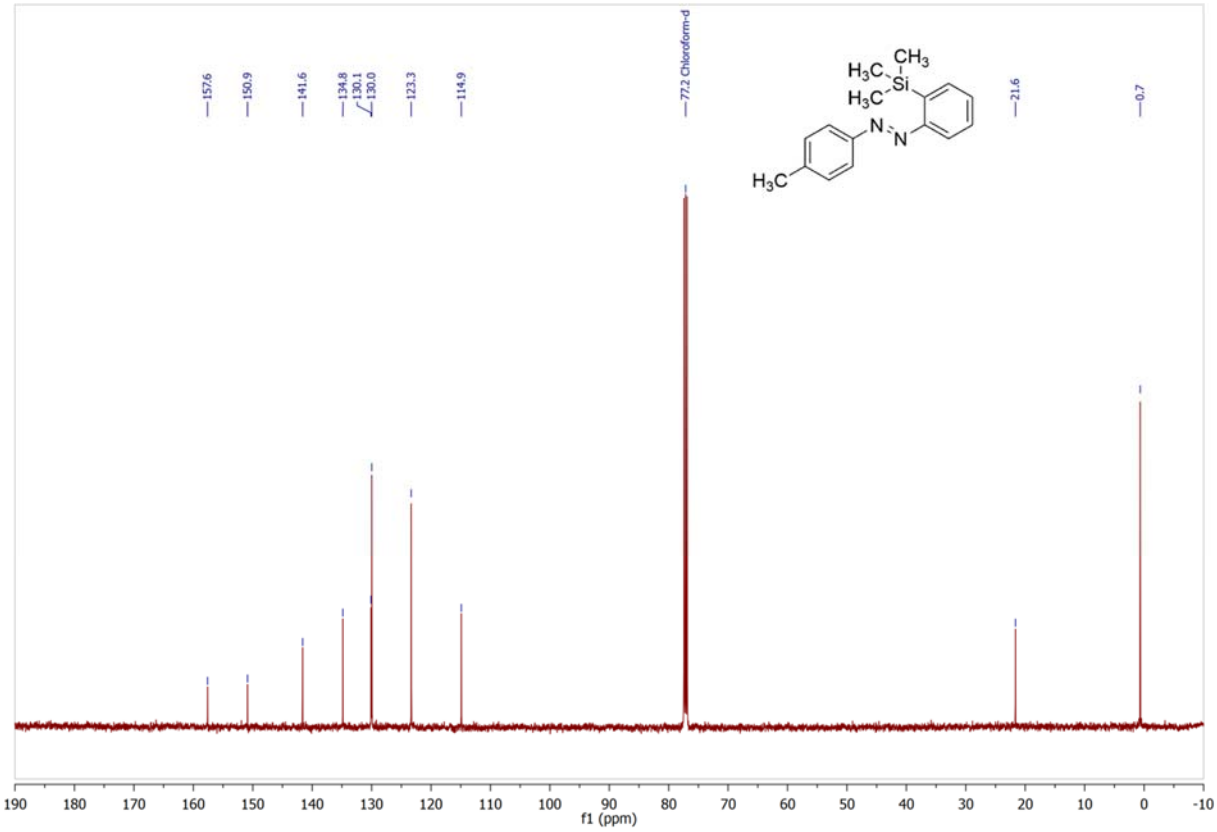

4-(1-Hydroxy-1-methylethyl)-4‘-methylazobenzene (18a) in chloroform-*d*

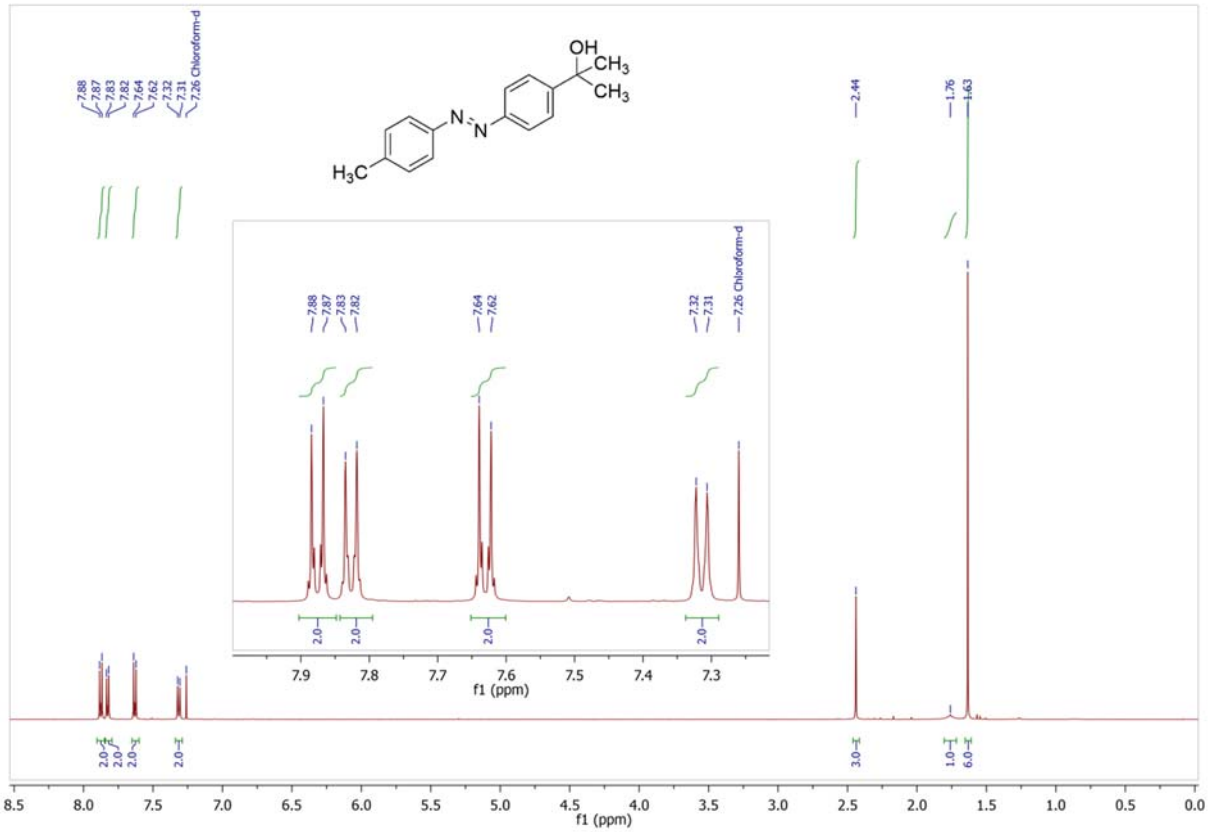

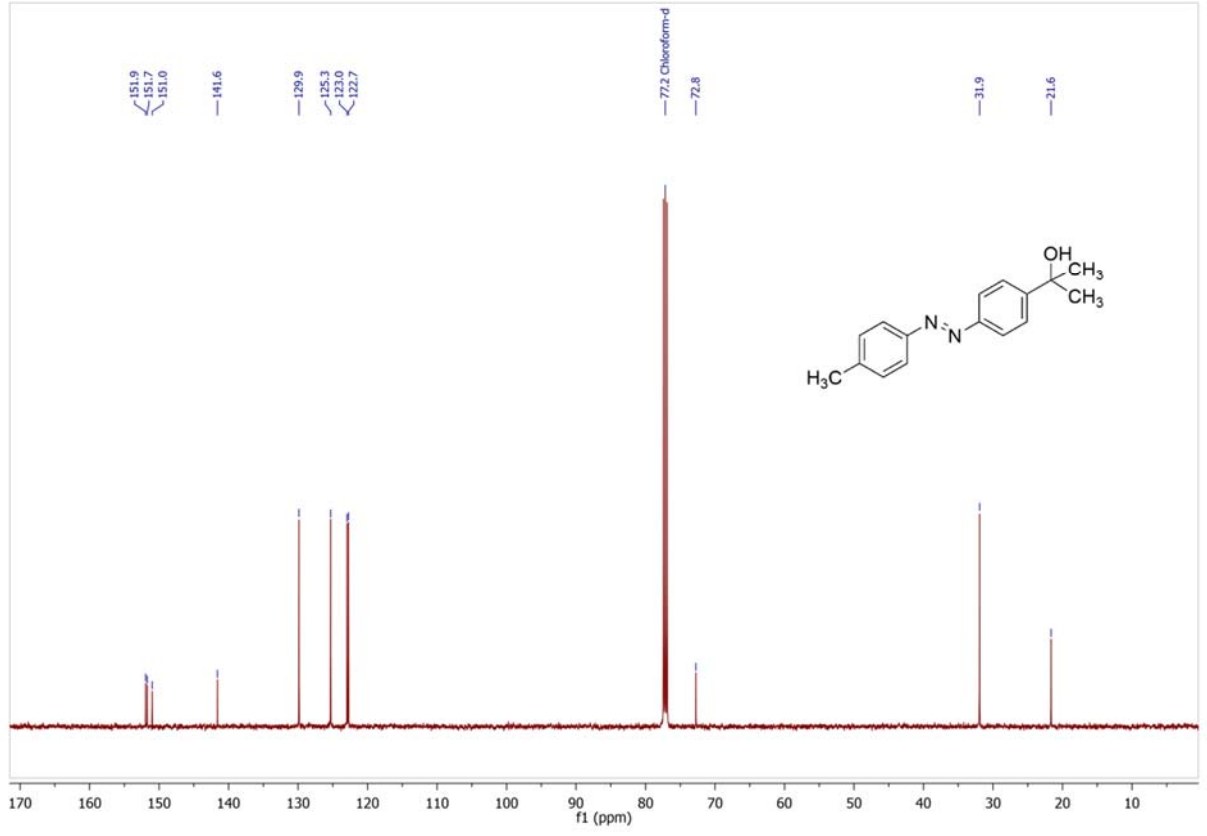

3-(1-Hydroxy-1-methylethyl)-4‘-methylazobenzene (18b) in chloroform-*d*

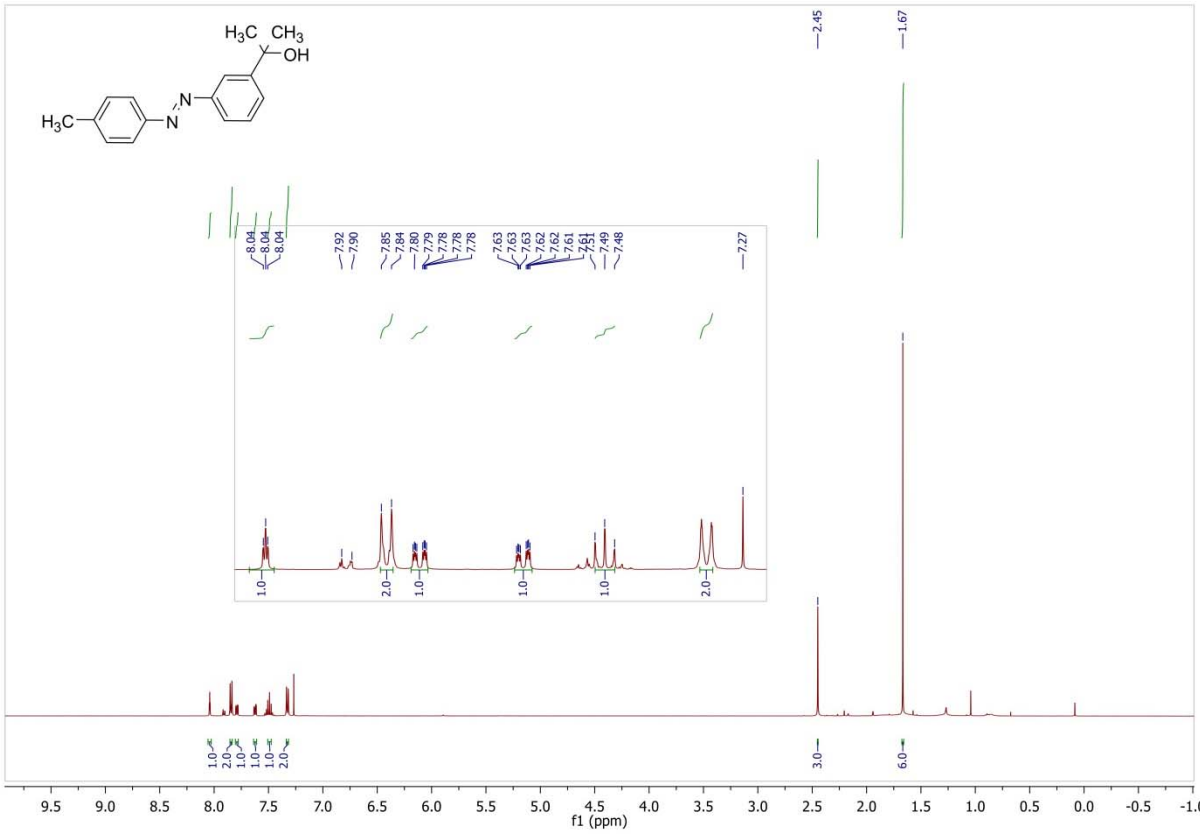

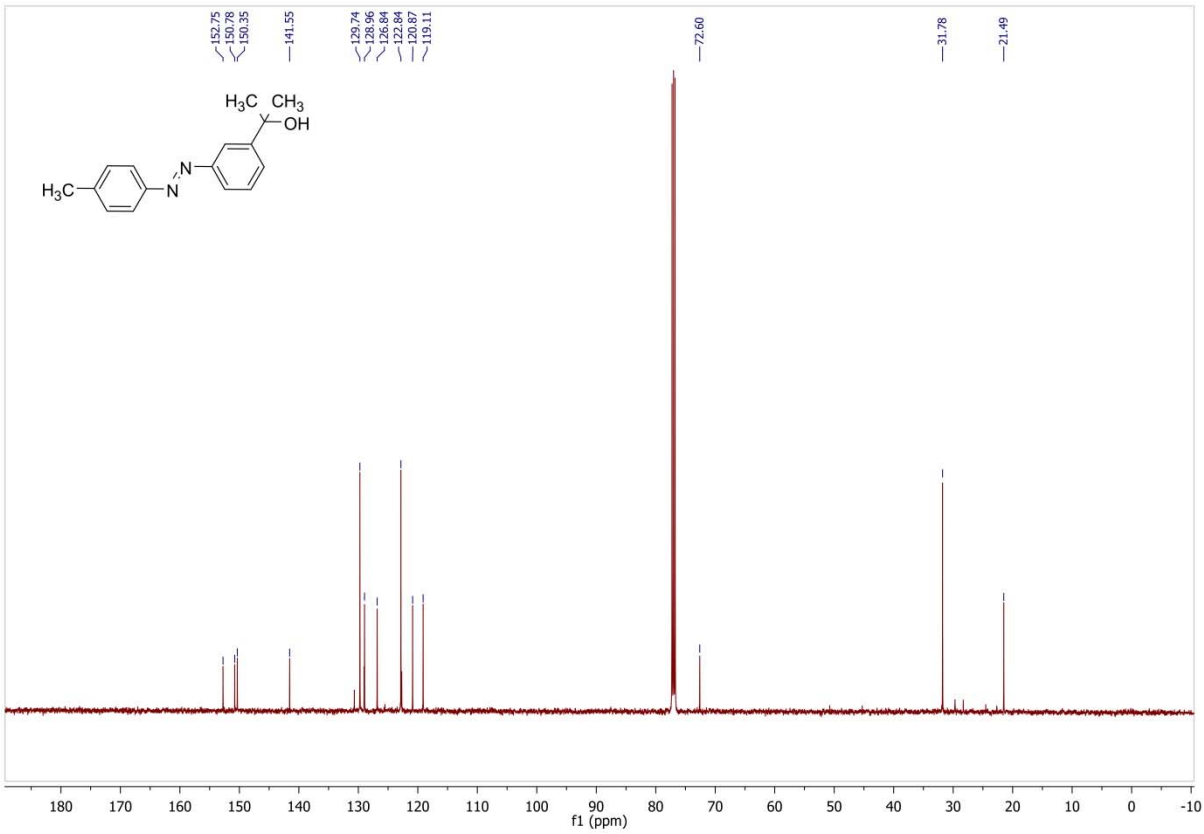

4-Tolyl-[4-(4-methylphenyl)azo-phenyl)]methanol (19a) in chloroform-*d*

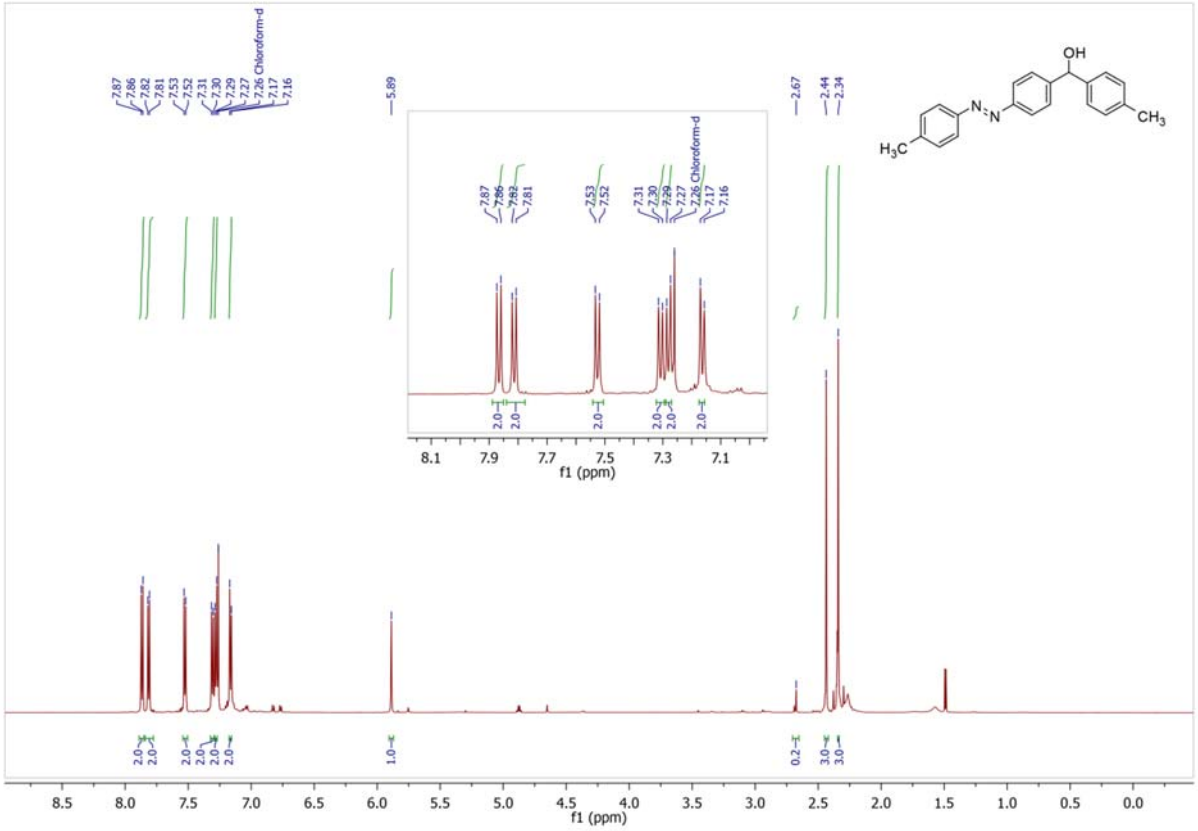

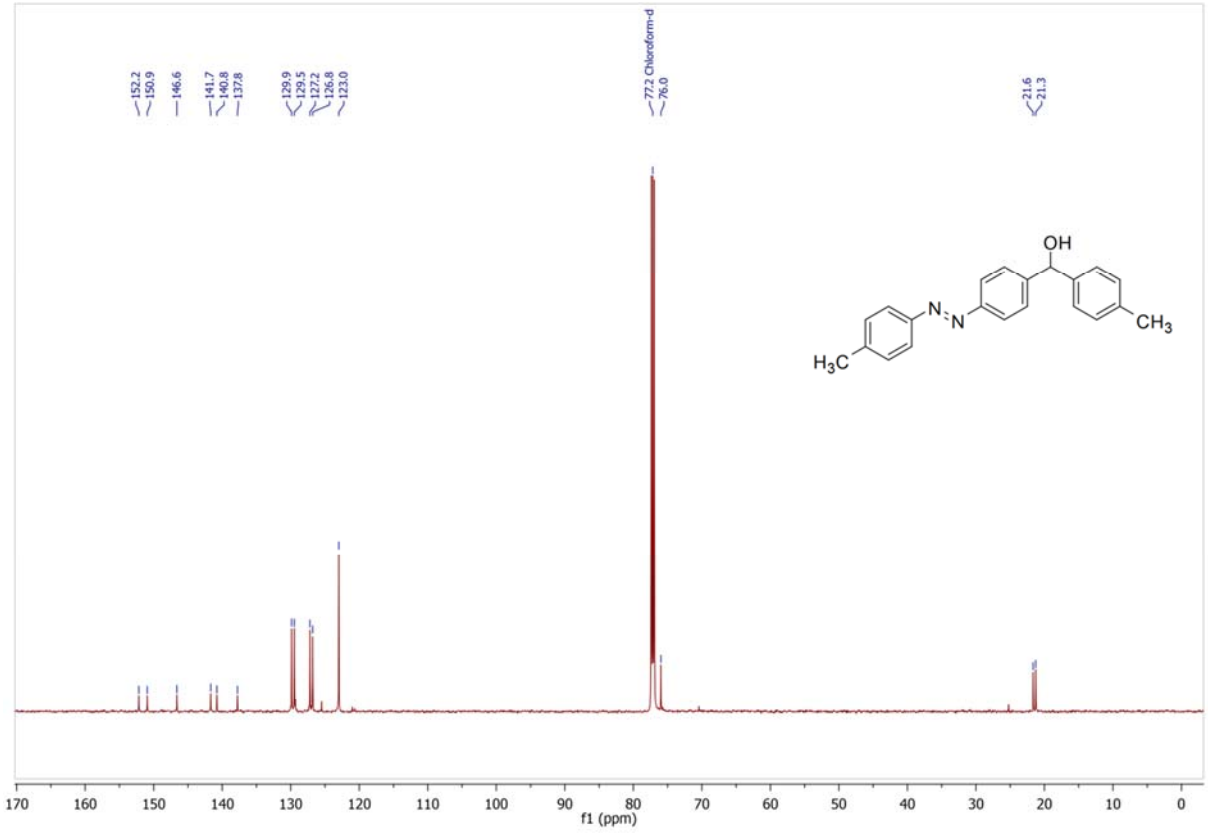

4-Tolyl-[3-(4-methylphenyl)azo-phenyl)]methanol (19b) in DMSO-d_6

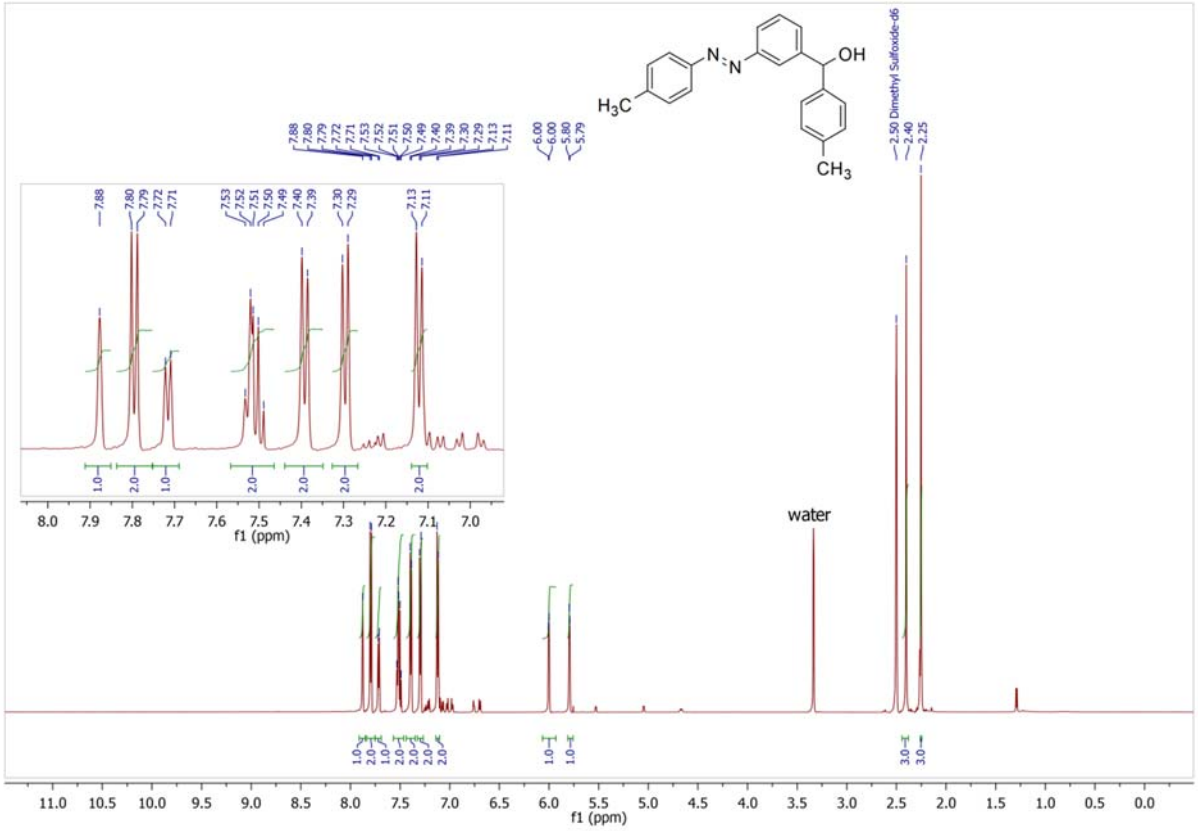

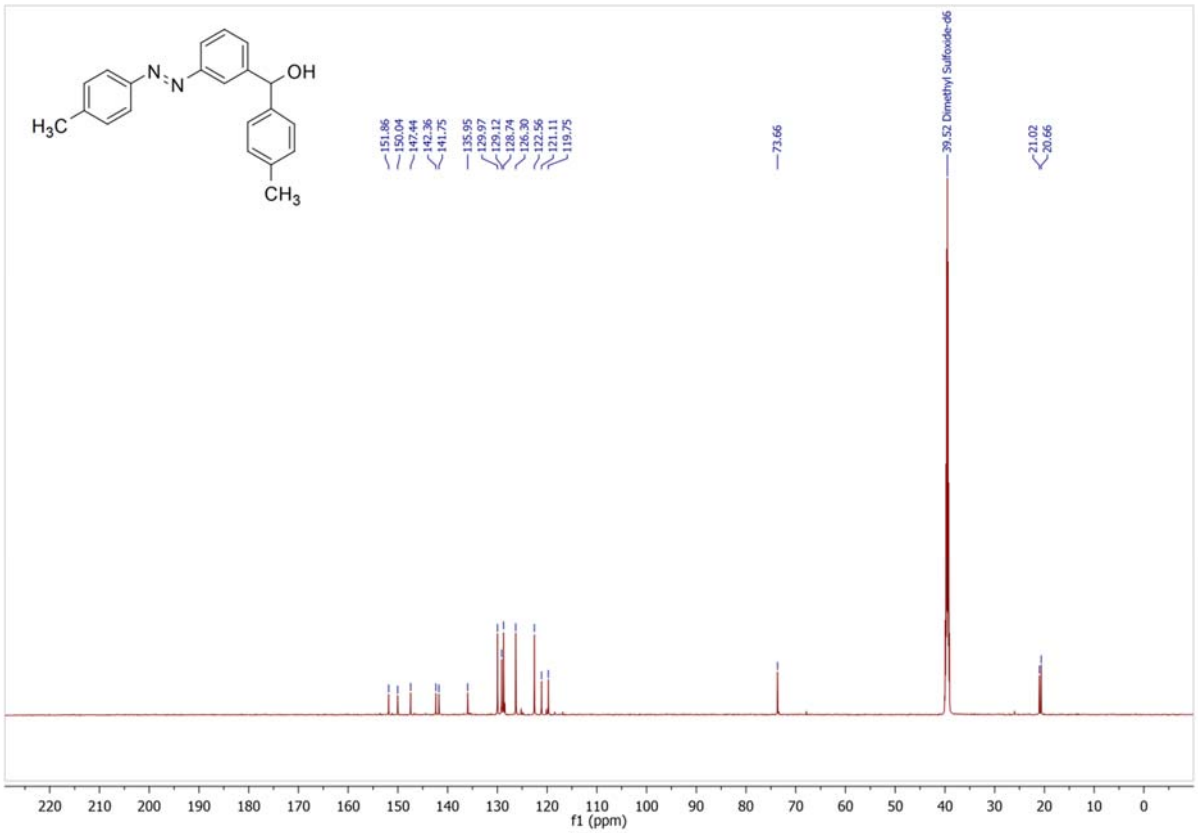

4-Formyl-4‘-methylazobenzene (20a) in chloroform-*d*

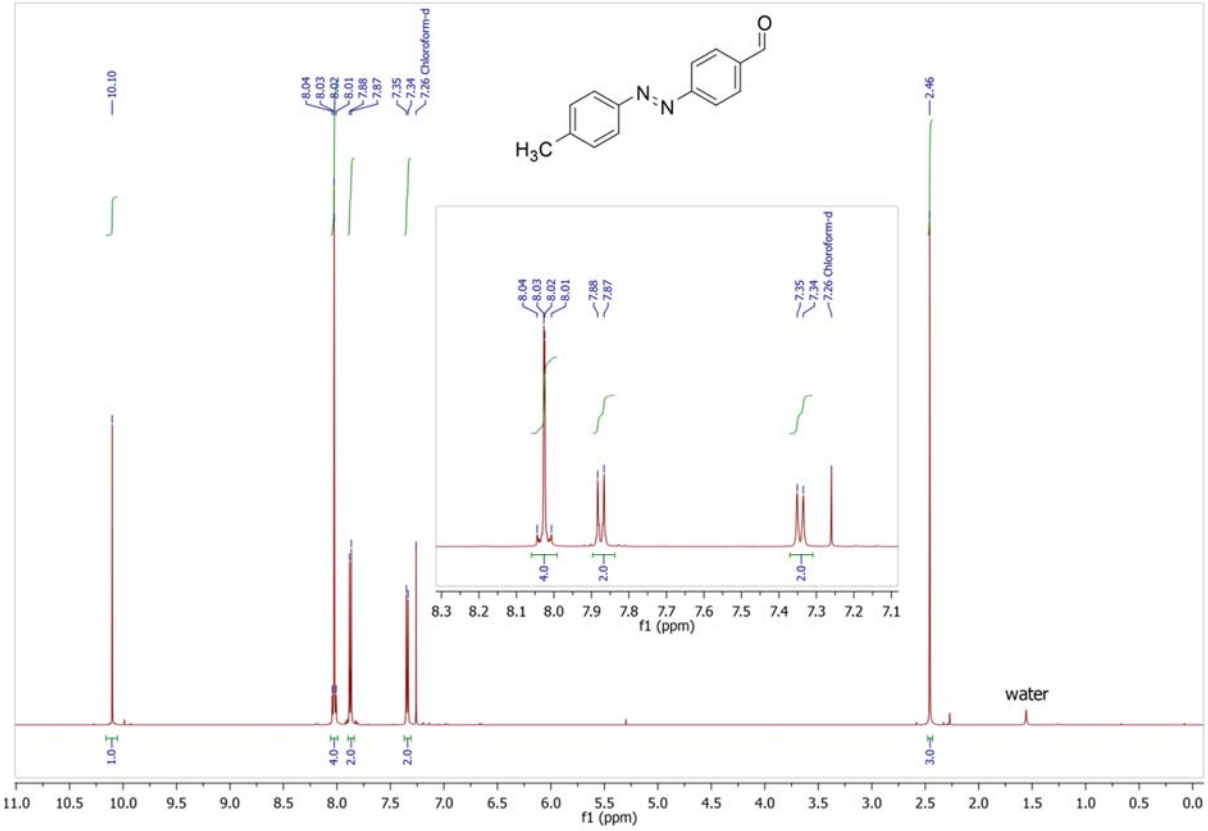

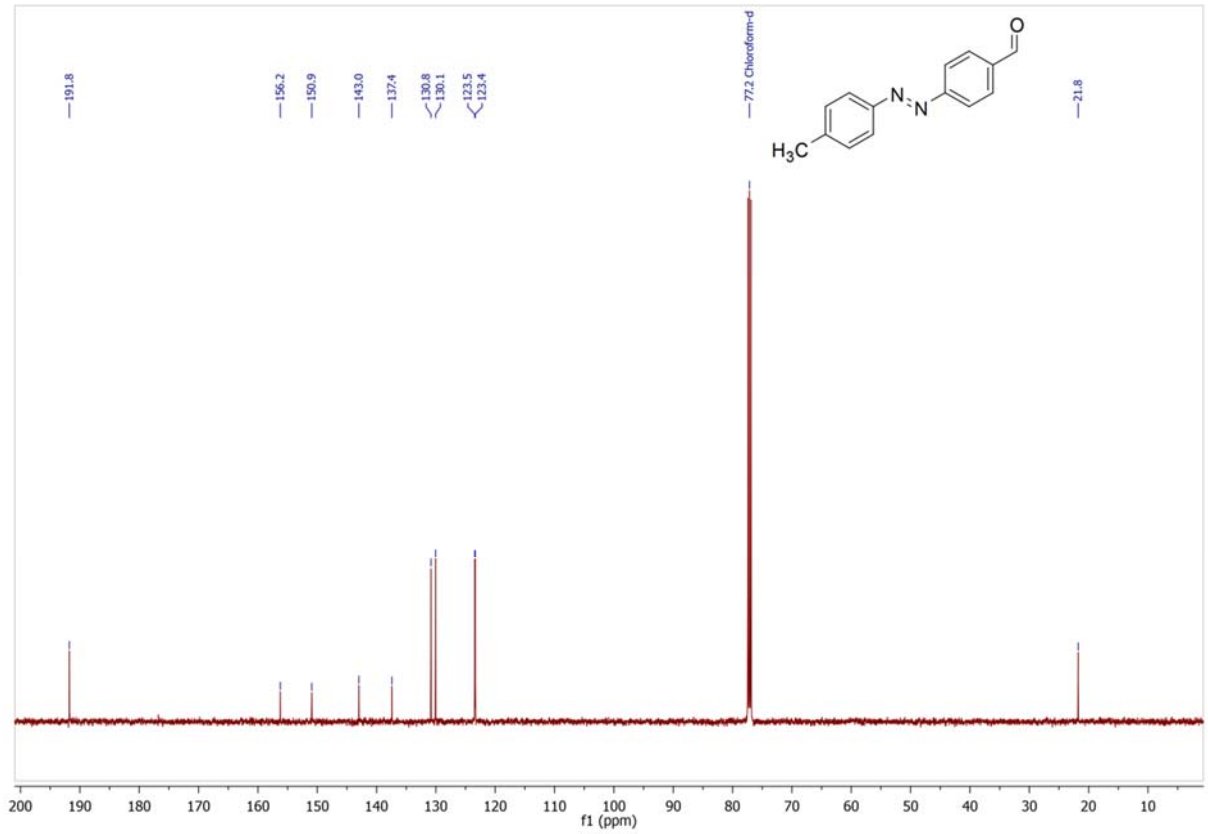

4-Methyl-3’formylazobenzene (20b) in chloroform-*d*

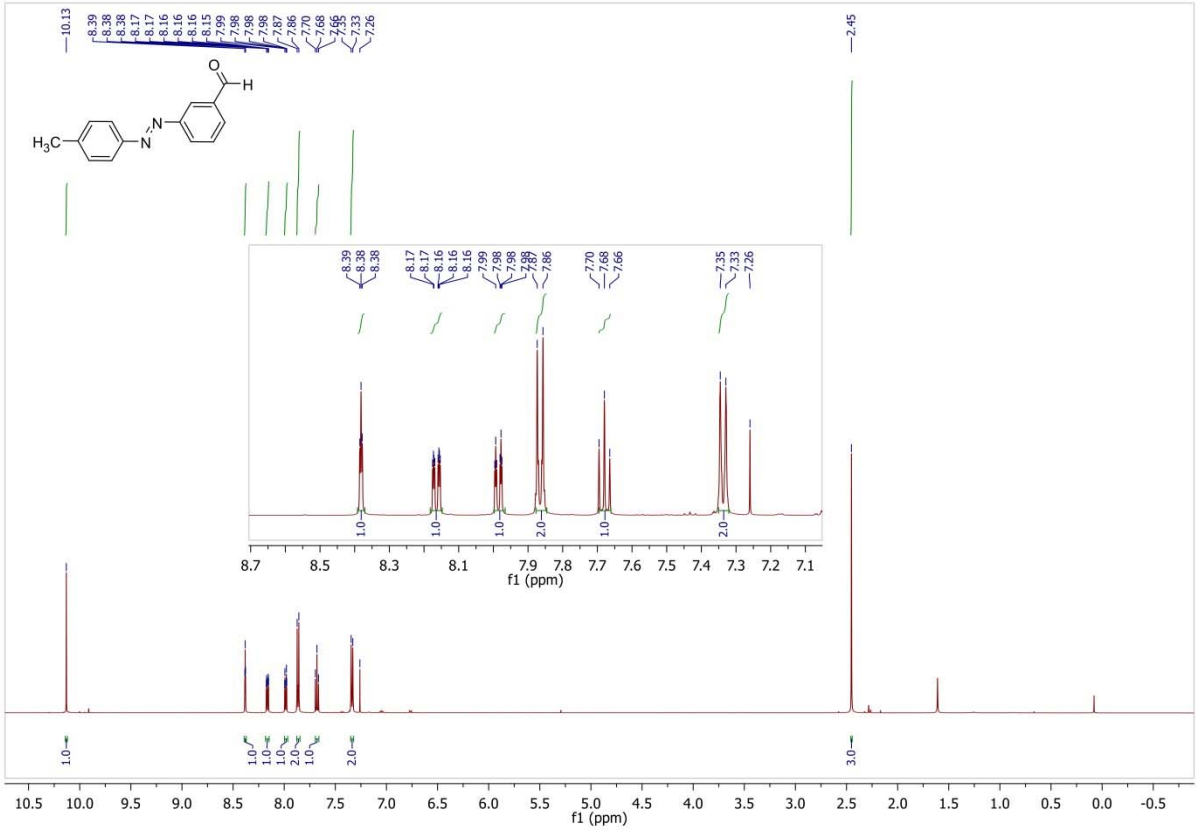

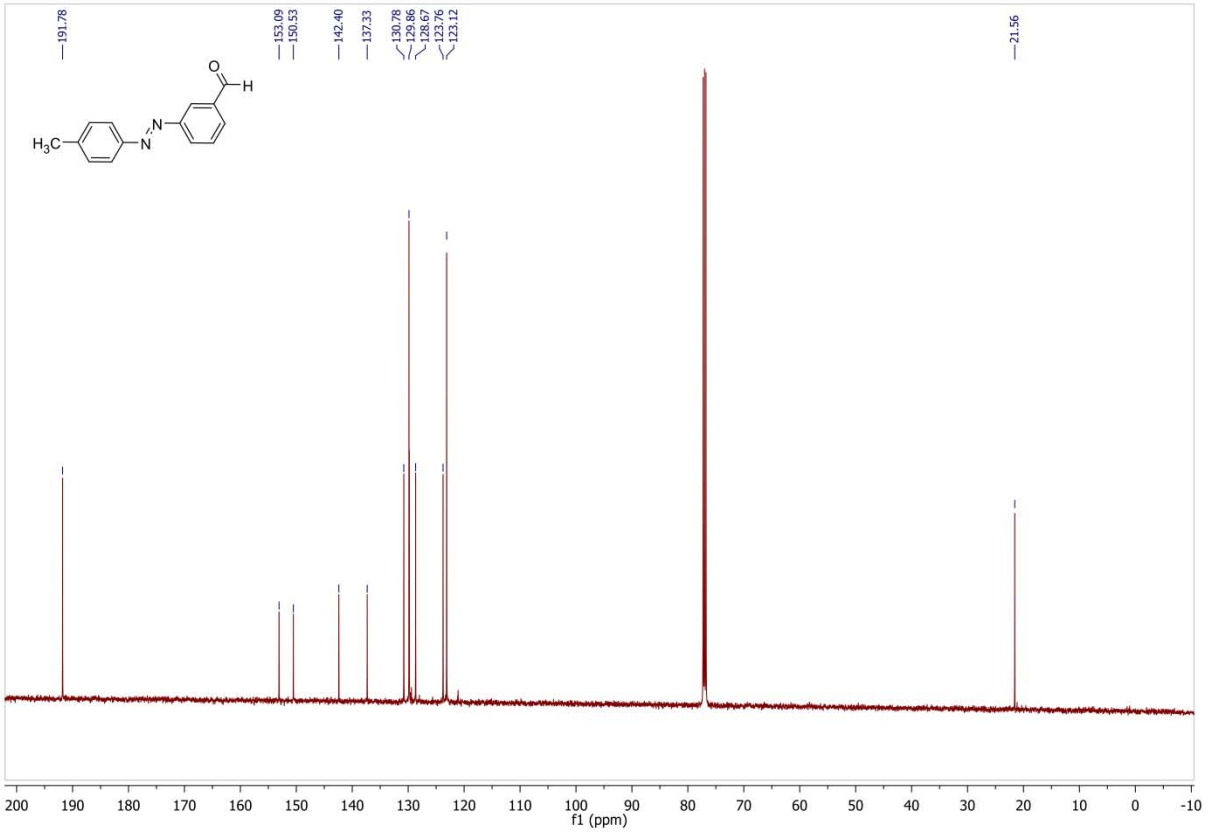

N*-Methoxy-*N*-methylbenzamide (21) in chloroform-*d

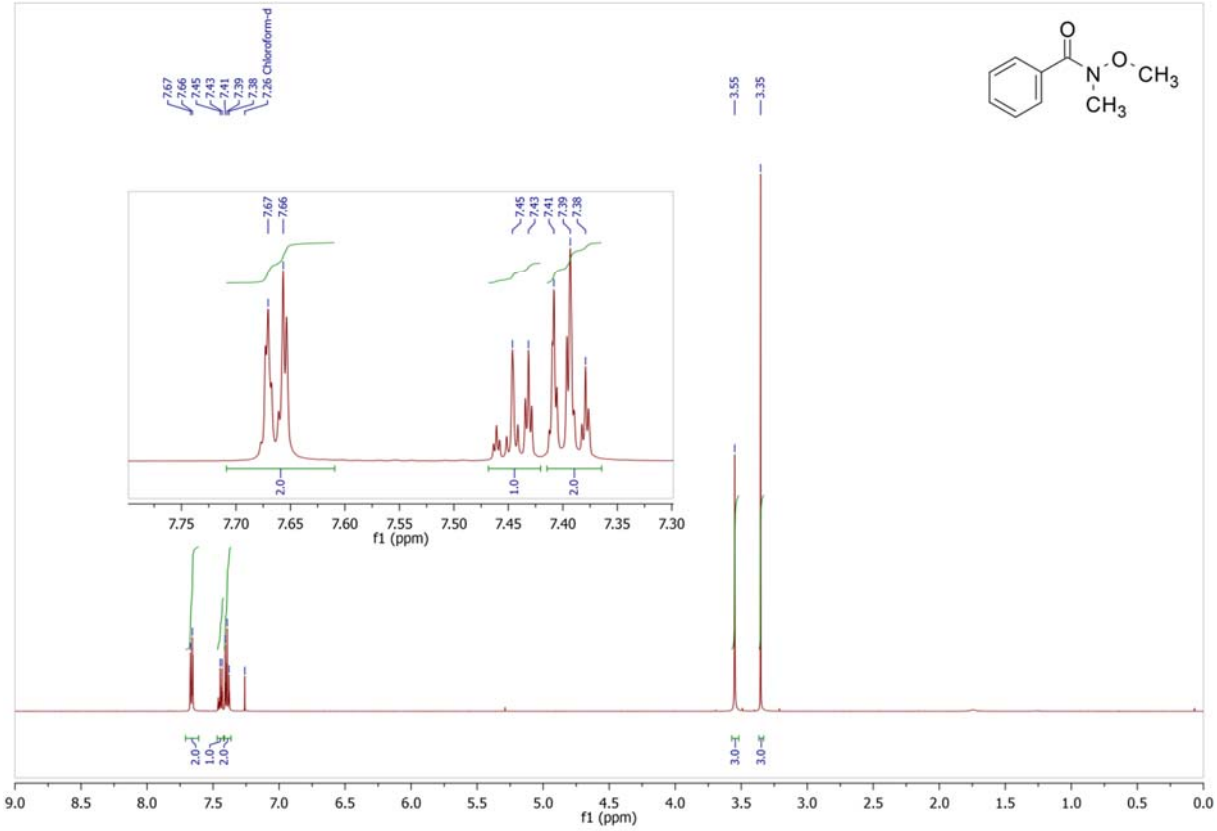

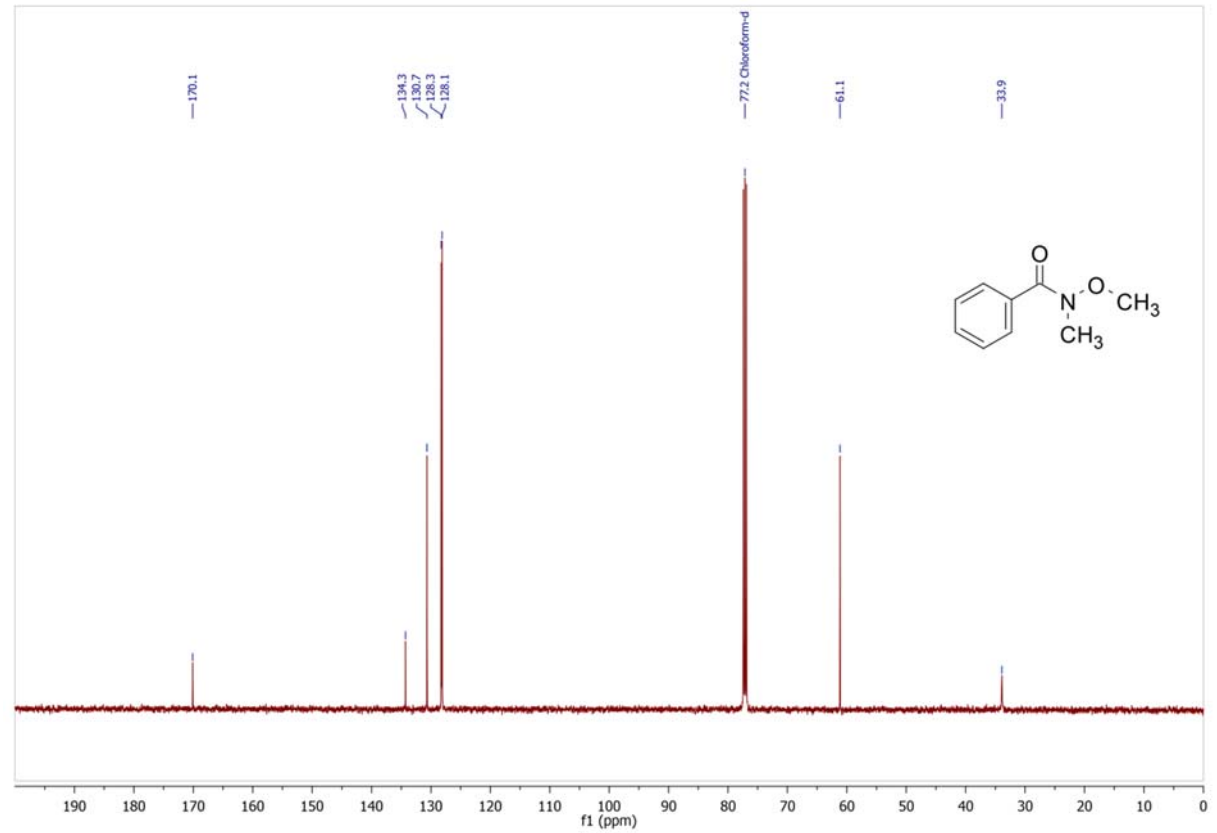

Phenyl-[4-(4-methylphenyl)azo-phenyl)]ketone (22a) in dichloromethane-d_2

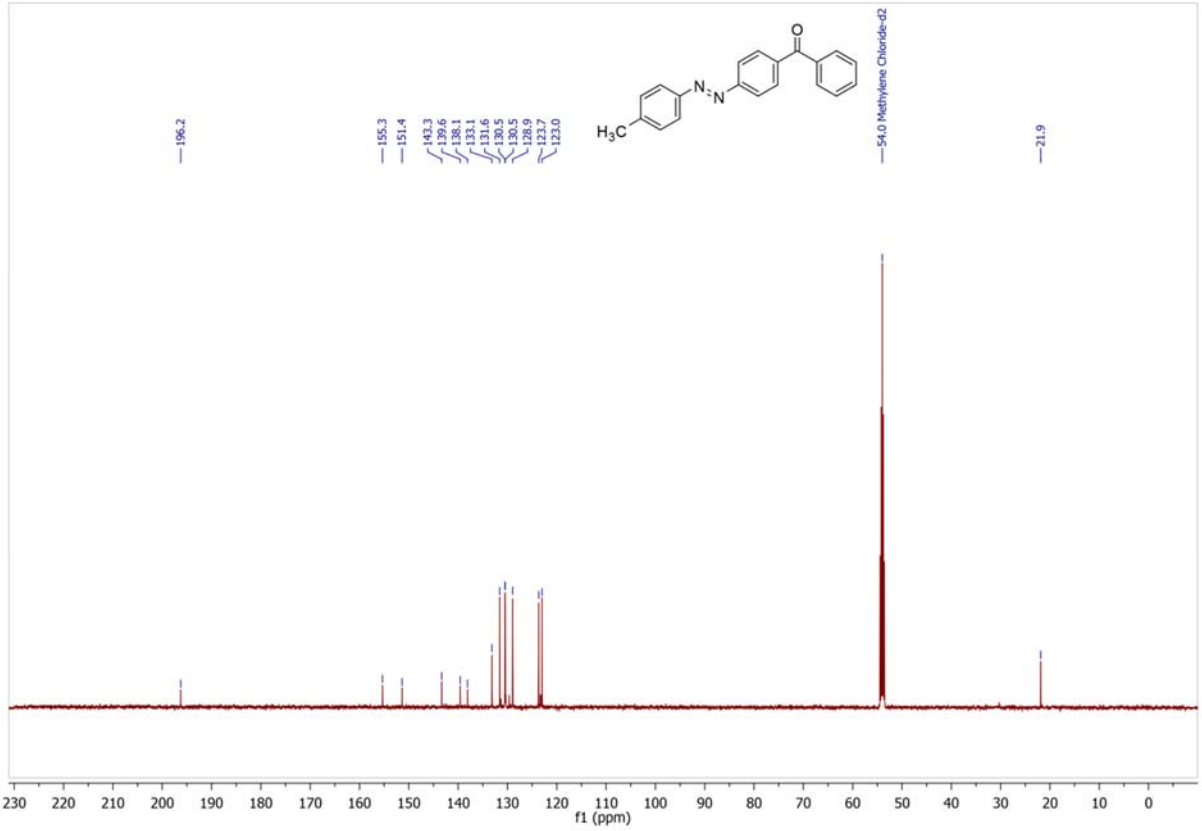

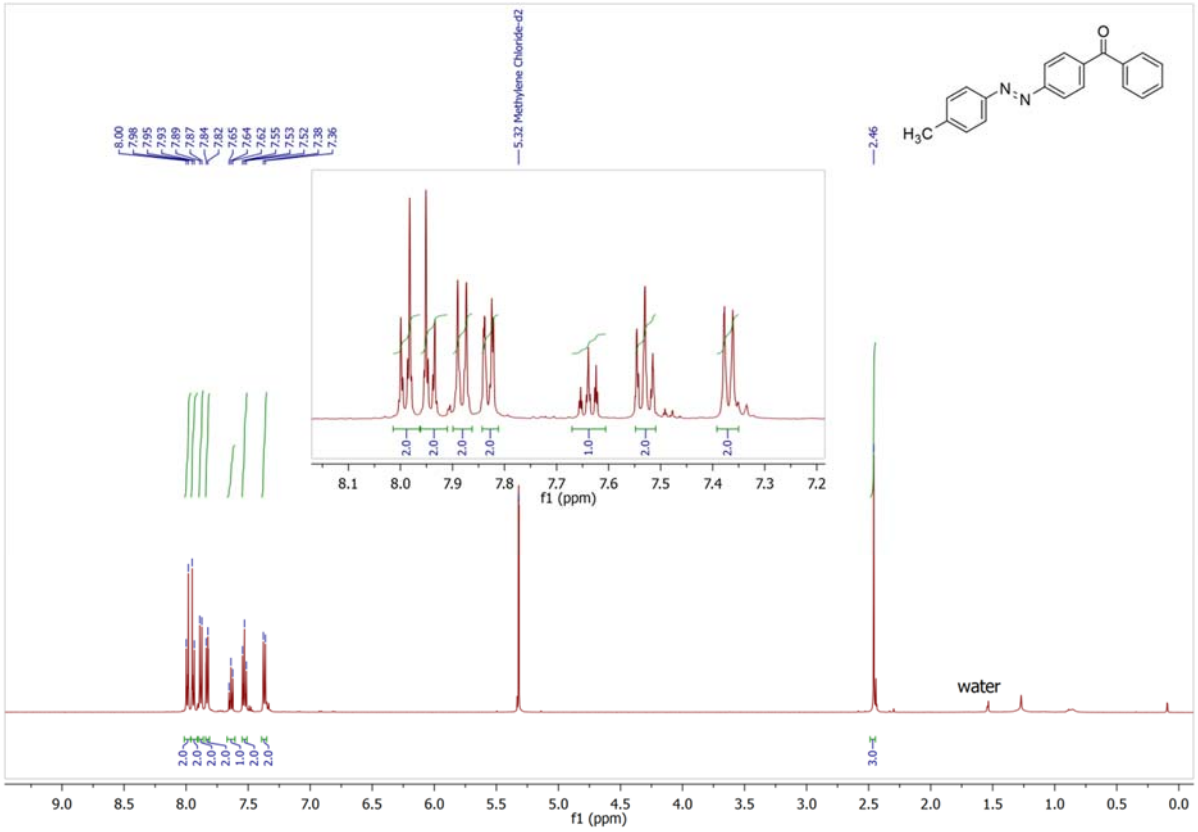

Phenyl-[3-(4-methylphenyl)azo-phenyl)]ketone (22b) in chloroform-*d*

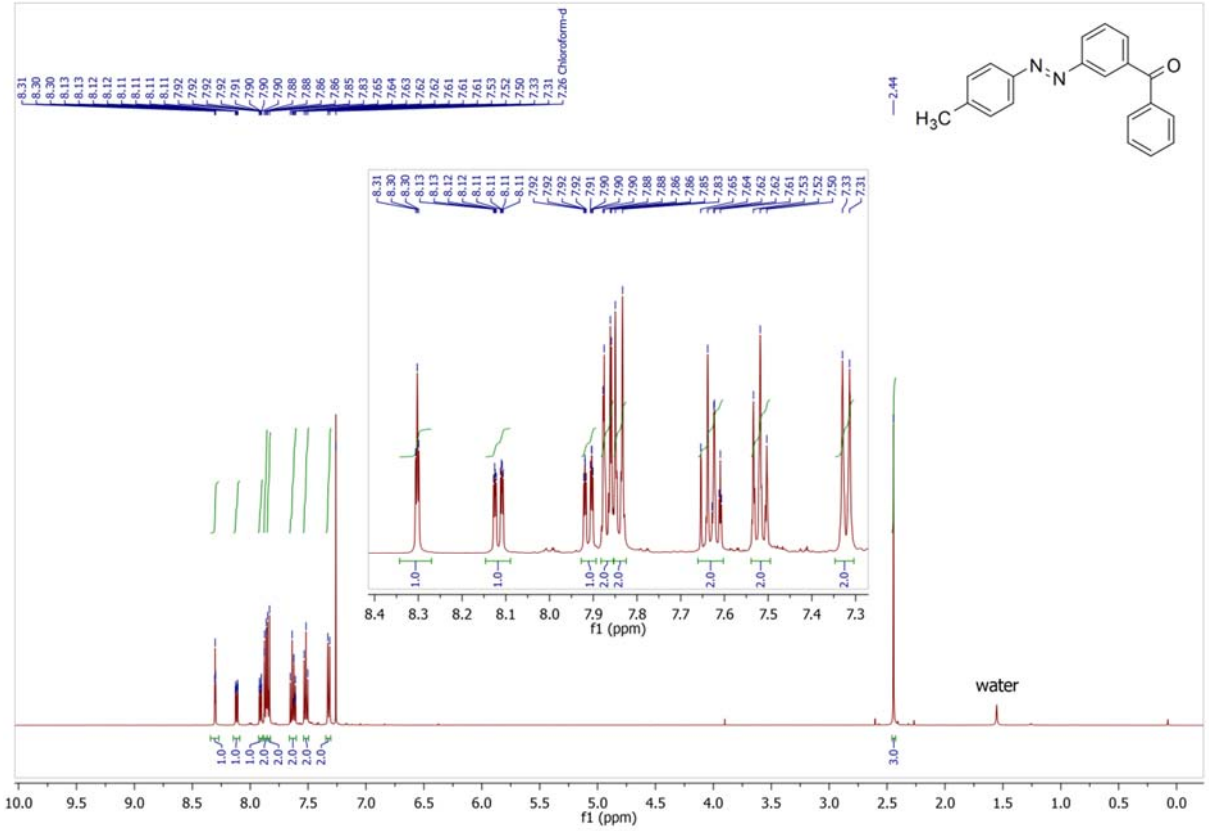

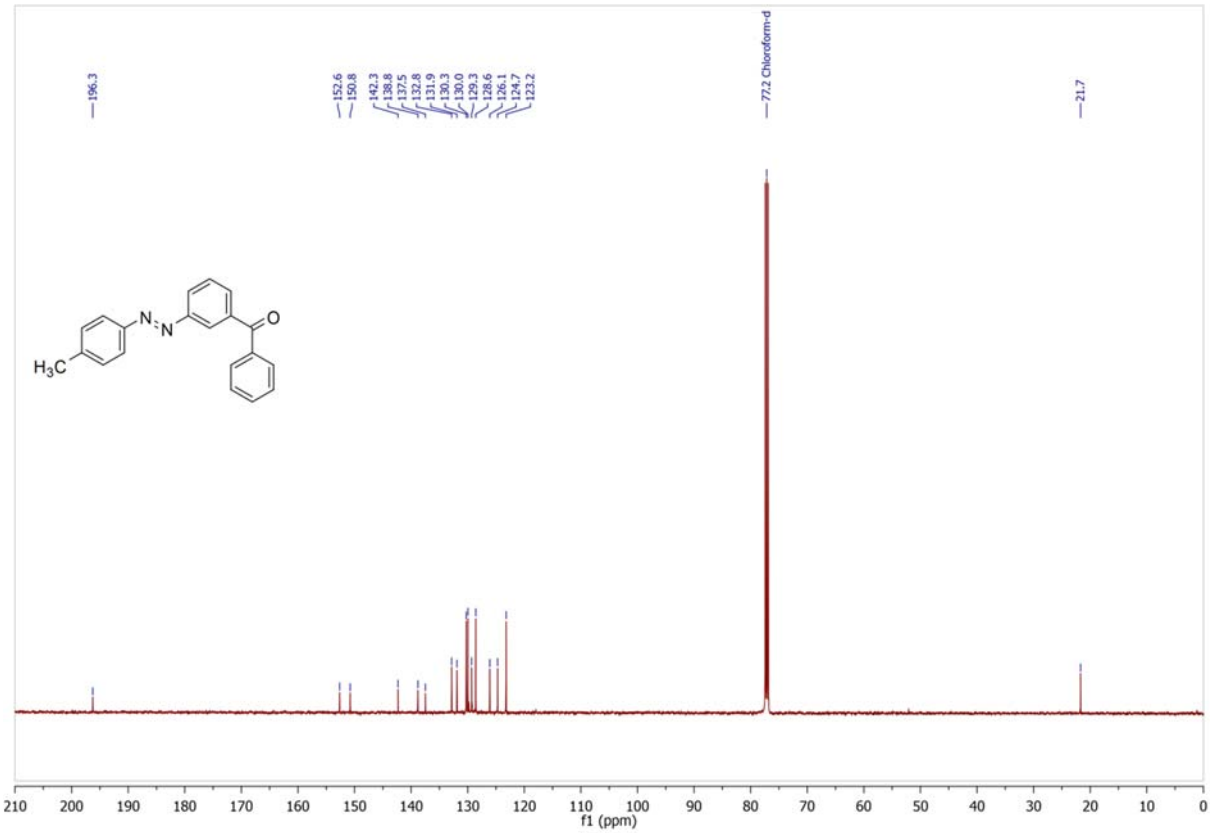

4-Methy-(4'-*N*-Phenylformamid)azobenzene (23a) in DMSO-d_6

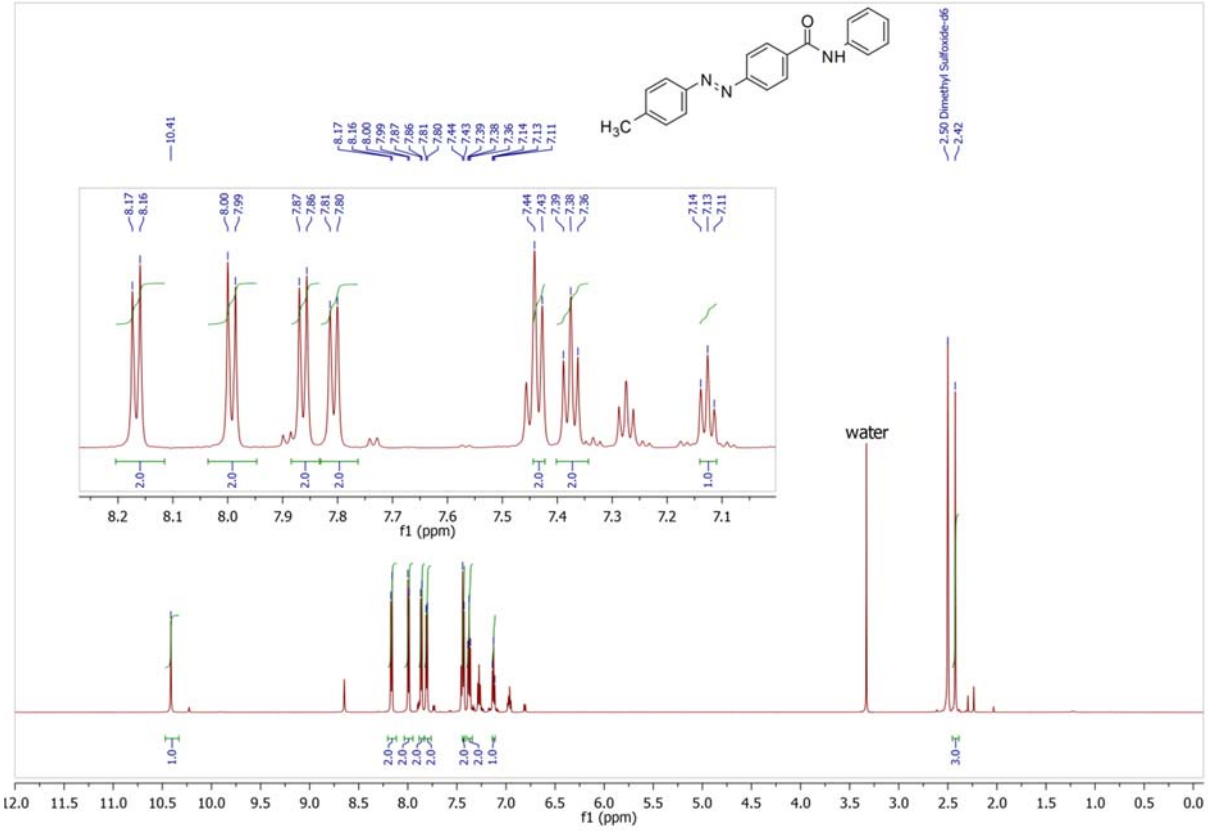

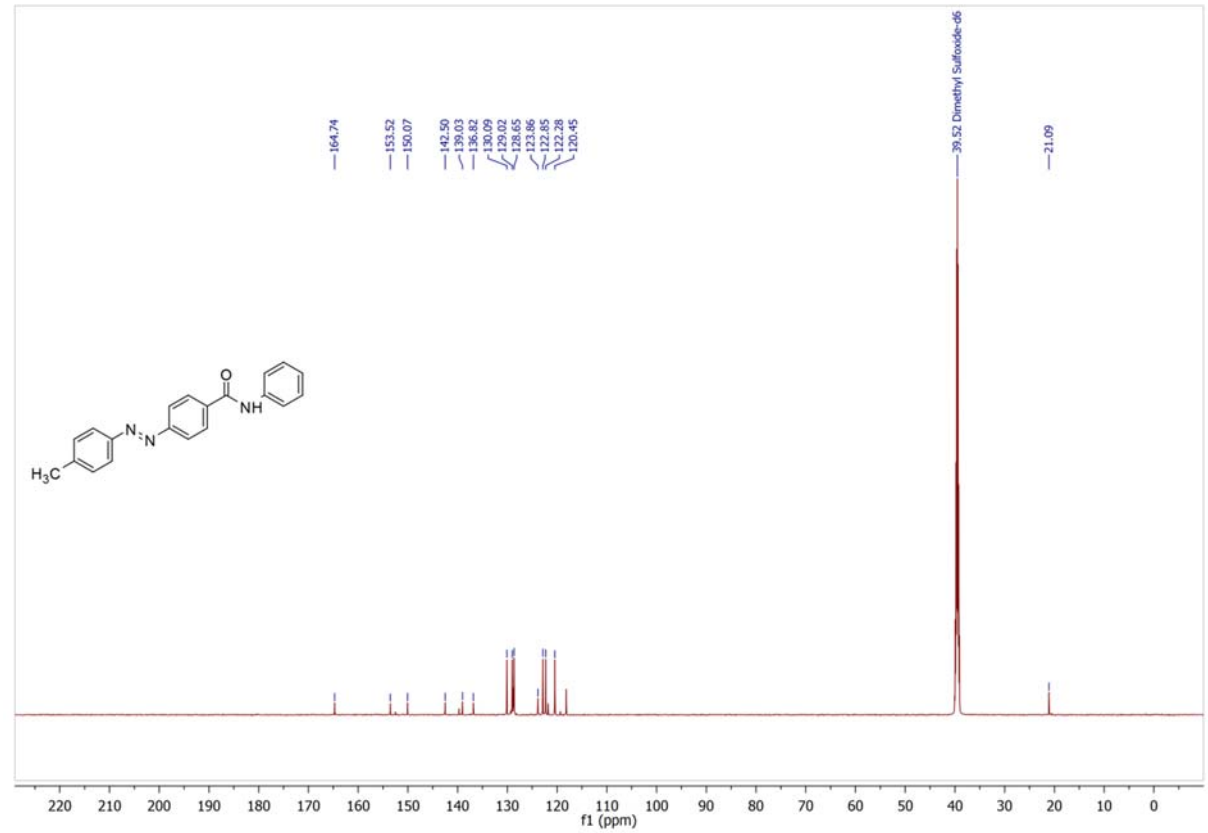

4-Methy-(3‘-*N*-Phenylformamid)azobenzene (23b) in chloroform-*d*

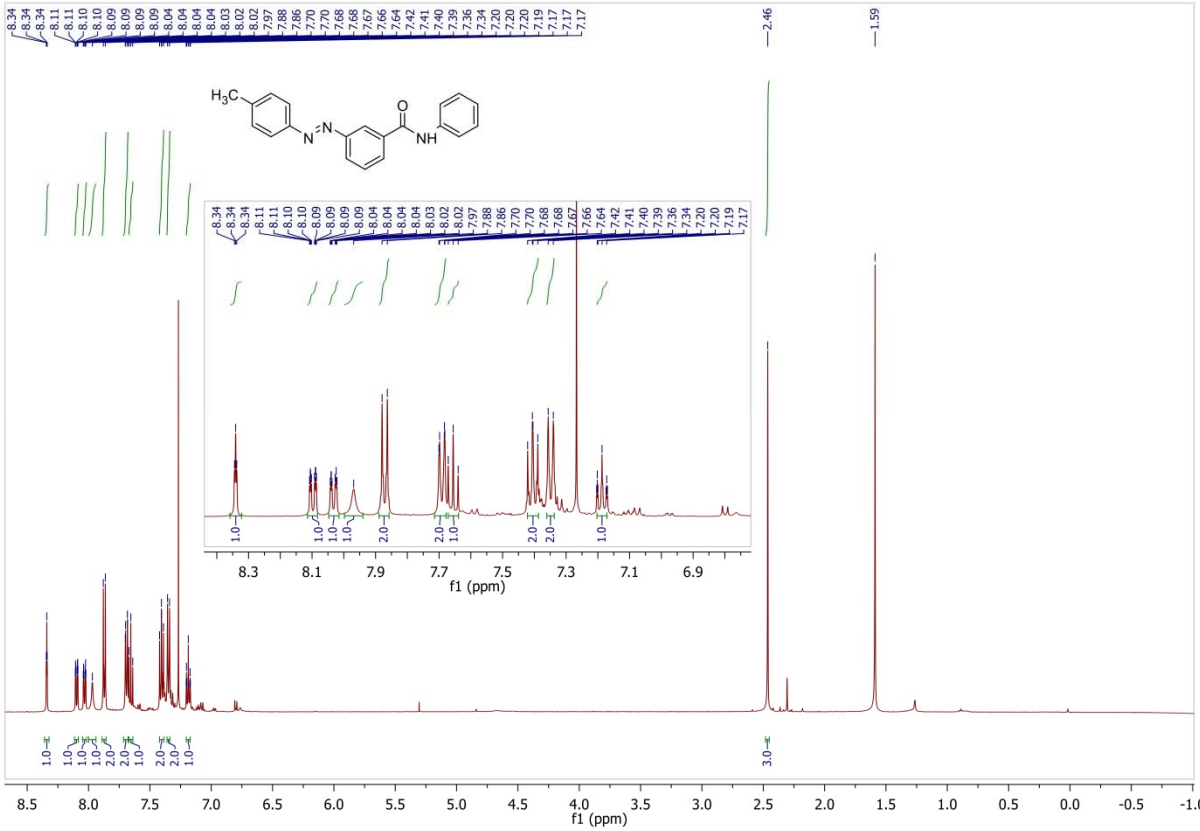

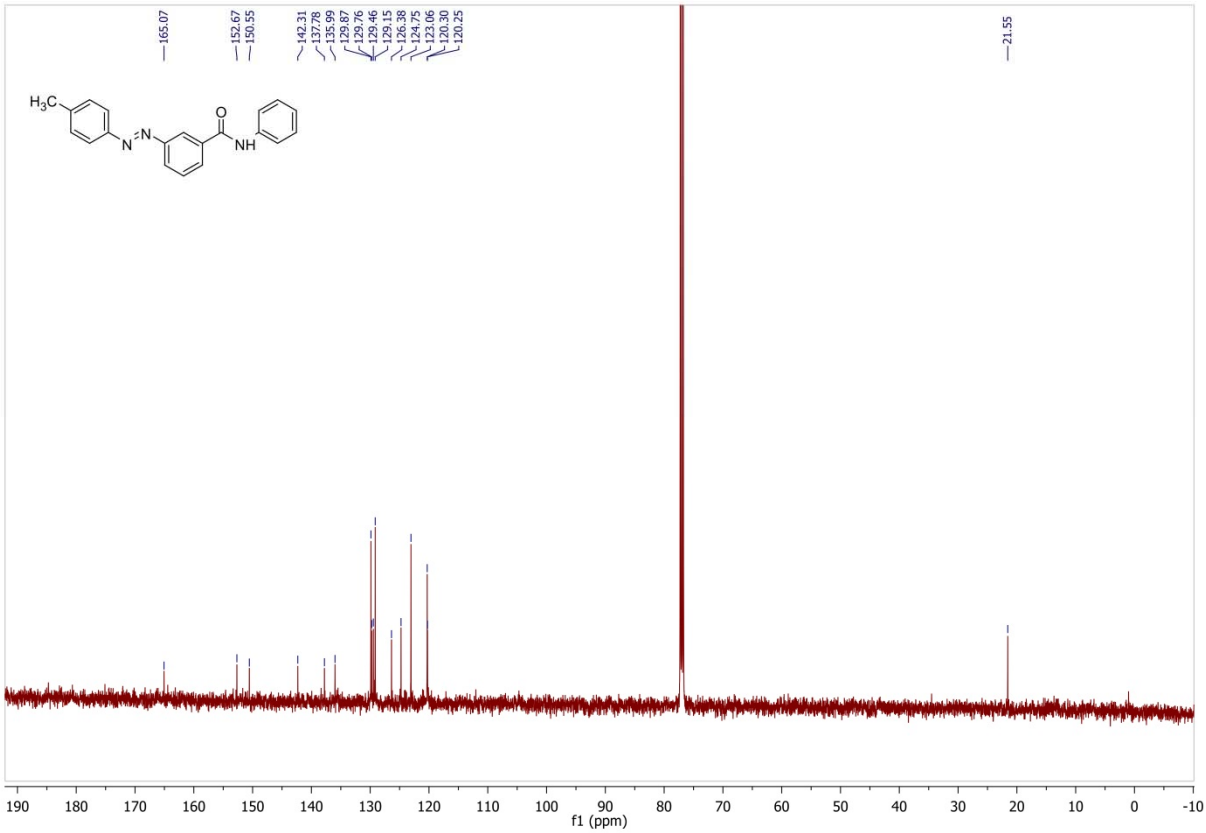

4-Methy-(4'-*N*-Phenylthioformamid)azobenzene (24a) in DMSO-d_6

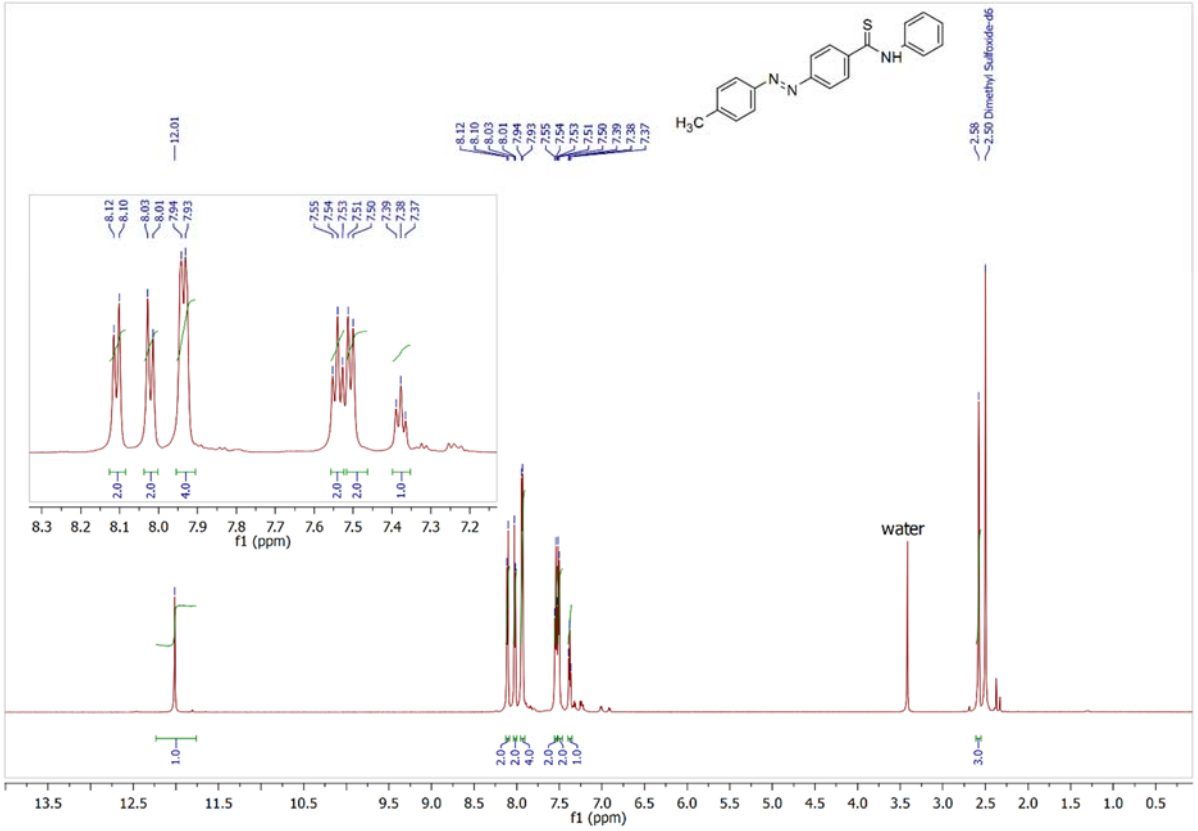

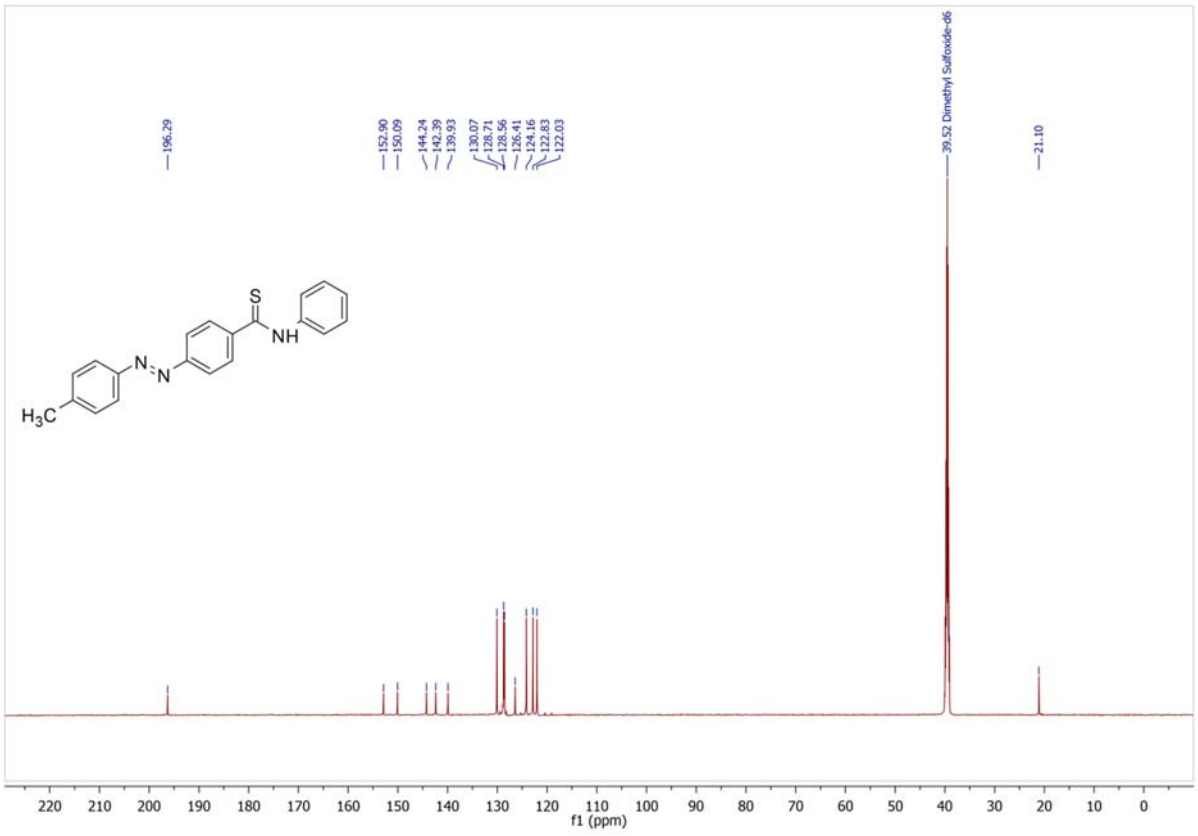

4-Methy-(3'-*N*-Phenylthioformamid)azobenzene (24b) in DMSO-d_6

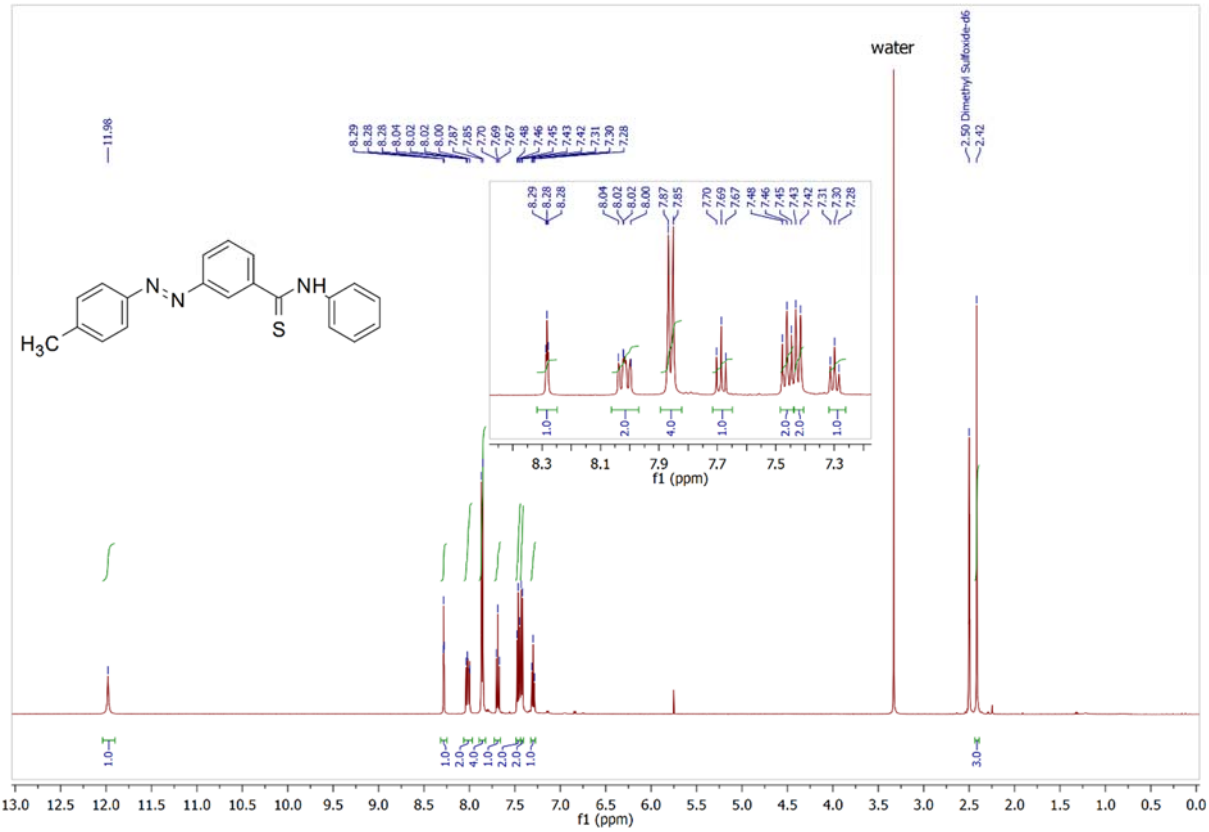

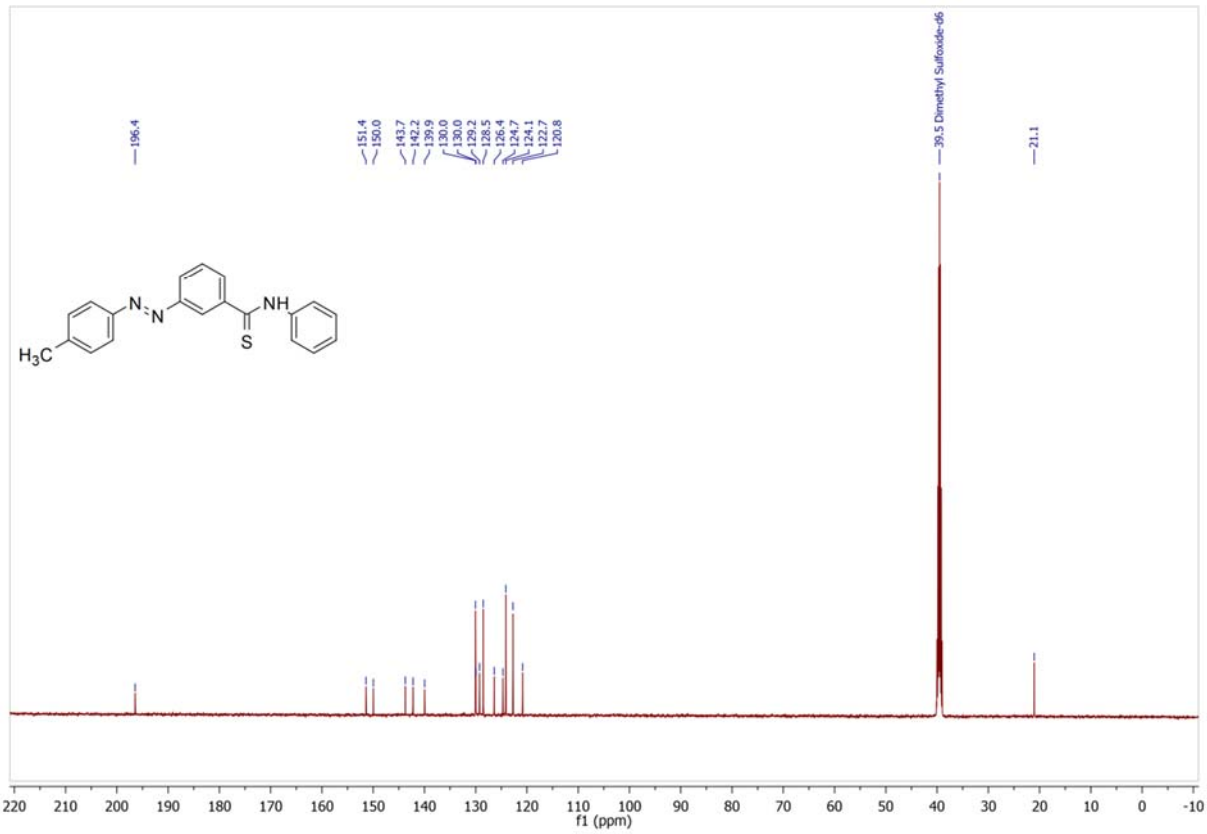

1.4 Compounds with Multiple Azobenzene Units

4-Phenyl-di-[4-(4-methylphenyl)azo-phenyl)]methanol (25a) in dichloromethane-d_2

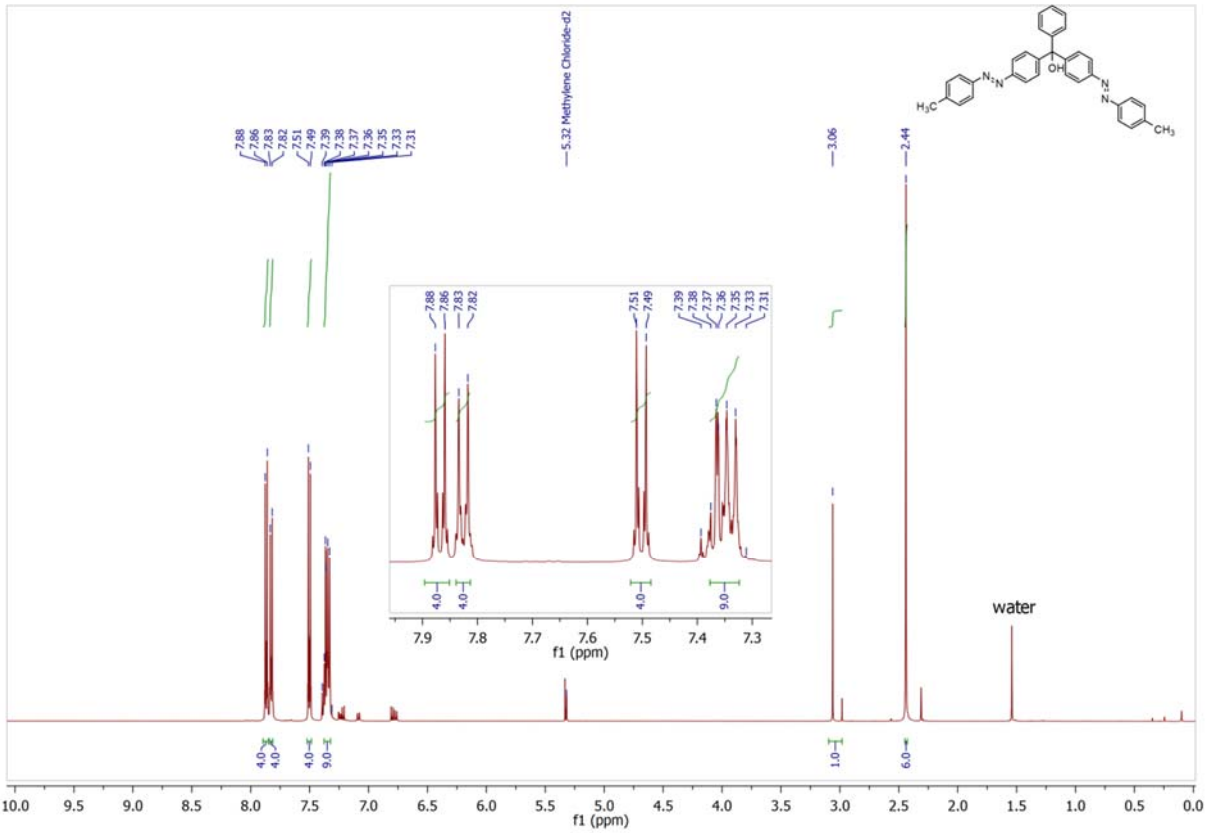

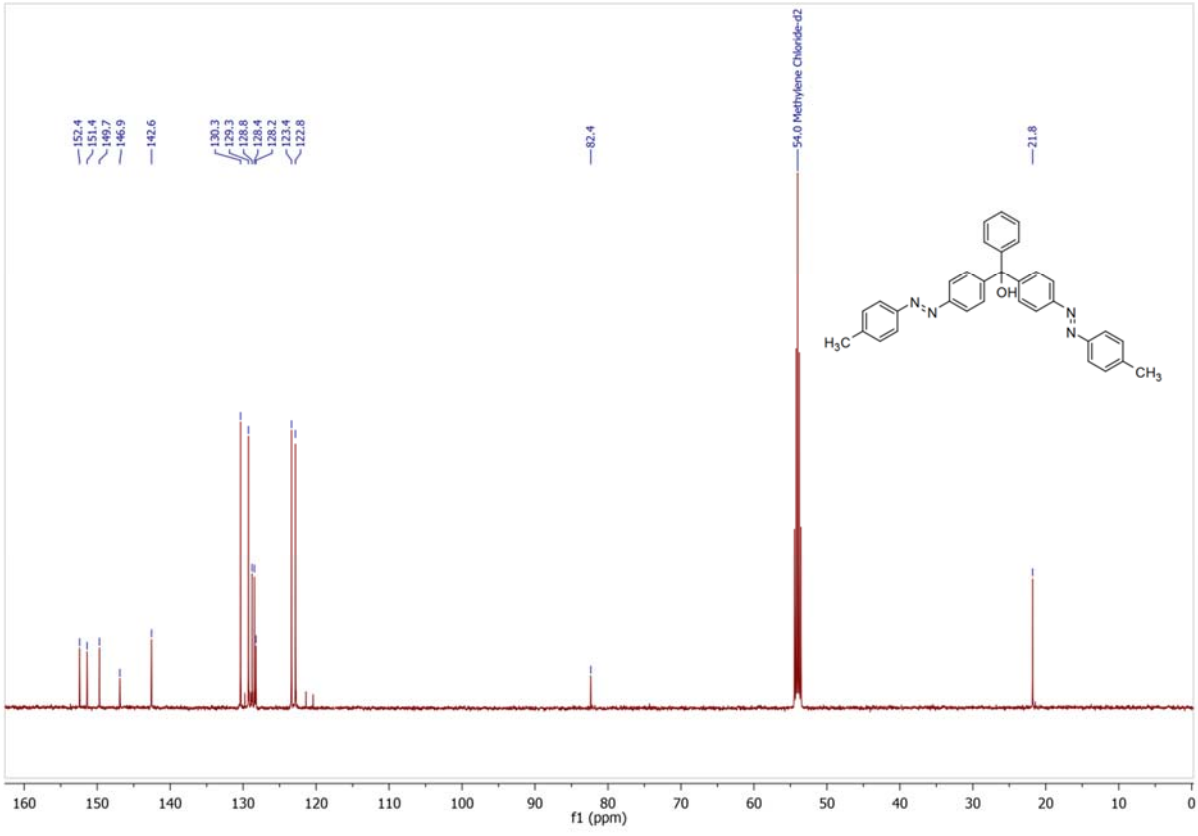

Phenyl-di-[3-(4-methylphenyl)azo-phenyl)]methanol (25b) in chloroform-*d*

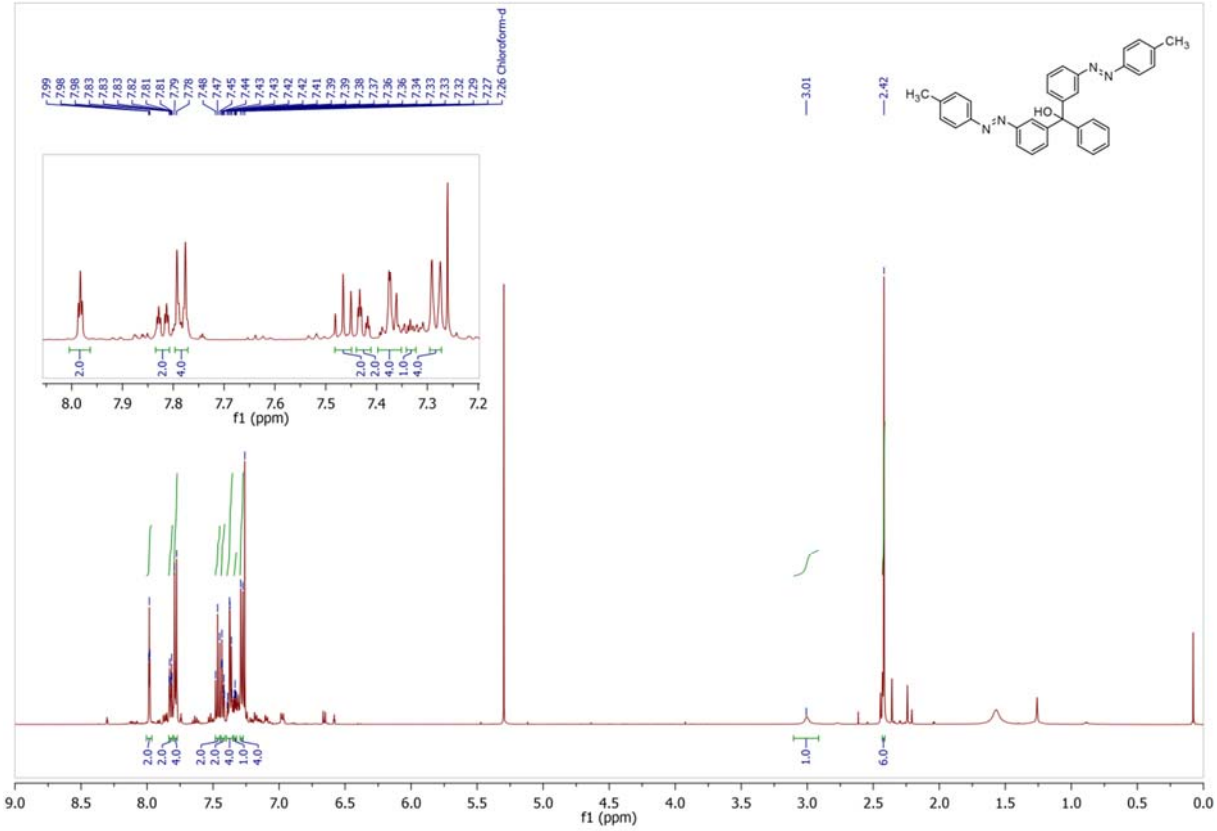

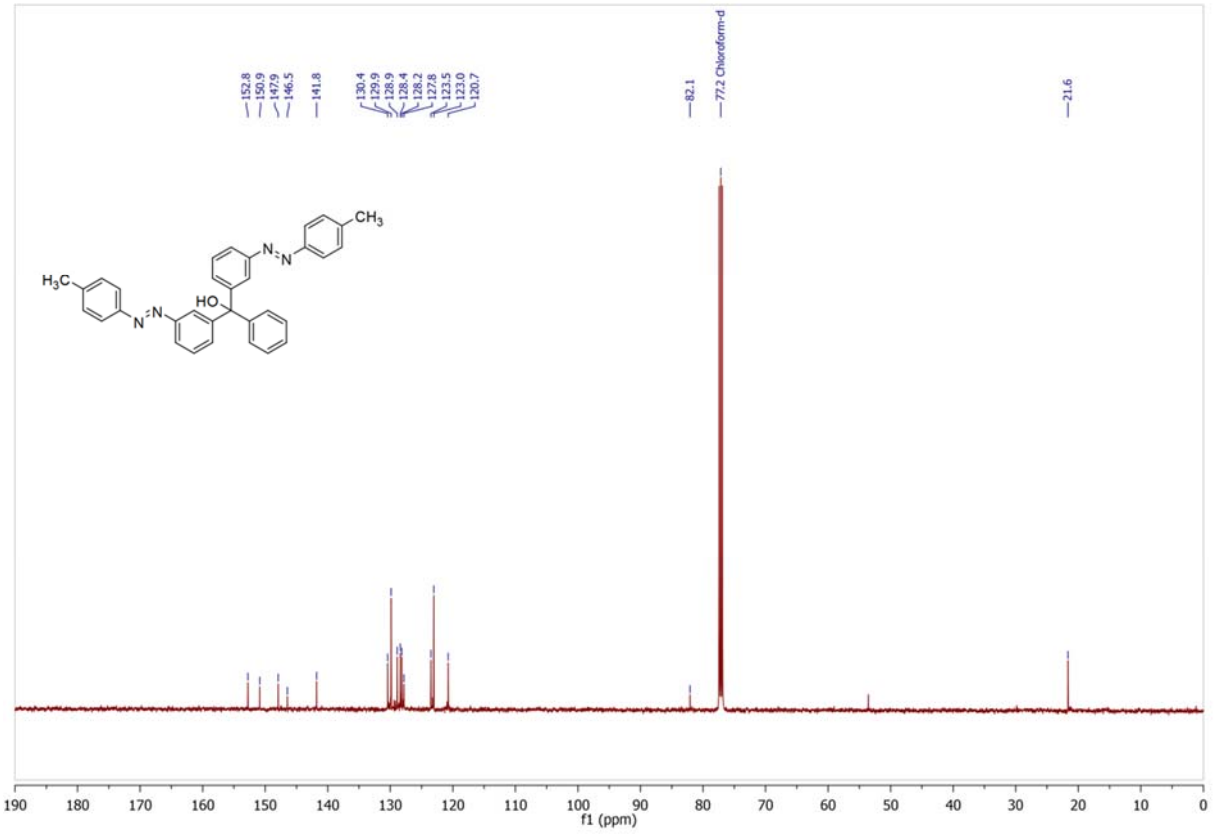

4-Tolyl-di-[4-(4-methylphenyl)azo-phenyl)]methanol (26a) in dichloromethane-d_2

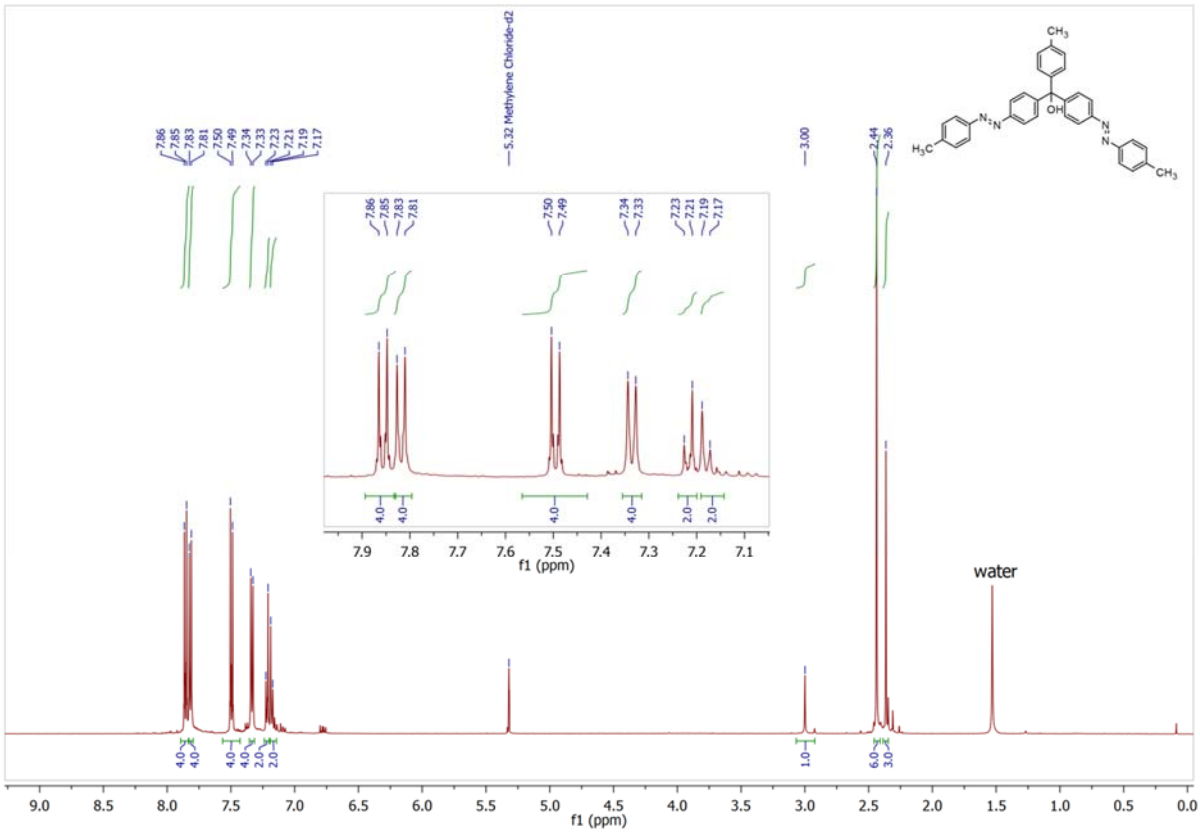

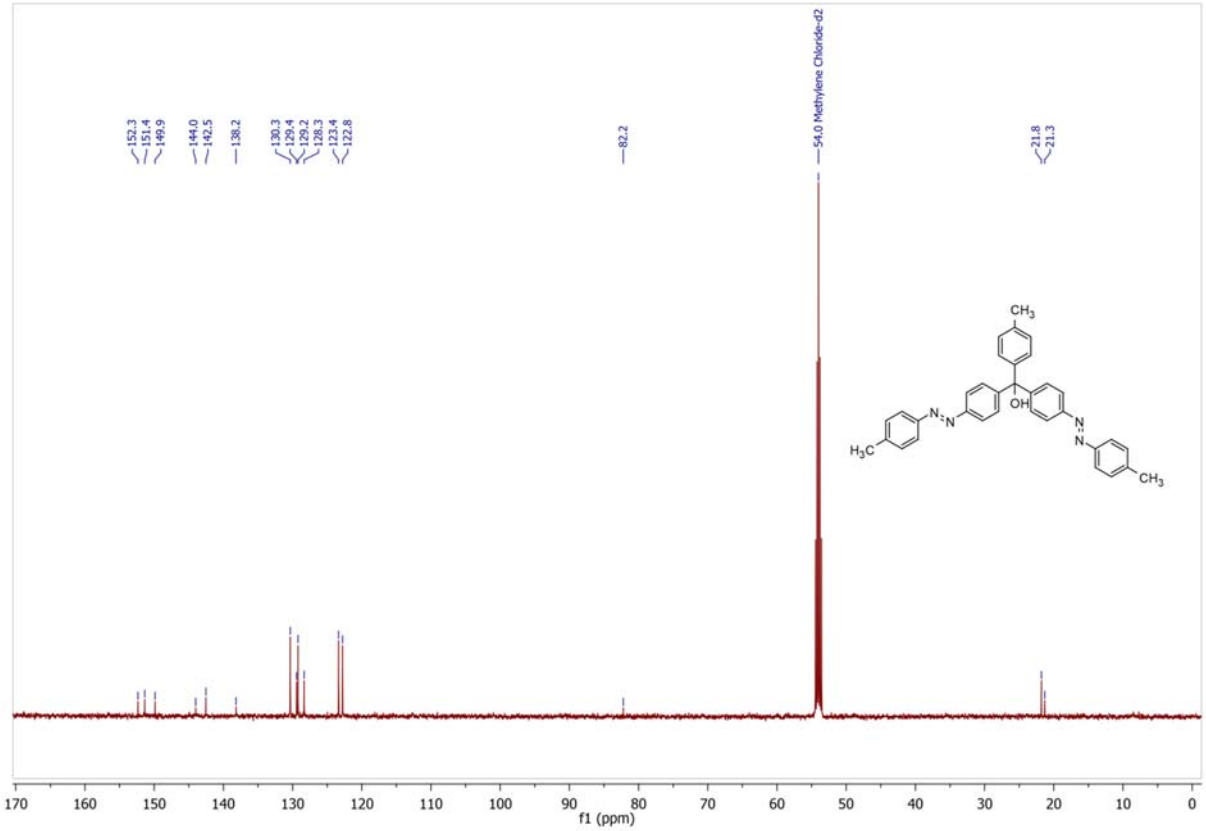

4-Tolyl-di-[3-(4-methylphenyl)azo-phenyl)]methanol (26b) in DMSO-d_6

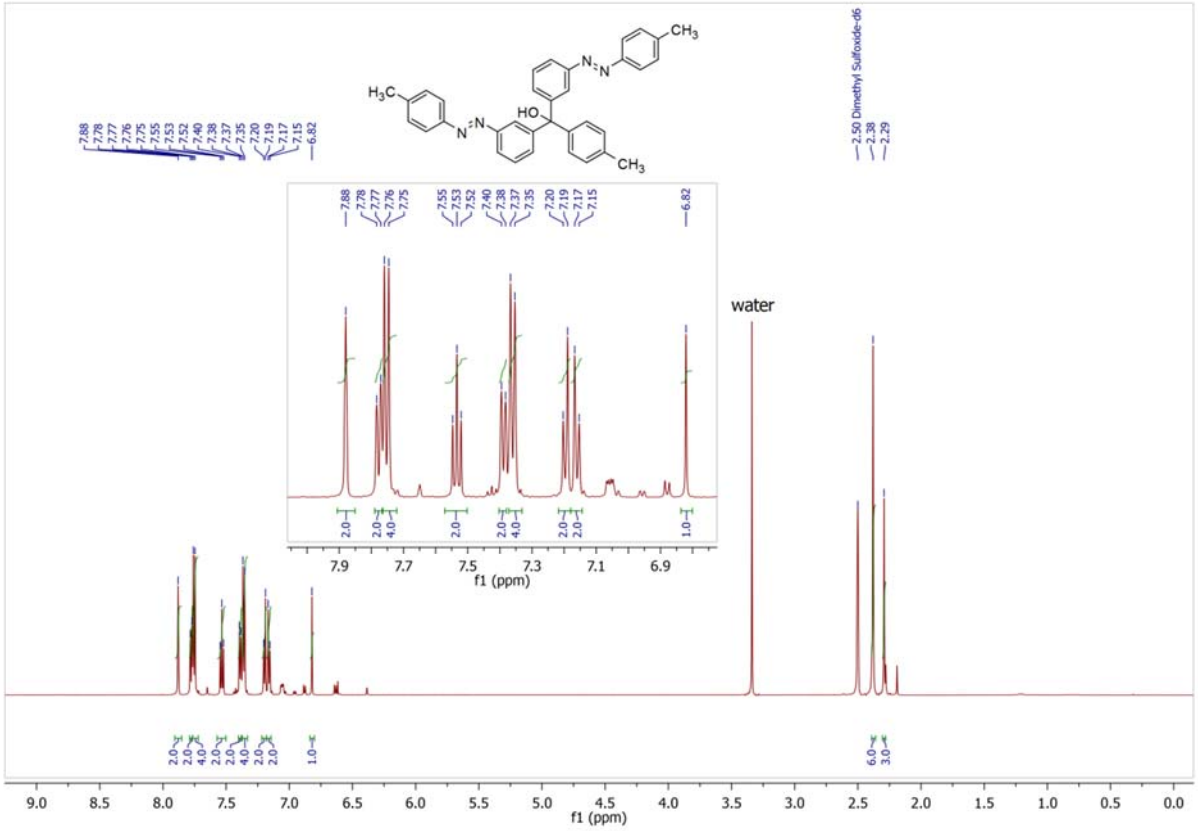

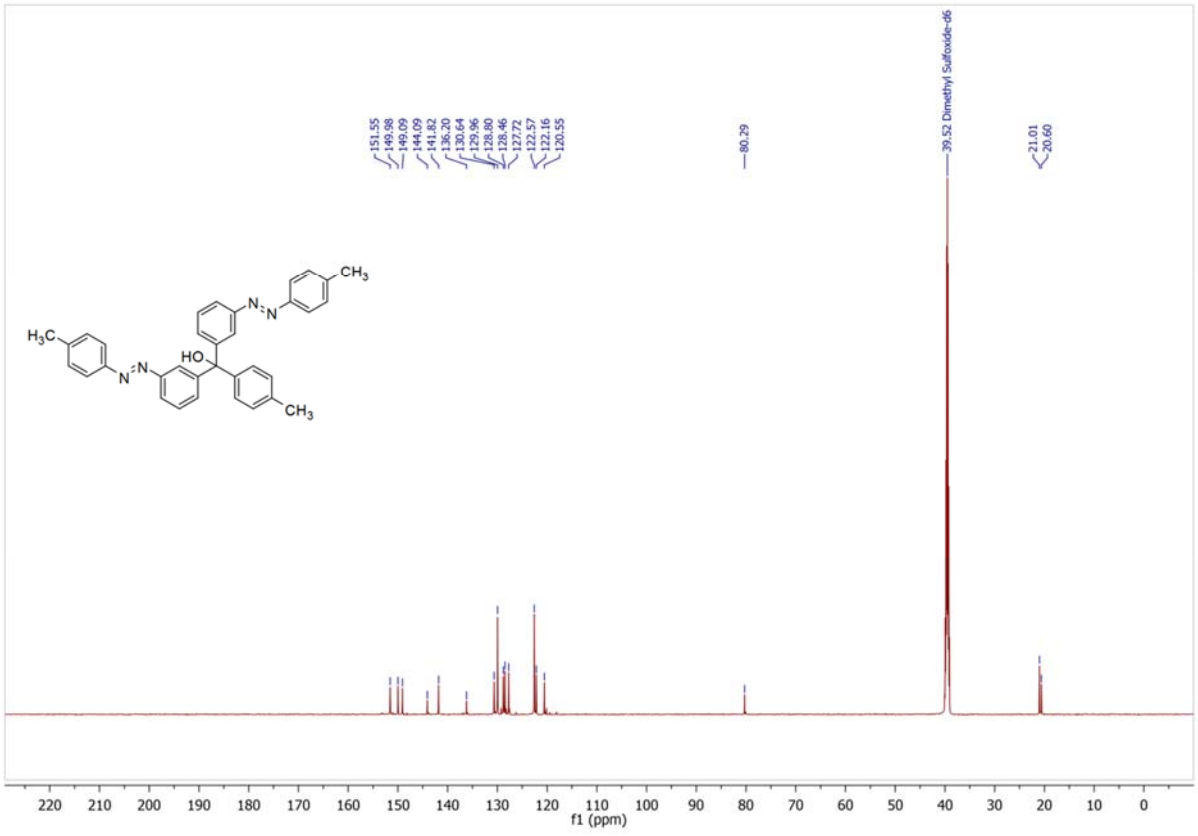

Tri-[4-(4-methylphenyl)azo-phenyl)]methanol (27a) in DMSO-d_6

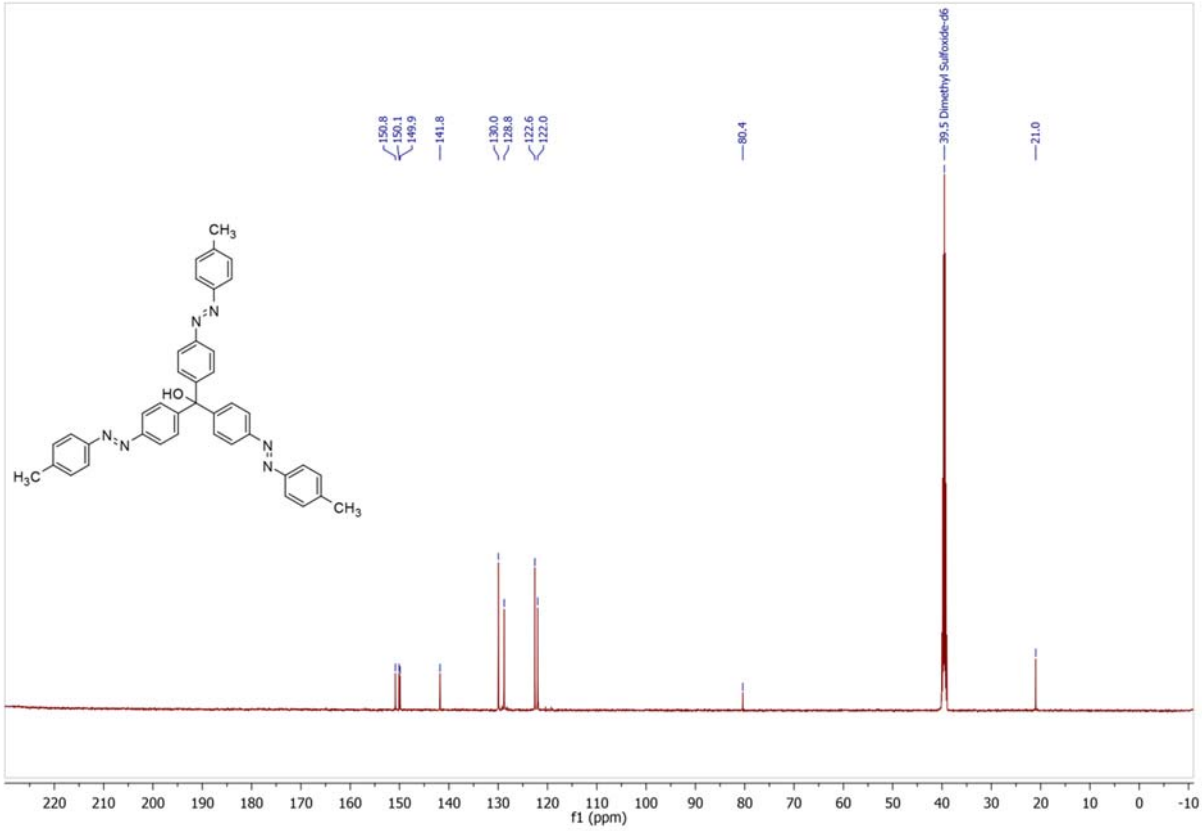

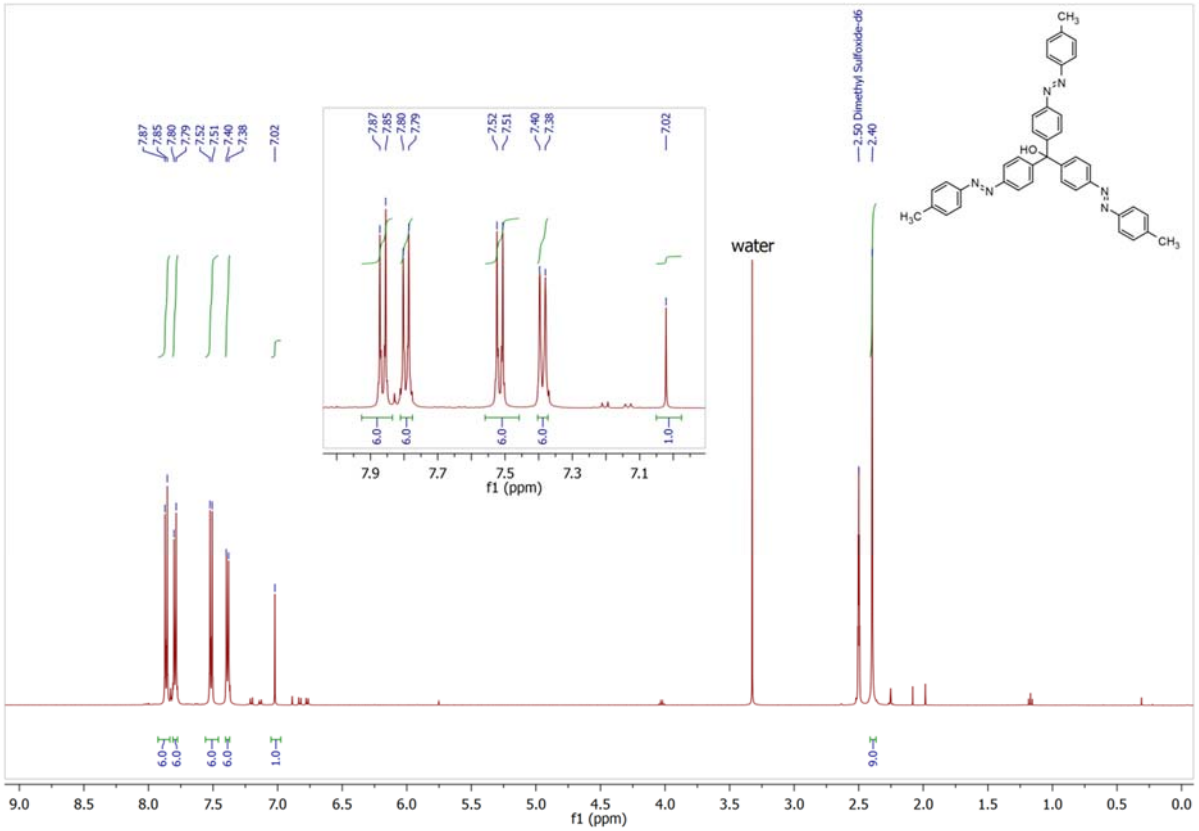

Side product: Di-[4-(4-methylphenyl)azo-phenyl)]ketone (27a) in chloroform-*d*

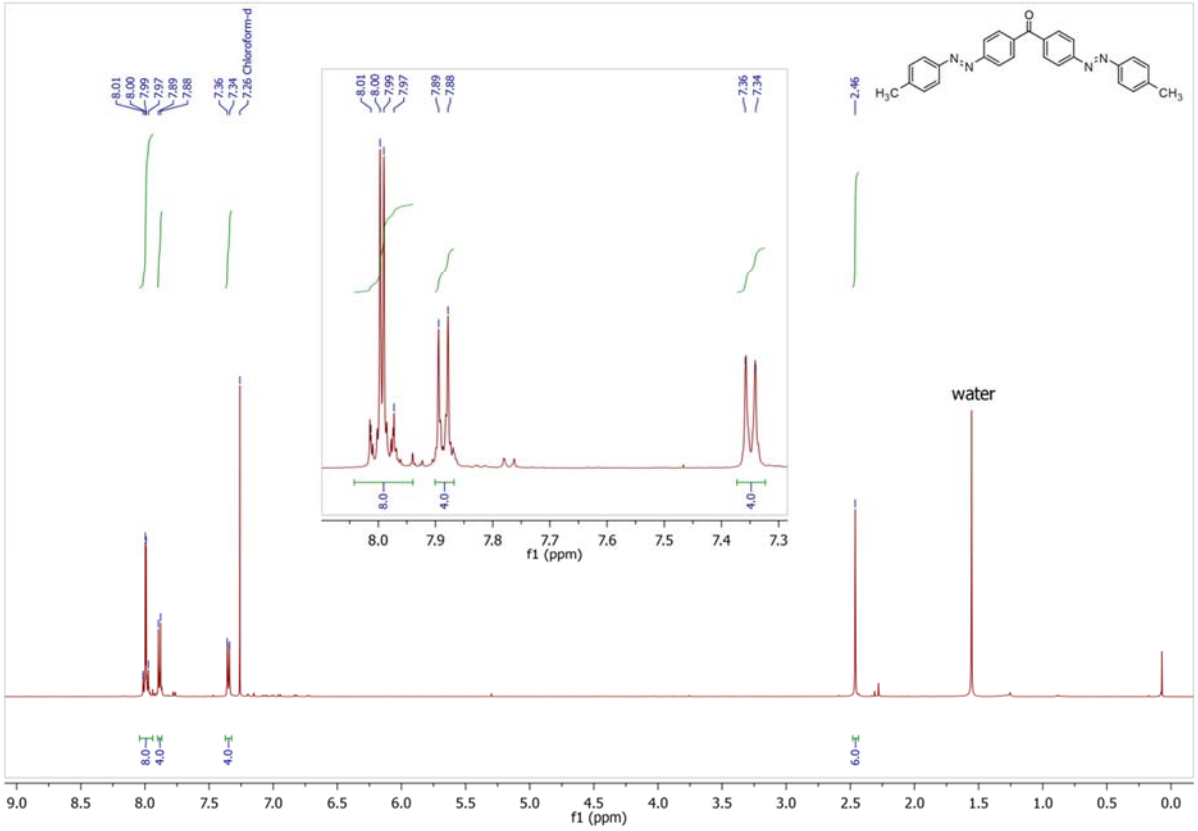

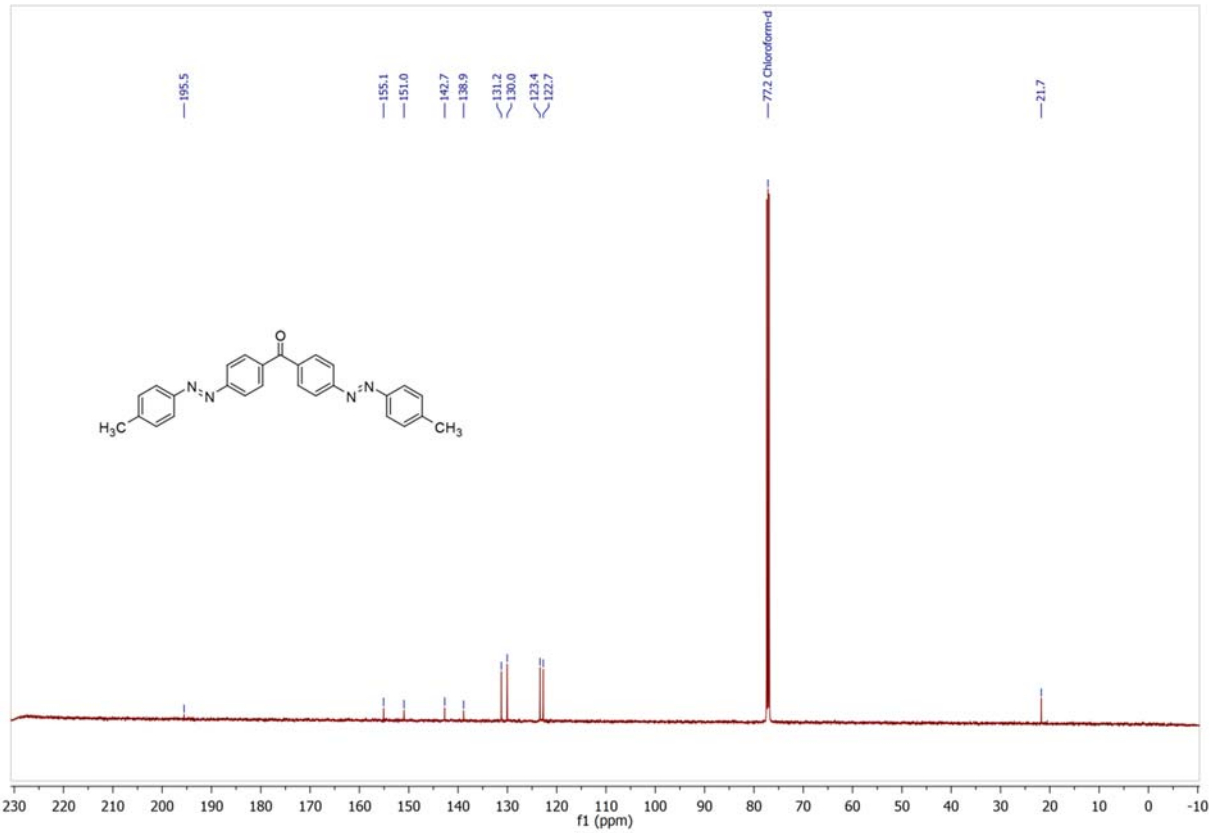

Tri-[3-(4-methylphenyl)azo-phenyl)]methanol (27b) in DMSO-d_6

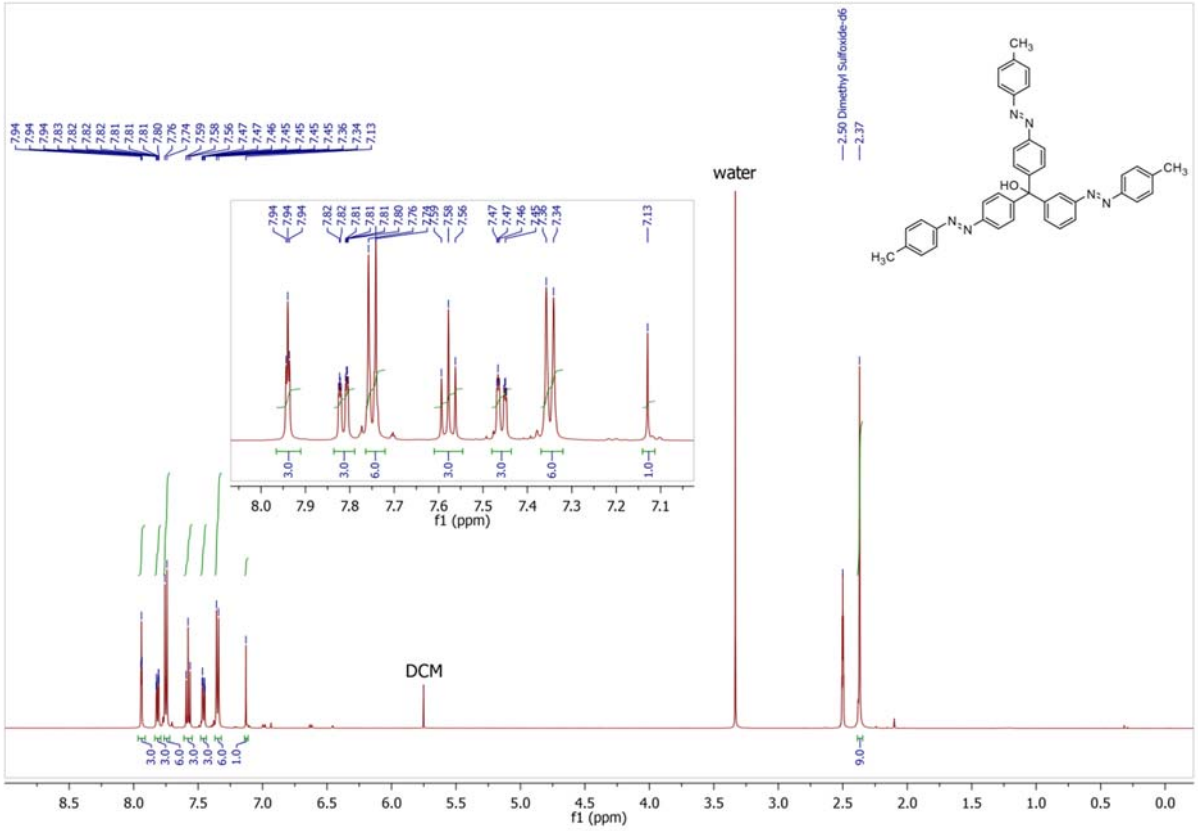

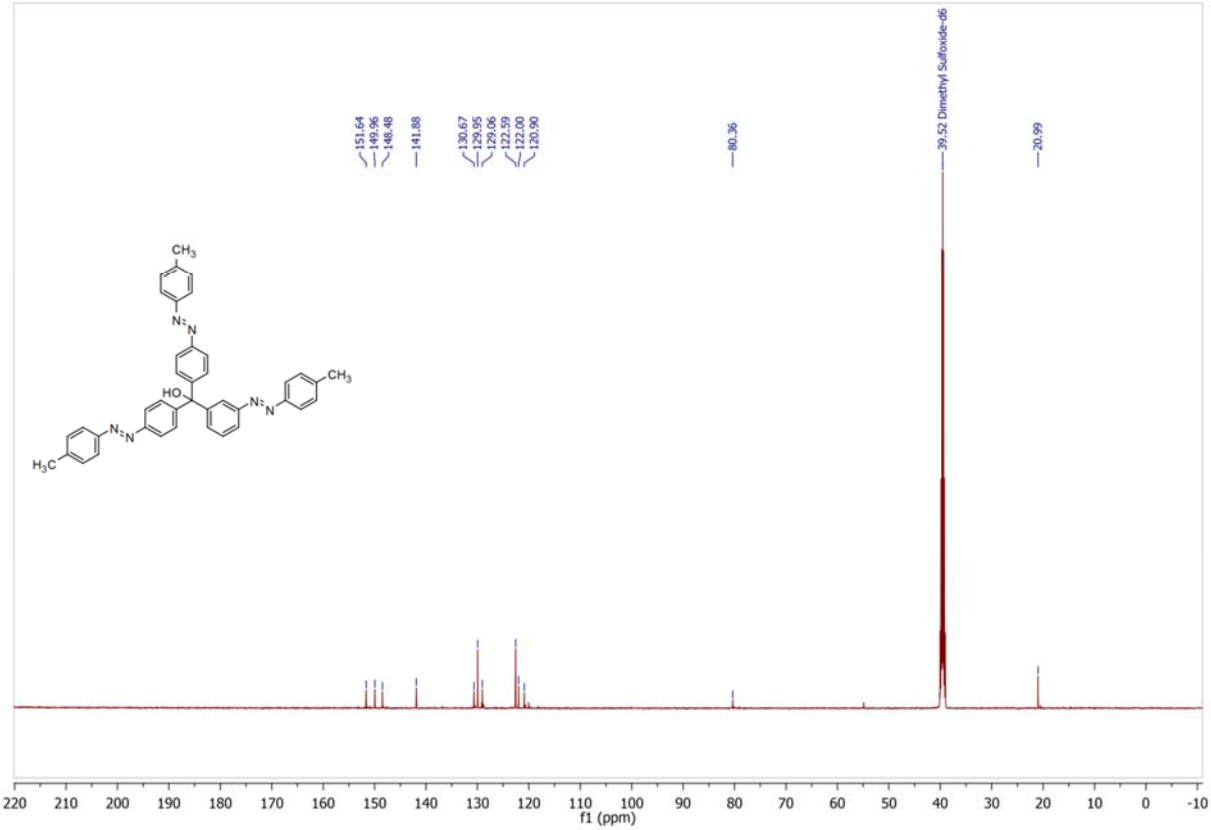

Side product: **Bis-[3-(4-methylphenyl)azo-phenyl)]ketone (28b) in chloroform-*d***

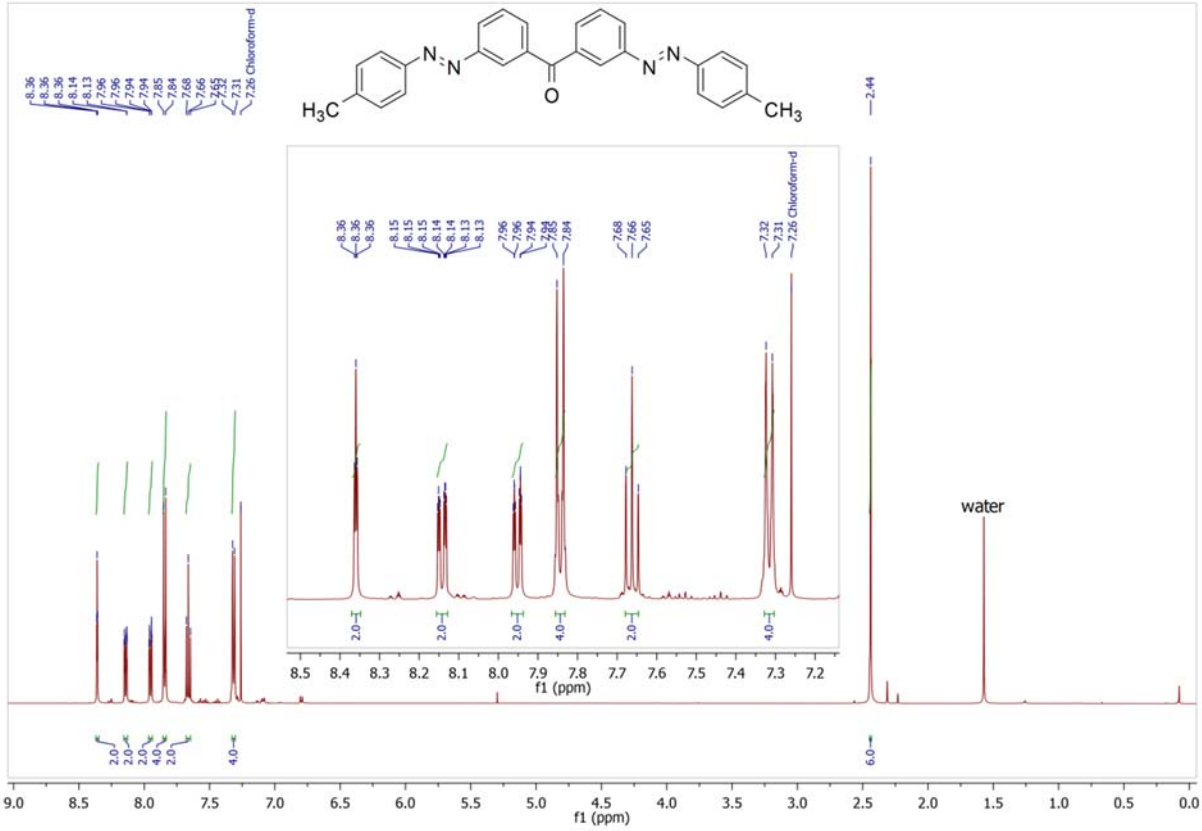

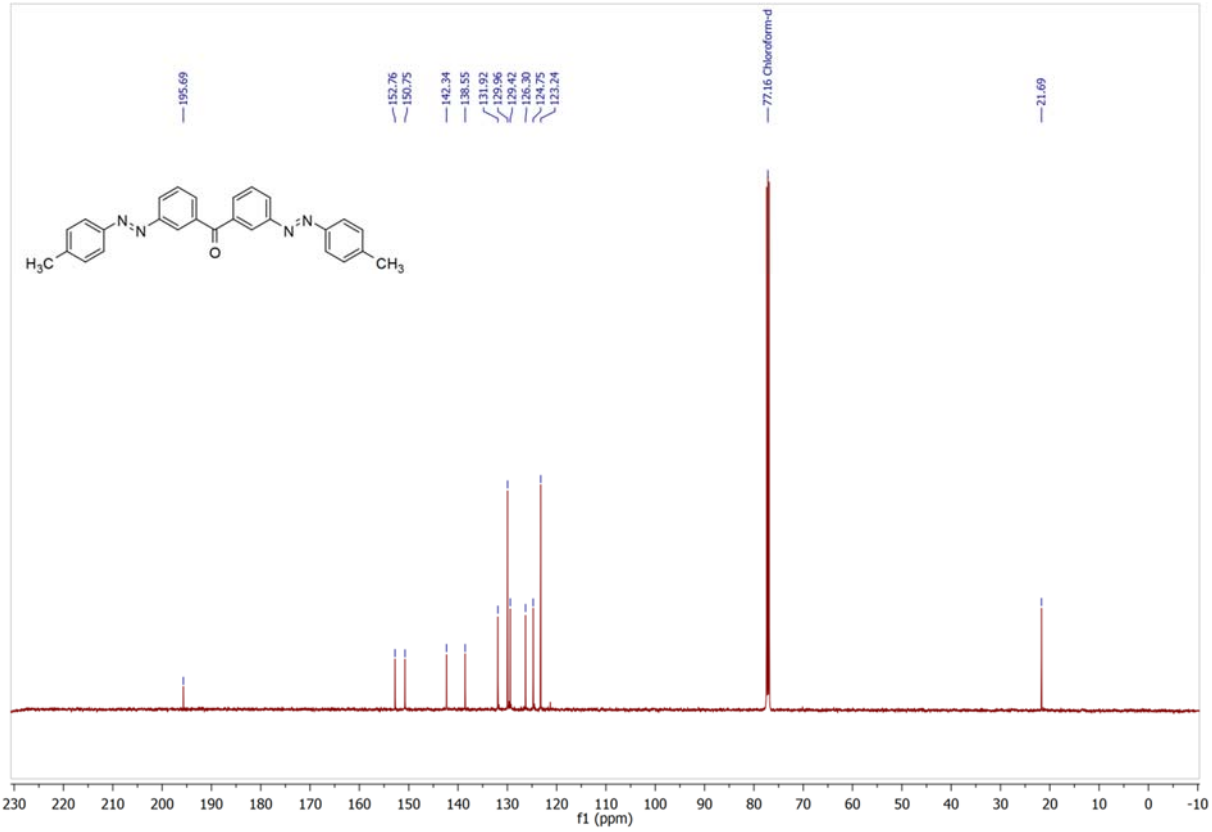

1.5 Mono Substituted Azobenzenes

4-Methylazobenzene (SI-2) in chloroform-*d*

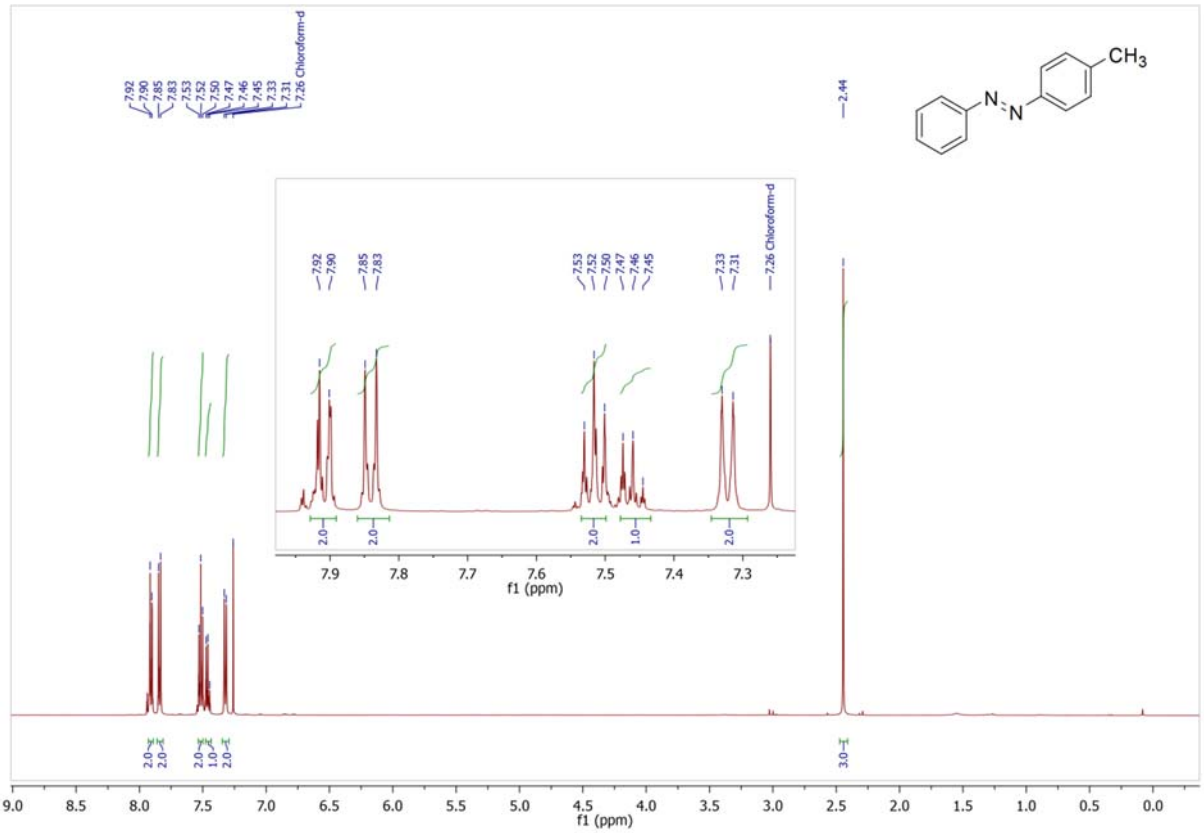

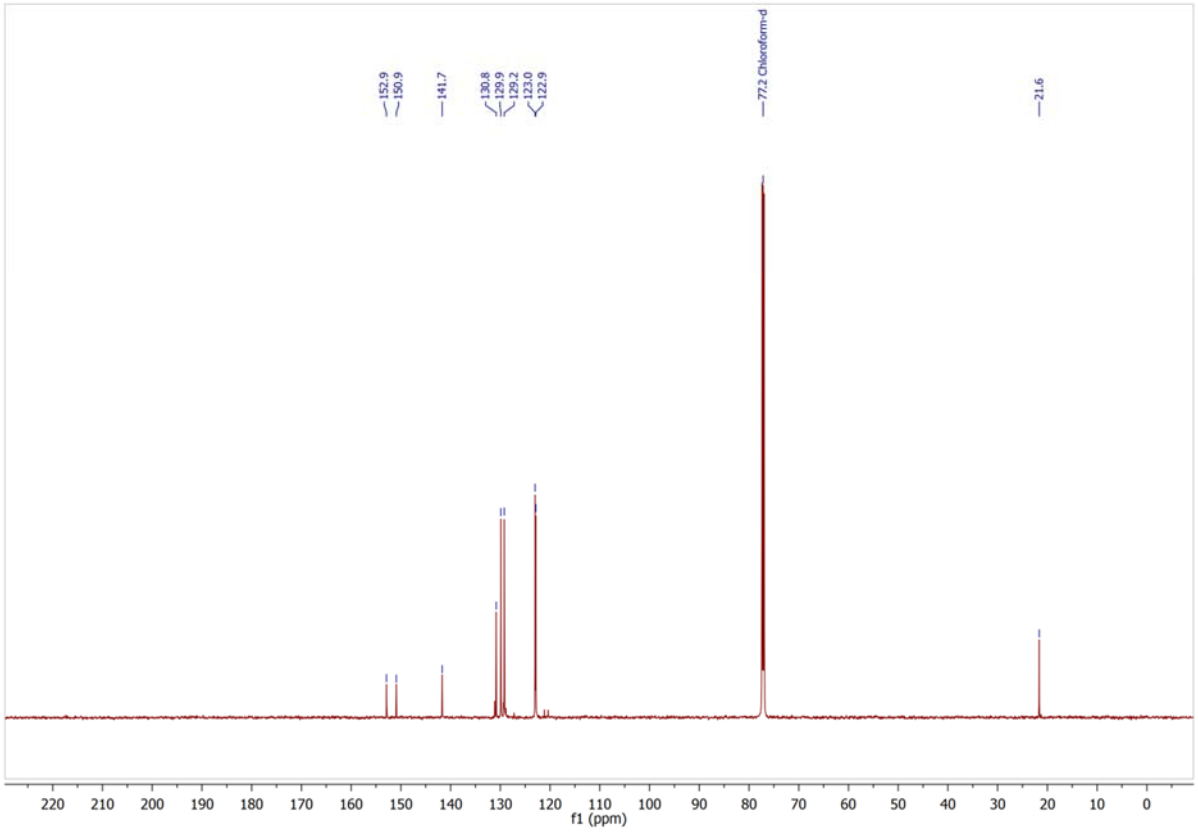

3-Methylazobenzene (SI-3) in chloroform-*d*

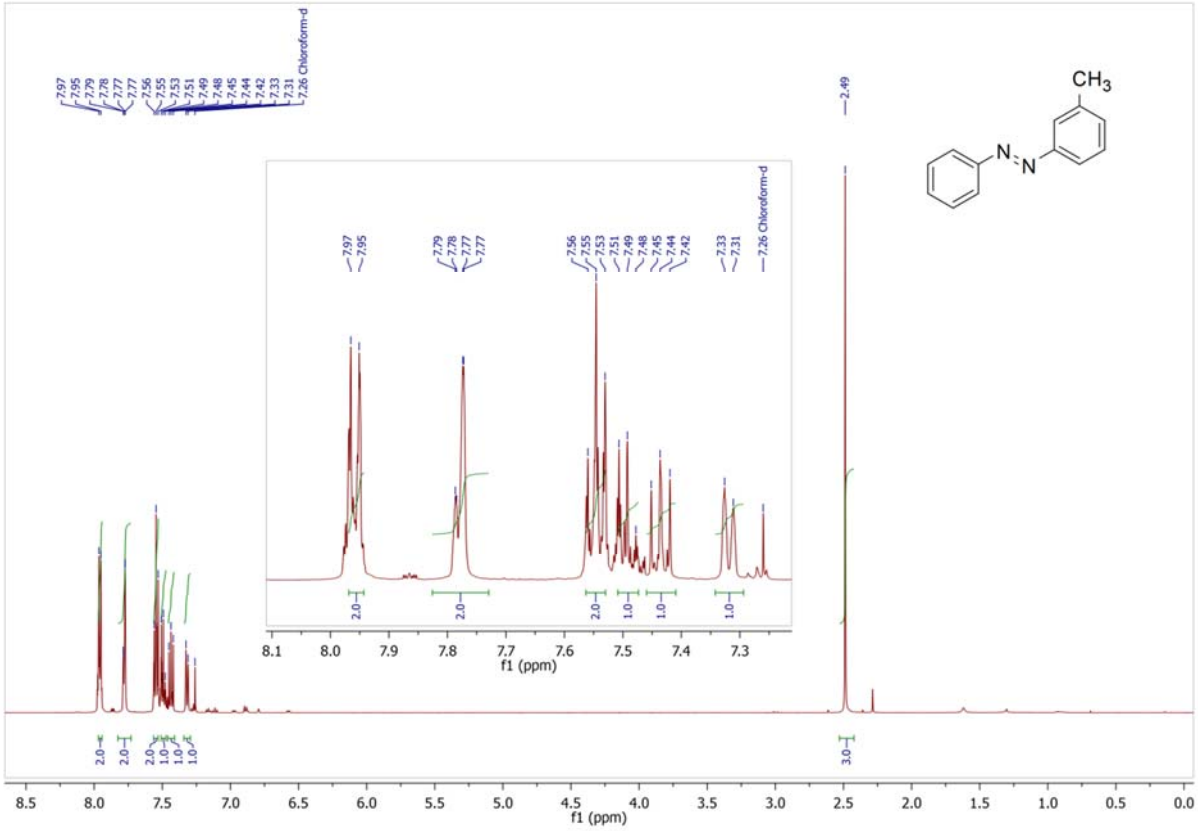

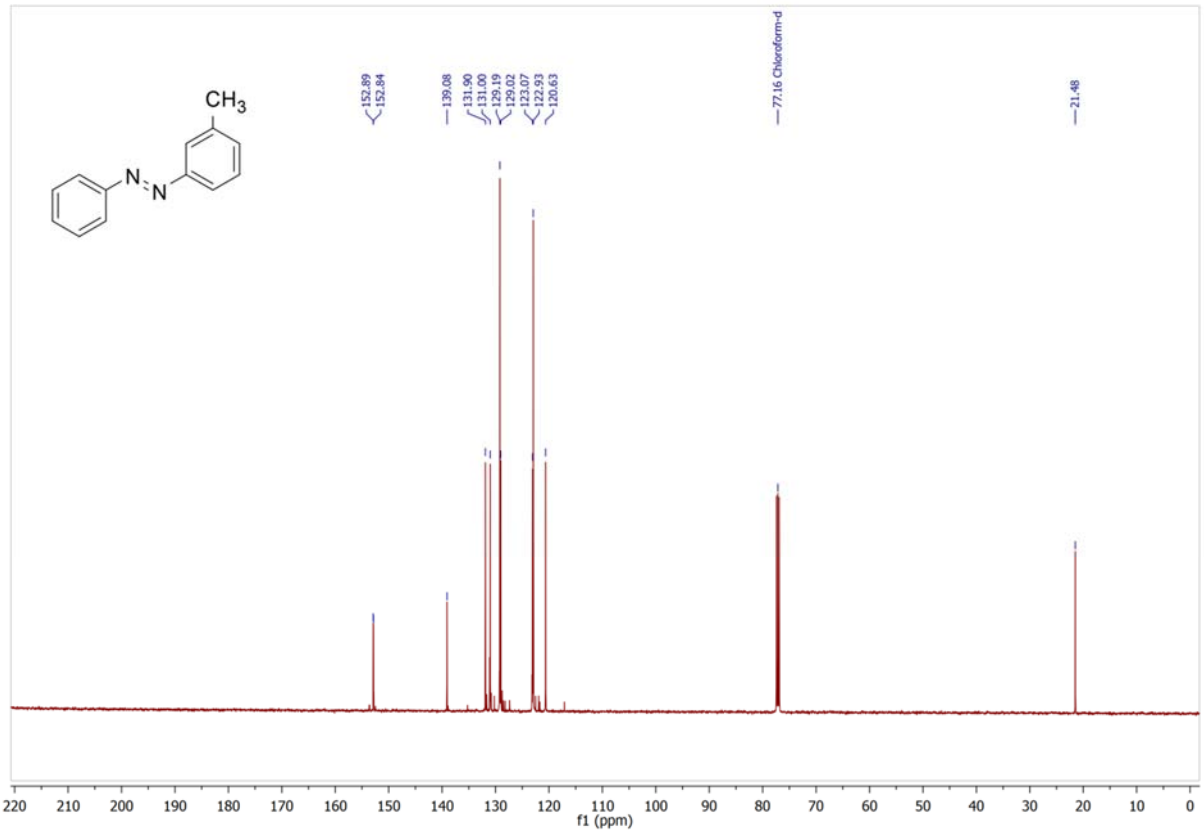

2-Methylazobenzene (SI-4) in chloroform-*d*

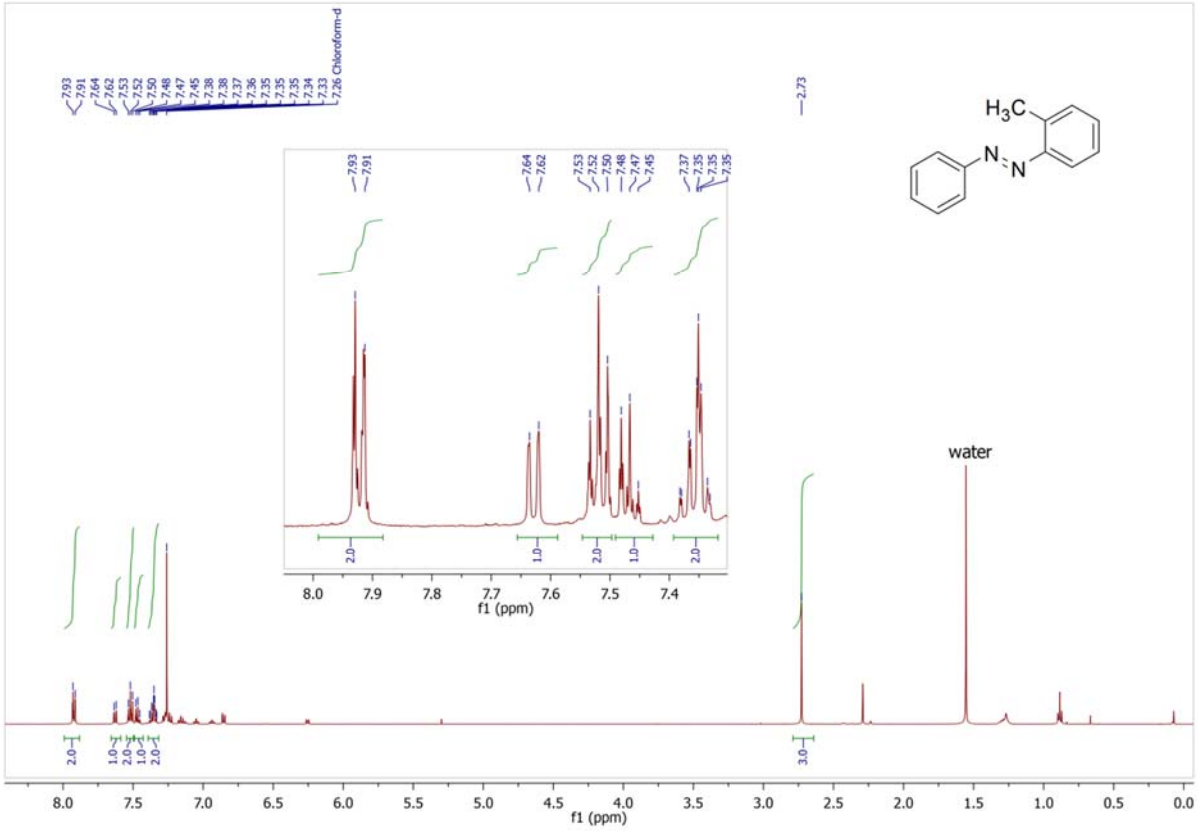

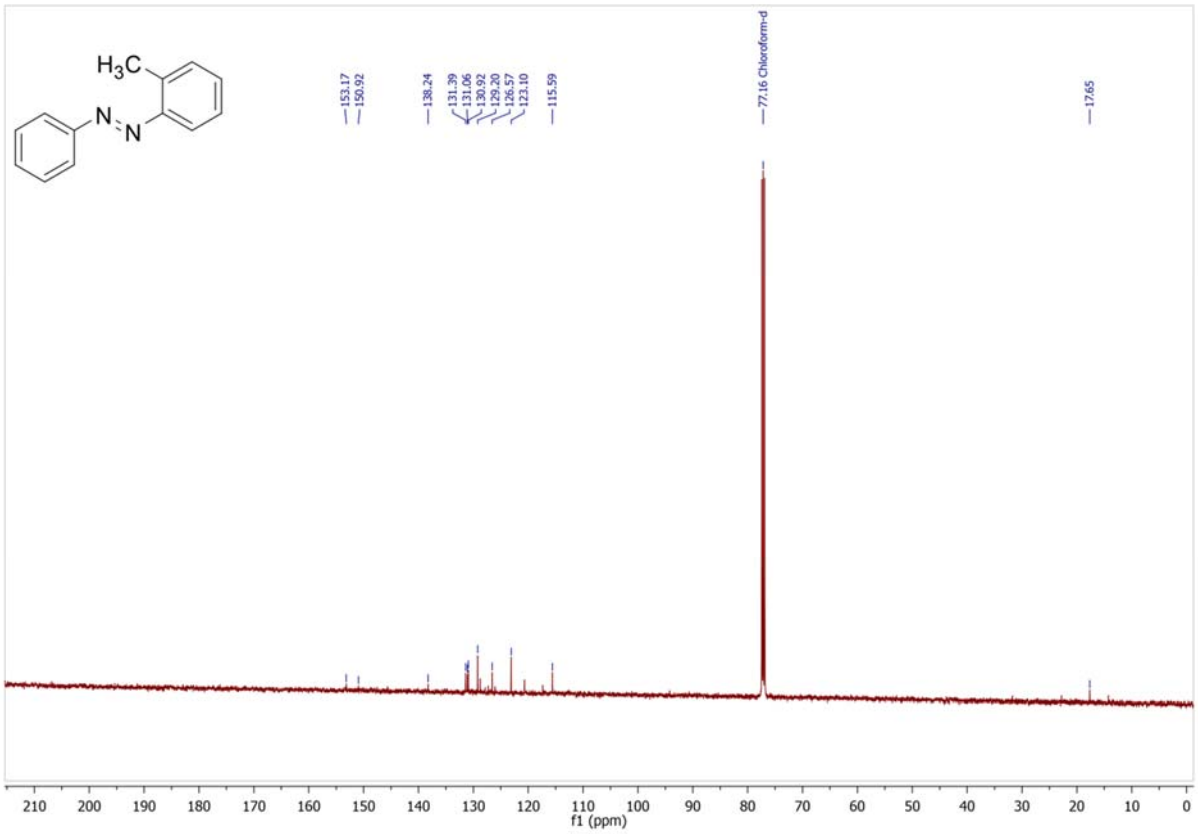

4-(Trimethylsilyl)azobenzene (SI-5) in chloroform-*d*

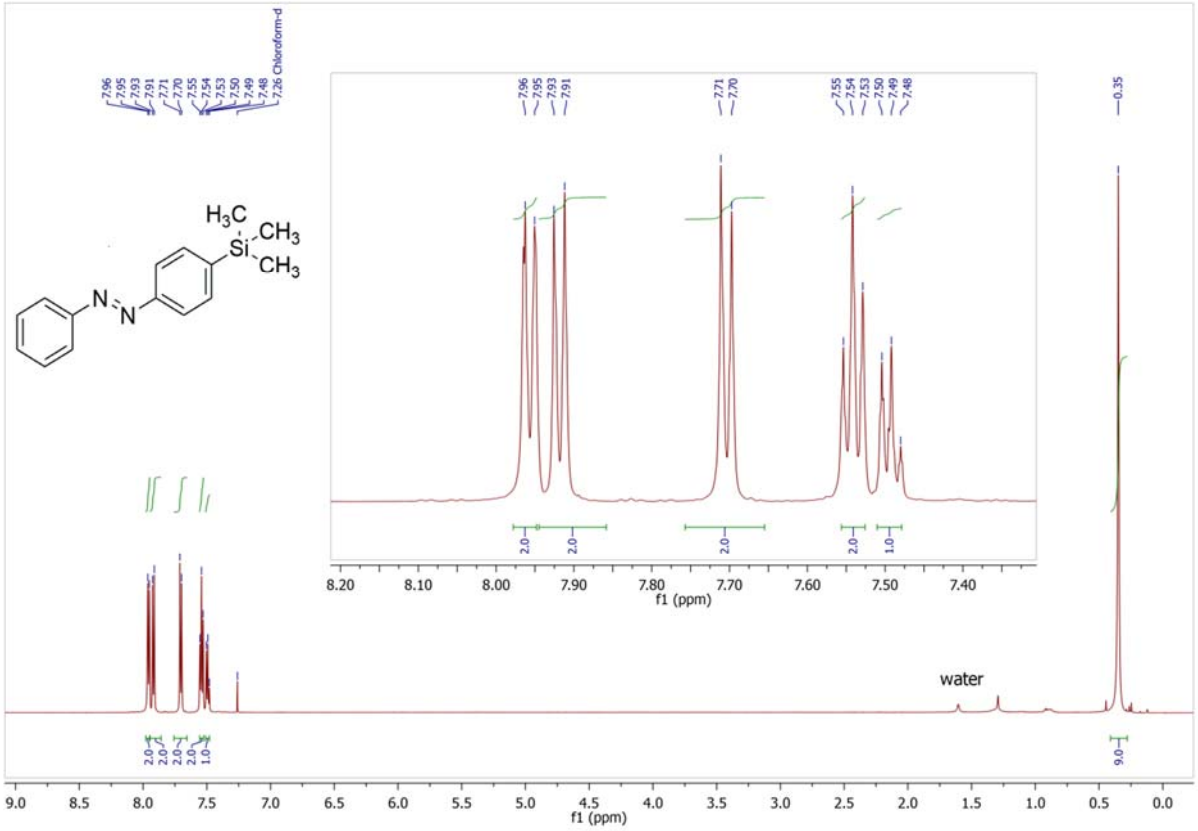

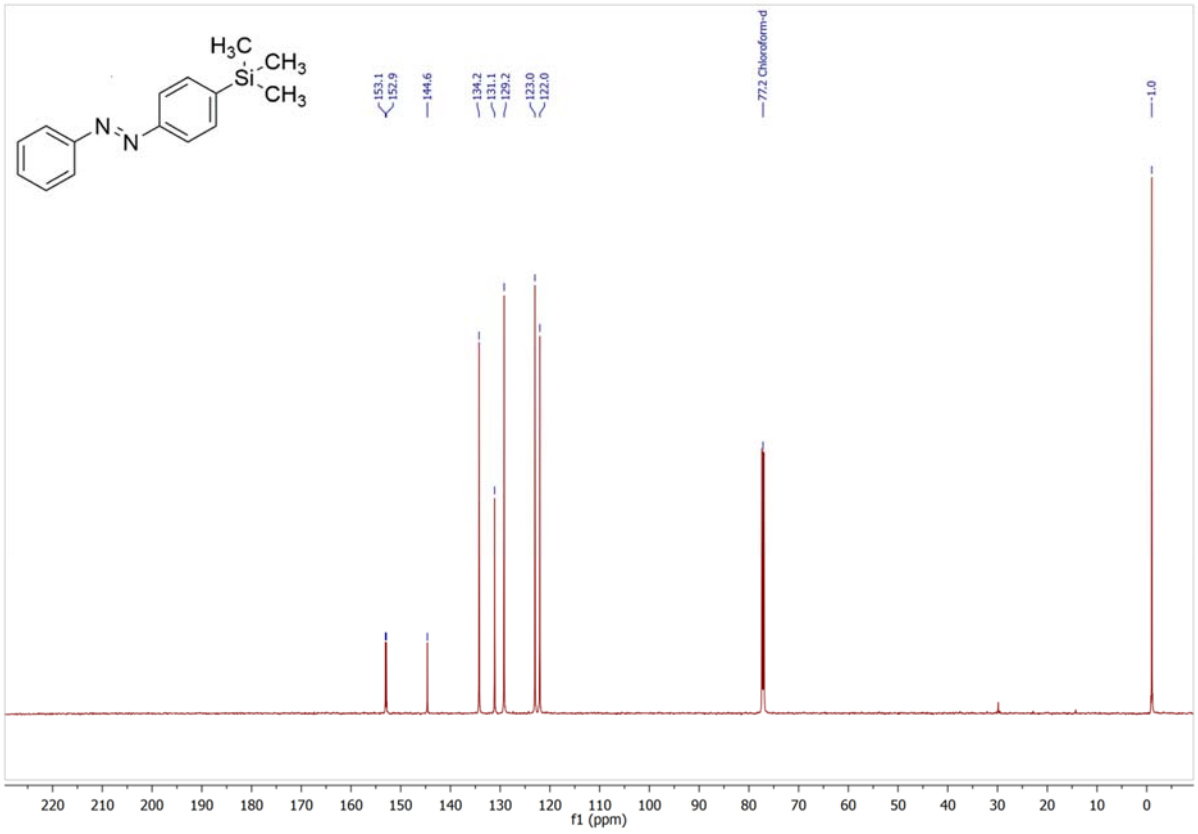

3-(Trimethylsilyl)azobenzene (SI-6) in chloroform-*d*

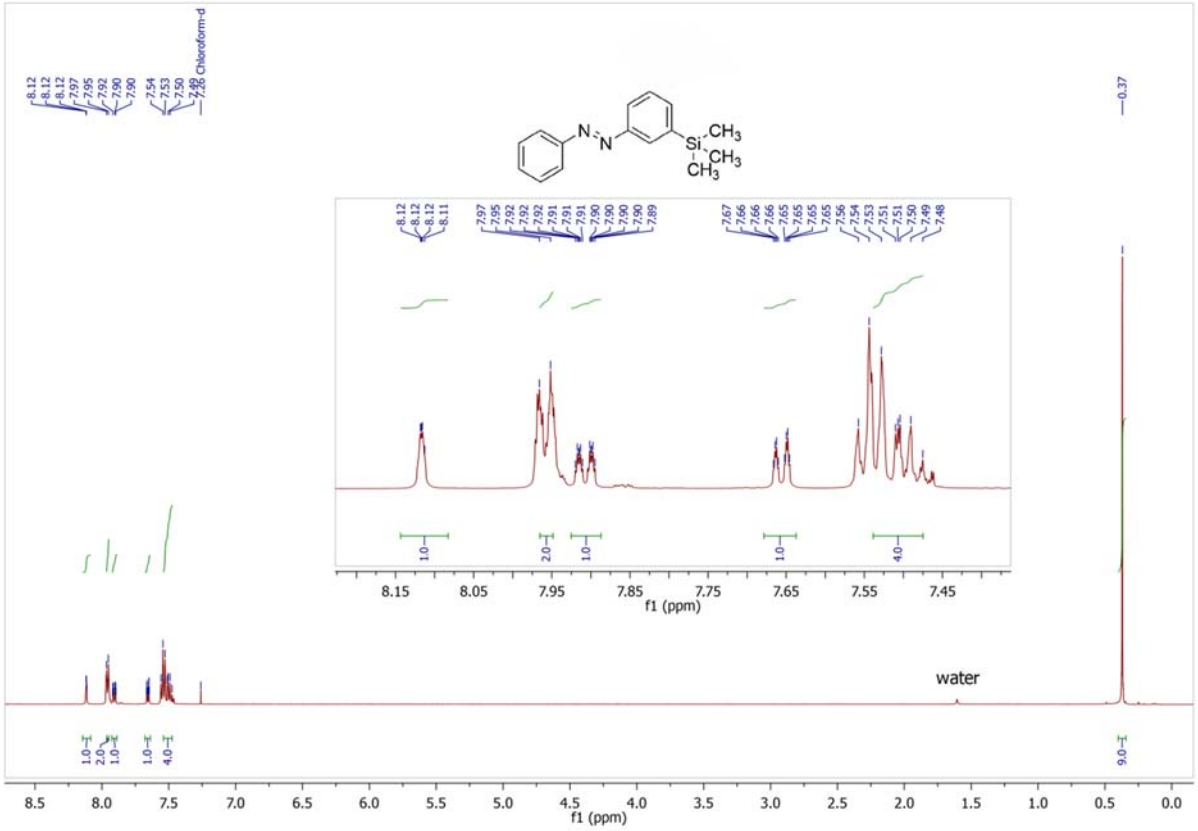

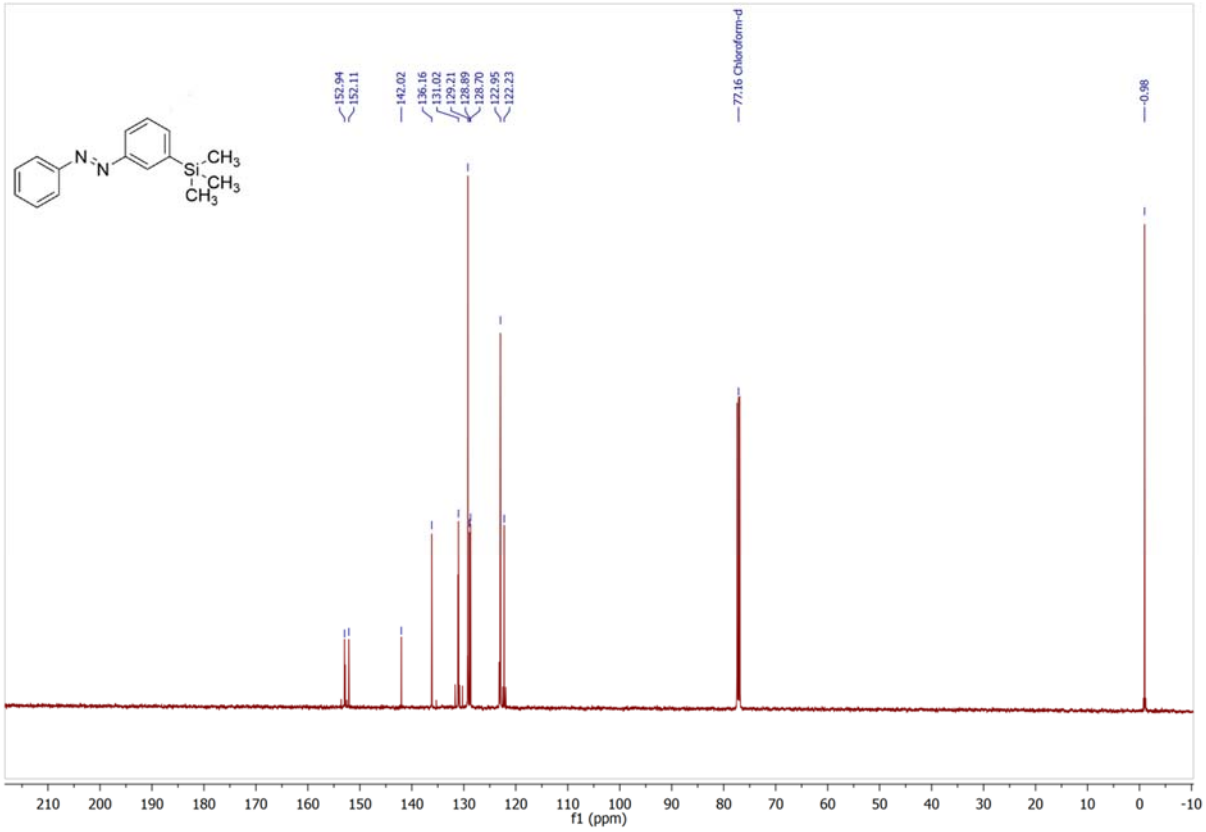

2-(Trimethylsilyl)azobenzene (SI-7) in chloroform-*d*

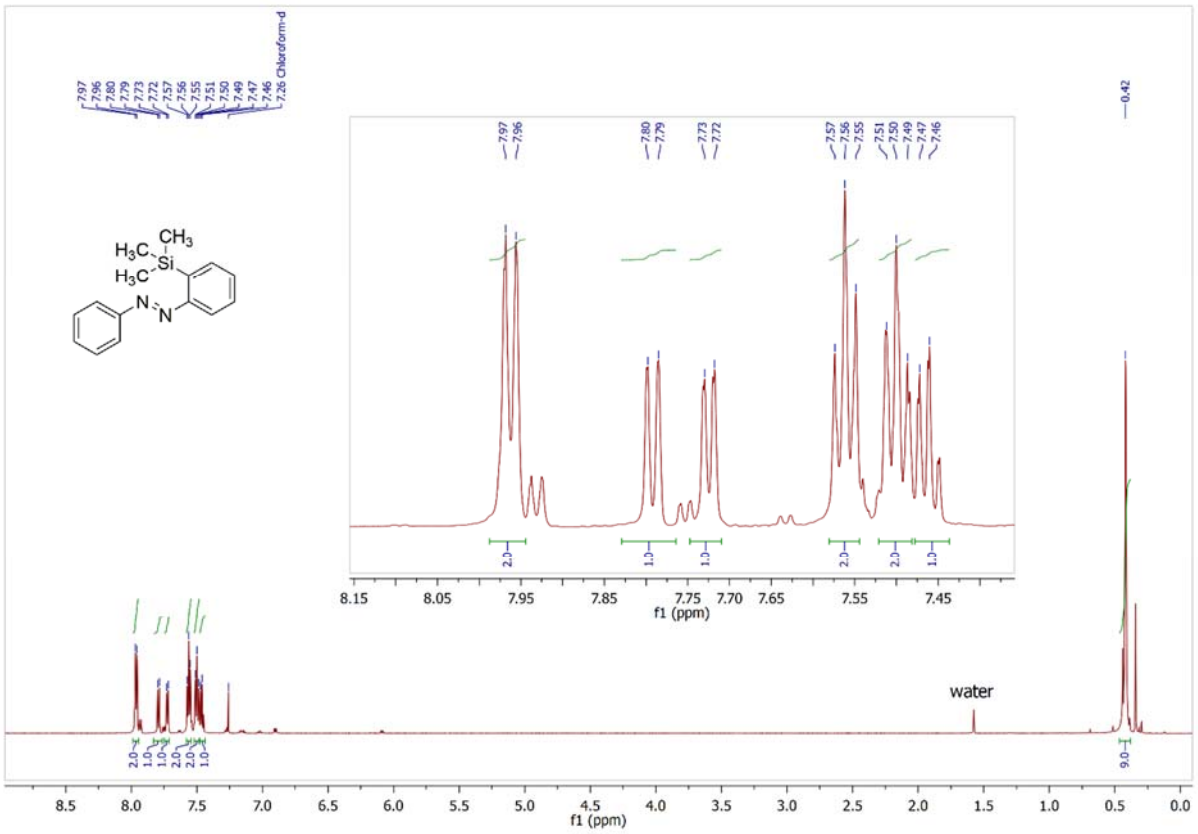

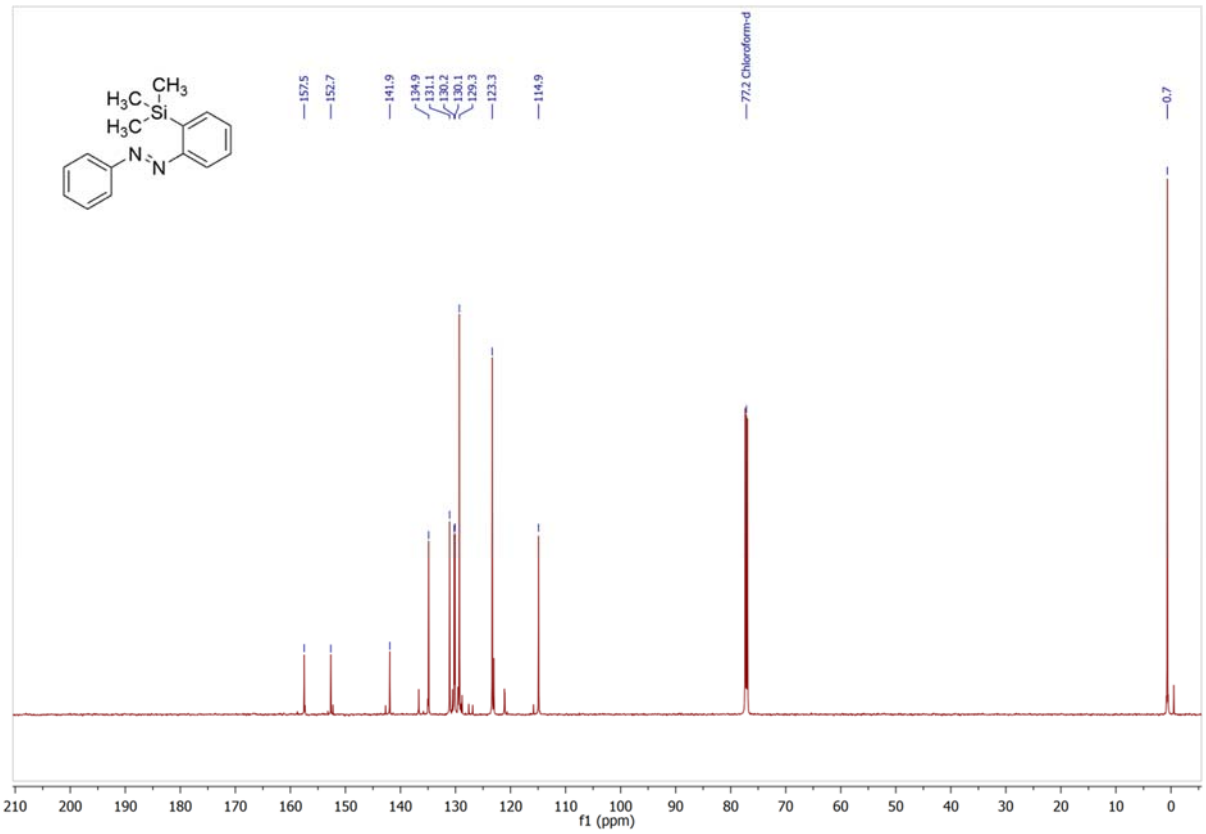

Supporting Information

for

High Yielding Lithiation of Azobenzenes by Tin-Lithium Exchange

-DFT Calculations-

Jan Strueben[a], Matthias Lipfert[a], Jan-O. Springer[a], Colin A. Gould[a], Paul J. Gates[b], Frank D. Sönnichsen[a], Anne Staubitz[a]*

[a] *Otto-Diels-Institute for Organic Chemistry, University of Kiel, Otto-Hahn-Platz 4, 24098 Kiel (Germany)*
* astaubitz@oc.uni-kiel.de

[b] *School of Chemistry, University of Bristol, Cantock's Close, Bristol BS7 1TS (UK)*

Table of Contents

Computational Details

The only tin-ate complex that has ever been isolated and both analysed by X-ray crystallography by DFT methods was the methyl lithium stannate of spirobistannafluorene described by Saito and co-workers.[1] To ensure good comparability with our results, the same DFT functional was uesd: The geometry of the compounds was optimized at the B3LYP level,[2] using the Programme Gaussian 9.0, revision D01.[3] The results were visualized with the program GaussView 5.0.[4] The LANL2DZ basis set and pseudo potential was used for Sn,[5] while the 6-31G basis set was used for Li, C, N and H.[6] To estimate the key thermochemical properties, full geometry optimization was followed by vibrational frequency calculations. These confirmed that true minima (only positive frequencies) or transition states (one negative frequency) were obtained. They also allowed to obtain corrections for zero-point energy, internal energy, and free energy (at 298.15K) in the rigid-rotor harmonic oscillator limit. Dipole moments were derived from calculating natural bond orbital (NBO) charges for optimized structures.[7,8] The solvent effect of tetrahydrofuran (THF) has been taken into account using the polarized continuum model (PCM)[9] on the optimized structures without further geometrical optimization. Calculated solvation free energies were combined with gasphase reaction free energies to obtain the reaction free energies in solution.

All energies presented in this work are given in kilocalories per mole unless stated otherwise and for comparison, the electronic energies, E, the zero-point energy corrected energies E_{ZPE} (at 0 K), enthalpies ΔH (at 298.15 K), and free energies ΔG (at 298.15 K) are given.

Structural Data and Energies of the Species Discussed

Structures Occurring in All Mechanisms

Li^+

Coordinates

Center	Atomic Number	x	y	z
1	3	0.000000	0.000000	0.000000

E = -7.284534
E_{ZPE} = -7.284535
H = -7.282174
G = -7.297283
PCM = -7.45442514

$SnMe_4$

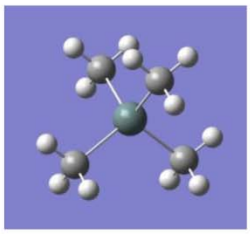

Coordinates

Center	Atomic Number	x	y	z
1	50	6.249169	1.593137	0.006300
2	6	6.361265	-0.546848	-0.183309
3	1	6.800958	-0.993654	0.715521
4	1	5.363332	-0.976729	-0.325417
5	1	6.980178	-0.828486	-1.042662
6	6	5.026888	2.099699	1.702613
7	1	4.955575	3.187027	1.818781
8	1	4.012934	1.701593	1.583147
9	1	5.450561	1.684668	2.624086
10	6	8.226925	2.393099	0.283053
11	1	8.689018	1.981591	1.187482
12	1	8.868239	2.146759	-0.570701
13	1	8.194033	3.483950	0.382177
14	6	5.381598	2.426597	-1.777156
15	1	4.371903	2.032416	-1.938400
16	1	5.314544	3.517850	-1.702767
17	1	5.988749	2.180659	-2.655645

E = -163.007331542
E_{ZPE} = -162.860824
H = -162.849445
G = -162.894246
PCM = -163.0082175

MeLi

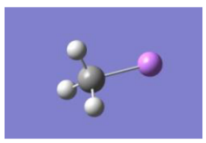

Coordinates

Center	Atomic Number	x	y	z
1	3	1.629878	1.284938	0.657495
2	6	-0.344359	1.284938	0.657495
3	1	-0.746926	1.766880	1.563896
4	1	-0.746926	1.828933	-0.213079
5	1	-0.746926	0.259001	0.621669

E = -47.3935035
E_{ZPE}= -47.359438
H = -47.355099
G = -47.380531
PCM = -47.42839112

Starting Materials

para-Trimethyltin azobenzene

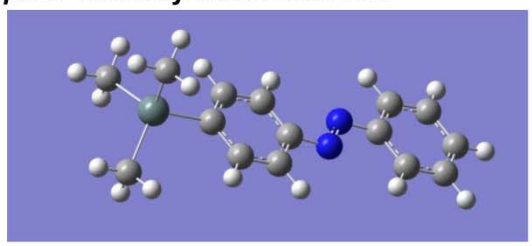

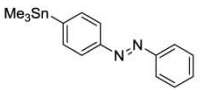

Coordinates

Center	Atomic Number	x	y	z
1	6	-4.888271	1.222928	-2.114437
2	6	-3.506011	1.398714	-2.015059
3	6	-2.833058	1.029276	-0.839970
4	6	-3.547753	0.480918	0.241676
5	6	-4.926785	0.308148	0.136381
6	6	-5.600760	0.677587	-1.039269
7	1	-5.407524	1.508833	-3.023273
8	1	-2.923993	1.818033	-2.828100
9	1	-3.006470	0.203691	1.137879
10	1	-5.482885	-0.114135	0.967530
11	1	-6.674905	0.539970	-1.113567
12	6	0.600586	1.139876	0.215937
13	6	1.317045	1.691468	-0.861636
14	6	1.277179	0.772452	1.388544
15	6	2.695785	1.866526	-0.752852
16	1	0.778468	1.972728	-1.758717
17	6	2.659254	0.952874	1.485536
18	1	0.698706	0.352517	2.204496
19	6	3.402000	1.501048	0.418185
20	1	3.230231	2.300466	-1.594436
21	1	3.157505	0.665385	2.407867
22	7	-0.805807	0.916531	0.221070
23	7	-1.425804	1.251880	-0.845474
24	50	5.532915	1.767993	0.561301
25	6	6.020368	2.254296	2.595198
26	1	5.530213	3.186030	2.896666
27	1	5.698722	1.460797	3.278823
28	1	7.102537	2.382140	2.708785
29	6	6.100293	3.366544	-0.755052
30	1	7.177562	3.553731	-0.685907
31	1	5.865172	3.122567	-1.796958
32	1	5.573879	4.289899	-0.491114
33	6	6.539626	-0.041802	-0.013233
34	1	6.260906	-0.867820	0.649744
35	1	6.276073	-0.322057	-1.038614
36	1	7.625780	0.092114	0.040203

E = -695.1075054
EZPE = -694.815627
H = -694.794470
G = -694.868835
PCM = -695.1127868

meta-Trimethyltin azobenzene

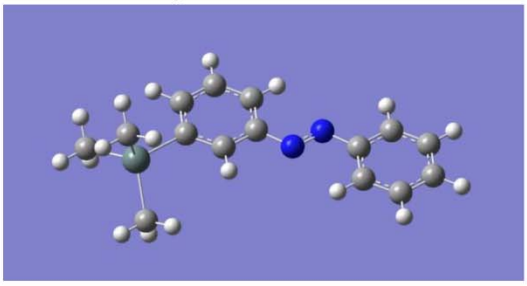

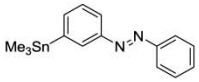

Coordinates

Center	Atomic Number	x	y	z
1	6	-0.264091	1.111405	7.233578
2	6	0.213644	1.272932	5.934159
3	6	-0.689340	1.564241	4.894553
4	6	-2.060490	1.690876	5.166287
5	6	-2.533183	1.527644	6.470765
6	6	-1.636116	1.237818	7.506193
7	1	0.427977	0.886803	8.039177
8	1	1.266990	1.180225	5.699917
9	1	-2.727354	1.915904	4.341487
10	1	-3.593414	1.625616	6.679726
11	1	-2.000511	1.110652	8.520734
12	6	1.306427	1.818886	1.914920
13	6	2.677207	1.682642	1.643317
14	6	0.406048	2.121770	0.877464
15	6	3.186123	1.840631	0.340734
16	1	3.322097	1.453819	2.487085
17	6	0.892808	2.285209	-0.417198
18	1	-0.647124	2.223154	1.109151
19	6	2.265783	2.147420	-0.683303
20	1	2.613672	2.286781	-1.703943
21	1	0.208132	2.522295	-1.226231
22	7	0.931371	1.632529	3.276853
23	7	-0.315491	1.750110	3.531895
24	50	5.285481	1.610388	-0.071110
25	6	5.754425	-0.469899	-0.337007
26	1	5.490699	-1.043886	0.557709
27	1	5.200545	-0.885641	-1.185478
28	1	6.825726	-0.600080	-0.526855
29	6	6.399721	2.397807	1.586526
30	1	7.474148	2.254478	1.427350
31	1	6.208732	3.469460	1.705957
32	1	6.124132	1.894802	2.519920
33	6	5.738262	2.693322	-1.869203
34	1	5.192400	2.283484	-2.726245
35	1	5.470070	3.749928	-1.763598
36	1	6.809613	2.631900	-2.090020

E = -695.1076259
E_{ZPE} = -694.815550
H = -694.794507
G = -694.867953
PCM = -695.112854

ortho-Trimethyltin azobenzene

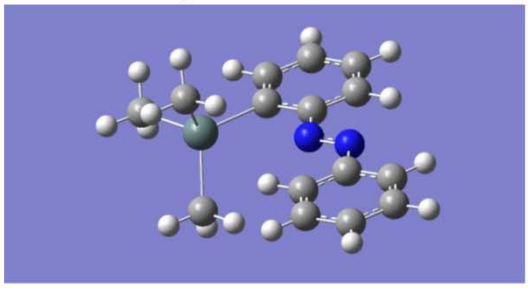

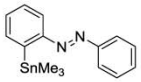

Coordinates

Center	Atomic Number	x	y	z
1	6	-0.354165	3.241484	4.184801
2	6	0.094740	2.731236	2.967415
3	6	-0.746883	2.782287	1.839823
4	6	-2.029456	3.344575	1.945947
5	6	-2.473335	3.854041	3.168233
6	6	-1.636650	3.803499	4.289920
7	1	0.292199	3.203632	5.055951
8	1	1.081269	2.295485	2.873758
9	1	-2.651873	3.368104	1.058594
10	1	-3.464723	4.287782	3.246870
11	1	-1.978481	4.198507	5.241297
12	6	1.084294	1.295320	-0.888884
13	6	2.372723	0.729118	-1.003183
14	6	0.208003	1.367616	-1.988007
15	6	2.759058	0.233920	-2.261824
16	1	3.742516	-0.209216	-2.390301
17	6	0.618218	0.868938	-3.222326
18	1	-0.770787	1.811249	-1.850389
19	6	1.894620	0.300963	-3.362101
20	1	2.211858	-0.087054	-4.325546
21	1	-0.049812	0.919729	-4.076487
22	7	0.752578	1.779162	0.412508
23	7	-0.407342	2.297063	0.545237
24	50	3.646208	0.661391	0.734198
25	6	5.470213	-0.272773	0.071577
26	1	5.285052	-1.285954	-0.303087
27	1	5.947505	0.307671	-0.726211
28	1	6.178451	-0.345887	0.905067
29	6	2.799970	-0.560878	2.282383
30	1	1.827856	-0.165690	2.590804
31	1	2.658048	-1.585814	1.922499
32	1	3.463587	-0.592847	3.153860
33	6	4.127560	2.632542	1.434034
34	1	4.783769	2.580551	2.310147
35	1	4.645655	3.197602	0.651445
36	1	3.216381	3.173673	1.704623

E = -695.1125253
E_{ZPE} = -694.820567
H = -694.799534
G = -694.872415
PCM = -695.1166414

para-Trimethyltin azobenzene: minimum with MeLi associated

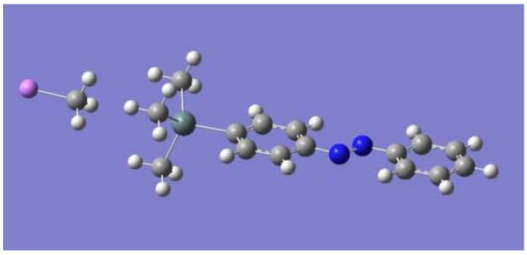

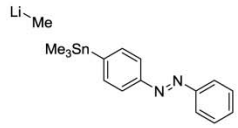

Coordinates

Center	Atomic Number	x	y	z
1	6	7.765346	1.291551	-0.032105
2	6	6.371994	1.392473	-0.037492
3	6	5.582539	0.232374	-0.007652
4	6	6.191910	-1.035944	0.027831
5	6	7.582639	-1.130150	0.033117
6	6	8.373075	0.030435	0.003232
7	1	8.374268	2.189439	-0.055203
8	1	5.869252	2.352781	-0.064337
9	1	5.561724	-1.916526	0.050554
10	1	8.057338	-2.106098	0.060566
11	1	9.455520	-0.051148	0.007616
12	6	2.042931	-0.391243	0.003173
13	6	1.426469	0.873107	-0.028422
14	6	1.253925	-1.551054	0.033760
15	6	0.035154	0.959330	-0.030262
16	1	2.050161	1.758959	-0.048414
17	6	-0.139651	-1.450393	0.031524
18	1	1.756201	-2.512315	0.061118
19	6	-0.784050	-0.195171	-0.003295
20	1	-0.422452	1.945545	-0.047908
21	1	-0.727283	-2.364408	0.062316
22	7	3.450074	-0.603734	0.010259
23	7	4.173920	0.450028	-0.015699
24	50	-2.937539	-0.037242	-0.020997
25	6	-3.729291	-1.668205	1.125809
26	1	-3.436903	-2.634484	0.699735
27	1	-3.372981	-1.625895	2.160559
28	1	-4.822660	-1.607375	1.128834
29	6	-3.643457	-0.143984	-2.045973
30	1	-4.734102	-0.046372	-2.051030
31	1	-3.214509	0.661036	-2.652205
32	1	-3.373495	-1.101325	-2.504571
33	6	-3.461088	1.850333	0.852880
34	1	-4.552001	1.935708	0.893728
35	1	-3.063969	1.933910	1.870160
36	1	-3.071279	2.685399	0.260137
37	6	-7.340385	0.365832	0.053786
38	1	-6.910314	0.359537	1.068626
39	1	-6.886550	1.202431	-0.502097
40	1	-7.046679	-0.571983	-0.445367
41	3	-9.312770	0.547378	0.120724

E = -742.504224287
E_{ZPE} = -742.177621
H = -742.150840
G = -742.242061
PCM = -742.5436877

meta-Trimethyltin azobenzene: minimum with MeLi associated

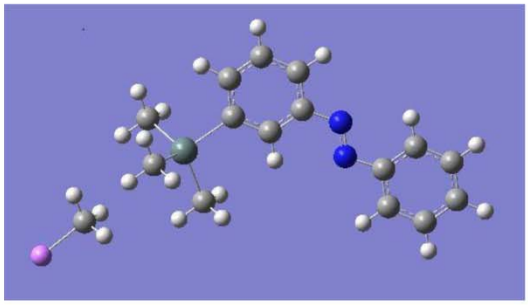

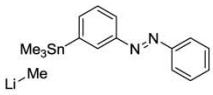

Coordinates

Center	Atomic Number	x	y	z
1	6	6.089397	-2.267369	0.107109
2	6	4.793542	-1.745651	0.083517
3	6	4.595252	-0.357167	0.034149
4	6	5.700568	0.513694	0.008266
5	6	6.991073	-0.012838	0.032061
6	6	7.190201	-1.402242	0.081467
7	1	6.240966	-3.341199	0.145217
8	1	3.919518	-2.387073	0.102204
9	1	5.522038	1.581295	-0.029825
10	1	7.846846	0.654895	0.012292
11	1	8.198203	-1.804694	0.099728
12	6	1.506219	3.152787	-0.102945
13	6	1.691589	1.763299	-0.052999
14	6	0.212489	3.677217	-0.128494
15	6	0.578505	0.899927	-0.028051
16	6	-0.890576	2.814326	-0.103383
17	1	0.062752	4.751828	-0.168882
18	6	-0.729938	1.408890	-0.051137
19	1	0.770761	-0.166986	0.007309
20	1	-1.888585	3.246098	-0.127652
21	7	3.049045	1.331021	-0.032267
22	7	3.234162	0.067196	0.013792
23	50	-2.432515	0.081312	-0.003538
24	6	-3.420012	0.270656	1.893881
25	1	-2.741836	0.008161	2.712834
26	1	-3.772981	1.295207	2.054512
27	1	-4.281675	-0.404693	1.919565
28	6	-1.707962	-1.917731	-0.278772
29	1	-2.557374	-2.608804	-0.270014
30	1	-1.184965	-2.019551	-1.235772
31	1	-1.019077	-2.204563	0.523328
32	6	-3.773565	0.638341	-1.584395
33	1	-4.118055	1.671881	-1.467321
34	1	-3.283700	0.547481	-2.559740
35	1	-4.645500	-0.023849	-1.565895
36	6	-5.881291	-2.696455	0.025148
37	1	-6.259734	-1.670254	0.161119
38	1	-5.354815	-2.738282	-0.942249
39	1	-5.145075	-2.894757	0.821154
40	3	-7.360148	-4.014336	0.084881
41	1	2.383946	3.789399	-0.121602

E = -742.503936396
E_{ZPE} = -742.177270
H = -742.150562
G = -742.241566
PCM = -742.5434611

ortho-Trimethyltin azobenzene: minimum with MeLi associated

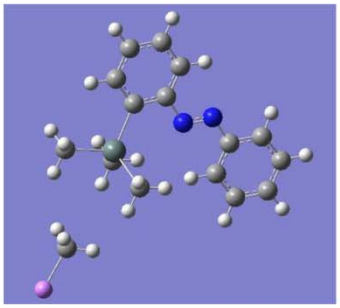

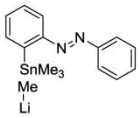

Coordinates

Center	Atomic Number	x	y	z
1	6	0.388326	-5.166114	0.180370
2	6	0.341954	-3.775380	0.091292
3	6	1.541740	-3.038726	0.094635
4	6	2.774525	-3.704890	0.186168
5	6	2.814271	-5.098157	0.276075
6	6	1.621250	-5.831431	0.273313
7	1	-0.535092	-5.736646	0.177448
8	1	-0.601832	-3.250099	0.018525
9	1	3.679202	-3.107366	0.184946
10	1	3.768433	-5.609932	0.347336
11	1	1.648698	-6.914360	0.342347
12	6	1.829779	1.132872	-0.180924
13	6	0.606765	0.436104	-0.145642
14	6	1.822147	2.522743	-0.270516
15	6	-0.634151	1.108396	-0.198616
16	6	0.602209	3.215853	-0.324346
17	1	2.759534	3.069746	-0.298886
18	6	-0.608662	2.512508	-0.288226
19	1	-1.541962	3.066881	-0.330643
20	1	0.598238	4.299795	-0.394362
21	7	0.519596	-0.985513	-0.055811
22	7	1.626692	-1.619394	0.008320
23	50	-2.471301	-0.030703	-0.136729
24	6	-2.650617	-1.101704	1.711904
25	1	-1.840462	-1.829266	1.815508
26	1	-2.607083	-0.411564	2.561641
27	1	-3.612439	-1.625106	1.736124
28	6	-2.638222	-1.314432	-1.846198
29	1	-3.592132	-1.851193	-1.805574
30	1	-2.607057	-0.728101	-2.771129
31	1	-1.817679	-2.037428	-1.867586
32	6	-4.046768	1.431744	-0.231321
33	1	-4.005826	2.123454	0.617903
34	1	-3.998948	2.016470	-1.157149
35	1	-5.010302	0.910851	-0.203616
36	6	-6.467104	-2.149171	0.014261
37	1	-5.684555	-2.886296	0.256931
38	1	-6.386790	-1.321020	0.737131
39	1	-6.251523	-1.745077	-0.988225
40	3	-8.269908	-2.968472	0.077354
41	1	2.754991	0.570661	-0.137598

E = -742.508333329
E_{ZPE} = -742.181654
H = -742.154946
G = -742.246719
PCM = -742.5472427

Ate-complexes

para-Tin-ate complex with the azobenzene in equatorial position

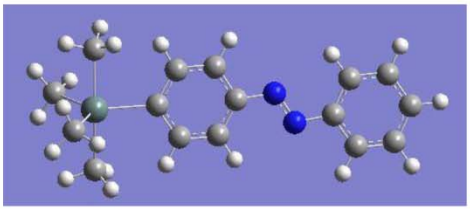

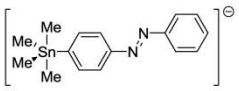

Coordinates

Center	Atomic Number	x	y	z
1	6	-7.375877	1.184989	-0.055525
2	6	-5.988167	1.348190	-0.063411
3	6	-5.141747	0.228788	-0.010399
4	6	-5.699844	-1.062700	0.051372
5	6	-7.085609	-1.220144	0.059308
6	6	-7.930379	-0.099867	0.005975
7	1	-8.023385	2.056021	-0.096939
8	1	-5.528251	2.329326	-0.110006
9	1	-5.027763	-1.911295	0.091775
10	1	-7.513972	-2.217604	0.107280
11	1	-9.008774	-0.229611	0.012516
12	6	-1.593255	-0.310583	0.010232
13	6	-0.792747	-1.468596	0.049344
14	6	-0.971193	0.955887	-0.032732
15	6	0.598802	-1.362205	0.039579
16	1	-1.294144	-2.432073	0.083477
17	6	0.419185	1.038882	-0.030640
18	1	-1.594050	1.843474	-0.063756
19	6	1.258786	-0.109046	0.001787
20	1	1.194208	-2.268196	0.057435
21	1	0.882252	2.019457	-0.051363
22	7	-2.985091	-0.529168	0.018241
23	7	-3.742426	0.508839	-0.022941
24	50	3.531463	0.052908	-0.002093
25	6	4.599601	0.495689	-1.887593
26	1	5.104824	-0.392126	-2.287183
27	1	3.882716	0.855205	-2.640209
28	1	5.337206	1.293348	-1.725772
29	6	3.690221	-2.179367	-0.402684
30	1	3.343922	-2.805496	0.434929
31	1	3.161046	-2.497028	-1.314531
32	1	4.761785	-2.389132	-0.548114
33	6	4.663790	-0.218759	1.879964
34	1	5.411506	-1.014929	1.768844
35	1	5.160921	0.710604	2.184862
36	1	3.973771	-0.516542	2.683348
37	6	3.373253	2.285064	0.404510
38	1	2.924878	2.856415	-0.423733
39	1	2.817715	2.518844	1.325999
40	1	4.404139	2.650917	0.534184

E = -734.9967693
E_{ZPE}= -734.672439
H = -734.648760
G = -734.728780
PCM = -735.0522379

para-Tin-ate complex with the azobenzene in apical position

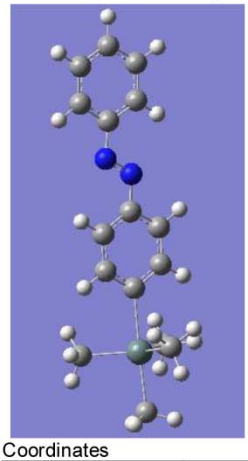

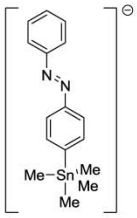

Coordinates

Center	Atomic Number	x	y	z
1	6	-5.091776	-0.572688	0.441848
2	6	-3.694983	-0.603677	0.454106
3	6	-2.954817	0.540623	0.112247
4	6	-3.633105	1.723031	-0.243794
5	6	-5.027576	1.748787	-0.254175
6	6	-5.764872	0.603817	0.087748
7	1	-5.654833	-1.462828	0.707790
8	1	-3.145676	-1.499115	0.724212
9	1	-3.043195	2.593676	-0.503534
10	1	-5.546932	2.663030	-0.529110
11	1	-6.850770	0.630726	0.077753
12	6	0.520809	1.387964	-0.135806
13	6	1.204583	2.567846	-0.497172
14	6	1.270134	0.243637	0.221996
15	6	2.598822	2.597774	-0.501584
16	1	0.607412	3.435340	-0.767951
17	6	2.660930	0.303371	0.209440
18	1	0.738309	-0.660931	0.499423
19	6	3.394495	1.472625	-0.153193
20	1	3.092619	3.524491	-0.788901
21	1	3.212991	-0.592947	0.487529
22	7	-0.880777	1.460643	-0.164501
23	7	-1.536614	0.399652	0.158827
24	50	5.784549	1.598109	-0.025220
25	6	5.876912	-0.546568	-0.488232
26	1	5.738653	-1.146880	0.422626
27	1	5.101191	-0.838236	-1.206296
28	1	6.863791	-0.787803	-0.902021
29	6	5.424542	2.294208	2.032170
30	1	4.786358	3.187836	2.022126
31	1	4.893741	1.521425	2.604560
32	1	6.368580	2.530536	2.538503
33	6	8.027249	1.752818	0.208667
34	1	8.382467	1.099820	1.022093
35	1	8.550301	1.456623	-0.714728
36	1	8.328584	2.784337	0.452050
37	6	5.759953	3.015232	-1.702885
38	1	4.930367	2.818246	-2.391738
39	1	5.663591	4.047727	-1.336908
40	1	6.709594	2.942739	-2.247723

E = -735.0022355
E_{ZPE} = -734.678181
H = -734.654189
G = -734.735784
PCM = -735.0566402

meta-Tin-ate complex with the azobenzene in equatorial position

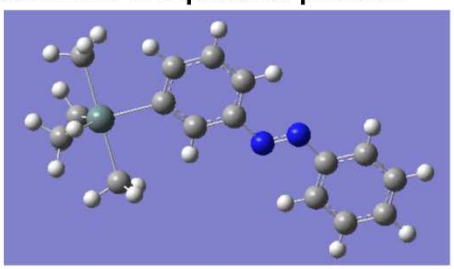

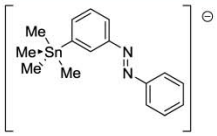

Coordinates

Center	Atomic Number	x	y	z
1	6	-2.942346	1.458415	4.180245
2	6	-1.974420	1.552635	3.180403
3	6	-2.359567	1.860298	1.861585
4	6	-3.715637	2.069410	1.564112
5	6	-4.681432	1.973742	2.569576
6	6	-4.298249	1.668060	3.881657
7	1	-2.643629	1.221132	5.197501
8	1	-0.922419	1.395460	3.385750
9	1	-3.979476	2.304950	0.538702
10	1	-5.728655	2.136964	2.331920
11	1	-5.046459	1.593414	4.665556
12	6	0.714521	1.905771	0.001638
13	6	2.059652	1.667786	0.350307
14	6	0.369829	2.231673	-1.327380
15	6	3.111371	1.766662	-0.584582
16	1	2.262348	1.397861	1.380899
17	6	1.385164	2.322403	-2.272209
18	1	-0.670163	2.404492	-1.578423
19	6	2.728756	2.105431	-1.901537
20	1	3.499251	2.210502	-2.658743
21	1	1.142712	2.571746	-3.303528
22	7	-0.221733	1.790487	1.055186
23	7	-1.456475	1.984644	0.762013
24	50	5.277913	1.411989	-0.013064
25	6	6.323632	-0.415968	-0.691508
26	1	6.443025	-1.141119	0.122867
27	1	5.747765	-0.891873	-1.498880
28	1	7.311307	-0.158511	-1.097929
29	6	4.600169	0.355485	1.881272
30	1	4.107820	1.020140	2.608628
31	1	3.926855	-0.491569	1.678418
32	1	5.506508	-0.044383	2.363021
33	6	6.348844	2.903081	1.220451
34	1	6.932187	2.395846	2.001276
35	1	7.017782	3.528734	0.616973
36	1	5.620474	3.554842	1.724548
37	6	5.946684	2.472005	-1.915568
38	1	5.718718	1.920339	-2.841857
39	1	5.531301	3.487718	-2.007226
40	1	7.042546	2.563541	-1.850004

E = -734.995427
E_{ZPE} = -734.671104
H = -734.647516
G = -734.726000
PCM = -735.0519655

meta-Tin-ate complex with the azobenzene in apical position

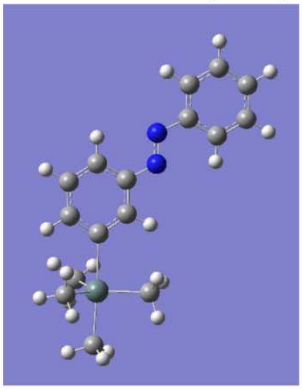

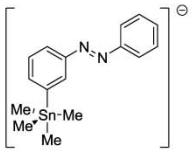

Coordinates

Center	Atomic Number	x	y	z
1	6	-6.024077	-1.837805	0.690630
2	6	-4.798931	-1.206668	0.475654
3	6	-4.764809	0.161028	0.142201
4	6	-5.967310	0.877378	0.029144
5	6	-7.192174	0.240404	0.245443
6	6	-7.225564	-1.120070	0.577131
7	1	-6.047779	-2.893241	0.947866
8	1	-3.858732	-1.738653	0.557061
9	1	-5.907803	1.929249	-0.229026
10	1	-8.117714	0.802003	0.155939
11	1	-8.176085	-1.618090	0.745926
12	6	-1.270937	0.919111	-0.219040
13	6	-0.095083	0.147069	-0.092843
14	6	-1.191618	2.288145	-0.554447
15	6	1.199907	0.676816	-0.289877
16	1	-0.233784	-0.899907	0.165958
17	6	0.066296	2.845551	-0.754070
18	1	-2.103099	2.866881	-0.648127
19	6	1.226827	2.053035	-0.623245
20	1	2.190280	2.534403	-0.793722
21	1	0.154395	3.899726	-1.013776
22	7	-2.483828	0.231924	0.009024
23	7	-3.571635	0.907644	-0.099332
24	50	3.243068	-0.534719	-0.011196
25	6	3.995457	0.406542	-1.850727
26	1	4.551353	-0.341927	-2.430744
27	1	3.190496	0.818202	-2.469556
28	1	4.696728	1.216924	-1.603283
29	6	2.104335	-2.406850	-0.160255
30	1	1.500028	-2.568092	0.743682
31	1	1.421149	-2.388145	-1.018871
32	1	2.793349	-3.252998	-0.267628
33	6	5.202456	-1.621643	0.305622
34	1	5.433259	-2.288900	-0.540588
35	1	6.036323	-0.908717	0.410264
36	1	5.170329	-2.235802	1.220164
37	6	3.404123	0.526465	1.909214
38	1	3.346251	1.611663	1.750845
39	1	2.563794	0.247704	2.559732
40	1	4.345506	0.286261	2.418753

E = -734.9998121
E_{ZPE} = -734.675608
H = -734.651777
G = -734.730462
PCM = -735.0554864

ortho-Tin-ate complex with the azobenzene in apical position

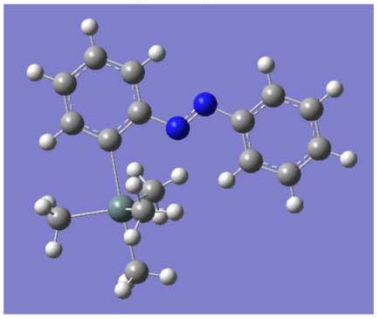

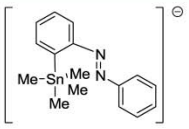

Coordinates

Center	Atomic Number	x	y	z
1	6	-0.061791	3.442015	4.084062
2	6	0.284246	2.928088	2.833932
3	6	-0.648604	2.967467	1.779731
4	6	-1.919551	3.523521	1.998375
5	6	-2.260806	4.036978	3.252505
6	6	-1.332393	3.998315	4.300772
7	1	0.660207	3.409505	4.895163
8	1	1.258257	2.493316	2.646933
9	1	-2.615605	3.538155	1.166333
10	1	-3.246271	4.465655	3.412812
11	1	-1.594026	4.396319	5.277302
12	6	1.055179	1.472661	-1.023629
13	6	2.354570	0.917000	-1.195287
14	6	0.092077	1.536337	-2.061276
15	6	2.614161	0.430628	-2.503937
16	1	3.586813	-0.006496	-2.715298
17	6	0.404338	1.041525	-3.320310
18	1	-0.877286	1.975479	-1.849822
19	6	1.678488	0.484531	-3.541853
20	1	1.931765	0.095349	-4.527636
21	1	-0.325139	1.084663	-4.125921
22	7	0.762629	1.978194	0.275249
23	7	-0.406910	2.472573	0.461485
24	50	4.006119	0.822410	0.585195
25	6	5.362716	-0.269797	-0.748775
26	1	6.254159	-0.569115	-0.184700
27	1	4.887005	-1.171349	-1.156602
28	1	5.682198	0.354263	-1.594636
29	6	2.619352	-0.445504	1.715610
30	1	2.135409	0.138206	2.510157
31	1	1.837297	-0.864097	1.073423
32	1	3.182689	-1.260008	2.191717
33	6	5.475384	0.830688	2.308413
34	1	5.737275	-0.194418	2.616677
35	1	6.405979	1.349246	2.025834
36	1	5.060322	1.348781	3.188435
37	6	4.046467	3.011350	0.432156
38	1	4.143552	3.311979	-0.619425
39	1	3.099877	3.419967	0.806596
40	1	4.878406	3.432051	1.010683

E = -734.9970561
E_{ZPE} = -734.672766
H = -734.649037
G = -734.726949
PCM = -735.0540134

Transition States

Transition state to form the *para*-lithiated azobenzene[10]

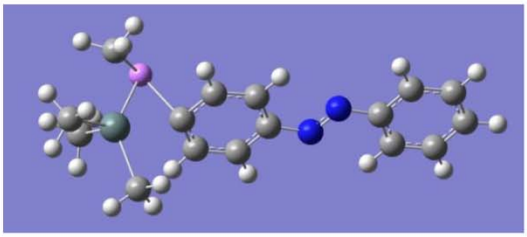

Coordinates

Center	Atomic Number	x	y	z
1	6	1.253374	2.315216	0.218531
2	6	0.012861	2.976913	0.250720
3	6	1.300017	0.929050	-0.003758
4	6	-1.160885	2.244029	0.054021
5	1	-0.005448	4.045693	0.430590
6	6	0.115150	0.209773	-0.185305
7	6	-1.155916	0.839067	-0.167616
8	1	-2.112289	2.773509	0.084172
9	1	0.179190	-0.866729	-0.334397
10	50	-3.142272	-0.467595	0.105576
11	6	-2.643195	-1.918538	-1.454998
12	1	-2.095592	-2.761300	-1.017659
13	1	-3.565687	-2.301576	-1.905358
14	1	-2.008332	-1.541999	-2.277337
15	6	-4.110168	1.182100	-1.404974
16	1	-4.654583	1.757716	-0.646103
17	1	-3.697010	1.967463	-2.079981
18	1	-4.861683	0.625855	-1.982047
19	6	-5.221432	-0.764911	0.702914
20	1	-5.901031	-0.770091	-0.155416
21	1	-5.308939	-1.719796	1.235665
22	1	-5.541822	0.031264	1.387207
23	6	-2.273298	-1.089159	2.013441
24	1	-2.319198	-0.264417	2.735684
25	1	-2.843374	-1.932883	2.421215
26	1	-1.223337	-1.378416	1.901763
27	3	-2.165534	0.688737	-1.964825
28	7	2.515028	2.951351	0.398610
29	7	2.477724	4.212160	0.607529
30	6	3.739808	4.846712	0.791481
31	6	4.978317	4.178457	0.757106
32	6	3.691131	6.230818	1.020220
33	6	6.153999	4.901237	0.951492
34	1	4.990194	3.110049	0.580089
35	6	4.873153	6.949569	1.214363
36	1	2.720095	6.712738	1.041271
37	6	6.105986	6.286293	1.180294
38	1	7.111779	4.390988	0.926613
39	1	4.834638	8.019317	1.391607
40	1	7.025980	6.842167	1.331341
41	1	2.272095	0.446752	-0.023712

E = -742.4992788
E_{ZPE} = -742.171395
H = -742.147222
G = -742.226337
PCM = -742.5230986

Transition state to form the *meta*-lithiated azobenzene

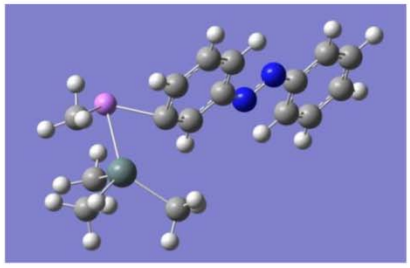

Coordinates

Center	Atomic Number	x	y	z
1	6	1.678003	-0.474587	-0.014984
2	6	0.831871	-1.558190	-0.237230
3	6	1.119243	0.778092	0.304884
4	6	-0.564275	-1.401153	-0.133988
5	1	1.251649	-2.527927	-0.490655
6	6	-0.275578	0.928902	0.379776
7	6	-1.162800	-0.153097	0.171494
8	1	-1.198260	-2.270114	-0.304232
9	1	-0.648127	1.926854	0.601848
10	50	-3.492380	0.246604	-0.198570
11	6	-3.728797	1.571960	1.529923
12	1	-3.736292	2.613421	1.187670
13	1	-4.683687	1.368678	2.027681
14	1	-2.928732	1.522134	2.290540
15	6	-3.748237	-1.814303	1.064363
16	1	-3.934560	-2.481323	0.213097
17	1	-3.073904	-2.412063	1.720371
18	1	-4.702814	-1.704323	1.596917
19	6	-5.479770	-0.254566	-0.954184
20	1	-6.142787	-0.613143	-0.160028
21	1	-5.922591	0.635599	-1.417471
22	1	-5.413927	-1.035314	-1.722865
23	6	-2.862785	1.389312	-1.951042
24	1	-2.516780	0.709945	-2.740260
25	1	-3.708826	1.966341	-2.343808
26	1	-2.038789	2.068617	-1.709373
27	3	-2.257801	-0.587599	1.876152
28	1	2.755372	-0.567860	-0.077649
29	7	1.880825	1.953607	0.569532
30	7	3.150594	1.820038	0.510638
31	6	3.910406	2.996742	0.773129
32	6	3.351550	4.256020	1.061790
33	6	5.304149	2.836922	0.728057
34	6	4.192341	5.341015	1.303722
35	1	2.273358	4.354976	1.088480
36	6	6.141498	3.928166	0.972230
37	1	5.699950	1.853348	0.501031
38	6	5.587179	5.181425	1.260458
39	1	3.766918	6.314689	1.525747
40	1	7.218808	3.803794	0.937583
41	1	6.235325	6.031303	1.449731

E = -742.4995674
E_{ZPE}= -742.171673
H= -742.147516
G= -742.226511
PCM = -742.5231702

Transition state to form the *ortho*-lithiated azobenzene

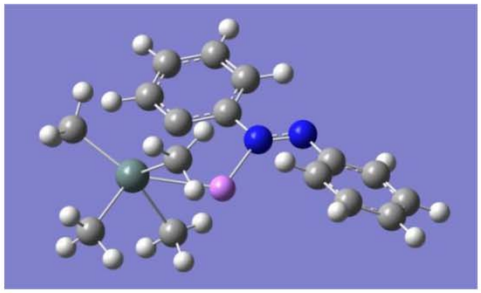

Coordinates

Center	Atomic Number	x	y	z
1	6	-4.350719	-1.652248	-0.677852
2	6	-3.271397	-0.764424	-0.703181
3	6	-3.387176	0.496851	-0.082707
4	6	-4.600831	0.870171	0.519616
5	6	-5.668546	-0.028450	0.552847
6	6	-5.545752	-1.292968	-0.039923
7	1	-4.267771	-2.614093	-1.173798
8	1	-2.376541	-1.012835	-1.266242
9	1	-4.676085	1.856906	0.962048
10	1	-6.598437	0.257669	1.032837
11	1	-6.381353	-1.984616	-0.023893
12	6	-0.048690	1.883738	-0.050034
13	6	1.251029	1.293251	0.044325
14	6	-0.276817	3.280840	-0.114046
15	6	2.301697	2.242548	0.123464
16	1	3.323330	1.891720	0.216300
17	6	0.799137	4.151676	-0.048748
18	1	-1.293709	3.645327	-0.202371
19	6	2.096802	3.625247	0.084243
20	1	2.946740	4.299699	0.151920
21	1	0.641795	5.224595	-0.093808
22	7	-1.151343	0.988258	-0.043739
23	7	-2.343784	1.461800	-0.056978
24	50	2.061660	-1.082705	0.108982
25	6	3.960233	-0.372386	-0.680792
26	1	4.442847	-1.243725	-1.137226
27	1	3.832509	0.410893	-1.432664
28	1	4.625864	0.000816	0.106600
29	6	0.598912	-1.720944	-1.425776
30	1	-0.065845	-2.538713	-1.097746
31	1	0.016784	-0.920454	-1.900322
32	1	1.220610	-2.161325	-2.214029
33	6	2.838823	-3.095556	0.577169
34	1	3.353776	-3.525132	-0.292820
35	1	3.562874	-3.053733	1.402939
36	1	2.035324	-3.783044	0.873116
37	6	0.856793	-1.165387	2.031010
38	1	0.196456	-0.323376	2.297789
39	1	0.336501	-2.129017	2.166383
40	1	1.646494	-1.155207	2.792181
41	3	-0.499133	-0.787676	0.356219

E = -742.5199952
E_{ZPE} = -742.191098
H = -742.167650
G = -742.243692
PCM = -742.5340509

Lithiated Products

para-Lithiated azobenzene

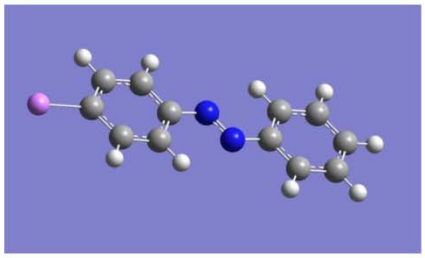

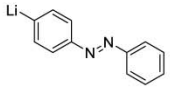

Coordinates

Center	Atomic Number	x	y	z
1	6	-0.191061	2.902507	4.266071
2	6	0.192056	2.483323	2.992707
3	6	-0.624838	2.782454	1.886227
4	6	-1.817748	3.499132	2.069195
5	6	-2.196735	3.916695	3.347557
6	6	-1.384558	3.619523	4.448995
7	1	0.437431	2.672975	5.121317
8	1	1.107821	1.929195	2.826846
9	1	-2.423837	3.712889	1.195766
10	1	-3.119891	4.470714	3.485287
11	1	-1.676659	3.942804	5.443383
12	6	1.065489	1.366223	-0.951147
13	6	2.262891	0.650771	-1.115019
14	6	0.268515	1.650016	-2.077040
15	6	2.655590	0.226192	-2.387600
16	6	0.681849	1.215678	-3.336170
17	1	-0.653836	2.203210	-1.937504
18	6	1.888815	0.485658	-3.557552
19	1	0.038423	1.454467	-4.183730
20	7	0.755624	1.751861	0.378195
21	7	-0.333676	2.405214	0.541533
22	1	2.859315	0.444932	-0.230898
23	1	3.592315	-0.325831	-2.466788
24	3	2.450814	-0.118571	-5.349715

E = -579.5023179
E_{ZPE} = -579.320692
H = -579.307621
G = -579.360624
PCM = -579.5481634

meta-Lithiated azobenzene

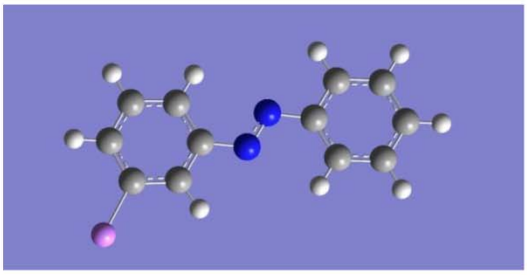

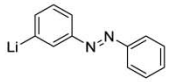

Coordinates

Center	Atomic Number	x	y	z
1	6	-0.186381	2.894145	4.260280
2	6	0.197994	2.482786	2.984678
3	6	-0.624088	2.777511	1.881136
4	6	-1.823360	3.481970	2.068786
5	6	-2.203590	3.892000	3.349330
6	6	-1.386253	3.599150	4.448012
7	1	0.445970	2.667927	5.113619
8	1	1.118666	1.937977	2.814878
9	1	-2.433455	3.692531	1.197374
10	1	-3.131761	4.436596	3.490677
11	1	-1.679390	3.916401	5.444038
12	6	1.072002	1.386285	-0.969597
13	6	2.278220	0.681126	-1.138271
14	6	0.259254	1.673444	-2.082569
15	6	2.739887	0.227842	-2.400280
16	6	0.674415	1.246898	-3.341000
17	1	-0.666336	2.217134	-1.935640
18	6	1.884655	0.542480	-3.490471
19	1	2.161109	0.232188	-4.498769
20	1	0.059208	1.459857	-4.212336
21	7	0.762317	1.764953	0.365315
22	7	-0.331897	2.406932	0.534198
23	1	2.847578	0.500092	-0.227404
24	3	4.438117	-0.755947	-2.568751

E = -579.5021988
E_{ZPE} = -579.320526
H = -579.307463
G = -579.360407
PCM = -579.5474803

ortho-Lithiated azobenzene

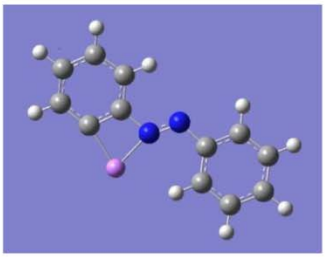

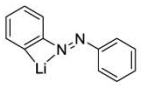

Coordinates

Center	Atomic Number	x	y	z
1	6	-0.280789	2.643989	4.280538
2	6	0.071812	2.212607	3.000729
3	6	-0.596788	2.731612	1.875478
4	6	-1.635553	3.661756	2.052981
5	6	-1.975748	4.099073	3.334174
6	6	-1.298431	3.593603	4.451796
7	1	0.226472	2.231916	5.147382
8	1	0.830368	1.448114	2.871122
9	1	-2.149941	4.027718	1.171680
10	1	-2.771174	4.825626	3.463306
11	1	-1.570130	3.924015	5.449017
12	6	1.120795	1.405038	-1.033197
13	6	2.468706	0.949844	-1.154156
14	6	0.179635	1.421661	-2.088204
15	6	2.821890	0.498087	-2.447725
16	1	3.830897	0.134238	-2.630084
17	6	0.590811	0.963328	-3.332297
18	1	-0.828808	1.781830	-1.916235
19	6	1.914085	0.501357	-3.511338
20	1	2.222269	0.144342	-4.491448
21	1	-0.102265	0.956779	-4.168222
22	7	0.815717	1.847635	0.287565
23	7	-0.333066	2.354802	0.529821
24	3	2.700864	1.399255	0.757575

E = -579.5322215
E_{ZPE} = -579.349766
H = -579.337247
G = -579.388534
PCM = -579.5597994

Scans

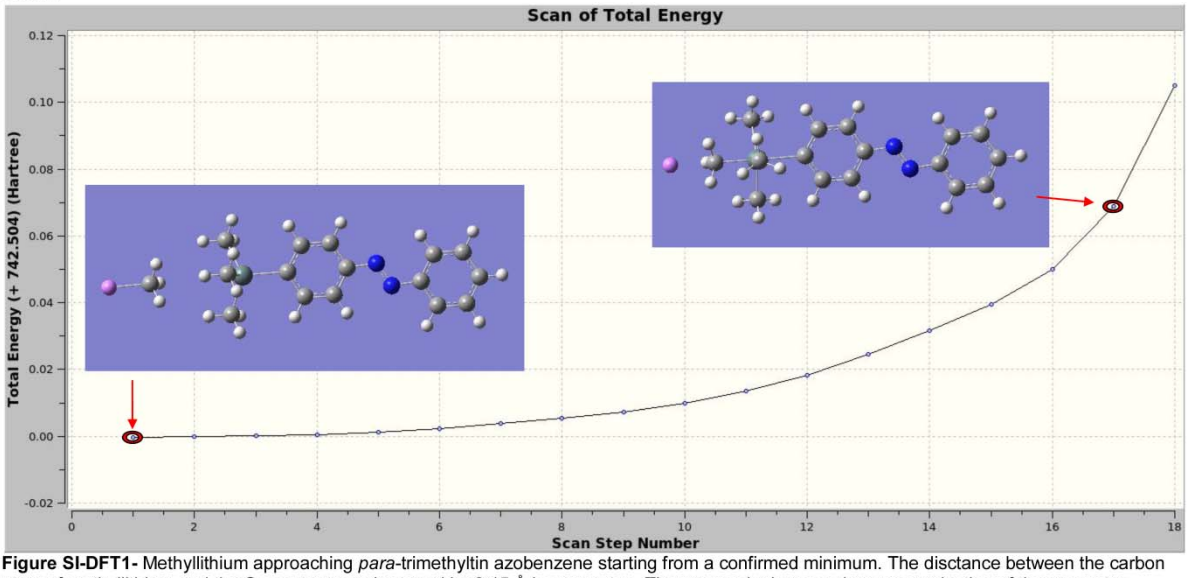

Figure SI-DFT1- Methyllithium approaching *para*-trimethyltin azobenzene starting from a confirmed minimum. The disctance between the carbon atom of methyllithium and the Sn center was shortened by 0.15 Å in every step. The approach shows a clear reorganisation of the geometry around the Sn atom towards a trigonal bipyramid. The energy rises steadily and no transition state could be found.

SI-DFT-13

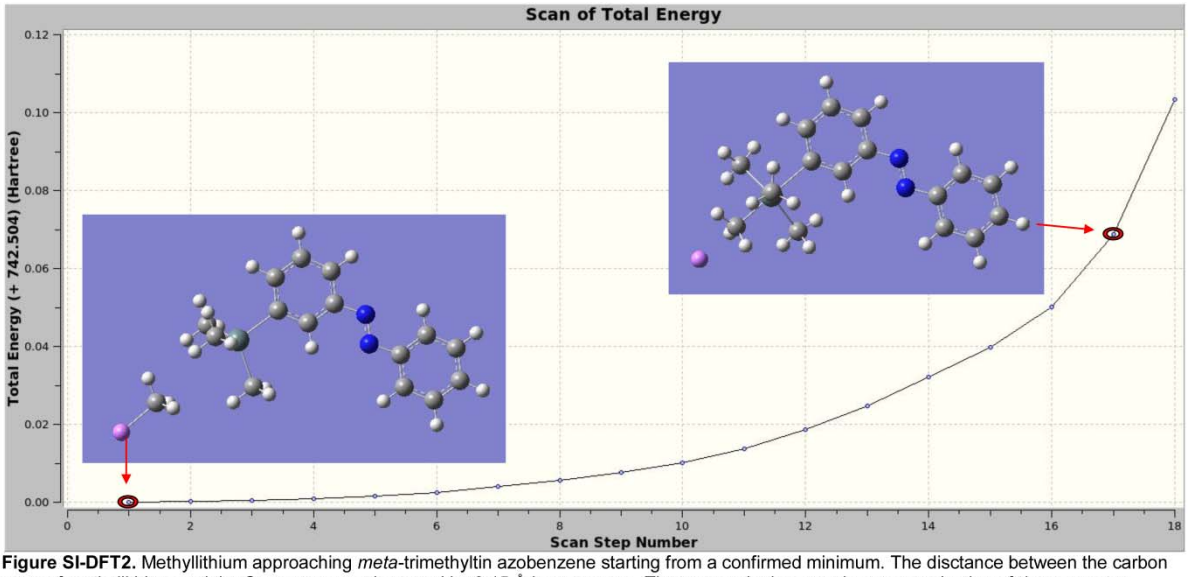

Figure SI-DFT2. Methyllithium approaching *meta*-trimethyltin azobenzene starting from a confirmed minimum. The disctance between the carbon atom of methyllithium and the Sn center was shortened by 0.15 Å in every step. The approach shows a clear reorganisation of the geometry around the Sn atom towards a trigonal bipyramid. The energy rises steadily and no transition state could be found.

SI-DFT-14

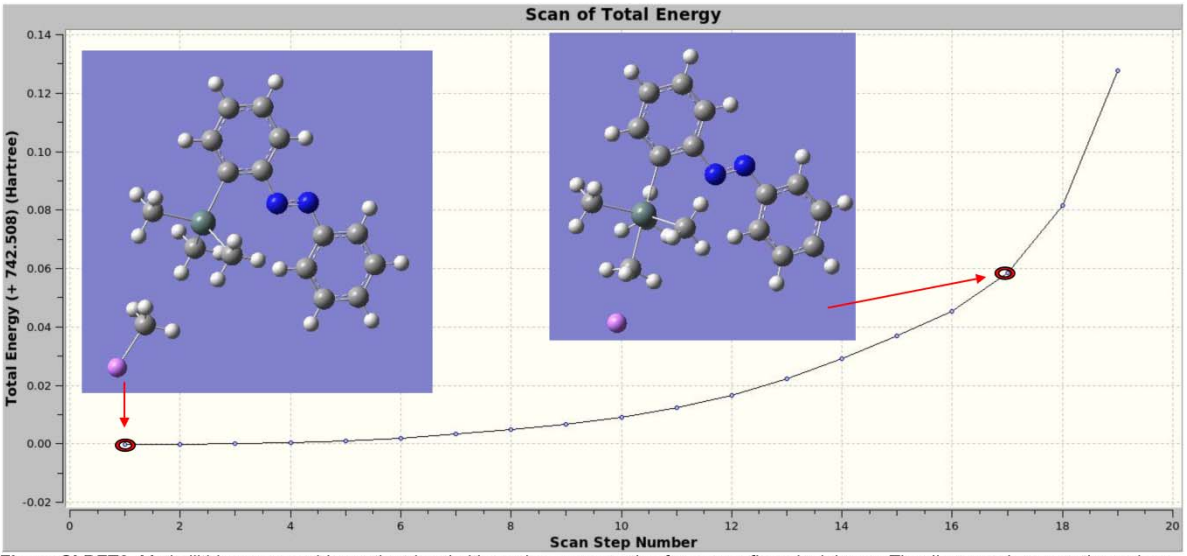

Figure SI-DFT3. Methyllithium approaching *ortho*-trimethyltin azobenzene starting from a confirmed minimum. The disctance between the carbon atom of methyllithium and the Sn center was shortened by 0.15 Å in every step. The approach shows a clear reorganisation of the geometry around the Sn atom towards a trigonal bipyramid. The energy rises steadily and no transition state could be found.

References

[1] M. Saito, S. Imaizumi, T. Tajima, K. Ishimura, S. Nagase, *J. Am. Chem. Soc.* **2007**, *129*, 10975.

[2] a) A. D. Becke, *J. Chem. Phys.* **1993**, *98*, 5648; b) C. Lee, W. Yang, R. G. Parr, *Phys. Rev. B* **1988**, *37*, 785.

[3] Gaussian 09, Revision D.01, M. J. Frisch, G. W. Trucks, H. B. Schlegel, G. E. Scuseria, M. A. Robb, J. R. Cheeseman, G. Scalmani, V. Barone, B. Mennucci, G. A. Petersson, H. Nakatsuji, M. Caricato, X. Li, H. P. Hratchian, A. F. Izmaylov, J. Bloino, G. Zheng, J. L. Sonnenberg, M. Hada, M. Ehara, K. Toyota, R. Fukuda, J. Hasegawa, M. Ishida, T. Nakajima, Y. Honda, O. Kitao, H. Nakai, T. Vreven, J. A. Montgomery, Jr., J. E. Peralta, F. Ogliaro, M. Bearpark, J. J. Heyd, E. Brothers, K. N. Kudin, V. N. Staroverov, T. Keith, R. Kobayashi, J. Normand, K. Raghavachari, A. Rendell, J. C. Burant, S. S. Iyengar, J. Tomasi, M. Cossi, N. Rega, J. M. Millam, M. Klene, J. E. Knox, J. B. Cross, V. Bakken, C. Adamo, J. Jaramillo, R. Gomperts, R. E. Stratmann, O. Yazyev, A. J. Austin, R. Cammi, C. Pomelli, J. W. Ochterski, R. L. Martin, K. Morokuma, V. G. Zakrzewski, G. A. Voth, P. Salvador, J. J. Dannenberg, S. Dapprich, A. D. Daniels, O. Farkas, J. B. Foresman, J. V. Ortiz, J. Cioslowski, and D. J. Fox, Gaussian, Inc., Wallingford CT, 2013.

[4] Gaussian, Inc. 340 Quinnipiac St Bldg 40, Wallingford, CT 06492 USA, Copyright 2000-2008 Semichem. Inc. Authors: R. D. Dennington II, T. A. Keith, J. M. Millan.

[5] a) W. R. Wadt, P. J. Hay, *J. Chem. Phys.* **1985**, *82*, 284; b) C. E. Check, T. O. Faust, J. M. Bailey, B. J. Wright, T. M. Gilbert, L. S. Sunderlin, *J. Phys. Chem. A* **2001**, *105*, 8111.

[6] a) W. J. Hehre, R. Ditchfield, J. A. Pople, *J. Chem. Phys.* **1972**, *56*, 2257; b) P. Hariharan, J. A. Pople, *Theor. Chim. Acta* **1973**, *28*, 213; c) R. Ditchfield, W. J. Hehre, J. A. Pople, *J. Chem. Phys.* **1971**, *54*, 724.

[7] A. E. Reed, L. A. Curtiss, F. Weinhold, *Chem. Rev.* **1988**, *88*, 899.

[8] NBO Version 3.1, E. D. Glendening, A. E. Reed, J. E. Carpenter, and F. Weinhold.

[9] a) S. Miertuš, J.Tomasi, *J. Chem. Phys.* **1982**, *65*, 239; b) E. Cancès, B. Mennucci, J.Tomasi, *J. Chem. Phys.* **1997**, *107*, 3032; c) M.Cossi, V. Barone, B. Mennucci, J. Tomasi, *J. Chem. Phys. Lett.* **1998**, *286*, 253; d) B. Mennucci, J. Tomasi, *J. Chem. Phys.* **1997**, *106*, 5151.

[10] Optimization completed on the basis of negligible forces.

4.3 Unpublished Results: Exactly Alternating Azobenzene-Siloxane Copolymers

General Methods and Materials

All preparations for the stannylation reactions were performed in a nitrogen filled glovebox and carried out in a sealed vial under nitrogen. All reagents and solvents for the lithiation reactions were stored in a nitrogen filled glovebox. Solutions of starting materials and solutions of methyl lithium were prepared in the glovebox. All other oxygen and water sensitive reactions were carried out using standard Schlenk techniques under an argon atmosphere. Schlenk Glassware was flame dried prior to use. The water and oxygen concentration in the glovebox was always below 1 ppm. Argon of the grade “N46” was dried by passing it through a column with a diameter of 5 cm and a length of 40 cm filled with activated 3 Å molecular sieves. Molecular sieves were activated by heating at 300 °C and at a reduced pressure of 0.05 mbar. The activated molecular sieves were stored in a nitrogen filled glovebox. As cooling bath for low temperature reactions, a mixture of acetone and dry ice was used.

Analyses

^{1}H NMR, ^{13}C NMR, ^{119}Sn NMR spectra were recorded at 300 K. ^{1}H NMR spectra were recorded on a Bruker DRX 500 (500 MHz) spectrometer or a Bruker Avance 600 (600 MHz). ^{13}C NMR spectra were recorded on a Bruker DRX 500 (126 MHz) spectrometer or a Bruker Avance 600 (151 MHz) spectrometer. ^{119}Sn NMR spectra were recorded on a Bruker DRX 500 (187 MHz) spectrometer. All ^{1}H NMR and ^{13}C NMR spectra were referenced against the solvent residual proton signals (^{1}H) or the solvent itself (^{13}C). ^{119}Sn and ^{29}Si NMR spectra were referenced externally against TMS.

The exact assignment of the peaks was performed by two-dimensional NMR spectroscopy such as ^{1}H COSY, ^{1}H/^{13}C HSQC or ^{1}H/^{13}C HMBC when possible.

Ultra high resolution ESI mass spectra were recorded on a Bruker Daltonics Apex IV Fourier transform Ion Cyclotron resonance mass spectrometer. High-resolution accurate-mass EI

mass spectra were recorded on a Jeol AccuTOF JMS-T100GCV mass spectrometer. CI spectra were recorded on a VG Analytical Autospec apparatus with isobutane as ionisation gas. IR spectra were recorded on a Perkin Elmer Paragon 1000 FT-IR spectrometer with an A531-G Golden-Gate-ATR-unit. All melting points were recorded on an electrothermal melting point apparatus LG 1586 and are uncorrected. Analytical gel permeation chromatography was performed on a Viscotek GPCMax VE2001 with a refractive index detector (using chloroform as an eluent and a flow rate of 1 mL/min) and the calibration was done with polystyrene standards. Dynamic scanning calorimetry (DSC) was performed in a Perkin Elmer Pyris apparatus with a heating / cooling rate of 10 K/min. X-ray diffraction was performed on a STOE Stadi P transmission diffractometer. Tensile tests were performed on a "quickTest QTS 3" by Prüfpartner GmbH. The Differential thermal analysis – Thermogravimetry (DTA-TG) measurements were performed in a nitrogen atmosphere in Al_2O_3 crucibles using a STA-409CD instrument from Netzsch. The measurements were performed with a flow rate of 75 $mL \times min^{-1}$ and were corrected for buoyancy and current effects. CHNS analysis was performed on a EURO EA elemental analyzer by EURO VECTOR Intruments.

Optical Equipment

For the UV irradiation of NMR tubes and for irradiating solutions for the preparation of films at the photostationary equilibrium, a circular aligned lamp consisting of nine high power UV-LED with 300 mW each by “Sahlmann Photochemichal Solutions” was used (Figure 20, a). For irradiation of polymer films, a Honle LED Power Pen with 500 mW was used. For irradiation with 450 nm, an individually designed LED pen by “Sahlmann Photochemichal Solutions” was used. The LED used in this device is a Luxeon LXML-PR01 with a total optical power of 900 mW with a peak wavelength of 443 nm (Figure 20, b). The emission power at 450 nm was measured with 80% of the peak intensity using an Ocean Optics USB 4000 spectrometer.

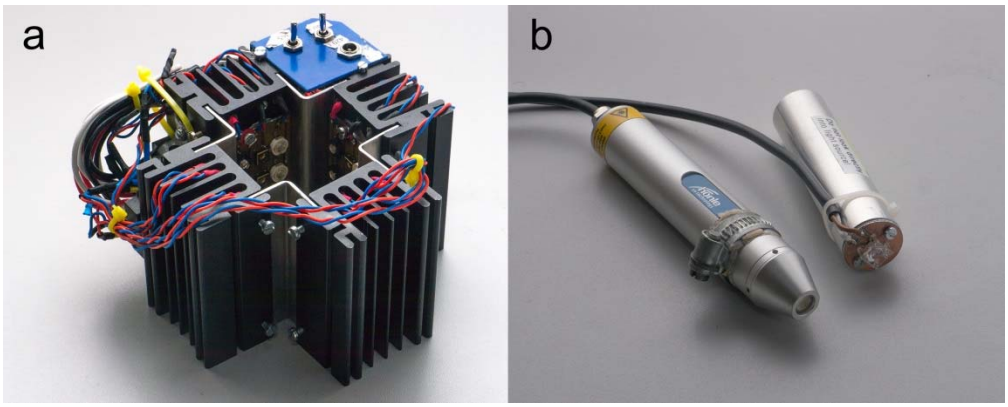

Figure 22. a) Circular aligned LEDs for irradiation of NMR tubes and UV cuvettes; b) LED Pens

Reagents

If not otherwise noted, all reagents were used as received.

Reagent	Supplier	Purity	Additional Purification
Copper (I) Chloride	Merck AG	99.8%	
Dimethyldichlorosilane	ABCR Inc.	99%	Degassed and freshly distilled from calcium hydride
Dichloroethenylmethylsilane	ABCR Inc.	99%	Degassed and freshly distilled from calcium hydride
Hexamethyldistannane	Sigma-Aldrich	98%	
3-Iodoaniline	ABCR Inc.	99%	
4-Iodoaniline	ABCR Inc.	99%	
Magnesium sulfate	Grüssing GmbH	99.9%	
Methyl lithium (1.6 M in diethylether)	Acros Organics		Titration gave 1.60 M[69]
Monopotassium phosphate	Sigma-Aldrich Inc.	99.7%	
Potassium Hydroxide	Grüssing Inc.	99%	
Phenyl Isocyanate	Alfa-Aesar Inc.	99%	Degassed and dried over 3 Å molecular sieves for 7 d
Pyrrolidine	Merck AG	99%	Degassed and dried over 3 Å molecular sieves for 7 d
Sodium methoxide	TCI Inc.	99%	
Tetrakis(triphenylphosphine)palladium(0)	Sigma-Aldrich Inc.	> 98%	

Solvents

All solvents were freshly distilled, if used for purification. Where noted, solvents were dried over the specified drying agent by refluxing for several hours before distillation. Dry solvents were degassed by three freeze-pump-thaw cycles and stored in a nitrogen filled glove box over 3 Å molecular sieves. The water contamination of diethyl ether, THF and toluene was less than 5 ppm and was determined by Karl Fischer titration on a "Mettler-Toledo C20 Coulometric KF Titrator" with "Hydranal - Coulomat AD" by Fluka.

Solvent	Supplier; drying procedure
Chloroform	BCD; -
Chloroform-d_1	Predried over a column of aluminum oxide and dried over molecular sieves 3 Å for 7d
DCM	BCD;-
Diethylether	Merck-Polaro, dried and degassed with an PS-MD-5 by Innovation Technology.
Methanol	BCD; (for synthesis: distilled from sodium, stored over sieves 3 Å)
Pyridine	Sigma Aldrich (purity: 99.9%, used as received)
THF	Merck-Polaro, dried and degassed with an PS-MD-5 by Innovation Technology.
Toluene	BCD; distilled from sodium with benzophenone as indicator.

Synthetic and Purification Equipment

All microwave syntheses were performed on a CEM Discover Explorer. Column-chromatography of tin functionalized azobenzenes was performed manually using Merck Silica Gel 60 (15 – 40 μm). Thin layer chromatography (TLC) was performed with pre-coated TLC-sheets from Macherey-Nagel GmbH & Co. KG with silica 60 and fluorescent indicator UV254.

Photochemical Properties

The photostationary equilibrium and half-life of the *cis*-state of the linear polymers were determined by ^{1}H NMR spectroscopy. 15 mg of the polymer were dissolved in 550 µL chloroform-d_1 and irradiated with a 365 nm high power LED (circular aligned lamp, see optical equipment) for 3 h. The NMR tube was then directly transferred to the NMR spectrometer while it was protected from ambient light. Every 30 min, a ^{1}H NMR spectrum was recorded until all azobenzene units were completely switched to the *trans*-isomer. The photostationary equilibrium was determined by the ratio of the integrals of *cis* and *trans*-signals with the of the aromatic *cis* and *trans* specific signals. The half-life was determined by the change of the ratio over the time.

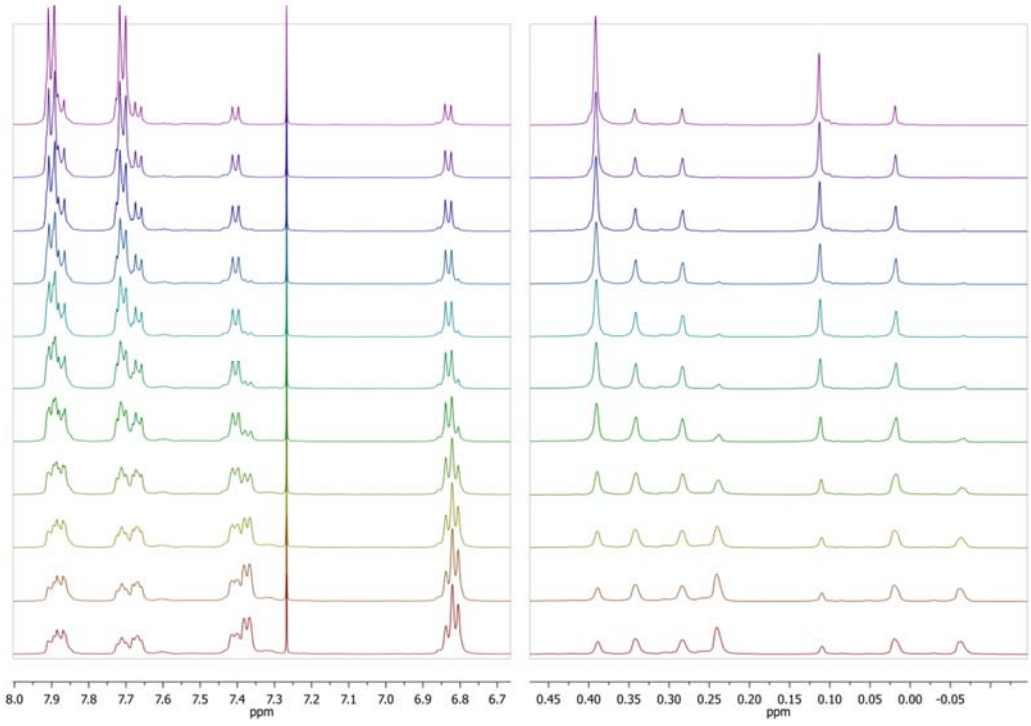

Figure 23. ^{1}H NMR-Spectra of polymer **1** and at the photostationary equilibrium (bottom) and the back switching over the course of 6 d. Because of the high intensities of the methyl protons, the intensities of the aromatic and alkyl region of the NMR spectrum were adjusted for plotting purposes.

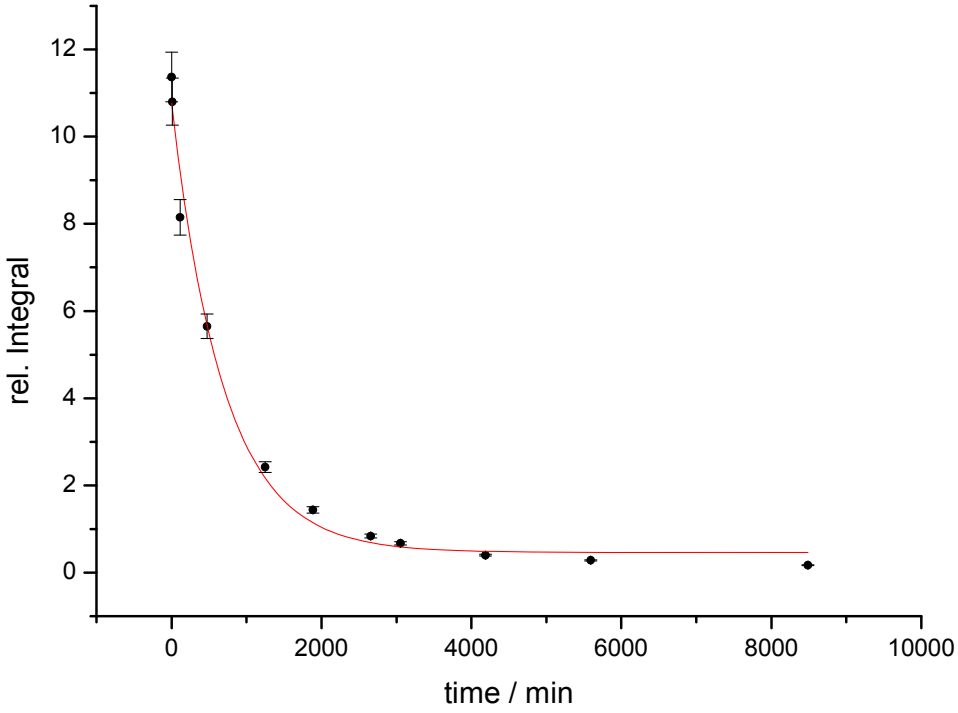

Figure 24. The half life was determined from the change of the integral of the signal at 0.24 ppm which does not overlap with a *trans* signal. The half-life was determined with 481 min. The data points were fitted using an exponential fit: $y = y_0 + A*\exp(R_0*x)$ with $y_0 = 0.46231$; $A = 10.29925$; $R_0 = 0.00144$. The fit correlates to $R^2 = 0.9882$.

For the solid state UV spectra, polymers were casted onto a quartz glass slide with chloroform as a solvent. For the determination of the half-life in solid state, a solution of the polymer **1** (1 mg/mL) was irradiated with UV light (365 nm) for 3 h and casted on a quartz glass slide. Over the course of 14 h, UV/vis spectra were recorded every 10 min. The change of the relative intensity at 330 nm was used to determine the half life time.

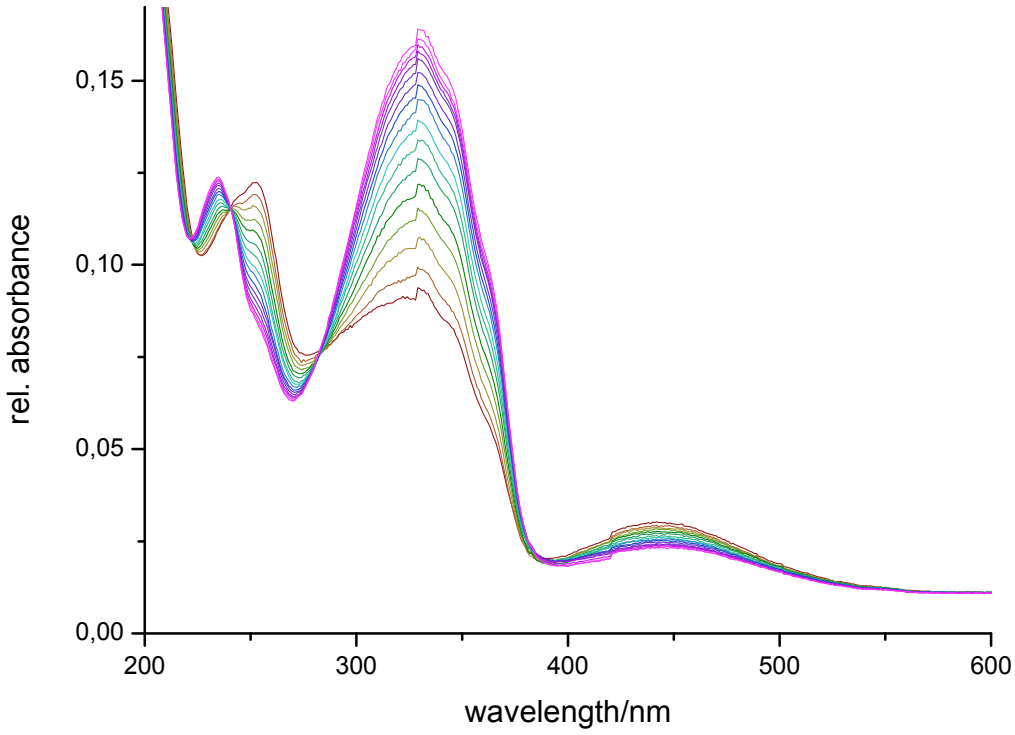

Figure 25. UV Spectra of a polymer film (**1**) over the course of 14 h. Spectra were recorded every 10 min. Only one spectrum per hour is displayed. The artifact at 327 nm is due to the change to the deuterium lamp in the spectrometer.

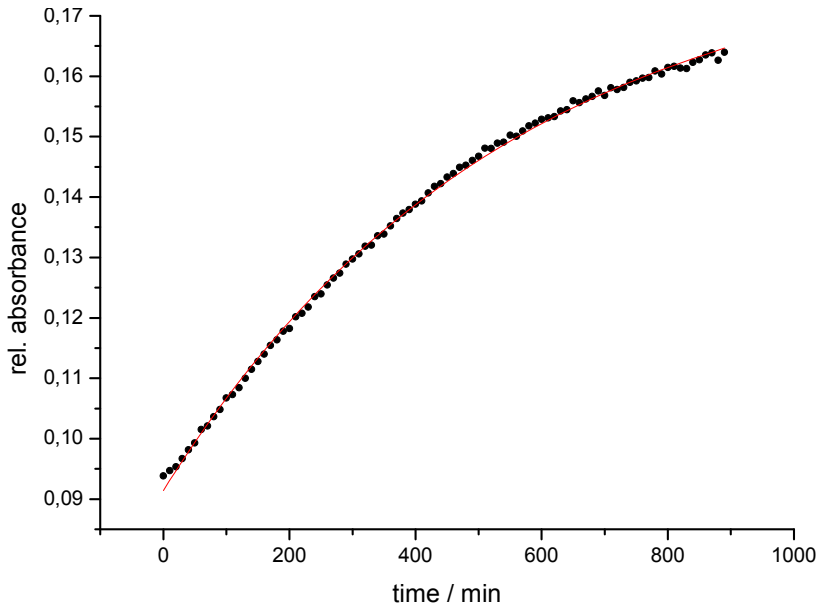

Figure 24. Half life time over the course of 14 h for the spin coated film. Every 10 min, a spectrum was recorded. The half life of the bulk material was determined to be 377 min. The relative absorbance at 330 nm was used for the determination of the half-life. The data points were fitted using an exponential fit: $y = y_0 + A*\exp(R_0*x)$ with y_0=0.0.18241; A = -0.9098; R_0 = -0.00184. The fit correlates to R^2 = 0.99896.

DSC and DTA-TG

The DSC was measured in three cycles from -40 °C to 80 °C at a heating rate of 10 K/min. The DSC gave following values:

Glass transition temperature T_g = 22.67 °C

Extrapolated onset temperature T_{gO}^{E} = 20.09 °C

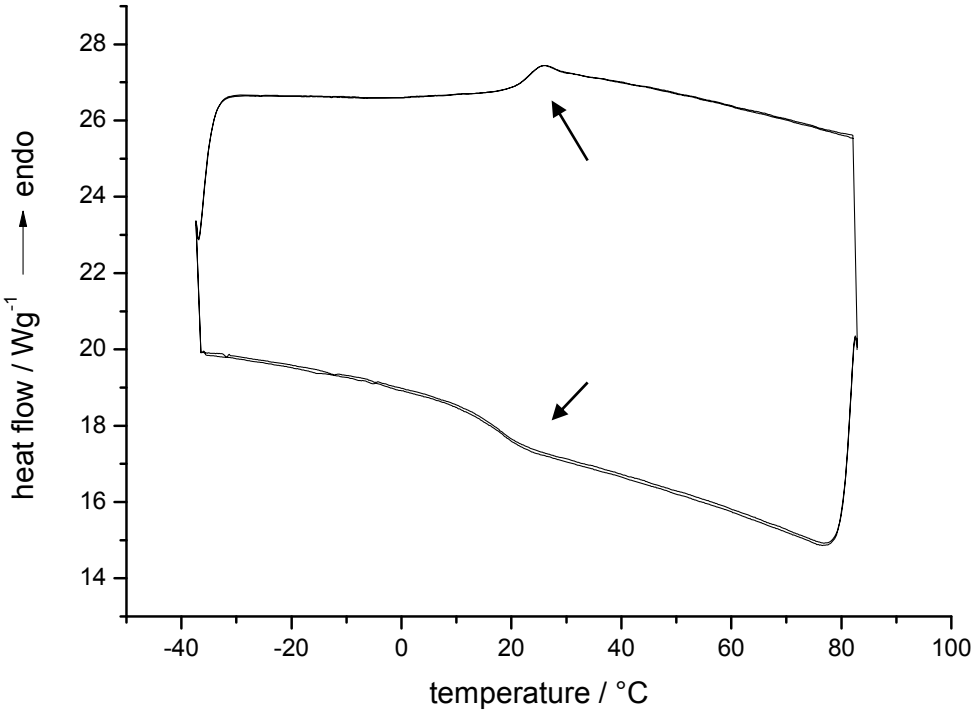

Figure 26. DSC of polymer **1**. Three cycles were performed at a heating rate of 10 °C in a temperature range of -40°C to 80°C. The glass transition temperature was determined as T_g = 22.67 °C; T_{gO}^{E} = 20.09 °C.

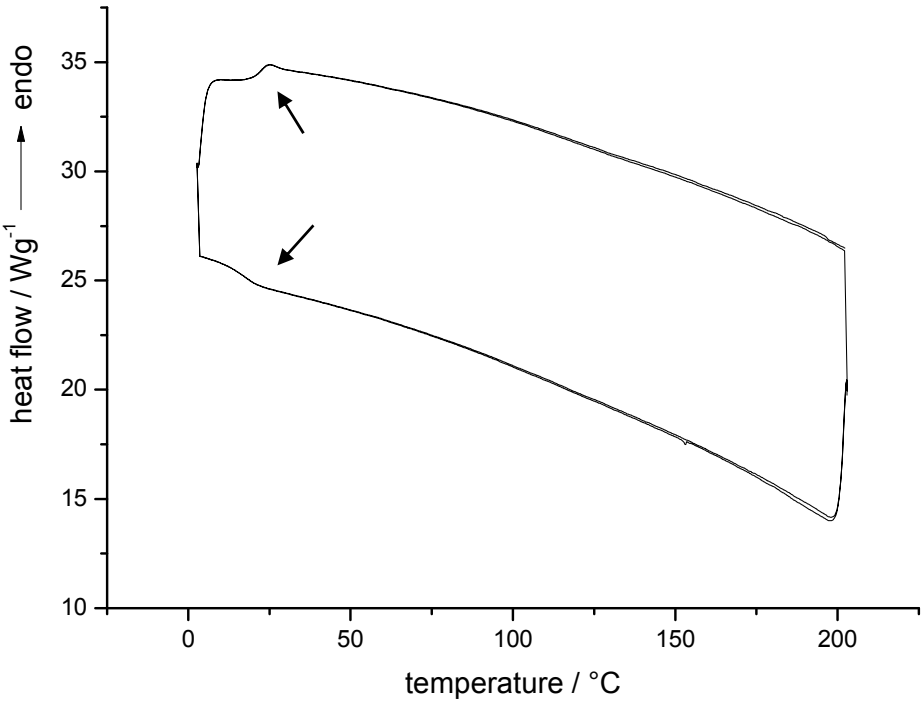

Figure 27. DSC of polymer **1**. Three cycles were performed at a heating rate of 10 °C in a temperature range of 0 °C to 200 °C. Besides the glass transition temperature at 23 °C, no further phase transition could be observed.

The thermal stability of the material was determined by differential thermal analysis and thermogravimetry (DTA-TG). The initial degradation temperature of 419 °C was found (Figure 27 and 28)

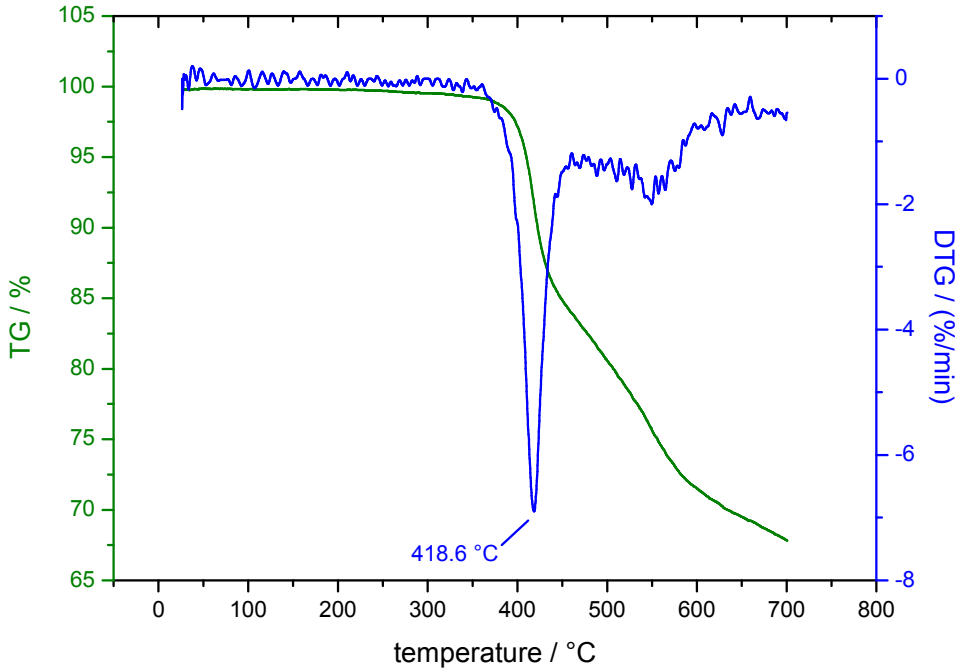

Figure 28. Thermogravimetry of **1** (green) and DTG of **1**. A degradation temperature of 418.6 °C could be determined.

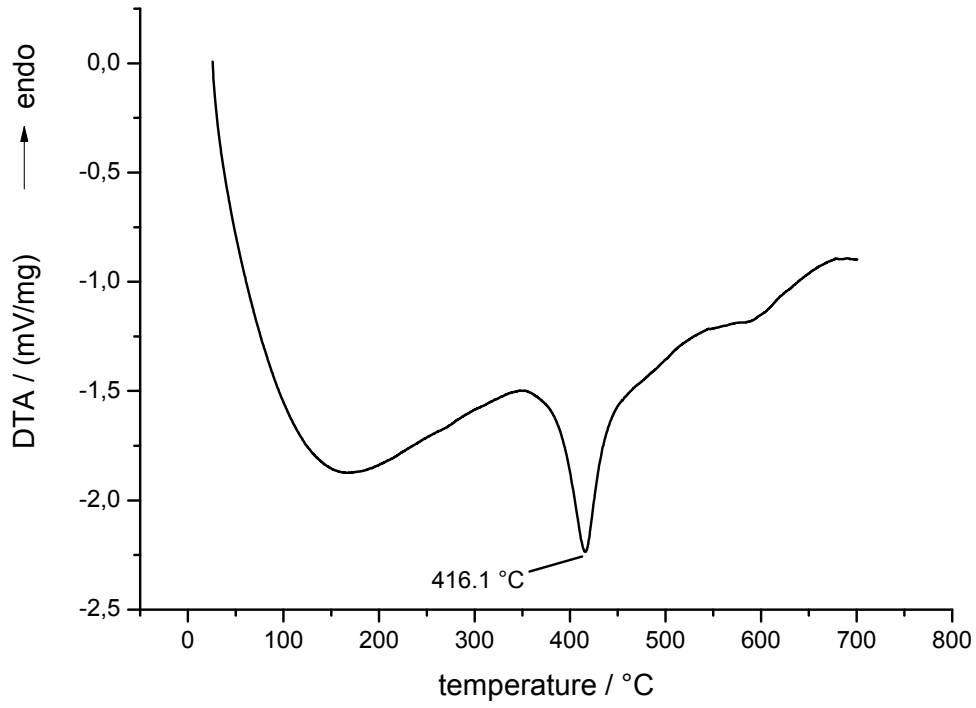

Figure 29. Differential thermal analysis of **1**. An exothermic event at 416.1 °C could be observed. This is initially the degradation temperature.

Tensile Tests

A solution of 34.1 mg poly(azobenzene-tri(dimethylsiloxane)) (**1**) in 0.5 mL chloroform was put in a PTFE mold (20 mm x 0.5 mm). The sample was dried at 20 °C for 1 d. The material was cooled to -20 °C for 1 h. The rigid polymer film was removed from the mold by the help of a razor blade. The material was dried at 4 x 10^{-3} mbar for 2 d. The polymer film was cut into a piece with the dimensions of width x thickness x length = 3.90 mm x 1.98 mm x 19.93 mm. Both ends of the polymer film were clamped into the tensile testing device. The length of the polymer film which was actually stretched was 11.35 mm. The polymer was stretched at 22 °C with a speed of 20 mm/min. The polymer was stretched to a length of 23.9 mm until the material failure.

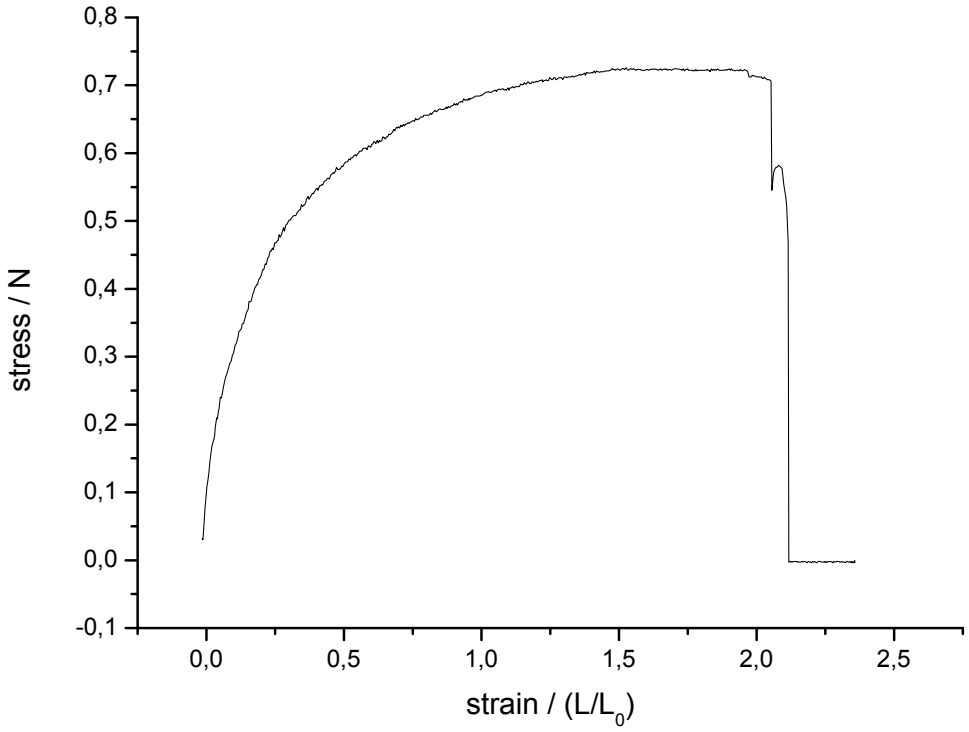

Figure 30. Stress/strain curve of poly(azobenzene-tri(dimethylsiloxane)) for a film of polymer **1** with the dimensions width x thickness x length = 3.90 mm x 1.98 mm x 19.93 mm. Due to the fixation of the film, the streched length was 11.35 mm.

X-Ray Diffraction

X-ray data of the polymer show reflections at very small angles which indicate a certain order within the system. For the preparation of the film, 10 mg of the polymer **1** were dissolved in 2 mL of chloroform. The solvent was evaporated at 20 °C in a PTFE mold for 24 h. The polymer was removed from the mold and dried for 3 d at a pressure of 0.04 mbar.

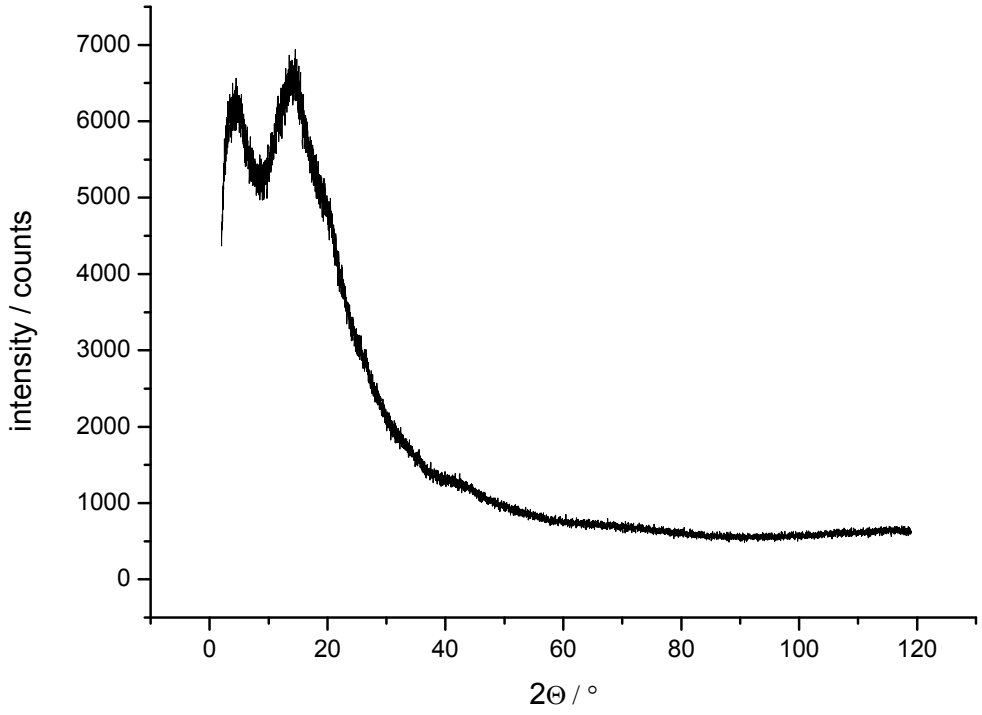

Figure 30. XRD of polymer **1**.

Preparation of Polymer Films

Polymer films for deformation experiments were produced by casting a solution of 60 mg poly(azobenzene-tri(dimethylsiloxane)) (**1**) in chloroform (1 mL) on a PTFE substrate. The sample dried for 1 d at atmospheric pressure and at a temperature of 20 °C. The sample was cooled to -20 °C for 1 h and removed by the help of a razor blade. The resulting film was then dried at 4 x 10^{-3} mbar for two days at 20 °C.

Syntheses

4,4´-*bis*(Iodo-)azobenzene[70] **(5)**

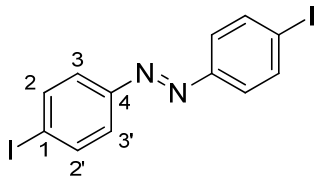

Copper (I) chloride (5.00 g, 45.7 mmol) was dissolved in pyridine (50 mL). The mixture was stirred for 30 min at 20 °C. The remaining solid was filtered off. The filtrate and 4-iodoaniline (14.3 g, 65.3 mmol) were mixed. The reaction mixture was stirred while air was bubbled through the solution with the help of a frit for 9 h at 20 °C. The solvent was evaporated. The crude product was filtered through a column of silica (eluent: dichloromethane). The product was recrystallized from methanol and dark red crystals could be obtained (9.49 g, 67%, Lit.: 87%[70]).

Mp.: T = 210 °C (Lit.: 210-211 °C)[70]

^{1}H NMR (500 MHz, $CDCl_3$): δ = 8.07 (d, ^{3}J = 8.7 Hz, 4 H, H-2, 2'), 7.79 (d, ^{3}J = 8.7 Hz, 4 H, H-3,3') ppm.

^{13}C NMR (126 MHz, $CDCl_3$): δ = 151.8 (*C-1*), 138.4 (*C-2, 2'*), 124.5 (*C-3, 3'*), 98.1 (*C-4*) ppm.

IR (ATR): ṽ = 3078 (w), 1560 (m), 1573 (m), 1469 (m), 1393 (m), 1156 (m), 1051 (m), 1001 (m), 833 (s), 539 (s) cm^{-1}.

HRMS (CI-sector*) m/z*: $[M+H]^+$ calcd for $[C_{12}H_8N_2I_2 + H]^+$ 434.8855, found 434.8848.

4,4´-*bis*(Trimethylstannyl-)azobenzene[60] (6)

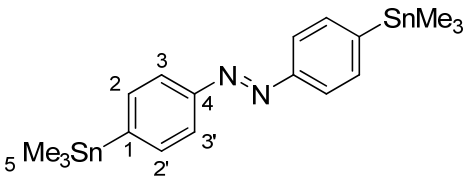

4,4´-*bis*(iodo)azobenzene (**5**, 3.00 g, 6.90 mmol), hexamethyldistannane (5.00 g, 15.3 mmol) and $Pd(PPh_3)_4$ (400 mg, 346 µmol, 4 mol%) were dissolved in toluene (15.0 mL). The reaction mixture was heated at 150 °C for 10 min in a microwave. The solvent was evaporated and the product was purified by column chromatography (eluent: *n*-hexane, R_f = 0.6). Subsequently, residual excess of hexamethyldistannane was removed *in vacuo* (3 x 10^{-2} mbar, 28 h). The product was obtained as an orange solid in a yield of 2.21 g (89%, Lit.: 81%[60]).

Mp.: T = 54.3 °C (Lit.: 54 °C)[60]

^{1}H NMR (500 MHz, $CDCl_3$): δ = 7.87 (d, ^3J = 8.2 Hz, 4 H, H-3, 3'), 7.65 (d, ^3J = 8.2 Hz, 4 H, H-2, 2'), 0.34 (s, 18 H, H-5) ppm.

^{13}C NMR (126 MHz, $CDCl_3$): δ = 152.8 (*C-4*), 147.1 (*C-1*), 136.6 (*C-2, 2'*), 122.0 (*C-3, 3'*), -9.4 (*C-5*) ppm.

^{119}Sn NMR (187 MHz, $CDCl_3$): δ = -25.20 ppm.

IR (ATR): $\tilde{\nu}$ = 3067 (w), 3024 (w), 2987 (w), 2917 (w), 1925 (w), 1437 (m), 1383 (m), 1306 (m), 1067 (m), 1011 (m), 831 (s), 761 (s), 583 (s), 508 (s) cm^{-1}.

HRMS (ESI-FTMS) *m/z*: $[M+H]^+$ calcd for $[C_{18}H_{26}N_2Sn_2 + H]^+$ 511.0213, found 511.0227.

4,4´-*bis*(Hydroxydimethylsilane-)azobenzene (2)

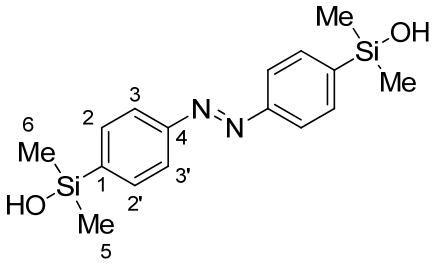

4,4´-*Bis*(trimethylstannyl-)azobenzene (**6**, 3.80 g, 7.48 mmol) was dissolved in dry THF (100 mL). A solution of methyl lithium (19.0 mmol, 12.0 mL of a 1.6 M solution in diethylether) in THF (18.0 mL) was added at -78 °C. The orange solution turned dark and was stirred 10 min. Then dichlorodimethylsilane (30.0 mL, 32.1 g, 249 mmol) was added to quench the reaction. The reaction was allowed to warm to 25 °C by removing the cooling bath. The solvent and the excess of dichlorodimethylsilane were evaporated. The residual orange solid was dissolved in diethyl ether (25 mL) and added dropwise over the course of 15 min to a solution of sodium methoxide (4.00 g, 74.0 mmol) in methanol (50 mL). Both of the latter steps were performed under inert conditions. To this mixture, a solution of sodium hydroxide (17.5 g, 435 mmol) in methanol (105 mL) and water (10 mL) was added. The resulting mixture was stirred 15 minutes and then a further portion of sodium hydroxide (17.5 g) in water (105 mL) was added. The reaction mixture was stirred 1 h. This mixture was poured into a vigorously stirred solution of monopotassium phosphate (155 g, 1.14 mol) in water (200 mL). The orange precipitate was filtered and purified by three recrystallization cycles from diethyl ether/*n*-hexane (*v/v*, 1:1). The product was isolated as a bright-orange solid in a yield of 864 mg (35%).

Mp.: T = 141 °C

^{1}H NMR (500 MHz, $CDCl_3$): δ = 7.92 (d, ^{3}J = 8.3 Hz, 4 H, H-3, 3'), 7.75 (d, ^{3}J = 8.3 Hz, 4 H, H-2, 2'), 1.99 (s, 2H, H-6), 0.46 (s, 12 H, H-5) ppm.

^{13}C NMR (126 MHz, $CDCl_3$): δ = 153.3 (*C-4*), 142.8 (*C-1*), 133.9 (*C-2,2´*), 122.1 (*C-3,3´*), 0.0 (*C-5*) ppm.

^{29}Si NMR (187 MHz, $CDCl_3$): δ = 7.77 ppm.

IR (ATR): ṽ = 3141 (m), 2956 (w), 1385 (m), 1251 (m), 1106 (w), 859 (s), 833 (s), 815 (s), 776 (s), 667 (s), 553 (s), 529 (m), 491 (m) cm^{-1}.

HRMS (EI-sector) *m/z*: $[M]^+$ calcd for $[C_{16}H_{22}N_2O_2Si_2]^+$ 330.1220, found 330.1221.

***bis*(Pyrrolidinyl)dimethylsilane[62] (10)**

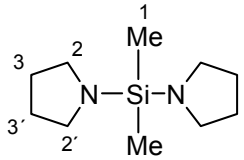

This reaction was performed entirely under inert conditions. To a solution of dichlorodimethylsilane (80.0 mL, 85.6 g, 663 mmol) in *n*-hexane (150 mL), pyrrolidine (230 mL, 196 g, 2.76 mmol) was added dropwise over the course of 1 h at 0 °C. After completion of the addition the ice bath was removed and the reaction was stirred for 15 h. A precipitate of the amino hydrochloride which had formed, was removed by filtration. The liquid was placed in a J. Young's flask and the remaining solvent was removed *in vacuo*. A colorless liquid in a yield of 116 g (87%, Lit.: 95 %[62]) was obtained.

^{1}H NMR (500 MHz, $CDCl_3$): δ = 2.91 (m, 8 H, H-2,2´), 1.66 (m, 8 H, H-3,3´), 0.04 (s, 6 H, H-1) ppm.

^{13}C NMR (126 MHz, $CDCl_3$): δ = 46.8 (*C-2,2´*), 26.7 (*C-3,3´*), -3.3 (*C-1*) ppm

^{29}Si NMR (187 MHz, $CDCl_3$): δ = -8.11 ppm.

Anal. calcd for $C_{10}H_{22}N_2Si$: C 60.54, H 11.18, N 14.12; **found:** C 60.61, H 11.27, N 14.27.[1]

[1]Due to the very high sensivitity of this compound, no mass spectra could be measured.

***bis*(*N*-phenyl-*N´*-pyrrolidinyl)dimethylsilane[61] (11)**

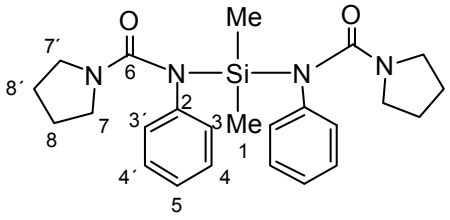

The reaction was performed entirely under inert conditions. *Bis*(pyrrolidinyl)dimethylsilane (**X,** 40.0 g, 201 mmol) was dissolved in dry diethyl ether (250 mL) and cooled in an ice bath. Then phenyl isocyanate (45.0 mL, 49.3 g, 410 mmol) was added dropwise at 0 °C during 3 h and the reaction mixture was allowed to warm to 25 °C over the course of 15 h. The white precipitate of *bis*(*N*-phenyl-*N´*-pyrrolidinyl)dimethylsilane was collected by filtration. The product was washed with diethyl ether and dried at 5 x 10^{-2} mbar for 12 h to receive 79.6 g (91%, Lit.: 85%[61]) of a colorless solid.

Mp.: T = 72 °C

^{1}H NMR (500 MHz, $CDCl_3$): δ = 7.18 (t, ^{3}J = 7.5 Hz, 4 H, H-4,4´), 7.07 (t, ^{3}J = 7.5 Hz, 2 H, H-5), 6.94 (t, ^{3}J = 7.5 Hz, 4 H, H-3,3´), 2.88 (m, 8 H, H-7,7´), 1.58 (m, 8 H, H-8,8´), 0.37 (s, 6 H, H-1) ppm.

^{13}C NMR (126 MHz, $CDCl_3$): δ = 159.67 (*C-6*), 143.10 (*C-2*), 128.78 (*C-3,3´*), 128.43 (*C-4,4´*), 124.97 (*C-5*), 47.62 (*C-7,7´*), 25.46 (*C-8,8´*), -1.38 (*C-1*) ppm.

^{29}Si NMR (187 MHz, $CDCl_3$): δ = -3.57 ppm.

Anal. calcd for $C_{25}H_{35}N_4O_2Si$: C 66.48, H 7.81, N 12.40, O 7.08; **found:** C 66.60, H 7.90, N 12.56, O 7.13. [2]

[2]Due to the very high sensivitity of this compound, no mass spectra could be measured.

Poly(azobenzene-tri(dimethylsiloxane)) (1)

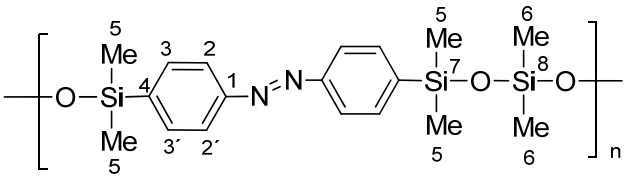

4,4´-bis(hydroxydimethylsilane-)azobenzene (**X**, 800 mg, 2.48 mmol) was placed in a flask without solvent. A solution of *bis*(*N*-phenyl-*N´*-pyrrolidinyl)dimethylsilane (**11**) (1.01 g, 2.48 mmol) was dissolved in chlorobenzene (8.00 mL) and added dropwise over the course of 8 h at -40 °C by the help of a syringe pump. The solution was stirred over the course of 8 d at 22 °C, while the progress of the reaction was monitored GPC. Once a sufficiently high molecular weight had been obtained, the reaction was removed from the glove box and the solvent was evaporated. The polymer was purified by dissolving it in chloroform (10 mL) and precipitation into methanol (100 mL). This step was repeated three times. The red rubber-like precipitate was dried at 20 °C under vacuum (5 x 10^{-3} mbar) for 4 d, to obtain 550 mg (55%) of the desired polymer.

^{1}H NMR (500 MHz, $CDCl_3$): δ = 7.90 (d, ^{3}J = 8.0 Hz, 8 H, H-2,2´), 7.70 (d, ^{3}J = 8.0 Hz, 8 H, H-3,3´), 0.39 (s, 12 H, H-5), 0.11 (s, 6 H, H-6) ppm.

^{13}C NMR (126 MHz, $CDCl_3$): δ = 153.2 (*C-1*), 143.3 (*C-4*), 133.4 (*C-3, 3'*), 122.0 (*C-2,2´*), 2.0 (*C-5*), 0.8 (*C-6*) ppm.

^{29}Si NMR (187 MHz, $CDCl_3$): δ = -2.4 ppm (s, Si-7), -19.0 (s, Si-8).

IR (ATR): ṽ = 2957 (m), 1386 (w), 1255 (m), 1109 (m), 1012 (s), 1029 (s), 818 (s), 835 (s), 782 (s), 702 (m), 685 (m), 665 (m), 621 (m), 555 (s) 528 (m) cm^{-1}.

DSC (10 K/min): T_g = 23.2 °C

GPC ($CHCl_3$, 1 mL/min): M_n = 32 kDa; M_w = 53 kDa; M_n/M_w = 1.7

3.3´-*bis*(Iodo-)azobenzene (13)

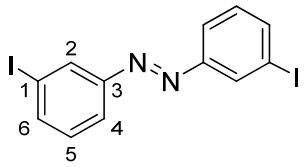

Initially, the catalyst for the reaction was prepared. For this, copper (I) chloride (5.00 g, 45.7mmol) was dissolved in pyridine (50 mL) and the mixture was stirred 30 min at 20 °C. Then the solution was filtered to remove the excess of insoluble copper chloride, and *3*-iodoaniline (14.3 g, 65.3 mmol) was added. The reaction mixture was stirred while air was bubbled through for 14 h at 20 °C. The solvent was evaporated. The crude product was filtrated over silica (eluent: dichloromethane) and recrystallized from methanol. The product was obtained in a yield of 6.12 g (43%, Lit.: 82%[71] [3])

Mp.: T = 155 °C[4]

^{1}H NMR (500 MHz, $CDCl_3$): δ = 8.24 (at, ^{4}J = 1.8 Hz, 2 H, H-2), 7.91 (ddd, ^{3}J = 7.9 Hz, ^{4}J = 1.8 Hz, 2 H, H-4), 7.82 (ddd, ^{3}J = 7.9 Hz, ^{4}J = 1.8 Hz, 2 H, H-6), 7.28 (at, ^{3}J = 7.9 Hz, 2 H, H-5) ppm.

^{13}C NMR (126 MHz, $CDCl_3$): δ = 153.4 (*C-1*), 140.1 (*C-6*), 130.7 (*C-2*), 130.7 (*C-5*), 123.8 (*C-4*), 94.6 (*C-3*) ppm.

IR (ATR): ṽ = 3053 (w), 1759 (m), 1574 (m), 1556 (s), 1464 (w), 1453 (s), 1403 (s), 1294 (w), 1191 (m), 1147 (m), 1080 (m), 991 (m), 909 (m), 882 (s), 847 (s), 791 (s), 681 (s), 652 (s), 532 (s), 521 (s) cm^{-1}.

HRMS (CI-sector*) m/z*: $[M+H]^+$ calcd for $[C_{12}H_8N_2I_2 + H]^+$ 434.8855, found 434.8851.

[3] In this report, the substance was synthesized in a reductive azo-coupling reaction from 3-iodonitrobenzene.
[4] No melting point is reported before

3,3´-*bis*(Trimethylstannyl-)azobenzene (14)

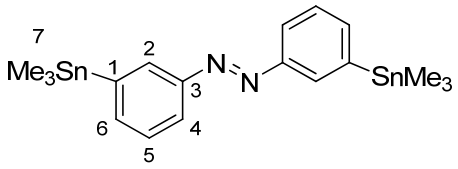

Under inert conditions, *3,3´-bis*(iodo-)azobenzene (**14**, 3.00 g, 6.90 mmol), hexamethyldistannane (5.00 g, 15.3 mmol) and [$Pd(PPh_3)_4$] (400 mg, 346 µmol, 4 mol%) were dissolved in toluene (15.0 mL) in a microwave reaction vessel. The reaction mixture was heated for 10 min to 150 °C. Then the solvent was removed under reduced pressure followed by purification by column chromatography (eluent: *n*-hexane, R_f = 0.65). The product was obtained as an orange solid 2.51 g (70%).

Mp.: T = 61.2 °C

^{1}H NMR (500 MHz, $CDCl_3$): δ = 8.09 (dd, ^4J = 2.1, ^4J = 1.3, 2 H, H-2), 7.88 (ddd, ^3J = 7.9, ^4J = 2.1, ^4J = 1.3 Hz, 2 H, H-4), 7.63 (dt, ^3J = 7.9, ^4J = 1.3 Hz, 2 H, H-6), 7.52 (at, ^3J = 7.9 Hz, 2 H, H-5), 0.41 (s, 18 H, H-7) ppm.

^{13}C NMR (126 MHz, $CDCl_3$): δ = 152.5 (*C-3*), 143.6 (*C-1*), 138.5 (*C-6*), 130.5 (*C-2*), 128.7 (*C-5*), 122.5 (*C-4*), -9.4 (*C-7*) ppm

^{119}Sn NMR (187 MHz, $CDCl_3$): δ = -24.23 ppm

IR (ATR): ṽ = 2975 (w), 2911 (w), 1925 (w), 1434 (m), 1397 (m), 1193 (w), 1156 (m), 1101 (w), 1056 (w), 925 (m), 802 (s), 771 (s), 760 (s), 740 (s), 713 (s), 694 (s), 528 (s), 512 (s) cm^{-1}.

HRMS (ESI-FTMS) *m/z*: $[M+H]^+$ calcd for $[C_{18}H_{26}N_2Sn_2 + H]^+$ 511.0213, found 511.0217.

3,3´-*bis*(Hydroxydimethylsilane-)azobenzene (12)

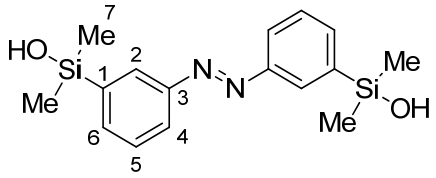

3,3´-bis(trimethylstannyl-)azobenzene (**12**, 3.80 g, 7.48 mmol) was dissolved in dry THF (100 mL). Then at -78 °C, methyl lithium (19.0 mmol, 12.0 mL of a 1.6 M solution in diethyl ether) in THF (18.0 mL) was added and the mixture was stirred for 10 min at -78 °C. The reaction was quenched with dichlorodimethylsilane (30.0 mL, 32.1 g, 249 mmol). The reaction was allowed to warm to 25 °C in the cooling bath and the solvent and the excess of dichlorodimethylsilane were evaporated. The residual orange solid was dissolved in diethyl ether (25 mL) and added dropwise over the course of 15 min to a solution of sodium methoxide (4.00 g, 74.0 mmol) in methanol (50 mL). Both of the latter steps were performed under inert conditions. To this mixture, a solution of sodium hydroxide (17.5 g, 438 mmol) in methanol (105 mL) and water (10.0 mL) of water) was added. The resulting solution was stirred 15 minutes and then a further portion of sodium hydroxide (17.5 g, 438 mmol) in water (105 mL)was added. The reaction mixture was stirred 1 h. This mixture was finally poured into a vigorously stirred solution of monopotassium phosphate (155 g, 1.14 mol) in water (200 mL). The orange precipitate was filtered and purified by three recrystallizations from diethyl ethyl ether/*n*-hexane (*v/v* 1:1). The final product was isolated as an orange solid in a yield of 500 µg (20%).

Mp.: T = 101 °C

^{1}H NMR (500 MHz, $CDCl_3$): δ = 8.14 (at, ^{4}J = 4.6 Hz , 2 H, H-2), 7.92 (adt, ^{3}J = 7.9 Hz, ^{4}J = 4.6 Hz, 2 H, H-4), 7.70 (adt, ^{3}J = 7.9 Hz, ^{4}J = 4.6 Hz, 2 H, H-6), 7.53 (atd, ^{3}J = 7.9 Hz, 2 H, H-5), 2.5 (s, 2 H, H-8), 0.46 (s, 18 H, H-7) ppm.

^{13}C NMR (126 MHz, $CDCl_3$): δ = 152.0 (*C-3*), 140.5 (*C-1*), 135.7 (*C-6*), 128.8 (*C-5*), 128.0 (*C-2*), 123.4 (*C-4*), 0.1 (*C-8*) ppm.

^{29}Si NMR (187 MHz, $CDCl_3$): δ = 7.61 ppm.

IR (ATR): ṽ = 3189 (m), 2955 (w), 1398 (m), 1251 (m), 1111 (w), 1068 (m), 897 (s), 863 (s), 820 (s), 799 (s), 764 (s), 691 (s), 645 (m), 534 (m) cm^{-1}.

HRMS (EI-sector) *m/z*: $[M]^+$ calcd for $[C_{16}H_{22}N_2O_2Si_2]^+$ 330.1220, found 330.1222.

***bis*(Pyrrolidinyl)methylvinylsilane[72] (17)**

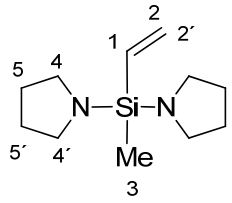

The reaction was performed entirely under inert conditions. Dichloromethylvinylsilane (40.0 mL, 43.2 g, 306 mmol) was dissolved in *n*-hexane (75.0 mL). Then pyrrolidine (113.0 mL, 97.9 g, 1.38 mmol) was added dropwise at 0 °C over the course of 1 h. The reaction was allowed to warm to 25 °C by removal of the cooling bath and stirred 15 h. The precipitate of the amino hydrochloride was removed by filtration under inert conditions. The solvent was evaporated. The product could be obtained in a yield of 58.0 g (87%, Lit.: 74%[72]) as a colorless liquid.

^{1}H NMR (500 MHz, $CDCl_3$): δ = 6.12 (dd, ^{3}J = 20.4, ^{3}J = 14.8 Hz, 1 H, H-1), 5.94 (dd, ^{3}J = 14.8, ^{2}J = 4.3 Hz, H-2), 5.71 (dd, ^{2}J = 20.3, ^{2}J = 4.3 Hz, H-2´), 2.96 (ddd, ^{3}J = 6.4, ^{4}J = 3.6, ^{4}J = 2.8 Hz, H-4,4´), 1.69 (ddd, ^{3}J = 6.4, ^{4}J = 3.6, ^{4}J = 2.8 Hz, H-5,5´), 0.16 – 0.08 (s, 3 H, H-3) ppm.

^{13}C NMR (126 MHz, $CDCl_3$): δ = 137.0 (*C-1*), 131.8 (*C-2,2´*), 46.7 (*4,4´*), 26.3 (*5,5´*), -5.0 (*C-3*) ppm.

^{29}Si NMR (187 MHz, $CDCl_3$): δ = -19.1 ppm.

Anal. calcd for $C_{11}H_{22}N_2Si$: C 62.80, H 10.54, N 13.31; **found:** C 62.86, H 10.61, N 13.16

***bis*(*N*-phenyl-*N´*-pyrrolidinyl)methylvinylsilane[72] (18)**

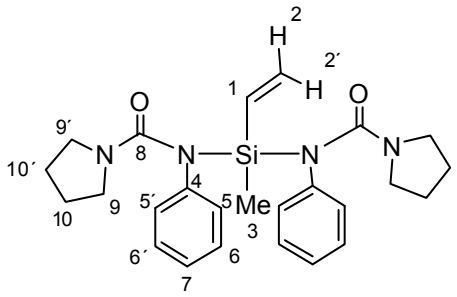

The entire reaction was performed under inert conditions. *Bis*(pyrrolidinyl)methylvinylsilane (**17**, 20.0 g, 95.0 mmol) was dissolved in dry diethyl ether (125 mL) at 0 °C and phenyl isocyanate (22.5 mL, 24.6 g, 205 mmol) was added dropwise over the course of 3 h. The reaction mixture was allowed to warm to 25 °C by removal of the cooling bath. The reaction stirred for 15 h at 25 °C. The crude product was recrystallized from diethyl ether at -30 °C (under inert conditions). A colorless solid could be obtained in a yield of 40.1 g (91%, Lit.: 62%[72]).

Mp: T = 46 °C

^{1}H NMR (500 MHz, $CDCl_3$): 7.15 (t, ^{3}J = 7.8, 4 H, H-6,6´), 7.06 (t, ^{3}J = 7.8 Hz, 2 H, H-7), 6.97 (t, ^{3}J = 7.8 Hz, 4 H, H-5,5´), 6.35 (dd, ^{3}J = 20.5, ^{3}J = 14.8 Hz, 1 H, H-1), 5.82 (dd, ^{3}J = 14.8, ^{2}J = 3.1, 1H, H-2), 5.64 (dd, ^{3}J = 20.5, ^{2}J = 3.1, 1 H, H-2´), 2.87 (m, 8 H, H-9,9´), 1.55 (m, 8 H, H-10,10´), 0.37 (s, 3 H, H-3) ppm.

^{13}C NMR (126 MHz, $CDCl_3$): 159.6 (*C-8*), 142.3 (*C-4*), 137,0 (*C-1*), 131.2 (*C-2,2´*), 128.9 (*C-3,3´*), 128.4 (*C-6,6´*), 125.1 (*C-7*), 47.6 (*C-9,9´*), 25.1 (*C-10,10´*), -2.0 (*C-3*) ppm.

^{29}Si NMR (187 MHz, $CDCl_3$): δ = -18.27 ppm.

Anal. calcd for $C_{25}H_{35}N_4O_2Si$: C 67.35, H 7.61, N 12.08, O 6.90; **found:** C 67.30, H 7.66, N 12.13, O 6.99.

Single Crystal Data for 4,4´-bis(Hydroxydimethylsilane-)azobenzene (2)

Table 1. Crystal data and structure refinement for $C_{16}H_{22}N_2O_2Si_2$ at 200 K in $P2_1/n$ (p-Silanol).

Identification code	staubit6	
Empirical formula	$C_{16}H_{22}N_2O_2Si_2$	
Formula weight	330.54	
Temperature	200(2) K	
Wavelength	0.71073 Å	
Crystal system	monoclinic	
Space group	$P2_1/n$	
Unit cell dimensions	a = 17.8705(4) Å	□= 90°.
	b = 10.0016(3) Å	□= 97.013(2)°.
	c = 20.5323(5) Å	□ = 90°.
Volume	3642.36(16) $Å^3$	
Z	8	
Density (calculated)	1.206 Mg/m^3	
Absorption coefficient	0.202 mm^{-1}	
F(000)	1408	
Crystal size	0.10 x 0.15 x 0.15 mm^3	
Theta range for data collection	1.61 to 27.00°.	
Index ranges	-21<=h<=22, -12<=k<=12, -26<=l<=26	
Reflections collected	30514	
Independent reflections	7877 [R(int) = 0.0256]	
Completeness to theta = 27.00°	99.1 %	
Refinement method	Full-matrix least-squares on F^2	
Data / restraints / parameters	7877 / 0 / 409	
Goodness-of-fit on F^2	1.042	
Final R indices [I>2sigma(I)]	R1 = 0.0374, wR2 = 0.0917	
R indices (all data)	R1 = 0.0463, wR2 = 0.0958	
Largest diff. peak and hole	0.315 and -0.201 e.$Å^{-3}$	

Comments:
All non-hydrogen atoms were refined anisotropically. The C-H and O-H H atoms were located in difference map but were positioned with idealized geometry (methyl and hydroxyl H atoms allowed to rotate but not to tip) and refined isotropically with $U_{iso}(H) = 1.2\ U_{eq}(C)$ (1.5 for methyl and hydroxyl H atoms).

Table 2. Atomic coordinates (x 10^4) and equivalent isotropic displacement parameters ($Å^2$x 10^3). U(eq) is defined as one third of the trace of the orthogonalized U^{ij} tensor.

	x	y	z	U(eq)
C(1)	1906(1)	2367(2)	5940(1)	36(1)
C(2)	2214(1)	1753(2)	5427(1)	38(1)
C(3)	2991(1)	1616(2)	5462(1)	37(1)
C(4)	3478(1)	2071(1)	6006(1)	33(1)
C(5)	3147(1)	2639(2)	6522(1)	37(1)
C(6)	2371(1)	2797(2)	6488(1)	39(1)
Si(1)	4533(1)	2026(1)	6024(1)	33(1)
O(1)	4817(1)	520(1)	5846(1)	41(1)
C(7)	4843(1)	3152(2)	5391(1)	52(1)
C(8)	4991(1)	2526(2)	6846(1)	46(1)
N(1)	1119(1)	2648(2)	5960(1)	43(1)
N(2)	689(1)	2094(2)	5517(1)	45(1)
C(9)	-93(1)	2435(2)	5537(1)	42(1)
C(10)	-613(1)	1632(2)	5170(1)	49(1)
C(11)	-1377(1)	1869(2)	5171(1)	45(1)
C(12)	-1640(1)	2929(2)	5522(1)	36(1)
C(13)	-1102(1)	3742(2)	5875(1)	48(1)
C(14)	-334(1)	3507(2)	5886(1)	51(1)
Si(2)	-2673(1)	3281(1)	5488(1)	34(1)
O(2)	-3151(1)	1984(1)	5165(1)	40(1)
C(15)	-2926(1)	4716(2)	4941(1)	53(1)
C(16)	-2939(1)	3644(2)	6317(1)	49(1)
C(21)	6151(1)	7120(2)	1559(1)	38(1)
C(22)	6568(1)	5947(2)	1584(1)	42(1)
C(23)	7345(1)	6015(2)	1632(1)	41(1)
C(24)	7726(1)	7242(2)	1663(1)	35(1)
C(25)	7292(1)	8400(2)	1643(1)	41(1)
C(26)	6510(1)	8347(2)	1583(1)	44(1)
Si(3)	8778(1)	7274(1)	1698(1)	34(1)
O(3)	9011(1)	6678(1)	1002(1)	39(1)
C(27)	9217(1)	6144(2)	2346(1)	53(1)
C(28)	9136(1)	9003(2)	1832(1)	53(1)
N(3)	5346(1)	7174(2)	1515(1)	42(1)
N(4)	5048(1)	6055(2)	1561(1)	44(1)
C(29)	4244(1)	6111(2)	1533(1)	40(1)
C(30)	3902(1)	4941(2)	1692(1)	61(1)
C(31)	3128(1)	4912(2)	1697(1)	62(1)
C(32)	2678(1)	6017(2)	1534(1)	40(1)
C(33)	3040(1)	7174(2)	1366(1)	54(1)
C(34)	3816(1)	7227(2)	1365(1)	55(1)
Si(4)	1632(1)	5927(1)	1540(1)	39(1)
O(4)	1314(1)	4969(1)	915(1)	40(1)
C(35)	1418(1)	5168(3)	2317(1)	61(1)
C(36)	1203(1)	7614(2)	1438(1)	62(1)

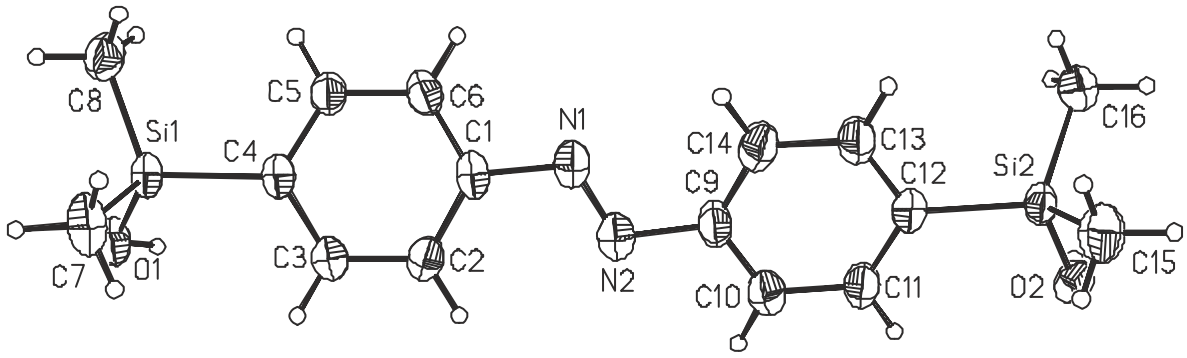

Table 3. Bond lengths [Å] and angles [°].

C(1)-C(6)	1.383(2)	N(2)-C(9)	1.4439(19)
C(1)-C(2)	1.390(2)	C(9)-C(10)	1.380(2)
C(1)-N(1)	1.4403(19)	C(9)-C(14)	1.388(3)
C(2)-C(3)	1.389(2)	C(10)-C(11)	1.386(2)
C(3)-C(4)	1.406(2)	C(11)-C(12)	1.395(2)
C(4)-C(5)	1.395(2)	C(12)-C(13)	1.394(2)
C(4)-Si(1)	1.8827(14)	C(12)-Si(2)	1.8723(15)
C(5)-C(6)	1.388(2)	C(13)-C(14)	1.390(2)
Si(1)-O(1)	1.6446(12)	Si(2)-O(2)	1.6473(11)
Si(1)-C(8)	1.8527(18)	Si(2)-C(15)	1.8438(19)
Si(1)-C(7)	1.8536(18)	Si(2)-C(16)	1.8578(19)
N(1)-N(2)	1.246(2)		
C(6)-C(1)-C(2)	119.98(13)	N(1)-N(2)-C(9)	112.70(14)
C(6)-C(1)-N(1)	114.13(14)	C(10)-C(9)-C(14)	120.03(15)
C(2)-C(1)-N(1)	125.87(14)	C(10)-C(9)-N(2)	115.89(15)
C(3)-C(2)-C(1)	119.34(15)	C(14)-C(9)-N(2)	124.07(15)
C(2)-C(3)-C(4)	121.79(15)	C(9)-C(10)-C(11)	119.84(16)
C(5)-C(4)-C(3)	117.20(13)	C(10)-C(11)-C(12)	121.69(16)
C(5)-C(4)-Si(1)	120.80(11)	C(13)-C(12)-C(11)	117.22(14)
C(3)-C(4)-Si(1)	121.88(12)	C(13)-C(12)-Si(2)	121.58(12)
C(6)-C(5)-C(4)	121.44(15)	C(11)-C(12)-Si(2)	121.15(12)
C(1)-C(6)-C(5)	120.19(15)	C(14)-C(13)-C(12)	121.79(16)
O(1)-Si(1)-C(8)	109.59(7)	C(9)-C(14)-C(13)	119.39(16)
O(1)-Si(1)-C(7)	105.95(8)	O(2)-Si(2)-C(15)	106.97(8)
C(8)-Si(1)-C(7)	109.78(9)	O(2)-Si(2)-C(16)	110.13(8)
O(1)-Si(1)-C(4)	110.68(6)	C(15)-Si(2)-C(16)	109.57(9)
C(8)-Si(1)-C(4)	109.91(8)	O(2)-Si(2)-C(12)	109.08(7)
C(7)-Si(1)-C(4)	110.86(7)	C(15)-Si(2)-C(12)	109.64(8)
N(2)-N(1)-C(1)	114.15(14)	C(16)-Si(2)-C(12)	111.35(8)

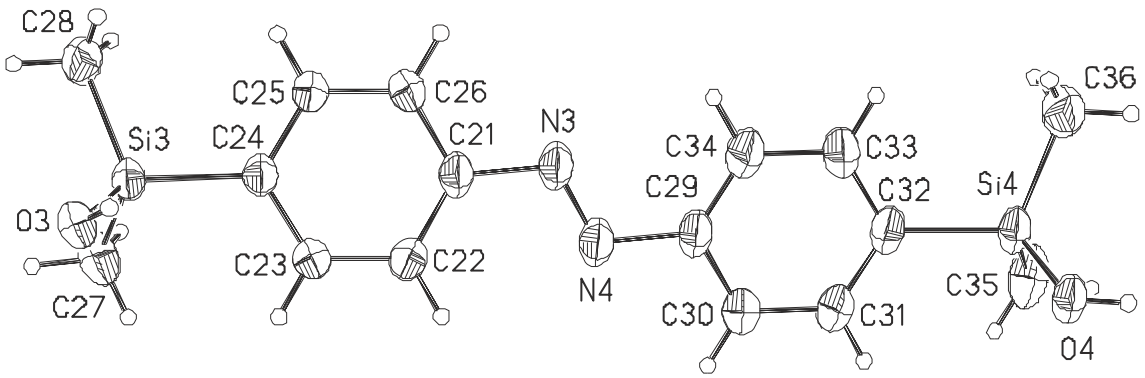

Table 3. Bond lengths [Å] and angles [°].

C(21)-C(26)	1.383(2)	N(4)-C(29)	1.4321(19)
C(21)-C(22)	1.387(2)	C(29)-C(34)	1.373(3)
C(21)-N(3)	1.4307(19)	C(29)-C(30)	1.378(3)
C(22)-C(23)	1.382(2)	C(30)-C(31)	1.385(2)
C(23)-C(24)	1.402(2)	C(31)-C(32)	1.385(3)
C(24)-C(25)	1.392(2)	C(32)-C(33)	1.390(3)
C(24)-Si(3)	1.8723(15)	C(32)-Si(4)	1.8719(15)
C(25)-C(26)	1.389(2)	C(33)-C(34)	1.387(2)
Si(3)-O(3)	1.6487(12)	Si(4)-O(4)	1.6469(12)
Si(3)-C(27)	1.8466(19)	Si(4)-C(35)	1.849(2)
Si(3)-C(28)	1.8528(18)	Si(4)-C(36)	1.854(2)
N(3)-N(4)	1.248(2)		
C(26)-C(21)-C(22)	120.25(14)	N(3)-N(4)-C(29)	113.40(14)
C(26)-C(21)-N(3)	115.31(14)	C(34)-C(29)-C(30)	120.02(15)
C(22)-C(21)-N(3)	124.44(14)	C(34)-C(29)-N(4)	124.57(15)
C(23)-C(22)-C(21)	119.49(15)	C(30)-C(29)-N(4)	115.41(16)
C(22)-C(23)-C(24)	121.62(15)	C(29)-C(30)-C(31)	119.46(18)
C(25)-C(24)-C(23)	117.48(13)	C(32)-C(31)-C(30)	122.21(18)
C(25)-C(24)-Si(3)	122.72(12)	C(31)-C(32)-C(33)	116.73(15)
C(23)-C(24)-Si(3)	119.77(11)	C(31)-C(32)-Si(4)	120.74(13)
C(26)-C(25)-C(24)	121.45(15)	C(33)-C(32)-Si(4)	122.53(13)
C(21)-C(26)-C(25)	119.69(15)	C(34)-C(33)-C(32)	121.88(17)
O(3)-Si(3)-C(27)	105.89(8)	C(29)-C(34)-C(33)	119.67(17)
O(3)-Si(3)-C(28)	110.33(8)	O(4)-Si(4)-C(35)	110.22(8)
C(27)-Si(3)-C(28)	110.81(10)	O(4)-Si(4)-C(36)	110.10(8)
O(3)-Si(3)-C(24)	108.57(6)	C(35)-Si(4)-C(36)	110.14(11)
C(27)-Si(3)-C(24)	110.72(8)	O(4)-Si(4)-C(32)	105.83(6)
C(28)-Si(3)-C(24)	110.40(8)	C(35)-Si(4)-C(32)	109.69(8)
N(4)-N(3)-C(21)	113.33(14)	C(36)-Si(4)-C(32)	110.79(9)

Table 4. Anisotropic displacement parameters ($Å^2 x\ 10^3$). The anisotropic displacement factor exponent takes the form: $-2\pi^2[h^2 a^{*2} U^{11} + ... + 2 h k a^* b^* U^{12}]$

	U^{11}	U^{22}	U^{33}	U^{23}	U^{13}	U^{12}
C(1)	24(1)	36(1)	49(1)	6(1)	8(1)	4(1)
C(2)	28(1)	44(1)	42(1)	2(1)	1(1)	-1(1)
C(3)	29(1)	41(1)	42(1)	0(1)	7(1)	2(1)
C(4)	24(1)	32(1)	42(1)	4(1)	5(1)	2(1)
C(5)	28(1)	39(1)	43(1)	-1(1)	5(1)	1(1)
C(6)	31(1)	41(1)	47(1)	-2(1)	12(1)	3(1)
Si(1)	21(1)	35(1)	44(1)	3(1)	5(1)	2(1)
O(1)	26(1)	39(1)	60(1)	-1(1)	10(1)	2(1)
C(7)	33(1)	57(1)	67(1)	18(1)	12(1)	3(1)
C(8)	34(1)	47(1)	57(1)	-5(1)	-1(1)	4(1)
N(1)	28(1)	50(1)	50(1)	2(1)	6(1)	1(1)
N(2)	31(1)	53(1)	52(1)	-3(1)	5(1)	4(1)
C(9)	26(1)	52(1)	48(1)	1(1)	6(1)	6(1)
C(10)	34(1)	56(1)	56(1)	-12(1)	3(1)	9(1)
C(11)	30(1)	48(1)	55(1)	-9(1)	1(1)	3(1)
C(12)	26(1)	41(1)	42(1)	0(1)	3(1)	2(1)
C(13)	30(1)	52(1)	61(1)	-15(1)	4(1)	1(1)
C(14)	29(1)	58(1)	63(1)	-10(1)	-1(1)	-4(1)
Si(2)	22(1)	38(1)	42(1)	-1(1)	2(1)	2(1)
O(2)	32(1)	45(1)	41(1)	3(1)	0(1)	-6(1)
C(15)	45(1)	46(1)	66(1)	9(1)	4(1)	7(1)
C(16)	34(1)	61(1)	52(1)	-9(1)	8(1)	3(1)
C(21)	25(1)	46(1)	43(1)	-6(1)	8(1)	-2(1)
C(22)	32(1)	39(1)	55(1)	-7(1)	9(1)	-6(1)
C(23)	31(1)	36(1)	56(1)	-4(1)	8(1)	1(1)
C(24)	27(1)	38(1)	40(1)	-3(1)	7(1)	-1(1)
C(25)	29(1)	36(1)	60(1)	-3(1)	10(1)	-2(1)
C(26)	30(1)	39(1)	64(1)	-4(1)	10(1)	4(1)
Si(3)	24(1)	38(1)	41(1)	-2(1)	4(1)	0(1)
O(3)	29(1)	45(1)	42(1)	0(1)	5(1)	7(1)
C(27)	41(1)	71(1)	47(1)	7(1)	7(1)	14(1)
C(28)	34(1)	48(1)	75(1)	-15(1)	6(1)	-7(1)
N(3)	26(1)	50(1)	51(1)	-6(1)	8(1)	-3(1)
N(4)	27(1)	52(1)	55(1)	-10(1)	7(1)	-4(1)
C(29)	25(1)	51(1)	46(1)	-10(1)	6(1)	-5(1)
C(30)	32(1)	47(1)	104(2)	-1(1)	6(1)	-2(1)
C(31)	31(1)	48(1)	107(2)	3(1)	10(1)	-9(1)
C(32)	27(1)	51(1)	43(1)	-10(1)	3(1)	-6(1)
C(33)	29(1)	55(1)	76(1)	9(1)	5(1)	0(1)
C(34)	32(1)	54(1)	79(1)	11(1)	9(1)	-7(1)
Si(4)	24(1)	51(1)	42(1)	-9(1)	5(1)	-5(1)
O(4)	24(1)	52(1)	45(1)	-9(1)	5(1)	-4(1)
C(35)	39(1)	100(2)	46(1)	-5(1)	7(1)	-15(1)
C(36)	39(1)	59(1)	87(2)	-18(1)	9(1)	2(1)

Table 5. Hydrogen coordinates (x 10^4) and isotropic displacement parameters ($Å^2$x 10^3).

	x	y	z	U(eq)
H(2)	1896	1430	5055	46
H(3)	3200	1204	5108	44
H(5)	3459	2925	6904	44
H(6)	2159	3201	6842	47
H(1O)	4497	-46	5934	61
H(7A)	5386	3043	5378	77
H(7B)	4736	4081	5500	77
H(7C)	4570	2927	4962	77
H(8A)	4817	1941	7180	69
H(8B)	4859	3454	6934	69
H(8C)	5539	2446	6860	69
H(10)	-447	918	4918	58
H(11)	-1730	1295	4927	53
H(13)	-1265	4477	6115	57
H(14)	22	4076	6131	61
H(2O)	-3238	1456	5465	60
H(15A)	-2787	4522	4504	79
H(15B)	-2655	5513	5119	79
H(15C)	-3470	4876	4910	79
H(16A)	-3477	3865	6281	73
H(16B)	-2642	4401	6509	73
H(16C)	-2839	2856	6598	73
H(22)	6321	5105	1568	50
H(23)	7628	5209	1645	49
H(25)	7536	9246	1672	50
H(26)	6223	9149	1558	53
H(3O)	8680	6894	693	58
H(27A)	8987	5256	2290	79
H(27B)	9139	6501	2777	79
H(27C)	9759	6075	2316	79
H(28A)	9685	9008	1837	79
H(28B)	9007	9336	2253	79
H(28C)	8906	9581	1477	79
H(30)	4195	4160	1797	73
H(31)	2898	4106	1816	74
H(33)	2749	7951	1249	64
H(34)	4050	8030	1248	66
H(4O)	847	4862	908	60
H(35A)	881	4944	2281	92
H(35B)	1542	5804	2677	92
H(35C)	1718	4354	2404	92
H(36A)	1370	8051	1054	92
H(36B)	1360	8151	1831	92
H(36C)	652	7532	1377	92

Single Crystal Data for 3,3´-bis(Hydroxydimethylsilane-)azobenzene (12)

Table 1. Crystal data and structure refinement for $C_{16}H_{22}N_2O_2Si_2$ at 200 K in P-1 (Staubitz7; m-Silanol).

Identification code	staubit7	
Empirical formula	$C_{16}H_{22}N_2O_2Si_2$	
Formula weight	330.54	
Temperature	200(2) K	
Wavelength	0.71073 Å	
Crystal system	triclinic P	
Space group	P-1	
Unit cell dimensions	a = 6.6731(4) Å	□= 83.992(4)°.
	b = 9.8806(6) Å	□= 82.810(4)°.
	c = 21.4108(10) Å	□ = 87.508(5)°.
Volume	1392.25(14) Å^3	
Z	3	
Density (calculated)	1.183 Mg/m^3	
Absorption coefficient	0.199 mm^{-1}	
F(000)	528	
Crystal size	0.1 x 0.2 x 0.3 mm^3	
Theta range for data collection	1.93 to 25.00°.	
Index ranges	-7<=h<=7, -9<=k<=11, -25<=l<=25	
Reflections collected	11236	
Independent reflections	4845 [R(int) = 0.0397]	
Completeness to theta = 25.00°	98.9 %	
Refinement method	Full-matrix least-squares on F^2	
Data / restraints / parameters	4845 / 0 / 308	
Goodness-of-fit on F^2	1.034	
Final R indices [I>2sigma(I)]	R1 = 0.0503, wR2 = 0.1139	
R indices (all data)	R1 = 0.0758, wR2 = 0.1262	
Extinction coefficient	0.029(4)	
Largest diff. peak and hole	0.220 and -0.263 e.Å^{-3}	

Comments:
All non-hydrogen atoms were refined anisotropically. The C-H and O-H H atoms were located in difference map but were positioned with idealized geometry (methyl and hydroxyl H atoms allowed to rotate but not to tip) and refined isotropically with $U_{iso}(H) = 1.2\ U_{eq}(C)$ (1.5 for methyl and hydroxyl H atoms).
One of the two crystallogrtaphically independent molecules is located around a center of inversion.

Table 2. Atomic coordinates (x 10^4) and equivalent isotropic displacement parameters ($Å^2$x 10^3). U(eq) is defined as one third of the trace of the orthogonalized U^{ij} tensor.

	x	y	z	U(eq)
C(1)	8173(4)	1655(3)	4615(1)	59(1)
C(2)	9324(4)	1796(3)	4027(1)	59(1)
C(3)	9809(4)	679(3)	3679(1)	59(1)
C(4)	9071(5)	-579(3)	3950(1)	66(1)
C(5)	7927(5)	-728(3)	4535(1)	68(1)
C(6)	7477(4)	383(3)	4874(1)	64(1)
Si(1)	11414(1)	794(1)	2897(1)	60(1)
O(1)	11934(3)	2393(2)	2665(1)	62(1)
C(7)	13851(5)	-109(4)	2978(2)	86(1)
C(8)	10036(6)	100(4)	2311(2)	86(1)
N(1)	7784(4)	2872(3)	4925(1)	64(1)
N(2)	6495(4)	2720(3)	5405(1)	66(1)
C(9)	6026(4)	3926(3)	5721(1)	61(1)
C(10)	4536(4)	3763(3)	6234(1)	60(1)
C(11)	3852(4)	4840(3)	6591(1)	58(1)
C(12)	4745(4)	6092(3)	6398(1)	62(1)
C(13)	6230(5)	6259(3)	5883(1)	65(1)
C(14)	6878(4)	5178(3)	5544(1)	64(1)
Si(2)	1874(1)	4584(1)	7286(1)	58(1)
O(2)	1366(3)	6048(2)	7584(1)	61(1)
C(15)	-549(5)	4071(3)	7056(2)	73(1)
C(16)	2840(5)	3318(3)	7882(1)	74(1)
C(21)	8037(5)	9557(3)	9573(1)	68(1)
C(22)	7417(5)	8341(3)	9407(1)	69(1)
C(23)	5797(5)	8287(3)	9056(1)	69(1)
C(24)	4812(5)	9522(4)	8890(1)	75(1)
C(25)	5405(5)	10746(4)	9059(2)	78(1)
C(26)	7043(5)	10774(4)	9399(1)	76(1)
Si(3)	4967(1)	6664(1)	8809(1)	70(1)
O(3)	4598(3)	6900(2)	8061(1)	68(1)
C(27)	6904(6)	5296(4)	8920(2)	100(1)
C(28)	2455(6)	6217(5)	9235(2)	103(1)
N(3)	9716(4)	9442(3)	9935(1)	74(1)

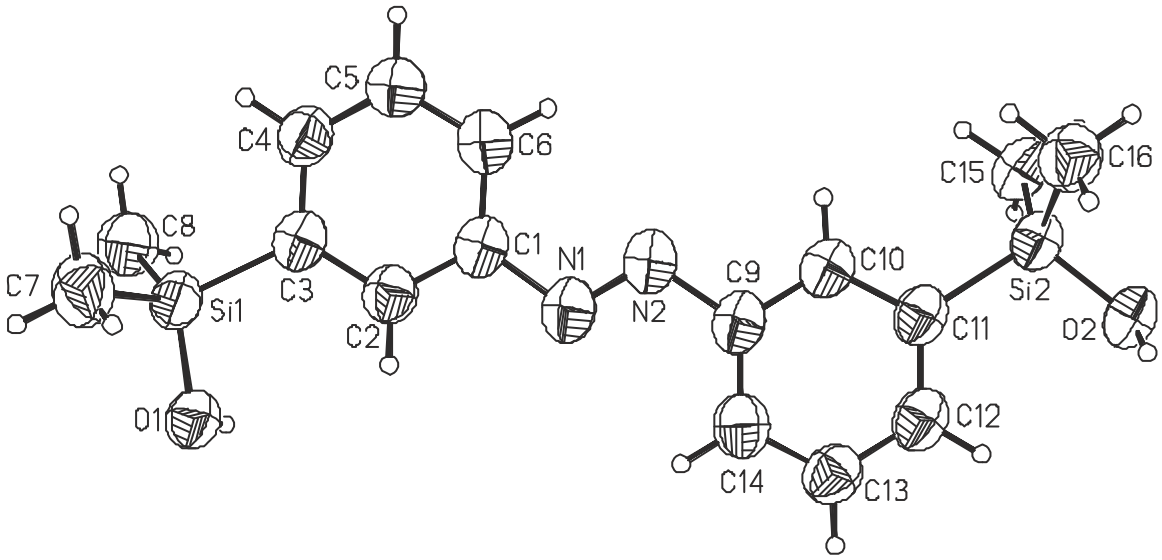

Table 3. Bond lengths [Å] and angles [°].

C(1)-C(2)	1.386(4)	N(2)-C(9)	1.434(3)
C(1)-C(6)	1.394(4)	C(9)-C(14)	1.381(4)
C(1)-N(1)	1.432(3)	C(9)-C(10)	1.387(4)
C(2)-C(3)	1.400(4)	C(10)-C(11)	1.402(4)
C(3)-C(4)	1.398(4)	C(11)-C(12)	1.396(4)
C(3)-Si(1)	1.867(3)	C(11)-Si(2)	1.865(3)
C(4)-C(5)	1.381(4)	C(12)-C(13)	1.389(4)
C(5)-C(6)	1.379(4)	C(13)-C(14)	1.378(4)
Si(1)-O(1)	1.644(2)	Si(2)-O(2)	1.6468(18)
Si(1)-C(7)	1.839(3)	Si(2)-C(16)	1.847(3)
Si(1)-C(8)	1.848(3)	Si(2)-C(15)	1.853(3)
N(1)-N(2)	1.256(3)		
C(2)-C(1)-C(6)	120.3(2)	N(1)-N(2)-C(9)	114.5(3)
C(2)-C(1)-N(1)	116.0(3)	C(14)-C(9)-C(10)	120.2(2)
C(6)-C(1)-N(1)	123.7(2)	C(14)-C(9)-N(2)	125.7(3)
C(1)-C(2)-C(3)	121.3(3)	C(10)-C(9)-N(2)	114.1(3)
C(4)-C(3)-C(2)	116.9(2)	C(9)-C(10)-C(11)	122.0(3)
C(4)-C(3)-Si(1)	119.7(2)	C(12)-C(11)-C(10)	116.3(3)
C(2)-C(3)-Si(1)	123.3(2)	C(12)-C(11)-Si(2)	122.7(2)
C(5)-C(4)-C(3)	122.1(3)	C(10)-C(11)-Si(2)	121.0(2)
C(6)-C(5)-C(4)	120.2(3)	C(13)-C(12)-C(11)	121.8(3)
C(5)-C(6)-C(1)	119.2(3)	C(14)-C(13)-C(12)	120.5(3)
O(1)-Si(1)-C(7)	106.33(15)	C(13)-C(14)-C(9)	119.2(3)
O(1)-Si(1)-C(8)	109.67(14)	O(2)-Si(2)-C(16)	110.15(12)
C(7)-Si(1)-C(8)	112.18(18)	O(2)-Si(2)-C(15)	105.38(12)
O(1)-Si(1)-C(3)	109.77(11)	C(16)-Si(2)-C(15)	111.68(16)
C(7)-Si(1)-C(3)	109.72(14)	O(2)-Si(2)-C(11)	108.83(12)
C(8)-Si(1)-C(3)	109.13(14)	C(16)-Si(2)-C(11)	108.79(13)
N(2)-N(1)-C(1)	112.8(2)	C(15)-Si(2)-C(11)	111.93(14)

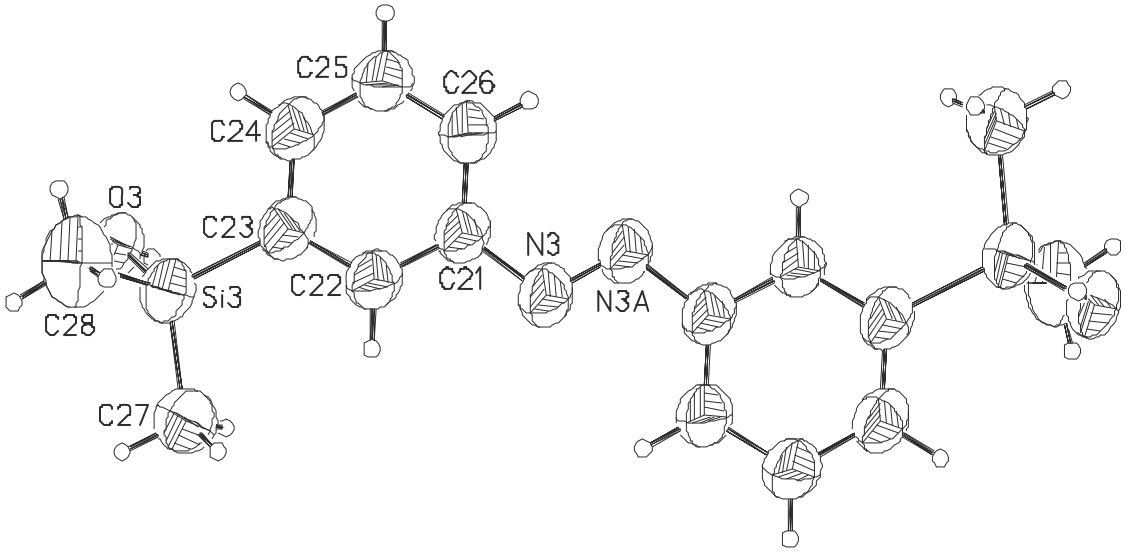

Table 3. Bond lengths [Å] and angles [°].

C(21)-C(22)	1.382(4)	C(24)-C(25)	1.386(5)
C(21)-C(26)	1.387(4)	C(25)-C(26)	1.389(4)
C(21)-N(3)	1.434(4)	Si(3)-O(3)	1.642(2)
C(22)-C(23)	1.398(4)	Si(3)-C(27)	1.848(4)
C(23)-C(24)	1.394(4)	Si(3)-C(28)	1.853(4)
C(23)-Si(3)	1.867(3)	N(3)-N(3A)	1.250(5)
C(22)-C(21)-C(26)	120.5(3)	C(21)-C(26)-C(25)	118.8(3)
C(22)-C(21)-N(3)	115.2(3)	O(3)-Si(3)-C(27)	109.67(15)
C(26)-C(21)-N(3)	124.3(3)	O(3)-Si(3)-C(28)	104.44(15)
C(21)-C(22)-C(23)	121.9(3)	C(27)-Si(3)-C(28)	112.7(2)
C(24)-C(23)-C(22)	116.6(3)	O(3)-Si(3)-C(23)	109.09(13)
C(24)-C(23)-Si(3)	120.7(2)	C(27)-Si(3)-C(23)	110.39(17)
C(22)-C(23)-Si(3)	122.7(2)	C(28)-Si(3)-C(23)	110.32(17)
C(25)-C(24)-C(23)	122.1(3)	N(3A)-N(3)-C(21)	114.0(3)
C(24)-C(25)-C(26)	120.1(3)		

Symmetry transformations used to generate equivalent atoms: A: -x+2,-y+2,-z+2

Table 4. Anisotropic displacement parameters ($Å^2 x\ 10^3$). The anisotropic displacement factor exponent takes the form: $-2\pi^2[h^2 a^{*2} U^{11} + ... + 2 h k a^* b^* U^{12}]$

	U^{11}	U^{22}	U^{33}	U^{23}	U^{13}	U^{12}
C(1)	61(2)	61(2)	56(2)	-13(1)	-11(1)	7(1)
C(2)	61(2)	60(2)	56(2)	-7(1)	-9(1)	3(1)
C(3)	61(2)	60(2)	57(2)	-13(1)	-12(1)	7(1)
C(4)	73(2)	61(2)	64(2)	-15(1)	-6(1)	2(1)
C(5)	72(2)	66(2)	66(2)	-9(1)	-4(1)	-4(1)
C(6)	62(2)	73(2)	58(2)	-11(1)	-6(1)	3(1)
Si(1)	67(1)	56(1)	56(1)	-10(1)	-4(1)	7(1)
O(1)	62(1)	60(1)	64(1)	-8(1)	-8(1)	7(1)
C(7)	85(2)	81(2)	84(2)	3(2)	5(2)	24(2)
C(8)	108(3)	87(2)	63(2)	-20(2)	-3(2)	-15(2)
N(1)	66(1)	71(2)	56(1)	-14(1)	-10(1)	8(1)
N(2)	68(2)	71(2)	60(1)	-16(1)	-5(1)	5(1)
C(9)	65(2)	65(2)	55(2)	-15(1)	-11(1)	8(1)
C(10)	65(2)	58(2)	59(2)	-12(1)	-11(1)	4(1)
C(11)	63(2)	58(2)	56(2)	-12(1)	-17(1)	7(1)
C(12)	70(2)	61(2)	59(2)	-12(1)	-19(1)	9(1)
C(13)	75(2)	59(2)	62(2)	-8(1)	-16(1)	1(1)
C(14)	66(2)	73(2)	55(2)	-8(1)	-11(1)	4(1)
Si(2)	63(1)	56(1)	56(1)	-14(1)	-13(1)	8(1)
O(2)	61(1)	61(1)	65(1)	-20(1)	-15(1)	9(1)
C(15)	71(2)	71(2)	81(2)	-25(2)	-18(2)	4(2)
C(16)	83(2)	68(2)	70(2)	-9(2)	-13(2)	10(2)
C(21)	70(2)	80(2)	58(2)	-17(2)	-17(1)	2(2)
C(22)	74(2)	77(2)	60(2)	-17(1)	-19(1)	5(2)
C(23)	69(2)	88(2)	53(2)	-18(1)	-14(1)	1(2)
C(24)	76(2)	92(2)	61(2)	-16(2)	-20(2)	2(2)
C(25)	87(2)	82(2)	68(2)	-16(2)	-25(2)	9(2)
C(26)	87(2)	81(2)	64(2)	-21(2)	-24(2)	5(2)
Si(3)	75(1)	83(1)	56(1)	-13(1)	-15(1)	-7(1)
O(3)	67(1)	87(1)	53(1)	-16(1)	-11(1)	-7(1)
C(27)	120(3)	85(3)	104(3)	-11(2)	-49(2)	-3(2)
C(28)	106(3)	137(4)	68(2)	-19(2)	2(2)	-31(2)
N(3)	77(2)	85(2)	67(2)	-21(1)	-22(1)	-2(1)

Table 5. Hydrogen coordinates (x 10^4) and isotropic displacement parameters ($Å^2$x 10^3).

	x	y	z	U(eq)
H(2)	9793	2669	3858	71
H(4)	9367	-1356	3724	79
H(5)	7448	-1597	4705	82
H(6)	6702	283	5278	77
H(1O)	10878	2822	2574	93
H(7A)	14698	-33	2568	129
H(7B)	13620	-1071	3119	129
H(7C)	14535	297	3289	129
H(8A)	8789	642	2265	129
H(8B)	9701	-847	2455	129
H(8C)	10886	135	1902	129
H(10)	3961	2895	6347	72
H(12)	4325	6850	6626	75
H(13)	6802	7125	5763	77
H(14)	7899	5293	5193	77
H(2O)	2396	6300	7723	92
H(15A)	-1505	3862	7437	109
H(15B)	-314	3263	6824	109
H(15C)	-1109	4818	6785	109
H(16A)	4026	3672	8031	110
H(16B)	3222	2470	7691	110
H(16C)	1786	3140	8240	110
H(22)	8111	7519	9535	83
H(24)	3698	9524	8653	90
H(25)	4691	11568	8942	93
H(26)	7473	11611	9510	91
H(3O)	5699	7075	7837	102
H(27A)	6439	4448	8795	150
H(27B)	7132	5164	9366	150
H(27C)	8169	5549	8658	150
H(28A)	1436	6892	9099	155
H(28B)	2491	6210	9691	155
H(28C)	2108	5314	9140	155

Table 6. Hydrogen bonds with H..A < r(A) + 2.000 Angstroms and <DHA > 110 deg.

D-H	d(D-H)	d(H..A)	<DHA	d(D..A)	A
O1-H1O	0.840	1.872	173.15	2.708	O2 [-x+1, -y+1, -z+1]
O2-H2O	0.840	1.861	177.22	2.701	O3
O3-H3O	0.840	1.858	175.44	2.696	O1 [-x+2, -y+1, -z+1]

Supporting Information

for

Photoswitching of Porous Liquid Crystal Elastomers

Emre Kizilkan[1], Jan Strueben[2], Xin Jin[3], Clemens Schaber[1], Rainer Adelung[3,*], Anne Staubitz[2,*], Stanislav N. Gorb[1,*]

[1]*Zoological Institute of the University of Kiel, Am BotanischenGarten 1–9, 24118 Kiel, Germany*
e-mail: sgorb@zoologie.uni-kiel.de

[2]*Otto-Diels-Institute for Organic Chemistry, University of Kiel, Otto-Hahn-Platz 4, 24098 Kiel (Germany)*
e-mail: astaubitz@oc.uni-kiel.de

[3]*Institute for Materials Science, Kaiserstrasse 2, 24143 Kiel, Germany Tel: +49-431-880-6116*
e-mail: ra@tf.uni-kiel.de

Table of Contents

Abbreviations

ATR	attenuated total reflectance
at	apparent triplet (NMR)
calcd.	calculated
COSY	correlated spectroscopy
d	doublet (NMR)
DMF	*N*,*N*-dimethylformamide
DSC	dynamic scanning calorimetry
HMBC	heteronuclear multiple bondcoherence
HSQC	heteronuclearsinglequantumcoherence
IR	infrared
m	medium (concerning the intensity) (IR)
m	multiplet (NMR)
M.p.	melting point
MS	mass spectrometry
Ph	phenyl
R_f	retention factor
s	strong (concerning the intensity) (IR)
s	singlet (NMR)
t	triplet (NMR)
THF	tetrahydrofuran
w	weak (concerning the intensity) (IR)

General Methods and Materials

Reagents/Reactants

If not noted otherwise, all reagents were used as received.

Reagent	Supplier	Purity
Acroylchloride	Alfa Aesar Inc.	99%
Benzene-1,4-diol	Merck	99.5 %
9-Bromo-1-nonanol	Sigma-Aldrich Inc.	99%
Hydrochloricacid (37 %)	Grüssing	98%
Magnesium sulfate	Grüssing	99 %
4-Nitrophenol	Sigma-Aldrich Inc.	99 %
Phenol	Alfa Aesar Inc.	97%
Pottassiumcarbonate	Grüssing	>95%
Palladium on carbon (10 %)	Alfa Aesar Inc.	98%
Sodiumnitrite	Alfa Aesar Inc.	98%
Sodiumhydroxide	Grüssing	99%
Sodiumhydride	VWR	98%
Triethylamine	Alfa Aesar Inc.	99%

Solvents

All solvents were freshly distilled, if used for purification. Where noted, solvents were dried over the specified drying agent by refluxing for several hours before distillation. Dry solvents were degassed by three freeze-pump-thaw cycles and stored in a nitrogen filled glove box over 3 Å molecular sieves.

Solvent	Supplier; drying procedure
Acetonitrile	Sigma Aldrich; Dried over phosphorus pentoxide
Chloroform	VWR; -
Cyclohexane	VWR; -
DMF	Acros Organics, extra dry, stored over 3 Å molecular sieves, flushed with nitrogen.
Ethyl acetate	BCD;-
Methanol	BCD; -
THF	Merck-Polaro, dried and degassed with an PS-MD-5 by Innovation Technology.

Analyses

^{1}H NMR spectra, and ^{13}C NMR, spectra were recorded at 300 K. ^{1}H NMR spectra were recorded on a Bruker DRX 500 (500 MHz) spectrometer or a Bruker Avance 600 spectrometer. ^{13}C NMR spectra were recorded on a Bruker DRX 500 (126 MHz) spectrometer or a Bruker Avance 600 (151 MHz) spectrometer. ^{3}C NMR spectra were referenced against the solvent residual proton signals (^{1}H) or the solvent itself (^{13}C). The exact assignment of the peaks was performed by two-dimensional NMR spectroscopy such as ^{1}H COSY, ^{1}H/^{13}C HSQC or ^{1}H/^{13}C HMBC when possible.

Ultra High resolution mass spectra were recorded on a JEOL ACCUTOF GCV JMS-T100GCVat 70 eV ionisation energy. IR spectra were recorded on a Perkin Elmer Paragon 1000 FT-IR spectrometer with a A531-G Golden-Gate-ATR-unit. Dynamic

scanning calorimetry was performed on a Perkin Elmer Pyris with a temperature ramp of 10 K/minute. All melting points were recorded on an Electrothermal melting point apparatus LG 1586 and are uncorrected.

Synthetic and Purification Equipment

Polymerizations were performed on a Linkam LTS-420 heating stage inbetween PTFE coated glass slides (see description below). Thin layer chromatography (TLC) was performed with pre-coated TLC-sheets from Macherey-Nagel GmbH & Co. KG with silica 60 and fluorescent indicator UV254. Column chromatography was performed with silica gel 60M from Macherey-Nagel GmbH & Co. KG with a size of 0.040 – 0.063 mm.

Porosity Calculations

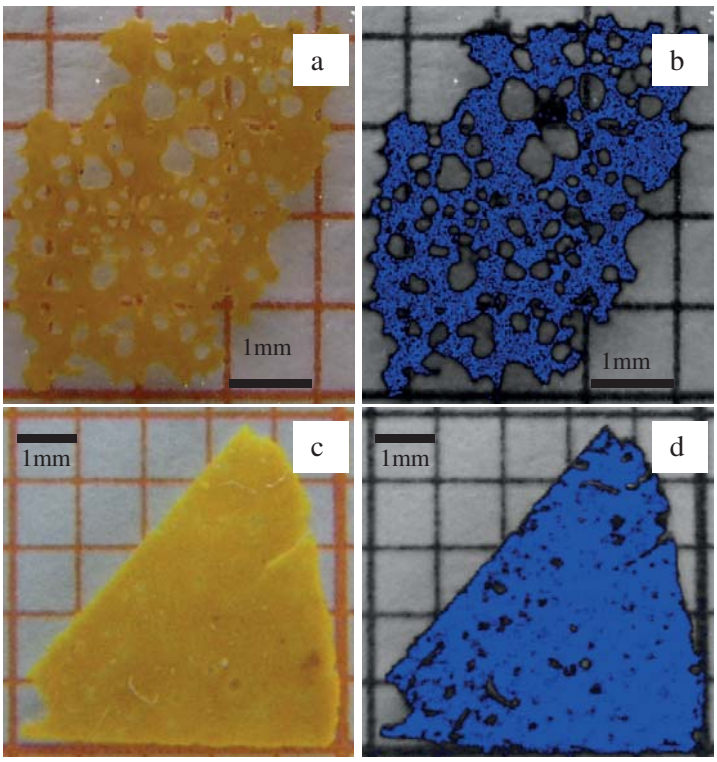

Supplementary Figure S1: Surface porosity calculation of LCE films, (a) 67% porous LCE, (b) porosity calculation of 67% porous LCE film via colour threshold, (a) 5% porous LCE, (b) porosity calculation of 5% porous LCE film via colour threshold.

The porosities of the samples were calculated with the image analysis software ImageJ 1.47v (NIH, USA). The colours of the image were separated into blue, green and red channels. The blue channel was used in the colour threshold analysis of the software, which allowed the calculation of the area of the pores of the apparent surface area of the film (Figure S1). The ratio of the calculated area to the total area was then used to estimate the porosity of the film.

Bending and Force Measurements

In the bending and force measurements, a UV LED source with λ = 365 nm (Hoenle LED UV Pen 2.0, approx. 5 W), and a homemade LED visible light source (approx. 3 W) with λ = 455nm, were used for illumination. For the photoactuation, the free standing film samples were fixed with tweezers while the lateral side of the films was illuminated with the light source.

The different light intensities were obtained by varying the distances of sample to the UV light source. The distances to the film substrate were 1.2 cm, 1.5 cm, 2cm and 3 cm. At a distance of 1.2 cm, the light was in focus and light intensity was 7.5 W/cm^2 at the center of the Gaussian beam (2w=~0.4 mm). At 1.5 cm, 2 cm and 3 cm, the light intensities were 80% (6

W/cm^2), 40% (3 W/cm^2) and ~15% (~1.1 W/cm^2) at the center of light beam, respectively[1].The bending of the film during photoactivation was recorded with a high-speed video camera (Photron Fastcam SA1.1) in epi-illumination mode (video 1 and video 2). The bending angle was evaluated from the displacement of the film at the point furthest from the fixed tweezer using the image analysis software ImageJ 1.47v (NIH, USA)(Figure S2). The statistical analyses were performed by one-way ANOVA Tukey test (SigmaPlot 12.5 software, Systat Software, Inc., Richmond, CA, USA).

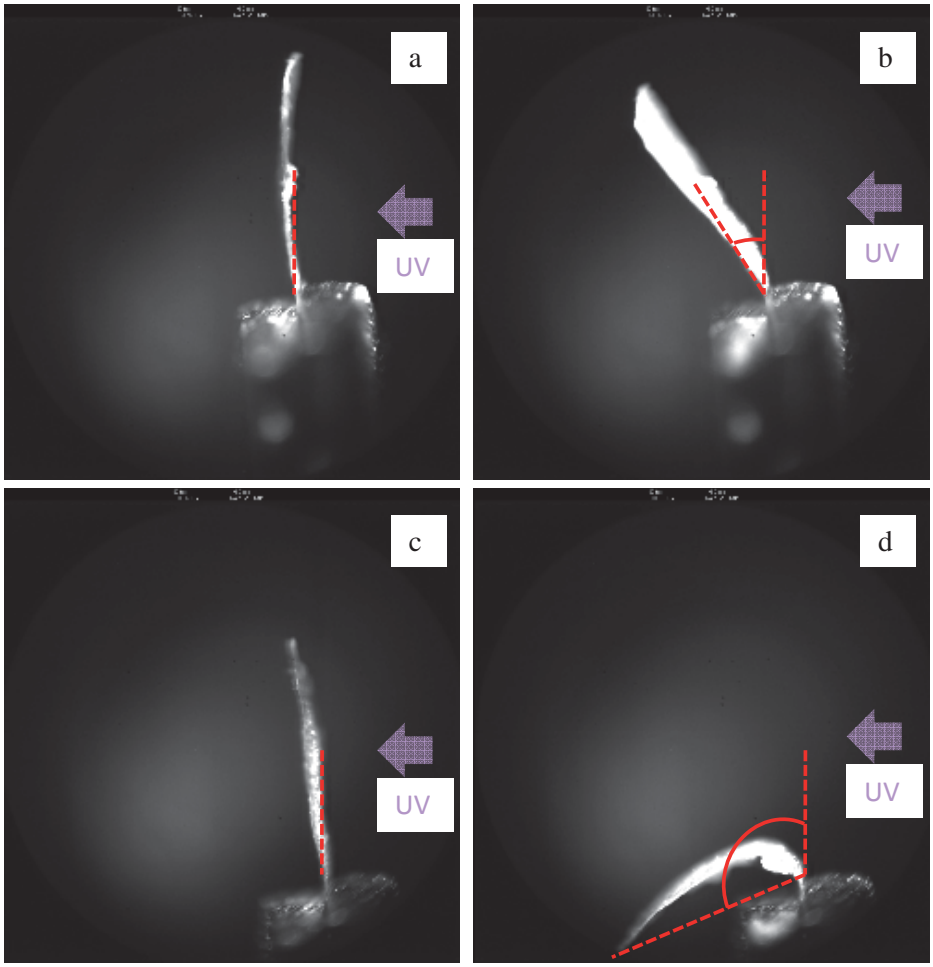

Supplementary Figure S2. Calculation of bending angles of LCE films with 5% (a: 0 s – b: 20 s') and 67% (c: 0 sec – d: 20 s) porosity under illumination of UV light. The displacement of free standing edge of the film was compared with the initial position and the angle is calculated corresponding to y-axis.

Figure S3 shows the measurement of forces during photoisomerisation of LCE film with 67% porosity with a size 5 x 2 x 0.1 mm. To measure forces exerted by the azobenzene LCE films during photoisomerisation, a tube-shaped glass cantilever with a diameter of 15 µm was used as force probe. The glass cantilever was marked with paint to obtain a point of reference to measure the deflection of the cantilever during the experiments. In order to calibrate the glass cantilever, a highly precise ultra micro balance (MT-SICS-UMX2, MettlerToledo GmbH, Greifensee, Switzerland) and a motor driven micromanipulator (DC3001R with controller MS314, World Precision Instruments Inc., Sarasota, FL, USA) were used. The glass cantilever was driven by the micromanipulator onto a vertically mounted razor blade on the ultra micro balance. For each 10 µm distance driven, the weight was recorded and converted to the corresponding forces. The LCE films were brought into contact with the cantilever, so that the reference point was visible. Using a monochrome high-speed digital camera (Kodak Motion Corder Analyzer SR-Ultra, Eastman Kodak Co., San Diego, CA, USA) and an optical stereomicroscope (Leica MZ 12.5,

Leica GmbH, Wetzlar, Germany), the bending of the free standing LCE films were recorded. Three LCE films with 67% porosity were used and forces were measured 40 times for each: 20 measurements under UV and 20 measurements under visible light illumination. The forces exerted by the samples on the force probe were evaluated by measuring the distance between the initial and the final positions of the reference point using Image J.

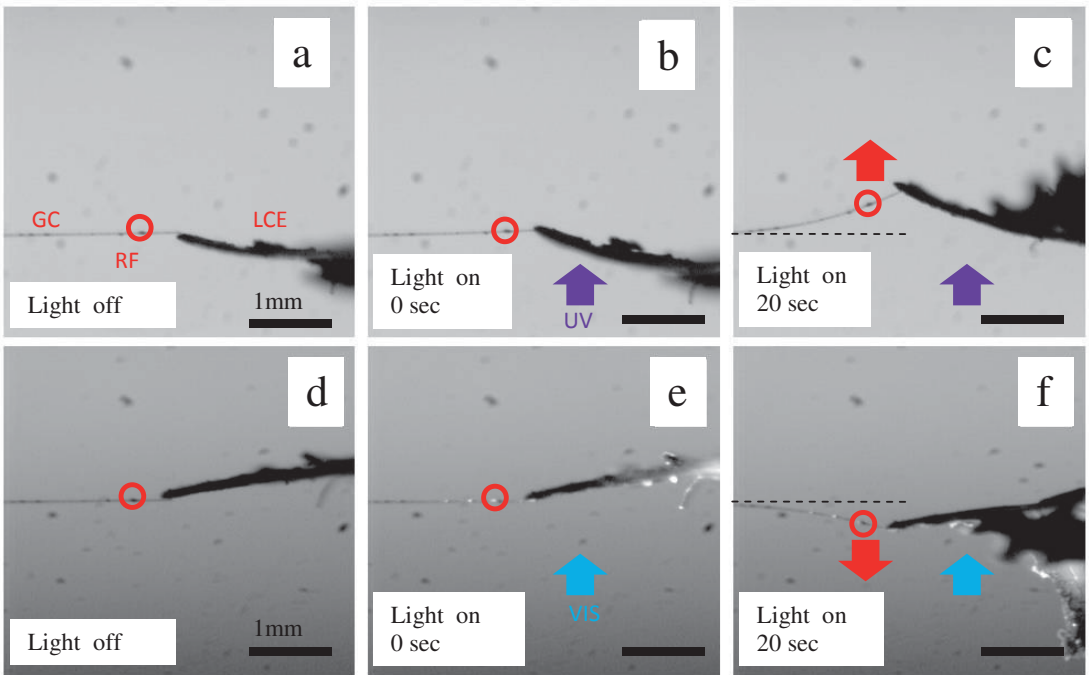

Supplementary Figure S3. Force measurements of LCE film with 67% porosity using a glass cantilever as a force probe. GC=glass cantilever, RF=reference point. (a-c) The film was illuminated with UV light (λ = 365 nm) was performed; (a) light source is off ; (b) light source is on, 0 sec; (c) light source is on, 20sec.The film bentaway from the UV light illumination.This was followed by illumination with visible light (λ = 455nm) (d-f): (d) light source is off ; (e) light source is on, 0 sec; (f) light source is on, 20sec.After this second illumination, the film bentback again towards the source of illumination. The reference point on the glass cantilever was observed via high-speed camera and the deflections after each illumination were calculated by ImageJ.

Polymerization

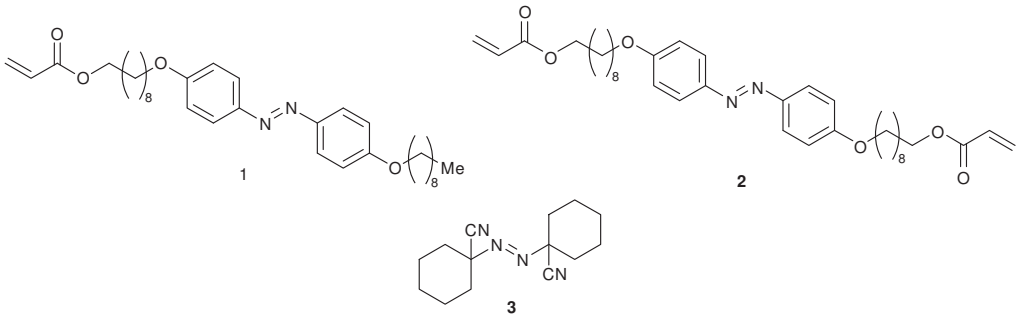

4(9-(acryloyloxy)nonyloxy-4'nonyloxyazobenzene (**1**, 9 eq, 18.8 mg, 31.1 µmol), 4,4'-bis[9-(acryloyloxy)nonyloxy]azobenzene (**2**, 1 eq, 150 mg, 280 µmol) and 1,1′-azobis(cyclohexanecarbonitrile) (**3**, 1.1 mg, 4.48 µmol, 1.6mol% and 1.6 mg, 6.44 µmol, 2.3mol% - experiment A and B) were dissolved in dichloromethane. The solvent was evaporated and the solid mixture was introduced into a homemade LC cell on a heating stage (see description below). The mixture was melted at 100 °C. Then, the temperature was decreased to 91 °C over the course of 120 min. This temperature was held for 12 h (temperature stability < 0.1 °C). During the polymerization process, the gas evolution due to the decomposition of the initiator **3**produced bubbles in the polymer film. For the extraction of the polymer film from the LC cell, it was introduced in a bath of chloroform. Unreacted monomers dissolved, while the polymer film delaminated from the substrate. The resulting polymer film was extracted by soxleth extraction with chloroform for 10 h. The film was dried in a vacuum oven at 50 °C at a pressure of 10 mbar for 24 h.

Glass Cell and Polymerization Methodology

a) Fabrication of the glass cell:

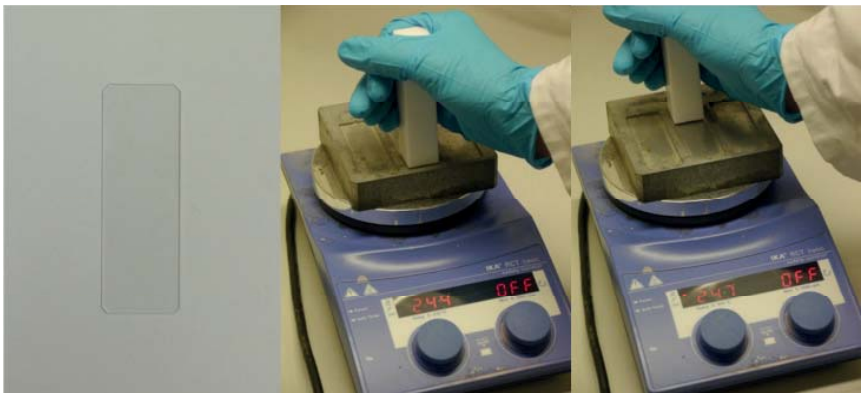

Fig. SI-3A glass slide was heated on a magnetic stirrer to approx. 250 °C. A bulk PTFE stick was rubbed with a speed of approx. 7 cm/30s over the surface of the glass slide.

b) Using the glass slides as polymerization reactors for the LCE films.

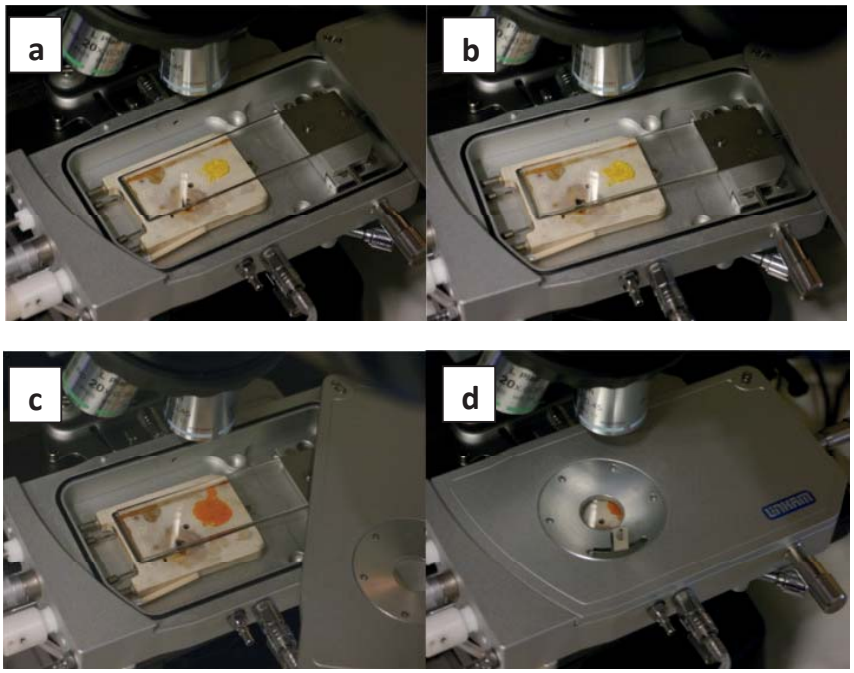

Fig. SI-4 APTFE coated glass slide was placed on the heating stage. The mixture of monomersand initiator (see experimental procedure) was placed on the glass slide (a).The mixture was covered with another glass PTFE coated glass slide (b) and subsequently heated to 100 °C (at this temperature, the mixture gives an isotropic melt) (c). The stage was closed and cooled down to 94 °C over the course of 60 min (d)The temperature was hold for 18 h while the mixture is polymerizing.

Syntheses

The analysis of all compounds is consistent with the original characterization by Ikeda and co-workers.[2]

4-(9-Hydroxynonanyloxy)nitrobenzene (1)

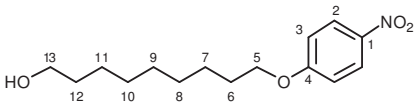

The procedure by Ikeda and coworkers was performed under Schlenk conditions in an atmosphere of dry nitrogen and modified as follows: Sodium hydride (8.96 mmol, 215 mg) was suspended in a solution of 4-nitrophenol (8.96 mmol, 1.25 g) in DMF (50,0 mL).The reaction mixture was cooled to 0 °C and a solution of 9-bromo-1-nonanol (8.96 mmol, 2.00 g) in DMF (10 mL) was added via syringe over the course of 5 min. The reaction mixture was heated at 120 °C for 90 h. After cooling to 20 °C, the residue was filtered. The solvent was evaporated in *vacuo*. The crude product was purified by column chromatography (cyclohexane : ethyl acetate, *v/v*, 2:1, R_f=0.28). A brownish white solid was obtained in a yield of 90 % (8.09 mmol, 2.28 g, Lit.:=78 %).

M. p.: 52 °C

^{1}H NMR (500 MHz, $CDCl_3$): 8.18 (d, ^3J = 9.3 Hz, 2 H, H-2), 6.93 (d, ^3J = 9.3 Hz, 2 H, H-3), 4.04 (t, ^3J = 6.5 Hz, 2 H, H-5), 3.64 (t, ^3J = 6.6 Hz, 2 H, H-13), 1.81 (m, 2 H, H-6), 1.56 (m, 2 H, H-12), 1.51-1.42 (m, 4H, H-7, H-11), 1.39-1.30 (m, 6 H, H-8, 9, 10).

^{13}C NMR (125 MHz, $CDCl_3$): 164.2 (C-4), 141.3 (C-1), 125.9 (*C-2*), 114.4 (C-3), 68.9 (C-5), 63.0 (C-13), 32.7 (C-12), 29.4 (C-9), 29.3 (C-10), 29.2 (c-8), 28.9 (C-6), 25.9 (c-7), 25.7 (C-11) ppm.[1]

IR (ATR): $\tilde{\nu}$ = 3527.6 (m), 3210 (w), 3089 (w), 2920 (s), 2879 (m), 2850 (m), 1590 (s), 1501 (s), 1473 (m), 1396 (m), 1336 (s), 1307 (m), 1253 (s), 1183 (m), 1116 (m), 1056 (m), 1031 (m), 1005 (s), 859 (s), 754 (m), 719 (m), 693 (m), 658 (s), 499 (s) cm^{-1}.

HRMS (EI): *m/z* found 281.1629; calcd. for$C_{15}H_{23}NO_4$281.1627.

4-(9-Hydroxynonanyloxy)aniline (2)

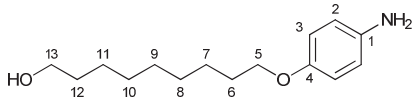

The original synthesis by Ikeda and co-workers.was modified as follows: A mixture of4-(9-hydroxynonanyloxy)nitrobenzene (**1**)(2.8 g, 10mmol) and Pd-C (0.11 g; Pd: 10 %) was added to THF (15 mL), and the resulting suspension was stirred at 50 °C in an autoclave in a hydrogen atmosphere (150 bar) for 12 h. A precipitate formed, which was filtered and the solvent was evaporated. The crude product was dissolved in chloroform and filtered through a short column of silica with ethyl acetate as eluent. The solvent was evaporated anda yellow/brownish solid was obtained in a yield of 87 % (Lit.: 82 %).

M. p.: 87 °C

^{1}H NMR (500 MHz, $CDCl_3$): 6.73 (d, ^3J = 8.9 Hz, 2 H, 3-H), 6.62 (d, ^3J = 8.9 Hz, 2 H, 2-H), 3.86 (t, ^3J = 6.6 Hz, 2 H, H-5), 3.60 (t, ^3J = 6.7 Hz, 2 H, H-13), 1.72 (m, , 2 H, H-6), 1.53 (m, 2 H, H-12), 1.46-1.37 (m, 4H, H-7, H-11), 1.35-1.27 (m, 6 H, H-8, H-9, H-10).[2]

^{13}C NMR (125 MHz, $CDCl_3$): 153.3 (C-4), 139.7 (C-1), 116.5 (*C-2,2'*), 115.6 (C-3,3'), 68.7 (C-5), 62.8 (C-13), 32.7 (C-12), 29.5 (C-9), 29.4 (C-10), 29.3 (c-8), 29.3 (C-6), 26.0 (c-7), 25.7 (C-11) ppm.

IR (ATR): $\tilde{\nu}$ = 3337 (w), 3270 (w), 3047 (w), 2923 (s), 2853 (m), 1613 (w), 1590 (w), 1514 (s), 1475 (m), 1383 (w), 1298 (w), 1237 (s), 1104 (m), 1072 (s), 1046 (s), 1037 (m), 979 (w), 900 (m), 814 (s), 763 (s), 728 (m), 559 (m), 527 (s) cm^{-1}.

HRMS (EI): *m/z* found 251.1878; calcd. for $C_{15}H_{25}N_O$251.1885.

4-Hydroxy-4'-(9-hydroxynonanyloxy)azobenzene (3)

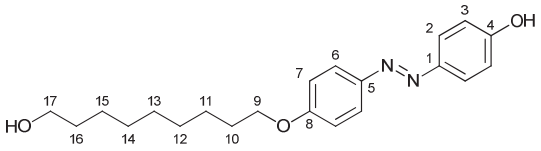

The original synthesis by Ikeda and co-workers was modified as follows: A solution of4-(9-hydroxynonanyloxy)aniline (**2**) (8.46 g, 33.7 mmol) in hydrochloric acid (80.0 mL, 6 M) was cooled to -8 °C. A solution of sodium nitrite (2.51 g, 36.4 mmol) in water (25 ml) was cooled to 0 °C and added dropwise to the reaction mixture over the course of 15 min. A solution of phenol (3.17 g, 33.7 mmol) in an aqueous sodium hydroxide solution (100 mL, 0.75 M), cooled to - 5 °C was added dropwise over the course of 90 min. The temperature of the reaction mixture was held at - 5 °C for 30 min without stirring while the product precipitates.The precipitate was filtered and washed with water (3x 100 mL). The product was recrystallized from ethanol.A brown solid was obtained in a yield of89 % (10.7 g) (Lit.: 59%).

DSC.: Phase Transitions at 127 °C and 148°C

^{1}H NMR (500 MHz, DMSO-d_6): 10.23 (Ar-OH), 7.78 (d, ^{3}J = 9.0 Hz, 2 H, H-6), 7.74 (d, ^{3}J = 8.9 Hz, 2 H, H-2), 7.06 (d, ^{3}J = 9.0 Hz, 2 H, H-7), 6.93 (d, ^{3}J = 8.9 Hz, 2 H, H-3), 4.03 (t, ^{3}J = 6.5 Hz, 2 H, H-9), 3.72 (s, 1 H, CH2-OH), 3.37 (t, J = 6.6 Hz, 2 H, H-17), 1.72 (m,2 H, H-10), 1.44-1.37 (m, 4 H, H-11, 16), 1.32 (m, 8 H, H-12-15) ppm.

^{13}C NMR (126 MHz, $CDCl_3$): 161.1 (C-8 or C-4)[3], 161.0 (C-8 or C-4)3, 146.6 (C-1 or C5)3, 145.7 (C1 or C5)3, 124.8 (C-2), 124.4 (C-6), 116.33 (C-3), 115.3 (C-7), 68.4 (C-9), 61.2 (C-17), 33.0 (C-16), 29.5 (C-13), 29.4 (C-14), 29.2 (C-12), 29.1 (C-10), 26.0 (C-11), 25.9 (C-15) ppm.

IR (ATR): $\tilde{\nu}$ = 3304 (b), 3073 (w), 2922 (m), 2923 (s), 2852 (s), 1519 (m), 1581 (s), 1501 (m), 1470 (m), 1238 (s), 1143 (s), 1105 (m), 1070 (w), 1049 (w), 1018 (s), 970 (w), 909 (w), 843 (s), 811 (m), 772 (m), 752 (m), 723 (m), 643 (w), 548 (s), 536 (m), 502 (w) cm^{-1}.

HRMS (EI): *m/z* found 356.2091; $[M]^+$ calcd. for $C_{21}H_{28}N_2O_3$ 356.2100.

[2]The proton signals of the amine were invisible, presumably due to rapid H/D exchange.
[3]The resolution of HSQC- and HMBC-NMR spectry was insufficient to allow a precise assignment of the carbon signals because the chemical shifts were too close.

4,4'-Bis(9-hydroxynonanyloxy)azobenzene (4)

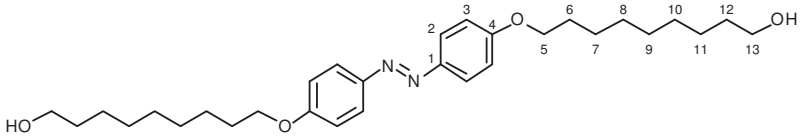

A mixture of 4-hydroxy-4'-(9-hydroxynonanyloxy)azobenzene (4.00 g, 11.0mmol) and 9-bromo-1-nonanol (2.94 g, 13.0mmol) was dissolved in DMF (50 mL), and potassium carbonate (1.80 g, 13.0 mmol) was added to the solution in one portion. The reaction mixture was heated to reflux for 36 h. Water (700 mL) was added and the mixture was allowed to settle for 30 min without stirring. The precipitate was filtered and washed with water (3x 250 mL). The crude product was dried *in vacuo* for 24 h. The product was recrystallized from THF/ methanol (9/1, *v/v*). 2.63 g (5.28 mmol, 48 %, Lit=65 %) of a yellow solid could be obtained.

DSC.: Phase Transitions at 64 °C and 178 °C

^{1}H NMR (500 MHz, $CDCl_3$): 7.79 (d, ^3J = 8.7 Hz, 4 H, H-2), 6.92 (d, ^3J = 8.7 Hz, 4 H, H-3), 3.96 (t, ^3J = 6.4 Hz, 4 H, H-5), 3.67 (t, ^3J = 6.4 Hz, 4 H, H-13), 1.74 (m, 4 H, H-6), 1.56-1.46 (m, 8 H, CH_2), 1.44-1.36 (m, 4 H, CH_2), 1.34-1.24 (m, 14 H, CH_2) ppm.[4]

^{13}C NMR (126 MHz, $CDCl_3$): 161.4 (C-4), 146.6 (C-1), 124.3 (C-2), 114.7 (C-3), 68.3 (C-5), 63.1 (C-13), 32.8, 29.5, 29.3, 29.3, 29.3, 29.2, 26.0, 25.7 ppm.4

IR (ATR): $\tilde{\nu}$ = 3317 (b), 2929 (m), 2923 (m), 2850 (m), 1606 (m), 1580 (m), 1501 (m), 1472 (m), 1463 (m), 1393 (m), 1316 (m), 1246 (s), 1151 (s), 1062 (m), 1024 (s), 846 (s), 750 (m), 556 (m) cm^{-1}.

HRMS (EI): *m/z* found 498.3461; $[M]^+$ calcd. for$C_{30}H_{46}N_2O_4$498.3458.

4-(9-Hydroxynonanyloxy)-4'-(nonanyloxy)azobenzene(5)

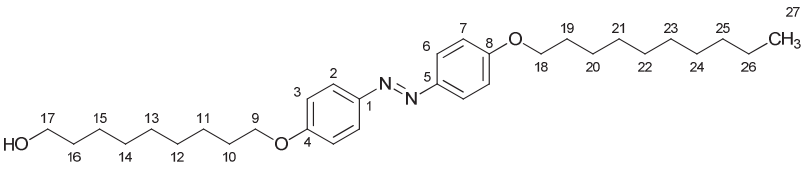

A mixture of 4-hydroxy-4'-(9-hydroxynonanyloxy)azobenzene (6.00 g, 16.8mmol) and 9-bromo-1-nonane (3.97 mL, 19.0mmol) were dissolved in DMF (50 mL).Potassium carbonate (2.63 g, 19.0mmol) was added to the solution in one portion. The reaction mixture was heated to reflux for 27 h. After the reaction mixture was cooled to 20 °C, water (500 mL)

[4]The proton and carbon signals that were not assigned could not be resolved byCOSY-, HSQC- or HMBC- NMR spectra.

was added to the mixture. The precipitate was filtered and washed with water (3 x 150 mL).The product was recrystallized from THF/ methanol (9/1, *v/v*). 4.92 g (9.91 mmol, 59%) of a yellow solid could be obtained.

M.p.: 116 °C

^{1}H NMR (600 MHz, $CDCl_3$): 7.89 (ad, ^3J = 8.2 Hz, 4 H, H-3, 7), 7.01 (ad, ^3J = 8.2 Hz, 4 H, H-2, 6), 4.06 (d, ^3J = 6.6 Hz, 4 H, H-9, H-18), 3.67 (at, ^3J = 6.6 Hz, 2 H, H-17), 1.84 (m, 4 H, H-10, H-19), 1.65-1.55 (m, 6 H), 1.54-1.56 (m, 4 H), 1.42-1.27 (m, 18 H), 0.92 (t, ^{3}J = 6.9 Hz, 3 H, H-27) ppm.[5]

^{13}C NMR (150 MHz, $CDCl_3$): 161.3 (C-4, C-8), 146.8 (C-1, C-5), 124.4 (C-2, C-6), 114.7 (C-3. C-7), 68.4 (C-9), 68.3 (C-18), 63.1 (C-17), 32.8, 31.9, 29.5, 29.5, 29.4, 29.3, 29.3, 29.3, 29.2, 26.1, 25.7, 22.7 (C-26), 14.12 (C-23) ppm.[2]

IR (ATR): $\tilde{\nu}$ = 3314 (b), 3072 (w), 3053 (w), 2936 (m), 2920 (s), 2850 (s), 1603 (m), 1580 (m), 1498 (m), 1396 (m), 1246 (s), 1151 (m), 1110 (m), 1017 (s), 846 (s), 776 (m), 642 (m), 557 (s) cm^{-1}.

HRMS (EI): *m/z* found 482.3510; $[M]^+$ calcd. for $C_{30}H_{46}N_2O_3$482.3508.

4,4'-Bis[9-(acryloyloxy)nonanyloxy]azobenzene (6)

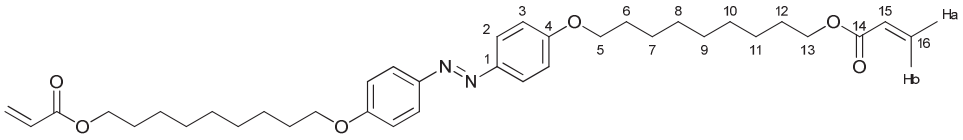

4,4'-Bis(9-hydroxynonanyloxy)azobenzene, (2.5 g, 5.0 mmol), triethylamine (4.33 mL, 31.6 mmol) and benzene-1,4-diol[6] (5.00 mg, 45.0 µmol) were dissolved in THF (500 mL). The reaction mixture was cooled to 0 °C.Acryloyl chloride (2.52 mL, 31.6 mmol) in THF (50 mL) was addeddropwise over the course of 30 min. The reaction mixture was stirred for 24 h at 20 °C. It was then poured into water (500 mL), and the product was extracted with chloroform. (3 x 300 mL).The organic layer was separated and dried over magnesium sulfate.The solvent was evaporated. The crude product was purified by column chromatography (chloroform, R_f=0.56). The product wasrecrystallized from methanol. 1.33 g (42 %, 2.10 mmol, Lit:=25 %) of a yellow solid wasobtained.

DSC.: Phase Transitions at 78 °C and 91 °C

^{1}H NMR (500 MHz, $CDCl_3$): 7.86 (d, ^3J = 8.9 Hz, 2 H, H-2), 6.98 (d, ^3J = 8.9 Hz, 2 H, H-3), 6.39 (dd, ^3J = 17.3, 1.4 Hz, 2 H, H-16b), 6.12 (6.12 (dd, ^3J = 17.3, 10.4 Hz, 2 H, H-15), 5.81 (dd, ^3J = 10.4, 1.4 Hz, 2 H, H-16a), 4.15 (at, J = 6.7 Hz, 4 H, H-13), 4.02 (at, J = 6.5 Hz, 4 H, H-5), 1.81 (m, 4 H, H-6), 1.67 (m, 4 H, H-12), 1.51 – 1.44 (m, 4 H, H-7), 1.42-1.31 (m, 16 H, H-8,9,10,11) ppm.

[2]The proton and carbon signals that are not assigned could not be resolved byCOSY-, HSQC- or HMBC- NMR spectra.

[6] This reagent was added as an inhibitor to prevent premature polymerization of compound **6**.

^{13}C NMR (126 MHz, $CDCl_3$): 166.3 (C-14), 161.14 (C-4), 146.95 (C-1), 130.4 (C-16), 128.6 (C-15), 124.3 (C-2), 114.7 (C-3), 68.3 (C-5), 64.7 (C-13), 29.4, 29.3, 29.2, 29.2, 28.6, 26.0, 25.9 ppm.[7]

IR (ATR): $\tilde{\nu}$ = 3070 (w), 2961 (w), 2939 (m), 2920 (s), 2853 (m), 1724 (s), 1603 (m), 1580 (m), 1498 (m), 1476 (m), 1412 (m), 1393 (m), 1320 (m), 1301 (m), 1246 (s), 1202 (s), 1018 (s), 846 (s), 556 (m) cm^{-1}.

HRMS (EI): *m/z* found 606.3671; $[M]^+$ calcd. for $C_{36}H_{50}N_2O_6$634.3669.

4-[9-(Acryloyloxy)nonanyloxy]-4'-(nonanyloxy)azobenzene (7)[3]

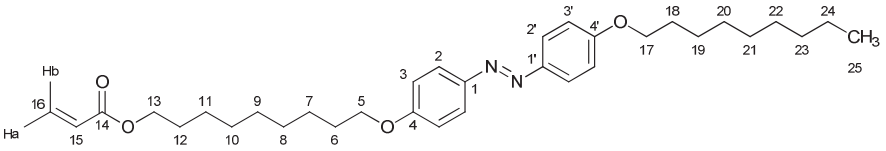

4-(9-Hydroxynonanyloxy)-4'-(nonanyloxy)azobenzene (4.50 g, 9.66 mmol), triethylamine (4.17 mL, 30.5mmol) and benzene-1,4-diol (2.1 mg, 18.9 µmol) were dissolved in THF (500 mL). The reaction mixture was cooled to 0 °C. Acryloyl chloride (2.43 mL, 30.5mmol) in THF (50 mL) was addeddropwise over the course of 30 min. The reaction mixture stirred at 20 °C for 24 h. The reaction mixture was poured into water (500 mL), and the product was extracted with chloroform (3 x 300 mL). The organic layer was separated and dried over magnesium sulfate. The solvent was evaporated. The crude product was purified by column chromatography (chloroform, R_f=0.85). The product was recrystallized from methanol. 2.74 g (49 %, 2.10 mmol) of a yellow solid were obtained.

DSC.: Phase Transitions at 69 and 94 °C

^{1}H NMR (500 MHz, $CDCl_3$): 7.86 (d, ^3J = 8.9 Hz, 2 H, H-2), 6.98 (d, ^3J = 8.9 Hz, 2 H, H-3), 6.40 (dd, J = 17.3, 1.5 Hz, 1 H, H-16b), 6.12 (6.12 (dd, ^3J = 17.3, 10.4 Hz, 1 H, H-15), 5.81 (dd, J = 10.4, 1.5 Hz, 1 H, H-16a), 4.15 (t, ^3J = 6.7 Hz, 2 H, H-13), 4.02 (at, ^3J = 6.5 Hz, 4 H, H-5, 17), 1.81 (m, 4 H, H-6, 18), 1.68 (m, 2 H, H-12), 1.48 (m, 4 H, H-7,19), 1.42-1.22 (m, 18 H, H-8-11; H-20-23), 0.89 (t, ^3J = 7.0 Hz, 3 H-25) ppm.

^{13}C NMR (126 MHz, $CDCl_3$): 166.3 (C-14), 161.2 (C-4,4'), 147.0 (C-1,1'), 130.4 (C-16), 128.7 (C-15), 124.3 (C-2), 114.65 (C-3), 68.3 (C-5), 68.3 (C-17), 64.7 (C-13), 31.9, 29.5, 29.4, 29.3, 29.2, 29.2, 29.2, 28.6, 26.0, 26.0, 22.7, 14.09 (C-25) ppm.[8]

IR (ATR): $\tilde{\nu}$ = 3104 (w), 3079 (w),3044 (w),2939 (m), 2923 (m), 2853 (m), 2853 (m), 1727 (m), 1711 (s), 1600 (m), 1581 (m), 1472 (m), 1476 (m), 1412 (m), 1320 (m), 1301 (m), 1240 (s), 1192 (s), 1107 (m), 1021 (s), 992 (m), 811 (m), 779 (m), 725 (m), 642 (m), 550 (m) cm^{-1}.

HRMS (EI): *m/z* found 536.3612; $[M]^+$ calcd. for $C_{36}H_{54}N_2O_4$536.3614

[4]The proton and carbon signalsthat are not assigned could not be resolved byCOSY-, HSQC- or HMBC- NMR spectra.
[8]The protonand carbon signalsthat are not assigned could not be resolved by COSY-, HSQC- or HMBC- NMR spectra.

NMR Spectra – ^{1}H NMR Spectra followed by ^{13}C NMR Spectra

4-(9-Hydroxynonanyloxy)nitrobenzene (1)

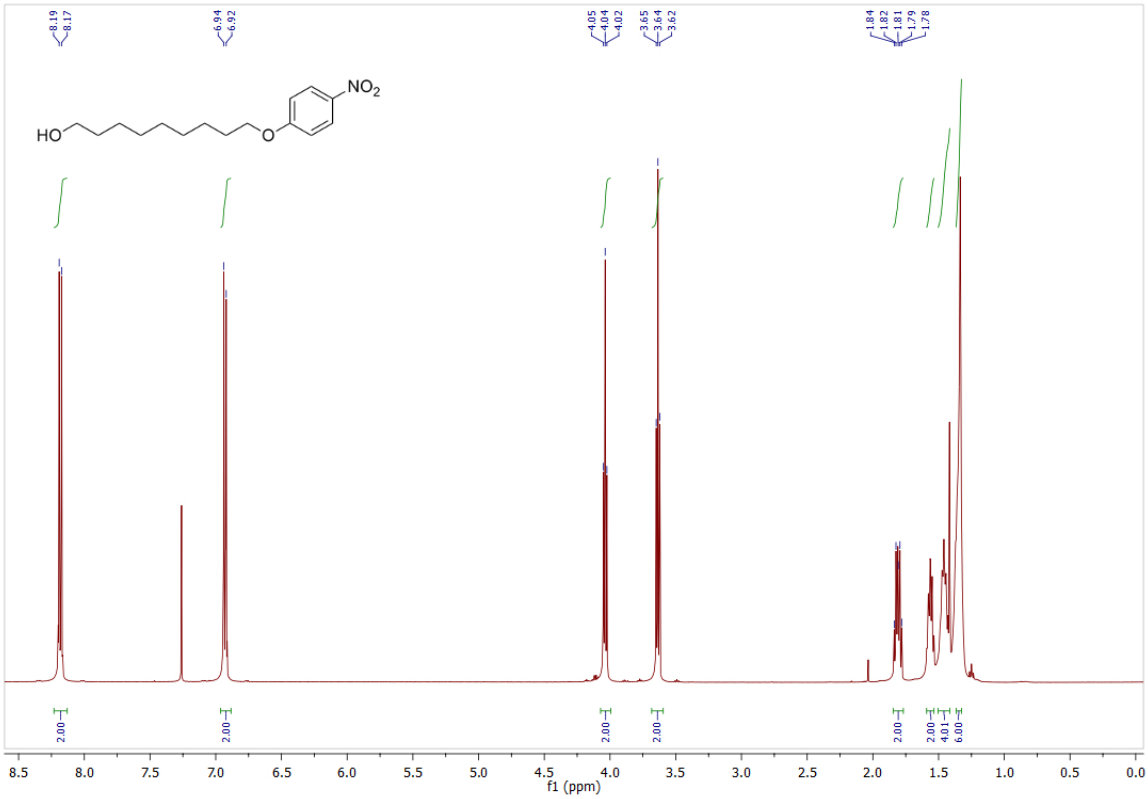

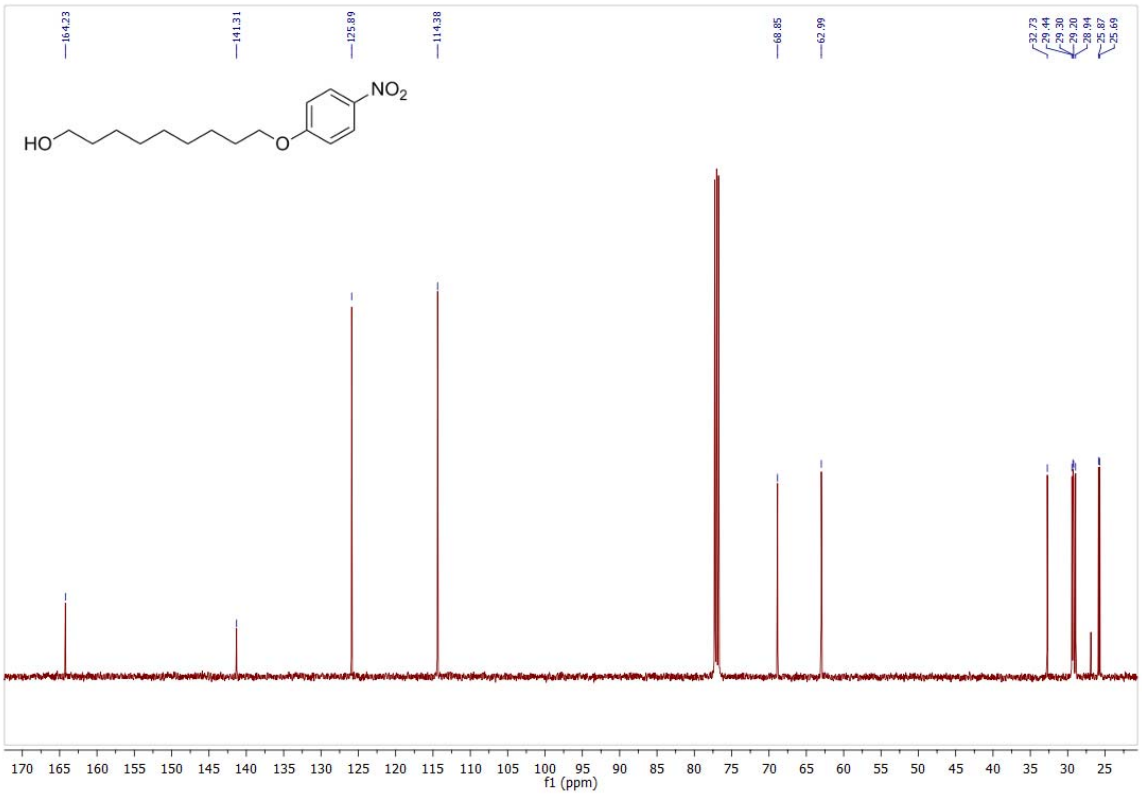

4-(9-Hydroxynonanyloxy)aniline (2)

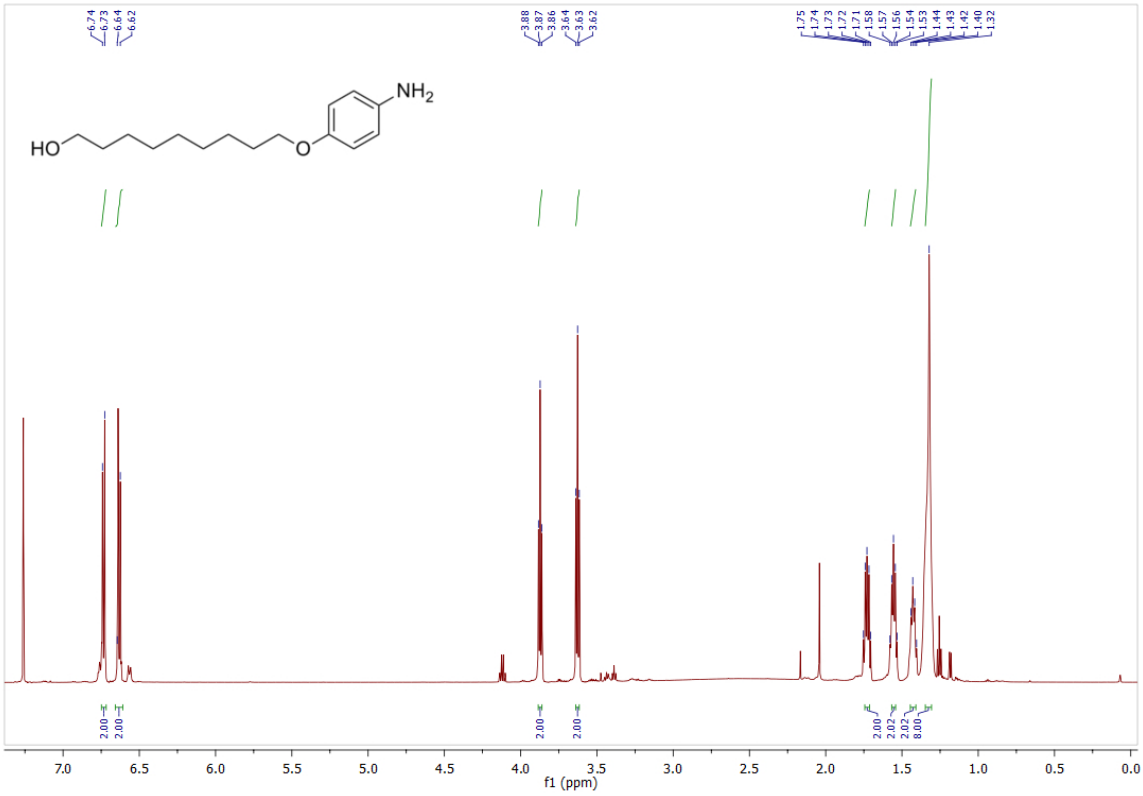

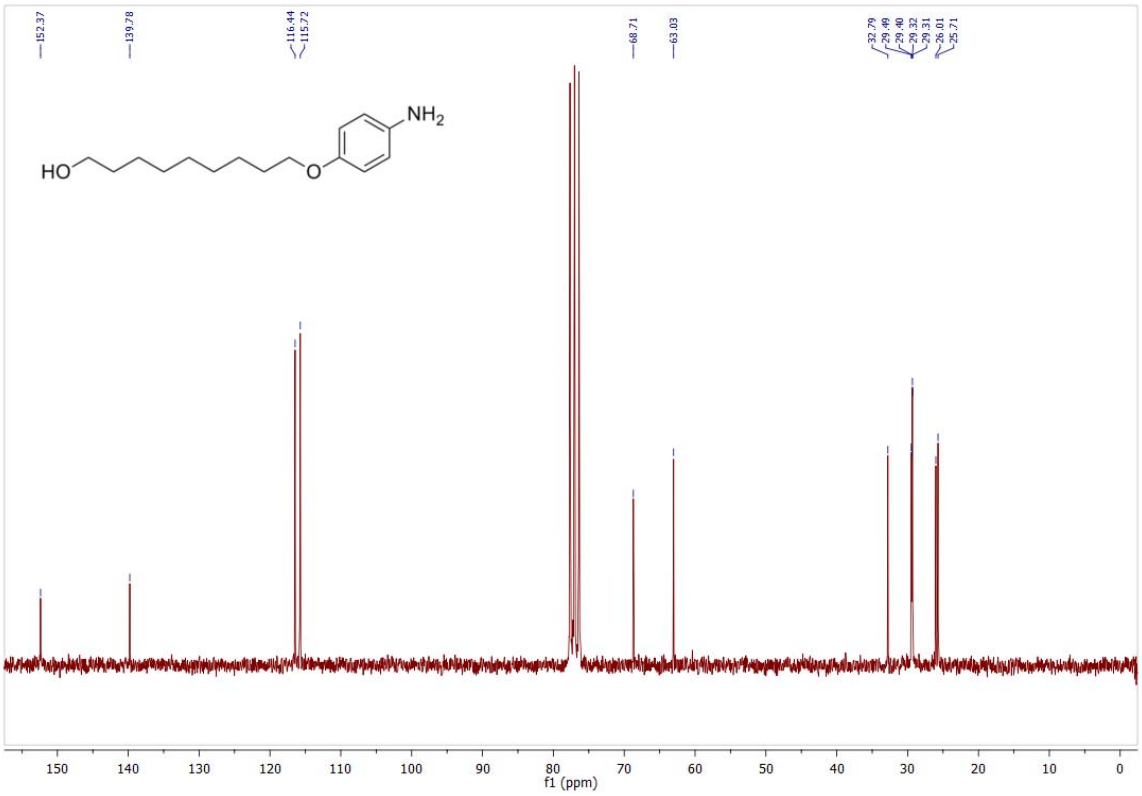

4-Hydroxy-4’-(9-hydroxynonanyloxy)azobenzene (3)

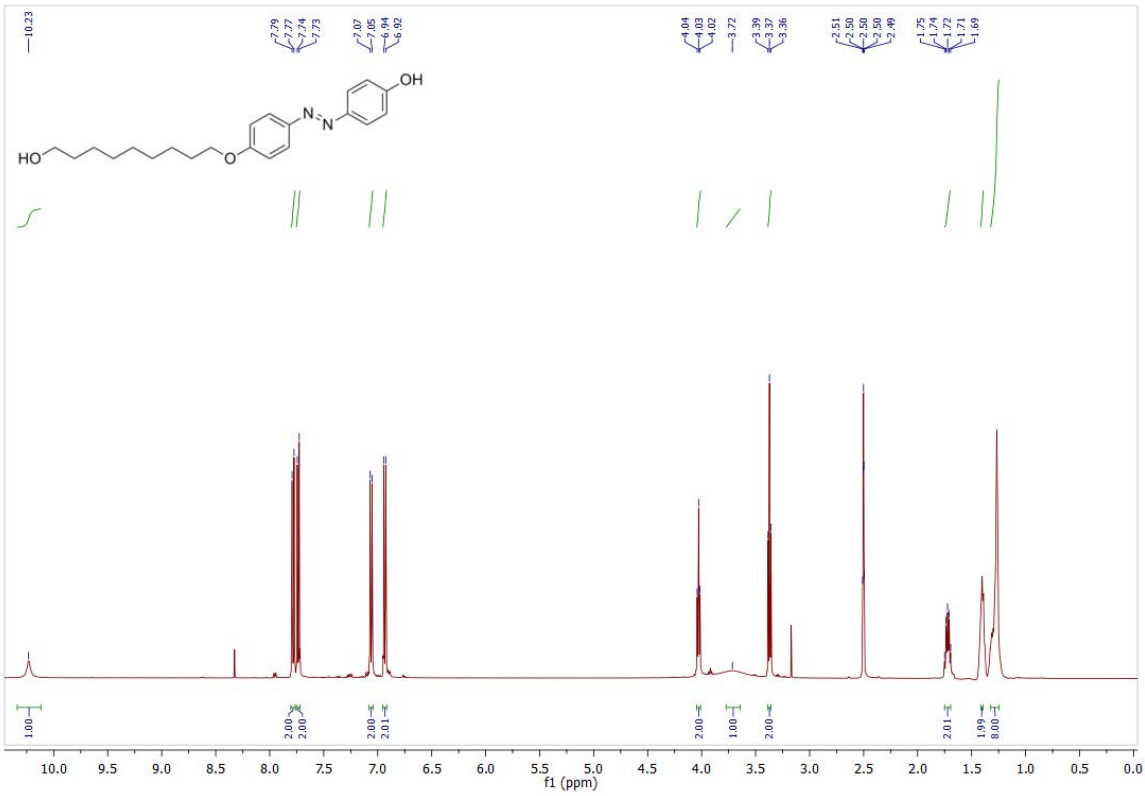

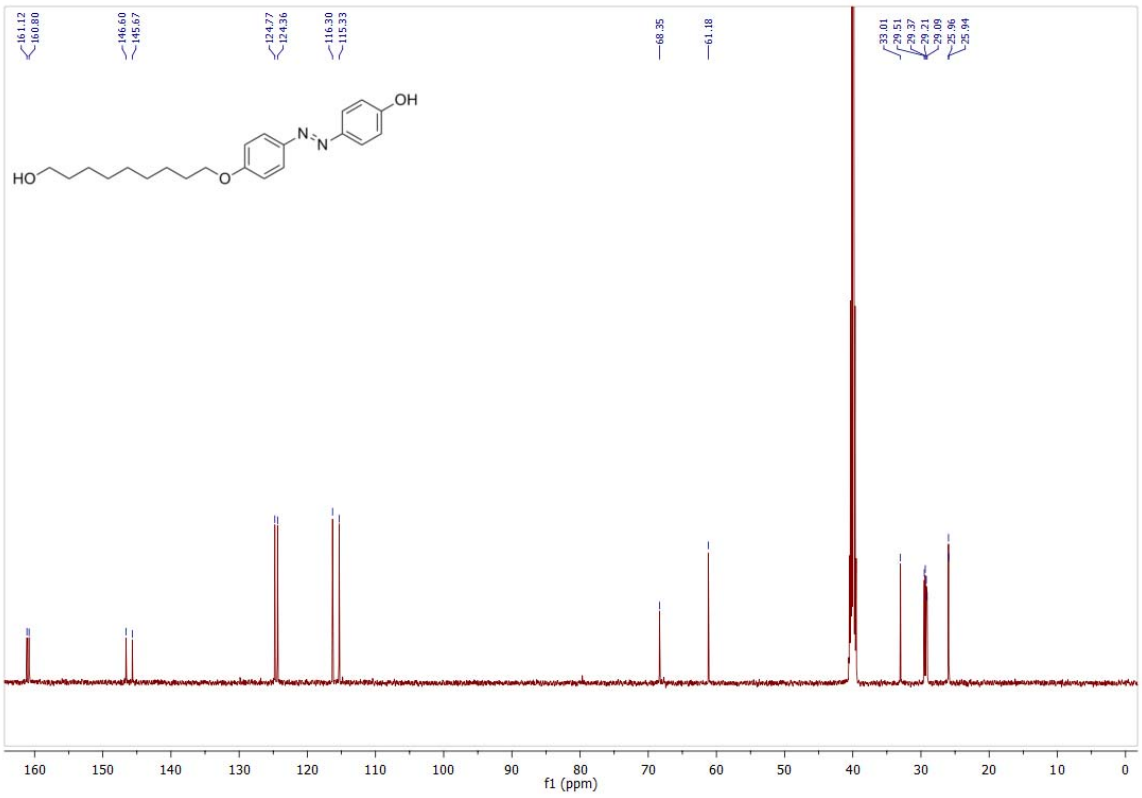

4,4’-Bis(9-hydroxynonanyloxy)azobenzene (4)

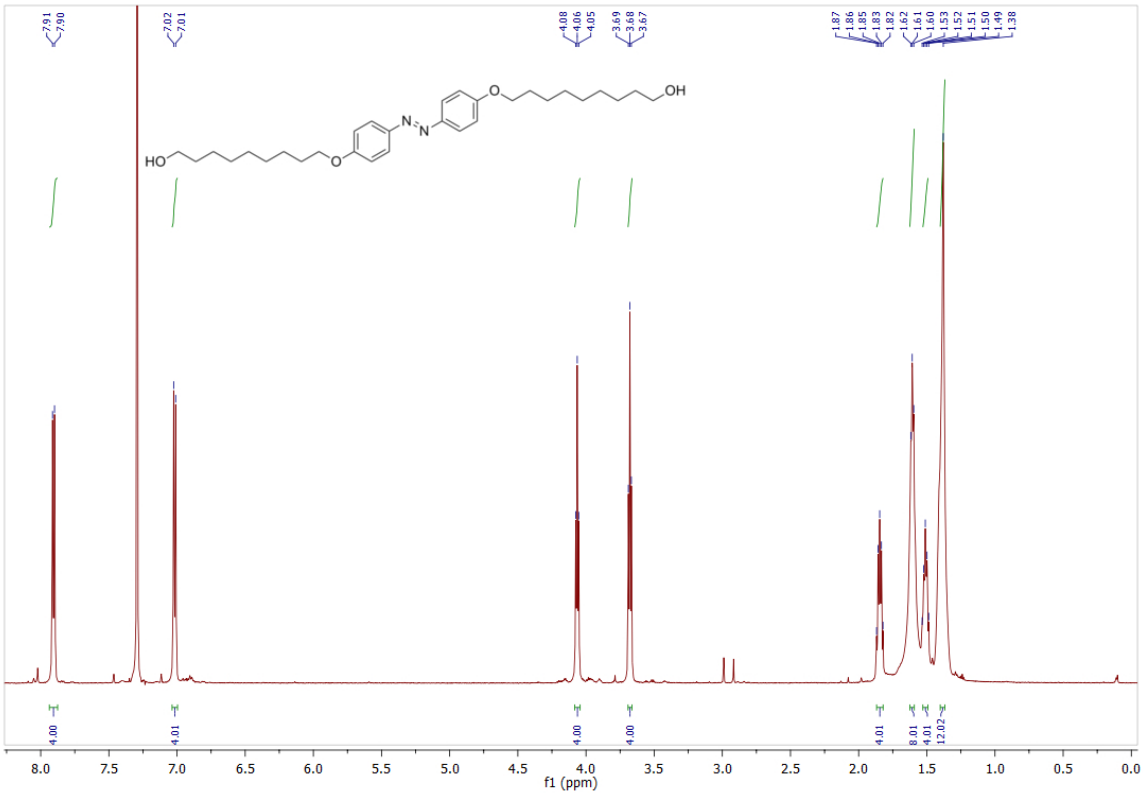

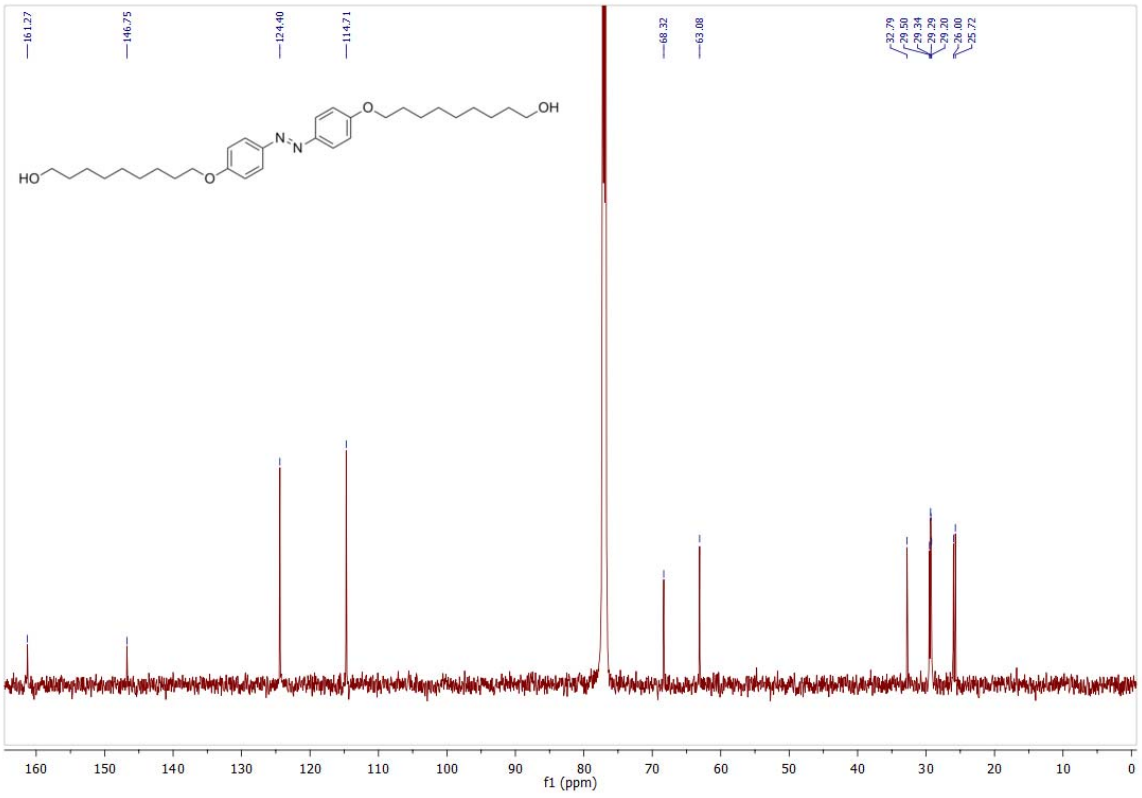

4-(9-Hydroxynonanyloxy)-4’-(nonanyloxy)azobenzene (5)

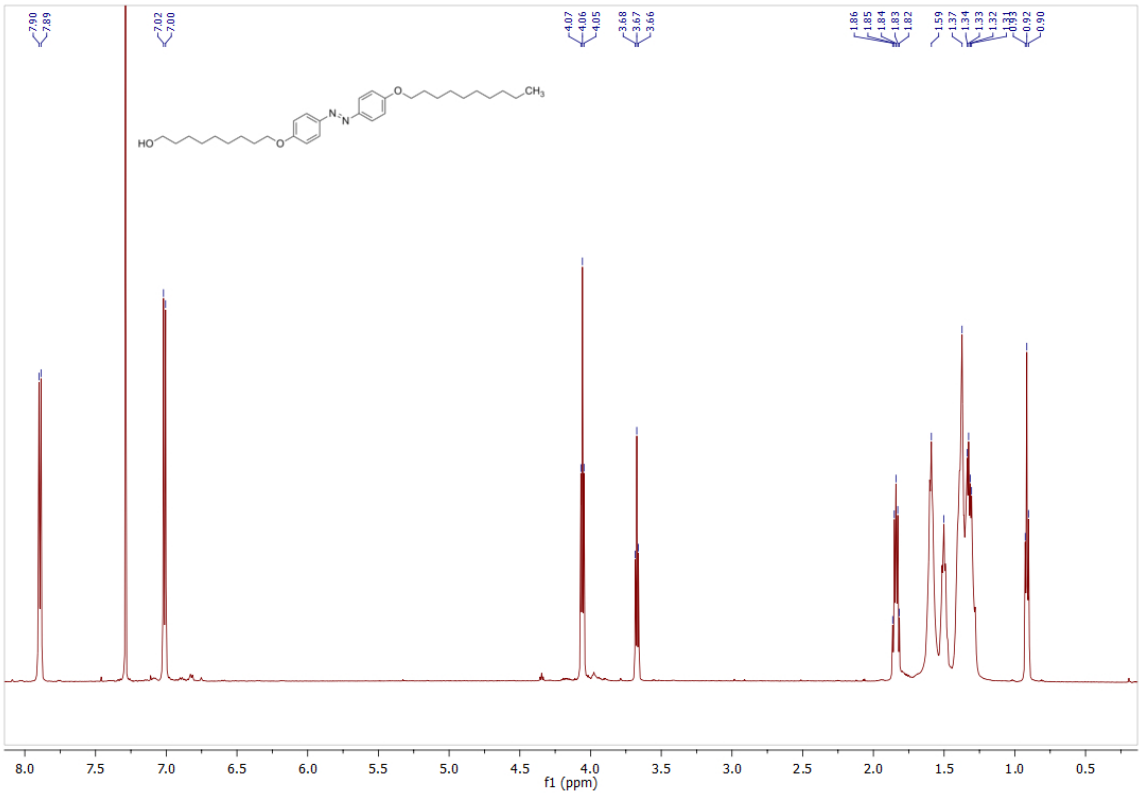

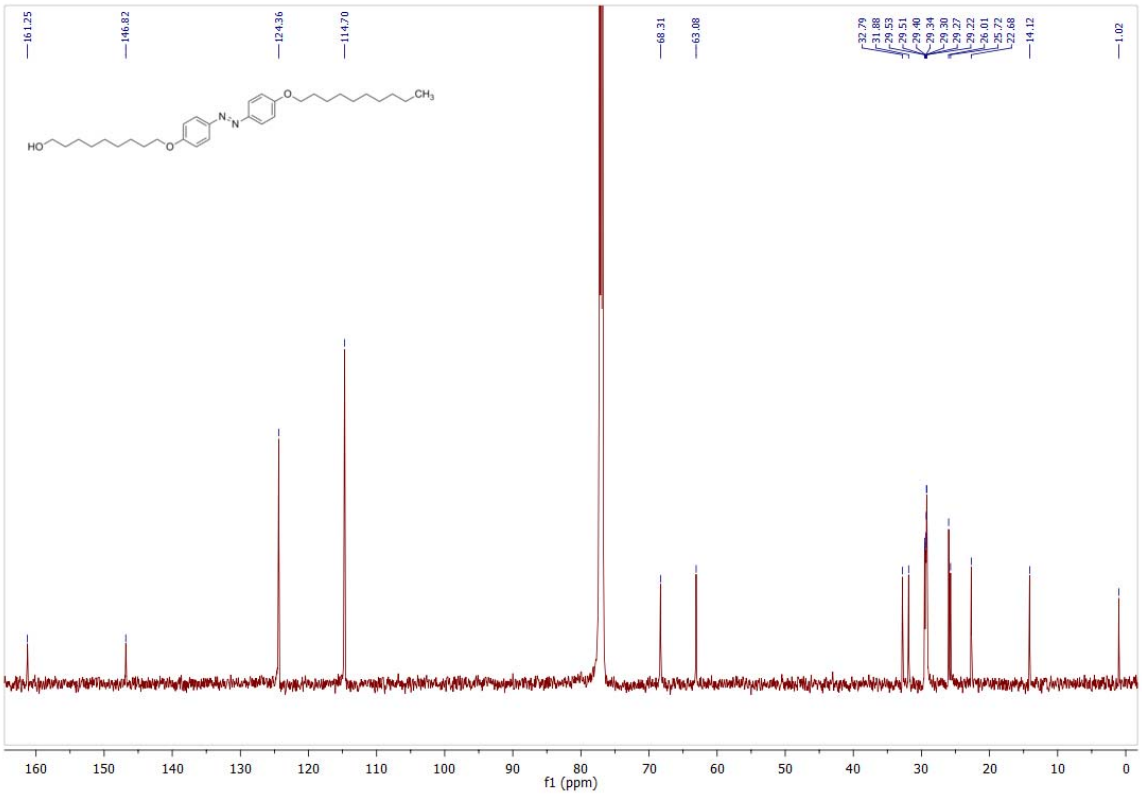

4,4’-Bis[9-(acryloyloxy)nonanyloxy]azobenzene (6)

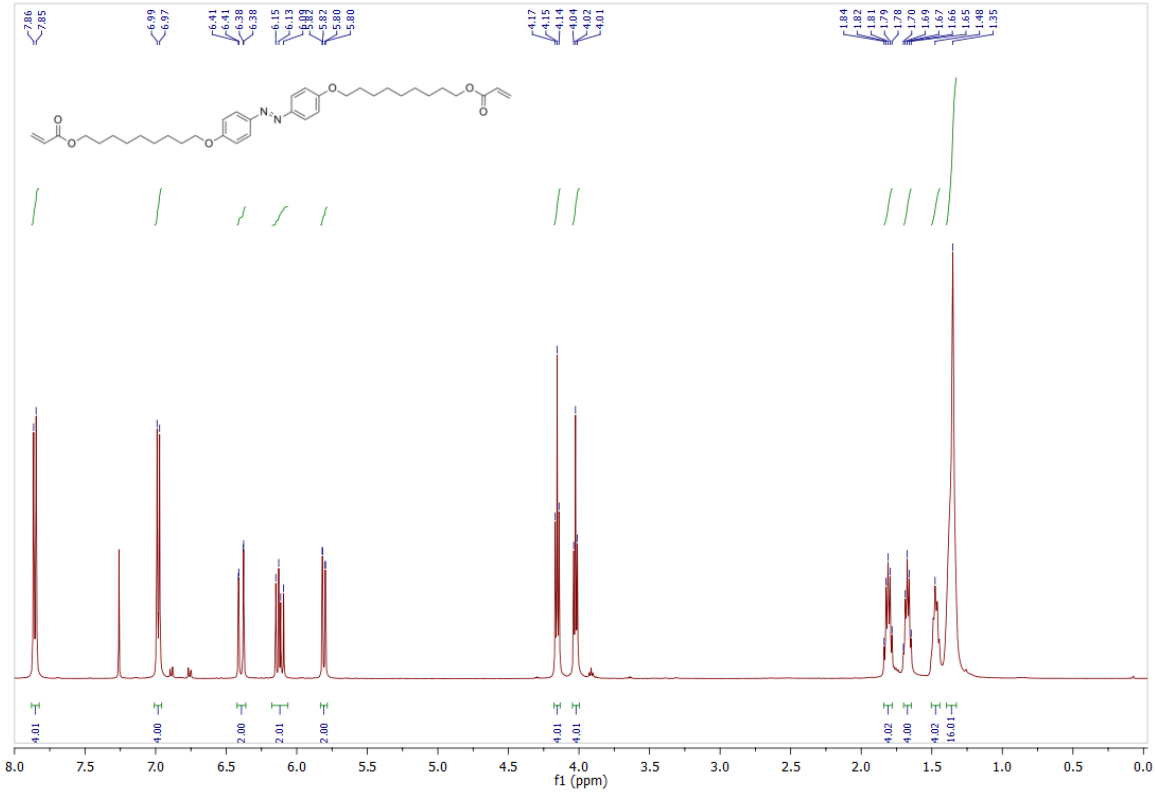

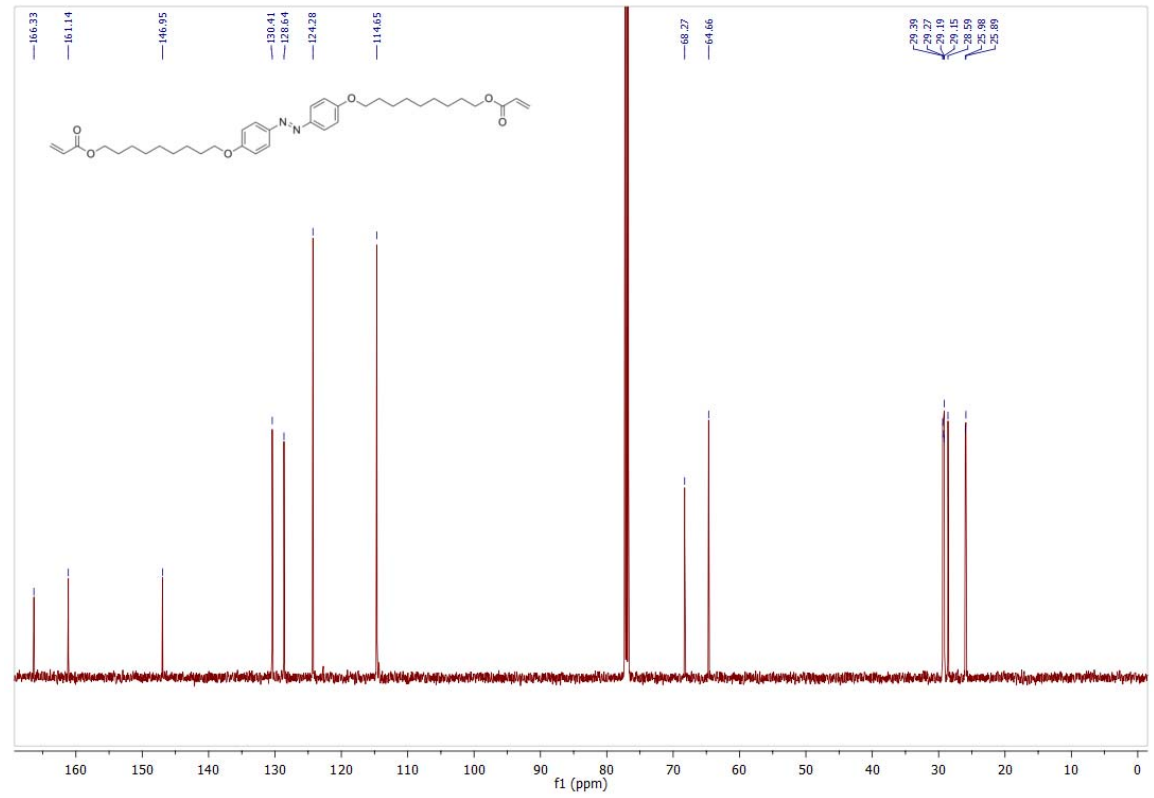

4-[9-(Acryloyloxy)nonanyloxy]-4’-(nonanyloxy)azobenzene (7)

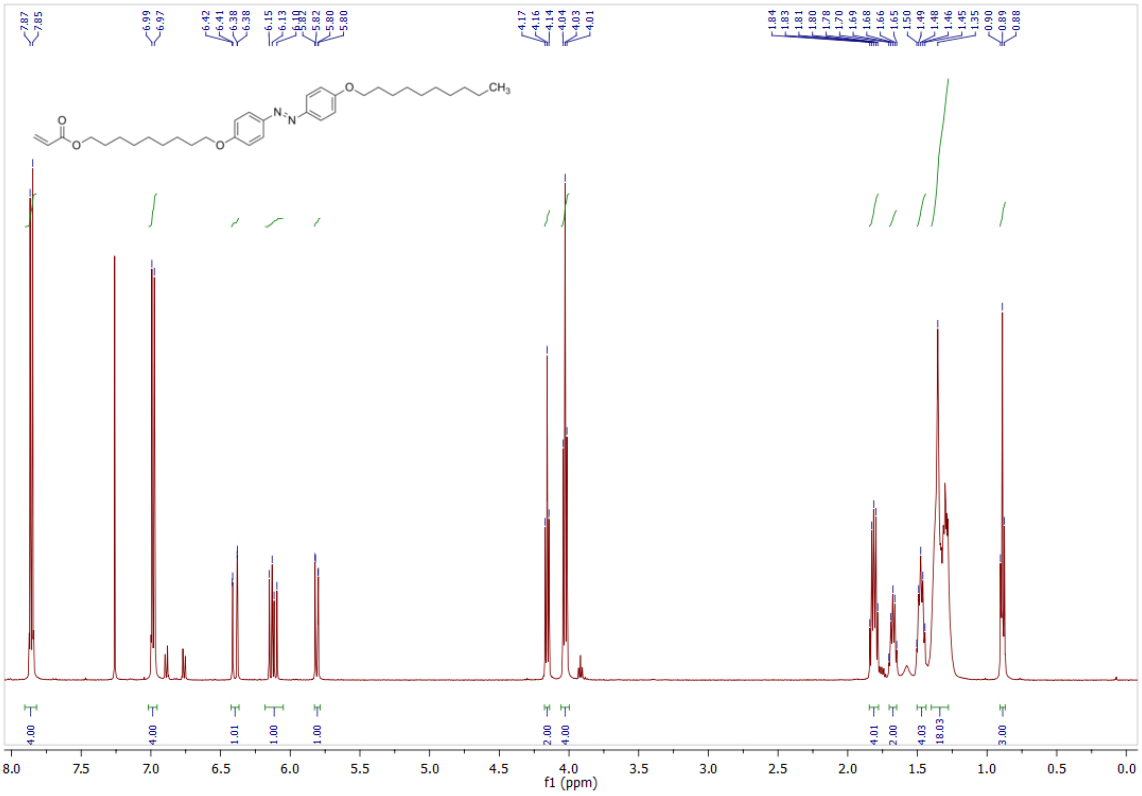

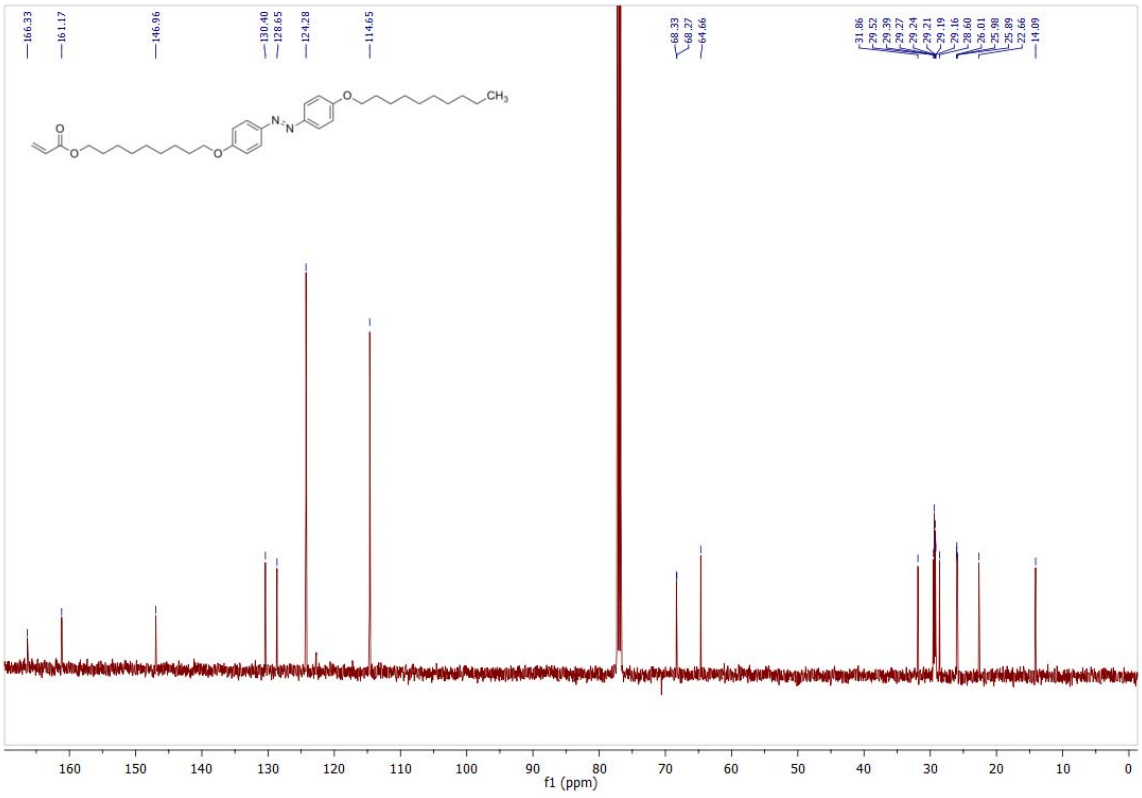

DSC-Plots

DSC scan rate 10 K/min, second time heating curves are shown with baseline corrections.

4-Hydroxy-4’-(9-hydroxynonanyloxy)azobenzene (3)

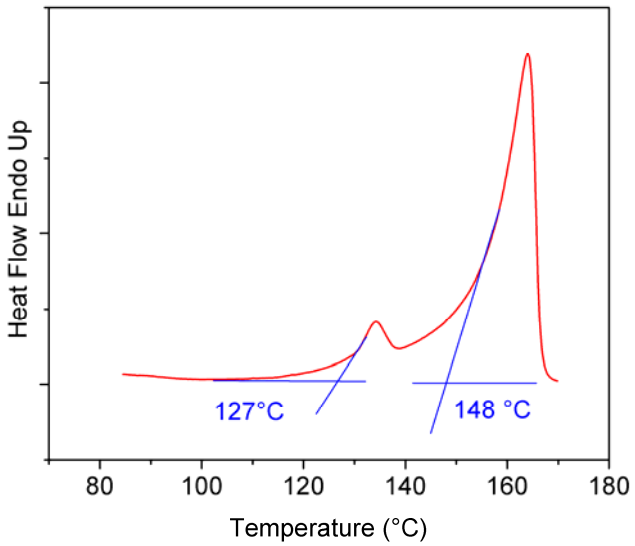

4,4’-Bis(9-hydroxynonanyloxy)azobenzene (4)

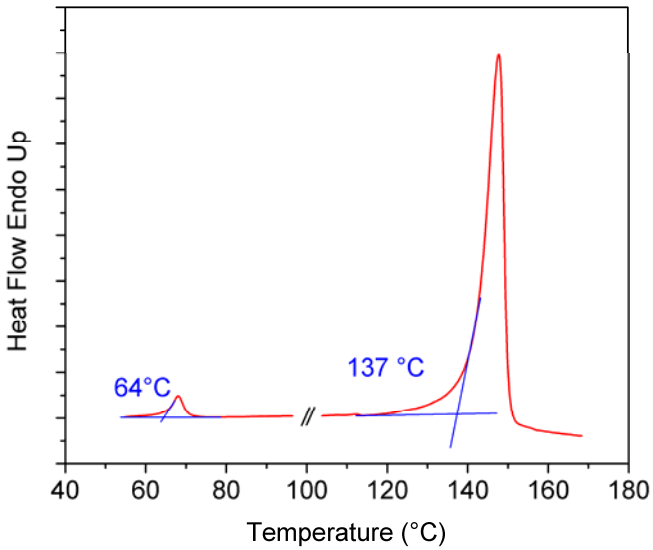

4-(9-Hydroxynonanyloxy)-4’-(nonanyloxy)azobenzene (5)

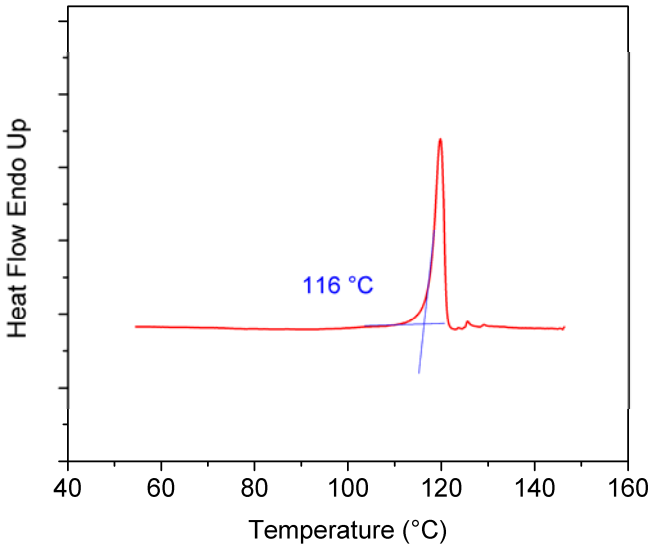

4,4’-Bis[9-(acryloyloxy)nonanyloxy]azobenzene (6)

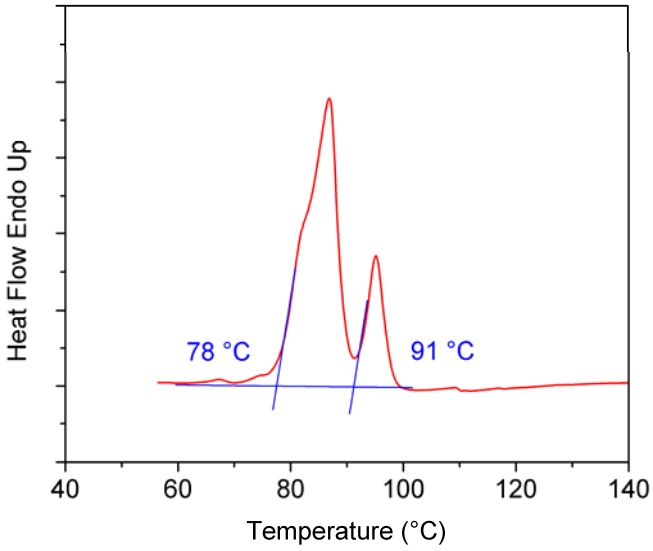

Supporting Information for *Adv. Mater.* 2012, *24*, 5676-5680.

ADVANCED MATERIALS

Supporting Information

for *Adv. Mater.*, DOI: 10.1002/adma.201201780

Joining the Un-Joinable: Adhesion Between Low Surface Energy Polymers Using Tetrapodal ZnO Linkers

Xin Jin, Jan Strueben, Lars Heepe, Alexander Kovalev, Yogendra K. Mishra, Rainer Adelung, Stanislav N. Gorb,* and Anne Staubitz**

Submitted to ADVANCED MATERIALS

Supporting Information

for

Joining the Un-Joinable: Adhesion Between Low Surface Energy Polymers Using Tetrapodal ZnO Linkers

By *Xin Jin*,[1] *Jan Strueben*,[2] *Lars Heepe*,[3] *Alexander Kovalev*,[3] *Yogendra K. Mishra*,[1] *Rainer Adelung*,*[,1] *Stanislav N. Gorb**[,3] and *Anne Staubitz**[,2]

1) Materials

ZnO tetrapods were fabricated by a flame transport method. [20] Ground ZnO was fabricated by grinding the T-ZnO with a ball milling machine (Fritsch planetary mill pulverisette 5) at 110 rpm (rounds per minute) for 15 min. PTFE was purchased from Sigma Aldrich as dispersion (60% *w*/*w* in water). PVB was supplied by Kuraray Europe GmbH as in powder form. PDMS (Silicone Elastomer, Dow Corning Sylgard 184) was purchased from Dow Corning Cooperation as a two part kit.

2) Peel Test Sample Preparation

Cross-linked PDMS elastomer: the two part kits (pre-polymer and cross-linker) of a weight ratio of 10:1 were mixed, then the mixture was placed in a vacuum oven for 5 minutes before use, until there were no visible air bubbles left.

PTFE / PDMS samples: A PTFE dispersion (70 μL) was coated onto glass substrate (25 mm by 75 mm) by slip-casting. Then the substrate was heated on a hotplate to 120 °C and kept for 10 min to completely remove the residual water, 290 °C for 10 min to remove the surfactant present in the purchased PTFE as a dispersion stabiliser, and eventually 350°C for 30 min to melt the polymer. A transparent layer was then observed. Then the heating was stopped to solidify the PTFE layer. After the sample was cooled down to room temperature, a second layer of the PTFE dispersion (140 μL) was coated onto the sample. Then part of the sample was shielded. ZnO fillers were added on the coated liquid layer (before heating) with the help of a sieve. Then this layer was solidified by repeating the procedure described above. After the PTFE had cooled down to room temperature, the PDMS pre-polymer and cross-linker mixture (ca. 1.5 g) was flow coated on top, then heated on a hotplate at 100 °C for 40 min to cure.

PVB / PDMS samples: A mixture of PVB in ethanol was prepared with weight ratio of 1 PVB: 3 ethanol. The mixture was sealed in a glass bottle and left for 24 hours until a transparent bubble free solution was formed. The solution was coated on glass substrate by slip casting. Part of the sample was then shielded. ZnO fillers were added with help of a sieve. Another glass slide (weight 4 g) was placed on top of the ZnO region for a few seconds to press the filler into the viscous PVB solution layer. Then the ethanol was evaporated at room temperature for 24 hours. The thickness of the PVB layer was ca. 20 μm. The PDMS layer was coated on top as described above.

3) Peel Tests

The samples were cut into 10 mm or 20 mm wide sheets. The upper polymer layer (PDMS) was about 1 mm thick and was back-taped with tesa® PSA adhesive tape (tesa AG Hamburg, Germany) before the peeling. The sample was fixed on the peel tester stage with double-sided tesa tape (tesa AG, Hamburg, Germany). The peeling angle was set at 90°. The peeling speed was 0.5 mm s^{-1}. The peel tester was equipped with an additional force sensor in the

perpendicular direction of peeling, which sends a signal to a feedback circuit for the control system to adjust the speed of horizontal stage movement.

4) Additional SEM Images

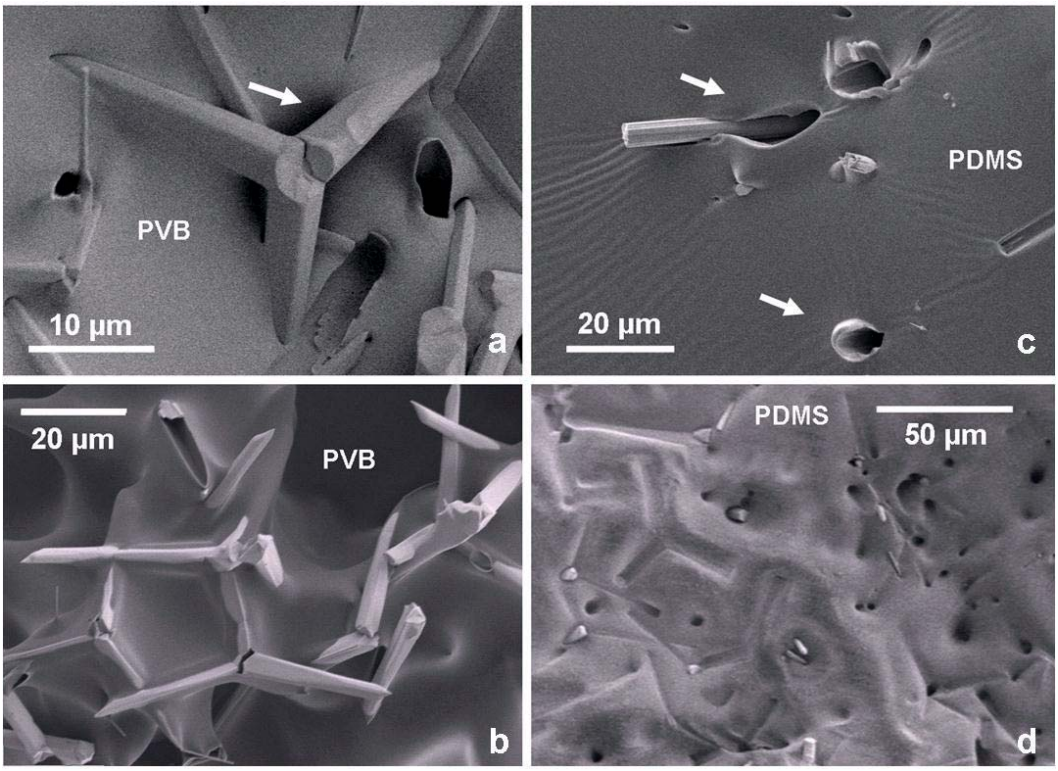

Figure SI 1. PVB surface after peeling (a, b) and peeled PDMS surface (c, d) of PVB / PDMS samples. The white arrows in the images indicate bridging (a) and pull-out (c) of a tetrapod.

5) Optical Images

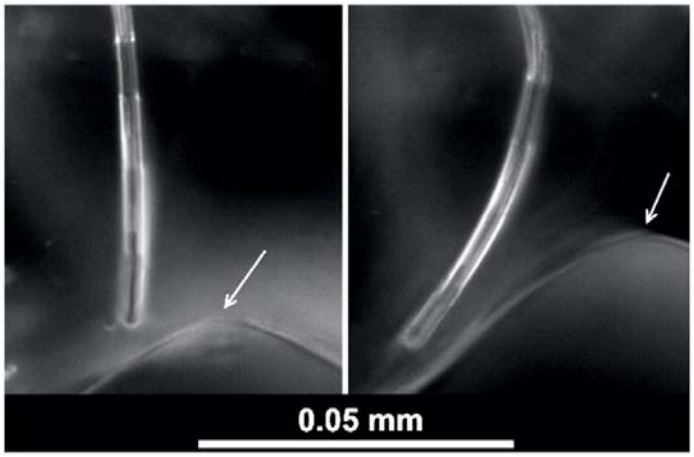

Figure SI 2. Tetrapodal ZnO embedded in a PDMS matrix. The bending of ZnO leg under stress is shown on the right. White arrows point to the front of crack propagation.

6) Error Estimation

The errors for filling factor and peeling strength were calculated from the following error transfer formula:

$$ff = \frac{m}{A} = \frac{m}{d \times l}$$

$$\frac{\Delta ff}{ff} = \frac{\Delta m}{m} + \frac{\Delta d}{d} + \frac{\Delta l}{l}$$

where *ff* is the filling factor, and *m* and *A* are the filler weight and the covered area. *d* and *l* are the width and length of the filled area. The precision of length measurement was Δd = ±0.1 cm, the weight measurement variance Δm = ±0.001 g.

The peeling strength is given by:

$$Ps = \frac{F}{b}$$

where *Ps* is the peeling strength, *F* is measured peeling force, *b* is the sample width. The errors were then calculated by

$$\Delta Ps = \frac{\Delta F}{F} + \frac{\Delta b}{b}$$

The force measurement has a variance of $\Delta F = \pm 0.01$N. Width measurement has a precision of $\Delta b = \pm 0.1$ cm.

Abbreviations

A	area
Ac	acetate
as	apparent singlet (NMR)
adt	apparent dublet triplet (NMR)
ATR	attenuated total reflectance
Bu	butyl
calcd.	calculated
CI	chemical ionization
COSY	correlated spectroscopy
d	doublet (NMR)
DCM	dichloromethane
DMF	*N*,*N*-dimethylformamide
DMSO	dimethylsulfoxide
DSC	dynamic scanning calorimetry
DFT	density functional theory
DTA	differential thermo analysis
EI	electron ionization
ESI	electrospray ionization
FT-IR	Fourier transform infrared sprectroscopy
GC	gas chromatography
GC/MS	gas chromatography-mass spectrometry
GPC	gel permeation chromatography
HMBC	heteronuclear multiple bond coherence
HSQC	heteronuclear single quantum coherence
IR	infrared
LC	liquid crystalline
LCP	liquid crystalline polymer
LCE	liquid crystalline elastomer
m	medium (concerning the intensity) (IR)
m	multiplet (NMR)

Me	methyl
MeTHF	methyl tetrahydrofuran
M.p.	melting point
MS	mass spectrometry
PDI	poly dispersity index
PDMS	poly(dimethylsiloxane)
MCLCP	main chain liquid crystalline polymer
M_n	number average molecular weight (GPC)
M_w	weight average molecular weight (GPC
MW	microwave
Ph	phenyl
PTFE	polytetrafluoroethylene
RF	response factor
R_f	retention factor
s	strong (concerning the intensity) (IR)
s	singlet (NMR)
SCLCE	side chain liquid crystalline elastomer
SCLCP	side chain liquid crystalline polymer
t	triplet (NMR)
THF	tetrahydrofuran
TG	thermo gravimetry
T_g	glass transition temperature
UV	ultra violet
vis	visible
w	weak (concerning the intensity) (IR)
XRD	X-ray diffraction

References

[1] a) B. Bhushan, in *Nanotribology and Nanomechanics*, Springer Berlin Heidelberg, **2008**, pp. 1073-1134; b) L. Heepe, S. N. Gorb, *Ann. Rev. Mater. Res.* **2014**, *44*, 173-203.

[2] a) A. Jagota, S. J. Bennison, *Integr. Comp. Biol.* **2002**, *42*, 1140-1145; b) T. Tang, C.-Y. Hui, N. J. Glassmaker, *J. R. Soc. Interface* **2005**, *2*, 505-516; c) J. Y. Chung, M. K. Chaudhury, *J. R. Soc. Interface* **2005**, *2*, 55-61.

[3] a) B. N. J. Persson, *J. Chem. Phys.* **2003**, *118*, 7614-7621; b) B. N. J. Persson, S. Gorb, *J. Chem. Phys.* **2003**, *119*, 11437-11444; c) T. W. Kim, B. Bhushan, *J. Adhes. Sci. Technol.* **2007**, *21*, 1-20; d) A. Filippov, V. L. Popov, S. N. Gorb, *J. Theor. Biol.* **2011**, *276*, 126-131.

[4] R. Spolenak, S. Gorb, E. Arzt, *Acta Biomater.* **2005**, *1*, 5-13.

[5] S. N. Gorb, M. Varenberg, *J. Adhes. Sci. Technol.* **2007**, *21*, 1175-1183.

[6] a) K. Autumn, Y. A. Liang, S. T. Hsieh, W. Zesch, W. P. Chan, T. W. Kenny, R. Fearing, R. J. Full, *Nature* **2000**, *405*, 681-685; b) H. Gao, X. Wang, H. Yao, S. Gorb, E. Arzt, *Mechanics of Materials* **2005**, *37*, 275-285; c) S. Niederegger, S. Gorb, *J. Insect Physiol.* **2003**, *49*, 611-620.

[7] A. Donald, A. Windle, S. Hanna, *Liquid Crystalline Polymers*, 2nd ed., Cambridge University Press, Cambridge, **2006**.

[8] a) C. Lagrasta, I. R. Bellobono, M. Bonardi, *J. Photoch. Photobio. A* **1997**, *110*, 201-205; b) S. K. Yesodha, C. K. Sadashiva Pillai, N. Tsutsumi, *Prog. Polym. Sci.* **2004**, *29*, 45-74.

[9] P.-G. de Gennes, *Cr. Acad. Sci. II B* **1997**, *324*, 343-348.

[10] J. M. Mark, H. R. Allcock, R. West., *Inorganic Polymers*, 2nd ed., Oxford University Press, New York, **2005**.

[11] a) M. Shansong, T. Mei, T. Shunqing, Z. Changren, *J. Mater. Sci. Lett.* **2003**, *22*, 343-344; b) D. Fallahi, H. Mirzadeh, M. T. Khorasani, *J. Appl. Polym. Sci.* **2003**, *88*, 2522-2529.

[12] a) J. E. Mark, *Silicon-Based Polymer Science, Vol. 224*, American Chemical Society, Washington D. C., **1990**; b) P. R. Dvornic, J. D. Jovanovic, M. N. Govedarica, *J. Appl. Polym. Sci.* **1993**, *49*, 1497-1507; c) M. M. Somoza, M. I. Sluch, M. A. Berg, *Macromolecules* **2003**, *36*, 2721-2732.

[13] V. Candrasekhar, *Inorganic and Organometallic Polymers*, Springer Verlag, Berlin Heidelberg, **2005**.

[14] A. A. Yaroshevsky, *Geochem. Int+* **2006**, *44*, 48-55.

[15] M. Rehahn, W. L. Mattice, U. W. Suter, *Adv. Polym. Sci.* **1997**, *131/132*, 1.

[16] B. C. Cope, D. E. Packham, G. Leggett, J. C. Beech, G. B. Lowe, D. Briggs, D. M. Brewis, A. D. Crocombe, D. G. Dixon, W. J. Van Ooij, B. Parbhoo, C. M. Warwick, J. Pritchard, S. Millington, C. Chatfield, J. Comyn, D. A. Dillard, B. Kneafsey, M. E. R. Shanahan, A. V. Pocius, in *Handbook of Adhesion*, John Wiley & Sons, Ltd, **2005**, pp. 439-525.

[17] G. Wypych, in *Handbook of Polymers* (Ed.: G. Wypych), Elsevier, Oxford, **2012**, pp. 328-332.

[18] J. E. Mark, B. Erman, *Rubberlike Elasticity. A Molecular Primer*, Wiley-Interscience, New York, **1988**.

[19] *Polymer Data Handbook*, Oxford University Press, New York, **1999**.

[20] P. R. Dvornic, R. W. Lenz, *Macromolecules* **1992**, *25*, 3769-3778.

[21] G. S. Hartley, *Nature* **1937**, *140*, 281.

[22] H. Zollinger, *Colour Chemistry, Synthesis, Properties, and Applications of Organic Dyes*, VCH, Weinheim, **1987**.

[23] H. M. D. Bandara, S. C. Burdette, *Chem. Soc. Rev.* **2012**, *41*, 1809-1825.

[24] G. S. Hartley, R. J. W. Le Fevre, *J. Chem. Soc.* **1939**, 531-535.

[25] T. Nägele, R. Hoche, W. Zinth, J. Wachtveitl, *Chem. Phys. Lett.* **1997**, *272*, 489-495.

[26] a) H. Rau, E. Lueddecke, *J. Am. Chem. Soc.* **1982**, *104*, 1616-1620; b) C. R. Crecca, A. E. Roitberg, *J. Phys. Chem. A* **2006**, *110*, 8188-8203; c) J. L. Magee, W. Shand, H. Eyring, *J. Am. Chem. Soc.* **1941**, *63*, 677-688; d) D. Y. Curtin, E. J. Grubbs, C. G. McCarty, *J. Am. Chem. Soc.* **1966**, *88*, 2775-2786.

[27] K. G. Yager, C. J. Barrett, in *Smart Light-Responsive Materials*, John Wiley & Sons, Inc., **2009**, pp. 1-46.
[28] a) C. Zhang, N. Jiao, *Angew. Chem. Int. Edit* **2010**, *49*, 6174-6177; b) E. Merino, *Chem. Soc. Rev.* **2011**, *40*, 3835-3853.
[29] S. Gowda, D. C. Gowda, *Synthesis* **2002**, *2002*, 0460-0462.
[30] B.-C. Yu, Y. Shirai, J. M. Tour, *Tetrahedron* **2006**, *62*, 10303-10310.
[31] K. Haghbeen, E. W. Tan, *J. Org. Chem.* **1998**, *63*, 4503-4505.
[32] a) A. R. Katritzky, J. Wu, S. V. Verin, *Synthesis* **1995**, *1995*, 651-653; b) E. Ciganek, in *Org. Reactions*, John Wiley & Sons, Inc., **2004**; c) T. T. T. Nguyen, A. Boussonnière, E. Banaszak, A.-S. Castanet, K. P. P. Nguyen, J. Mortier, *J. Org. Chem.* **2014**, *79*, 2775-2780.
[33] H. J. Shine, H. Zmuda, H. Kwart, A. G. Horgan, M. Brechbiel, *J. Am. Chem. Soc.* **1982**, *104*, 5181-5184.
[34] S. Farhadi, S. Sepahvand, *J. Mol. Catal. A-Chem.* **2010**, *318*, 75-84.
[35] M. Matsui, Y. Iwata, T. Kato, K. Shibata, *Dyes Pigments* **1988**, *9*, 109-117.
[36] a) A. Alberti, N. Bedogni, M. Benaglia, R. Leardini, D. Nanni, G. F. Pedulli, A. Tundo, G. Zanardi, *J. Org. Chem.* **1992**, *57*, 607-613; b) A. Nose, T. Kudo, *Chem. Pharm. Bull.* **1988**, *36*, 1529-1533.
[37] H. Baumgärtel, E. U. Franck, W. Grünbein, H. Stegemeyer, *Liquid Crystals, Vol. 3*, Springer, New York, **1994**.
[38] X.-J. Wang, Q.-F. Zhou, *Liquid Crystalline Polymers*, World Scientific Publishing Co. Pte. Ltd., Singapore, **2004**.
[39] M. Schadt, *Annu. Rev. Mater. Sci.* **1997**, *27*, 305-379.
[40] T. Ganicz, W. Stańczyk, *Materials* **2009**, *2*, 95-128.
[41] V. S. Papkov, Y. K. Godovsky, V. S. Svistunov, V. M. Litvinov, A. A. Zhdanov, *J. Polym. Sci. A1* **1984**, *22*, 3617-3632.
[42] S. Dai, P. Ravi, K. C. Tam, *Soft Matter* **2008**, *4*, 435-449.
[43] M. Heskins, J. E. Guillet, *J. Macromol. Sci. A* **1968**, *2*, 1441-1455.
[44] D. A. Davis, A. Hamilton, J. Yang, L. D. Cremar, D. Van Gough, S. L. Potisek, M. T. Ong, P. V. Braun, T. J. Martinez, S. R. White, J. S. Moore, N. R. Sottos, *Nature* **2009**, *459*, 68-72.
[45] a) F. D. Jochum, P. Theato, *Chem. Soc. Rev.* **2013**, *42*, 7468-7483; b) D. Iqbal, M. Samiullah, *Materials* **2013**, *6*, 116-142.
[46] E. Merian, *Text. Res. J.* **1966**, *36*, 612-618.
[47] H. Finkelmann, E. Nishikawa, G. G. Pereira, M. Warner, *Phys. Rev. Lett.* **2001**, *87*, 015501.
[48] a) N. B. Holland, T. Hugel, G. Neuert, A. Cattani-Scholz, C. Renner, D. Oesterhelt, L. Moroder, M. Seitz, H. E. Gaub, *Macromolecules* **2003**, *36*, 2015-2023; b) T. Hugel, N. B. Holland, A. Cattani, L. Moroder, M. Seitz, H. E. Gaub, *Science* **2002**, *296*, 1103-1106.
[49] a) D. Y. Kim, S. K. Tripathy, L. Li, J. Kumar, *Appl. Phys. Lett.* **1995**, *66*, 1166-1168; b) P. Rochon, E. Batalla, A. Natansohn, *Appl. Phys. Lett.* **1995**, *66*, 136-138.
[50] a) H. Murakami, A. Kawabuchi, R. Matsumoto, T. Ido, N. Nakashima, *J. Am. Chem. Soc.* **2005**, *127*, 15891-15899; b) B. Hesseler, M. Zindler, R. Herges, U. Lüning, *Eur. J. Org. Chem.* **2014**, *2014*, 3885-3901.
[51] Y. Yu, M. Nakano, T. Ikeda, *Nature* **2003**, *425*, 145-145.
[52] a) M. Yamada, M. Kondo, J.-i. Mamiya, Y. Yu, M. Kinoshita, C. J. Barrett, T. Ikeda, *Angew. Chem. Ger. Edit.* **2008**, *120*, 5064-5066; b) M. Yamada, M. Kondo, J.-i. Mamiya, Y. Yu, M. Kinoshita, C. J. Barrett, T. Ikeda, *Angew. Chem. Int. Edit.* **2008**, *47*, 4986-4988.
[53] a) S. Pandey, S. P. Mishra, B. Kolli, T. Kanai, A. B. Samui, *J. Polym. Sci. A1* **2012**, *50*, 2659-2668; b) U. Hrozhyk, S. Serak, N. Tabiryan, T. J. White, T. J. Bunning, *Opt. Express* **2009**, *17*, 716-722; c) K. D. Harris, R. Cuypers, P. Scheibe, C. L. van Oosten, C. W. M. Bastiaansen, J. Lub, D. J. Broer, *J. Mater. Chem.* **2005**, *15*, 5043-5048; d) D. H. Wang, K. M. Lee, Z. Yu, H. Koerner, R. A. Vaia, T. J. White, L.-S. Tan, *Macromolecules* **2011**, *44*, 3840-3846.
[54] S. Iamsaard, S. J. Aßhoff, B. Matt, T. Kudernac, J. L. M. CornelissenJeroen, S. P. Fletcher, N. Katsonis, *Nat. Chem.* **2014**, *6*, 229-235.

[55] T. Ikeda, M. Nakano, Y. Yu, O. Tsutsumi, A. Kanazawa, *Adv. Mater.* **2003**, *15*, 201-205.
[56] Y. Yu, M. Nakano, T. Ikeda, in *Pure Appl. Chem., Vol. 76*, **2004**, p. 1467.
[57] Y. Yu, T. Ikeda, in *Smart Light-Responsive Materials*, John Wiley & Sons, Inc., **2009**, pp. 95-144.
[58] M. Kondo, Y. Yu, T. Ikeda, *Angew. Chem. Int. Edit* **2006**, *118*, 1406-1410.
[59] H. Yang, A. Buguin, J.-M. Taulemesse, K. Kaneko, S. Méry, A. Bergeret, P. Keller, *J. Am. Chem. Soc.* **2009**, *131*, 15000-15004.
[60] J. Strueben, P. J. Gates, A. Staubitz, *J. Org. Chem.* **2014**, *79*, 1719-1728.
[61] P. R. Dvornic, R. W. Lenz, *J. Appl. Polym. Sci.* **1980**, *25*, 641-652.
[62] V. Passarelli, F. Benetollo, P. Zanella, G. Carta, G. Rossetto, *Dalton T.* **2003**, 1411-1418.
[63] P. R. Dvornic, R. W. Lenz, *J. Polym. Sci. A1* **1982**, *20*, 951-966.
[64] a) G. Marrucci, *Macromol. Sy.* **1996**, *101*, 131-138; b) F. Giavazzi, S. Crotti, A. Speciale, F. Serra, G. Zanchetta, V. Trappe, M. Buscaglia, T. Bellini, R. Cerbino, *Soft Matter* **2014**, *10*, 3938-3949.
[65] C. Brown, *Acta Crystallog.* **1966**, *21*, 146-152.
[66] A. Mostad, C. Romming, *Acta Chem. Scand.* **1971**, *25*, 3561-3568.
[67] a) F. C. Krebs, *Sol. Energ. Mat. Sol. C.* **2009**, *93*, 465-475; b) F. C. Krebs, *Sol. Energ. Mat. Sol. C.* **2009**, *93*, 394-412.
[68] A. Knobloch, A. Manuelli, A. Bernds, W. Clemens, *J. Appl. Phys.* **2004**, *96*, 2286-2291.
[69] A. F. Burchat, J. M. Chong, N. Nielsen, *J. Organomet. Chem.* **1997**, *542*, 281-283.
[70] B. Jousselme, P. Blanchard, N. Gallego-Planas, E. Levillain, J. Delaunay, M. Allain, P. Richomme, J. Roncali, *Chem.- Eur. J.* **2003**, *9*, 5297-5306.
[71] S. H. Gund, R. S. Shelkar, J. M. Nagarkar, *RSC Advances* **2014**, *4*, 42947-42951.
[72] E. Hedaya, J. H. Kawakami, P. W. Kopf, G. T. Kwiatkowski, D. W. McNeil, D. A. Owen, E. N. Peters, R. W. Tulis, *J. Polym. Sci. A1* **1977**, *15*, 2229-2238.